THE CHEMISTRY OF FUNCTIONALISED CAGE COMPLEXES

A Thesis Submitted for

the Degree of

Doctor of Philosophy of

The Australian National University

Research School of Chemistry

by

Anthony James Elliott

(April 1998)

DECLARATION

The work presented in this thesis is the original work of the candidate, except where due reference is made in the text.

The X-ray structures throughout this thesis were determined by Dr A. C. Willis at the Australian National University.

The antiviral testing of some of the alkyl tail complexes presented in this thesis was performed and coordinated by Dr S. Marcuccio and his team at the Division of Molecular Science, CSIRO, Clayton, Victoria.

THE AUSTRALIAN
LIBRARY
NATIONAL UNIVERSITY

Anthony James Elliott

Acknowledgements

I wish to express my sincere appreciation to my supervisor Professor Alan Sargeson for his guidance and encouragement during the course of this work.

I would specially like to thank Dr Patricia Angus, Dr Paul Bernhardt, Dr Bruce Wild, Dr Chris Crane, Dr Peter Osvath and Dr Mark Lynch for many helpful discussions, contributions and their patience during my time at the RSC.

My gratitude is extended to the following people for their assistance and advice: Dr Anthony Willis, who solved all of the crystal structures appearing in this work, Dr Stuart Macgregor, Tim Lovell, Dr Mark Bown, Richard Baldwin, Dr Kylie Brown, Paul Gugger, Nick Perkins, Chris Blake and Tin Culnane. I would also like to thank the staff of the RSC including the Analytical Services Unit, the NMR unit, the Workshop staff, the computer unit, and Joan Smith the librarian.

The antiviral testing of some of the alkyl tail complexes presented in this thesis was performed and coordinated by Dr S. Marcuccio and his team at the Division of Molecular Science, CSIRO, Clayton, Victoria.

Thankyou to my co-students and fellow Sargo group members who have made my time at the RSC enjoyable and worthwhile.

Receipt of an ANU Postgraduate PhD Scholarship from the RSC is gratefully acknowledged. The financial assistance from the RSC to attend conferences in Perth and Townsville was also appreciated.

Finally, I would like to thank my friends from Fenner Hall for their support and encouragement throughout my years of study at the ANU.

To my parents Mike and Joan and my sister Bronwyn whom without their love and support this thesis would not have been possible.

Abstract

Reaction of the hexadentate template $[Co^{III}(sen)]^{3+}$ ([(tris(4-amino-2-azabutyl)amine)cobalt(III)]$^{3+}$) with various carbon acids (diethyl malonate, ethyl acetoacetate and ethyl cyanoacetate) and formaldehyde in aqueous base resulted in a series of amide, amidine, saturated cage and macrocyclic complexes. The hexadentate amide cage ligand Me,COOH-2-oxosar (1-carboxy-8-methyl-2-oxo-3,6,10,13,16,19-hexaazabicyclo[6.6.6]icosane) was removed from the Co(III) ion and new metal complexes and structures were established which have varying properties.

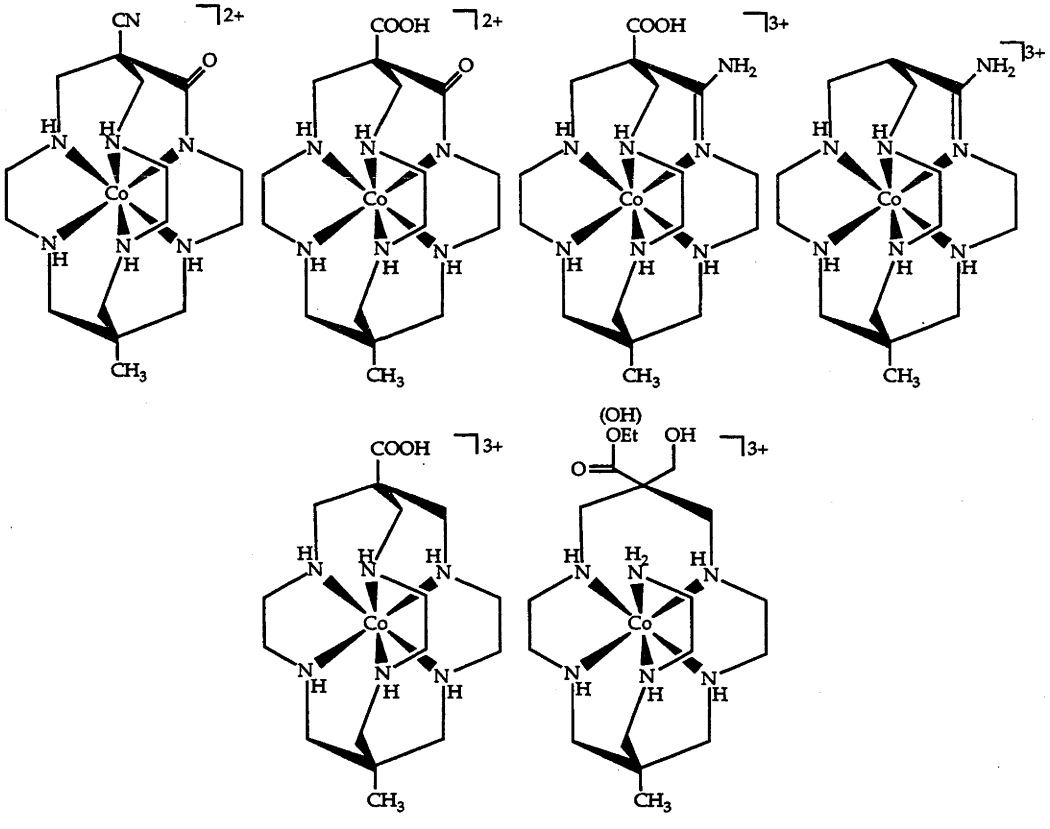

Amide cages were also synthesised by oxidation of the ligand in the presence of the Co(III) ion using mercuric acetate. Both oxo and dioxo cages were isolated, the metal ion was extruded and different metals were substituted. This strategy expanded the metal amido cage chemistry considerably.

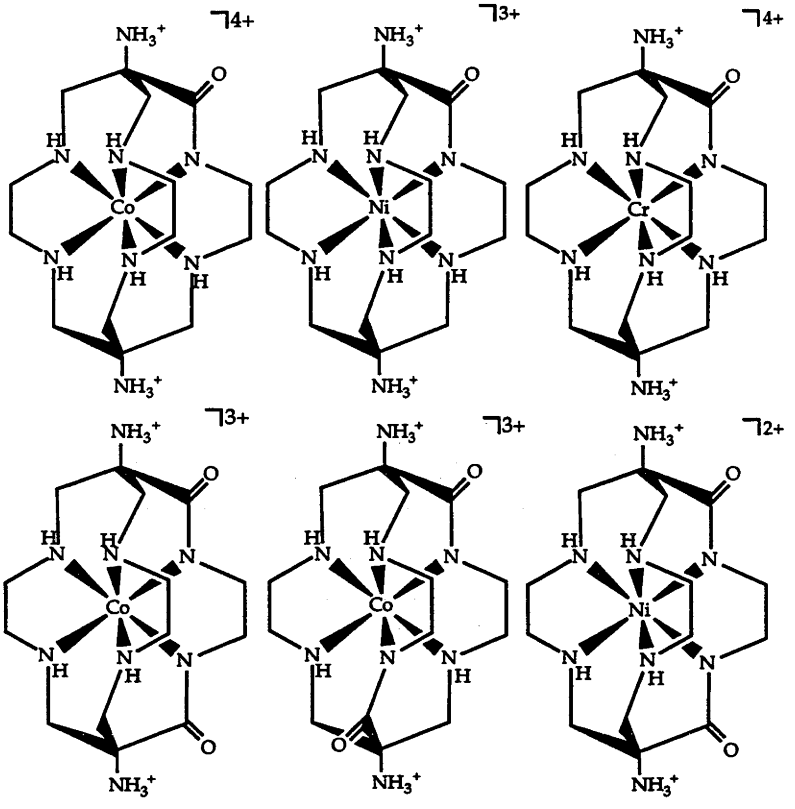

Trigonally symmetrical triamide complexes were constructed from tripodal ligands. The first method involved condensing ethane-1,2-diamine directly with ethyl tricarboxylate triethylester. In the second method 1,1,1-tris(aminomethyl)ethane was reacted with 2-bromo-2-methylpropionyl bromide. The ligand was then converted into the triamide triamine by a two step process. Both ligands were then complexed to cobalt(III) to give new non electrolyte triamido tripodal hexadentate complexes which unfortunately resisted attempts to encapsulate the metal.

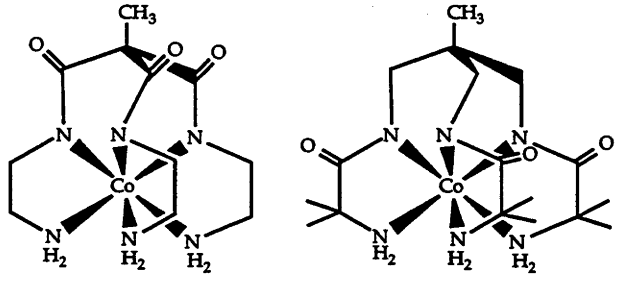

The syntheses, spectroscopic and structural properties of many of the complexes are reported. The bound amido ions alter the redox potentials of

the systems by as much as 0.2 V relative to the saturated analogue. The nature of the apical substituents also influences the redox couples. The Ni(III) ion for example, is now readily accessible in water with both the monoamido and diamido ligand systems and routes to Ni(IV) and Fe(IV) complexes at least are evident.

Antiviral activity for complex ligands such as two linked nitrogen macrocycles has been published and it prompted an examination for many of the cage complexes. Dialkylated derivatives of the sar cages have been simply synthesised by condensing $[Co(en)_3]^{3+}$ ([(tris(ethane-1,2-diamine)cobalt(III)]$^{3+}$) with formaldehyde and 1-butanal or 1-pentanal in the presence of aqueous base. Reduction of the diethyl di-imine species to $[Co(Et_2\text{-sar})]^{3+}$ ([(1,8-diethyl-3,6,10,13,16,19-hexaazabicyclo-[6.6.6]icosane)-cobalt(III)]$^{3+}$) with $NaBH_4$ followed by resolution of this complex was achieved. Attempts to add various carbon acids to the imine carbon were also undertaken. The antiviral properties of the diethyl di-imine cage complex, $[Co(Et_2\text{-sar})]^{3+}$ and others were examined. $[Co(Et_2\text{-sar})]^{3+}$ has been shown to have substantial inhibitory properties towards the Hepatitis B virus.

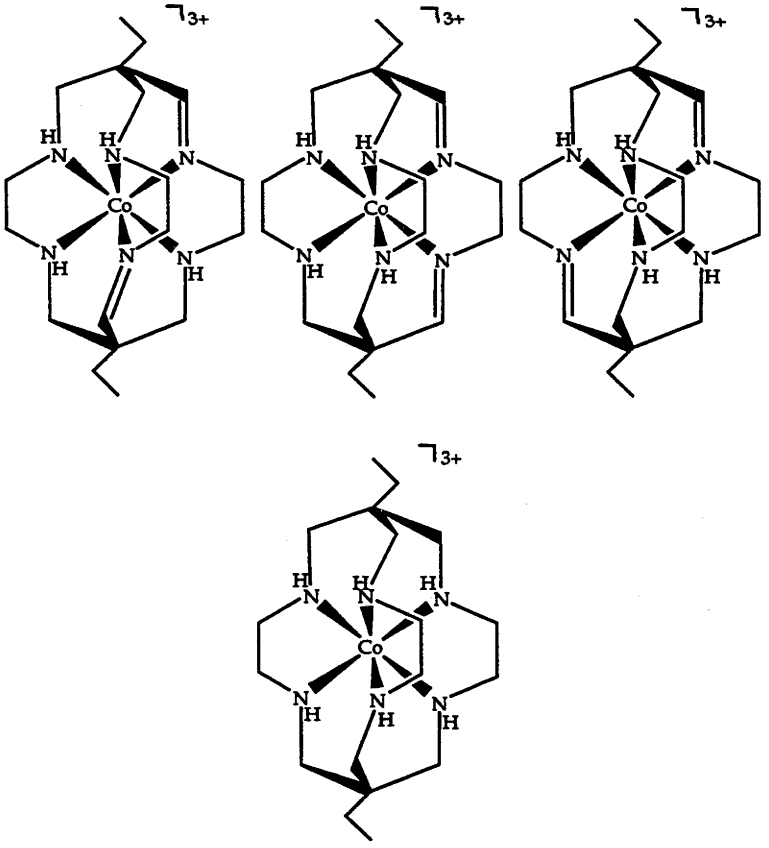

Table of Contents

Abbreviations

AIDS	Acquired Immune Deficiency Syndrome
AR	analytical reagent
CD	circular dichroism
$CDCl_3$	deutero chloroform
chxn	cyclohexanediamine
COSY	Correlation Spectroscopy
CV	cyclic voltammogram
DEPT	distortionless polarisation transfer
diamsar	1,8-diaminosarcophagine; 1,8-diamino-3,6,10,13,16,19-hexaazabicyclo[6.6.6]icosane
D_2O	deuterium oxide
en	ethane-1,2-diamine
ESMS	electrospray mass spectrometry
FT	Fourier Transform
HBV	Hepatitis B Virus
HIV	Human Immunodeficiency Virus
IR	infra-red
NaTSP	sodium(trimethylsilyl)propanesulfonate
NMR	nuclear magnetic resonance
ORD	optical rotary dispersion
RT	reverse transcriptase

sar	sarcophagine; 3,6,10,13,16,19-hexaazabicyclo[6.6.6]icosane
SCE	saturated calomel electrode
sen	1,1,1-tris(4-amino-2-azabutyl)ethane
sep	sepulchrate; 1,3,6,8,10,13,16,19-octaazabicyclo[6.6.6]icosane
SHE	standard hydrogen electrode
tacn	1,4,7-triazacyclononane
tame	1,1,1-tris(aminomethyl)ethane
TMS	tetramethylsilane
UV	ultra violet
vis	visible

CHAPTER 1.

Introduction to the Synthesis, Structure and Properties of Cage Complexes Bearing Amide and Imine Groups.

1.1 Introduction to Functionalised Cage Chemistry.

1.1.1 Preamble

Saturated polyazapolymacrocyclic or cage complexes have occupied a significant place in chemistry for the last two and a half decades. This prominence has arisen as a result of their interesting properties including fully encapsulating metal ions, possessing enhanced thermodynamic and kinetic stability relative to their unencapsulated counterparts, displaying relevance to biological and industrial processes. In some instances, the syntheses of such cages can be very simply carried out using template procedures around cobalt(III), and two such examples are shown in Figure 1.

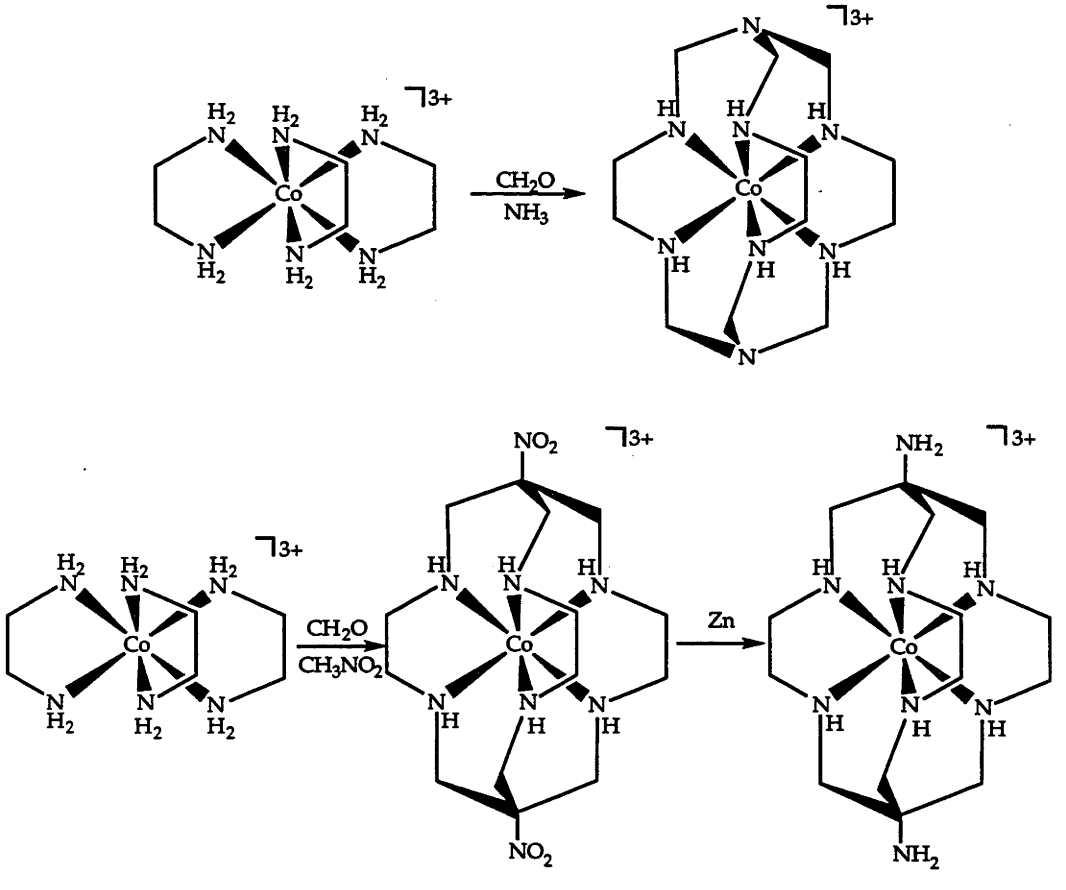

Figure 1

The examples shown above are unusual in that the Co(II) forms of the complexes have been found to be inert to hydrolysis in acidic aqueous media. This is in contrast to $[Co^{II}(NH_3)_6]^{2+}$ which loses ammonia in less than a millisecond under the same conditions. This observation alone shows that cage complexes are remarkably stable. In fact, rigorous conditions are required to remove the cobalt from the ligand. Once this is

achieved, the free ligand can then be recoordinated to other transition metals ions and the resulting complexes often show a similar stability to that of the cobalt cage compounds. It has also been shown that the cage ligands are versatile enough to incorporate a range of metal ions, in different oxidation states, from Co(III) to Hg(II), and the metals are bound to all six nitrogen donor atoms. At this stage most of the first row, along with some second and third row, transition metal ions have been encapsulated by cage ligands like sar (3,6,10,13,16,19-hexaazabicyclo[6.6.6]icosane) or diamsar (1,8-diamino-3,6,10,13,16,19-hexaazabicyclo[6.6.6]icosane) (Figure 1). For such a series of metal ions to be encapsulated by a single ligand is certainly unusual and cage ligands have provided an opportunity to study their properties systematically under similar conditions.

More importantly, the ability to encapsulate metal ions in different oxidation states has allowed the use of cage compounds in redox reactions. Furthermore, incorporation of functional groups into the saturated cage ligand extends the range of these complexes for these reactions and allows modulation of the redox potential without altering the electron self exchange rate significantly for a particular metal. Functional groups have also been found to alter the spectroscopic properties of the complexes to a degree. This also increases their practical value, including the possibility of using some of these complexes to produce H_2 from H_2O.

Two obvious functionalities to build into the skeleton of the cage complexes are amide and imine groups. Ligands functionalised with these types of moieties display some interesting characteristics. For example, the amide is often bonded as the deprotonated anion and in this form it can be used to stabilise metal ions in higher oxidation states.[1] On the other hand, imines tend to stabilise the low oxidation state preferentially. They are also activated towards addition of a nucleophile when bound to some metal ions. This property may allow the stereospecific introduction of substituents into the cage for a variety of chemical, physical and biological applications.

Despite a large amount of research on macrocyclic amide[1-8] and imine[9-11] complexes, there has been relatively little with amide and imine cage complexes. Therefore, one of the aims of this thesis research was to synthesise and characterise a number of amide and imine cage complexes as well as test the reactivity of the imine group to different carbon acids in the context of the cage. In addition, some exploration of the properties,

both physical and biological, of the compounds derived from this research was undertaken.

Various synthetic strategies exist for these types of complexes and some of these will now be outlined. The most common methods available that allow incorporation of functional groups into cage complexes include direct template synthesis, oxidative reactions and direct non-template organic synthesis. In most cases there is a need to demetallate the template complex so the new metal ions can be introduced.

1.2 Synthetic Strategies.

1.2.1 Template Methods

For template reactions, the metal plays a central role in the formation of the functionalised cage complex. It organises reactive fragments within its coordination sphere in such a way that they are activated for reaction with incoming substrates. The reactions are cheap, efficient and high-yielding which makes this strategy very appealing. Two classic examples are the synthesis of $[Co^{III}(sep)]^{3+}$ [12] and $[Co^{III}(\{NO_2\}_2\text{-sar})]^{3+}$ [13] from $[Co^{III}(en)_3]^{3+}$, formaldehyde and ammonia or nitromethane respectively in basic conditions (Figure 1). Other cage systems can be formed by simply varying the carbon acid and template in the above strategy. For example, by using formaldehyde, diethyl malonate and $[Co^{III}(sen)]^{3+}$ a less symmetrical system arises (Figure 2).[14] The resultant amide cage complex possesses different properties and apical substituents to that of $[Co^{III}(\{NH_2\}_2\text{-sar})]^{3+}$ for example and carries a dipositive charge. A further illustration is the reaction between $[Co^{III}(sen)]^{3+}$, formaldehyde and propanal in basic acetonitrile which also led to an unsymmetrical cage system possessing an imine group (Figure 3). Subsequent treatment of this complex with $NaBH_4$ then gave the fully saturated cage complex.

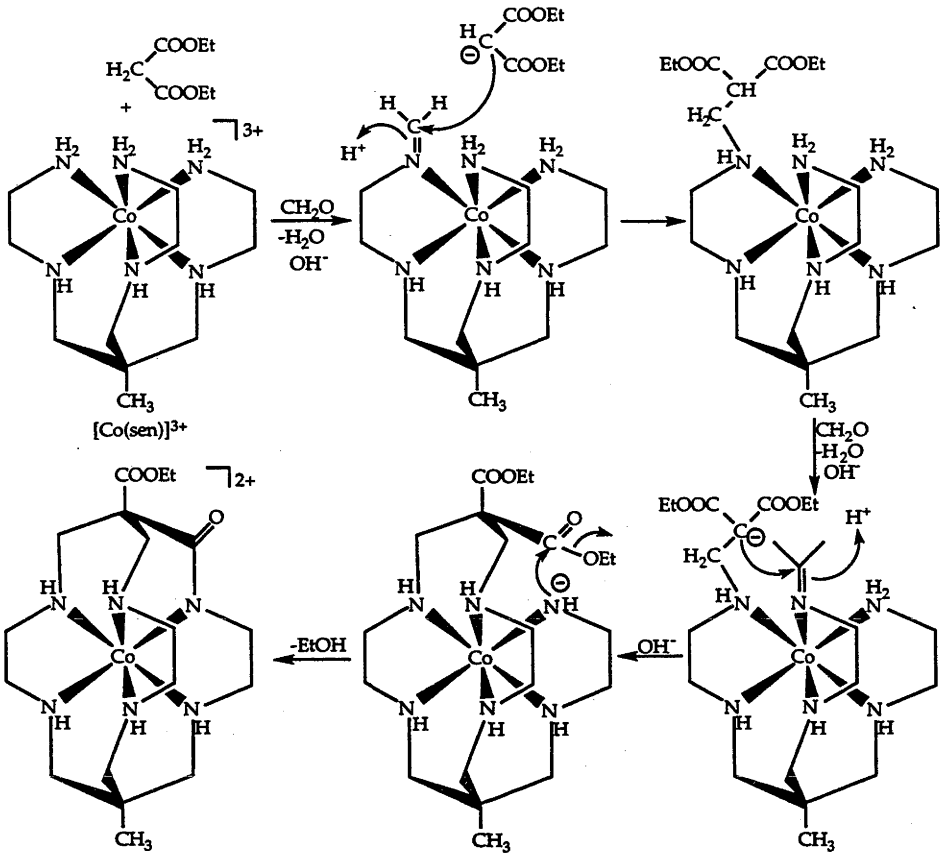

Figure 2

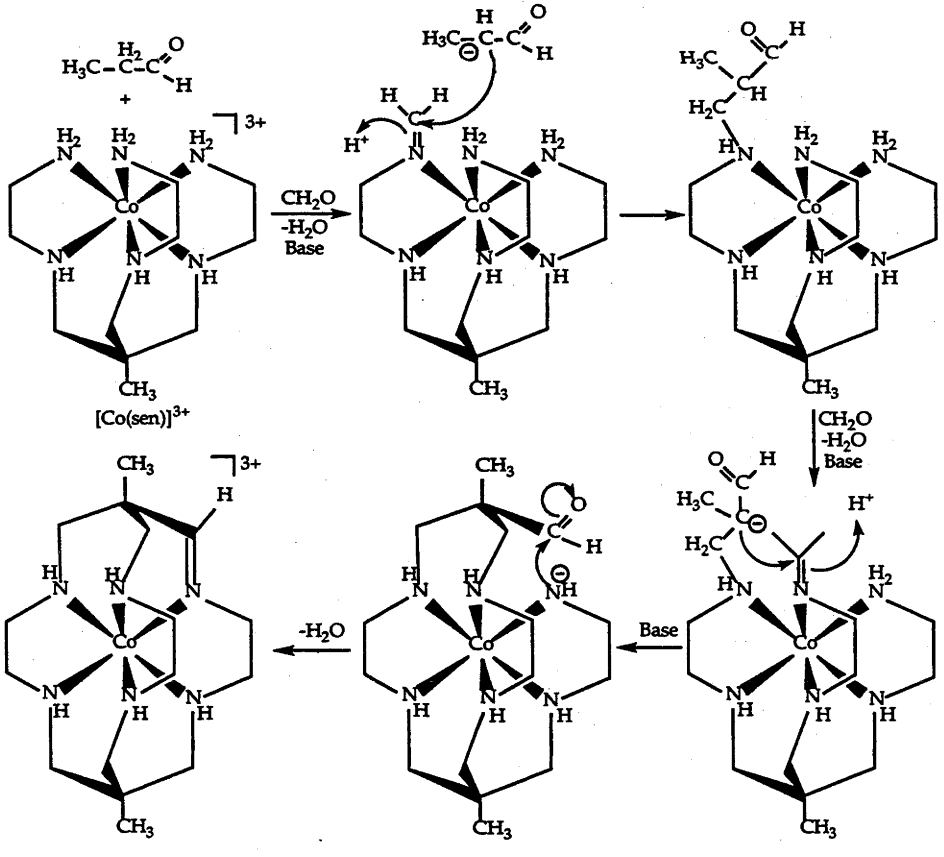

Figure 3

1.2.2 Oxidative Type Reactions

In a few instances, cages undergo oxidation resulting in either amide[15] or imine[16] groups being embodied into the caps or ethylene fragments of the ligand. The complex may do this by an internal redox reaction coupled with an external oxidant. For example the $[Ru^{II}(sar)]^{2+}$ ion is readily oxidised to the Ru(III) complex, which then spontaneously disproportionates to the $[Ru^{II}(sar)]^{2+}$ and $[Ru^{IV}(sar\text{-}2H)]^{2+}$ ions. The latter then undergoes a spontaneous intramolecular redox reaction to give the $[Ru^{II}(sar\text{-}2\text{-}ene)]^{2+}$ complex (Figure 4). Treatment of the $[Ru^{II}(sar)]^{2+}$ ion with two equivalents of Ag^+ gave the $[Ru^{II}(sar\text{-}2\text{-}ene)]^{2+}$ ion in almost quantitative yield. Further additions of Ag^+ gave isomers of the diimine and then triimine complexes, finally yielding the Ru(II) hexaimine cage complex (Figure 4). An essential factor in the oxidation path seems to be donation of an electron pair at a deprotonated N centre to a d^4 Ru(IV) centre.[17] This increases the bond order between Ru and N, which in turn labilises the protons on the adjacent methylene group, triggering a concerted two electron transfer to the Ru(IV) ion and shifting the double bond order from Ru=N to N=C. Another important factor in the process is the stabilisation of the coordinated imine by the d^6 Ru(II) ion via the donation of non-bonding electrons on the d^6 Ru(II) ion to the empty π^* imine orbitals. However, such pathways are only evident where all three metal oxidation states are accessible.

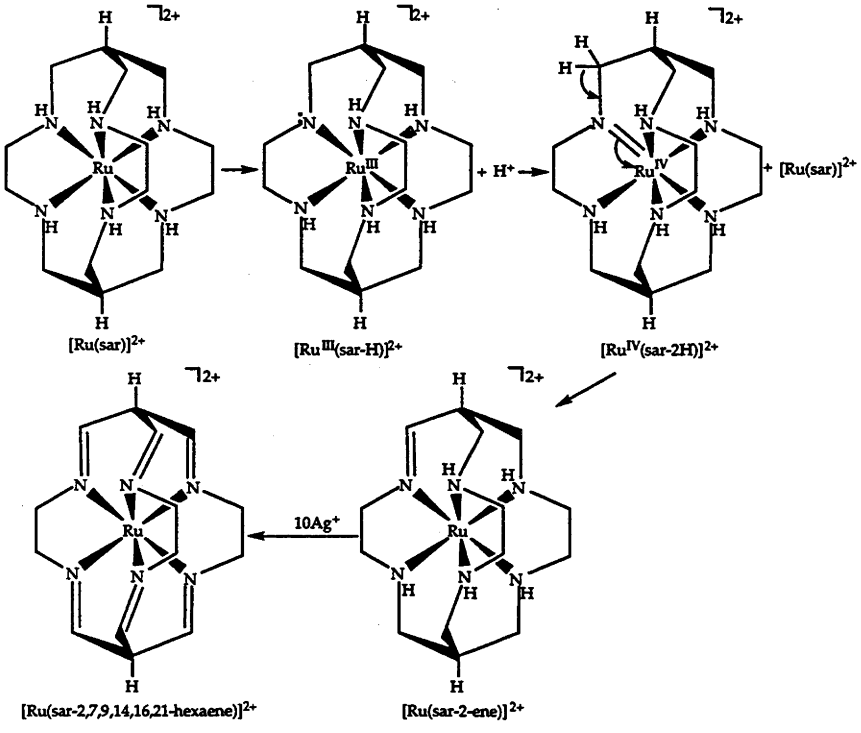

Figure 4

A few external oxidants, such as O_2 in the presence of a $Co^{II}Cl_2$-charcoal mixture and $Hg^{II}(OAc)_2$, have also been useful for the oxidation of Co(III) cage complexes. Both imine and amide complexes arise from the $O_2/Co^{II}Cl_2$-charcoal oxidation, with the main product being the diamido compound (Figure 5).[15] One of the most interesting results in the $Hg^{II}(OAc)_2$ oxidations of Co(III) cage complexes is the oxidation of the Co(III) cage derived from the capping of $[Co^{III}$(trans-1,2-cyclohexanediamine$)_3]^{3+}$ ($[Co^{III}(char)]^{3+}$).[17] Not only does the $Hg^{II}(OAc)_2$ generate the amide moieties, but it also aromatises one of the cyclohexane rings as well (Figure 6).

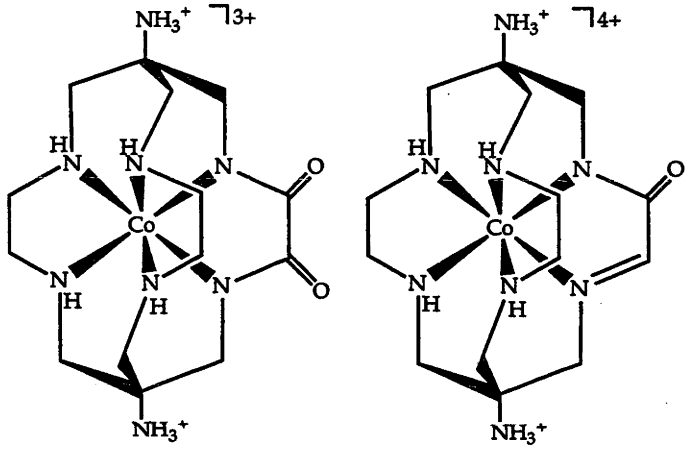

Figure 5

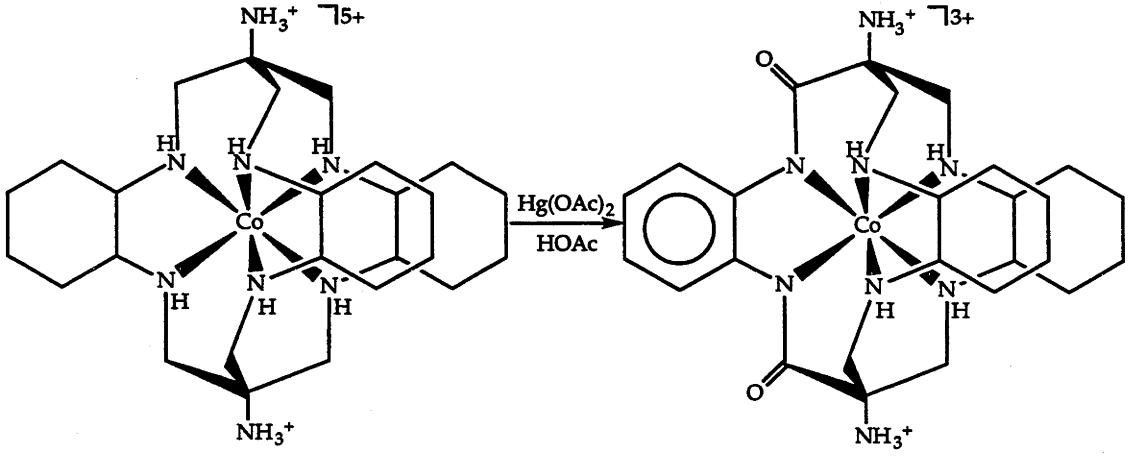

Figure 6

1.2.3 Apical Substituents

The incorporation of apical substituents into the cage ligand yields further derivatisation of the amide and imine cage complexes. The main reason for the introduction of substituents, such as CH_3, COOH, NH_2, NH_3^+, is that they have the ability to alter the redox potentials of these systems by at least 0.3 V for the Co(III)/(II) systems. The substituents can be built into the cage synthesis[18], as briefly shown earlier, or modified by regular organic synthetic methods.[19] Some examples will now be given to show how it is possible to introduce and alter cage apical substituents. For example $[Co^{III}(sar)]^{3+}$ (Figure 7)[18] was synthesised from $[Co^{III}(\{NO_2\}_2\text{-sar})]^{3+}$, by reacting it with Zn/HCl, reducing the two nitro groups to protonated amines. Treatment of the resultant $[Co^{III}(\{NH_3^+\}_2\text{-sar})]^{5+}$ ion with HNO_3/Cl^- converted the two amine groups into chloro substituents. Finally, the desired $[Co^{III}(sar)]^{3+}$ ion was formed from the reaction of $[Co^{III}(Cl_2\text{-sar})]^{3+}$ with Ni/Al alloy under basic conditions.

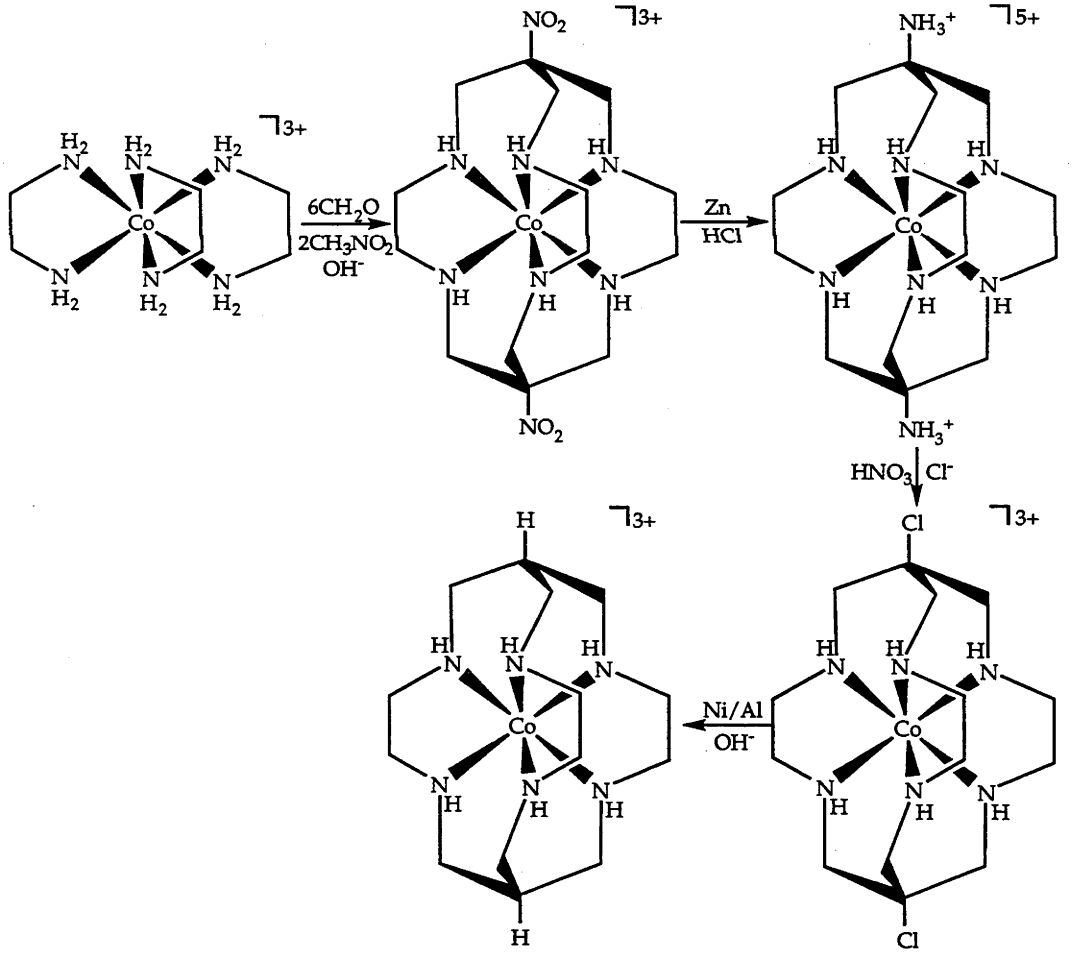

Figure 7

Other reactions are available to alter the apical functional groups of the cages resulting in different cage systems. For example, changes to only one apical group of the $[Co^{III}(Me,COOEt\text{-}2\text{-}oxosar\text{-}H)]^{2+}$ ion can give rise to a number of other compounds (Figure 8).[14] Other amide cage complexes, such as the $[Co^{III}(NO_2,COOEt\text{-}2\text{-}oxosar\text{-}H)]^{2+}$ ion, allow alterations to occur at both apical groups (Figure 9).[14] Also, here and in other examples, many different functional groups such as those shown in Figures 8 and 9 can exist at the bridgehead of these types of molecules.[20]

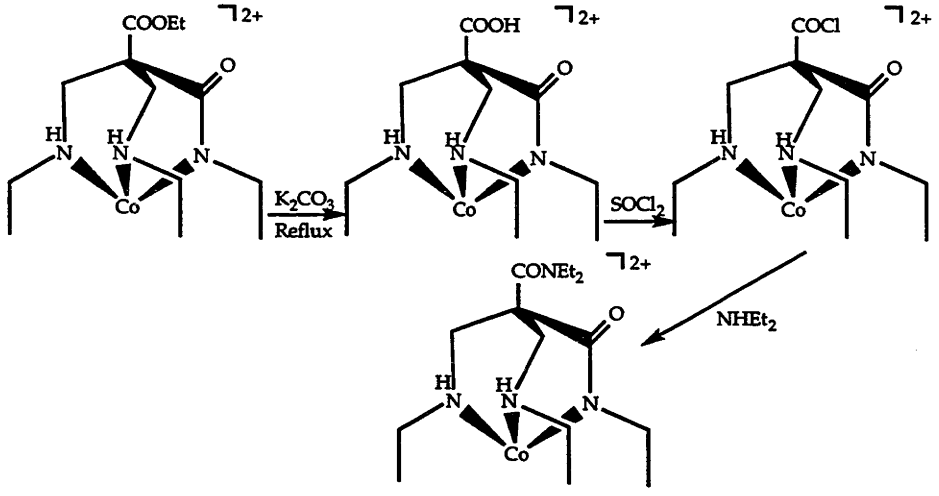

Figure 8

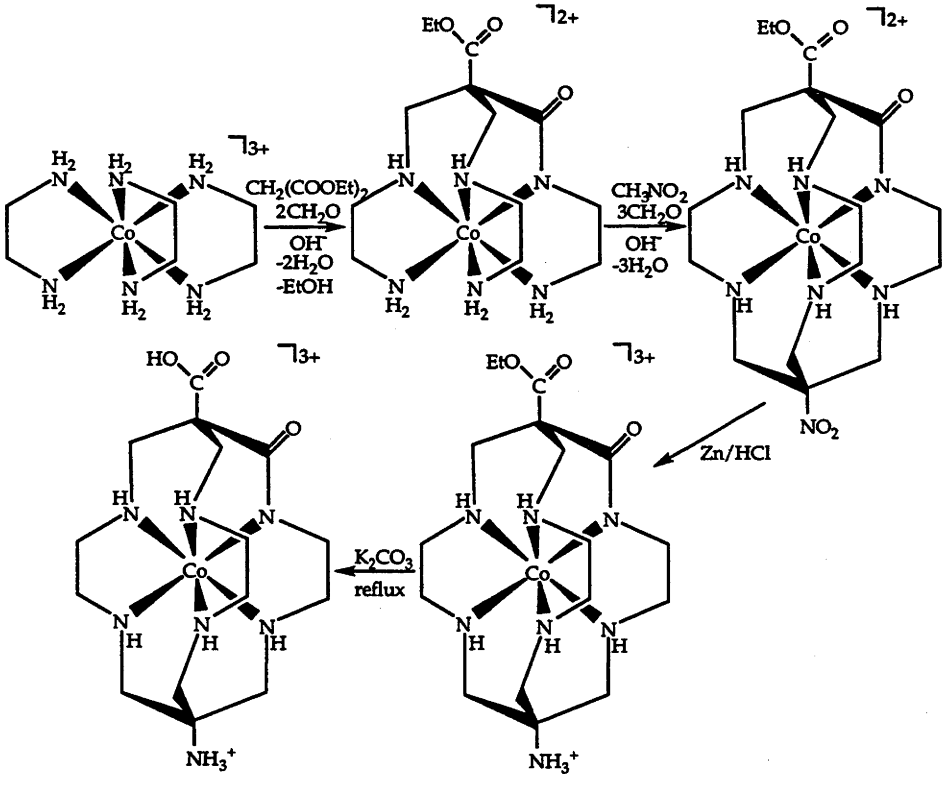

Figure 9

1.2.4 Organic Procedures

Generally, the most common method of introducing a functional group within the actual cage skeleton itself is via template methods. However, it should be possible to use straight organic syntheses, at least in part of the overall cage synthesis, to incorporate functional groups within a cage ligand. To date though there does not appear to be an N_6 amide cage complex partly produced in this way. Therefore, triamide tripodal ligands formed by reacting either a triester with ethane-1,2-diamine or a triamine with an acid chloride are interesting target molecules. Following complexation with Co(III), encapsulation of the metal ion to form a triamide cage complex by known methods is a feasible prospect.

1.2.5 Demetallation

Once a cobalt(III) cage complex has been formed, the free ligand can usually be obtained via reaction with cyanide and Co(II) ion. This method involves refluxing the Co(III) complex in a basic solution of potassium cyanide in the presence of $Co^{II}Cl_2$ according to equation 1. Finally the $[Co^{II}(CN)_6]^{4-}$ is oxidised to $[Co^{III}(CN)_6]^{3-}$ with O_2. Another method of refluxing the Co(II) cage in concentrated HBr has also been used but the acid-sensitive nature of the amide and imine bond off the metal precludes this route in this study. In fact, the instability of the unbound cage imine function prevents these types of complexes from undergoing demetallation under most conditions. Therefore only the amide cage systems will be demetallated in this thesis. Once the free amide ligand is obtained it should then possible to recomplex this with a range of other transition metal ions.

$$[Co^{III}(cage)]^{3+} + Co_{aq}^{2+} + 12CN^- \rightarrow [Co^{III}(CN)_6]^{3-} + [Co^{II}(CN)_6]^{4-} + cage \quad (1)$$

The removal of the Co(III) ion from a cage amide ligand has not yet been reported. Therefore there is a need to develop demetallation procedures especially for complexes with more than one amide group. For the Co(III) cages with more than one amide function, within the skeletal structure, a modified cyanide procedure may be necessary since $[Co^{II}(CN)_6]^{4-}$ may not be adequate to reduce the amide Co(III) cage.

1.3 Nomenclature

A number of macrobicyclic, macrocyclic and tripodal complexes have been synthesised within this thesis and since IUPAC names are clearly too long for frequent use a practical trivial nomenclature has been adopted. A systematic IUPAC name can be assigned for each basic unsubstituted cage ligand, by using IUPAC replacement nomenclature for both cyclic and acyclic compounds. The trivial nomenclature for much of this thesis is therefore based on the assignment of the IUPAC name to the substituted parent hydrocarbon. Substituents are ordered and numbered according to the normal IUPAC rules.

The basic and most common cage ligand discussed has the 3,6,10,13,16,19-hexaazabicyclo[6.6.6]icosane structure of Figure 10a; this is given the abbreviation sar (sarcophagine). The other type of ligand dealt with in this thesis has the 1,1,1-tris(4-amino-2-azabutyl)ethane structure of 10b, which is abbreviated to sen. In this thesis most of the cage complexes possess substituents in the 1, 2, 7 and 8 positions. In naming metal compounds the substituents appear as prefixes to the ligand in alphabetical order. However, for the trivial nomenclature adopted here substituents in the apical or 1,8 positions are named before any other ligand substituents. Therefore for the sar ligand for example the name becomes abbreviated to $[M(A,B\text{-sar})]^{n+}$ with the lower molecular weight substituent appearing in the A position. However, if A is H then the name is $[M(B\text{-sar})]^{n+}$ since the substituent simply replaces H in the parent hydrocarbon. If the same substituent exists in the 1 and 8 positions then the name becomes $[M(\{A_2\}_2\text{-sar})]^{n+}$. Also, throughout this work various substituents have also been abbreviated by using an extended trivial nomenclature. Thus, the 2-oxo-substituted sar cage ligand of Figure 10c will be called 2-oxosar. When two or three oxo groups are present within the sar or sen ligand skeletons the prefix x,y-di or x,y,z-tri (eg $(NH_2)_2$-2,7-dioxosar) is used before the oxosar parent name to denote the positions of the oxo groups within the ligand skeleton. In addition, when the amide group is deprotonated a suffix of -H follows the substituent's name while the number preceeding the H indicates the number of protons lost from the complex (Figure 10d). Some macrocyclic ligands have also been examined in this work and the macrocyclic ligands (Figure 10e and f) are called desar and cyclam (1,4,8,11-tetraazacyclotetradecane) respectively.

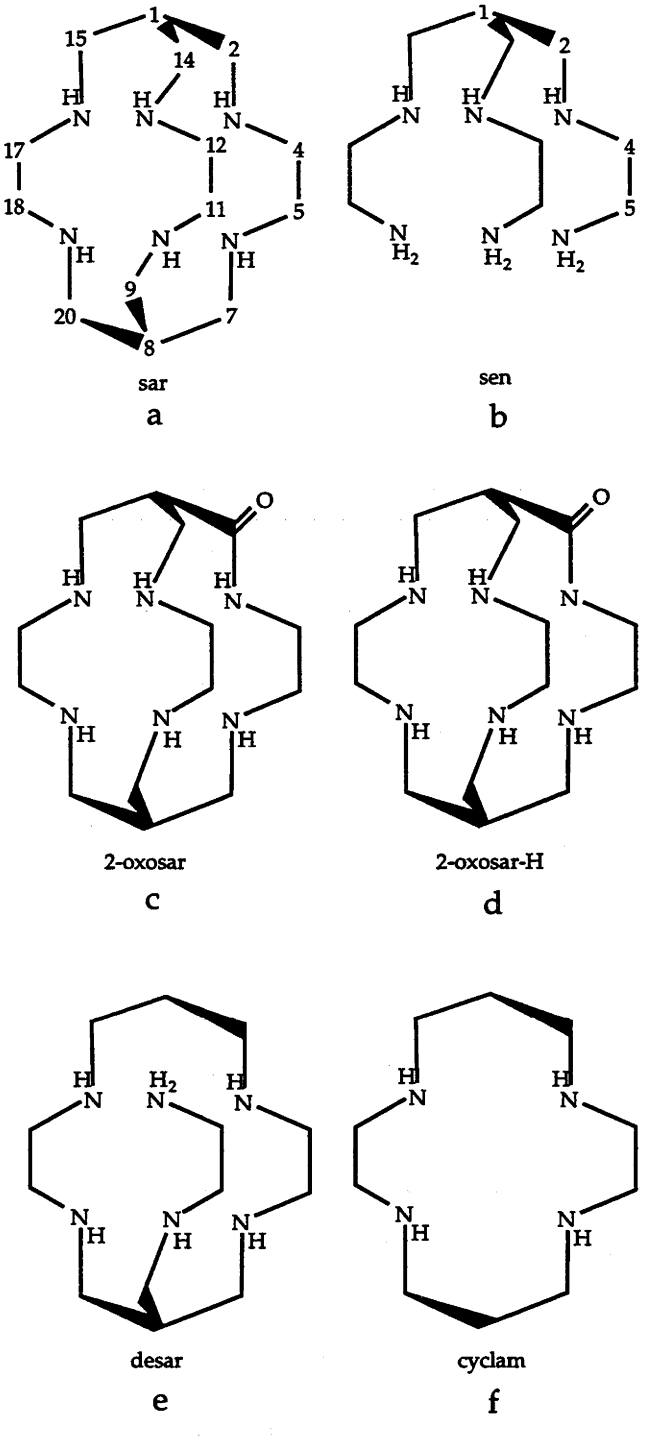

Figure 10

The partially unsaturated sar ligand of Figure 11a is denoted as sar-2-ene. Again with a doubly unsaturated sar cage, for instance Figures 11b, 11c and 11d, the prefix of x,y-di is used to denote the position of the diene functional group. In the absence of a metal ion however the di-imine ligands of Figure 11c and d are identical. It is only when they are complexed to a metal eg Co(III) that the two can be distinguished.

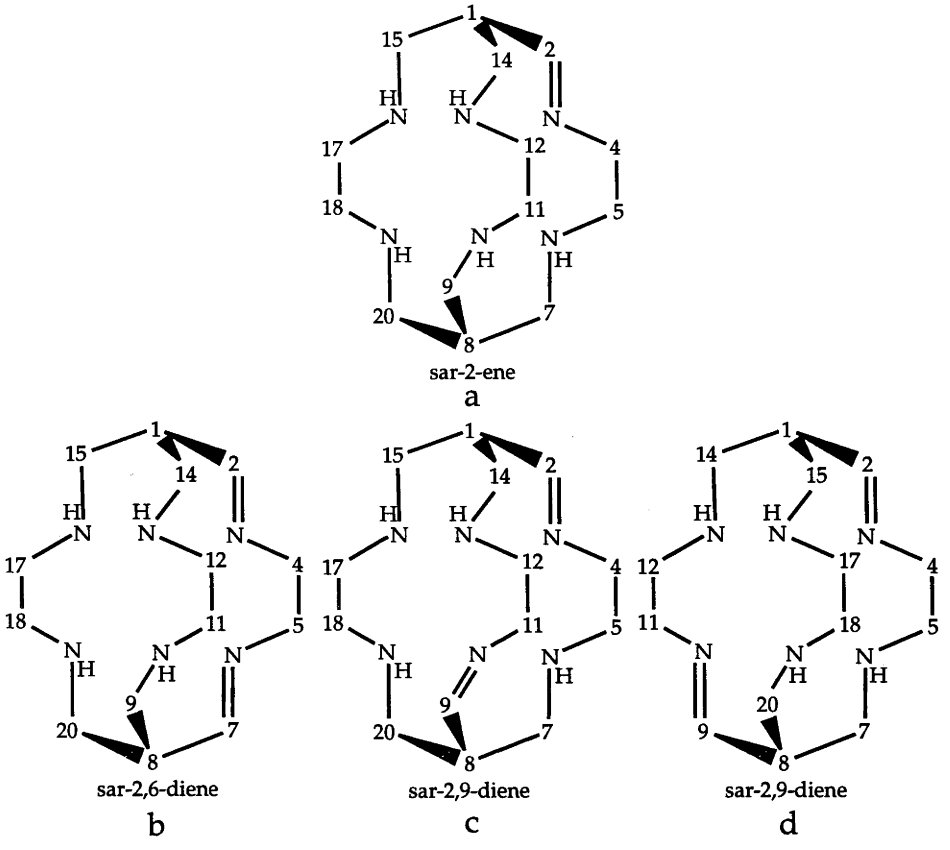

Figure 11

1.4 Physical Properties of Cage Complexes.

1.4.1 Structural Features

Although a wide variation of properties exists among cage complexes they still display some common features and it is pertinent to illustrate the more interesting facets. The complexity of the stereochemistry is exemplified by the fully saturated hexamine cages such as $[Co^{III}(sar)]^{3+}$. This complexity increases with skeletal substitution. Firstly a variety of conformations are possible with these ligands. Two features define the type of conformation that a cage complex possesses (Figures 12a - d and 13). The first is the orientation of the C-C bond of the ethylenediamine link, relative to the C_3- or pseudo C_3- axis going through the caps and metal atom. It can either be parallel (*lel*) or oblique (*ob*) to this axis. The second property is the twist angle of the caps which determines if the molecule possesses C_3 or D_3 symmetry (Figure 13). If the molecule contains a mixture of both *lel* and *ob* rings then the symmetry is reduced. Therefore the six conformations that a cage can adopt are D_3lel_3, D_3lel_3', C_3lel_3, D_3ob_3, C_2lel_2ob and C_2ob_2lel (Figure 13).[21]

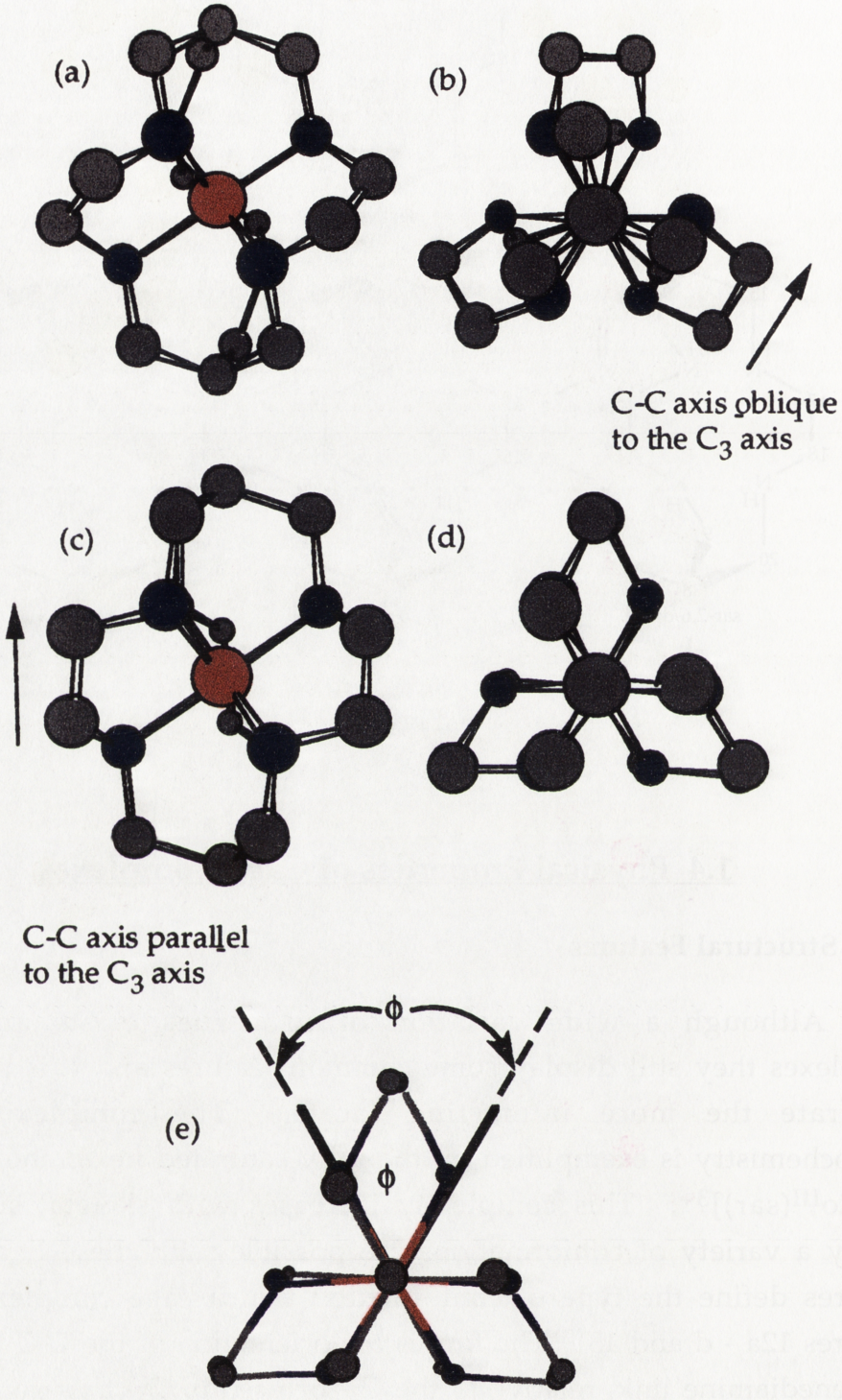

Figure 12 (a) *D3ob3* Δ-[M(sar)]$^{n+}$ (b) *D3ob3* viewed down C_3 axis (c) *D3lel3* Δ-[M(sar)]$^{n+}$ (d) *D3lel3* viewed down C_3 axis (e) definition of twist angle ϕ (Protons omitted for clarity).

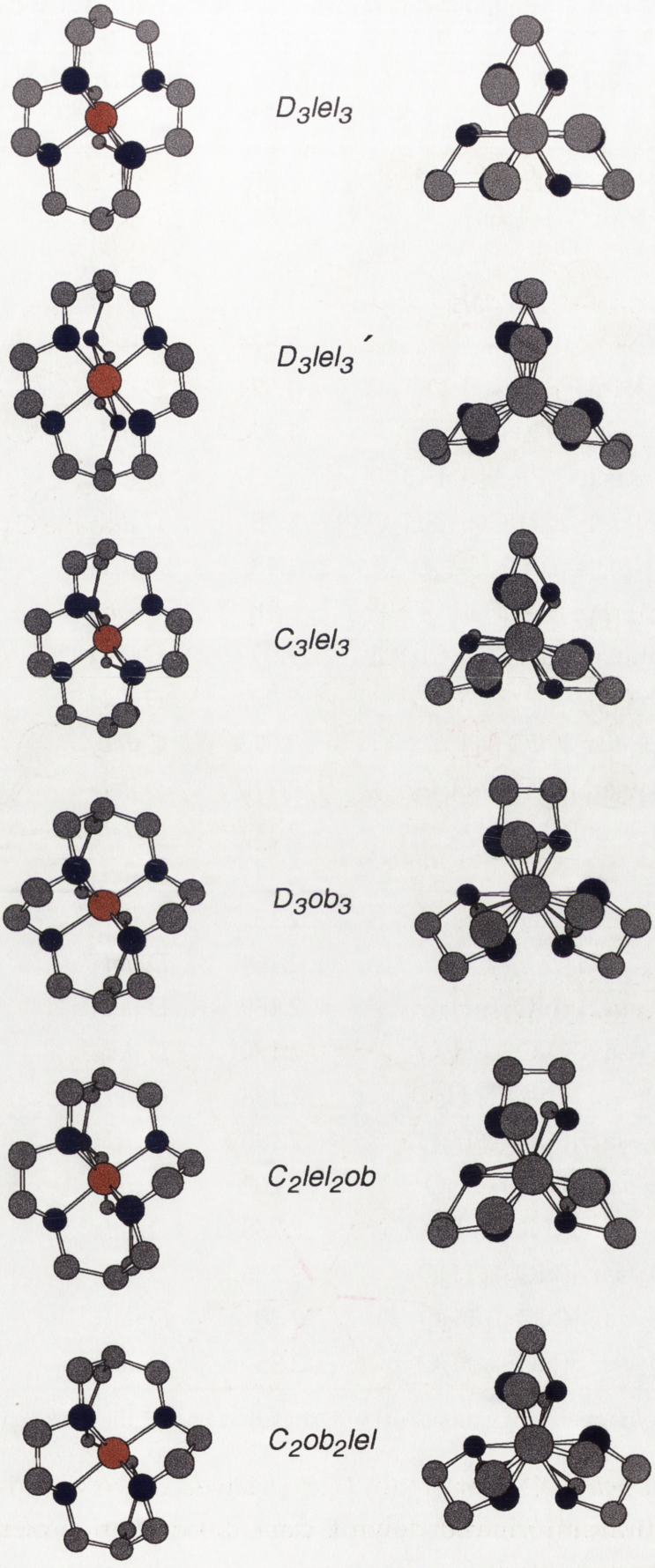

Figure 13 Conformations of Δ-$[M(sar)]^{n+}$ reproduced from reference 11.

Table 1: Experimental structural parameters for small cavity cages.

complex	M-N_{av} (Å)	conformation	(f_{av}) (°)	ref
$[Co^{III}((NMe_3)_2\text{-sar})]Cl_5\cdot 6H_2O$ (i)	1.96	D_3ob_3	57	22
$[Co^{III}(PyCH_2NH,Me\text{-sar})](CF_3SO_3)_3\cdot H_2O$	1.960	D_3ob_3	58	19
$[Co^{III}((NMe_3)_2\text{-sar})](NO_3)_5\cdot 3H_2O$	1.961	D_3ob_3	58	22
$[Co^{III}(sep)](NO_3)_3$	1.974	D_3lel_3	57	23
$[Co^{III}(NH_2OH\text{-sar})]Cl_5\cdot 4H_2O$	1.974	D_3ob_3	58	21
$[Co^{III}(ZnCl_3\text{-sar})]Cl\cdot 2H_2O$	1.976	D_3lel_3	55	24
$[Co^{III}(Me\text{-arsasar})](PF_6)_3\cdot 3H_2O$	1.979	D_3ob_3	57	25
rac-$[Co^{III}((NH_3)_2\text{-sar})]Cl_5\cdot 1.5H_2O$ (i)	1.98	D_3lel_3	54	26
Λ-$[Co^{III}((NH_3)_2\text{-sar})]Cl_5\cdot 5H_2O$	1.98	D_3lel_3	56	26
$[Co^{III}((NO_2)_2\text{-sar-H})]Cl_2\cdot 4H_2O$ (ii)	1.98	D_3ob_3	57	13
$[Co^{III}(Me\text{-phosphasar})](ZnCl_4)Cl$	1.99	D_3lel_3	55	27
$[Fe^{III}(sar)](NO_3)_3$	2.007	D_3lel_3	53	28
$[Cr^{III}((NH_3)_2\text{-sar})](NO_3)_4$	2.073	C_3lel_3	49	28
$[Ni^{II}((NH_3)_2\text{-sar})](NO_3)_4\cdot H_2O$	2.110	D_3lel_3	47	29
$[Ni^{II}((NH_3)_2\text{-sar})]Cl_4\cdot H_2O$	2.111	C_2lel_2ob	46	28
$[Ni^{II}(sep)](ClO_4)_2$	2.111	D_3lel_3	48	30
$[Mn^{III}(sar)](NO_3)_3\cdot H_2O$	2.13	D_3lel_3'	28	31
$[Co^{II}(sep)]S_2O_6\cdot H_2O$	2.164	D_3lel_3	42	12
$[Cu^{II}((NH_3)_2\text{-sar})](NO_3)_4\cdot H_2O$	2.169	D_3lel_3'	30	28
$[Co^{II}((NH_3)_2\text{-sar})](NO_3)_4\cdot H_2O$	2.170	D_3lel_3'	29	28
$[Mg^{II}((NH_3)_2\text{-sar})](NO_3)_4\cdot H_2O$	2.188	D_3lel_3'	28	18
$[Zn^{II}((NH_3)_2\text{-sar})](NO_3)_4\cdot H_2O$	2.190	D_3lel_3'	29	28
$[Fe^{II}((NH_3)_2\text{-sar})](NO_3)_4\cdot H_2O$	2.202	D_3lel_3'	29	28
$[Mn^{II}((NH_3)_2\text{-sar})](NO_3)_4\cdot H_2O$	2.238	D_3lel_3'	28	32
$[Ag^{II}((NH_3)_2\text{-sar})](NO_3)_4\cdot H_2O$	2.286	D_3lel_3'	29	28
$[Cd^{II}((NH_3)_2\text{-sar})](NO_3)_4\cdot H_2O$	2.30	D_3lel_3'	27	28
$[Hg^{II}((NH_3)_2\text{-sar})](NO_3)_4\cdot H_2O$	2.35	D_3lel_3'	26	28

(i) A and B are independent cations. (ii) indicates that one of the nitrogen donor atoms is deprotonated.

Structural information about cage complexes comes from X-ray crystal studies of the cage compounds. This allows an analysis of the competition between the preferred metal stereochemistry and the demands

of the ligand. It gives rise to a third cage property, the trigonal twist angle ϕ (Figure 12e) about the C_3 axis. A selection of structures for a range of different metal ions, ranging from d^0 - d^{10}, appears in Table 1.[21,28] The observed complexes then fall into two groups. A plot of the twist angle ϕ as a function of the number of d electrons for the metal ions shows this grouping (Figure 14).[28] The first group of complexes all possess twist angles close to ~28° and display a *D3lel3'* conformation. The ligand structure in these cases also resembles that of the metal-free ligand. All the complexes of this type display weak ligand fields and the ligand itself appears to dictate the structure of the complex. On the other hand, the second grouping lie more towards an octahedral structure, in the order of Ni(II) < Cr(III) < Fe(III) < Co(III). These complexes display twist angles between 45° - 60° and have shorter bond lengths than any in the former group. Therefore, for these complexes, a stronger ligand field arises and stereochemical preference of the metal dominates the overall structure. A range of conformations including *D3lel3*, *C3lel3*, *D3ob3* and *C2lel2ob* arise in these instances.

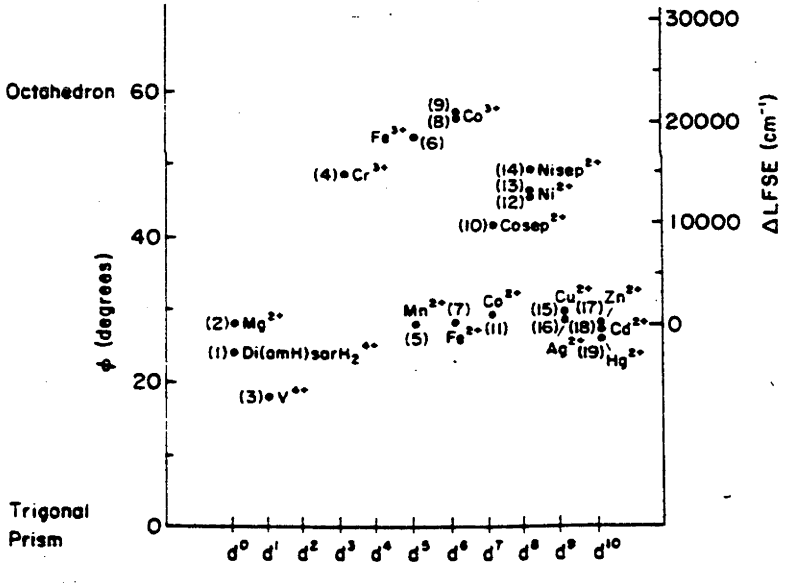

Figure 14

1.4.2 Optical Activity

Since the $[Co^{III}(en)_3]^{3+}$ template is chiral (Λ or Δ) then the cage product is also chiral and formed stereospecifically. If the template is in a racemic form the resulting cage complexes can be resolved by various means into their catoptric forms.[12-14,22,29] Using this retention property in

combination with X-ray crystallography, the absolute configurations of many of the chiral cage complexes have been assigned.

When Co(III) cages are reduced to Co(II) with Zn dust at 20° C they have been observed to retain their chirality. On reoxidation to their parent Co(III) complex full activity is restored, provided the cage itself is not decomposed.[14] This remarkable feature has allowed the CD and ORD spectra of Co(II) cage complexes to be recorded, and is very unusual since high spin Co(II) complexes normally exchange ligands on the ms→μs time scale[33] and presumably racemise at a comparable rate or faster. The inertness of $[Co^{III}(diazasar)]^{2+}$ was confirmed by isotopic exchange with $^{60}Co^{2+}_{(aq)}$, since no incorporation of the labelled Co(II) was observed (< 1%) within seventeen hours at 25° C.[12] Some relevant CD spectra for Co(III) and Co(II) cage complexes exist and for the Co(III) complexes the CD arising from the first d-d transition ($^1A_{1g}\rightarrow{}^1T_{1g}$ parentage) has its sign inverted in comparison to that of the parent $[Co^{III}(en)_3]^{3+}$ isomer of the same absolute configuration.[12,22] This phenomenon is due to the A_2 component of the transition for the cage complex being dominant in the circular dichroism, while the E component (of opposite sign) prevails for the $[Co^{III}(en)_3]^{3+}$ ion.

1.4.3 Electron Transfer Properties

Another aspect that was surprising for the cage compounds was in the area of electron transfer. A range of apically substituted Co(III) sar molecules covering a wide span of redox potentials exists. Redox reactions between partners in this series, cover approximately ten orders of magnitude in equilibrium constant and three orders of magnitude in reaction rate.[34,35]

Both the Co(III) and Co(II) oxidation states of cage complexes are reasonably accessible, and are inert to substitution and dissociation. It is thus possible to measure the electron self exchange rates simply and accurately by following the rate of racemisation of an equimolar mixture of Δ-$[Co^{III}(cage)]^{3+}$ and Λ-$[Co^{II}(cage)]^{2+}$.[12] Electron transfer leads to a change in oxidation state for the enantiomeric configuration and thus racemisation.

$$\Delta\text{-}[Co^{III}(cage)]^{3+} + \Lambda\text{-}[Co^{II}(cage)]^{2+} \rightleftharpoons \Delta\text{-}[Co^{II}(cage)]^{2+} + \Lambda\text{-}[Co^{III}(cage)]^{3+}$$

The self exchange rates of the Co(II)/(III) cages are much higher (10^6 - 10^5 fold) than those of the monodentate $[Co^{III}(NH_3)_6]^{3/2+}$ and bidentate $[Co^{III}(en)_3]^{3/2+}$ systems.[12,22,35,36] This unexpected result[37] led to a detailed

examination of the structures and strain in both oxidation states.[38-40] The most convincing argument is that there is a correlation between redox potential, electron transfer rate and steric factors, and that the dominant contribution to the rate is the inner-sphere reorganisation term for both oxidation states.[37-39]

A study of electron transfer reactions between pairs of caged cobalt ions, showed that their electron transfer rates conform well to the Marcus-Hush theoretical model.[36] For example, the experimentally determined rate constant for the cross-reaction between $[Co^{III}(sar)]^{2+}$ and $[Co^{III}(azamesar)]^{3+}$ is 10(1) $M^{-1}s^{-1}$ while the calculated rate constant using the Marcus cross-relation is 8 - 14 $M^{-1}s^{-1}$.[36] This agreement between theory and experiment arises because of the spherical nature of the ions and the weak electronic interactions between the reaction partners which is consistent with the theoretical model.[36,41]

1.4.4 Charge Transfer Photochemistry

The photochemical properties of cages are completely different from those of $[Co^{III}(NH_3)_6]^{3+}$. Ultraviolet irradiation (250 nm) of the ammine complex leads to both photoaquation and photoreduction. Owing to the encapsulating nature of the cage ligand no net dissociation occurs in the Co(II) state following ligand to metal charge transfer (LMCT) excitation. By itself, $[Co^{III}(sep)]^{3+}$ is inert in the visible region but by forming ion pairs with oxidisable anions, the complex can act as an electron transfer photosensitiser as shown in Figure 15.

$$Co(sep)^{3+} + X^- \rightleftharpoons \{[Co(sep)]^{3+}, X^-\}$$

$$\{[Co(sep)]^{3+}, X^-\} \overset{h\nu(IPCT)}{\rightleftharpoons} \{Co(sep)^{2+}, X^-\}$$

$$\{[Co(sep)]^{2+}, X^-\} \longrightarrow Co(sep)^{2+} + X$$

$$X \longrightarrow \text{products}$$

$$Co(sep)^{2+} + A \longrightarrow Co(sep)^{3+} + A^-$$

Figure 15 $[Co(sep)]^{3+}$ as an electron transfer photosensitiser. X^- is either iodide, oxalate or citrate, and A is an electron acceptor.[42,43]

the peptide ligand, a lowering of the redox potentials occurred.[54] This highlighted the fact that it was also possible to vary the redox potential in these types of compounds.

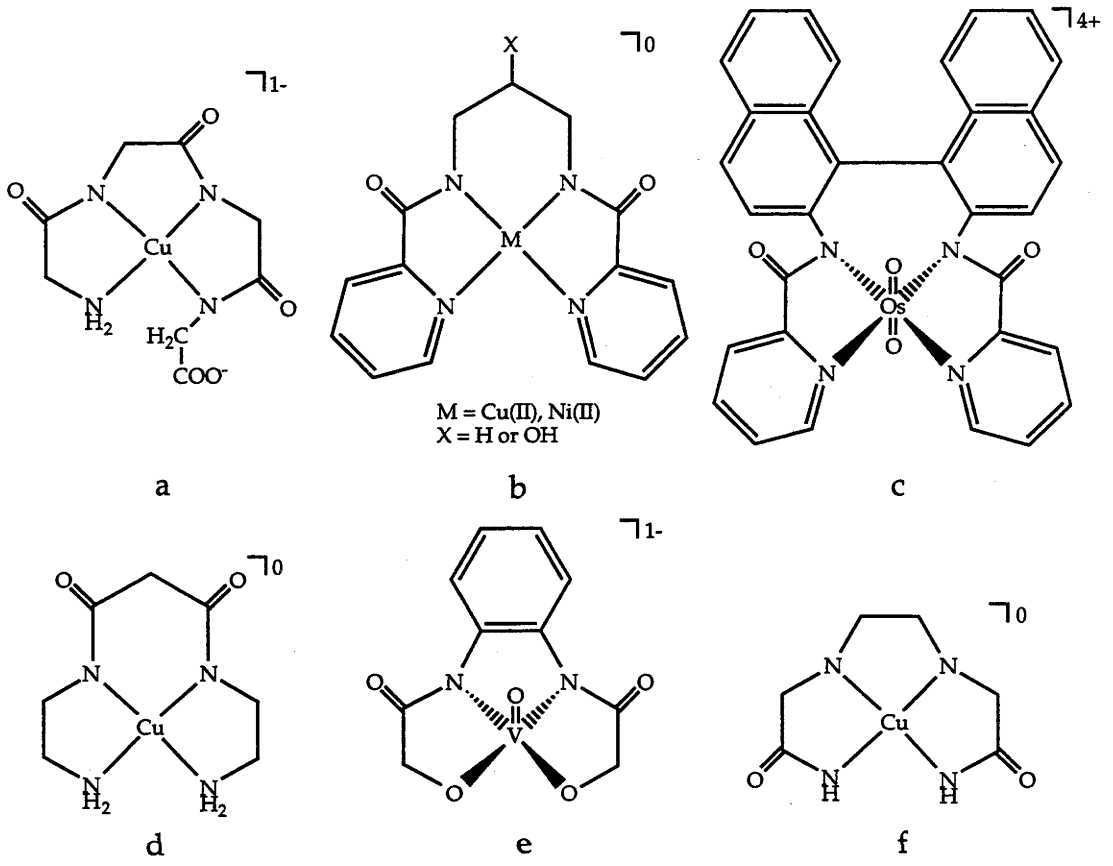

Figure 17

Quite a few acyclic ligands now exist as a result of the peptide chemistry and a selection of these appear in Figure 17. Much of the early work has revolved around Cu and Ni compounds,[55-57] but many other transition metal complexes now exist.[58,59] Much of what is known about the fundamental properties of amide groups stems from this research. For example, the crystal structures of these types of compounds have allowed an examination of the bonding properties between that of the metal and the amide ligand. Also, studies for copper, at least, show that the metals generally interact with the acyclic amide ligand in stages.[4] Some amide complexes of copper[60]and cobalt[61] undergo ligand photodecomposition by a ligand-to-metal charge transfer mechanism. Again the acyclic amide ligands have the ability to stabilise a variety of metals in higher oxidation states and the Os(VI) and V(V) diamide complexes (Figure 17c and e) are examples of this. One limitation of the acyclic systems is that in general they are less stable than the macrocyclic amide complexes.[62]

1.5.2 Macrocyclic Amide Complexes

The production of amide-bearing macrocycles occurs mainly through direct organic synthesis, and a range of different metal complexes exist with Cu(II) and Ni(II) compounds being the most prominent (Figure 18).[4,63,64] These ligands produce metal complexes with high stability, as well as high ligand field strengths, for metals that fit into the ligand cavity. Therefore, they are more selective in their interactions with different metal ions than the saturated analogues.[4] However, many first row transition metal complexes exist with these types of ligands.[1] Also most of the ligands tend to favour square-planar coordination induced by the planar amide groups.[4] Also, metals in higher oxidation states exist with these ligands. The Fe(IV)[8] and possibly Co(IV)[1] complexes with the ligand systems below are good examples (Figure 18).

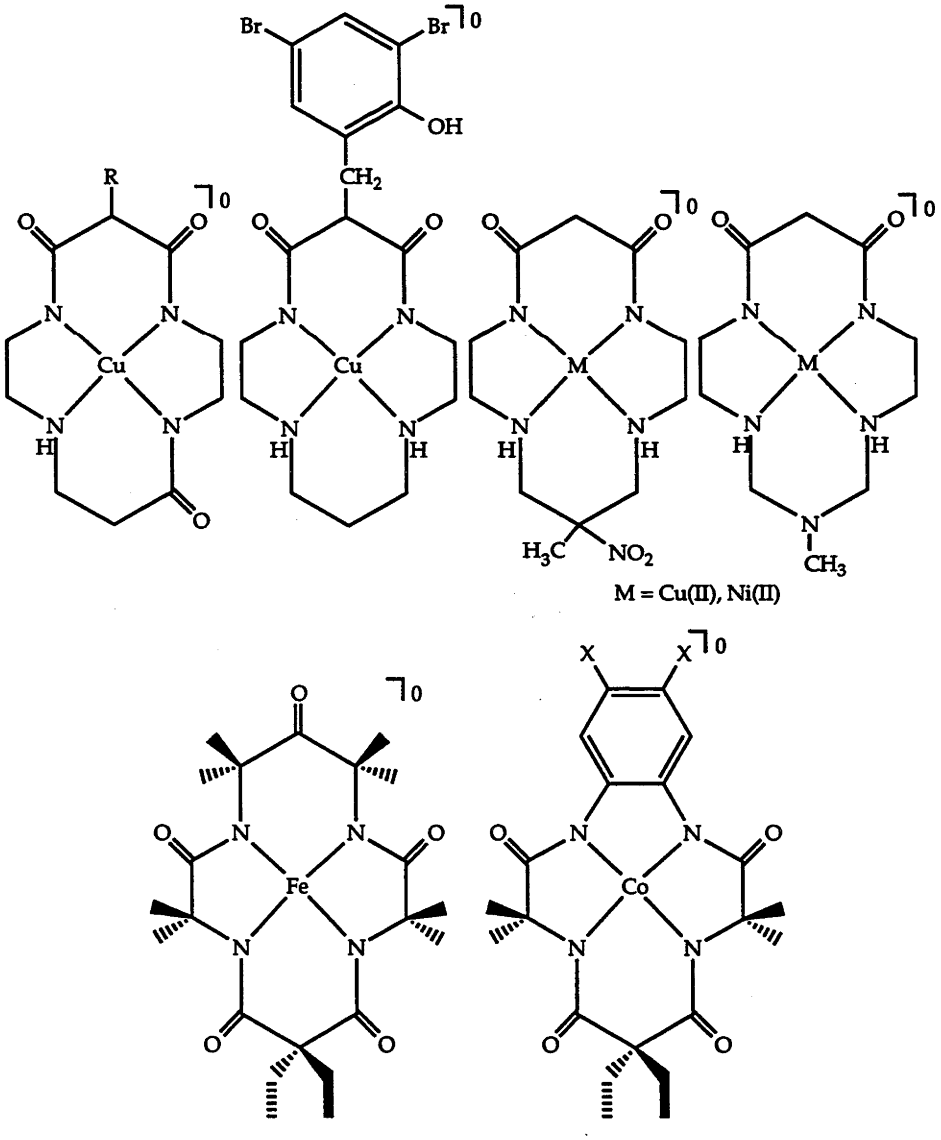

Figure 18

1.5.3 Applications of Amide Complexes

Amide complexes have the potential to be useful in a large number of areas. For example, the [Ru^{III}(bbpc)(PPh_3)Cl] complex (Figure 19) acts as a catalyst for the cyclopropanation of styrene by ethyl diazoacetate.[65] The reaction is rather stereoselective giving a trans:cis ratio of 6:1 (Figure 19). The complex is also an efficient catalyst for the mediation of atom transfer reactions to C=C bonds. In this case the most likely intermediate is a Ru(IV) species stabilised by the chelating diamide ligand. The triamide compound (A) found in Figure 20 finds use as a renal-function imaging agent.[66] The [$^{99m}Tc^{V}O(MAG)_3]^-$ complex images only the kidney function of patients and replaces a more harmful choice. Two other related $^{99m}Tc^{V}$ compounds show promise in the areas of liver and kidney imaging, although they are still in the experimental stage.[67] Experiments show that in mice at least, both the liver and kidneys clear the acyclic amide (B) from the body, while only the liver becomes targeted by the cyclic tetraamide (C) (Figure 20). The carboxyl group of the acyclic ligand B reacts with the free amine group because of its proximity to the amine, resulting in the formation of a fourth amide and cyclization of the ring. This intramolecular cyclization may offer an alternative to the normal methods used in the production of macrocyclic amide compounds.

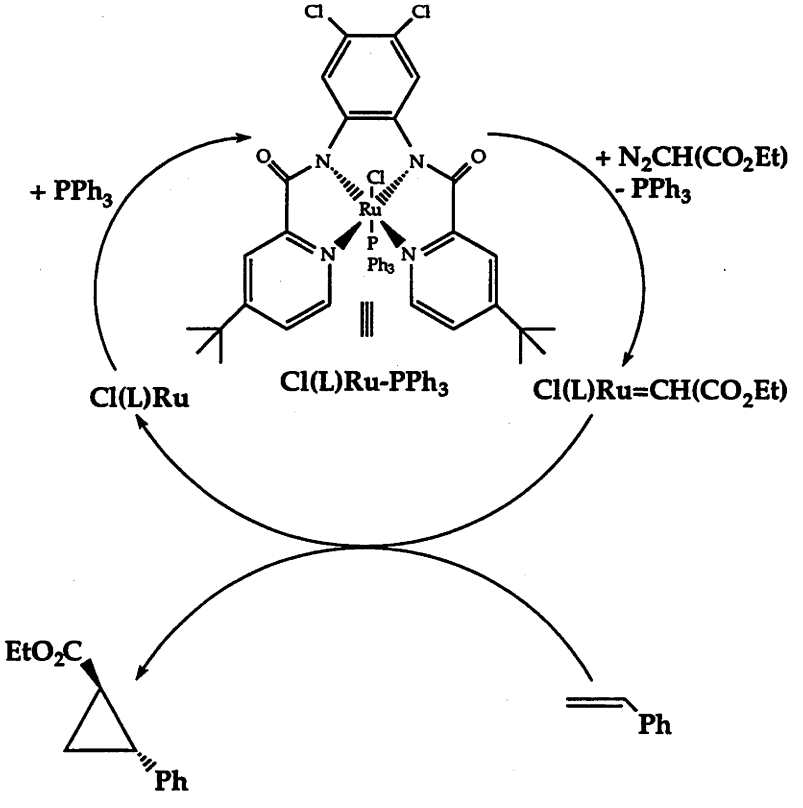

Figure 19

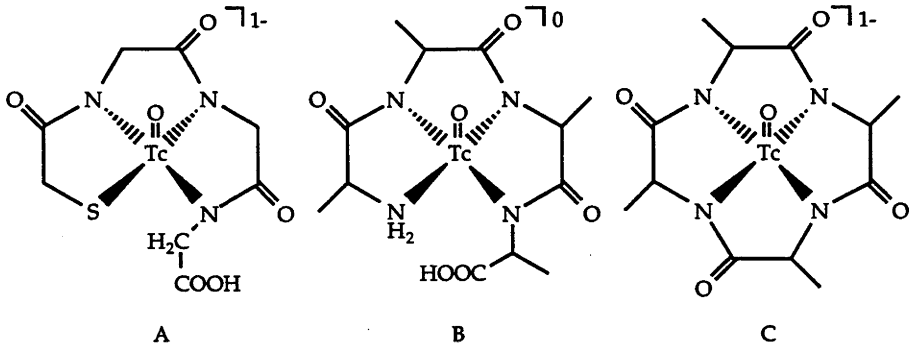

Figure 20

1.6 Cage Complexes Containing Imine Functions.

The reactions that occur between carbonyl compounds and amines, in the presence of metal ions, have been exploited widely in macrocyclic chemistry. Recently the strategy has provided a fruitful route to the production of imine cage complexes which display properties different from those of the saturated cages. For example, the presence of an imine moiety within the cage can alter ring conformation, spectroscopic, electrochemical and electron transfer properties. This arises from the contraction and distortion of the CoN_6 cavity as well as electronic and conformational effects.

The $[Co^{III}(sen)]^{3+}$ ion has proved to be a useful template in the production of these types of cages. For example, the capping reaction of $[Co^{III}(sen)]^{3+}$ with formaldehyde and 2-phenylethanal results in an imine cage with a phenyl apical substituent (Figure 21). This type of reaction is not just restricted to this one template, others also have been used, eg; $[Co^{III}(tame)_2]^{3+}$ and $[Co^{III}(tach)_2]^{3+}$. This strategy is also important because it also allows the introduction of different groups into the caps of the cage ligand as well as different cavity sizes for the cages.

The properties of the imine function in these complexes have not been explored except for reduction with $NaBH_4$ to give the saturated analogues. Therefore, one of the aims of this work was to examine the properties of a series of Co(III) di-imine cage complexes. A study of this nature should generally extend knowledge of metal imine ligand complexes.[68,69] Also an interesting facet of imine cage complexes is that they allow the prospect of further chemistry. For example, adjacent methine or methylene carbon groups may be sufficiently acidic to facilitate

the introduction of functional groups for a variety of chemical, physical and biological applications. Reactions of this nature have been shown to occur with macrocyclic imine systems.[70]

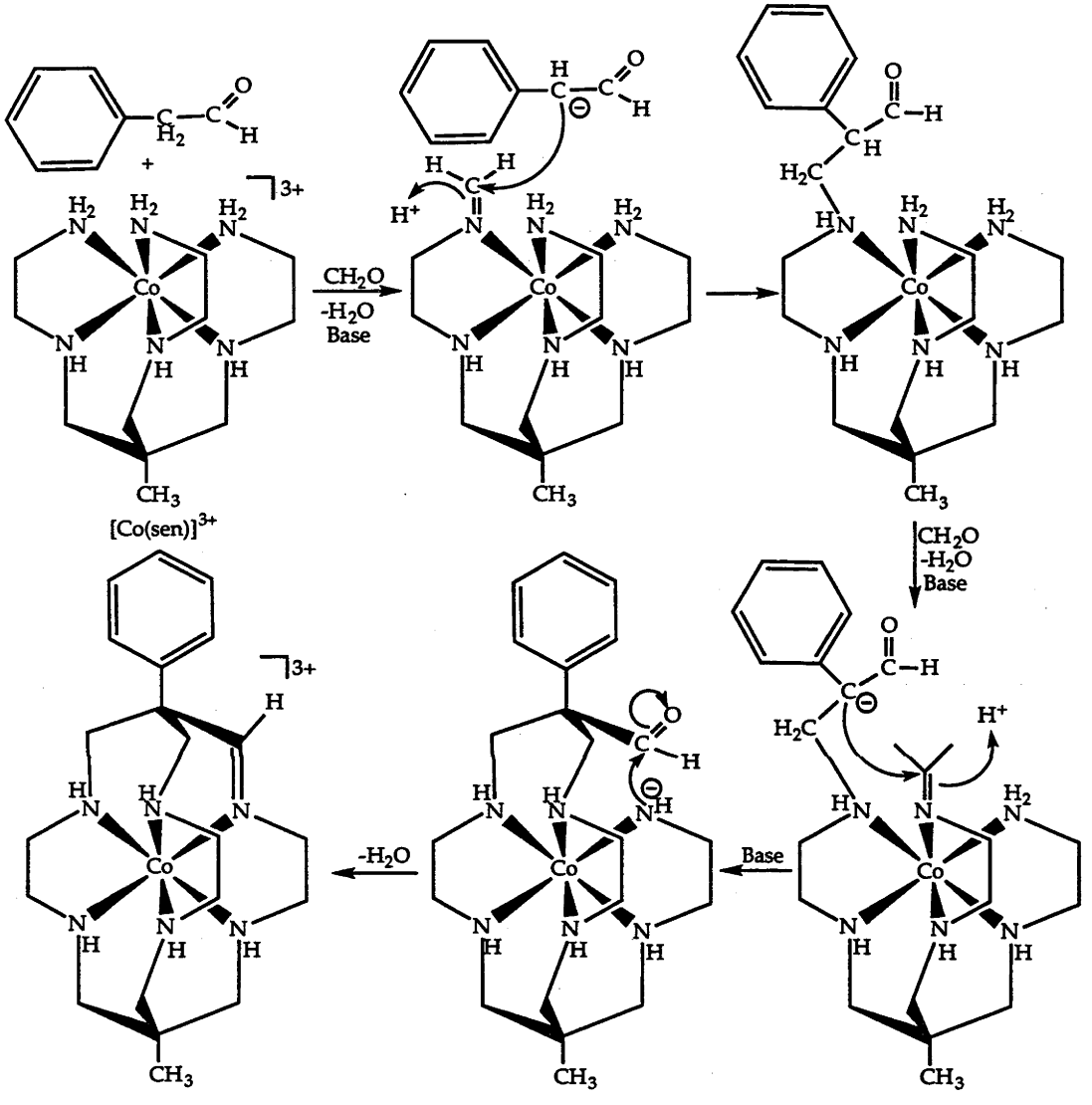

Figure 21

The production of imine cage complexes is also important for another reason. It allows the introduction, as mentioned previously, of specific photo sensitive functional groups in the cap of the formed cages. Once reduced, to the saturated cage, the complexes can then be used as combined photoactive and electron transfer agents and to target specific areas of biology. This will be another area of exploration in this work. Some background to previous biological uses of cage complexes follows.

1.7 Biological Applications of Cage Complexes.

Cage compounds have been known for more than twenty years and are certainly active in a biological sense.[20] They have been used to remove toxic metals, for example Cu, from biological systems by complexation followed by normal elimination of the stable complex.[71] Because of the stability of the metal complexes in the body they have been proposed as carriers of isotopes of heavy metals for radionuclide therapy or NMR imaging.[20] Also, for example, the anthracene complex $[Co^{III}(Me,AnCH_2NHCH_2CH_2CH_2NH\text{-}sar)]^{3+}$ (Figure 16) intercalates with DNA with a binding constant of $\sim 10^5$.[48] The subsequent irradiation of the Co(III) complex with UV light resulted in the cleavage of the DNA.[72]

In addition, it has been reported that cage compounds with long alkyl tails, which are consequently surface-active agents, have the power to disrupt biological membranes in nematodes and may be useful generally as anthelmintics.[73,74] Insertion of the surfactant into biological membranes could also influence other biological conditions. One important feature appeared to be that the metal cage complex was extracted unchanged i.e., without loss of the metal ion. The cage ligands or complexes with varying substituents have not previously been used as control agents for infections by retroviruses, hepadnaviruses and flaviviruses but not dissimilar bicyclam chelates[75] appear to be active in this context. Therefore testing the cage complexes against certain viral diseases seemed a relevant exploration.

1.8 Aims and Scope of this Work.

The previous brief survey highlights some areas of cage chemistry and exposes others that require further exploration. That is, the chemistry of amide and imine cage complexes, as well as the antiviral properties of Co(III) cage compounds. Therefore the work in this thesis examines these specific areas in two parts.

Part 1. Amide Cage Complexes

To date, relatively little is known about the properties of amide cage complexes. Therefore one aim was to produce a number of amide cage complexes with different metals, by different methods, to expand this area

of chemistry. The study involves their synthesis and structures and an investigation of the redox and electronic properties of these types of amide complexes, including their ability to stabilise various metals in higher oxidation states. By combining the properties of the cage and amido ligands some stable powerful oxidants were envisaged.

Part 2. Imine and Saturated Amine Cages and their Biological Activity

The synthesis and properties of imine cage complexes needs to be explored systematically especially those with alkyl substituents. These two aspects are linked synthetically since the imine syntheses readily allow different substituents to be introduced into the apical positions and the imines are easily reduced to the fully saturated cage complexes. Although long chain alkyl groups have been tied to the cage to give new surface active agents which are toxic systemically since they lyse red blood cells easily, the biological properties of the lesser alkylated cages have not been explored. What is significant in this context is that dicyclam a related twin macrocyclic ligand has been shown to be active towards inhibiting the AIDS and hepatitis B viruses[75] so it seemed relevant that the properties of the cages should be explored in this context.

1.9 References.

(1) Collins, T. J.; Powell, R. D.; Slebodnick, C.; Uffelman, E. S. *J. Am. Chem. Soc.* **1991**, *113*, 8419.

(2) Margerum, D. W.; Rybka, J. S. *Inorg. Chem.* **1981**, *20*, 1453.

(3) Margerum, D. W.; Rybka, J. S. *Inorg. Chem.* **1980**, *19*, 2784.

(4) Kimura, E. *J. Coord. Chem.* **1986**, *15*, 1.

(5) Collins, T. J.; Slebodnick, C.; Uffelman, E. S. *Inorg. Chem.* **1990**, *29*, 3433.

(6) Collins, T. J.; Powell, R. D.; Slebodnick, C.; Uffelman, E. S. *J. Am. Chem. Soc.* **1990**, *112*, 899.

(7) Collins, T. J.; Nichols, T. R.; Uffelman, E. S. *J. Am. Chem. Soc.* **1991**, *113*, 4708.

(8) Kostka, K. L.; Fox, B. G.; Hendrich, M. P.; Collins, T. J.; Rickard, C. E. F.; Wright, L. J.; Münck, E. *J. Am. Chem. Soc.* **1993**, *115*, 6746.

(9) Curtis, N. F.; Einstein, F. W. B.; Willis, A. C. *Inorg. Chem.* **1984**, *23*, 3444.

(10) Chen, J.; Ye, N.; Alcock, N. W.; Busch, D. H. *Inorg. Chem.* **1993**, *32*, 904.

(11) Chia, P. S. K.; Masarwa, M.; Warburton, P. R.; Wu, W.; Kojima, M.; Nosco, D.; Alcock, N. W.; Busch, D. H. *Inorg. Chem.* **1993**, *32*, 2736.

(12) Creaser, I. I.; Geue, R. J.; Harrowfield, J. M.; Herlt, A. J.; Sargeson, A. M.; Snow, M. R.; Springborg, J. *J. Am. Chem. Soc.* **1982**, *104*, 6016.

(13) Geue, R. J.; Hambley, T. W.; Harrowfield, J. M.; Sargeson, A. M.; Snow, M. R. *J. Am. Chem. Soc.* **1984**, *106*, 5478.

(14) Geue, R. J.; Petri, W. R.; Sargeson, A. M.; Snow, M. R. *Aust. J. Chem.* **1992**, *45*, 1681.

(15) McCarthy, M. G. Ph.D. Thesis, Australian National University, 1984.

(16) Bernhard, P.; Sargeson, A. M. *J. Am. Chem. Soc.* **1989**, *111*, 597.

(17) Sargeson, A. M. *Pure & Appl. Chem.* **1986**, *58*, 1511.

(18) Bottomly, G. A.; Clark, I. J.; Creaser, I. I.; Engelhardt, L. M.; Geue, R. J.; Hagen, K. S.; Harrowfield, J. M.; Lawrance, G. A.; Lay, P. A.; Sargeson, A. M.; See, A. J.; Skelton, B. W.; White, A. H.; Wilner, F. R. *Aust. J. Chem.* **1994**, *47*, 143.

(19) Gajhede, M.; Hammershøi, A.; Skov, L. K. *Acta Chem. Scand.* **1991**, *45*, 474.

(20) Sargeson, A. M. *Chemistry in Australia* **1991**, 176.

(21) Comba, P. *Inorg. Chem.* **1989**, *26*, 4122.

(22) Bernhardt, P. V.; Bygott, A. M. T.; Geue, R. J.; Hendry, A. J.; Korybut-Daszkiewicz, B. R.; Sargeson, A. M.; Willis, A. C. *Inorg. Chem.* **1994**, *33*, 4553.

(23) Dubicki, L.; Ferguson, J.; Geue, R. J.; Sargeson, A. M. *Chem. Phys. Lett.* **1980**, *74*, 393.

(24) Creaser, I. I.; Lydon, J. D.; Sargeson, A. M.; Horn, E.; Snow, M. R. *J. Am. Chem. Soc.* **1984**, *106*, 5729.

(25) Höhn, A.; Geue, R. J.; Sargeson, A. M.; Willis, A. C. *J. Chem. Soc., Chem. Commun.* **1989**, 1648.

(26) Tiekink, E. R. T. *unpublished results*

(27) Höhn, A.; Geue, R. J.; Sargeson, A. M.; Willis, A. C. *J. Chem. Soc., Chem. Commun.* **1989**, 1644.

(28) Comba, P.; Sargeson, A. M.; Engelhardt, L. M.; Harrowfield, J. M.; White, A. H.; Horn, E.; Snow, M. R. *Inorg. Chem.* **1985**, *24*, 2325.

(29) Clark, I. J.; Creaser, I. I.; Engelhardt, L. M.; Harrowfield, J. M.; Krausz, E. R.; Moran, G. M.; Sargeson, A. M.; White, A. H. *Aust. J. Chem.* **1993**, *46*, 111.

(30) Suh, M. P.; Shin, W.; Kim, S. *Inorg. Chem.* **1984**, *23*, 618.

(31) Anderson, P. A.; Creaser, I. I.; Dean, C.; Harrowfield, J. M.; Horn, E.; Martin, L. L.; Sargeson, A. M.; Snow, M. R.; Tiekink, E. R. T. *Aust. J. Chem.* **1993**, *46*, 449.

(32) Creaser, I. I.; Engelhardt, L. M.; Harrowfield, J. M.; Sargeson, A. M.; Skelton, B. W.; White, A. H. *Aust. J. Chem.* **1993**, *46*, 465.

(33) Basolo, F.; Pearson, R. G. *Mechanisms Of Inorganic Reactions;* 2nd ed.; John Wiley and Sons: New York, 1967, p 145.

(34) Lawrance, G. A.; Lay, P. A.; Sargeson, A. M. *Inorg. Chem.* **1990**, *29*, 4808.

(35) Bond, A. M.; Lawrance, G. A.; Lay, P. A.; Sargeson, A. M. *Inorg. Chem.* **1983**, *22*, 2010.

(36) Creaser, I. I.; Sargeson, A. M.; Zanella, A. W. *Inorg. Chem.* **1983**, *22*, 4022.

(37) Sargeson, A. M. *Pure & Appl. Chem.* **1984**, *56*, 1603.

(38) Bond, A. M.; Hambley, T. W.; Snow, M. R. *Inorg. Chem.* **1985**, *24*, 1920.

(39) Hambley, T. W. *Inorg. Chem.* **1988**, *27*, 2496.

(40) Geue, R. J.; Pizer, R.; Sargeson, A. M. *Abs. 183rd National Meeting of the American Chem. Soc.;* American Chemical Society, Washington DC: Las Vagas, NV, 1982, p INOR 62.

(41) Bernhard, P.; Sargeson, A. M. *Inorg. Chem.* **1987**, *26*, 4122.

(42) Horvath, O.; Stevenson, K. L. *Charge Transfer Photochemistry of Coordination Compounds.;* VCH Publishers: 1993.

(43) Balzani, V. *Gazz. Chim. Ital.* **1989**, *119*, 311.

(44) Creaser, I. I.; Gahan, L. R.; Geue, R. J.; Launikonis, A.; Lay, P. A.; Lydon, J. D.; McCarthy, M. G.; Mau, A. W.; Sargeson, A. M.; Sasse, W. H. F. *Inorg. Chem.* **1985**, *24*, 2671.

(45) Balzani, V.; Juris, A.; Scandola, F. In *Homogeneous and Heterogeneous Photocatalysis;* E. Pelizzetti and N. D. Serpone, Eds.; Reidel Publishing Company, NATO ASI Series C, Mathematical and Physical Sciences: 1986; Vol. 174; p 1.

(46) Launikonis, A.; Lay, P. A.; Mau, A. W.; Sargeson, A. M.; Sasse, W. H. F. *Scientific Papers of the Institute of Physical and Chemical Research* **1984**, *78*, 198.

(47) Creaser, I. I.; Hammershøi, A.; Launikonis, A.; Mau, W. H.; Sargeson, A. M.; Sasse, W. H. F. *Photochemistry and Photobiology* **1989**, *49*, 19.

(48) Mau, A. H.; Sasse, W. H. F.; Creaser, I. I.; Sargeson, A. M. *Nouv. J. Chem.* **1986**, *10*, 589.

(49) Fabbrizzi, L. *Comments Inorg. Chem.* **1985**, *4*, 33.

(50) Martin, R. B.; Sigel, H. *Chem. Rev.* **1982**, *82*, 385.

(51) Margerum, D. W.; Dukes, G. R. In *Metal Ions in Biological Systems*; H. Sigel, Ed.; Marcel Dekker: New York, 1974; Vol. 1; Chapter 5, p 157.

(52) Margerum, D. W. In *Oxidases Related. Redox Syst., Proc. Int. Symp.*; 3rd ed.1982; p 193.

(53) Margerum, D. W.; Chellappa, K. L.; Bossu, F. P.; Burce, G. L. *J. Am. Chem. Soc.* **1975**, *97*, 6894.

(54) Bossu, F. P.; Chellappa, K. L.; Margerum, D. W. *J. Am. Chem. Soc.* **1977**, *99*, 2195.

(55) Sakurai, T.; Hongo, J.-I.; Nakahara, A.; Nakao, Y. *Inorg. Chim. Acta* **1980**, *46*, 205.

(56) Lim, M.-C. *Aust. J. Chem.* **1982**, *35*, 483.

(57) Bertoncello, K.; Fallon, G. D.; Murray, K. S. *Polyhedron* **1990**, *9*, 2867.

(58) Cornman, C. R.; Geiser-Bush, K. M.; Singh, P. *Inorg. Chem.* **1994**, *33*, 4621.

(59) Lin, J.-H.; Che, C.-M.; Lai, T.-F.; Poon, C.-K.; Cui, Y. X. *J. Chem. Soc., Chem. Commun.* **1991**, 468.

(60) Hamburg, A. W.; Margerum, D. W. *Inorg. Chem.* **1983**, *22*, 3884.

(61) Lee, G. H.; Larson, J. L.; Perkins, T. A.; Schanze, K. S. *Inorg. Chem.* **1990**, *29*, 2015.

(62) Bernhardt, P. V.; Comba, P.; Hambley, T. W.; Massoud, S. S.; Stebler, S. *Inorg. Chem.* **1992**, *31*, 2644.

(63) Gavrish, S. P.; Lampeka, Y. D. *Russ. J. Inorg. Chem.* **1993**, *38*, 1211.

(64) Lin, H.-K.; Zhu, S. R.; Gu, Z.-X.; Chen, Y. T. *J. Chem. Soc., Dalton Trans.* **1995**, 1879.

(65) Ko, P.-H.; Chen, T.-Y.; Zhu, J.; Cheng, K.-F.; Peng, S.-M.; Che, C.-M. *J. Chem. Soc. Dalton Trans.* **1995**, 2215.

(66) Grummon, G.; Rajagopalan, R.; Palenik, G. J.; Koziol, A. E.; Nosco, D. L. *Inorg. Chem.* **1995**, *34*, 1764.

(67) Bormans, G.; Peeters, O. M.; Vanbilloen, H.; Blaton, N.; Verbruggen, A. *Inorg. Chem.* **1996**, *35*, 6240.

(68) Lindoy, L. F. *The Chemistry of Macrocyclic Ligand Complexes*; Cambridge University Press: Cambridge, 1989.

(69) *Coordination Chemistry of Macrocyclic Complexes*; Melson, G. A., Ed.; Plenum: New York, 1982.

(70) Kang, S.-G.; Kim, M.-S.; Kim, S.-J.; Ryu, K. *Polyhedron* **1996**, *15*, 1835.

(71) McArdle, H. J.; Gross, S. M.; Creaser, I. I.; Sargeson, A. M.; Danks, D. M. *The American Physiological Society* **1989**, *256*, 667.

(72) Hendry, P.; Dixon, N. E.; Sargeson, A. M. *unpublished results*

(73) Behm, C. A.; Creaser, I. I.; Korybut-Daszkiewicz, B.; Geue, R. J.; Sargeson, A. M.; Walker, G. W. *J. Chem. Soc., Chem. Commun.* **1993**, 1844.

(74) Behm, C. A.; Boreham, P. F. L.; Creaser, I. I.; Korybut-Daszkiewicz, B.; Maddalena, D. J.; Sargeson, A. M.; Snowdon, G. M. *Aust. J. Chem.* **1995**, *48*, 1009.

(75) De Clercq, E.; Yamamoto, N.; Pauwels, R.; Baba, M.; Schols, D.; Nakashima, H.; Balzarini, J.; Debyser, Z.; Murrer, B. A.; Schwartz, D.; Thornton, D.; Bridger, G.; Fricker, S.; Henson, G.; Abrams, M.; Picker, D. *Proc. Natl. Acad. Sci. USA* **1992**, *89*, 5286.

CHAPTER 2.

General Experimental Strategies

Unless otherwise specified the following general physical equipment and procedures were used.

2.1 Starting Materials and Solvents

All chemicals (AR grade) were used as received unless otherwise specified. General starting materials were prepared according to literature methods and are referenced in the text. Distilled water was used for all chromatography while both water and ethanol were used for recrystallisations. Solvents (AR grade) were used as received. Evaporations were performed at reduced pressures (~20 Torr) and in a water bath at ≤ 50°C using a Büchi rotary evaporator.

Standard inert atmosphere techniques were used where stated in the text using nitrogen. Where required, solvents were thoroughly purged with inert gas immediately prior to use.

2.2 Chromatography

For chromatography SP Sephadex C-25 (Pharmacia Fine Chemicals) and Dowex 50Wx2 (Bio-Rad, 200-400 mesh) cation exchange resins were used for complex separations and desalting respectively. All column dimensions are given as length by diameter in cm.

2.3 Hazards and Special Precautions

In synthetic procedures acetic acid was used to quench the condensation reactions. However on a few occasions hydrochloric acid was used, care was taken to avoid contact with the fumes when quenching this reaction as carcinogenic haloethers may have formed. All quenching reactions were performed in a well ventilated fumehood. Perchlorate salts were handled carefully as they are potentially explosive.

2.4 NMR Spectroscopy

^{1}H and ^{13}C NMR spectra were acquired on a Varian 300 MHz spectrometer using standard Varian software. Spectra were referenced externally against 1,4-dioxane (3.70 ppm vs TMS for ^{1}H NMR spectra and 67.4 ppm vs TMS for ^{13}C NMR spectra). Chemical shifts (δ) are in ppm and are reported as positive chemical shifts downfield from the tetramethyl silane (TMS (=0)) reference. The 500 MHz ^{1}H NMR spectra were acquired with a Varian 500 MHz spectrometer using standard Varian software. These spectra were referenced internally against

sodium(trimethylsilyl)propanesulfonate (NaTSP). The two dimensional COSY experiments were obtained using an Inova 600 MHz NMR spectrometer in conjunction with standard Inova software. Uncertainties in the chemical shift are typically 0.05 ppm for ^{1}H and 0.5 ppm of ^{13}C. The quaternary peak assignments were made using DEPT spectra and by analogy with complexes containing similar chromophores.

2.5 Infra-red Spectroscopy

Infra-red spectra were recorded with either a Perkin-Elmer 683 Spectrometer as KBr disks and the 1601 cm^{-1} absorption of a polystyrene film as calibration or a Perkin-Elmer 1800 Fourier-Transform Infra-red (FTIR) Spectrometer as KBr disks or in D_2O.

2.6 Electrospray Mass Spectrometry

Electrospray mass spectra (ESMS) were recorded by Dr Carl Braybrook (ANU). ESMS of aqueous solutions were recorded using a Fisons/VG Biotech Quatro II mass spectrometer. The solvent stream was water.

2.7 Structure Determinations

The X-ray structures throughout this thesis were determined by Dr. A. C. Willis at the Australian National University. The equipment used and the conditions under which the experimental data were aquired are described in the relevant experimental sections.

2.8 Electrochemistry

(a) Electrolytes

The electrolytes used in the aqueous electrochemistry were of AR grade and used without further purification. The electrolyte concentration in the aqueous electrochemistry was typically 0.05 M or 0.1 M.

The concentration of the electroactive species was generally 1mM. All samples were purged for ~15 minutes with a continuous flow of nitrogen prior to data aquisition. Measurements were acquired under a blanket of nitrogen at ~293(1) K unless otherwise specified.

(b) Cyclic Voltammetry

Standard electrochemical measurements were performed on a BAS 100 Electrochemical Analyser. Using BAS File Transfer Software, the data

was transfered to a personal computer, which was then converted to Macintosh-readable form. The CV's were displayed using a suitable graphics programme. In all cases, a three electrode system was used with full iR compensation. The auxiliary electrode consisted of a Pt wire and the reference electrode was $Hg/Hg_2Cl_2/KCl$ (saturated) (SCE), (241 mV vs SHE). The working electrode consisted of either an edge plane pyrolytic graphite (EPG) carbon or mercury electrode. The mercury electrode (Metrohm 663 VA stand, interfaced with an RSC Model-411 interface unit) was generally used as a hanging mercury drop electrode (HMDE). The EPG electrode was polished using a suspension of BAS polishing alumina on a polishing cloth prior to each measurement. The electrode was then rinsed thoroughly with distilled water and carefully wiped dry with lens tissue. For the HMDE a new mercury drop was formed prior to commencement of each measurement. In aqueous solutions the reference electrode was separated from the cell using a salt bridge containing an aqueous solution of saturated KCl.

2.9 Electronic Spectroscopy

Electronic absorption spectra were obtained with a Hewlett Packard 8450A UV/Visible spectrophotometer in 1 cm quartz cells. The data were converted to Macintosh readable forms and the spectra displayed using a suitable graphics programme. The electronic spectra of the Ni(III) compounds were obtained by in situ oxidation of the Ni(II) species in 0.1 cm quartz cell in a Perkin-Elmer Lambda 9 UV/Visible/NIR spectrophotometer coupled to a RSC 424 Thompson Potentiostat Monitor Unit and a Thompson Electrochemical Ministat Potentiostat.

CHAPTER 3.

The Synthesis and Properties of Functionalised Cage and Macrocyclic Metal Complexes.

3.1 Introduction

Ligands possessing amide groups have been extensively investigated in the last twenty years, as they can stabilise higher oxidation states of some transition metal ions. These ligands take on many forms, although macrocyclic amide complexes form the bulk of the examples. A number of different methods and reagents exist for the preparation of the various amide ligands. One of the most common procedures is to condense an ester with a primary amine giving an amide linkage. The use of a template to perform this condensation is not as prominent in the literature.

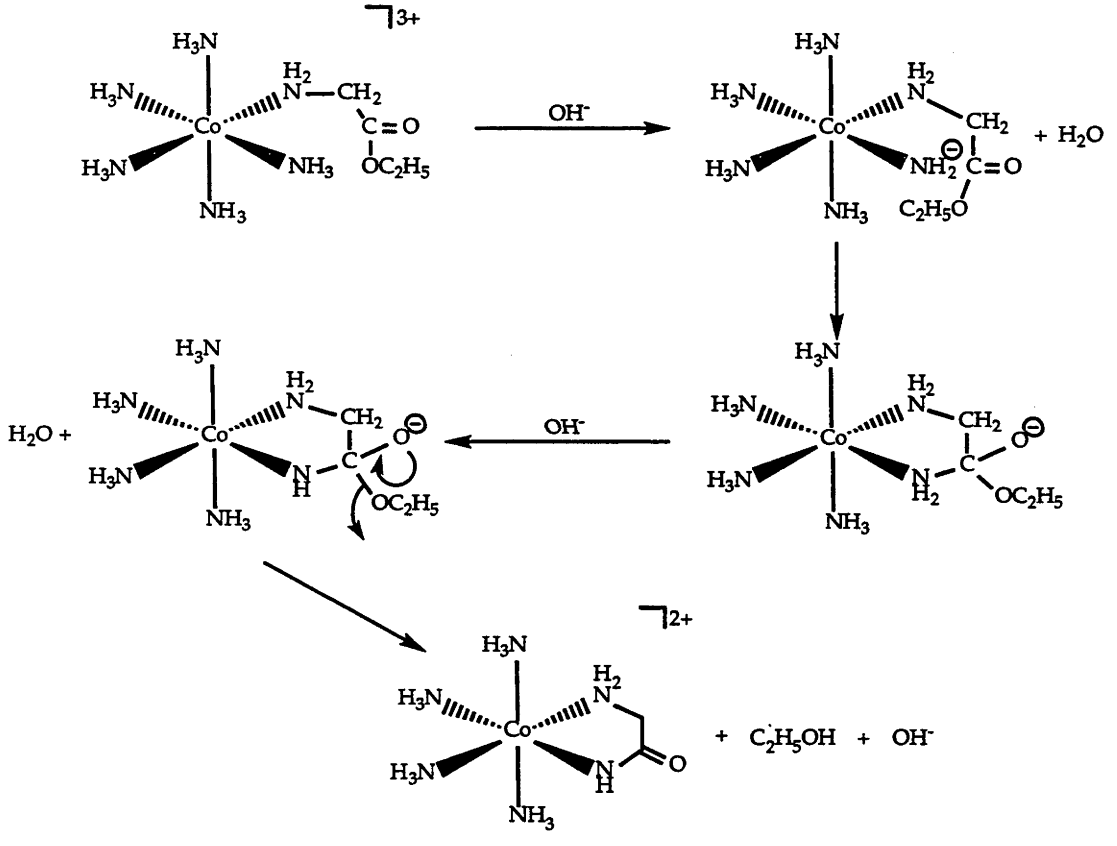

Figure 1

One of the first examples of a template reaction between an ester and amine, leading to an amido bond, was the hydrolysis of the $[Co^{III}(NH_3)_5HN_2CH_2COOC_2H_5]^{3+}$ ion in base (Figure 1).[1] The metal contributes to this condensation reaction by making the condensation intramolecular and therefore much faster and also by increasing the acidity of NH_3. When the metal ion is absent, refluxing conditions and high

dilution techniques are essential for amide bond formation and generally the yields of these reactions are low. However, the template synthesis strategy makes cyclic amide ligand production simpler, faster and higher yielding.

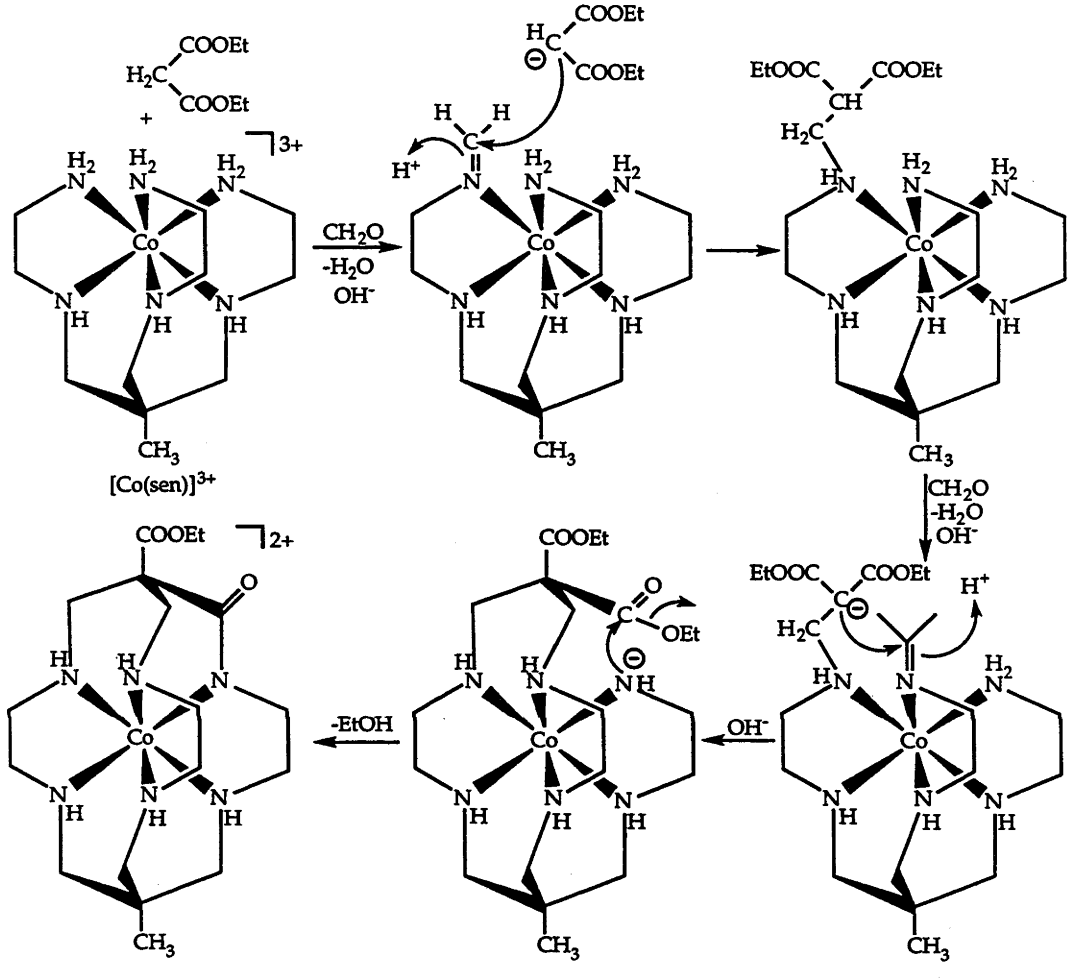

Figure 2

Another template approach that can lead to the production of a coordinated amide involves the reaction of a coordinated primary amine with formaldehyde and a carbon acid ester, such as diethyl malonate in the presence of base (Figure 2).[2] Other acidic ester compounds of the form X-CH_2-COOEt may be used in these types of reactions. However, not all of these template reactions produce amide linkages. The template reaction may produce a new six membered ring macrocycle containing pendant groups, but no amide bond (Figure 3).[3] The ester condensation does not compete effectively with the Mannich type reaction and sometimes does

not take part in the condensation reaction. However, when three amines are available on a trigonal face, of a template, the ester moiety can be condensed finally to form an amide bond.[2]

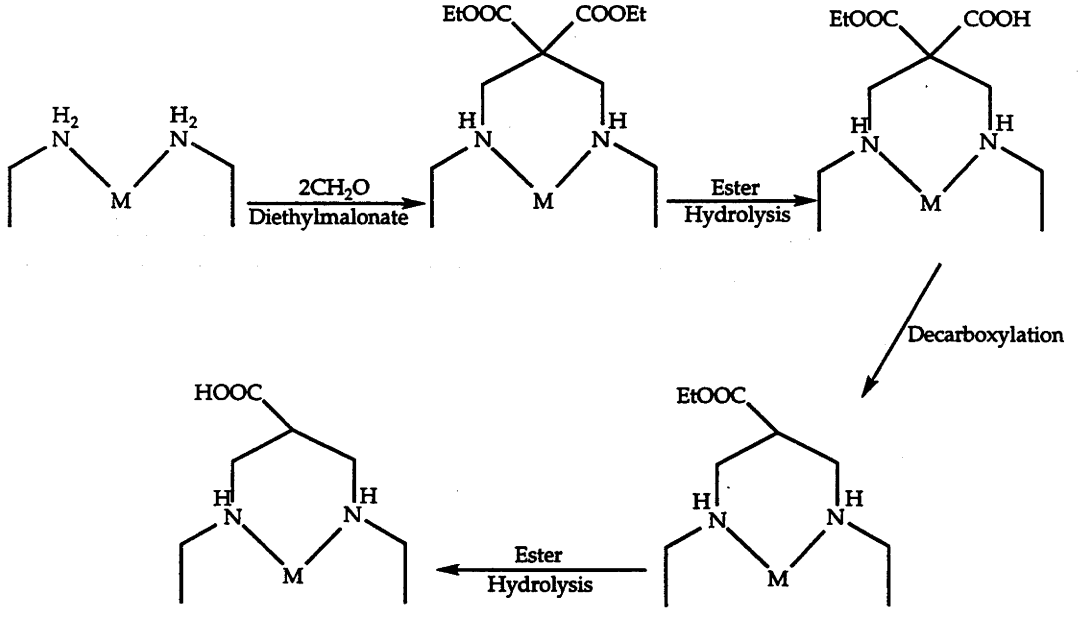

Figure 3

This chapter describes the reaction of the $[Co^{III}(sen)]^{3+}$ ion with three different ester compounds leading to the production of two different Co(III) monoamido complexes, as well as a number of other Co(III) compounds. One of these amide complexes has been demetallated and the free ligand recomplexed to a range of different metal ions. The main aim of this study was to examine the effect that amide functionalisation has upon the basic sar cage with different metal ions.

3.2 Experimental

3.2.1 Section 1. Reaction of $[Co^{III}(sen)]^{3+}$ with ethyl cyanoacetate and formaldehyde in aqueous base.

3.2.1.1 Syntheses

[1,1,1-Tris(4-amino-2-azabutyl)ethane)cobalt(III)]chloride.H_2O $[Co^{III}$-(sen)]$Cl_3.H_2O$ was prepared according to literature methods.[4-6] Anal. Calc. for $C_{11}H_{30}N_6Cl_3Co.H_2O$: C, 30.8; H, 7.5; N, 19.6; Cl, 24.8. Found C, 30.6; H, 7.7; N, 19.7; Cl, 24.9. ^{13}C NMR (δ, D_2O): 20.4 ($CqCH_3$); 40.6 ($CqCH_3$); 43.4, 55.1 (NCH_2); 57.5 (NCH_2Cq). IR in KBr (ν-$_{max}$/cm^{-1}): 3230, 3180 (NH stretch); 2970, 2960 (C-H stretch); 1630, 1610 (NH, NH_2); 1460, 1410 (C-H deformation); 1080, 1060, 1020 (CH_2 rock). Low resolution ESMS (80 V) [m/z, obs (calc) (%) assignment where cage = $[^{12}C_{11}{}^{1}H_{30}{}^{14}N_6{}^{59}Co]^{3+}$]: 302.8 (303) (100%) [Cocage^{3+} - $2H^+]^+$; 338.7 (339) (9%) [Cocage^{3+} - H^+ + $^{35}Cl^-]^+$.

[(1-cyano-8-methyl-2-oxo-3,6,10,13,16,19-hexaazabicyclo[6.6.6]icosanato)-cobalt(III)]chloride.3.5H_2O, $[Co^{III}$(Me,CN-2-oxosar-H)]Cl_2.3.5H_2O, [(2-amino-1-carboxy-8-methyl-3,6,10,13,16,19-hexaazabicyclo[6.6.6]icosanato-2-ene)-cobalt(III)]chloride.0.5C_2H_5OH.3.5H_2O, $[(Co^{III}$(Me,COOH-2-aminosar-2-ene)]Cl_3.0.5C_2H_5OH.3.5H_2O, [(1,3,6,10,13,-16,19-heptaaza-8-methylbicyclo-[6.6.6]icosane)cobalt(III)]chloride.3H_2O, [Co-(Meazasar)]Cl_3.3H_2O, [(4-methyl-amino-2-azabutyl-bis-1,1-(4-amino-2-azabutyl)ethane)cobalt(III)]chloride.-H_2O, $[Co^{III}$(N-Me-sen)]$Cl_3.H_2O$ and [(2-amino-8-methyl-3,6,10,13,-16,19-hexaazabicyclo[6.6.6]icosanato-2-ene)cobalt(III)]chloride.3H_2O, $[Co^{III}$(Me-2-aminosar-2-ene)]Cl_3.3H_2O

$[Co^{III}(sen)]Cl_3.H_2O$ (10 g; 0.023 mol), formaldehyde (20 mL, 36% solution, 0.24 mol), ethyl cyanoacetate (4 mL; 0.035 mol) and Na_2CO_3 (7.2 g; 0.07 mol) were stirred in water (40 mL) at 60° C for two hours. The reaction was quenched with acetic acid, diluted to five litres and adsorbed onto Dowex 50Wx2 cation exchange resin (25 cm x 5cm). After washing with water and 1 M HCl elution with 3 M HCl produced two bands; the first red band (Fraction 1) separated cleanly from an orange fraction which represented the bulk of the material. The red band was collected and evaporated to dryness via rotary evaporation to yield the chloride salt. This was then redissolved in ethanol and taken back to dryness in an attempt to remove the last traces of HCl. **Fraction 1** the ^{13}C NMR spectrum of displayed sixteen signals consistent with the formation of a unsymmetrical cage complex. The NMR spectra of this band were consistent with the

species $[Co^{III}(Me,CN\text{-}2\text{-}oxosar\text{-}H)]^{2+}$. Yield = 2.7 g (23%). Anal. Calc. for $C_{16}H_{30}N_7Cl_2CoO.3.5H_2O$: C, 37.4; H, 7.3; N, 19.1; Cl, 13.8. Found C, 37.5; H, 7.0; N, 19.1; Cl, 13.4. ^1H NMR (**δ**, D_2O): 0.86 (s, 3H, CH_3 tail); 2.30 - 3.51 (complex pattern, 21H, NCH_2); 3.82 (m, 1H, CH_2). ^{13}C NMR (**δ**, D_2O): 20.8 ($CqCH_3$); 41.4 ($CqCH_3$); 58.0 ($CqC{=}O$); 47.1, 50.5, 52.1, 52.6, 52.8, 53.3, 55.0, 55.1, 55.3, 55.6, 55.7 (NCH_2); 116.8 ($C{\equiv}N$); 171.3 ($C{=}O$). IR in KBr ($\nu\text{-}_{max}/cm^{-1}$): 3148, 3072 (NH stretch); 2960, 2868 (C-H stretch); 2250 (C≡N); 1621, 1605 (C=O amide stretch); 1448, 1420, 1400 (C-H deformation); 1370, 1323, 1277, 1173 (C-H twist); 1173, 1121, 1058, 1022, 916, 882, 846, 755 (C-H rock). Low resolution ESMS (50 V) [m/z, obs (calc) (%) assignment where cage = $[^{12}C_{16}{}^1H_{30}{}^{14}N_7{}^{59}Co^{16}O_2]^{2+}$]: 393.8 (394) (100%) $[Cocage^{2+} - H^+]^+$; 411.9 (412) (35%) $[Cocage^{2+} + {}^{35}Cl^-]^+$; 429.8 (430) (20%) $[Cocage^{2+} - H^+ + H_2O]^+$. A small amount of the chloride complex (0.10 g) was converted into the perchlorate salt by adding solid $NaClO_4$ to an aqueous solution of the compound and upon slow evaporation in the air crystals suitable for x-ray analysis formed. After taking the orange fraction to dryness it was rechromatographed on SP-Sephadex C-25 cation exchange resin. Elution with 0.2 M NaCl produced two bands the first of which was collected, desalted on Dowex, and dried (Fraction 2). The second fraction was desalted on Dowex, rechromatographed on Sephadex, and elution with 0.25 M K_2SO_4 gave three more bands (Fractions 3, 4 and 5). All three fractions were desalted on Dowex, eluted with 3 M HCl, and dried. Each fraction was then redissolved in ethanol and taken back to dryness in an attempt to remove the last traces of HCl.

Fraction 2. The ^{13}C NMR spectrum of Fraction 2 displayed sixteen signals consistent with an unsymmetrical cage complex. The NMR spectra are consistent with the species $[Co^{III}(Me,CO_2H\text{-}2\text{-}aminosar\text{-}2\text{-}ene)]^{3+}$. Yield = 1.9 g (14%). Anal. Calc. for $C_{16}H_{33}N_7Cl_3CoO_2.0.5C_2H_5OH.3.5H_2O$: C, 33.6; H, 6.6; N, 16.2; Cl, 17.5. Found C, 33.3; H, 6.5; N, 16.2; Cl, 17.2. ^1H NMR (**δ**, D_2O): 0.86 (s, 3H, CH_3 tail); 2.25 - 3.42 (complex pattern, 21H, NCH_2); 3.72 (m, 1H, CH_2). ^{13}C NMR (**δ**, D_2O): 20.7 ($CqCH_3$); 42.0 ($CqCH_3$); 62.1 ($CqCNH_2$); 49.2, 52.5, 53.6, 54.3, 54.7, 54.8 (double intensity), 55.0, 55.3, 55.9, 56.3, 55.7 (NCH_2); 169.4 ($N{=}CNH_2$); 173.6 ($CqCOOH$). IR in KBr ($\nu\text{-}_{max}/cm^{-1}$): 3479, 3426, 3359, 3140 (NH stretch); 3088, 3041 (OH stretch); 2962, 2863 (C-H stretch); 2553, 2469 (OH stretch); 1723 (C=O stretch); 1671 (C=N stretch); 1599 (NH_2 in-plane bending); 1465, 1433 (C-H deformation); 1390 ($C\text{-}CH_3$); 1329, 1262 (C-H twist); 1250 (OH bend); 1144, 1118 (C-N-C stretch); 1068, 1055, 1020, 917, 716 (CH_2 rock). Low resolution ESMS (80 V) [m/z, obs (calc) (%)

assignment where cage = $[^{12}C_{16}{}^{1}H_{33}{}^{14}N_7{}^{59}Co^{16}O_2]^{3+}$]: 367.8 (368) (100%) [Cocage^{3+} - 2H$^+$ - CO_2]$^+$; 411.8 (412) (20%) [Cocage^{3+} - 2H$^+$]$^+$.

Fraction 3. Yield = 0.29 g (3%). The NMR spectra are consistent with the species $[Co^{III}(azamesar)]^{3+}$. Anal. Calc. for $C_{14}H_{33}N_7Cl_3Co.3H_2O$: C, 32.4; H, 7.6; N, 18.9; Cl, 20.5. Found C, 32.2; H, 7.2; N, 19.2; Cl, 20.2. ^{1}H NMR (**δ**, D_2O): 1.02 (s, 3H, CH_3 tail); 2.31 - 3.52 (complex pattern, 18H, NCH_2); 3.57, 4.42 (AB quartet, 6H, CH_2). ^{13}C NMR (**δ**, D_2O): 20.3 (CqCH_3); 43.2 (CqCH_3); 53.4, 54.7 (NCH_2); 56.2 (NCH_2C); 67.9 (NCH_2N). IR in KBr (ν-$_{max}$/cm^{-1}): 3060 (NH stretch); 2960, 2860 (C-H stretch); 1450, 1405 (C-H deformation); 1070, 1060, 1030, 1005, 990, 840, 720 (CH_2 rock). Low resolution ESMS (80 V) [m/z, obs (calc) (%) assignment where cage = $[^{12}C_{14}{}^{1}H_{33}{}^{14}N_7{}^{59}Co]^{3+}$]: 355.8 (356) (100%) [Cocage^{3+} - 2H$^+$]$^+$; 391.7 (392) (23%) [Cocage^{3+} - H$^+$ + ^{35}Cl$^-$]$^+$.

Fraction 4. Yield = 1.8 g (18%). The NMR spectra are consistent with the species $[Co^{III}(N\text{-}Me\text{-}sen)]^{3+}$. Anal. Calc. for $C_{12}H_{32}N_6Cl_3Co.H_2O$: C, 32.5; H, 7.7; N, 18.9; Cl, 24.0. Found C, 32.8; H, 7.2; N, 18.7; Cl, 23.8. ^{1}H NMR (**δ**, D_2O): 0.72 (s, 3H, CH_3 tail); 2.01 - 3.10 (complex pattern, 21H, NCH_2, NCH_3). ^{13}C NMR (**δ**, D_2O): 20.3 (CqCH_3); 38.5 (NCH_3); 43.2 (CqCH_3); 42.9, 44.1, 54.6 (double intensity), 54.9 (double intensity), 56.0, 57.5, 58.0 (NCH_2). IR in KBr (ν-$_{max}$/cm^{-1}): 3260 (NH stretch); 2860 (C-H stretch); 1600 (NH_2); 1415, 1405 (C-H deformation); 1165 (N-CH_3); 1090, 1050, 1040 (CH_2 rock). Low resolution ESMS (80 V) [m/z, obs (calc) (%) assignment where cage = $[^{12}C_{12}{}^{1}H_{32}{}^{14}N_6{}^{59}Co]^{3+}$]: 316.9 (317) (100%) [Cocage^{3+} - 2H$^+$]$^+$; 352.8 (353) (42%) [Cocage^{3+} - H$^+$ + ^{35}Cl$^-$]$^+$; 302.8 (303) (37%) [Cocage^{3+} - H$^+$ - CH_3]$^+$.

Fraction 5. The ^{13}C NMR spectrum of Fraction 5 displayed fifteen signals consistent with the formation of an unsymmetrical cage complex. The NMR spectra are consistent with the species $[Co^{III}(Me\text{-}2\text{-}aminosar\text{-}2\text{-}ene)]^{3+}$. Yield = 1.2 g (10%). Anal. Calc. for $C_{15}H_{33}N_7Cl_3Co.3H_2O$: C, 33.9; H, 7.4; N, 18.5; Cl, 20.0. Found C, 33.9; H, 7.4; N, 18.4; Cl, 20.0. ^{1}H NMR (**δ**, D_2O): 0.87 (s, 3H, CH_3 tail); 2.22 - 3.43 (complex pattern, 21H, NCH_2); 3.55 (m, 1H, CH_2). ^{13}C NMR (**δ**, D_2O): 20.8 (CqCH_3); 42.5 (CqCH_3); 50.1 (CqCNH_2); 46.9, 47.8, 48.5, 54.2, 54.7, 54.8, 55.2, 55.3, 55.6, 55.7, 56.1 (NCH_2); 169.4 (N=CNH_2). IR in KBr (ν-$_{max}$/cm^{-1}): 3415, 3072 (NH stretch); 2960, 2860 (C-H stretch); 1654 (C=N stretch); 1618 (NH_2 in-plane bending); 1445, 1404 (C-H deformation); 1328, 1287, 1261, 1229, 1171 (C-H twist); 1073, 1050, 1034 (C-H rock). Low resolution ESMS (80 V) [m/z, obs (calc) (%) assignment where cage = $[^{12}C_{15}{}^{1}H_{33}{}^{14}N_7{}^{59}Co]^{3+}$]: 367.8 (368) (100%) [Cocage^{3+} - 2H$^+$]$^+$; 403.8 (404) (28%) [Cocage^{3+} - H$^+$ + ^{35}Cl$^-$]$^+$; 439.8 (440) (12%) [Cocage^{3+} - H$^+$ + ^{35}Cl$^-$ + 2H_2O]$^+$.

Attempted demetallation of [(1-cyano-8-methyl-2-oxo-3,6,10,13,16,19-hexaazabicyclo[6.6.6]icosanato)cobalt(III)]chloride.3.5H_2O, [Co^{III}(Me,CN-2-oxo-sar-H)]Cl_2.3.5H_2O.

[Co^{III}(Me,CN-2-oxosar-H)]Cl_2.3.5H_2O (28.8 g; 0.06 mol) was dissolved in 200 mL of water and to this was added a solution of $CoCl_2$.6H_2O (14.28 g; 0.06 mol) in 100 mL of water. KCN (74.6 g; 1.15 mol) was also dissolved in 150 mL of water and both solutions were deoxygenated with N_2 for approximately one hour. After this time the KCN solution was added dropwise over a period of ten minutes. As the cyanide was added a green precipitate formed, however this redissolved shortly after all of the KCN was added. The resulting mixture was heated to 40° C and stirred for one week; over this time the solution changed from red to pale yellow. Separation of the ligand from the cyanide consisted of precipitating out the KCN with ethanol (2 L) filtering the solution and removing the solvent under vacuum. The residue was then redissolved in ethanol (200 mL), refiltered to remove more KCN and once again taken to dryess. This procedure was repeated until no more KCN could be observed. NMR studies confirmed that the white solid obtained was a mixture of products none of which corresponded to the desired amide free ligand. The apical nitrile group was noticeably absent from the ^{13}C NMR while both the ^{1}H and ^{13}C NMR indicated the solid comprised largely decomposition products and characterisation was not pursued further.

Attempted oxidation and reduction of amidine complexes to produce a saturated cage.

Reaction with $NaNO_2$ and HCl.

A solution of [Co^{III}(Me-2-aminosar-2-ene)]Cl_3.3H_2O (3.6 g; 6.3x10^{-3} mol) and LiCl (8 g; 0.19 mol) in water (40 mL) was cooled in ice to below 5° C. $NaNO_2$ (1.74 g; 0.025 mol) was added and the mixture stirred until all the solid had dissolved. A slight effervescence occurred and the solution was left standing for thirty minutes. After this time conc. HCl (1.3 mL; 0.013 mol) was added and cooling was continued for a further thirty minutes. Finally, more conc. HCl (5 mL) was added producing a yellow/orange precipitate, and the solution was then allowed to warm to room temperature. After diluting with water (1 L) the reaction mixture was loaded onto a Dowex column (10 cm x 5 cm). The column was washed

with water (1 L), 1 M HCl and then eluted with 3 M HCl to produce a single orange band. The NMR spectra of the collected band showed that the starting material was recovered unchanged.

Reaction with concentrated HNO_3

$[Co^{III}$(Me-2-aminosar-2-ene)$]Cl_3.3H_2O$ (1 g; $2.1x10^{-3}$ mol) was added to conc. HNO_3 (50 mL) at 100° C rapidly with stirring and the complex dissolved immediately. The resultant solution was heated and stirred for sixty minutes. After this period the mixture was diluted with water (1 L) and sorbed onto Dowex 50Wx2 cation exchange resin where it was washed with water (1 L), 1 M HCl and finally eluted with 3 M HCl to produce a single orange band. The NMR spectra of the collected band showed that the starting material was recovered unchanged.

Reaction with $NaBH_4$.

$[Co^{III}$(Me-2-aminosar-2-ene)$]Cl_3.3H_2O$ (1 g; $2.1x10^{-3}$ mol) was dissolved in a carbonate buffer solution (pH 10) and to this was added $NaBH_4$ (1 g; 0.03 mol). This solution was stirred for one hour. The reaction was quenched with acetic acid, diluted to four litres with water and sorbed onto Dowex 50Wx2 cation exchange resin. The column was washed with water (1 L), and 0.5 M HCl (1 L), and finally eluted with 3 M HCl to yield a single orange band. The NMR spectra of the collected band showed that the starting material was recovered unchanged.

Attempted reduction with Pd/C.

$[Co^{III}$(Me-2-aminosar-2-ene)$]Cl_3.3H_2O$ (1 g; $2.1x10^{-3}$ mol) was partly dissolved in dry methanol and to this was added 10% Pd/C (0.5 g). The mixture was placed in a hydrogenator at 30 psi (1 week) and during this time the vessel was evacuated and refilled with H_2 five times. The charcoal was removed by filtration and the methanol filtrate taken to dryness under reduced pressure. The residue was dissolved in water and placed on a SP-Sephadex C-25 cation exchange column. After washing with water (1 L), the column was eluted with 0.05 M Na_3citrate producing two separate orange bands. These were collected, and then desalted on Dowex 50Wx2 cation exchange resin. NMR spectra of each band indicated that the complexes isolated were [Co(sen)]Cl_3 (0.34 g) and starting material (0.25 g). This indicated that the process had partly destroyed the amidine cage.

3.2.1.2 X-ray Crystallography of $[Co^{III}(Me,CN\text{-}2\text{-}oxosar\text{-}H)](ClO4)_{3/2}.Cl_{1/2}.H_2O$

Data Collection

A small orange crystal of the Co(III) monoamido complex having approximate dimensions of 0.17 x 0.09 x 0.07 mm was mounted on a quartz fibre. All measurements were made on a Rigaku AFC6R diffractometer with graphite monochromated Cu-Kα radiation and a 12 kW rotating anode generator. A LN2 refrigeration fixed tube low temperature system was used to cool the crystal to -60° C. Cell constants and an orientation matrix for data collection were obtained from a least squares refinement using the setting angles of 24 carefully centered reflections in the range $104.41° < 2\theta < 109.82°$ and corresponded to a C-centered monoclinic cell with dimensions a = 26.143(1) Å, b = 10.794(2) Å c = 17.061(2) Å and V = 4564.9(9) $Å^3$. For Z = 8 and F.W. = 580.31, the calculated density is 1.69 g/cm^3. Based on the systematic absences of: hkl: $h+k \neq 2n$, h0l: $l \neq 2n$ packing considerations, a statistical analysis of intensity distribution and the successful solution and refinement of the structure, the space group was determined to be C2/c (# 15). The data were collected at a temperature of -60 ± 1° C using the $\omega - 2\theta$ scan technique to a maximum 2θ value of 120.0°. Omega scans of several intense reflections, made prior to data collection, had an average width at half height of 0.33° with a take-off angle of 6.0°. Scans of $(1.10 + 0.30 \tan \theta)°$ were made at a speed of 16.0°/min (in omega). The weak reflections ($I < 10.0\sigma(I)$) were rescanned (maximum of four scans) and the counts were accumulated to ensure good counting statistics. Stationary background counts were recorded on each side of the reflection. The ratio of peak counting time to background counting time was 2:1. The diameter of the incident beam collimator was 0.5 mm, the crystal to detector distance was 400 mm, and the detector aperture was 15.0 x 8.0 mm (horizontal x vertical).

Data Reduction

Of the 3734 reflections collected, 3598 were unique ($R_{int} = 0.028$). The intensities of three representative reflections were measured after every 150 reflections. No decay correction was applied. The linear absorption coefficient, μ, for Cu-Kα radiation is 85.9 cm^{-1}. An analytical absorption correction was applied which resulted in transmission factors ranging from 0.40 to 0.58. The data were corrected for Lorentz and polarisation effects.

Structure Solution and Refinement

The structure was solved by direct methods[7] and refined using Fourier techniques.[8] The non-hydrogen atoms were refined anisotropically. The hydrogen atom coordinates were refined but their isotopic B values were fixed. The final cycle of full-matrix least-squares refinement was based on 2284 observed reflections ($I > 3.00\sigma(I)$) and 404 variable parameters and converge (largest parameter shift was 0.04 times its esd) with unweighted and weighted agreement of: $R = \Sigma \| |Fo| - |Fc| \| / \Sigma |Fo| = 0.033$ and $R_w = ((\Sigma\omega(|Fo| - |Fc|)^2/\Sigma\omega Fo^2)))^{1/2} = 0.026$. The standard deviation of an observation of unit weight was 1.64. The weighting scheme was based on counting statistics and included a factor (p = 0.006) to downweight the intense reflections. Plots of $\Sigma\omega(|Fo| - |Fc|)^2$ verses $|Fo|$, reflection order in data collection, $\sin\theta/\lambda$ and various classes of indices showed no unusual trends. The maximum and minimum peaks on the final difference Fourier map corresponded to 0.30 and -0.32 $e^-/Å^3$, respectively. Neutral atom scattering factors were taken from Cromer and Waber.[9] Anomalous dispersion effects were included in F_{calc}[10]; the values for $\Delta f'$ and $\Delta f''$ were those of Creagh and McAuley.[11] The values for the mass attenuation coefficients are those of Creagh and Hubbel.[12] All calculations were performed using the texsan[13] crystallographic software package of the Molecular Structure Corporation.

3.2.2 Section 2. Reaction of $[Co^{III}(sen)]^{3+}$ with ethyl acetoacetate and formaldehyde in aqueous base.

3.2.2.1 Syntheses

[(1-carboxy-8-methyl-3,6,10,13,16,19-hexaazabicyclo[6.6.6]icosanato)cobalt-(III)]chloride.0.5C_2H_5OH.H_2O, $[Co^{III}$(Me,COOH-sar)$]Cl_3$.0.5C_2H_5OH.H_2O, [(6-(4-amino-2-azoniabutyl)-13-ethoxycarbonyl-13-methylenehydroxy-6-methyl-1,4,8,11-tetraazacyclotetradecane)cobalt(III)]chloride.0.5C_2H_5OH.-2.5H_2O, $[Co^{III}$({CO_2H,CH_2OH}-Me-de-sar)$]Cl_3$.0.5C_2H_5OH.2.5H_2O and [(6-(4-amino-2-azoniabutyl)-13-carboxy-13-methylenehydroxy-6-methyl-1,4,8,11-tetraazacyclotetradecane)cobalt(III)]chloride.0.5C_2H_5OH.2.5H_2O, $[Co^{III}$({CO_2Et,CH_2OH}-Me-de-sar)$]Cl_3$.0.5C_2H_5OH.2.5H_2O.

$[Co^{III}(sen)]Cl_3.H_2O$ (20 g; 0.05 mol), formaldehyde (50 mL; 36% solution; 0.6 mol), ethyl acetoacetate (10 mL; 0.08 mol) and Na_2CO_3 (10 g; 0.1 mol) were stirred in water (200 mL) for two hours. The reaction was

quenched with acetic acid, diluted to five litres and absorbed onto a SP-Sephadex C-25 cation exchange column (100 cm x 10 cm). After the column was washed with water, the complexes were eluted with 0.05 M trisodium citrate. In this case an initial yellow band (1) was followed successively by an orange band (2), a small dark orange band (not isolated) and three separate orange bands (3), (4) and (5). All the collected fractions were then desalted on Dowex 50Wx2 cation exchange columns with HCl; then reloaded separately onto Sephadex and eluted again with 0.05 M trisodium citrate to free each of the complexes of minor impurities. The recovery of the isolated fractions consisted of desalting each band on Dowex/HCl and drying; each band was then redissolved in ethanol and taken to dryness in an attempt to remove the last traces of HCl.

Fraction 1. The ^{13}C NMR spectrum displayed eight signals indicating that the complex possessed C_3 symmetry. The NMR spectra were consistent with the species $[Co^{III}(Me,CO_2H\text{-}sar)]^{3+}$ and comparison with an authentic sample confirmed this. Yield = 4.4 g (16%). Anal. Calc. for $C_{16}H_{34}N_6Cl_3CoO_2.0.5C_2H_5OH.H_2O$: C, 37.8; H, 7.4; N, 14.7; Cl, 18.6. Found C, 37.4; H, 7.7; N, 14.6; Cl, 18.8. ^1H NMR (δ, D_2O): 0.80 (s, 3H, CH_3 tail); 2.23, 2.89 (AA'BB' coupling pattern, 12H, CH_2 en); 2.55, 3.11 (Distorted AB doublet of doublets, 8H, CH_2 caps). ^{13}C NMR (δ, D_2O) 20.2 (CqCH_3); 42.8 (CqCH_3); 55.1 (CqCOOH); 52.6, 55.3, 55.4 (double intensity) (NCH_2); 174.1 (CqCOOH). IR in KBr (ν-$_{max}$/cm^{-1}): 3040 (NH stretch); 2970, 2870 (C-H stretch); 1725 (COOH stretch); 1460, 1450, 1405 (C-H deformation); 1050, 710 (CH_2 rock). Low resolution ESMS (50 V) [m/z, obs (calc) (%) assignment where cage = $[^{12}C_{16}{}^1H_{34}{}^{14}N_6{}^{59}Co^{16}O_2]^{3+}$]: 398.8 (399) (100%) [Cocage^{3+} - 2H$^+$]$^+$; 354.8 (355) (1%) [Cocage^{3+} - 2H$^+$ - CO_2]$^+$; 434.8 (435) (4%) [Cocage^{3+} - H$^+$ + $^{35}Cl^-$]$^+$.

Fraction 2. The ^{13}C NMR spectrum displayed sixteen signals consistent with the formation of a unsymmetric cage complex. The NMR spectra were consistent with the species $[Co^{III}(\{CO_2H,CH_2OH\}\text{-Me-desar})]^{3+}$. Yield = 2.0 g (7%). Anal. Calc. for $C_{16}H_{36}N_6Cl_3CoO_3.0.5C_2H_5OH.2.5H_2O$: C, 33.7; H, 7.2; N, 14.7; Cl, 18.6. Found C, 33.9; H, 7.8; N, 14.6; Cl, 18.6. ^1H NMR (δ, D_2O): 0.78 (s, 3H, CH_3 tail); 2.11 - 3.35 (complex pattern, 22H, NCH_2); 3.51 (d, 1H, CH_2OH); 3.63 (d, 1H, CH_2OH). ^{13}C NMR (δ, D_2O): 20.2 (CqCH_3); 42.9 (CqCH_3); 57.7 (HOOCCqCH_2OH); 39.5, 47.1, 49.5, 51.1, 53.7, 54.0, 54.2, 54.4, 55.8, 56.1, 57.8 (NCH_2); 66.2 (CH_2OH); 173.4 ($HOCH_2$CqCOOH). IR in KBr (ν-$_{max}$/cm^{-1}): 3060 (NH stretch); 2860 (C-H stretch); 1740 (COOH stretch); 1630 (NH_2); 1460, 1450, 1405 (C-H deformation); 1285 (CH_2OH bend); 1050

(CH_2OH, CH_2 rock). Low resolution ESMS (80 V) [m/z, obs (calc) (%) assignment where cage = $[^{12}C_{16}{}^{1}H_{36}{}^{14}N_6{}^{59}Co^{16}O_3]^{3+}$]: 386.9 (387) (100%) $[Cocage^{3+} - 2H^+ - CH_2O]^+$; 416.8 (417) (12%) $[Cocage^{3+} - 2H^+]^+$; 452.8 (453) (8%) $[Cocage^{3+} - H^+ + {}^{35}Cl^-]^+$; 342.9 (343) (6%) $[Cocage^{3+} - 2H^+ - CH_2O - CO_2]^+$.

Fraction 3. Yield = 4.1 g (13%). The ^{13}C NMR spectrum displayed eighteen peaks consistent with the formation of a partially-capped cage complex of low symmetry. The NMR spectra are consistent with the species $[Co^{III}(\{CO_2Et,CH_2OH\}\text{-Me-desar})]^{3+}$. Anal. Calc. for $C_{18}H_{40}N_6Cl_3CoO_3.0.5C_2H_5OH.2.5H_2O$: C, 37.3; H, 8.0; N, 13.0; Cl, 16.5. Found C, 37.0; H, 7.8; N, 13.5; Cl, 16.9. ^1H NMR (**δ**, 500 MHz, D_2O): 0.78 (s, 3H, CH_3 tail); 1.16 (m, 3H, $OCH_2C\underline{H}_3$); 2.10 - 3.31 (complex pattern, 22H, NCH_2); 3.51 (d, 1H, $C\underline{H}_2OH$); 3.63 (d, 1H, $C\underline{H}_2OH$); 4.14 (m, 1H, $OC\underline{H}_2CH_3$); 4.21 (m, 1H, $OC\underline{H}_2CH_3$). ^{13}C NMR (**δ**, D_2O): 13.9 ($OCH_2\underline{C}H_3$); 20.2 ($Cq\underline{C}H_3$); 42.9 ($\underline{C}qCH_3$); 57.7 ($\underline{C}qCOOEt$); 43.1, 48.2, 51.0, 51.2, 53.5, 54.1, 54.3, 54.4, 54.6, 55.8, 55.9 ($N\underline{C}H_2$); 64.8 ($O\underline{C}H_2CH_3$); 66.4 ($Cq\underline{C}H_2OH$); 178.2 ($Cq\underline{C}OOEt$). IR in KBr ($\nu\text{-}_{max}/cm^{-1}$): 3050 (NH stretch); 2860 (C-H stretch); 1720 (COOEt stretch); 1600 (NH_2); 1460, 1450, 1405 (C-H deformation); 1280 (CH_2OH); 1070 (CH_2OH); 1050, 1035 (CH_2 rock). Low resolution ESMS (80 V) [m/z, obs (calc) (%) assignment where cage = $[^{12}C_{18}{}^{1}H_{40}{}^{14}N_6{}^{59}Co^{16}O_3]^{3+}$]: 480.8 (481) (18%) $[Cocage^{3+} - H^+ + {}^{35}Cl^-]^+$; 444.9 (445) (100%) $[Cocage^{3+} - 2H]^+$; 316.9 (317) (55%) $[Cocage^{3+} - C_6H_{10}O_3]^+$; 302.8 (303) (24%) $[Cocage^{3+} - C_7H_{12}O_3]^+$; 414.9 (415) (19%) $[Cocage^{3+} - 2H^+ - CH_2O]^+$; 386.8 (387) (15%) $[Cocage^{3+} - 2H^+ - CH_2O - C_2H_5]^+$; 330.8 (331) (9%) $[Cocage^{3+} - C_5H_8O_3]^+$.

Fraction 4. Yield = 3.6 g (16%). The NMR spectra were consistent with the species $[Co^{III}(N\text{-Me-sen})]^{3+}$.

Fraction 5. Yield = 7.2 g (36%). The NMR spectra are consistent with the species $[Co^{III}(sen)]^{3+}$.

3.2.3 Section 3. Reaction of $[Co^{III}(sen)]^{3+}$ with Diethyl Malonate and formaldehyde in aqueous base.

3.2.3.1 Syntheses

Preparation of $Fe^{II}Cl_2$

$Fe^{II}Cl_2$ was prepared by suspending partly oxidised $Fe^{II}Cl_2$ in methanol containing iron filings and a trace of HCl. The mixture was

stirred under nitrogen until the solution became a clear pale green whereupon the filings were then removed by filtration and the methanol evaporated off under vacuum. The resultant pale green powder was then stored under nitrogen until required.

[1-Carboxy-8-methyl-2-oxo-3,6,10,13,16,19-hexaazabicyclo[6.6.6]icosanato)-cobalt(III)]chloride.0.5C_2H_5OH.2H_2O, [Co^{III}(Me,CO_2H-2-oxosar-H)]Cl_2.-0.5C_2H_5OH.2H_2O

This compound was prepared according to a literature method.[2] Formaldehyde (103 mL; 36% solution; 1.23 mol), diethyl malonate (37 mL; 0.25 mol) and Na_2CO_3 (65.5 g; 0.62 mol) were added to a stirred solution of [Co^{III}(sen)]Cl_3.H_2O (50 g; 0.12 mol) in water (500 mL). The mixture was stirred, and every four hours (on average) formaldehyde and diethyl malonate were added (1 mL each). The solution slowly became dark red. After four days the reaction was diluted to 5 L with water, quenched with acid and sorbed onto SP-Sephadex C-25 cation exchange resin. Elution with 0.05 M trisodium citrate produced four separate bands comprising a major red band followed by three separate minor orange bands. The first red band was collected and desalted on Dowex 50Wx2 cation exchange resin, with HCl, while the other bands were not isolated. After drying the red band it was redissolved in a solution of ethanol (200 mL) and water (200 mL); potassium carbonate (10 g) was added and the resultant mixture heated at reflux for three hours to hydrolyse the ester group. The reaction mixture was neutralised with acetic acid, diluted to three litres with water and sorbed onto Dowex. The column was washed with water and 1 M HCl before a single red band was eluted with 3 M HCl. This was collected, dried and then recrystallised from ethanol. Yield = 44 g (67%). Anal. Calc. for $C_{16}H_{31}N_6Cl_2CoO_3$.0.5C_2H_5OH.2H_2O: C, 37.5; H, 7.0; N, 15.4; Cl, 13.0. Found C, 37.7; H, 7.4; N, 15.6; Cl, 12.9. ^1H NMR (**δ**, D_2O): 0.86 (s, 3H, CH_3 tail); 2.33 - 3.44 (complex pattern, 21H, NCH_2); 3.83 (m, 1H, $CH_2NC{=}O$). ^{13}C NMR (**δ**, D_2O): 21.0 (Cq$\underline{C}H_3$); 41.6 ($\underline{C}qCH_3$); 63.3 ($\underline{C}qCC{=}O$); 46.9, 53.2, 53.6, 54.0, 54.6, 55.1 (double intensity), 55.3, 55.5, 55.7, 57.0 ($N\underline{C}H_2$); 175.5 (Cq$\underline{C}OOH$); 178.2 (C=O). IR in KBr ($\tilde{\nu}_{max}/cm^{-1}$): 3412, 3090 (NH stretch); 2875 (C-H stretch); 1727 (C=O stretch); 1599 (C=O amide); 1465 (C-H deformation); 1365 (CH_3 symmetrical deformation); 1272 (OH bend); 1213, 1144 (C-H twist); 1076, 1050, 915, 843, 766, 708 (CH_2 rock). Low resolution ESMS (50 V) [m/z, obs (calc) (%) assignment where cage = [$^{12}C_{16}{}^1H_{31}{}^{14}N_6{}^{59}Co^{16}O_3$]$^{2+}$]: 412.8 (413) (65%) [Cocage^{2+} - H^+]$^+$; 369.9 (370) (11%) [Cocage^{2+} - H^+ - CO_2]$^+$.

1-Carboxy-8-methyl-2-oxo-3,6,10,13,19-hexaazabicyclo[6.6.6]icosane.-0.5C_2H_5OH.3.5H_2O, Me,CO_2K-2-oxosar.0.5C_2H_5OH.3.5H_2O

[Co^{III}(Me,CO_2H-2-oxosar-H)]Cl_2.0.5C_2H_5OH.2H_2O (50.0 g; 0.103 mol) was dissolved in 150 mL of H_2O and to this was added a solution of $Co^{II}Cl_2$.6H_2O (26.2 g; 0.11 mol) in 100 mL of H_2O. A second solution of KCN (134.2 g; 2.06 mol) in 250 mL of H_2O was added dropwise, over a period of ten minutes, after both solutions were deoxygenated with N_2 for approximately one hour. The resultant solution was stirred at ~20° C in the N_2 atmosphere for one week and over this time the colour changed from red to pale yellow. Separation of the ligand from the cyanide consisted of precipitating out the KCN with ethanol (2 L), filtering the solution and removing the solvent under vacuum. The residue was redissolved in ethanol (200 mL), refiltered to remove more cyanide and once again taken to dryness. This procedure was repeated until no more KCN was observed. Both the NMR of the product and the microanalysis showed the product to be contaminated with ethanol. Yield = 38 g. Anal. Calc. for $C_{16}H_{32}N_6O_3K$.0.5C_2H_5OH.3.5H_2O: C, 42.5; H, 8.8; N, 17.5. Found C, 42.7; H, 9.3; N, 17.7. ^{1}H NMR (**δ**, D_2O): 0.58 (s, 3H, CH_3 tail); 2.51 - 2.83 (complex pattern, 8H, NCH_2); 2.78, 3.20 (AA'BB' spin system, 12H, CH_2 en); 3.25 (m, 2H, NCH_2). ^{13}C NMR (**δ**, D_2O) 24.1 (CqCH_3); 37.3 (CqCH_3); 40.2 (CqCOO$^-$); 48.1, 48.2, 49.8, 53.7, 58.1, 60.5 (NCH_2); 176.2 (CqCOO$^-$); 178.6 (C=O). IR in KBr (ν-$_{max}$/cm^{-1}): 3417 (NH stretch); 2926, 2849 (C-H stretch); 1630 (C=O amide stretch); 1591 (COO^-K^+ antisymmetrical stretch); 1464 (C-H deformation); 1350 (COO^-K^+ symmetrical stretch); 1125 (C-N-C stretch).

[(1-Carboxy-8-methyl-2-oxo-3,6,10,13,19-hexaazabicyclo[6.6.6]icosanato)-nickel(II)]perchlorate.H_2O, [Ni^{II}(Me,CO_2^--2-oxosar)]ClO_4.H_2O

Me,CO_2K-2-oxosar.0.5C_2H_5OH.3.5H_2O (5.0 g; 0.01 mol) was dissolved in 100 mL of H_2O with stirring. A second solution of $Ni^{II}OAc_2$.4H_2O (2.6 g; 0.01 mol) and triethylamine (1.1 g; 0.01 mol) in 100 mL of H_2O was also prepared and both solutions were then deoxygenated, with N_2, for approximately thirty minutes. The nickel(II) solution was added dropwise to the ligand solution with stirring. After several hours the pink solution was diluted to 2 L with water, acidified with acetic acid and sorbed onto a SP-Sephadex C-25 cation exchange column (30 cm x 5 cm). The column was initially washed with water and elution with 0.25 M $NaClO_4$ produced two pink bands. The first fraction was collected and reduced in volume, while the second very minor band was not recovered. The isolated band was acidified with a few drops of acetic acid and kept at ~20° C for several days.

The pink product that precipitated was collected, washed with ethanol and ether and air dried. Further crops were obtained by allowing the acidified filtrate to continually evaporate in air. Finally, a crop of mauve crystals suitable for x-ray analysis were obtained. Yield = 2.0 g (37%). Anal. Calc. for $C_{16}H_{31}N_6ClNiO_7.H_2O$: C, 36.1; H, 6.3; N, 15.8; Cl, 6.7. Found C, 36.0; H, 6.8; N, 15.5; Cl, 6.8. IR in KBr (ν-$_{max}$/cm^{-1}): 3575, 3400, 3290, 3237 (NH stretch); 2933, 2880 (C-H stretch); 1709, 1691 (C=O amide stretch); 1602 (COO^- asymmetric stretch); 1457, 1432 (C-H deformation); 1374 (CH_3 symmetrical deformation); 1354 (COO^- symmetric stretch); 1277, 1218 (C-H twist); 1100 (ClO_4^-); 992, 912, 898, 870, 846, 799, 733 (C-H twist); 620 (ClO_4^-). IR of the deuterated complex in KBr (ν-$_{max}$/cm^{-1}): 2928, 2876 (C-H stretch); 2438 (ND stretch); 1685 (C=O amide stretch); 1604 (COO^- asymmetric stretch); 1467 (C-H deformation); 1359 (COO^- symmetric stretch); 1342, 1264 (C-H twist); 1105 (ClO_4^-); 926, 891, 854, 808, 753 (C-H twist); 624 (ClO_4^-). IR of the deuterated complex obtained from basic D_2O in KBr (ν-$_{max}$/cm^{-1}): 2958, 2925, 2873 (C-H stretch); 2444 (ND stretch); 1577 (COO^- asymmetric stretch, C=O amido stretch); 1455 (C-H deformation); 1350 (COO^- symmetric stretch); 1312, 1262, 1222, 1194 (C-H twist); 1093, 1027, 1013 (ClO_4^-); 978 (C-H twist); 623 (ClO_4^-). Low resolution ESMS (25 V) [m/z, obs (calc) (%) assignment where cage = $[^{12}C_{16}{}^{1}H_{31}{}^{14}N_6{}^{59}Ni{}^{16}O_3]^+$]: 413.0 (413) (100%) [Nicage$^+$]$^+$; 369.0 (369) (15%) [Nicage$^+$ - CO_2]$^+$.

[(8-Methyl-2-oxo-3,6,10,13,19-hexaazabicyclo[6.6.6]icosanato)copper(II)]-perchlorate.H_2O, [Cu^{II}(Me-2-oxosar-H)]$(ClO_4)_2.H_2O$

Me,CO_2K-2-oxosar.0.5C_2H_5OH.3.5H_2O (5.0 g; 0.01 mol) was dissolved in 100 mL of H_2O with stirring. A second solution of $Cu^{II}OAc_2.4H_2O$ (2.1 g; 0.01 mol) and triethylamine (1.1 g; 0.01 mol) in 100 mL of H_2O was also prepared and both solutions were then deoxygenated, with N_2, for approximately thirty minutes. The copper(II) solution was added dropwise to the ligand solution with stirring. After several hours the blue solution was diluted to 2 L with water, acidified with acetic acid and sorbed onto a SP-Sephadex C-25 cation exchange column (30 cm x 5 cm). The column was washed with water. Elution with 0.25 M $NaClO_4$ produced two blue bands. The first fraction was collected and reduced in volume, while the second very minor band was not recovered. The isolated band was acidified with a few drops of acetic acid and kept at ~20° C for several days. The blue product that precipitated during this time was collected, washed with ethanol and ether, and air dried. Further crops were obtained by allowing the acidified filtrate to continually evaporate in air. Finally, a crop of blue

crystals suitable for x-ray analysis were obtained. Analysis of the product indicated that the apical carboxyl group was absent from the complex and two perchlorate counter ions were present. Yield = 3.1 g (57%). Anal. Calc. for $C_{15}H_{32}N_6Cl_2CuO_9.H_2O$: C, 30.4; H, 5.8; N, 14.2; Cl, 12.0. Found C, 30.1; H, 5.9; N, 14.4; Cl, 12.1. IR in KBr (ν-$_{max}$/cm^{-1}): 3417, 3288, 3248 (NH stretch); 2880 (C-H stretch); 1656 (C=O amide stretch); 1461, 1425 (C-H deformation); 1090 (ClO_4^-); 955, 929, 874, 791 (C-H rock); 620 (ClO_4^-). IR of the deuterated complex in KBr (ν-$_{max}$/cm^{-1}): 2933, 2879 (C-H stretch); 2407 (ND stretch); 1649 (C=O amide stretch); 1461 (C-H deformation); 1352 (C-H twist); 1090 (ClO_4^-); 921 (C-H twist); 626 (ClO_4^-). IR of the deuterated complex obtained from basic D_2O in KBr (ν-$_{max}$/cm^{-1}): 2925 (C-H stretch); 2446 (ND stretch); 1645 (C=O amide stretch); 1460 (C-H deformation); 1318 (C-H twist); 1144, 1111, 1090 (ClO_4^-); 627 (ClO_4^-). Low resolution ESMS (80 V) [m/z, obs (calc) (%) assignment where cage = $[^{12}C_{15}{}^{1}H_{32}{}^{14}N_6{}^{63}Cu^{16}O]^{2+}$]: 373.8 (374) (100%) [$Cucage^{2+}$ - H^+]$^+$; 473.7 (474) (31%) [$Cucage^{2+}$ + $^{35}ClO_4^-$]$^+$.

[(1-Carboxy-8-methyl-2-oxo-3,6,10,13,19-hexaazabicyclo[6.6.6]icosanato)iron-(III)]chloride.HCl.0.5CH_3CH_2OH.2.5H_2O, [Fe^{III}(Me,CO_2H-2-oxosar-H)]Cl_2.-HCl.0.5CH_3CH_2OH.2.5H_2O

Freshly prepared $Fe^{II}Cl_2$ (0.79 g; 6.27 x 10^{-3} mol) was dissolved in 150 mL of H_2O that had been deoxygenated with N_2 for approximately half an hour before the dissolution of the Fe(II). A second solution containing Me,CO_2K-2-oxosar.0.5C_2H_5OH.3.5H_2O (3.0 g; 6.27 x 10^{-3} mol) and triethylamine (0.63 g; 6.27 x 10^{-3} mol) in 150 mL of H_2O was also prepared and both solutions were then deoxygenated with N_2 for a further thirty minutes. The iron solution was added to the ligand solution with stirring producing a dark green mixture. After several hours the solution was exposed to air whereupon it changed to an orange-brown colour. It was acidified with acetic acid and loaded onto a Dowex 50Wx2 cation exchange column and was washed with water and 1 M HCl. Elution with 3 M HCl produced two separate bands consisting of a red-purple band (not isolated) followed by a large orange-brown band. This was collected and dried. It was then redissolved in ethanol and evaporated to remove the residual traces of HCl and finally dried in a vacuum. Yield = 2.0 g (55%). Anal. Calc. for $C_{16}H_{31}N_6Cl_2FeO_3$.HCl.0.5C_2H_5OH.2.5H_2O: C, 35.9; H, 7.0; N, 14.8; Cl, 15.6. Found C, 35.5; H, 6.8; N, 14.7; Cl, 15.9. IR in KBr (ν-$_{max}$/cm^{-1}): 3417, 3251, 3179 (NH stretch); 2967, 2886 (C-H stretch); 1743 (C=O stretch); 1557 (C=O amide stretch); 1447 (C-H deformation); 1361 (CH_3 symmetric deformation); 1236 (C-H twist); 1213 (OH bend); 1093 (ClO_4^-); 1027, 1008, 941, 881, 756, 719

(CH_2 rock); 625 (ClO_4^-). Low resolution ESMS (50 V) [m/z, obs (calc) (%) assignment where cage = $[^{12}C_{16}{}^{1}H_{31}{}^{14}N_6{}^{56}Fe^{16}O_3]^{2+}$]: 409.8 (410) (100%) [Fecage^{2+} - 2H$^+$]$^+$; 365.9 (366) (5%) [Fecage^{2+} - H$^+$ - CO_2]$^+$. A small amount of the chloride complex (0.50 g) was converted into the perchlorate salt by adding solid $NaClO_4$ to an aqueous solution of the compound acidified with $HClO_4$. Upon evaporation in the air crystals suitable for X-ray analysis formed.

Di-[(1-carboxy-8-methyl-2-oxo-3,6,10,13,19-hexaazabicyclo[6.6.6]icosanato)-manganese(III)]dithionate.11H_2O, [Mn^{III}(Me,COO^--2-oxosar-H)]$_2$(S_2O_6).-11H_2O

$Mn^{II}Cl_2.4H_2O$ (0.86 g; 4.4 x 10^{-3} mol) was dissolved in H_2O (150 mL) that had been deoxygenated with N_2 for approximately half an hour before the dissolution of the Mn(II). A second solution containing Me,CO_2K-2-oxosar.0.5C_2H_5OH.3.5H_2O (2.1 g; 4.4 x 10^{-3} mol) and triethylamine (0.45 g; 4.4 x 10^{-3} mol) in 150 mL of H_2O was also prepared and both solutions were then deareated with N_2 for thirty minutes. The manganese solution was added to the ligand solution with stirring producing a clear solution. After several hours the mixture was exposed to air whereupon it became dark green. The solvent was removed from this solution producing a green-brown oil. This residue was redissolved in water and an excess of $LiS_2O_6.H_2O$ was added. The mixture was allowed to stand at four degrees overnight. The dark green product that precipitated during this time was collected, washed with ethanol and ether, and, air dried. Further crops were obtained by allowing the filtrate to continually stand at four degrees. However, the solution does eventually turn brown and decomposes to MnO_2 on standing for long periods. Analyses indicated that the apical carboxyl group remained deprotonated and that two cations shared a single dithionate anion. Yield = 1.9 g (37%). Anal. Calc. for $C_{32}H_{60}N_{12}Mn_2O_6S_2O_6.11H_2O$: C, 32.7; H, 7.0; N, 14.3; S, 5.5. Found C, 32.6; H, 5.6; N, 13.9; S, 5.4. IR in KBr (ν-$_{max}$/cm^{-1}): 3501, 3451, 3263, 3172 (NH stretch); 2932, 2860 (C-H stretch); 1610 (COO^- asymmetric stretch); 1595 (C=O amide); 1452, 1400 (C-H deformation); 1379 (CH_3 symmetrical deformation); 1310 (COO^- symmetric stretch); 1251, 1208 (C-H twist); 1105, 1084, 1069, 1055, 1024, 982, 913, 891, 860, 815, 782, 746, 725 (CH_2 rock). Low resolution ESMS (50 V) [m/z, obs (calc) (%) assignment where cage = $[^{12}C_{16}{}^{1}H_{30}{}^{14}N_6{}^{55}Mn^{16}O_3]^+$]: 408.8 (409) (100%) [Mncage$^+$]$^+$; 364.9 (365) (7%) [Mncage$^+$ - CO_2]$^+$.

[(1-Carboxy-8-methyl-2-oxo-3,6,10,13,19-hexaazabicyclo[6.6.6]icosanato)-chromium(III)]tetrachlorozincate, $[Cr^{III}(Me,CO_2H\text{-}2\text{-}oxosar\text{-}H)]ZnCl_4$

This compound has been prepared previously but is reported in detail here.[14] Dry ethanol (80 mL; 24 hr over freshly prepared 3 Å sieves) was degassed (Ar purged, using Schlenk-type apparatus) and placed in a glove compartment under O_2-free argon. The Me,COOH-2-oxosar ligand (0.45 g, 1.26×10^{-3} mol) and the chromium complexes $[Cr^{III}Cl_3pyridine_3]$[15] (0.40 g; 1.01×10^{-3} mol) and $[Cr^{II}(CH_3CO_2)_2.H_2O]_2$ (0.05 g, 0.13×10^{-3} mol, 0.27×10^{-3} mol in Cr^{III}) were also introduced into the glove box (under Ar). The ligand was first dissolved in the dry ethanol. Then the $[Cr^{II}(CH_3CO_2)_2.H_2O]_2$ dimer was added, followed by the $[Cr^{III}Cl_3pyridine_3]$ complex and the mixture stirred under Ar at 20° C. The reaction mixture quickly changed to a deep orange-red colour. It was removed from the glove box after 10 hr, quickly poured into water (200 mL), and sorbed onto Dowex 50Wx2 cation exchange resin (5 cm x 2.5 cm). The column was washed with water, 0.5 M HCl and then eluted off with 3 M HCl. The 3 M HCl eluent was evaporated to dryness, redissolved in water and chromatographed on a SP-Sephadex C-25 cation exchange column (30 cm x 2.5 cm) using 0.1 M K_2SO_4 as the eluent. Only one red/orange band was collected, desalted using Dowex 50Wx2 cation exchange resin with water, 0.5 M HCl eluents, and finally eluted of with 3 M HCl. The 3 M HCl eluent was reduced to dryness, redissolved in water, $Zn^{II}Cl_2$ solution added (pH ~3, Zn^{II}:Cr^{III} ~ 3:1) and the red/orange crystals were deposited by slow addition of EtOH. The crystals were filtered off, washed with EtOH and ether and air dried. Yield = 0.43 g (55% based on Cr). Anal. Calc. for $C_{16}H_{31}N_8Cl_4CrO_3Zn$: C, 31.3; H, 5.1; N, 16.7; Cl, 23.1. Found C, 31.2; H, 5.3; N, 16.5; Cl, 22.8. IR in KBr ($\tilde{\nu}_{max}/cm^{-1}$): 3420, 3030 (NH stretch); 2865 (C-H stretch); 1725 (C=O stretch); 1597 (C=O amide); 1470, 1415 (C-H deformation); 1360 (CH_3 symmetrical deformation); 1250 (OH bend); 1209, 1130 (C-H twist); 1070, 1050, 910, 837, 755, 720 (CH_2 rock). Low resolution ESMS (80 V) [m/z, obs (calc) (%) assignment where cage = $[^{12}C_{16}{}^{1}H_{31}{}^{14}N_6{}^{52}Cr^{16}O_3]^{2+}$]: 361.8 (362) (100%) $[Crcage^{2+} - H^+ - CO_2]^+$; 405.7 (406) (33%) $[Crcage^{2+} - H^+]^+$.

Attempts at Producing a Zn(II) Monoamide Cage Complex

Reaction of $Zn^{II}(ClO_4)_2$ with Me,CO_2K-2-oxosar.$0.5C_2H_5OH.3.5H_2O$

To a solution of Me,CO_2K-2-oxosar.$0.5C_2H_5OH.3.5H_2O$ (1.0 g; 2.1×10^{-3} mol) in 100 mL of H_2O was added $Zn^{II}(ClO_4)_2.2H_2O$ (0.62 g; 2.1×10^{-3} mol) in 100 mL of H_2O with stirring. After ten minutes of continuous stirring a saturated solution of $NaClO_4$ was added dropwise until precipitation was initiated. The resulting mixture was placed on ice, however, the colourless crystals subsequently collected by filtration were shown to be $KClO_4$. The filtrate was allowed to stand at room temperature for several days. The white product that precipitated during this time was collected and recrystallised from water. After several further days of standing at ~20° C a white solid again precipitated and was collected, washed with cold ethanol and ether, and, air dried. Investigation of the solid by ^{13}C NMR indicated a mixture of products were present, none of which were consistent with the expected cage formula.

Reaction of $Zn^{II}(NO_3)_2$ with Me,CO_2K-2-oxosar.$0.5C_2H_5OH.3.5H_2O$

To a solution of Me,CO_2K-2-oxosar.$0.5C_2H_5OH.3.5H_2O$ (1.0 g; 2.1×10^{-3} mol) in 100 mL of ethanol was added $Zn^{II}(NO_3)_2.H_2O$ (0.44 g; 2.1×10^{-3} mol) in 100 mL of ethanol with stirring; a white precipitate formed immediately upon the addition of the metal to the ligand solution. The resulting mixture was then placed in an ice bath for two hours. The white solid that formed was collected, washed with ethanol, and, ether and air dried. Again an investigation of this solid by ^{13}C NMR indicated a mixture of products were present, none of which were consistent with the expected cage formula.

3.2.3.2 X-ray Crystallography

Crystal Structure Solution and Refinement of $[Ni^{II}(Me,CO_2^-$-2-oxosar)$]_2(ClO_4)_2.3H_2O$

A mauve coloured rhomboid crystal of the Ni(II) monoamide complex was attached to a quartz fibre and mounted on a Rigaku AFC6S diffractometer equipped with a graphite monochromator. Using Cu-Kα radiation and a rotating anode generator, lattice parameters were determined by least-squares refinement of the setting angles of 24

reflections in the range of $108.98° < 2\theta < 110.03°$. The data were collected at a temperature of -60(1)° C using the ω-2θ scan technique to a maximum value of 120.1°. Scans of $(1.50 + 0.30 \tan \theta)°$ in ω were made at a speed of 32.0°/min. The weak reflections were rescanned (maximum of four scans) and the counts were accumulated to ensure good counting statistics. Stationary background counts were recorded on each side of the reflection. Three representative reflections were measured at intervals of 150 reflections. No decay correction was required. An analytical absorption correction factor was applied which resulted in transmission factors ranging from 0.53 to 0.75. The data set was reduced, an analytical absorption correction applied, and, Lorentz and polarisation effects were accounted for.

The structure was solved by direct methods[15a] and expanded using Fourier techniques.[17] A small degree of disorder was observed for C(20), which was modelled by assuming two sites, of occupancies p and (p-1), for this atom. Disorder was also observed for the O atoms of one perchlorate; restraints were imposed upon distances and angles for the minor orientation. In a subsequent difference map, two peaks 1.2 Å apart were observed within the lattice. They appear to be two mutually-exclusive sites for a water molecule and have been modelled as such. Non-hydrogen atoms attached to C atoms were included at geometrically determined positions; they were not refined but were periodically recalculated. Hydrogen atoms attached to the N atoms were all located in difference eletron-density maps and allowed to refine positionally. Water hydrogen atoms (except for O(19)/O(20)) were located in difference maps and refined positionally, but restraints were imposed on their bond lengths and angles.

Least-squares refinement was performed using full-matrix methods minimising the function $\Sigma\omega(|F_o| - |F_c|)^2$, where the weighting scheme was based on counting statistics and included a factor (p = 0.020) to downweight the intense reflections. Data reduction and refinement computations were performed with texsan[13] with the exception of the hydrogen-bonding network which was calculated using the Platon computing programme.[16] Neutral atom scattering factors were taken from Cromer and Waber.[9] Anomalous dispersion effects were included in Fcalc[10]; the values of $\Delta f'$ and $\Delta f''$ were those of Creagh and McAuley.[11] The values of the mass attenuation coefficients were those of Creagh and Hubbel.[12]

Crystal Structure Solution and Refinement of [Cu^{II}(Me-2-oxosar)]$(ClO_4)_2.1.3H_2O$

A dark-blue block-shaped crystal of the Cu(II) amide complex was attached to a quartz fibre and mounted on a Philips PW1100/20 diffractometer equipped with a graphite monochromator. Using Cu-Kα radiation, lattice parameters were determined by least-squares refinement of the setting angles of 25 reflections in the range of $31.30° < 2\theta < 35.90°$. The data were collected at a temperature of 23(1)° C using the ω scan technique to a maximum value of 50.1°. Omega scans of several intense reflections made prior to data collection showed that the peaks were rather broad, warning that the data would not be of the highest quality. Scans of $(1.80 + 0.30 \tan \theta)°$ were made at a speed of 2.0°/min in ω. Stationary background counts were recorded for ten seconds on each side of every scan. Three representative reflections were measured after every 360 minutes to monitor decomposition and consequently a decay correction of 2% was applied. The data set was reduced, an analytical absorption correction applied and Lorentz and polarisation effects were accounted for.

The structure was solved by heavy-atom Patterson methods[8] and expanded using Fourier techniques.[17] One perchlorate anion was found to be disordered, and this has been modelled by assuming two orientations for the oxygen atoms and refining their relative occupancies while the isotropic displacement factors were constrained to be equal; restraints were placed on Cl-O and O...O distances to give reasonable geometries. An area of electron density adjacent to this anion was assigned to be a water molecule, it's occupancy being set to 0.3. Full occupancy non-hydrogen atoms were refined with anisotropic displacement factors, while the rest were refined isotropically. Hydrogen atoms for the cation were included at calculated positions but not refined.

Least-squares refinement was performed using full-matrix methods minimising the function $\Sigma\omega(|F_o| - |F_c|)^2$ where the weighting scheme was based on counting statistics. Data reduction and refinement computations were performed with Xtal[18] and texsan[13] respectively. Neutral atom scattering factors were taken from Cromer and Waber.[9] Anomalous dispersion effects were included in F_{calc}[10]; the values of Δf' and Δf'' were those of Creagh and McAuley.[11] The values of the mass attenuation coefficients were those of Creagh and Hubbel.[12]

Crystal Structure Solution and Refinement of [Fe^{III}(Me,CO_2H-2-oxosar-H)]$(ClO_4)_2.0.5H_2O$

A red prismatic crystal of the Fe(III) monoamido complex was attached to a quartz fibre and mounted on a Rigaku AFC6S diffractometer equipped with a graphite monochromator. Using Cu-Kα radiation and a 12 kW rotating anode generator, lattice parameters were determined by least-squares refinement of the setting angles of 24 reflections in the range of $85.06° < 2\theta < 106.78°$. The data were collected at a temperature of -60(1)° C using the ω-2θ scan technique to a maximum value of 120.2°. Scans of (1.31 + 0.30 tan θ)° in ω were made at a speed of 32.0°/min. The weak reflections were rescanned (maximum of four scans) and the counts were accumulated to ensure good counting statistics. Stationary background counts were recorded on each side of the reflection. Three representative reflections were measured at intervals of 150 reflections. No decay correction was required. A linear correction factor was applied to the data to account for this phenomenon. The data set was reduced, an analytical absorption correction applied, and, Lorentz and polarisation effects were accounted for.

The structure was solved by direct methods[7] and expanded using Fourier techniques.[17] The non-hydrogen atoms were refined with anisotropic displacement factors. One perchlorate group was disordered, and has been modelled by assuming that there are two orientations for the group with one O_3 face common to both. The relative occupancies of each orientation have been refined; atoms with occupancies less than 1.0 were assigned isotropic displacement factors. Displacement factors are large for O9, O10, and O11 as they represent unresolved multiple sites. Hydrogen atoms attached to carbon and nitrogen atoms of the cation were included at calculated positions. A difference map at this stage revealed a peak with coordinates related to those of Fe1 by relationship (x, 1.5-y, z). This has been assumed to be a minor twinning component which is only apparent for the heaviest atom in the structure. For convenience the occupancy of Fe1 (and the rest of the structure) was kept at 1.0, but Fe2 has been included in the model (with coordinates constrained to be related to those of Fe1 and an isotropic displacement factor set equal to B_{eq} of Fe1) and its occupancy refined; the final value is 0.032(3). Hydrogen atoms for the carboxylate group and the water molecule were observed in difference maps and were included but not refined owing to the poor parameter/reflection ratio.

Least-squares refinement was performed using full-matrix methods minimising the function $\Sigma\omega(|F_o| - |F_c|)^2$, where the weighting scheme was

based on counting statistics and included a factor (p = 0.020) to downweight the intense reflections. Data reduction and refinement computations were performed with texsan[13] with the exception of the hydrogen-bonding network which was calculated using the Platon computing programme.[16] Neutral atom scattering factors were taken from Cromer and Waber.[9] Anomalous dispersion effects were included in Fcalc[10]; the values of $\Delta f'$ and $\Delta f''$ were those of Creagh and McAuley.[11] The values of the mass attenuation coefficients were those of Creagh and Hubbel.[12]

3.3 Results

3.3.1 Section 1. Reaction of $[Co^{III}(sen)]^{3+}$ with ethyl cyanoacetate and formaldehyde in aqueous base.

3.3.1.1 Syntheses

The reaction of $[Co^{III}(sen)]^{3+}$ with formaldehyde and ethyl cyanoacetate, in the presence of base, produced a variety of products that were separated into two different fractions on Dowex 50Wx2 resin with HCl as the eluent. The orange products were separated further on columns of SP-Sephadex C-25 by using NaCl or K_2SO_4 as eluents. The first band off the Dowex column comprised the red monoamido complex $[Co^{III}(Me,CN\text{-}2\text{-}oxosar\text{-}H)]^{2+}$; the second orange band consisted of four components identified as $[Co^{III}(Me,CO_2H\text{-}2\text{-}aminosar\text{-}2\text{-}ene)]^{3+}$, $[Co^{III}(Meazasar)]^{3+}$, $[Co^{III}(N\text{-}Me\text{-}sen)]^{3+}$ and $[Co^{III}(Me\text{-}2\text{-}aminosar\text{-}2\text{-}ene)]^{3+}$ respectively (Figure 4). The two amidine cage complexes produced in this reaction were previously unknown.

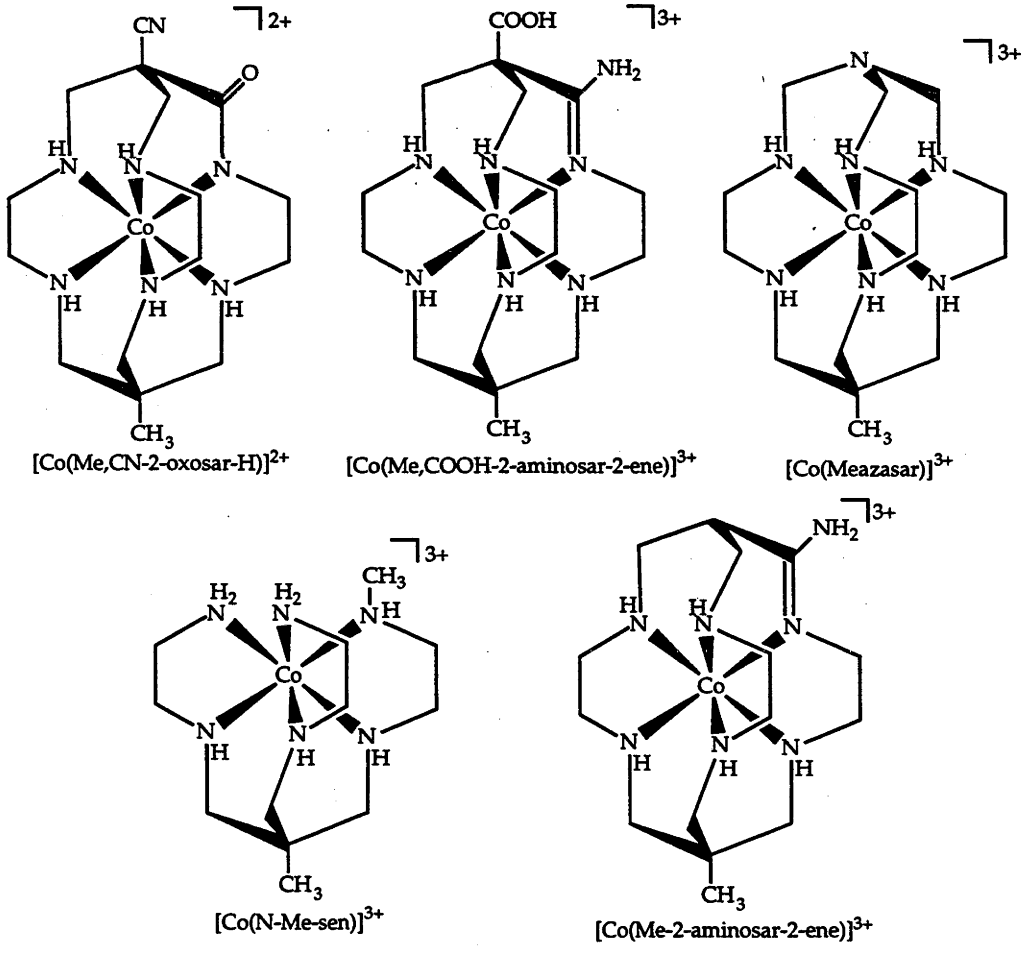

Figure 4

The attempt to demetallate $[Co^{III}(Me,CN\text{-}2\text{-}oxosar)]^{2+}$ with KCN to produce the free cage ligand was largely unsuccessful. Even though the reaction produced a white powder, the NMR spectra indicated the presence of a number of products, none of which corresponded to the desired cage ligand. The apical nitrile group appears to be reactive under the basic conditions employed as it is noticeably absent in the ^{13}C NMR spectrum of the product.

Attempts to produce a saturated cage species from $[Co^{III}(Me\text{-}2\text{-}aminosar\text{-}2\text{-}ene)]^{3+}$ also proved to be unsuccessful. The use of different oxidants or reductants, and the alteration of the reaction conditions produced none of the desired product. In most cases starting material was recovered. This indicates that the coordinated amidine group is an extremely stable moiety. However, with the use of high pressures and a Pd/C catalyst at 30 psi, some disruption of the amidine cage occurred and both $[Co^{III}(Me\text{-}2\text{-}aminosar\text{-}2\text{-}ene)]^{3+}$ and $[Co^{III}(sen)]^{3+}$ were present at the completion of the reaction. Clearly, this is not a useful path to pursue however.

3.3.1.2 NMR Spectroscopy

The ^{13}C NMR spectra of the amido and two amidine cage complexes (Figure 5a, b and c) highlight the general lack of symmetry within each of the molecules; all carbon atoms are inequivalent and a separate signal arises for each. For $[Co^{III}(Me,CN\text{-}2\text{-}oxosar\text{-}H)]^{2+}$ these signals arise from two quaternary, an amide, a methyl, a nitrile and eleven methylene carbons. Thus, the quaternaries, next to the methyl group and directly connected to the amide carbon give chemical shift values of 41.4 and 58.0 ppm respectively. The remaining methylene resonances have shifts at 47.1, 50.5, 52.1, 52.6, 52.8, 53.3, 55.0, 55.1, 55.3, 55.6 and 55.7 ppm; the amide, methyl and nitrile signals appear at 171.3, 20.8 and 116.8 ppm respectively. The ^{13}C NMR spectra of the two amidine cages display sixteen and fifteen signals but these appear at slightly different chemical shift values in each case. The signals arise from two quaternary, an amidine, a methyl and eleven methylene carbons. For $[Co^{III}(Me,CO_2H\text{-}2\text{-}aminosar\text{-}2\text{-}ene)]^{3+}$ they appear at 42.0, 62.1, 169.4, 20.7, 49.2, 52.5, 53.6, 54.3, 54.7, 54.8 (double intensity), 55.0, 55.3, 55.9 and 56.3 ppm. The second complex, $[Co(Me\text{-}2\text{-}aminosar\text{-}2\text{-}ene)]^{3+}$, has a similar set of signals at 42.5, 50.1, 169.4, 20.8, 46.9, 47.8, 48.5, 54.2, 54.7, 54.8, 55.2, 55.3, 55.6, 55.7 and 56.1 ppm. For $[Co^{III}(Me,CO_2H\text{-}2\text{-}aminosar\text{-}2\text{-}ene)]^{3+}$ an extra signal attributed to the apical acid group occurs at 173.6 ppm. The amidine chemical shifts in each

instance also bear a close resemblance to that found in $[Co^{III}(CO_2H\text{-}2\text{-amino}(N_3S_3\text{-sar})\text{-}2\text{-ene})]^{3+}$ (168 ppm).[19]

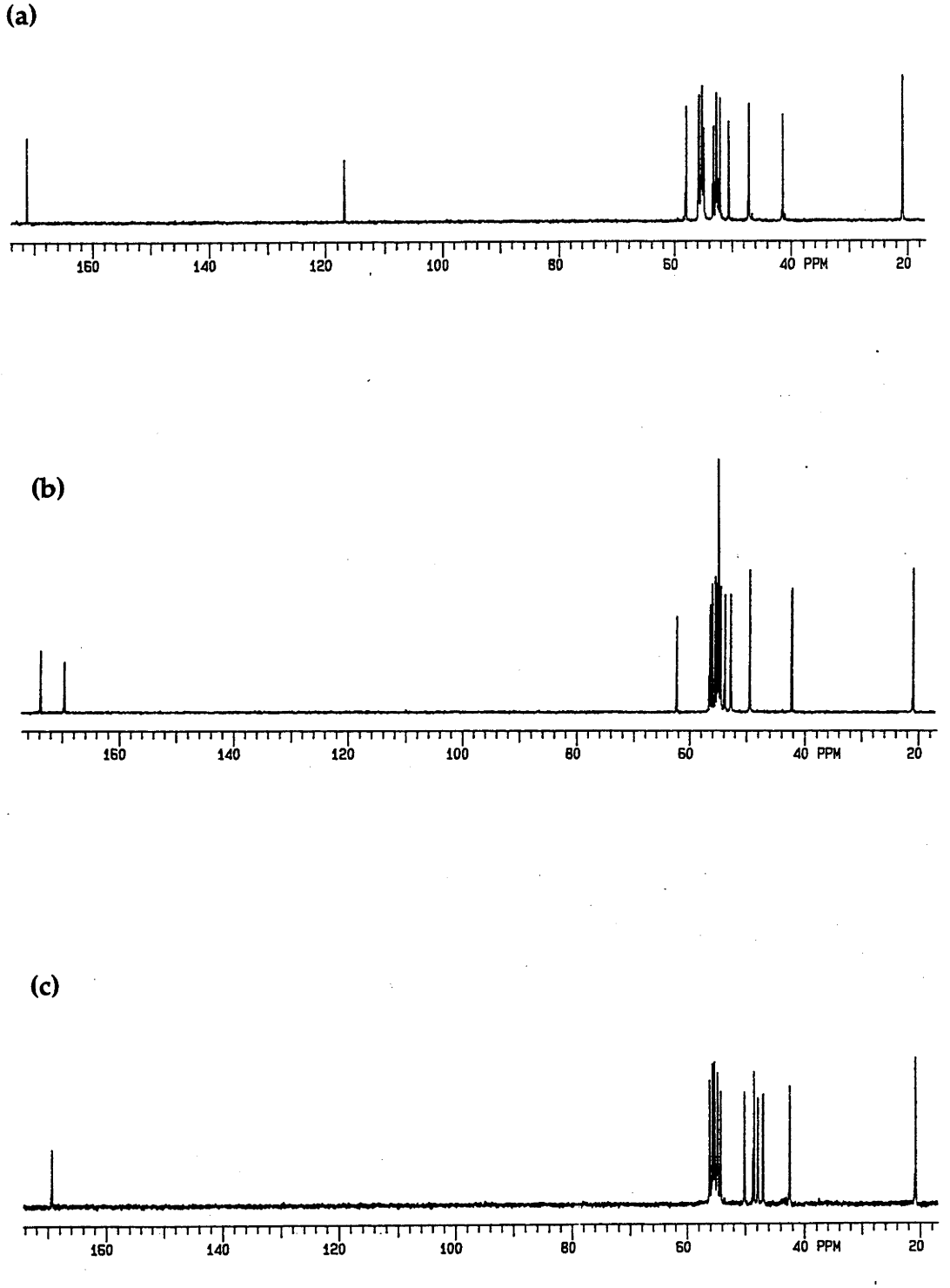

Figure 5. ^{13}C NMR spectra of (a) $[Co^{III}(Me,CN\text{-}2\text{-oxosar-H})]^{2+}$, (b) $[Co^{III}(Me,CO_2H\text{-}2\text{-aminosar-2-ene})]^{3+}$ and (c) $[Co^{III}(Me\text{-}2\text{-aminosar-2-ene})]^{3+}$ (Chloride salts in D_2O).

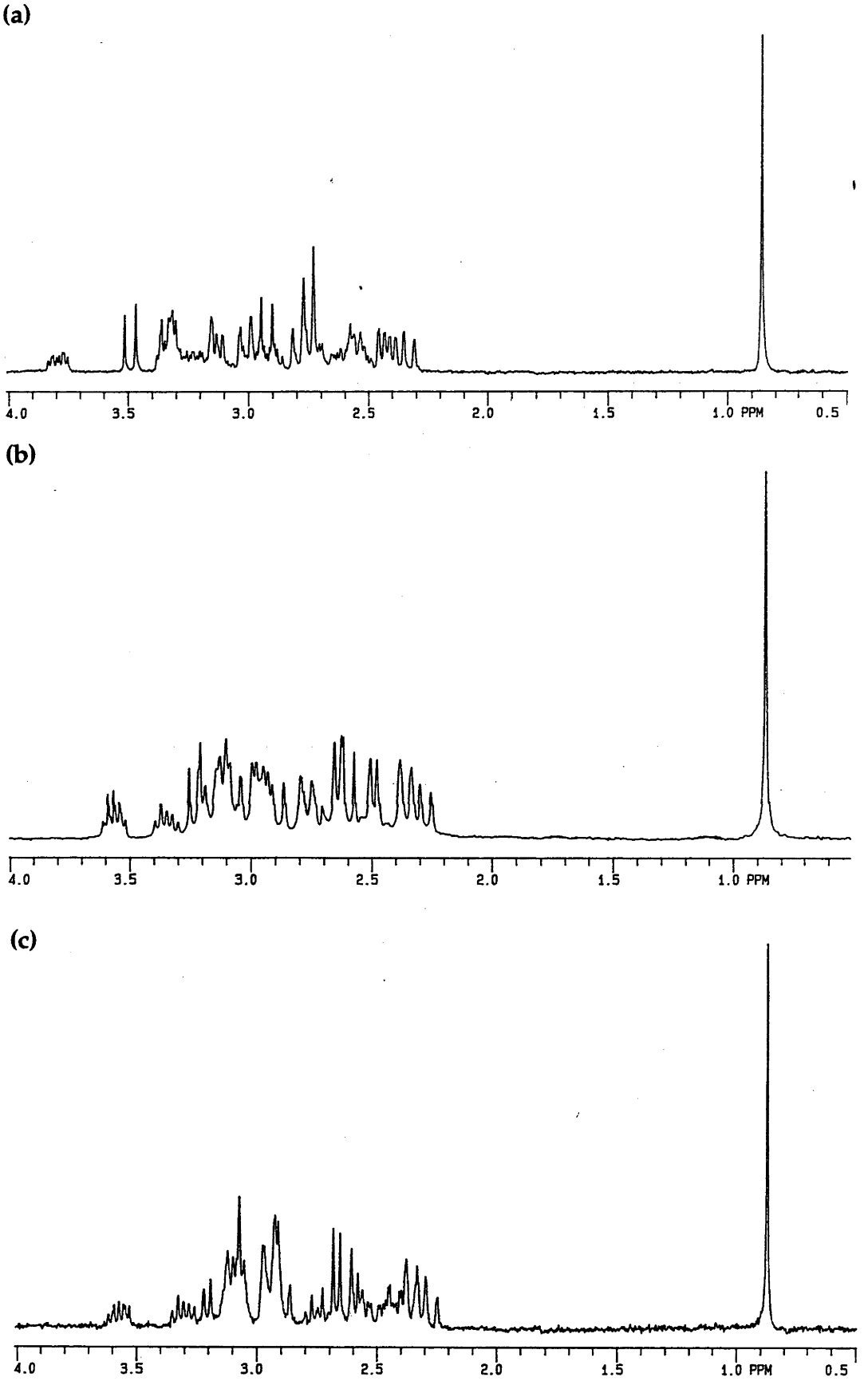

Figure 6. ^{1}H NMR spectra of (a) $[Co^{III}(Me,CN\text{-}2\text{-}oxosar\text{-}H)]^{2+}$, (b) $[Co^{III}(Me,CO_2H\text{-}2\text{-}aminosar\text{-}2\text{-}ene)]^{3+}$ and (c) $[Co^{III}(Me\text{-}2\text{-}aminosar\text{-}2\text{-}ene)]^{3+}$ (Chloride salts in D_2O).

The NMR data for these latter molecules and the crystallographic evidence (ahead) obtained for $[Co^{III}(Me,CO_2H\text{-}2\text{-}aminosar\text{-}2\text{-}ene)]^{3+}$, clearly confirm the presence of an amidine function in all instances. Therefore, along with the microanalytical, electrospray (ahead) and IR data (ahead) the second complex isolated has been assigned as the amidine cage compound, $[Co^{III}(Me\text{-}2\text{-}aminosar\text{-}2\text{-}ene)]^{3+}$ i.e., the first molecule has been decarboxylated.

The ^1H NMR spectra (Figure 6) of all three complexes were less informative than the ^{13}C NMR spectra due to the overlap of the methylene proton signals and their extensive spin-spin coupling. There is one feature however that does assist with the product identification. The methyl group (ca. 0.86 ppm) provides a gauge to the purity of the individual complexes. The methylene protons appear in the general region of 2.2 - 3.5 ppm. A noticeable feature of the amide complex, apart from the overlapping CH_2 resonances, is a multiplet centred on 3.8 ppm; integration of this peak indicates that it arises from a single proton. This trait also exists for the $[Co^{III}(Me,CO_2H\text{-}2\text{-}oxosar\text{-}H)]^{2+}$ ion (3.98 ppm).[2] Likewise the $[Co^{III}(Me,CO_2H\text{-}2\text{-}aminosar\text{-}2\text{-}ene)]^{3+}$ and $[Co^{III}(Me\text{-}2\text{-}aminosar\text{-}2\text{-}ene)]^{3+}$ complexes display the same feature centred on 3.57 ppm and 3.55 ppm respectively. Again integration showed that the peaks arose from a single proton in each case. In most sar cages, the axial and equatorial protons of each CH_2 group are chemically different.[20] This means that a separate set of signals arise for each of the two protons.

3.3.1.3 Infra-red Spectroscopy

Infra-red spectroscopy proved to be a useful tool in the investigation of the functionalised cage complexes and the relevant absorption vibrations appear in Table 1. For the $[Co^{III}(Me,CN\text{-}2\text{-}oxosar\text{-}H)]^{2+}$ complex two resolved bands appeared at 1621 cm^{-1} and 1605 cm^{-1} which are attributed to the C=O stretching mode in a delocalised deprotonated coordinated amido group. This value is similar to that observed for other Co(III) amido complexes.[2] Also, the two amidine complexes displayed absorptions attributed to C=N and C-NH_2 stretching vibrations at 1671 cm^{-1} and 1599 cm^{-1} for $[Co^{III}(Me,CO_2H\text{-}2\text{-}aminosar\text{-}2\text{-}ene)]^{3+}$ and 1654 cm^{-1} and 1618 cm^{-1} for $[Co^{III}(Me\text{-}2\text{-}aminosar\text{-}2\text{-}ene)]^{3+}$. The former compound possesses extra absorption bands at 1723 cm^{-1} and 1249 cm^{-1} resulting from the C=O stretching and OH bending modes of the apical COOH group.

Table 1. Selected functional group infra-red absorption frequencies of some Co(III) amido and amidine cage complexes.

Complex	$\tilde{\nu}$, cm^{-1}	Assignment
$[Co^{III}(Me,CN\text{-}2\text{-}oxosar\text{-}H)]^{2+}$	2250	C≡N stretch
	1621	$C{=}O_{(amido)}$ stretch
	1605	$C{=}O_{(amido)}$ stretch
$[Co^{III}(Me,CO_2H\text{-}2\text{-}aminosar\text{-}2\text{-}ene)]^{3+}$	3088, 3044	OH stretch
	2553, 2469	OH stretch
	1723	$C{=}O_{(COOH)}$ stretch
	1671	$C{=}N_{(amidine)}$ stretch
	1599	NH_2 in-plane bending
	1249	$OH_{(COOH)}$ bend
$[Co^{III}(Me\text{-}2\text{-}aminosar\text{-}2\text{-}ene)]^{3+}$	1654	$C{=}N_{(amidine)}$ stretch
	1618	NH_2 in-plane bending

3.3.1.4 Electrospray Mass Spectrometry

Background[21]

Electrospray mass spectrometry (ESMS) is a low energy technique in which the molecular or parent ion commonly occurs as the most abundant peak within the spectrum. It is a particularly effective tool for studying the cage complexes since it minimises cage fragmentation. A schematic diagram[21] of an electrospray mass spectrometer appears in Figure 7. A sample solution at flow rates usually between 1 and 20 μg/min enters the electrospray chamber through a stainless steel hypodermic needle. The needle is kept at a few kilovolts relative to the walls of the chamber and the surrounding cylindrical electrode that helps shape the distribution of potential and directs the flow of the bath gas. The resulting field at the needle tip charges the surface of the emerging liquid, dispersing it by Coulomb forces into a fine spray of charged droplets. Driven by the electric field, the droplets migrate toward the inlet end of the glass capillary at the end wall of the chamber. A counter-current flow of bath gas typically at 800 torr, an initial temperature from 320 to 350 K, and a flow rate of about 100 mL/s hastens evaporation of solvent from each droplet, decreasing its diameter as it drifts towards the end wall of the chamber. Consequently, the charge density on its surface increases until the Coulomb repulsion becomes the same order as the surface tension. The resulting instability,

sometimes called a "Coulomb explosion", tears the droplet apart, producing charged daughter droplets that also evaporate. This sequence of events repeats itself until the radius of curvature of a daughter droplet becomes small enough that the field due to the surface charge density is strong enough to desorb ions from the droplet into the ambient gas. The desorbing ions include cations, to which are attached solvent, or anions, thus producing so-called "quasi-molecular" ions suitable for mass analysis. Some of these ions become entrained in the flow of dry bath gas that enters the glass capillary to emerge at the exit end as a supersonic free jet in the first of two vacuum chambers. A core portion of this free jet passes through a skimmer into a second vacuum chamber, delivering ions to a quadrupolar mass spectrometer that measures the mass-to-charge ratio of the ions.

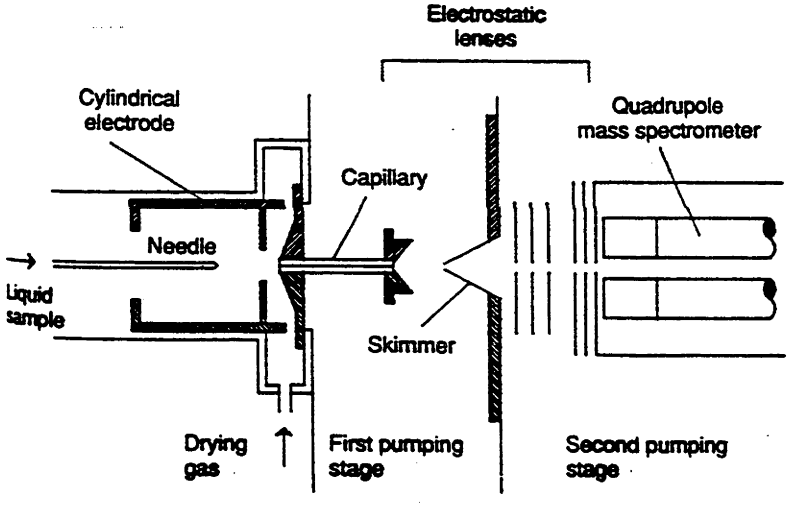

Figure 7. Schematic diagram of the apparatus.[21]

The ESM spectra of the amido and two amidine complexes in water appear in Figures 8, 9 and 10. In the ESM spectrum of the Co(III) cage amide ($[Co^{III}(Me,CN\text{-}2\text{-}oxosar\text{-}H)]^{2+}$) the most abundant peak appears at m/z = 393.8 and is attributed to a $[Cocage^{2+} - H^+]^+$ species. Two other peaks occurring at m/z = 429.8 and 411.9 are assigned to $[Cocage^{2+} + {}^{35}Cl^-]^+$ and $[Cocage^{2+} - H^+ + H_2O]^+$ species. For the Co(III) cage amidine complexes ($[Co^{III}(Me,COOH\text{-}2\text{-}aminosar\text{-}2\text{-}ene)]^{3+}$ and $[Co^{III}(Me\text{-}2\text{-}aminosar\text{-}2\text{-}ene)]^{3+}$) a peak corresponding to a $[Cocage^{3+} - 2H]^+$ species arises and for the

$[Co^{III}(Me\text{-}2\text{-}aminosar\text{-}2\text{-}ene)]^{3+}$ ion it is the base peak of that spectrum. In addition, for the $[Co^{III}(Me,COOH\text{-}2\text{-}aminosar\text{-}2\text{-}ene)]^{3+}$ ion, the spectrum displays a loss of forty-four mass units from the parent ion peak that corresponds to the loss of CO_2. This is consistent with the presence of the apical carboxylic acid group in this compound. In the spectrum of the $[Co^{III}(Me\text{-}2\text{-}aminosar\text{-}2\text{-}ene)]^{3+}$ ion, signals centred on m/z values of 404 and 440 are observed. These originate from the doubly charged species, $[Cocage^{3+} - H^+]^{2+}$, combined with a chloride ion and a chloride ion plus two water molecules respectively to produce a mono charged ion in each case. It is likely that the Cl^- ion and water molecule are H-bonded to the cation in the assemblies but the electrostatic forces for the cation and anion are likely to dominate the ion-pair formation. Solvent association is less common than ion pairing with these types of molecules. A number of other signals occur at masses around those of the observed ions especially $^{35}Cl^-$, $^{36}Cl^-$, ^{12}C and ^{13}C. These arise from the isotopic contributions of the various elements present. The observed patterns fit the respective simulated patterns of the observed ions. Lastly, the assignments support the microanalytical data.

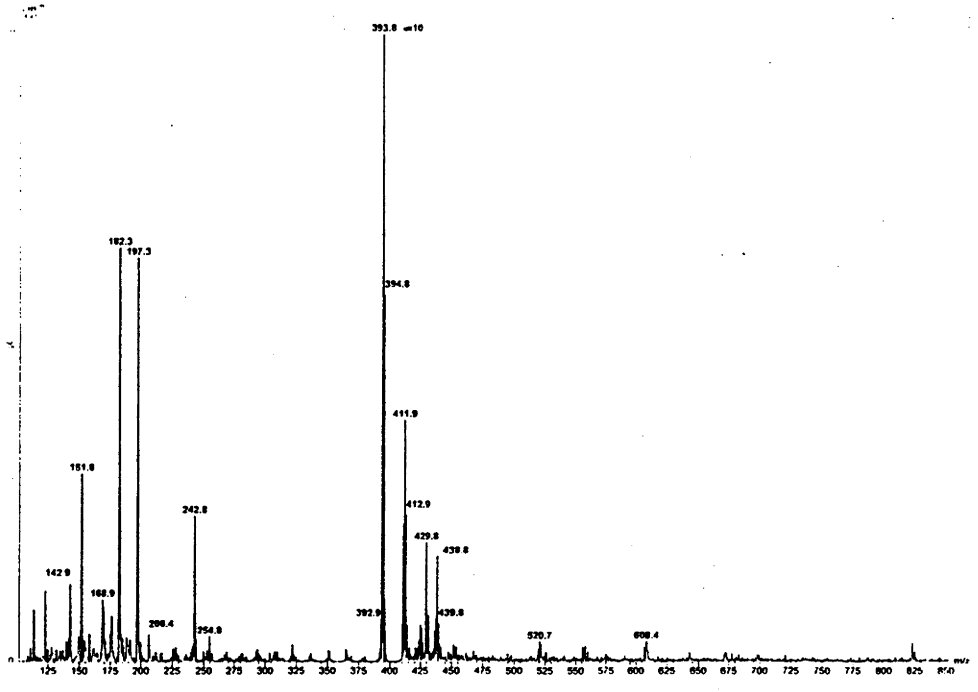

Figure 8. ESM spectrum of aqueous $[Co^{III}(Me,CN\text{-}2\text{-}oxosar\text{-}H)]^{2+}$ (Cone Voltage = 50 V).

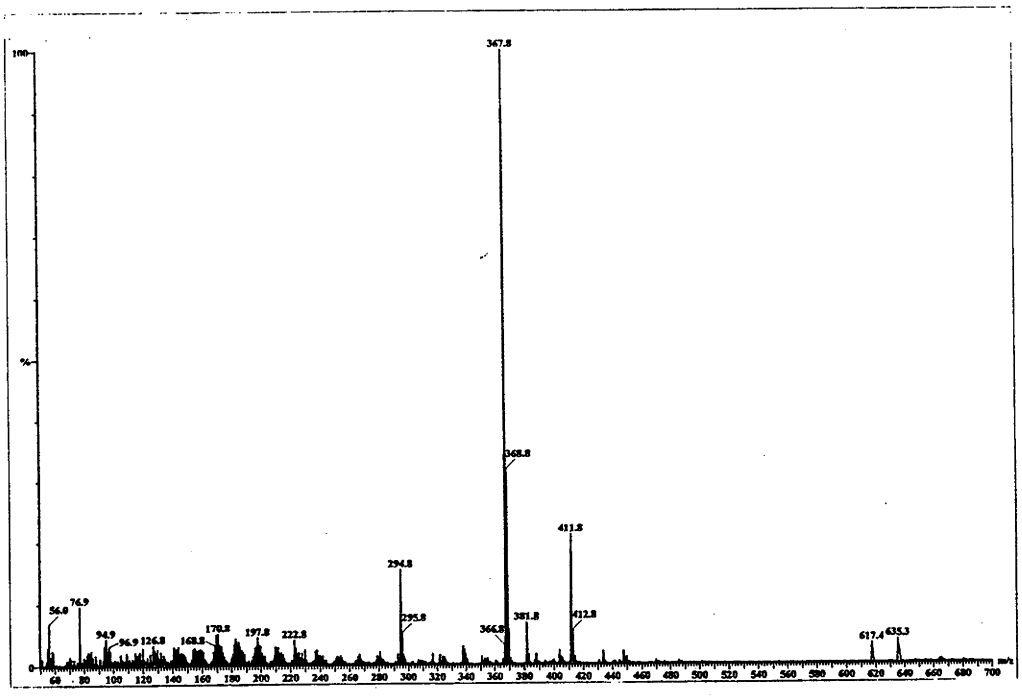

Figure 9. ESM spectrum of aqueous $[Co^{III}(Me,COOH\text{-}2\text{-}aminosar\text{-}2\text{-}ene)]^{3+}$ (Cone Voltage = 80 V).

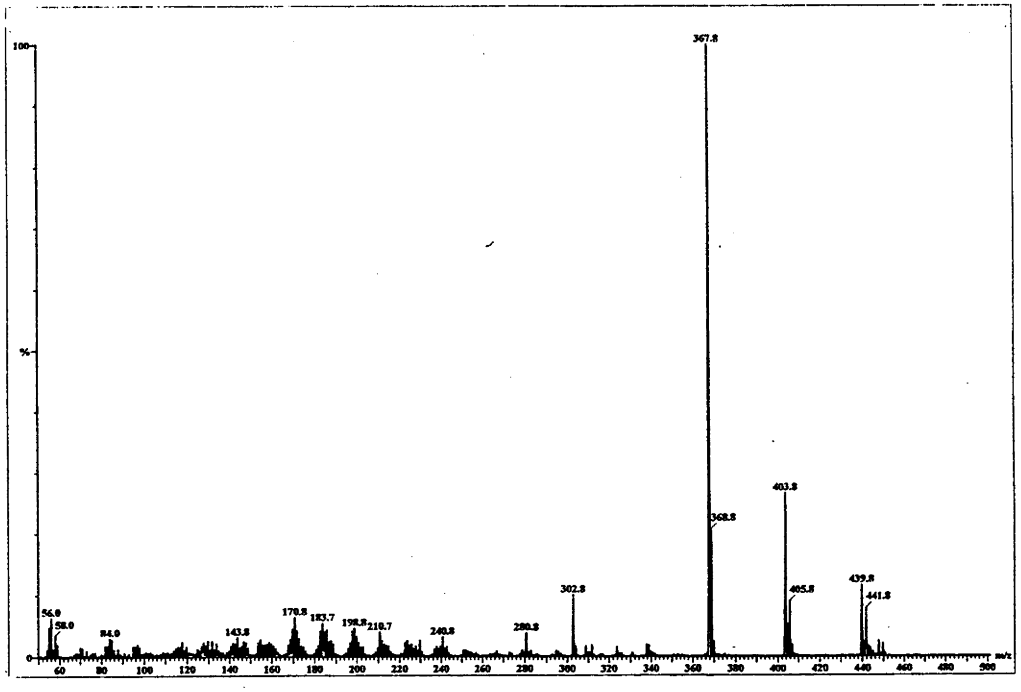

Figure 10. ESM spectrum of aqueous $[Co^{III}(Me\text{-}2\text{-}aminosar\text{-}2\text{-}ene)]^{3+}$ (Cone Voltage = 80 V).

3.3.1.5 X-ray Crystallographic Analysis

The structure of $[Co^{III}(Me,CN\text{-}2\text{-}oxosar\text{-}H)](ClO_4)_{3/2}Cl_{1/2}.H_2O$ and selected bond lengths and angles are shown in Figure 11, and, Tables 2 and 3 respectively. The structure shows that the ligand completely encapsulates the Co(III) ion and is six coordinate. Five of the coordination sites come from the secondary amines and the remaining one from the amide nitrogen after loss of a proton. In addition, two of the five membered chelate rings display a *lel* conformation while the remaining strap, containing the amido group, possesses an *ob* conformation which gives the complex the overall conformation of *lel*$_2$*ob*. This structure is similar to that observed for $[Co^{III}(Me,CO_2H\text{-}2\text{-}oxosar\text{-}H)]^{2+}$.[2]

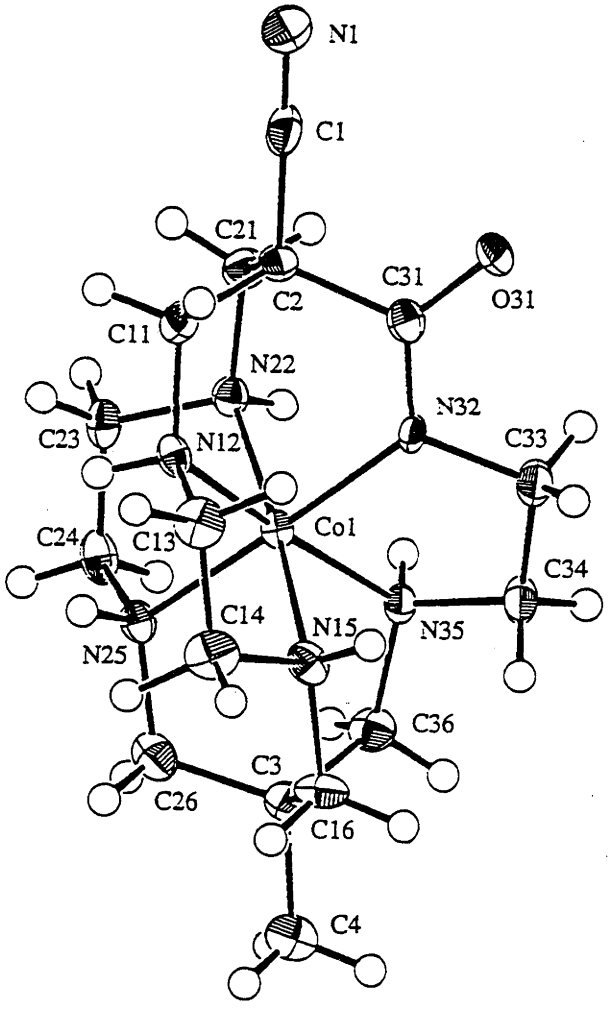

Figure 11. Thermal ellipsoid diagram of the $[Co^{III}(Me,CN\text{-}2\text{-}oxosar\text{-}H)](ClO_4)_{3/2}Cl_{1/2}.H_2O$ cation with labelling of selected atoms. Ellipsoids show 50% probability levels, except for hydrogen atoms which are drawn as spheres of arbitrary radius.

Table 2. Bond distances (Å) for $[Co^{III}(Me,CN\text{-}2\text{-}oxosar\text{-}H)](ClO_4)_{3/2}Cl_{1/2}.H_2O$

Atom	Distance (Å)	Atom	Distance (Å)
Co-N(12)	1.980(3)	Co-N(15)	1.971(4)
Co-N(22)	1.983(3)	Co-N(25)	1.976(3)
Co-N(32)	1.898(3)	Co-N(35)	1.971(3)
Cl(1)-O(11)	1.434(3)	Cl(1)-O(11)	1.434(3)
Cl(1)-O(12)	1.416(3)	Cl(1)-O(12)	1.416(3)
Cl(2)-O(21)	1.421(3)	Cl(2)-O(22)	1.412(3)
Cl(2)-O(23)	1.410(3)	Cl(2)-O(24)	1.426(4)
O(31)-C(31)	1.259(4)	N(1)-C(1)	1.129(5)
N(12)-C(11)	1.495(5)	N(12)-C(13)	1.482(5)
N(15)-C(14)	1.493(5)	N(15)-C(16)	1.503(5)
N(22)-C(21)	1.491(5)	N(22)-C(23)	1.497(5)
N(25)-C(24)	1.495(5)	N(25)-C(26)	1.494(5)
N(32)-C(31)	1.298(5)	N(32)-C(33)	1.467(5)
N(35)-C(34)	1.499(5)	N(35)-C(36)	1.492(5)
C(1)-C(2)	1.497(5)	C(2)-C(11)	1.534(5)
C(2)-C(21)	1.548(6)	C(2)-C(31)	1.548(5)
C(3)-C(4)	1.525(6)	C(3)-C(16)	1.527(6)
C(3)-C(26)	1.523(6)	C(3)-C(36)	1.527(6)
C(13)-C(14)	1.492(6)	C(23)-C(24)	1.497(6)
C(33)-C(34)	1.512(6)		

Table 3. Bond angles (°) for $[Co^{III}(Me,CN\text{-}2\text{-}oxosar\text{-}H)](ClO_4)_{3/2}Cl_{1/2}.H_2O$.

Atom	Angle(°)	Atom	Angle(°)	Atom	Angle(°)	Atom	Angle(°)
N(12)-Co-N(15)	86.5(1)	N(12)-Co-N(22)	90.2(1)	Co-N(32)-C(33)	117.1(3)	C(31)-N(32)-C(33)	116.2(3)
N(12)-Co-N(25)	92.5(1)	N(12)-Co-N(32)	90.5(1)	Co-N(35)-C(34)	107.9(2)	Co-N(35)-C(36)	115.9(3)
N(12)-Co-N(35)	170.9(1)	N(15)-Co-N(22)	175.1(1)	C(34)-N(35)-C(36)	110.9(3)	N(1)-C(1)-C(2)	178.4(5)
N(15)-Co-N(25)	89.9(1)	N(15)-Co-N(32)	94.6(1)	C(1)-C(2)-C(11)	107.1(3)	C(1)-C(2)-C(21)	107.2(4)
N(15)-Co-N(35)	87.9(1)	N(22)-Co-N(25)	86.7(1)	C(1)-C(2)-C(31)	109.3(3)	C(11)-C(2)-C(21)	111.3(3)
N(22)-Co-N(32)	89.0(1)	N(22)-Co-N(35)	95.9(1)	C(11)-C(2)-C(31)	113.8(3)	C(21)-C(2)-C(31)	107.9(3)
N(25)-Co-N(32)	174.8(1)	N(25)-Co-N(35)	94.6(1)	C(4)-C(3)-C(16)	108.5(4)	C(4)-C(3)-C(26)	108.1(4)
N(32)-Co-N(35)	82.9(1)	O(11)-Cl(1)-O(11)	110.0(3)	C(4)-C(3)-C(36)	107.6(4)	C(16)-C(3)-C(26)	109.5(4)
O(11)-Cl(1)-O(12)	108.3(2)	O(11)-Cl(1)-O(12)	109.5(2)	C(16)-C(3)-C(36)	112.5(4)	C(26)-C(3)-C(36)	110.4(4)
O(11)-Cl(1)-O(12)	109.5(2)	O(11)-Cl(1)-O(12)	108.3(2)	N(12)-C(11)-C(2)	112.2(3)	N(12)-C(13)-C(14)	107.6(4)
O(12)-Cl(1)-O(12)	111.2(4)	O(21)-Cl(2)-O(22)	109.0(2)	N(15)-C(14)-C(13)	106.7(4)	N(15)-C(16)-C(3)	113.3(4)
O(21)-Cl(2)-O(23)	109.9(2)	O(21)-Cl(2)-O(24)	108.5(3)	N(22)-C(21)-C(2)	112.1(3)	N(22)-C(23)-C(24)	106.6(3)
O(22)-Cl(2)-O(23)	111.1(2)	O(22)-Cl(2)-O(24)	109.3(2)	N(25)-C(24)-C(23)	107.0(3)	N(25)-C(26)-C(3)	114.3(4)
O(23)-Cl(2)-O(24)	109.0(2)	Co-N(12)-C(11)	117.8(3)	O(31)-C(31)-N(32)	126.1(4)	O(31)-C(31)-C(2)	119.7(4)
Co-N(12)-C(13)	107.3(3)	C(11)-N(12)-C(13)	111.6(3)	N(32)-C(31)-C(2)	113.9(3)	N(31)-C(33)-C(34)	108.3(3)
Co-N(15)-C(14)	107.1(3)	Co-N(15)-C(16)	117.9(3)	N(35)-C(34)-C(33)	110.9(3)	N(35)-C(36)-C(3)	113.7(4)
C(14)-N(15)-C(16)	112.8(3)	Co-N(22)-C(21)	117.7(3)				
Co-N(22)-C(23)	106.7(3)	C(21)-N(22)-C(23)	112.9(3)				
Co-N(25)-C(24)	107.2(3)	Co-N(25)-C(26)	117.3(3)				
C(24)-N(25)-C(26)	113.7(3)	Co-N(32)-C(31)	125.1(3)				

The Co-$N_{(amine)}$ bond distances (Table 2) are comparable to those reported for other amido sar-type Co(III) complexes, for example $[Co^{III}(Me,CO_2H\text{-}2\text{-}oxosar\text{-}H)]^{2+}$.[2] However, the remaining Co-$N_{(amido)}$ bond length, 1.898 Å, is shorter than the other Co-$N_{(amine)}$ distances besides being shorter than the Co-$N_{(amido)}$ distance observed for $[Co^{III}(Me,CO_2H\text{-}2\text{-}oxosar\text{-}H)]^{2+}$ (1.917(4) Å).[2] In addition, the Co-$N_{(amido)}$ bond distance observed for $[Co^{III}(Me,CN\text{-}2\text{-}oxosar\text{-}H)]^{2+}$ is shorter than the Co-$N_{(amido)}$ distance observed for the acyclic $[CH_3CONHCo^{III}(NH_3)_5]^{2+}$ cation (1.911(8) Å)[22] but longer than that reported for the chelate bis(glycylglycinato)cobalt(III) ion (1.87 Å).[23] Also, the N-$C_{(amido)}$ (1.298(5) Å) and C-$O_{(amido)}$ (1.259(4) Å) bond distances are shorter than the expected N-$C_{(peptide)}$ and C-$O_{(peptide)}$ bond distances of 1.30 Å and 1.27 Å respectively.[24] The other saturated C-N bonds, completing the caps, have distances that are similar to other sar type cages.[25-29]

The N-Co-N bond angles (Table 3) of $[Co^{III}(Me,CN\text{-}2\text{-}oxosar\text{-}H)]^{2+}$ deviate (~1° to 9°) slightly from the typical angles observed for octahedral symmetry. The average twist angle between the two N_3-planes, perpendicular to the long axis is 50°; the two N_3-planes also occur at an angle to one another of 1.07°. The metal possesses a pseudo-octahedral character resulting from all these small displacements. Typically in most sar cages each of the five membered chelate rings adopts a *lel* configuration similar to that found for $[Co^{III}(sepulchrate)]Cl_3.H_2O$.[30] However, this does not appear to be the case upon introduction of an amide function into the basic sar structure. Generally, the five membered chelate ring attached to the amide moiety becomes more *ob* in character as observed for $[Co^{III}(Me,CO_2H\text{-}2\text{-}oxosar\text{-}H)]^{2+}$ [2] and $[Co^{III}(Me,CN\text{-}2\text{-}oxosar\text{-}H)]^{2+}$. In this instance the two sectors free of the amide function, N(12)-C(13)-C(14)-N(15) and N(22)-C(23)-C(24)-N(25), have torsion angles of 54.7(5)° and 55.8(4)° respectively, while the remaining five membered chelate ring, N(32)-C(33)-C(34)-N(35), has a torsion angle of 21.8(5)°.

The partially solved structure of $[Co^{III}(Me,CO_2H\text{-}2\text{-}aminosar\text{-}2\text{-}ene)]^{3+}$ appears in Figure 12. Unfortunately, as a result of the disorder present in the apical carboxylic acid pendant a completely solved structure was not obtained. However, the ORTEP diagram of the complex does confirm that the nitrile has undergone condensation with a deprotonated amine to form an amidine complex with an apical carboxylic acid group. Also, the structure shows that the cobalt(III) ion is fully encapsulated and coordinated to all six nitrogens. It is estimated that the Co-$N_{(amidine)}$ bond

length is close to 1.898 Å which is the Co-$N_{(amidine)}$ bond distance reported for $\Lambda(+)_{546}$-[$Co^{III}(NH_2CH_2CH_2NC(NH_2)CH_2NH_2)(en)Cl]Cl_2.H_2O$.[31]

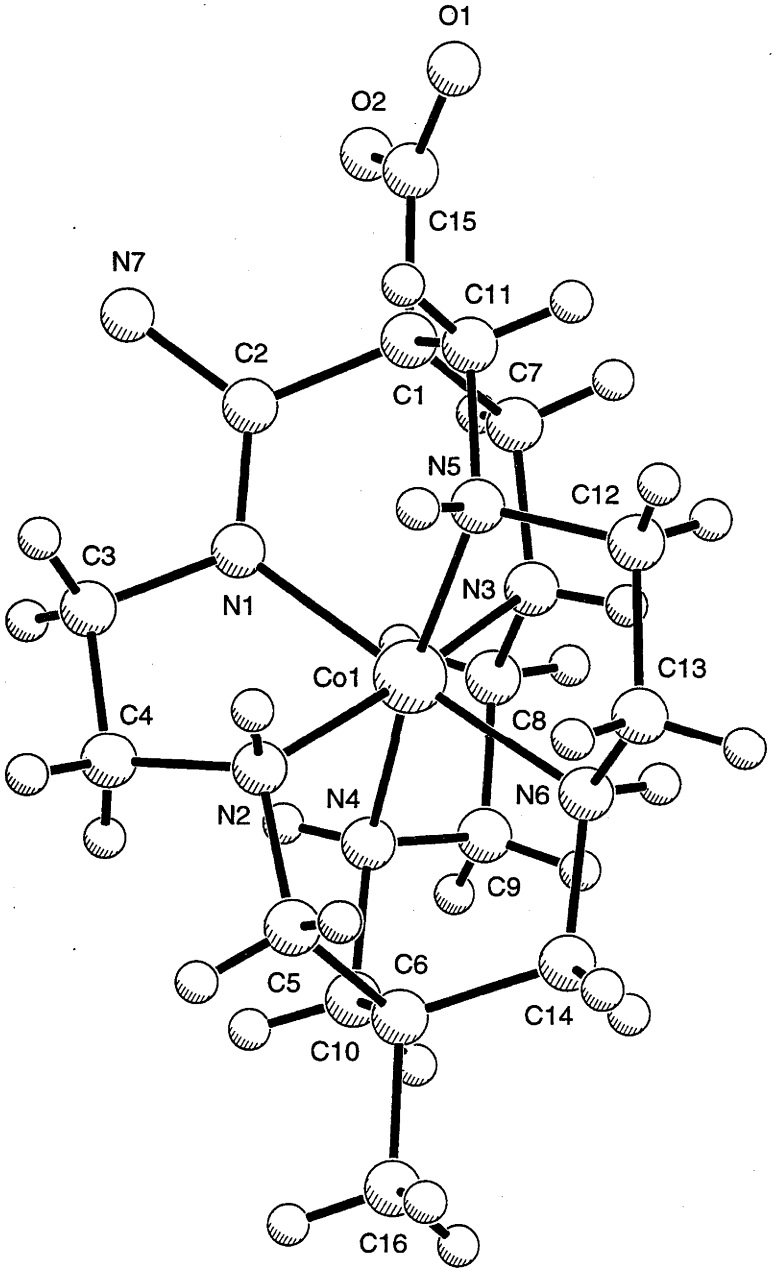

Figure 12. Thermal ellipsoid diagram of the partially solved structure of the [Co^{III}(Me,CO_2H-2-aminosar-2-ene)]$^{3+}$.

3.3.1.6 Electrochemistry

The cyclic voltammetry (CV) in aqueous solution of the Co(III) amido and amidine cage complexes, at a scan rate of 20 mVs^{-1}, appears in Figure 13 and the electrochemical data is displayed in Table 4. Simple observation of the CV's indicate that the Co(III) systems are basically reversible. Although in all cases, a quasireversible wave occurs under the conditions employed with $i_p \propto$ (scan rate)$^{1/2}$ and the peak to peak separation increasing with scan rate. For most coordination complexes, quasireversible behaviour is related to relatively slow heterogeneous or homogeneous electron transfer.[32] Also, repeated cycling of each complex at 100 mV/s produced no change in the observed results so the systems are chemically reversible and remain intact.

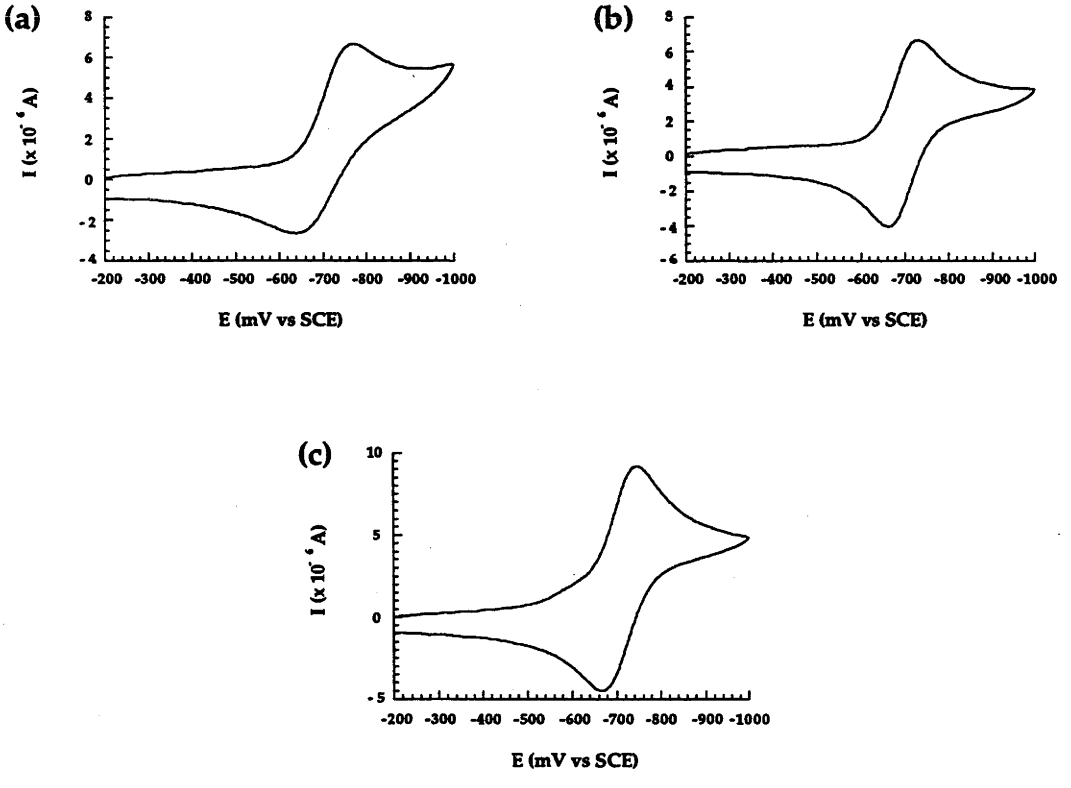

Figure 13. Co(III)/(II) cyclic voltammogram for (a) $[Co^{III}(Me,CN\text{-}2\text{-}oxosar\text{-}H)]^{2+}$ recorded in 0.05 M $KH_3(C_2O_4)_2.2H_2O$ and (b) $[Co^{III}(Me,CO_2H\text{-}2\text{-}aminosar\text{-}2\text{-}ene)]^{3+}$ and (c) $[Co^{III}(Me\text{-}2\text{-}aminosar\text{-}2\text{-}ene)]^{3+}$ recorded in 0.1 M $NaClO_4$ at 20° C with an EPG electrode and a scan rate of 20 mV s^{-1}.

Table 4. Electrochemical data for Co(III)/(II) couples of monoamide, amidine and saturated cage complexes (vs SCE). (EPG electrode; 1 mM solutions of complex in 0.05 M $KH_3(C_2O_4)_2.2H_2O$, 0.1 M $NaClO_4$ and 0.05 M Na_3PO_4 at 20° C with a scan rate of 20 mVs^{-1}).

Complex	pH	$E_{1/2}$ vs SCE (V)	E_{pc} vs SCE (mV)	E_{pa} vs SCE (mV)	i_{pc}/i_{pa}	ΔE_p (mV)
$[Co^{III}(Me,CN\text{-}2\text{-}oxosar\text{-}H)]^{2+}$	1.68 [a]	-0.71	-771	-641	0.90	130
$[Co^{III}(Me,CN\text{-}2\text{-}oxosar\text{-}H)]^{2+}$	-	-0.68[32]	-	-	-	-
$[Co^{III}(Me,CN\text{-}2\text{-}oxosar\text{-}H)]^{2+}$	12.04 [c]	-0.76	-794	-726	0.74	68
$[Co^{III}(Me,CO_2H\text{-}2\text{-}aminosar\text{-}2\text{-}ene)]^{3+}$	1.68 [a]	-0.68	-727	-626	0.92	101
$[Co^{III}(Me,CO_2H\text{-}2\text{-}aminosar\text{-}2\text{-}ene)]^{3+}$	~5 [b]	-0.70	-732	-665	1.01	67
$[Co^{III}(Me,CO_2^{-}\text{-}2\text{-}aminosar\text{-}2\text{-}ene)]^{2+}$	12.04 [c]	-0.77	-801	-730	0.99	71
$[Co^{III}(Me\text{-}2\text{-}aminosar\text{-}2\text{-}ene)]^{3+}$	1.68 [a]	-0.72	-766	-674	0.95	92
$[Co^{III}(Me\text{-}2\text{-}aminosar\text{-}2\text{-}ene)]^{3+}$	~5 [b]	-0.71	-749	-667	0.86	82
$[Co^{III}(Me\text{-}2\text{-}aminosar\text{-}2\text{-}ene)]^{3+}$	12.04 [c]	-0.74	-772	-704	0.87	68
$[Co^{III}(Mesar)]^{3+}$ [32]	-	-0.65	-	-	-	-
$[Co^{III}(sar)]^{3+}$	~6 [b]	-0.66	-698	-634	0.85	64

[a] 0.05 M $KH_3(C_2O_4)_2.2H_2O$, [b] 0.1 M $NaClO_4$, [c] 0.05 M Na_3PO_4.

For the $[Co^{III}(Me,CN\text{-}2\text{-}oxosar\text{-}H)]^{2+}$ ion a Co(III)/Co(II) wave occurs at $E_{1/2}$ = -0.68 V[32] in near neutral conditions. This value varied with pH. In acidic conditions, the $E_{1/2}$ value is similar to that found in neutral solution while in a freshly prepared basic solution, the amide displayed a potential at $E_{1/2}$ = -0.76 V. The $[Co^{III}(Me,CN\text{-}2\text{-}oxosar\text{-}H)]^{2+}$ complex displays a negative shift in the Co(III)/Co(II) redox potential, when compared to $[Co^{III}(sar)]^{3+}$ for example, as does the $[Co^{III}(Me,CO_2H\text{-}2\text{-}oxosar\text{-}H)]^{2+}$ ion. This trend is largely due to the incorporation of a deprotonated amido nitrogen into the cage structure and the resulting charge difference at the metal centre. Under all the pH conditions employed, higher oxidation states of cobalt, such as Co(IV), are inaccessible in water for the $[Co^{III}(Me,CN\text{-}2\text{-}oxosar\text{-}H)]^{2+}$ ion.

For the two amidine complexes, Co(III)/Co(II) waves occur at $E_{1/2}$ = -0.70 V for $[Co^{III}(Me,CO_2H\text{-}2\text{-}aminosar\text{-}2\text{-}ene)]^{3+}$ and $E_{1/2}$ = -0.71 V (vs SCE) for $[Co^{III}(Me\text{-}2\text{-}aminosar\text{-}2\text{-}ene)]^{3+}$ in neutral conditions. Again the potentials of these complexes varied under the pH conditions employed in a similar manner to that observed for the $[Co^{III}(Me,CN\text{-}2\text{-}oxosar\text{-}H)]^{2+}$ complex. The redox potential for each amidine complex is also slightly different. The potential for the $[Co^{III}(Me,CO_2H\text{-}2\text{-}aminosar\text{-}2\text{-}ene)]^{3+}$ complex appears at a slightly less negative potential than that observed for the $[Co^{III}(Me\text{-}2\text{-}aminosar\text{-}2\text{-}ene)]^{3+}$ ion. This is because the carboxyl substituent of the $[Co^{III}(Me,CO_2H\text{-}2\text{-}aminosar\text{-}2\text{-}ene)]^{3+}$ species has an influence on the potential. When the apical carboxyl group is protonated it is electron withdrawing which removes some charge from the metal hence the potential moves to more positive values. If the carboxyl is deprotonated then some extra charge is donated to the metal and the net positive charge on the complex decreases. It becomes harder to reduce the Co(III) to Co(II), and the potential appears at therefore somewhat more negative values. In addition, as for the $[Co^{III}(Me,CN\text{-}2\text{-}oxosar\text{-}H)]^{2+}$ ion, under all the pH conditions employed Co(IV) species were not attainable with either of the amidine ligand systems.

The data in general imply moderate electron transfer rates between the Co(III) and Co(II) states and inaccessible Co(IV) redox phenomena in water. The ligand anion alters the redox potential more than the neutral ligand and relatively stabilises the Co(III) state. This effect is more profound when the ligating atom is an anion. Peripheral charge on a substituent is less effective. In addition, the neutral amidine moiety also

relatively stabilises Co(III) compared to the neutral secondary amine ligating group.

3.3.1.7 Electronic Absorption Spectroscopy

The UV/Visible spectra of the cobalt(III) amido and amidine complexes appear in Figure 14 and Table 5. Each complex displays the two expected absorption envelopes that correspond to the $^1T_{2g} \leftarrow {}^1A_{1g}$ and $^1T_{1g} \leftarrow {}^1A_{1g}$ (O_h) parent transitions for low spin Co(III).

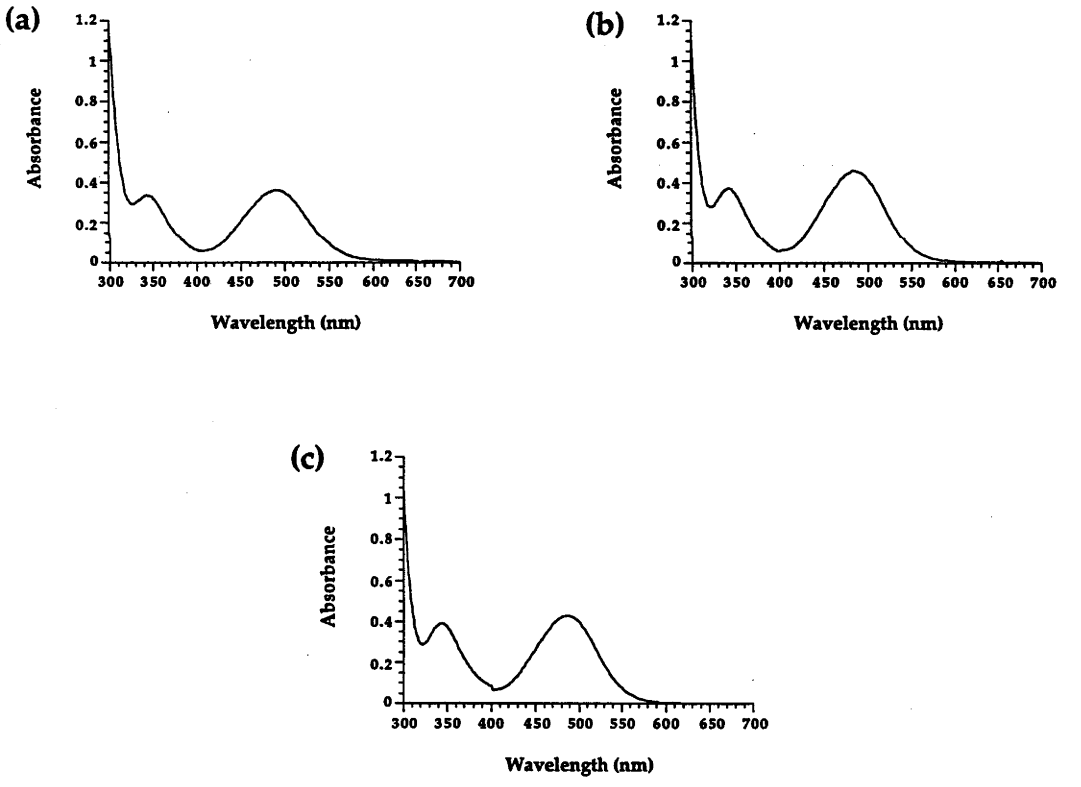

Figure 14. Electronic spectrum of (a) $[Co^{III}(Me,CN\text{-}2\text{-}oxosar\text{-}H)]^{2+}$ (b) $[Co^{III}(Me,CO_2H\text{-}2\text{-}aminosar\text{-}2\text{-}ene)]^{3+}$ and (c) $[Co^{III}(Me\text{-}2\text{-}aminosar\text{-}2\text{-}ene)]^{3+}$ in water at 20° C.

Table 5. Electronic absorption data on some Co(III) monoamido, amidine and saturated cage complexes (1mM solutions in water at 20° C, unless otherwise stated).

Complex	Band Origin Transition	λ_{max} nm (ε_{max} $M^{-1}cm^{-1}$)
$[Co^{III}(Me,CN\text{-}2\text{-}oxosar\text{-}H)]^{2+}$	$^1T_{2g}\leftarrow{}^1A_{1g}$	342 (216)
	$^1T_{1g}\leftarrow{}^1A_{1g}$	492 (233)
$[Co^{III}(Me,CO_2H\text{-}2\text{-}aminosar\text{-}2\text{-}ene)]^{3+}$	$^1T_{2g}\leftarrow{}^1A_{1g}$	343 (277)
	$^1T_{1g}\leftarrow{}^1A_{1g}$	488 (339)
$[Co^{III}(Me\text{-}2\text{-}aminosar\text{-}2\text{-}ene)]^{3+}$	$^1T_{2g}\leftarrow{}^1A_{1g}$	343 (208)
	$^1T_{1g}\leftarrow{}^1A_{1g}$	488 (228)
$[Co^{III}(Mesar)]^{3+}$	$^1T_{2g}\leftarrow{}^1A_{1g}$	345 (113)
	$^1T_{1g}\leftarrow{}^1A_{1g}$	472 (135)
$[Co^{III}(sar)]^{3+}$ [33] [a]	$^1T_{2g}\leftarrow{}^1A_{1g}$	343 (108)
	$^1T_{1g}\leftarrow{}^1A_{1g}$	471 (135)

[a] 0.1 M HCl

For the $[Co^{III}(Me,CN\text{-}2\text{-}oxosar\text{-}H)]^{2+}$ complex the two d-d absorption band maxima appear at 342 nm and 492 nm respectively. A red shift occurs in the lower energy d-d band of the amide complex compared to the analogous hexamine $[Co^{III}(sar)]^{3+}$; consequently the amide complex is red whereas $[Co^{III}(sar)]^{3+}$ is yellow. A similar red shift also occurs for the $[Co^{III}(\{NO_2\}_2\text{-}sar)]^{3+}$ complex after it loses a proton from a secondary nitrogen centre in a strong base.[33] This type of shift has been observed in other amide cage complexes. In addition, the absorptions of the amide are more intense than those of the usual $Co\text{-}N_6^{3+}$ transitions.

The UV/Visible spectra of the two amidine complexes are identical with the two d-d transitions occurring at 343 nm and 488 nm. The matching spectra arise because the apical groups in general have little influence on the position of the d-d bands[34] and the amidine is a neutral donor like the secondary amines. The two amidine complexes have their d-d absorption bands slightly red shifted when compared to the parent

hexamines $[Co^{III}(Me,COOH\text{-}sar)]^{3+}$ and $[Co^{III}(Mesar)]^{3+}$, and so have a slightly weaker ligand field. The two amidine species are however more intensely absorbing than the parent hexamine $[Co^{III}(Mesar)]^{3+}$.

3.3.2 Section 2. Reaction of $[Co^{III}(sen)]^{3+}$ with ethyl acetoacetate and formaldehyde in aqueous base.

3.3.2.1 Syntheses

The initial aim of using ethyl acetoacetate as a capping reagent for $[Co^{III}(sen)]^{3+}$ was to introduce two different functional groups, an amide and imine, into the one cap of the Co(III) cage complex. In addition, it was also envisaged that separate monoamido, monoimine and saturated cage compounds would have arisen from this reaction. However, the condensation of $[Co^{III}(sen)]^{3+}$ with formaldehyde and ethyl acetoacetate, in the presence of base, produced a number of different complexes some of which were unexpected. Separation of these compounds on SP-Sephadex - C25 resin, using trisodium citrate as the eluent, yielded five compounds. The first fraction was the Co(III) complex $[Co^{III}(Me,CO_2H\text{-sar})]^{3+}$; the remaining four fractions contained the compounds of $[Co^{III}(\{CO_2H,CH_2OH\}\text{-Me-desar})]^{3+}$, $[Co^{III}(\{CO_2Et,CH_2OH\}\text{-Me-desar})]^{3+}$ (Figure 15), $[Co^{III}(N\text{-Me-sen})]^{3+}$ and $[Co^{III}(sen)]^{3+}$ respectively. From these products, evidently, the ethyl acetoacetate undergoes reaction during the condensation process.

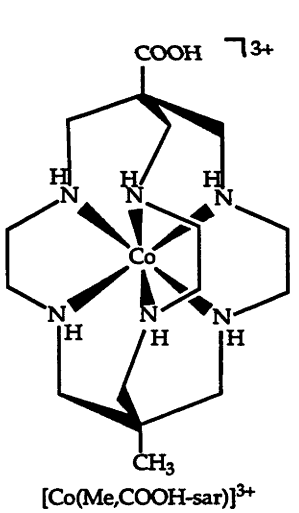

$[Co(Me,COOH\text{-sar})]^{3+}$

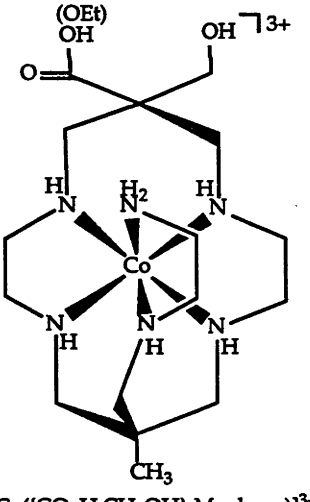

$[Co(\{CO_2H,CH_2OH\}\text{-Me-desar})]^{3+}$
$([Co(\{CO_2Et,CH_2OH\}\text{-Me-desar})]^{3+})$

Figure 15

3.3.2.2 NMR Spectroscopy

The ^{13}C NMR spectra of the two complexes of $[Co^{III}(\{CO_2H,CH_2OH\}\text{-Me-desar})]^{3+}$ and $[Co^{III}(\{CO_2Et,CH_2OH\}\text{-Me-desar})]^{3+}$ (Figure 16) from the above series highlight the general lack of symmetry within each molecule; all carbon atoms are inequivalent and a separate signal occurs for each.

NMR data on the remaining three complexes already exist. For $[Co^{III}(\{CO_2H,CH_2OH\}\text{-Me-desar})]^{3+}$, the carbon signals comprise two quaternary, one methyl, a pendent carboxylic acid, one methylene hydroxy and eleven methylene carbon atoms. These carbons have chemical shift values of 42.9, 57.7, 20.2, 173.4, 66.2, 39.5, 47.1, 49.5, 51.1, 53.7, 54.0, 54.2, 54.4, 55.8, 56.1 and 57.8 ppm respectively. For the complex of $[Co(\{CO_2Et,CH_2OH\}\text{-Me-desar})]^{3+}$ eighteen signals arise in its ^{13}C NMR spectrum which can be assigned to two quaternary, one methyl, a pendant ester, one methylene hydroxy and eleven methylene carbon atoms, which occur at 42.9, 57.7, 20.2, 13.9, 175.0, 64.8, 66.4, 43.1, 48.2, 51.0, 51.2, 53.5, 54.1, 54.3, 54.4, 54.6, 55.8 and 55.9 ppm respectively.

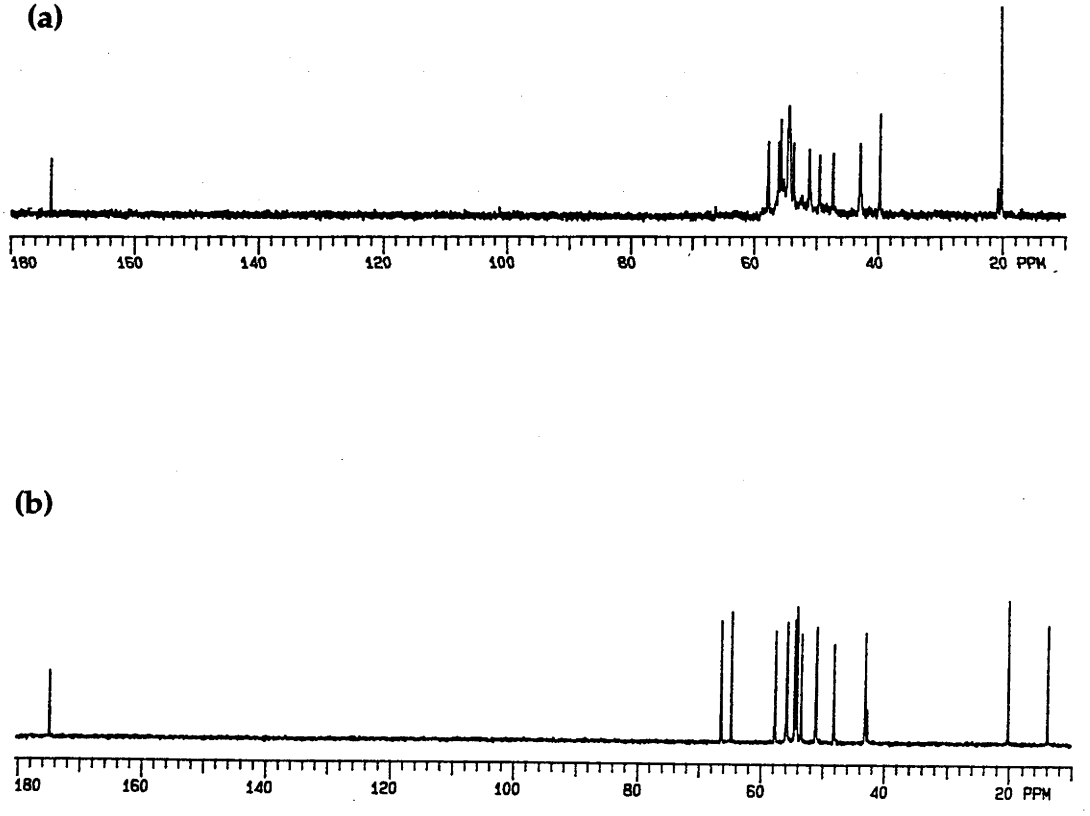

Figure 16. ^{13}C NMR spectra of (a) $[Co^{III}(\{CO_2H,CH_2OH\}\text{-Me-desar})]^{3+}$ and (b) $[Co^{III}(\{CO_2Et,CH_2OH\}\text{-Me-desar})]^{3+}$ (Chloride salts in D_2O).

The ^{1}H NMR spectrum of $[Co^{III}(\{CO_2H,CH_2OH\}\text{-Me-desar})]^{3+}$ (Figure 17) was less informative than the ^{13}C NMR spectra due to extensive overlap of the methylene proton signals and extensive spin-spin splitting and coupling. Assignments of the signals therefore are more difficult to make and are not especially revealing. The methylene protons appear in the general region of 2.1 - 3.4 ppm while the methyl group protons occur at 0.78 ppm. Also this, and the related complex $[Co^{III}(\{CO_2Et,CH_2OH\}\text{-Me-desar})]^{3+}$, are the only complexes reported in detail as the other compounds produced in this series have been characterised by NMR spectroscopy elsewhere.

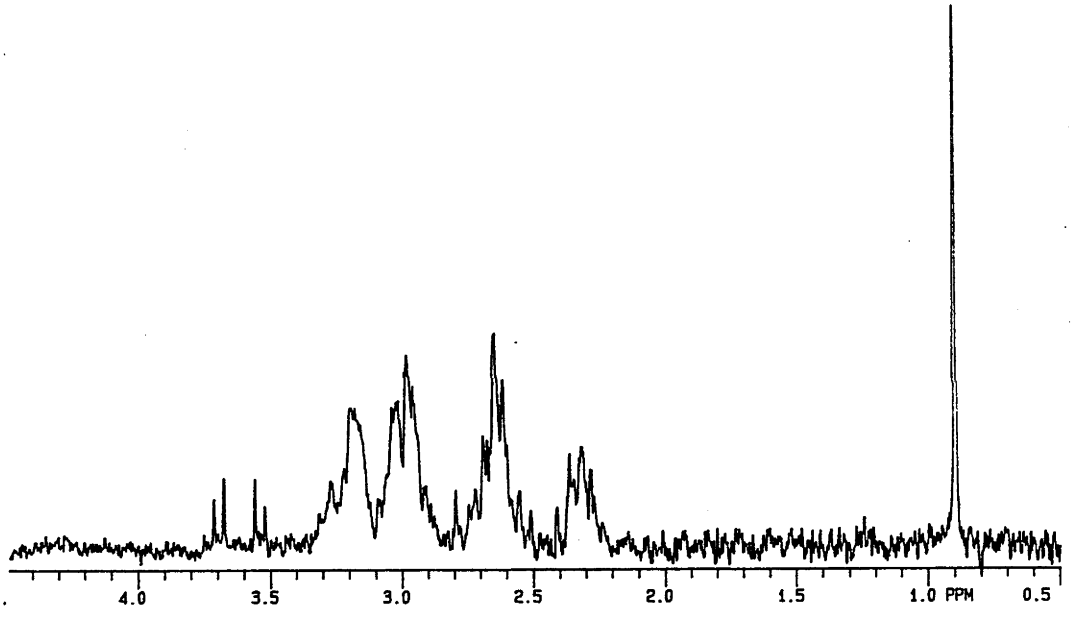

Figure 17. ^{1}H NMR spectra of $[Co^{III}(\{CO_2H,CH_2OH\}\text{-Me-desar})]^{3+}$ (Chloride salt in D_2O).

For the $[Co^{III}(\{CO_2Et,CH_2OH\}\text{-Me-desar})]^{3+}$ complex the 500 MHz ^1H NMR spectrum was more informative (Figure 18). Again a single methyl signal appears at 0.78 ppm while the methylene resonances occur between the values of 2.1 - 3.3 ppm. Separate signals arose for the pendant ester and methylene hydroxy groups. For the ester the protons on the CH_2 group are chemically different from each other and hence two multiplets result, that are centred on 4.14 and 4.21 ppm. Likewise, the three protons on the methyl group are coupled to the two inequivalent methylene protons and two doublets should arise. However, as the coupling between the methylene and methyl group is small the two doublets appear as a triplet centred at 1.16 ppm. Lastly, two doublets arise from the Cq-C$\underline{H_2}$OH protons and occur at 3.51 and 3.63 ppm respectively. A hexamine cage complex bearing the same apical pendant displays a similar chemical shift (3.67 ppm)[33,35] however, in this case the peak appears as a singlet. For the $[Co^{III}(\{CO_2Et,CH_2OH\}\text{-Me-desar})]^{3+}$ complex the CH_2 protons of the methylene hydroxy and ester groups are inequivalent due to the presence of the pro-chiral quaternary centre ($HNCH_2\underline{C}(COOEt)(CH_2OH)CH_2NH$) within the complex.

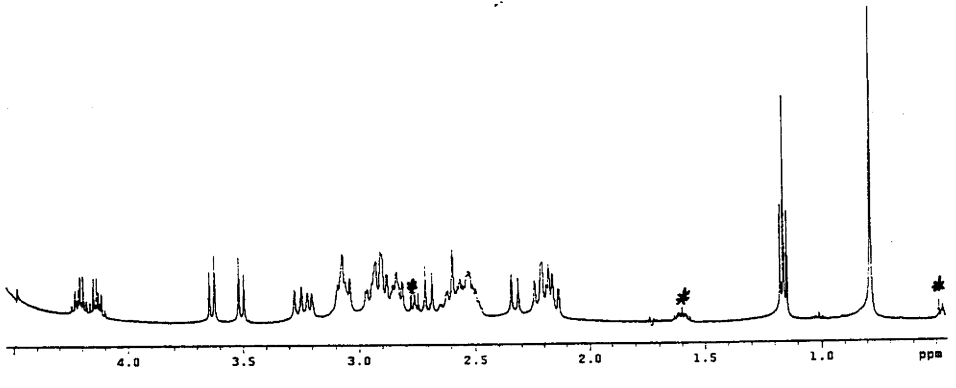

Figure 18. 500 MHz ^1H NMR spectrum of $[Co^{III}(\{CO_2Et,CH_2OH\}\text{-Me-desar})]^{3+}$ (Chloride salt in D_2O, * = NaTSP reference).

3.3.2.3 Infra-red Spectroscopy

Infra-red spectroscopy was also useful to help confirm the presence of various functional groups within the complexes of this series and their

absorption frequencies are tabulated in Table 6. Firstly, for the $[Co^{III}(Me,CO_2H\text{-sar})]^{3+}$ complex the presence of the COOH group gave rise to absorptions at 1725 cm^{-1} and 1280 cm^{-1}. The acid group was also evident in the $[Co^{III}(\{CO_2H,CH_2OH\}\text{-Me-desar})]^{3+}$ complex with the C=O stretch frequency appearing at 1740 cm^{-1} and 1250 cm^{-1}. In addition, this complex also displays absorptions at 1285 cm^{-1} and 1060 cm^{-1} which have been attributed to CH_2OH bending vibrations. Similarly, the compound $[Co^{III}(\{CO_2Et,CH_2OH\}\text{-Me-desar})]^{3+}$ also has CH_2OH absorptions at 1280 cm^{-1} and 1070 cm^{-1}. A C=O stretching band also appears at 1720 cm^{-1} which is consistent for the ester group.

Table 6. Selected functional group infra-red absorption frequencies of some Co(III) cage and macrocyclic complexes.

Complex	ν~, cm^{-1}	Assignment
$[Co^{III}(CO_2H\text{-sar})]^{3+}$	1725	$C{=}O_{(COOH)}$ stretch
	1280	$OH_{(COOH)}$ bend
$[Co^{III}(\{CO_2H,CH_2OH\}\text{-Me-desar})]^{3+}$	1740	$C{=}O_{(COOH)}$ stretch
	1630	NH_2 bend
	1285	$OH_{(CH_2OH)}$ bend
	1250	$OH_{(COOH)}$ bend
	1050	$OH_{(CH_2OH)}$ bend
$[Co^{III}(\{CO_2Et,CH_2OH\}\text{-Me-desar})]^{3+}$	1720	$C{=}O_{(COOEt)}$ stretch
	1600	NH_2 bend
	1280	$OH_{(CH_2OH)}$ bend
	1070	$OH_{(CH_2OH)}$ bend

3.3.2.4 Electrospray Mass Spectrometry

The ESM spectra of the Co(III) complexes of $[Co^{III}(Me,CO_2H\text{-sar})]^{3+}$, $[Co^{III}(\{CO_2H,CH_2OH\}\text{-Me-desar})]^{3+}$ and $[Co^{III}(\{CO_2Et,CH_2OH\}\text{-Me-desar})]^{3+}$ in water appear in Figures 19, 20 and 21. In all instances, the complexes display signals corresponding to a mono charged species after loss of one or

two hydrogens. For some of the complexes other singly charged species arise from the combination of doubly charged species with chloride ions. Again the charged ions observed in these cases are linked probably through hydrogen bonding. In the spectrum of $[Co^{III}(Me,CO_2H\text{-sar})]^{3+}$ signals for the $[Cocage^{3+} - 2H^+]^+$, $[Cocage^{3+} - H^+ + {}^{35}Cl]^+$ and $[Cocage^{3+} - 2H^+ - CO_2]^+$ ions appear at m/z = 398.8, 354.8 and 434.8 respectively. For the $[Co^{III}((CO_2H,CH_2OH)\text{-Me-desar})]^{3+}$ complex, the two signals centred on m/z values of 387 and 343 correspond to the sequential loss of CH_2O and CO_2. For the related complex $[Co^{III}((CO_2Et,CH_2OH)\text{-Me-desar})]^{3+}$, the ESM spectrum displays signals corresponding to the loss of the ethyl of the ester, and CH_2O groups. A number of other signals indicate that this species also loses the newly formed cap completely to leave a "sen" type Co(III) molecule.

Again signals arose in each of the spectra resulting from the isotopic contributions of the elements within each respective complex. The observed patterns fit the respective simulated isotope patterns of the observed ions in each case. Lastly, the assignments made in both cases support the information derived from the respective microanalytical data.

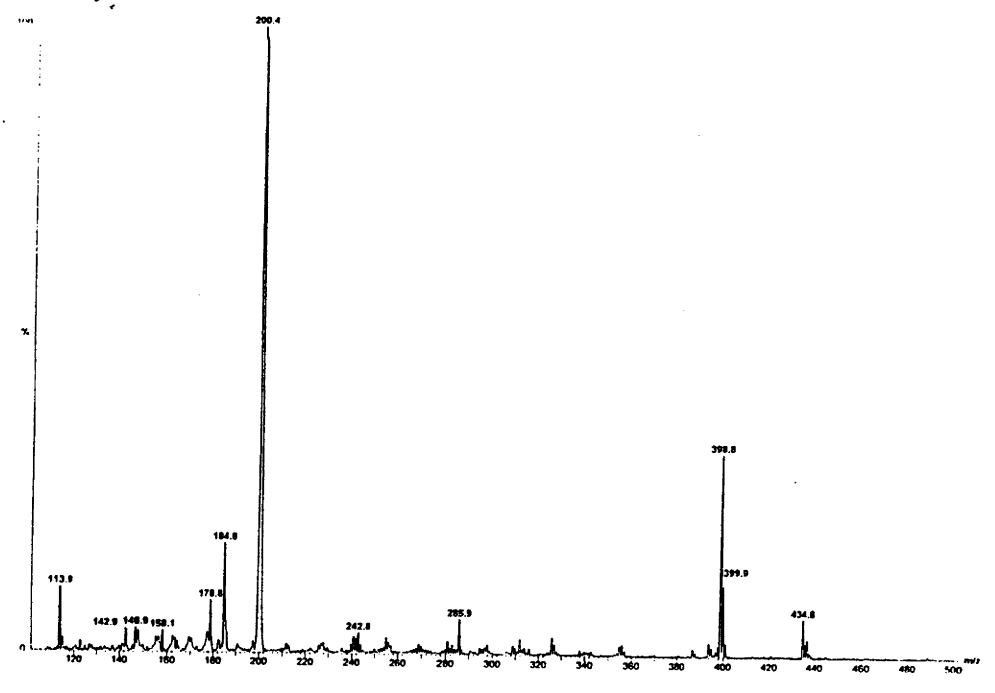

Figure 19. ESM spectrum of aqueous $[Co^{III}(Me,CO_2H\text{-sar})]^{3+}$ (Cone Voltage = 50 V).

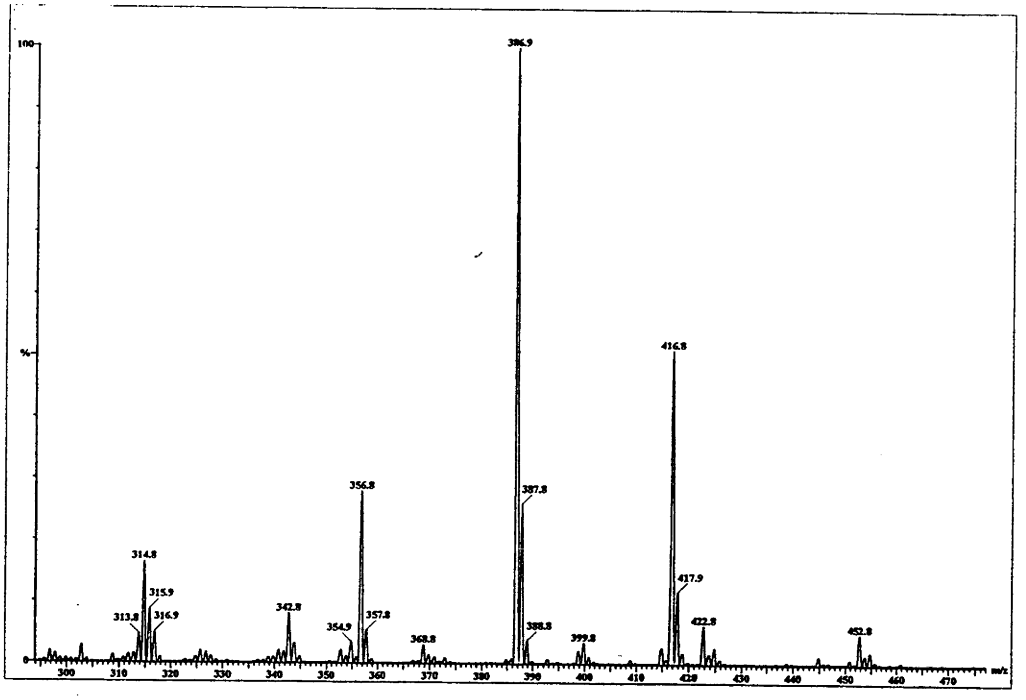

Figure 20. ESM spectrum of aqueous $[Co^{III}(\{CO_2H,CH_2OH\}\text{-Me-desar})]^{3+}$ (Cone Voltage = 80 V).

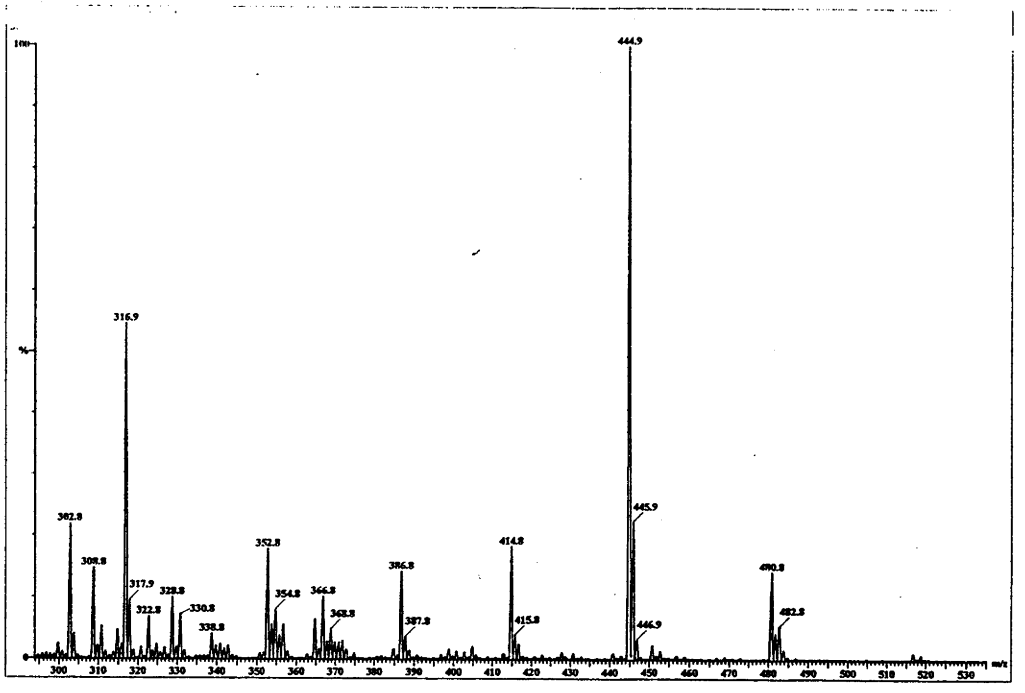

Figure 21. ESM spectrum of aqueous $[Co^{III}(\{CO_2Et,CH_2OH\}\text{-Me-desar})]^{3+}$ (Cone Voltage = 80 V).

3.3.2.5 Electrochemistry

The cyclic voltammetry, in aqueous solution at 20 mVs^{-1}, of the two Co(III) macrocyclic complexes in this series appear in Figure 22. The appearance of the two CV's show that these systems are basically reversible (quasireversible). The electrochemical data on the first three complexes in this series appear in Table 7. Usually, a quasireversible wave occurs under the various pH conditions employed with $i_p \propto$ (scan rate)$^{1/2}$, and peak to peak separation increasing with scan rate. For most coordination complexes, quasireversible behaviour indicates a moderate heterogeneous or homogeneous electron transfer.[32] Repeated cycling of the various complexes, at ≤ 100 mV/s, under all the conditions employed produced no changes in the observed results and the complexes are clearly chemically reversible.

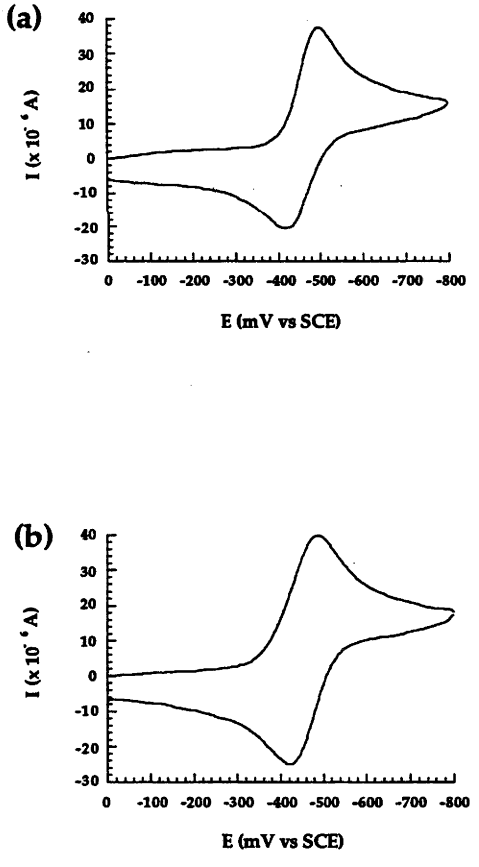

Figure 22. Co(III)/(II) cyclic voltammogram for (a) $[Co^{III}(\{CO_2H,CH_2OH\}$-Me-desar$)]^{3+}$ and (b) $[\{Co^{III}(\{CO_2Et,CH_2OH\}$-Me-desar$)]^{3+}$ recorded in 0.1 M $NaClO_4$ at 20° C with an EPG electrode and a scan rate of 20 mV s^{-1}.

Table 7. Electrochemical data for Co(III)/(II) couples of some saturated cage and macrocyclic complexes (vs SCE). (EPG electrode; 1 mM solutions of complex in 0.05 M $KH_3(C_2O_4)_2.2H_2O$, 0.1 M $NaClO_4$ and 0.05 M Na_3PO_4 at 20° C with a scan rate of 20 mVs^{-1}).

Complex	pH	$E_{1/2}$ vs SCE (V)	E_{pc} vs SCE (mV)	E_{pa} vs SCE (mV)	i_{pc}/i_{pa}	ΔE_p (mV)
$[Co^{III}(Me,CO_2H\text{-sar})]^{3+}$	1.68 [a]	-0.63	-665	-604	0.99	61
$[Co^{III}(Me,CO_2H\text{-sar})]^{3+}$ [32]	~6	-0.55	-	-	-	-
$[Co^{III}(Me,CO_2^-\text{-sar})]^{2+}$ [32]	~6	-0.60	-	-	-	-
$[Co^{III}(Me,CO_2^-\text{-sar})]^{2+}$	12.04 [c]	-0.74	-779	-714	0.96	65
$[Co^{III}(\{CO_2H,CH_2OH\}\text{-Me-de-sar})]^{3+}$	1.68 [a]	-	-478	-	-	-
$[Co^{III}(\{CO_2H,CH_2OH\}\text{-Me-de-sar})]^{3+}$	~6 [b]	-0.46	-500	-417	0.84	83
$[Co^{III}(\{CO_2^-,CH_2OH\}\text{-Me-de-sar})]^{2+}$	12.04 [c]	-0.59	-623	-557	1.10	66
$[Co^{III}(\{CO_2Et,CH_2OH\}\text{-Me-de-sar})]^{3+}$	1.68 [a]	-	-454	-	-	-
$[Co^{III}(\{CO_2Et,CH_2OH\}\text{-Me-de-sar})]^{3+}$	~6 [b]	-0.46	-489	-423	0.87	66
$[Co^{III}(Mesar)]^{3+}$ [32]	~6	-0.65	-	-	-	-
$[Co^{III}(sar)]^{3+}$	~6 [b]	-0.66	-698	-634	0.85	64

[a] 0.05 M $KH_3(C_2O_4)_2.2H_2O$, [b] 0.1 M $NaClO_4$, [c] 0.05 M Na_3PO_4.

The $[Co^{III}(Me,CO_2H\text{-sar})]^{3+/2+}$ couple is virtually reversible under all pH conditions at a 20 mVs^{-1} scan rate and the potentials are close to those of $[Co^{III}(Mesar)]^{3+/2+}$ and $[Co^{III}(sar)]^{3+/2+}$. By analogy all these systems would have similar homogeneous and heterogeneous electron transfer rates and would be expected to be reversible at low scan rates. The macrocyclic complexes however do display different patterns of behaviour. In acidic media (0.05 M $KH_3(C_2O_4).2H_2O$ (pH 1.68)) $[Co^{III}(\{CO_2H,CH_2OH\}\text{-Me-desar})]^{3+}$ and $[Co^{III}(\{CO_2Et,CH_2OH\}\text{-Me-desar})]^{3+}$ display irreversible redox waves. It is likely that in acid one of the N atoms of the hexadentate macrocycle peels off the Co(II) ion and is protonated thereby leading to irreversibility. This indicates that these molecules are not as inert as the cages. In addition, the complex $[Co^{III}(\{CO_2Et,CH_2OH\}\text{-Me-desar})]^{3+}$ is observed to change colour from orange to red/orange in basic conditions indicating that some change occurs to the compound under these conditions. The subsequent NMR spectra, in basic D_2O, indicated that at least three different products arose rapidly in these conditions. As a result in basic solution, a reversible redox couple for the $[Co^{III}(\{CO_2Et,CH_2OH\}\text{-Me-desar})]^{3+}$ complex was not obtained as it was not a single complex. Also, the position of the redox couple of the different metal complexes depended on the pH of the solution. For $[Co^{III}(Me,CO_2H\text{-sar})]^{3+}$ and $[Co^{III}(\{CO_2H,CH_2OH\}\text{-Medesar})]^{3+}$ the potentials become more negative when moving from acidic through to more basic conditions. Obviously, the carboxylate substituent, on both complexes, is influencing the observed redox potential in a similar manner to that outlined earlier. Lastly, the complexes of $[Co^{III}(\{CO_2H,CH_2OH\}\text{-Me-desar})]^{3+}$ and $[Co^{III}(\{CO_2Et,CH_2OH\}\text{-Me-desar})]^{3+}$ each possess Co(III)/(II) couples that are more negative than that observed for the $[Co^{III}(sen)]^{3+}$ ion.

3.3.2.6 Electronic Absorption Specroscopy

The UV/Visible spectra for the cobalt(III) macrocyclic complexes appear in Figure 23 while the spectral maxima for the first three complexes in this series appear in Table 8. Each compound displayed two bands that corresponded to the $^1T_{1g} \leftarrow {}^1A_{1g}$ and $^1T_{2g} \leftarrow {}^1A_{1g}$ (O_h) parent transitions for low spin Co(III). The intensities of two of the three complexes (Table 7) in this group are greater than the usual Co-N_6^{3+} d-d transitions while the absorptions of $[Co^{III}(Me,CO_2H\text{-sar})]^{3+}$ are consistent with that of the $[Co^{III}(sar)]^{3+}$ ion. The macrocyclic complexes display much the same spectroscopy as Co(III) hexaamines in general and given that they are basically saturated amine hexadentates it is not surprising.

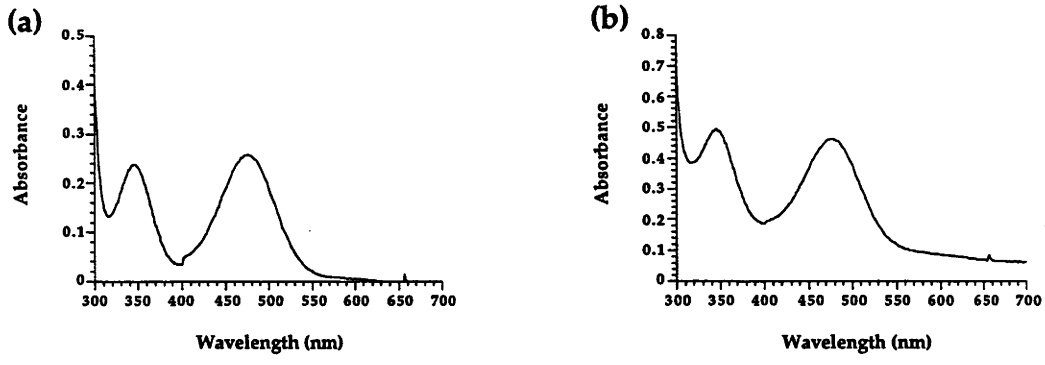

Figure 23. Electronic spectrum of (a) $[Co^{III}(\{CO_2H,CH_2OH\}\text{-Me-desar})]^{3+}$ and (b) $[Co^{III}(\{CO_2Et,CH_2OH\}\text{-Me-desar})]^{3+}$ in water at 20° C.

Table 8. Electronic absorption data on some Co(III) saturated cage and macrocyclic complexes (1mM solutions in water at 20° C, unless otherwise stated).

Complex	Band Origin Transition	λ_{max} nm (ε_{max} $M^{-1}cm^{-1}$)
$[Co^{III}(Me,CO_2H\text{-sar})]^{3+}$	$^1T_{2g}\leftarrow{}^1A_{1g}$	342 (134)
	$^1T_{1g}\leftarrow{}^1A_{1g}$	468 (166)
$[Co^{III}(Mesar)]^{3+}$	$^1T_{2g}\leftarrow{}^1A_{1g}$	345 (113)
	$^1T_{1g}\leftarrow{}^1A_{1g}$	472 (135)
$[Co^{III}(sar)]^{3+}$ [a]	$^1T_{2g}\leftarrow{}^1A_{1g}$	343 (108)
	$^1T_{1g}\leftarrow{}^1A_{1g}$	471 (135)
$[Co^{III}(\{CO_2H,CH_2OH\}\text{-Me-desar})]^{3+}$	$^1T_{2g}\leftarrow{}^1A_{1g}$	343 (141)
	$^1T_{1g}\leftarrow{}^1A_{1g}$	476 (130)
$[Co^{III}(\{CO_2Et,CH_2OH\}\text{-Me-desar})]^{3+}$	$^1T_{2g}\leftarrow{}^1A_{1g}$	347 (198)
	$^1T_{1g}\leftarrow{}^1A_{1g}$	476 (185)
cis-$[Co^{III}cyclam(OH_2)_2]^{3+}$ [36]	$^1T_{2g}\leftarrow{}^1A_{1g}$	367 (99)
	$^1T_{1g}\leftarrow{}^1A_{1g}$	506 (110)

[a] 0.1 M HCl

3.3.3 Section 3. Reaction of $[Co^{III}(sen)]^{3+}$ with diethyl malonate and formaldehyde in aqueous base.

3.3.3.1 Syntheses

The reaction of $[Co(sen)]^{3+}$ with formaldehyde and diethyl malonate, in the presence of base, led to the known complex $[Co^{III}(Me,CO_2Et\text{-}2\text{-}oxosar\text{-}H)]^{2+}$.[2] In the presence of K_2CO_3, the ester group hydrolysed, producing the final isolated product, $[Co^{III}(Me,CO_2H\text{-}2\text{-}oxosar\text{-}H)]^{2+}$ in relatively high yield. Demetallation of this product was achieved by reacting the amido complex with KCN and $CoCl_2.6H_2O$. Other metal amide and amido complexes were then produced with this ligand by complexation with Ni(II), Cu(II), Fe(III), Mn(III) and Cr(III) ions (Figure 24). Attempts to produce a Zn(II) complex by mixing the ligand and an appropriate zinc salt proved unsuccessful. Even substantial variation of the reaction conditions produced none of the required product.

The various transition metal complexes were characterised by microanalysis, visible spectroscopy, ESMS and to some extent by IR spectroscopy but finally by X-ray crystallographic analysis.

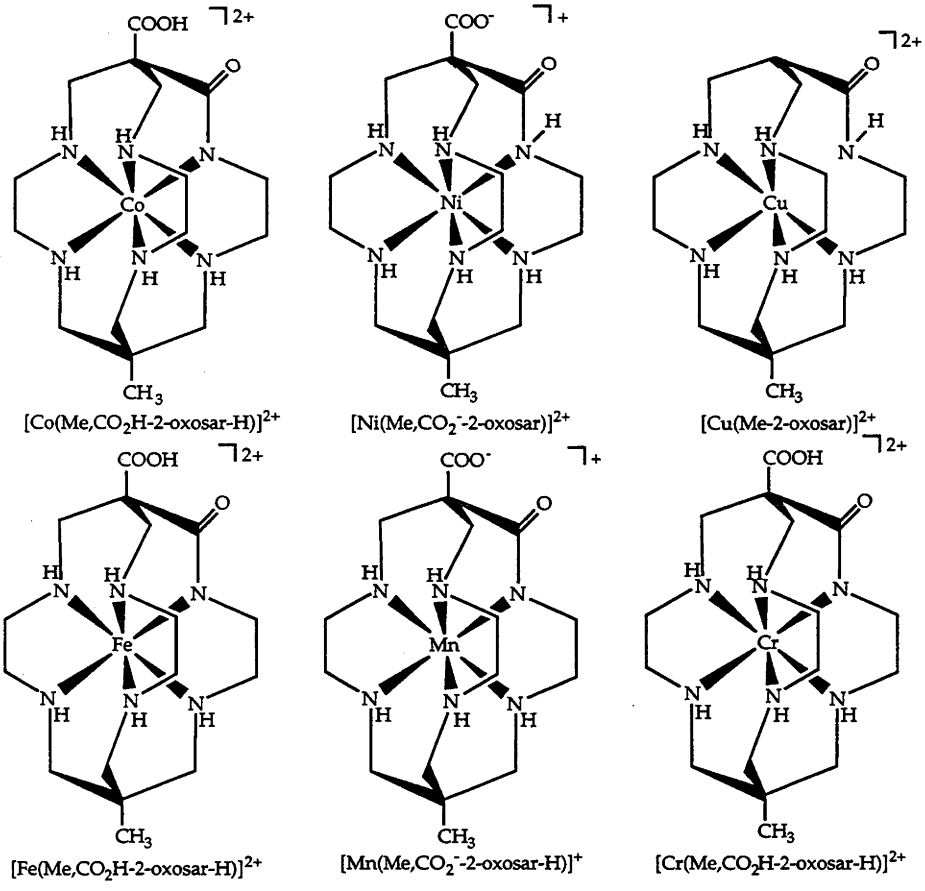

Figure 24

3.3.3.2 Infra-red Spectroscopy

Infra-red spectroscopy is a useful tool in the analysis of suspected amide complexes since the carbonyl stretching vibration is rather strong and characteristic of the bonding mode. Tabulated in Table 9 are the absorption frequencies of the functional groups of these complexes. For the $[Fe^{III}(Me,CO_2H\text{-}2\text{-}oxosar\text{-}H)]^{2+}$ complex an amido C=O stretching band appears at 1557 cm^{-1} while absorption bands for the COOH group appear at 1743 cm^{-1} (C=O stretch) and 1213 cm^{-1} (OH bend). These values match the amido and COOH frequencies of 1599 cm^{-1}, 1727 cm^{-1} and 1272 cm^{-1} observed for the $[Co^{III}(Me,CO_2H\text{-}2\text{-}oxosar\text{-}H)]^{2+}$ [2] species. The crystallographic evidence obtained on the Fe(III) and Co(III)[2] complexes shows that both metals are bound to an amido nitrogen. The observed frequencies of the amide carbonyl stretching vibration for the Fe(III) and Co(III) amido complexes also appear at lower values compared to those of unbound secondary amides (1680 cm^{-1} to 1630 cm^{-1}).[37]

By comparison, the copper(II) monoamide, $[Cu^{II}(Me\text{-}2\text{-}oxosar)]^{2+}$, (Figure 25a) displays an amide carbonyl stretching frequency of 1656 cm^{-1} consistent with an uncoordinated amide group. The crystal structure also shows that the copper is not bound to the amido nitrogen. Similarly, the free amide ligand, Me,CO_2K-2-oxosar, exhibits a characteristic amide carbonyl absorption band at 1630 cm^{-1} which is at the limit expected for an unbound secondary amide ligand. This compound also displays the antisymmetrical and symmetrical stretching vibrations anticipated for a COO^- group (1610 to 1550 cm^{-1} and 1420 to 1300 cm^{-1})[37] at 1591 cm^{-1} and 1349 cm^{-1} respectively. For the $[Cr^{III}(Me,CO_2H\text{-}2\text{-}oxosar\text{-}H)]^{2+}$ and $[Mn^{III}(Me,CO_2^-\text{-}2\text{-}oxosar\text{-}H)]^{+}$ complexes the amido carbonyl stretching frequencies appear at 1597 cm^{-1} and 1595 cm^{-1} respectively. In addition, carboxylate absorption frequencies for the Cr(III) amide complex appear at 1725 cm^{-1} and 1250 cm^{-1} respectively. For the Mn(III) amide complex the stretching vibrations at 1610 cm^{-1} and 1310 cm^{-1} are consistent with that expected for a COO^- group. Finally, the Ni(II) complex, $[Ni^{II}(Me,CO_2^-\text{-}2\text{-}oxosar)]^{+}$, (Figure 26a) displays an amide carbonyl stretching vibration, which is resolved into two bands, at 1709 cm^{-1} and 1691 cm^{-1}. In addition, the carboxylate ion stretching vibrations appear at 1602 cm^{-1} and 1354 cm^{-1}.

Table 9. Selected functional group infra-red absorption vibrations of the amide complexes and free ligand obtained in this work.

Complex	$\nu\tilde{}$, cm^{-1}	Assignment
$[Co^{III}(Me,CO_2H\text{-}2\text{-}oxosar\text{-}H)]^{2+}$	1727	$C{=}O_{(COOH)}$ stretch
	1599	$C{=}O_{(amido)}$ stretch
	1272	$OH_{(COOH)}$ bend
$Me,CO_2K\text{-}2\text{-}oxosar$	1630	$C{=}O_{(amide)}$ stretch
	1591	COO^-K^+ asym stretch
	1349	COO^-K^+ sym stretch
$[Ni^{II}(Me,CO_2^-\text{-}2\text{-}oxosar)]^+$	1709, 1691	$C{=}O_{(amide)}$ stretch
	1602	COO^- asym stretch
	1354	COO^- sym stretch
$[Cu^{II}(Me\text{-}2\text{-}oxosar)]^{2+}$	1656	$C{=}O_{(amide(I))}$ stretch
$[Fe^{III}(Me,CO_2H\text{-}2\text{-}oxosar\text{-}H)]^{2+}$	1743	$C{=}O_{(COOH)}$ stretch
	1557	$C{=}O_{(amido)}$ stretch
	1213	$OH_{(COOH)}$ bend
$[Mn^{III}(Me,CO_2^-\text{-}2\text{-}oxosar\text{-}H)]^+$	1610	COO^- asym stretch
	1595	$C{=}O_{(amido)}$ stretch
	1310	COO^- sym stretch
$[Cr^{III}(Me,CO_2H\text{-}2\text{-}oxosar\text{-}H)]^{2+}$	1725	$C{=}O_{(COOH)}$ stretch
	1597	$C{=}O_{(amido)}$ stretch
	1250	$OH_{(COOH)}$ bend

A small sample of the Cu(II) complex was then dissolved in D_2O and freeze-dried. The resultant IR spectrum (Figure 25b and Table 10) revealed that the two amide peaks were present at 1649 cm^{-1} and 1537 cm^{-1}. The copper complex was then redissolved in basic D_2O (pD ~ 9) and again freeze-dried. Examination of the freeze-dried complex in KBr (Figure 25c and Table 10) showed that the amide absorption bands appeared at similar values (1645 cm^{-1} and 1562 cm^{-1}) to that of the undeuterated complex. The Ni(II) monoamide complex was also treated exactly the same way as the $[Cu^{II}(Me\text{-}2\text{-}oxosar)]^{2+}$ ion above (Figures 26a, b and c and Table 10). However, for this complex the IR spectrum of the Ni(II) system, obtained from basic conditions (pD ~ 9) showed that the amide carbonyl stretch moves to a lower frequency (1577 cm^{-1}) overlapping with the carboxylate ion stretch stretching band.

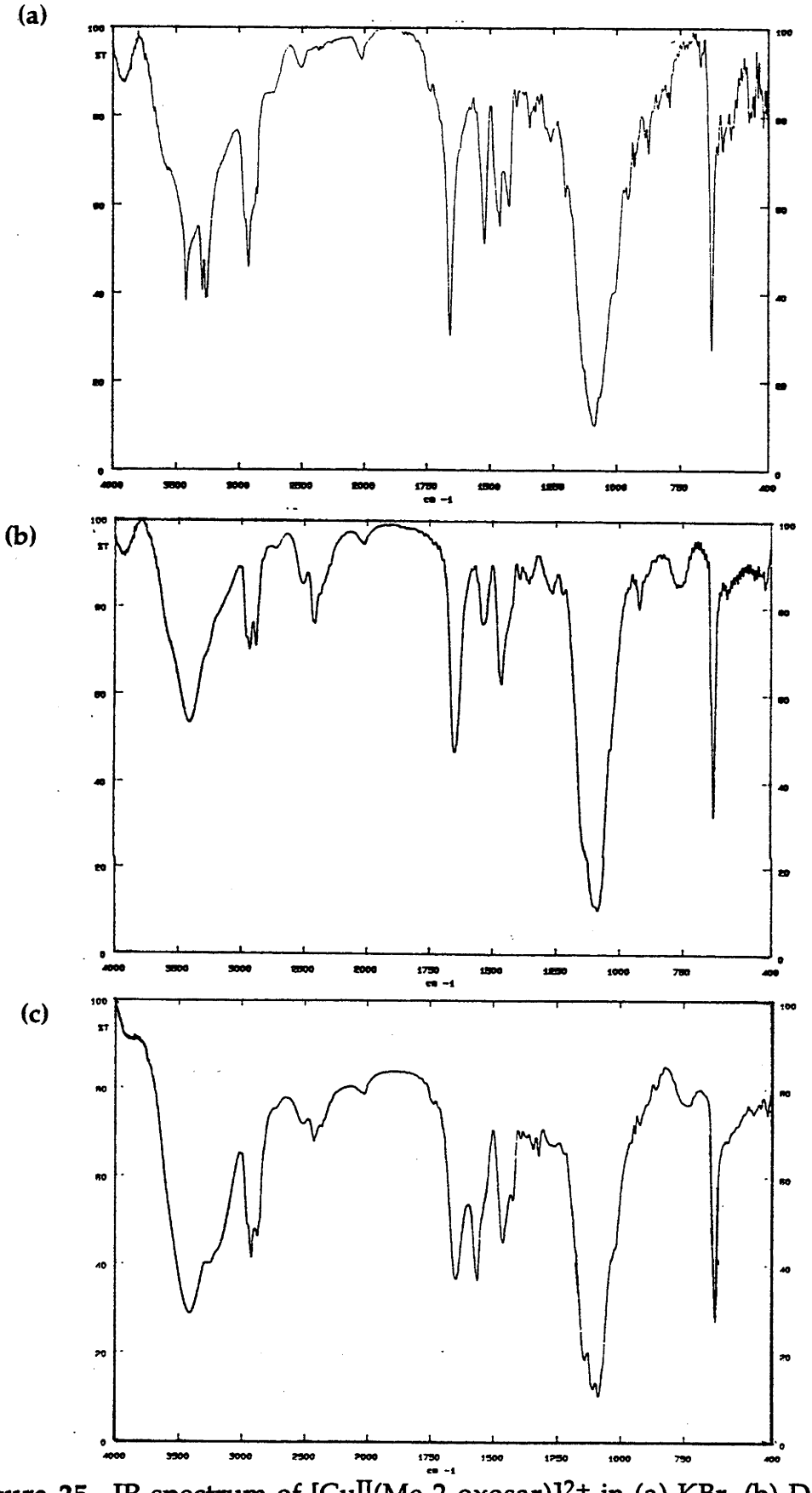

Figure 25. IR spectrum of $[Cu^{II}(Me\text{-}2\text{-}oxosar)]^{2+}$ in (a) KBr, (b) Deuterated complex in KBr and (c) Deuterated complex, obtained from basic D_2O, in KBr.

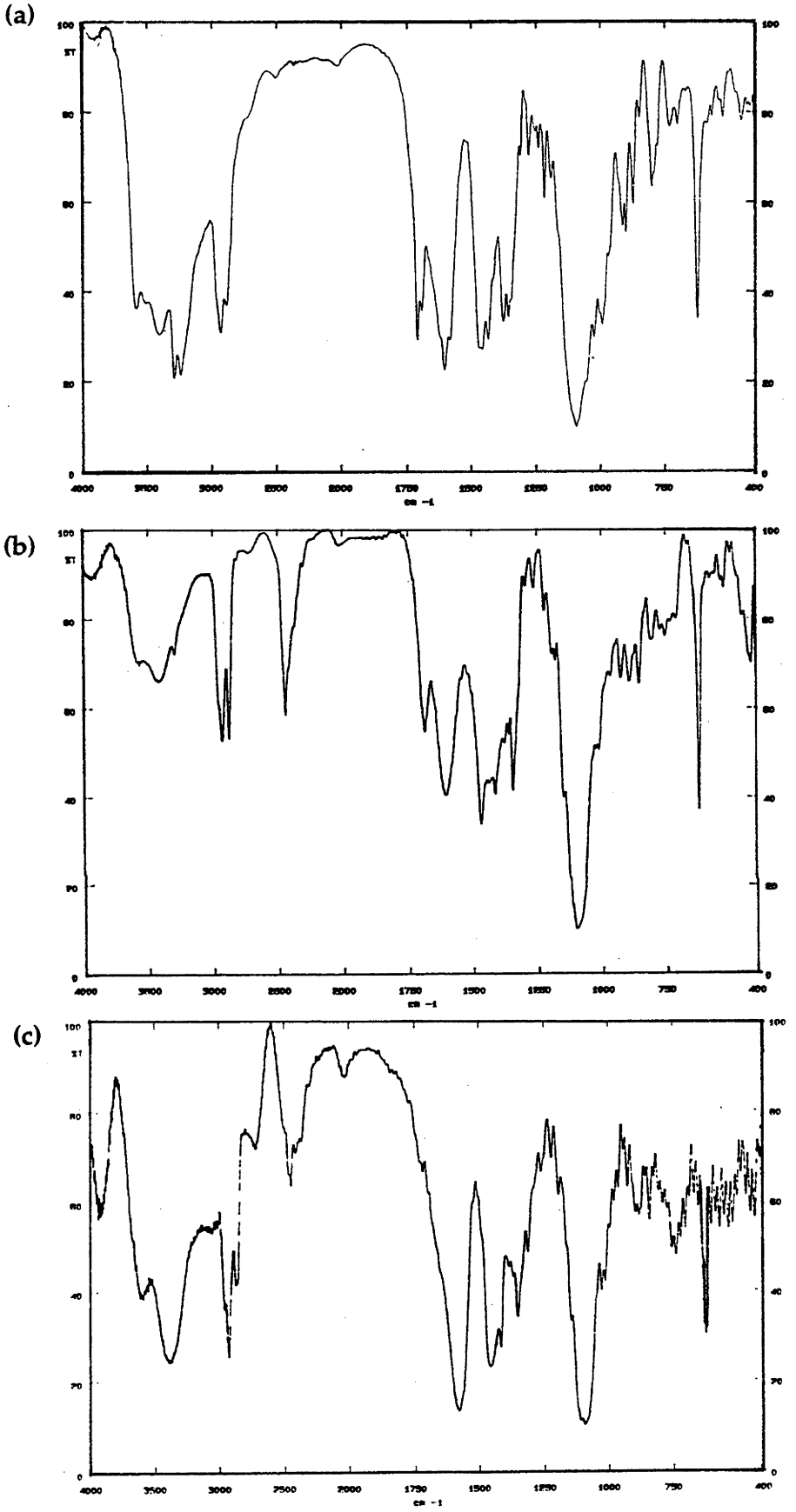

Figure 26. IR spectrum of $[Ni^{II}(Me,CO_2^-\text{-}2\text{-}oxosar)]^+$ in (a) KBr, (b) Deuterated complex in KBr and (c) Deuterated complex, obtained from basic D_2O, in KBr.

Table 10. Selected functional group infra-red absorption vibrations of the deuterated Cu(II) and Ni(II) amide complexes obtained in this work.

Complex	ν~, cm^{-1}	Assignment
$[Cu^{II}(Me\text{-}2\text{-}oxosar)]^{2+}$	1649	$C{=}O_{(amide(I))}$ stretch
	1537	$C{=}O_{(amide(II))}$ stretch
$[Cu^{II}(Me\text{-}2\text{-}oxosar)]^{2+}$	1645	$C{=}O_{(amide(I))}$ stretch
	1562	$C{=}O_{(amide(II))}$ stretch
$[Ni^{II}(Me,CO_2^-\text{-}2\text{-}oxosar)]^{+}$	1685	$C{=}O_{(amide)}$ stretch
	1604	COO^- asym stretch
	1359	COO^- sym stretch
$[Ni^{II}(Me,CO_2^-\text{-}2\text{-}oxosar\text{-}H)]^{0}$	1577	$C{=}O_{(amido)}$ stretch
	1350	COO^- sym stretch

3.3.3.3 Electrospray Mass Spectrometry

The ESM spectra of the Co(III), Ni(II), Cu(II), Fe(III), Mn(III) and Cr(III) amide complexes within this series in water appear in Figures 27 to 32. For the $[Co^{III}(Me,CO_2H\text{-}2\text{-}oxosar\text{-}H)]^{2+}$, $[Cu^{II}(Me\text{-}2\text{-}oxosar)]^{2+}$, $[Fe^{III}(Me,CO_2H\text{-}2\text{-}oxosar\text{-}H)]^{2+}$ and $[Cr^{III}(Me,CO_2H\text{-}2\text{-}oxosar\text{-}H)]^{2+}$ complexes all display a signal corresponding to a $[Mcage^{2+} - H^+]^+$ species and for the Cu(II) and Fe(III) complexes this is the most intense signal. For the $[Ni^{II}(Me,CO_2^-\text{-}2\text{-}oxosar)]^+$ and $[Mn^{III}(Me,CO_2^-\text{-}2\text{-}oxosar\text{-}H)]^+$ mono charged complexes, a base signal corresponding to a $[Mcage]^+$ species arises. Except for the Cu(II) complex that does not possess an apical CO_2 group, all the complexes display a loss of forty-four mass units from the base signal that corresponds to the elimination of a CO_2 group.

For the $[Cr^{III}(Me,CO_2H\text{-}2\text{-}oxosar\text{-}H)]^{2+}$ complex the $[Crcage^{2+} - H^+ - CO_2]^+$ ion appeared as the most abundant ion within the spectrum. In addition, for the Cu(II) complex a series of signals at an m/z of 474 occurs from the combination of the doubly charged ion, $[Cucage^{2+}]^{2+}$, with one perchlorate ion. In both instances, the charged ions combine presumably by hydrogen bonding to the cation in the ion pair. It is also of interest to note in all the spectra shown that signals occur at masses clustered around those of the observed ions. These signals arise from the isotopic contributions of the elements present within each molecule. The observed ions are consistant with the respective simulated patterns of the observed ions in each case and support the respective microanalytical assignments.

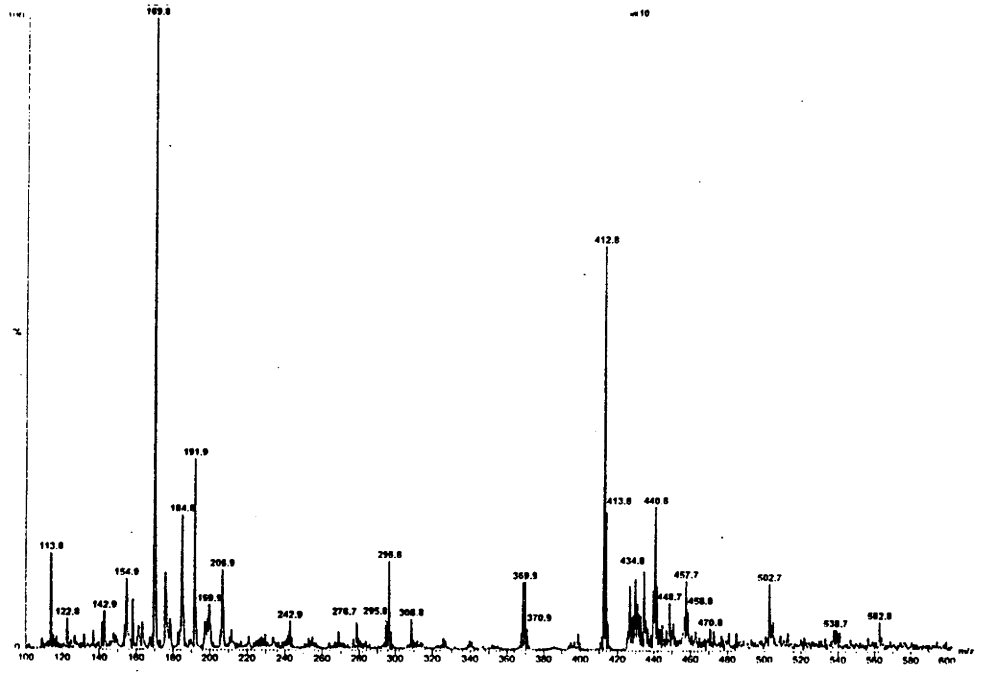

Figure 27. ESM spectrum of aqueous $[Co^{III}(Me,CO_2H\text{-}2\text{-}oxosar\text{-}H)]^{2+}$ (Cone Voltage = 50 V).

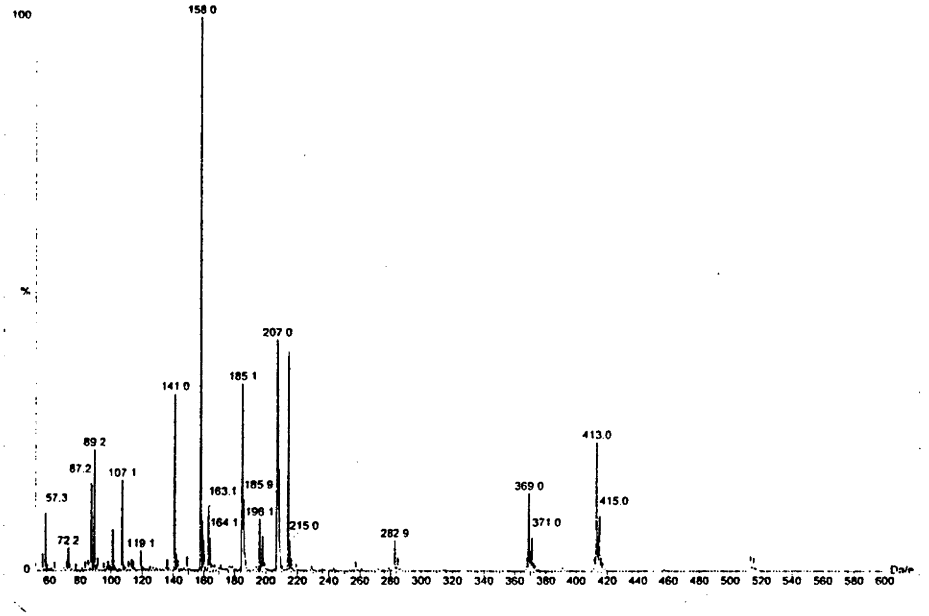

Figure 28. ESM spectrum of aqueous $[Ni^{II}(Me,CO_2^{-}\text{-}2\text{-}oxosar)]^{+}$ (Cone Voltage = 25 V).

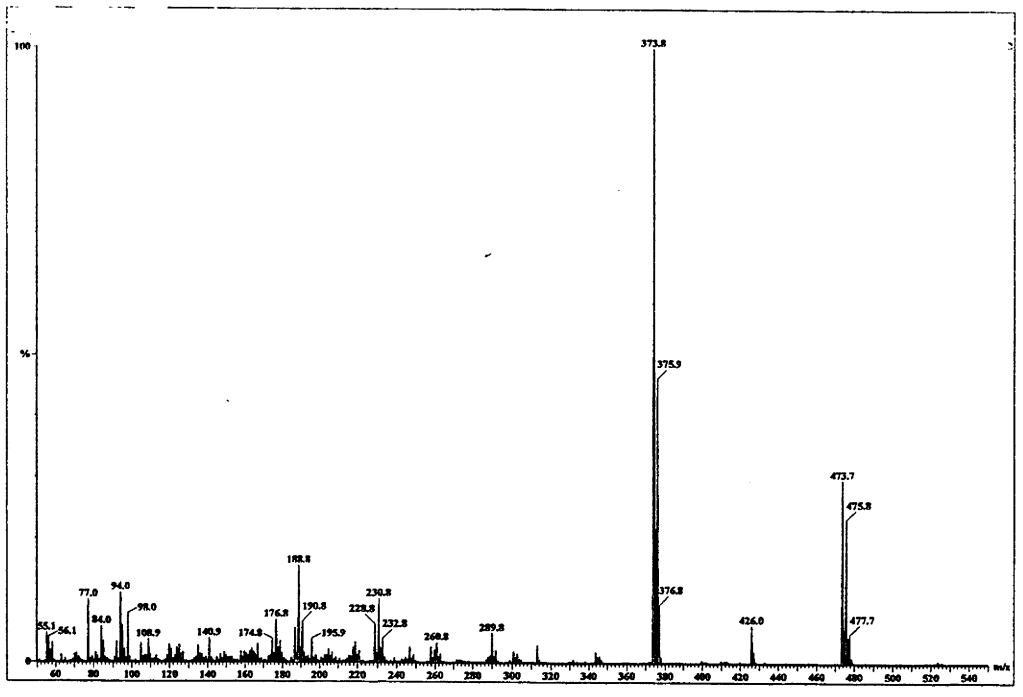

Figure 29. ESM spectrum of aqueous $[Cu^{II}(Me\text{-}2\text{-}oxosar)]^{2+}$ (Cone Voltage = 80 V).

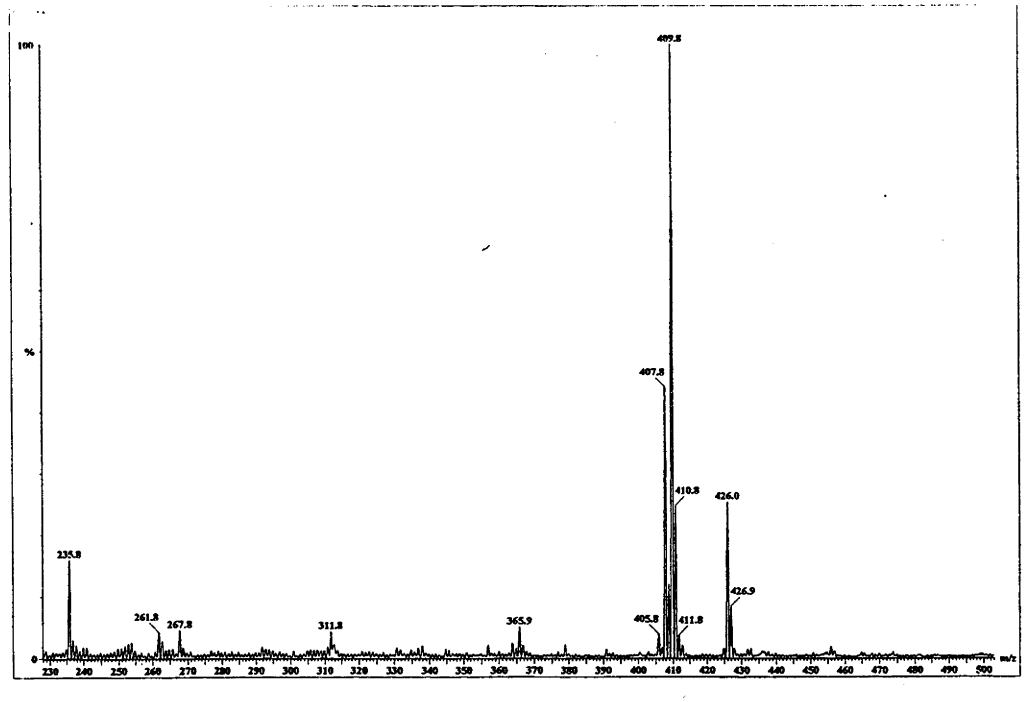

Figure 30. ESM spectrum of aqueous $[Fe^{III}(Me,CO_2H\text{-}2\text{-}oxosar\text{-}H)]^{2+}$ (Cone Voltage = 50 V).

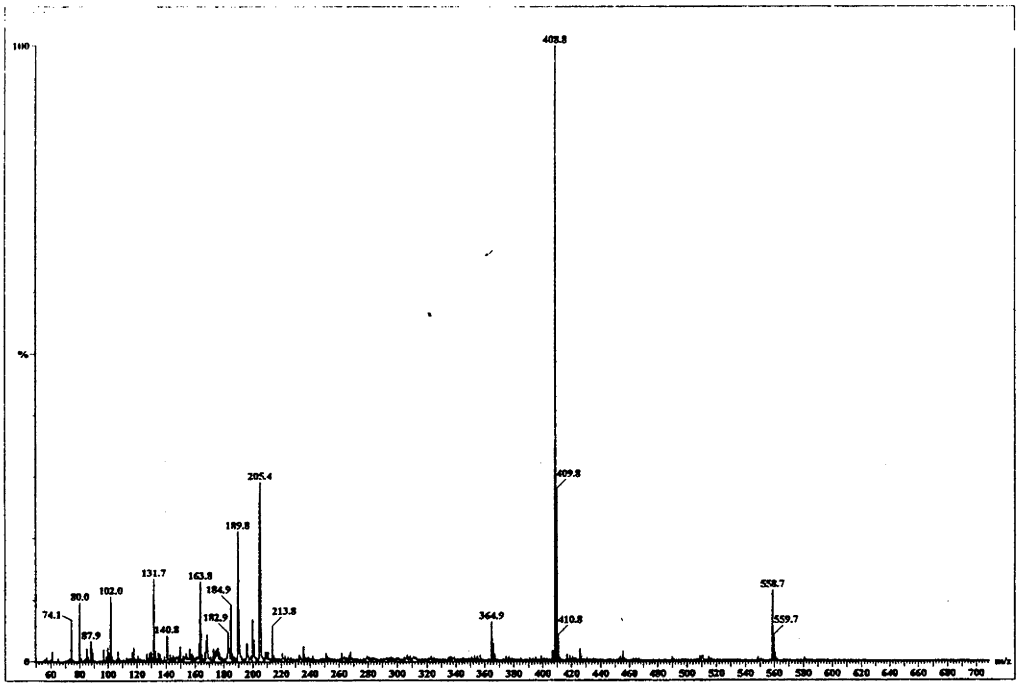

Figure 31. ESM spectrum of aqueous $[Mn^{III}(Me,CO_2^-\text{-}2\text{-oxosar-H})]^+$ (Cone Voltage = 50 V).

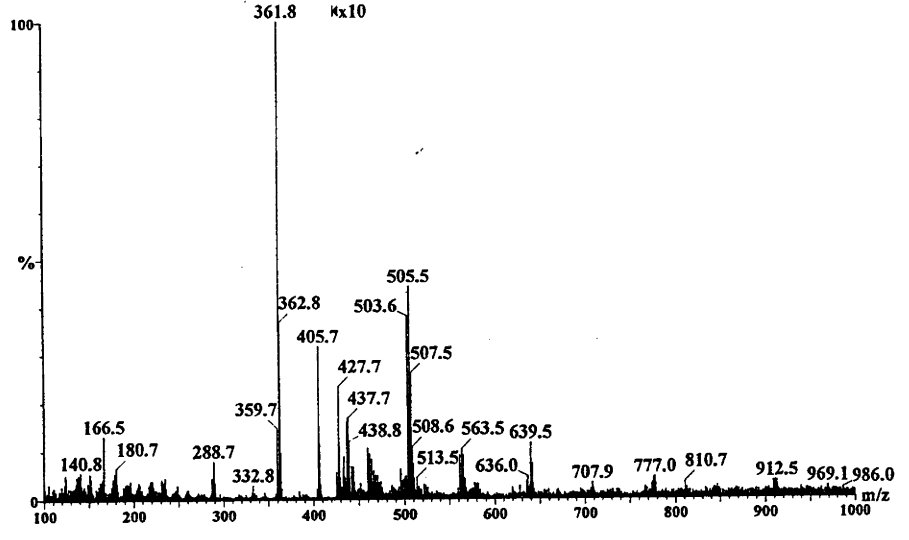

Figure 32. ESM spectrum of aqueous $[Cr^{III}(Me,CO_2H\text{-}2\text{-oxosar-H})]^{2+}$ (Cone Voltage = 80 V).

3.3.3.4 X-ray Crystallography

The Crystal Structure of $[Ni^{II}(Me,COO^{-}\text{-}2\text{-}oxosar)]_2(ClO_4)_2.3H_2O$

An X-ray crystallographic analysis of the perchlorate salt was obtained. The ORTEP diagrams of the two cations within the crystal are depicted in Figure 33 and 34. The bond distances and angles for each structure are compiled in Tables 11 and 12. Other relevant crystallographic data appears in Appendix 3.

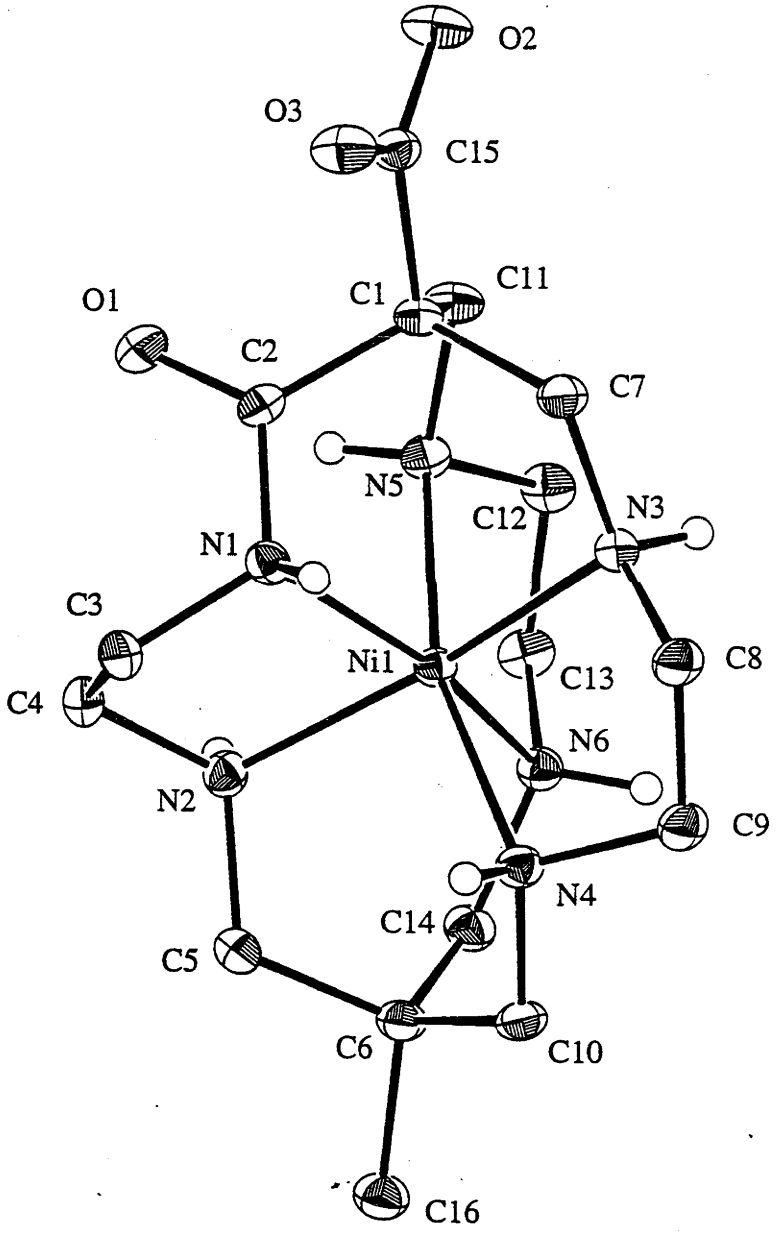

Figure 33. Thermal ellipsoid diagram of cation 1 of $[Ni^{II}(Me,COO^{-}\text{-}2\text{-}oxosar)]_2(ClO_4)_2.3H_2O$ with labelling of selected atoms. Ellipsoids show 30% probability levels. Hydrogen atoms bonded to nitrogen atoms are drawn as circles with small radii; all other hydrogen atoms have been omitted.

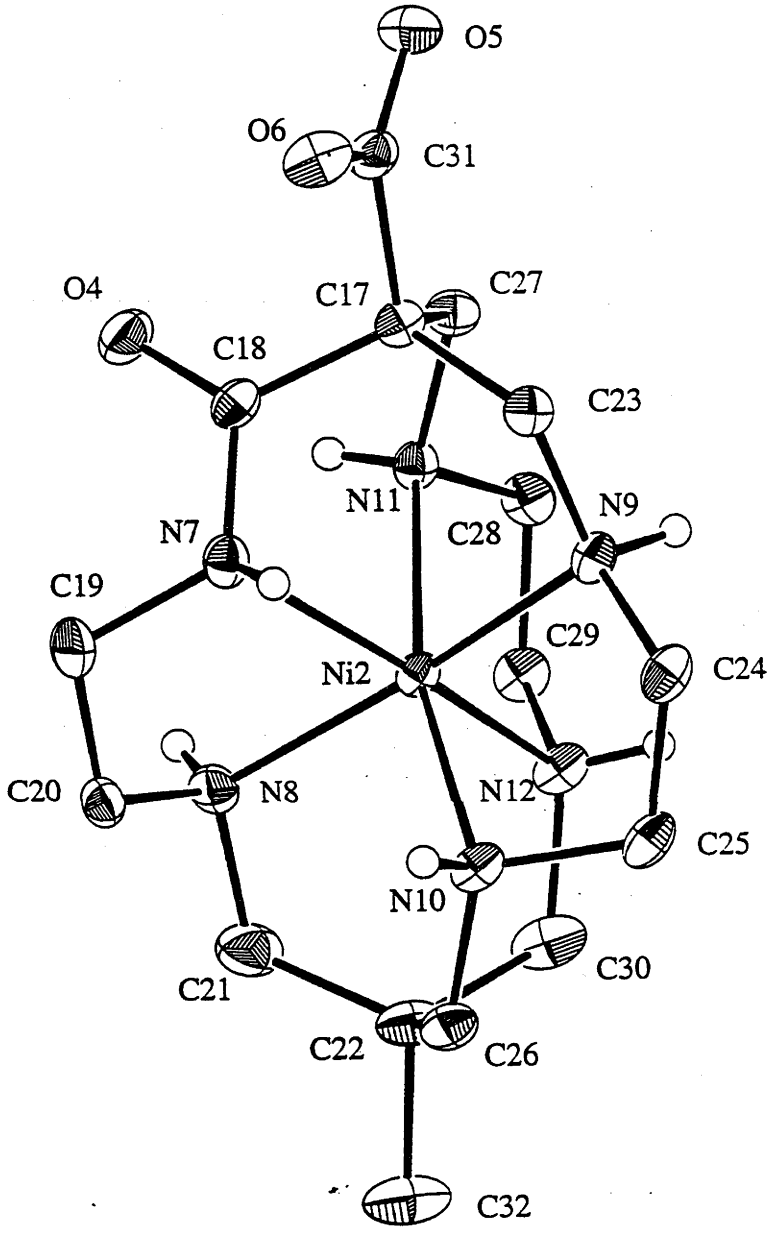

Figure 34. Thermal ellipsoid diagram of cation 2 of $[Ni^{II}(Me,COO^{-}\text{-}2\text{-}oxosar)]_2(ClO_4)_2.3H_2O$ with labelling of selected atoms. Ellipsoids show 30% probability levels. Hydrogen atoms bonded to nitrogen atoms are drawn as circles with small radii; all other hydrogen atoms have been omitted.

Table 11. Bond distances (Å) for cation 1 and 2 of $[Ni^{II}(Me,COO^{-}\text{-}2\text{-}oxosar)]_2(ClO_4)_2.3H_2O$

Atom	Distance (Å)	Atom	Distance (Å)
Ni(1)-N(1)	2.253(3)	Ni(1)-N(2)	2.076(3)
Ni(1)-N(3)	2.118(2)	Ni(1)-N(4)	2.095(3)
Ni(1)-N(5)	2.146(3)	Ni(1)-N(6)	2.101(2)
Ni(2)-N(7)	2.277(3)	Ni(2)-N(8)	2.076(3)
Ni(2)-N(9)	2.091(3)	Ni(2)-N(10)	2.088(3)
Ni(2)-N(11)	2.136(3)	Ni(2)-N(12)	2.070(3)
Cl(1)-O(7)	1.388(3)	Cl(1)-O(7a)	1.43(1)*
Cl(1)-O(8)	1.447(4)	Cl(1)-O(8a)	1.34(1)*
Cl(1)-O(9)	1.416(3)	Cl(1)-O(9a)	1.41(1)*
Cl(1)-O(10)	1.426(4)	Cl(1)-O(10a)	1.43(1)*
Cl(2)-O(11)	1.404(3)	Cl(2)-O(12)	1.369(3)
Cl(2)-O(13)	1.423(4)	Cl(2)-O(14)	1.391(4)
O(1)-C(2)	1.198(4)	O(2)-C(15)	1.247(4)
O(3)-C(15)	1.250(4)	O(4)-C(18)	1.218(4)
O(5)-C(31)	1.252(4)	O(6)-C(31)	1.256(4)
O(19)-O(20)	1.241(7)		
N(1)-C(2)	1.398(4)	N(1)-C(3)	1.481(4)
N(2)-C(4)	1.491(4)	N(2)-C(5)	1.490(4)
N(3)-C(7)	1.493(4)	N(3)-C(8)	1.481(4)
N(4)-C(9)	1.480(4)	N(4)-C(10)	1.485(4)
N(5)-C(11)	1.487(4)	N(5)-C(12)	1.489(4)
N(6)-C(13)	1.473(4)	N(6)-C(14)	1.499(4)
N(7)-C(18)	1.381(4)	N(7)-C(19)	1.476(4)
N(8)-C(20a)	1.58(2)	N(8)-C(20)	1.485(5)
N(8)-C(21)	1.488(5)	N(9)-C(23)	1.484(4)
N(9)-C(24)	1.490(4)	N(10)-C(25)	1.479(4)
N(10)-C(26)	1.487(4)	N(11)-C(27)	1.486(4)
N(11)-C(28)	1.482(4)	N(12)-C(29)	1.478(4)

* Restrained during refinement

Table 11 cont. Bond distances (Å) for cation 1 and 2 of $[Ni^{II}(Me,COO^{-}\text{-}2\text{-}oxosar)]_2(ClO_4)_2.3H_2O$

Atom	Distance (Å)	Atom	Distance (Å)
N(12)-C(30)	1.484(4)	C(1)-C(2)	1.526(4)
C(1)-C(7)	1.534(4)	C(1)-C(11)	1.540(4)
C(1)-C(15)	1.554(4)	C(3)-C(4)	1.508(5)
C(5)-C(6)	1.543(4)	C(6)-C(10)	1.526(4)
C(6)-C(14)	1.535(4)	C(6)-C(16)	1.533(4)
C(8)-C(9)	1.498(4)	C(12)-C(13)	1.508(4)
C(17)-C(18)	1.521(4)	C(17)-C(23)	1.538(4)
C(17)-C(27)	1.584(4)	C(17)-C(31)	1.561(4)
C(19)-C(20a)	1.36(2)	C(19)-C(20)	1.477(6)
C(21)-C(22)	1.497(5)	C(22)-C(26)	1.527(4)
C(22)-C(30)	1.553(5)	C(22)-C(32)	1.538(5)
C(24)-C(25)	1.511(5)	C(28)-C(29)	1.510(5)

* Restrained during refinement

Table 12. Bond angles (°) for $[Ni^{II}(Me,CO_2^-\text{-}2\text{-}oxosar)]_2(ClO_4)_2.3H_2O$.

Atom	Angle(°)	Atom	Angle(°)	Atom	Angle(°)	Atom	Angle(°)
N(1)-Ni(1)-N(2)	81.1(1)	N(1)-Ni(1)-N(3)	84.1(1)	O(8a)-Cl(1)-O(9a)	117(1)*	O(8a)-Cl(1)-O(10a)	111(1)*
N(1)-Ni(1)-N(4)	99.3(1)	N(1)-Ni(1)-N(5)	93.1(1)	O(9)-Cl(1)-O(10)	106.8(3)	O(9a)-Cl(1)-O(10a)	105.1(9)*
N(1)-Ni(1)-N(6)	165.7(1)	N(2)-Ni(1)-N(3)	164.4(1)	O(11)-Cl(2)-O(12)	110.8(3)	O(11)-Cl(2)-O(13)	107.3(2)
N(2)-Ni(1)-N(4)	94.0(1)	N(2)-Ni(1)-N(5)	100.2(1)	O(11)-Cl(2)-O(14)	112.1(3)	O(12)-Cl(2)-O(13)	110.3(3)
N(2)-Ni(1)-N(6)	85.9(1)	N(3)-Ni(1)-N(4)	83.1(1)	O(12)-Cl(2)-O(14)	108.9(3)	O(13)-Cl(2)-O(14)	107.5(3)
N(3)-Ni(1)-N(5)	85.9(1)	N(3)-Ni(1)-N(6)	109.2(1)	Ni(1)-N(1)-C(2)	99.3(2)	Ni(1)-N(1)-C(3)	106.8(2)
N(4)-Ni(1)-N(5)	162.5(1)	N(4)-Ni(1)-N(6)	87.6(1)	C(2)-N(1)-C(3)	117.4(3)	Ni(1)-N(2)-C(4)	111.6(2)
N(5)-Ni(1)-N(6)	83.2(1)	N(7)-Ni(2)-N(8)	79.7(1)	Ni(1)-N(2)-C(5)	110.7(2)	C(4)-N(2)-C(5)	114.1(2)
N(7)-Ni(2)-N(9)	88.5(1)	N(7)-Ni(2)-N(10)	98.1(1)	Ni(1)-N(3)-C(7)	114.2(2)	Ni(1)-N(3)-C(8)	107.5(2)
N(7)-Ni(2)-N(11)	90.0(1)	N(7)-Ni(2)-N(12)	168.9(1)	C(7)-N(3)-C(8)	110.0(2)	Ni(1)-N(4)-C(9)	106.4(2)
N(8)-Ni(2)-N(9)	166.1(1)	N(8)-Ni(2)-N(10)	90.7(1)	Ni(1)-N(4)-C(10)	115.4(2)	C(9)-N(4)-C(10)	111.6(2)
N(8)-Ni(2)-N(11)	100.7(1)	N(8)-Ni(2)-N(12)	92.5(1)	Ni(1)-N(5)-C(11)	116.5(2)	Ni(1)-N(5)-C(12)	104.5(2)
N(9)-Ni(2)-N(10)	83.7(1)	N(9)-Ni(2)-N(11)	86.4(1)	C(11)-N(5)-C(12)	112.2(2)	Ni(1)-N(6)-C(13)	108.5(2)
N(9)-Ni(2)-N(12)	100.2(1)	N(10)-Ni(2)-N(11)	167.0(1)	Ni(1)-N(6)-C(14)	113.2(2)	C(13)-N(6)-C(14)	112.6(2)
N(10)-Ni(2)-N(12)	89.7(1)	N(11)-Ni(2)-N(12)	83.7(1)	Ni(2)-N(7)-C(18)	99.3(2)	Ni(2)-N(7)-C(19)	107.9(2)
O(7)-Cl(1)-O(8)	111.7(2)	O(7)-Cl(1)-O(9)	115.4(3)	C(18)-N(7)-C(19)	118.1(3)	Ni(2)-N(8)-C(20a)	111.4(7)
O(7)-Cl(1)-O(10)	107.6(3)	O(7a)-Cl(1)-O(8a)	112(1)*	Ni(2)-N(8)-C(20)	106.2(2)	Ni(2)-N(8)-C(21)	113.1(2)
O(7a)-Cl(1)-O(9a)	106.5(9)*	O(7a)-Cl(1)-O(10a)	104.5(9)*	C(20a)-N(8)-C(21)	132.2(7)		
O(8)-Cl(1)-O(9)	107.7(2)	O(8)-Cl(1)-O(10)	107.2(3)	C(20)-N(8)-C(21)	109.4(3)	Ni(2)-N(9)-C(23)	112.0(2)

* Restrained during refinement

Table 12 cont. Bond angles (°) for $[Ni^{II}(Me,CO_2^-\text{-}2\text{-}oxosar)]_2(ClO_4)_2.3H_2O$.

Atom	Angle(°)	Atom	Angle(°)	Atom	Angle(°)	Atom	Angle(°)
Ni(2)-N(9)-C(24)	109.0(2)	C(23)-N(9)-C(24)	113.0(2)	N(6)-C(14)-C(6)	114.1(2)	O(2)-C(15)-O(3)	125.2(3)
Ni(2)-N(10)-C(25)	103.6(2)	Ni(2)-N(10)-C(26)	114.9(2)	O(2)-C(15)-C(1)	118.8(3)	O(3)-C(15)-C(1)	115.9(3)
C(25)-N(10)-C(26)	113.2(3)	Ni(2)-N(11)-C(27)	114.6(2)	C(18)-C(17)-C(23)	115.5(3)	C(18)-C(17)-C(27)	104.2(2)
Ni(2)-N(11)-C(28)	106.5(2)	C(27)-N(11)-C(28)	112.9(2)	C(18)-C(17)-C(31)	106.6(3)	C(23)-C(17)-C(27)	111.0(3)
Ni(2)-N(12)-C(29)	105.8(2)	Ni(2)-N912)-C(30)	115.2(2)	C(23)-C(17)-C(31)	106.6(2)	C(27)-C(17)-C(31)	113.0(3)
C(29)-N(12)-C(30)	114.0(3)	C(2)-C(1)-C(7)	115.1(2)	O(4)-C(18)-N(7)	122.9(3)	O(4)-C(18)-N(17)	118.9(3)
C(2)-C(1)-C(11)	105.3(2)	C(2)-C(1)-C(15)	108.4(2)	N(7)-C(18)-C(17)	117.3(3)	N(7)-C(19)-C(20a)	115.3(8)
C(7)-C(1)-C(11)	111.0(3)	C(7)-C(1)-C(15)	105.6(2)	N(7)-C(19)-C(20)	111.2(3)	N(8)-C(20a)-C(19)	113(1)
C(11)-C(1)-C(15)	111.5(2)	O(1)-C(2)-N(1)	121.7(3)	N(8)-C(20)-C(19)	112.1(3)		
O(1)-C(2)-C(1)	120.6(3)	N(1)-C(2)-C(1)	117.0(3)	N(8)-C(21)-C(22)	117.3(3)	C(21)-C(22)-C(26)	114.2(3)
N(1)-C(3)-C(4)	110.4(2)	N(2)-C(4)-C(3)	111.4(3)	C(21)-C(22)-C(30)	111.4(3)	C(21)-C(22)-C(32)	107.5(3)
N(2)-C(5)-C(6)	113.1(2)	C(5)-C(6)-C(10)	111.3(3)	C(26)-C(22)-C(30)	110.7(3)	C(26)-C(22)-C(32)	106.4(3)
C(5)-C(6)-C(14)	110.7(3)	C(5)-C(6)-C(16)	108.8(3)	C(30)-C(22)-C(32)	106.2(3)	N(9)-C(23)-C(17)	112.9(2)
C(10)-C(6)-C(14)	111.2(3)	C(10)-C(6)-C(16)	107.0(3)	N(9)-C(24)-C(25)	109.7(3)	N(10)-C(25)-C(24)	109.6(3)
C914)-C(6)-C(16)	107.5(3)	N(3)-C(7)-C(1)	113.5(2)	N(10)-C(26)-C(22)	115.2(3)	N(11)-C(27)-C(17)	110.4(2)
N(3)-C(8)-C(9)	109.1(3)	N(4)-C(9)-C(8)	109.0(3)	N(11)-C(28)-C(29)	109.6(2)	N(12)-C(29)-C(28)	108.2(3)
N(4)-C(10)-C(6)	113.1(3)	N(5)-C(11)-C(1)	111.2(2)	N(12)-C(30)-C(22)	115.1(3)	O(5)-C(31)-O(6)	126.5(3)
N(5)-C(12)-C(13)	109.0(2)	N(6)-C(13)-C(12)	109.6(2)	O(5)-C(31)-C(17)	119.0(3)	O(6)-C(31)-C(17)	114.5(3)

* Restrained during refinement

Both cations show that the Ni(II) is six coordinate being bound to five secondary amines and an amide nitrogen atom. The most interesting aspect of each structure is that while the metal is bound to the amide nitrogen the nitrogen atom is also protonated. Basically the metal ion bonds π to the amide group to give a pseudo-tetrahedral geometry about the N atom. Both cations also possess a deprotonated carboxyl group in the apical position giving each cation an overall charge of 1+. The main difference between the two cations comes through the conformation of the five membered chelate rings. For cation 1 (Figure 33) the two amide free five membered chelate rings have adopted a *lel* conformation while for the remaining amide strap, the chelate ring displays an *ob* conformation about the long axis through the metal. Overall, the cation displays a lel_2ob conformation which is similar to that observed for $[Co^{III}(Me,CO_2H\text{-}2\text{-}oxosar\text{-}H)](ClO_4)_2.0.5H_2O$.[2] The second cation (Figure 34) displays a slightly different conformation in that all three five membered chelate rings possess a *lel* configuration giving the complex a lel_3 configuration. This is similar to the conformation observed for $[Ni^{II}(\{NH_3^+\}_2\text{-}sar)]^{4+}$.[38]

The $Ni\text{-}N_{(amine)}$ distances for both cations are similar to those observed for $[Ni^{II}(\{NH_3^+\}_2\text{-}sar)]^{4+}$ (2.097 Å to 2.119 Å).[38] However, the $Ni\text{-}N_{(amide)}$ distance normally associated with deprotonated amido cage complexes does not arise for either cation. In fact, the $Ni\text{-}N_{(amide)}$ distance for both systems is slightly longer than the $Ni\text{-}N_{(amine)}$ bond lengths of each respective cation. Again this is due to each amide nitrogen atom being protonated and bonded π to the Ni(II) ion. The type of bonding observed in these systems also affects the bond distances in the actual amide group. Normally, for a deprotonated metal bound amido group the $C\text{-}N_{(amido)}$ and $C\text{-}O_{(amido)}$ distances should be approximately 1.30 Å and 1.24 Å respectively.[24] Also for an unbound secondary amide group the $C\text{-}N_{(amide)}$ and $C\text{-}O_{(amide)}$ bond lengths are 1.325 Å and 1.24 Å.[24] For cation 1 the $C\text{-}N_{(amide)}$ distance (1.398 Å) is longer than both of the expected $C\text{-}N_{(amido/amide)}$ distances while the $C\text{-}O_{(amide)}$ length (1.198 Å) is shorter than the usual $C\text{-}O_{(amido/amide)}$ distances. The same situation exists of cation 2 where the $C\text{-}N_{(amide)}$ and $C\text{-}O_{(amide)}$ distances are 1.381 Å and 1.218 Å respectively. However, the $C\text{-}N_{(amide)}$ distances of each cation are still shorter than that expected for a $C\text{-}N_{(amine)}$ distance of 1.45 Å.

The N-Ni-N bond angles of each cation show that the Ni(II) ion displays a distorted octahedral symmetry. However this is not unexpected as the $[Ni^{II}(\{NH_3^+\}_2\text{-}sar)]^{4+}$ ion possesses a similar type of distorted NiN_6

octahedral core.[38] The average twist angles for cation 1 and 2 are 42° and 45° respectively. In addition, as a consequence of this distortion the two N_3 planes, for each cation, are not set parallel to each other. For cation 1 the angle between the two planes is 5.52° while for cation 2 it is 0.86°. Also, the torsion angles of the five membered chelate rings are somewhat different for each cation. In cation 1 the five membered chelate ring, N(1)-C(3)-C(4)-N(2) containing the amide nitrogen atom, possesses a torsion angle of 50° while the two remaining amide free chelate rings, namely N(3)-C(8)-C(9)-N(4) and N(5)-C(12)-C(13)-N(6), display angles of -56° and -57° respectively. For cation 2 the amide chelate ring, N(7)-C(19)-C(20)-N(8), has a torsion angle of 41° while the two remaining chelate rings, N(9)-C(24)-C(25)-N(10) and N(11)-C(28)-C(29)-N(12), have angles of -52° and -57° respectively.

The Crystal Structure of $[Cu^{II}(Me\text{-}2\text{-}oxosar)](ClO_4)_2.1.3H_2O$

The structure of the complex along with the bond distances and angles are listed in Figure 35, and Tables 13 and 14 respectively. The structure confirms that the ligand acts as a pentadentate, and has lost the carboxyl group from the apex. The amide nitrogen atom remains unbound and has retained its proton. In addition the two five-membered chelate rings adopt a *lel* configuration with respect to the long axis through the complex. The remaining strand is skewed so that the plane of the amide group is perpendicular to the axis joining the amide N and Cu atoms but they are separated by ~3 Å and are therefore not considered bonded. This is a very similar orientation to that of the Ni complex but without the distortion of the planar amide group.

Interestingly, the Cu(II) amide system displays four short and one long $Cu\text{-}N_{(amine)}$ distances while the remaining non-bonded amide nitrogen atom is approximately 3 Å from the Cu(II) ion. This is in contrast to the hexadentate $[Cu^{II}(\{NH_3^+\}_2\text{-}sar)]^{4+}$ ion which posesses two short, two medium and two long $Cu\text{-}N_{(amine)}$ bond lengths.[39] The $Cu\text{-}N_{(amine)}$ distances are generally shorter than the average $Cu\text{-}N_{(amine)}$ bond lengths observed for $[Cu^{II}(\{NH_3^+\}_2\text{-}sar)]^{4+}$, (2.169 Å),[40] with the exception of Cu-N(2), that has a distance of 2.279(6) Å. The $Cu\text{-}N_{(amine)}$ distances observed for the amide complex, except for Cu-N(2), are also shorter than the $Cu\text{-}N_{(amine)}$ range exhibited for a series of secondary amine Cu(II) complexes (2.15 Å to 2.18 Å).[39] However, the $Cu\text{-}N_{(amine)}$ distances of the pentadentate $[Cu^{II}(N\text{-}Me_5sar)(OClO_3)]^+$ and $[Cu^{II}(N\text{-}Me_7sar)(OClO_3)]^{2+}$ ions are comparable to those of $[Cu^{II}(Me\text{-}2\text{-}oxosar)](ClO_4)_2.1.3H_2O$.[41] The unbound $N\text{-}C_{(amide)}$ distance is shorter than the expected $N\text{-}C_{(free\ peptide)}$

bond length of 1.325 Å, but the C-$O_{(amide)}$ is similar to the normal C-$O_{(free\ peptide)}$ value of 1.24 Å.[24]

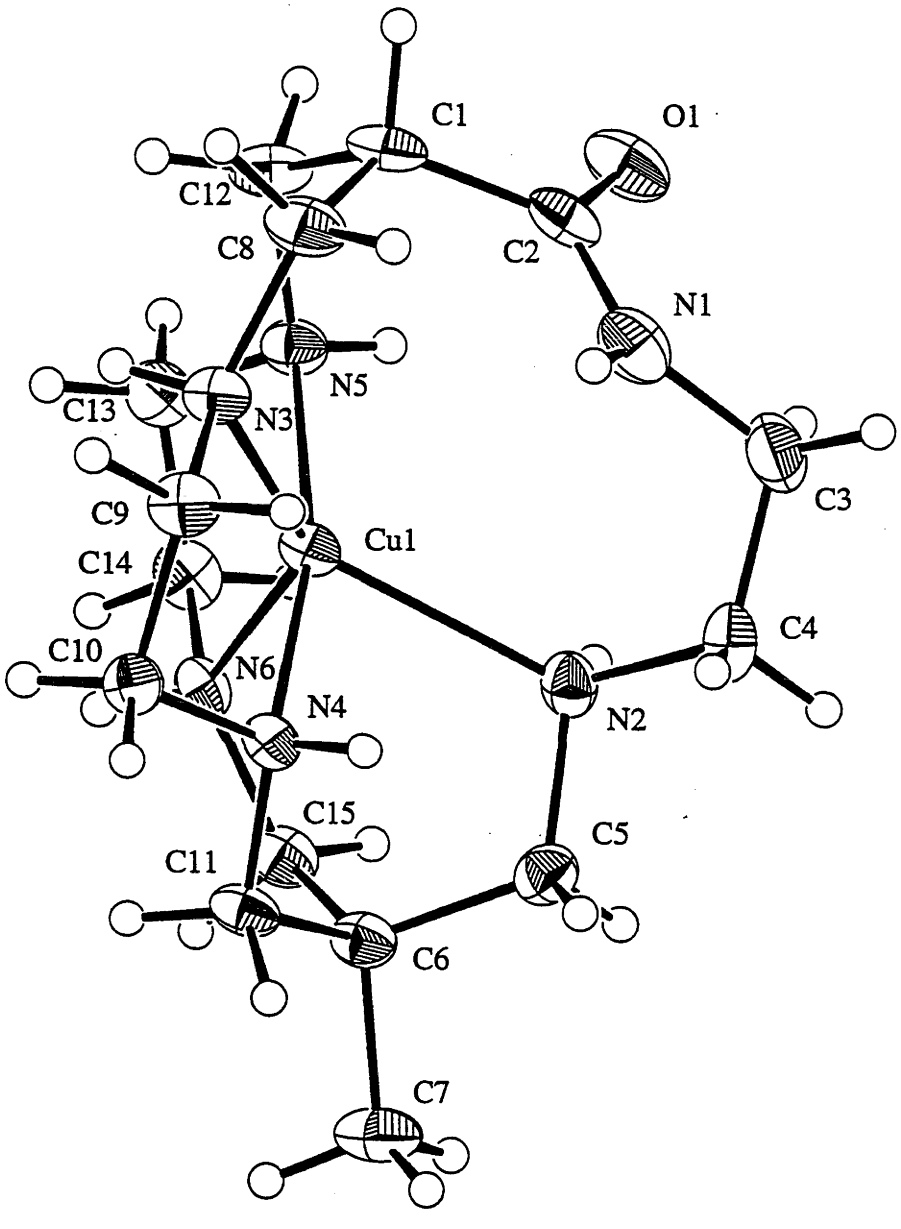

Figure 35. Thermal ellipsoid diagram of the $[Cu^{II}(Me\text{-}2\text{-}oxosar)](ClO_4)_2.1.3H_2O$ cation with labelling of selected atoms. Ellipsoids show 50% probability levels, except for hydrogen atoms which are drawn as spheres of arbitary radius.

Table 13. Bond distances (Å) for $[Cu^{II}(Me\text{-}2\text{-}oxosar)](ClO_4)_2.1.3H_2O$

Atom	Distance (Å)	Atom	Distance (Å)
Cu-N(1)	3.075(6)		
Cu-N(2)	2.279(6)	Cu-N(3)	2.040(5)
Cu-N(4)	1.995(5)	Cu-N(5)	2.031(5)
Cu-N(6)	2.059(5)	Cl(1)-O(2a)	1.535(8)*
Cl(1)-O(2b)	1.456(8)*	Cl(1)-O(3a)	1.373(8)*
Cl(1)-O(3b)	1.152(8)*	Cl(1)-O(4a)	1.428(8)*
Cl(1)-O(4b)	1.414(8)*	Cl(1)-O(5a)	1.433(8)*
Cl(1)-O(5b)	1.374(8)*	Cl(2)-O(6)	1.393(7)*
Cl(2)-O(7)	1.391(7)	Cl(2)-O(8)	1.393(7)
Cl(2)-O(9)	1.401(7)	O(1)-C(2)	1.236(9)
N(1)-C(2)	1.315(9)	N(1)-C(3)	1.439(10)
N(2)-C(4)	1.479(9)	N(2)-C(5)	1.491(8)
N(3)-C(8)	1.493(9)	N(3)-C(9)	1.483(8)
N(4)-C(10)	1.476(8)	N(4)-C(11)	1.467(8)
N(5)-C(12)	1.486(8)	N(5)-C(13)	1.470(8)
N(6)-C(14)	1.480(8)	N(6)-C(15)	1.463(8)
C(1)-C(2)	1.53(1)	C(1)-C(8)	1.538(10)
C(1)-C(12)	1.54(1)	C(3)-C(4)	1.51(1)
C(5)-C(6)	1.530(10)	C(6)-C(7)	1.525(9)
C(6)-C(11)	1.541(9)	C(6)-C(15)	1.536(10)
C(9)-C(10)	1.520(9)	C(13)-C(14)	1.495(10)

*Restrained during refinement

Table 14. Bond angles (°) for $[Cu^{II}(Me\text{-}2\text{-}oxosar)](ClO_4)_2.1.3H_2O$.

Atom	Angle (°)	Atom	Angle (°)	Atom	Angle (°)	Atom	Angle (°)
N(2)-Cu-N(3)	132.7(2)	N(2)-Cu-N(4)	83.8(2)	C(12)-N(5)-C(13)	113.7(6)	Cu-N(6)-C(14)	109.4(4)
N(2)-Cu-N(5)	107.6(2)	N(2)-Cu-N(6)	90.2(2)	Cu-N(6)-C(15)	115.7(4)	C(14)-N(6)-C(15)	114.7(5)
N(3)-Cu-N(4)	84.4(2)	N(3)-Cu-N(5)	90.3(2)	C(2)-C(1)-C(8)	117.6(7)	C(2)-C(1)-C(12)	105.4(6)
N(3)-Cu-N(6)	136.0(2)	N(4)-Cu-N(5)	167.9(3)	C(8)-C(1)-C(12)	111.9(6)	O(1)-C(2)-N(1)	123.0(8)
N(4)-Cu-N(6)	92.3(2)	N(5)-Cu-N(6)	83.9(2)	O(1)-C(2)-C(1)	118.4(7)	N(1)-C(2)-C(1)	118.1(7)
O(2a)-Cl(1)-O(3a)	107.7(6)*	O(2a)-Cl(1)-O(4a)	101.2(6)*	N(1)-C(3)-C(4)	110.4(6)	N(2)-C(4)-C(3)	112.6(6)
O(2a)-Cl(1)-O(5a)	103.0(6)	O(3a)-Cl(1)-O(4a)	116.6(7)*	N(2)-C(5)-C(6)	116.7(6)	C(5)-C(6)-C(7)	106.9(6)
O(3a)-Cl(1)-O(5a)	115.0(6)*	O(4a)-Cl(1)-O(5a)	111.3(6)*	C(5)-C(6)-C(11)	111.3(6)	C(5)-C(6)-C(15)	111.6(6)
O(2b)-Cl(1)-O(3b)	103.9(7)*	O(2b)-Cl(1)-O(4b)	107.0(7)*	C(7)-C(6)-C(11)	108.4(6)	C(7)-C(6)-C(15)	107.9(6)
O(2b)-Cl(1)-O(5b)	113.2(7)*	O(3b)-Cl(1)-O(4b)	104.7(7)*	C(11)-C(6)-C(15)	110.6(6)	N(3)-C(8)-C(1)	111.5(5)
O(3b)-Cl(1)-O(5b)	107.9(7)*	O(4b)-Cl(1)-O(5b)	118.7(7)*	N(3)-C(9)-C(10)	108.1(5)	N(4)-C(10)-C(9)	106.6(5)
O(6)-Cl(2)-O(7)	110.3(5)	O(6)-Cl(2)-O(8)	106.4(5)	N(4)-C(11)-C(6)	112.5(5)	N(5)-C(12)-C(1)	110.8(6)
O(6)-Cl(2)-O(9)	106.0(6)	O(7)-Cl(2)-O(8)	115.5(5)	C(5)-C(13)-C(14)	109.4(6)	N(6)-C(14)-C(13)	108.0(5)
O(7)-Cl(2)-O(9)	109.6(5)	O(8)-Cl(2)-O(9)	108.7(6)	N(6)-C(15)-C(6)	113.3(5)		
C(2)-N(1)-C(3)	122.9(7)	Cu-N(2)-C(4)	123.5(4)	N(1)-Cu-N(2)	63.5(2)	N(1)-Cu-N(3)	77.9(2)
Cu-N(2)-C(5)	109.2(4)	C(4)-N(2)-C(5)	108.5(6)	N(1)-Cu-N(4)	109.7(2)	N(1)-Cu-N(5)	79.7(2)
Cu-N(3)-C(8)	119.2(4)	Cu-N(3)-C(9)	10.9(4)	N(1)-Cu-N(6)	142.5(2)		
C(8)-N(3)-C(9)	114.3(5)	Cu-N(4)-C(10)	107.0(4)				
Cu-N(4)-C(11)	114.4(4)	C(10)-N(4)-C(11)	115.8(5)				
Cu-N(5)-C(12)	116.5(4)	Cu-N(5)-C(13)	106.1(4)				

*Restrained during refinement

The symmetry about the Cu(II) ion for $[Cu^{II}(Me\text{-}2\text{-}oxosar)](ClO_4)_2.1.3H_2O$ can best be described as a distorted square pyramid with the N-Cu-N angles varying considerably from ideal square pyramid values. However, this type of distorted geometry has been observed previously in other five-coordinate Cu(II) amine complexes.[42-46] In total, the evidence indicates the Cu complex should be viewed as a five-coordinate distorted square pyramidal complex with the amide group not bonded to the Cu^{II} ion.

The Crystal Structure of $[Fe^{III}(Me,CO_2H\text{-}2\text{-}oxosar\text{-}H)](ClO_4)_2.0.5H_2O$

The structure of the Fe(III) complex appears in Figure 36, and the bond distances and angles appear Tables 15 and 16 respectively. The structure confirms that the ligand is hexadentate; five coordination sites come from the secondary amines and the other from the deprotonated amide nitrogen. For the two sectors excluding the amide group, the five membered chelate rings adopt a *lel* configuration, while for the remaining amide strap, its five membered chelate ring possesses an *ob* conformation about the long axis through the metal. Therefore the cage complex displays a lel_2ob conformation. In addition the structure shows that the six N donors are at the corners of a slightly distorted octahedron. These properties are also seen for $[Co^{III}(Me,CN\text{-}2\text{-}oxosar\text{-}H)](ClO_4)_{3/2}Cl_{1/2}.H_2O$ and $[Co^{III}(Me,CO_2H\text{-}2\text{-}oxosar\text{-}H)](ClO_4)_2.0.5H_2O$.[2]

The $Fe\text{-}N_{(amine)}$ distances are similar to the average $Fe\text{-}N_{(amine)}$ bond lengths observed for $[Fe^{III}(sar)]^{3+}$, (2.007 Å)[47], with the exception of Fe-N(4) and Fe-N(6), that have distances of 1.970(9) Å and 2.017(8) Å respectively. The $Fe\text{-}N_{(amine)}$ distances observed are similar to the average distance reported for $[Fe(tacn)_2]^{3+}$ (1.998 Å).[48,49] Like the Co(III) complexes the $Fe\text{-}N_{(amido)}$ bond, 1.886(8) Å, is shorter than the other saturated amine distances and is also shorter than the average $Fe\text{-}N_{(amido)}$ distance (1.927 Å) reported for the five coordinate $[Fe^{III}Cl(\eta^4\text{-}MAC)]^{2-}$ tetraamido macrocyclic complex.[50] The N(1)-C(2) amide bond length (1.33(1) Å) is longer than the $N\text{-}C_{(peptide)}$ distance (1.30 Å)[24], while the remaining cap C-N bonds have distances comparable to those observed for $[Fe^{III}(sar)]^{3+}$.[47] The C(2)-O(1) bond length (1.25(1) Å) is also shorter than the anticipated $C\text{-}O_{(peptide)}$ value of 1.27 Å.[24]

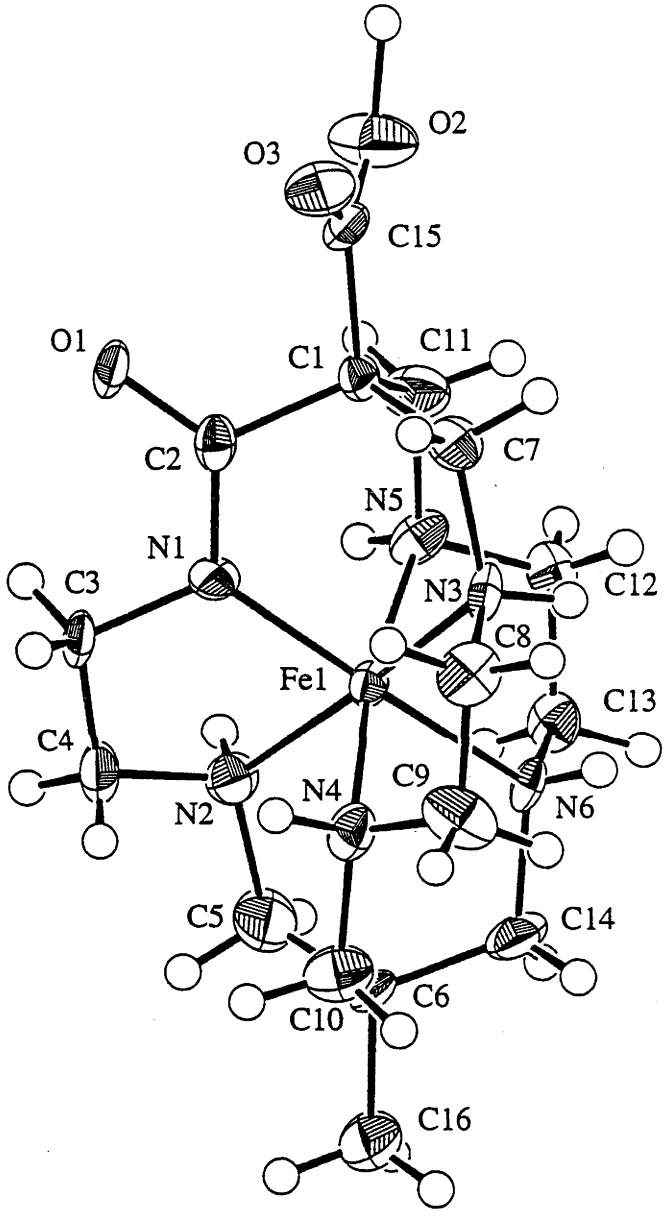

Figure 36. Thermal ellipsoid diagram of the $[Fe^{III}(Me,CO_2H\text{-}2\text{-}oxosar\text{-}H)](ClO_4)_2.0.5H_2O$ cation with labelling of selected atoms. Ellipsoids show 50% probability levels, except for hydrogen atoms which are drawn as spheres of arbitary radius.

Table 15. Bond distances (Å) for $[Fe^{III}(Me,CO_2H\text{-}2\text{-}oxosar\text{-}H)](ClO_4)_2.0.5H_2O$

Atom	Distance (Å)	Atom	Distance (Å)
Fe-N(1)	1.886(8)	Fe-N(2)	2.008(9)
Fe-N(3)	2.010(9)	Fe-N(4)	1.970(9)
Fe-N(5)	2.002(9)	Fe-N(6)	2.017(8)
Cl(1)-O(5)	1.41(1)	Cl(1)-O(6)	1.40(1)
Cl(1)-O(7)	1.40(1)	Cl(1)-O(8)	1.35(1)
Cl(21)-O(9)	1.25(1)		
Cl(21)-O(10)	1.40(2)	Cl(21)-O(11)	1.24(1)
Cl(21)-O(121)	1.33(3)	Cl(22)-O(9)	1.44(2)
Cl(22)-O(10)	1.12(2)	Cl(22)-O(11)	1.38(1)
Cl(22)-O(122)	1.27(2)	O(1)-C(2)	1.25(1)
O(2)-C(15)	1.32(1)	O(3)-C(15)	1.18(1)
N(1)-C(2)	1.33(1)	N(1)-C(3)	1.47(1)
N(2)-C(4)	1.50(1)	N(2)-C(5)	1.50(1)
N(3)-C(7)	1.49(1)	N(3)-C(8)	1.50(1)
N(4)-C(9)	1.49(1)	N(4)-C(10)	1.48(1)
N(5)-C(11)	1.50(1)	N(5)-C(12)	1.46(1)
N(6)-C(13)	1.48(1)	N(6)-C(14)	1.50(1)
C(1)-C(2)	1.55(1)	C(1)-C(7)	1.51(1)
C(1)-C(11)	1.55(1)	C(1)-C(15)	1.53(1)
C(3)-C(4)	1.50(2)	C(5)-C(6)	1.53(1)
C(6)-C(10)	1.53(1)	C(6)-C(14)	1.52(1)
C(6)-C(16)	1.50(1)	C(8)-C(9)	1.48(2)
C(12)-C(13)	1.49(2)		

Table 16. Bond angles (°) for $[Fe^{III}(Me,CO_2H\text{-}2\text{-}oxosar\text{-}H)](ClO_4)_2.0.5H_2O$.

Atom	Angle(°)	Atom	Angle(°)	Atom	Angle(°)	Atom	Angle(°)
N(1)-Fe-N(2)	82.2(4)	N(1)-Fe-N(3)	91.6(3)	Fe-N(3)-C(7)	115.6(6)	Fe-N(3)-C(8)	106.9(7)
N(1)-Fe-N(4)	99.3(4)	N(1)-Fe-N(5)	88.8(4)	C(7)-N(3)-C(8)	111.4(9)	Fe-N(4)-C(9)	108.2(7)
N(1)-Fe-N(6)	169.7(4)	N(2)-Fe-N(3)	170.0(4)	Fe-N(4)-C(10)	119.8(7)	C(9)-N(4)-C(10)	112.9(9)
N(2)-Fe-N(4)	86.9(4)	N(2)-Fe-N(5)	97.6(4)	Fe-N(5)-C(11)	116.4(6)	Fe-N(5)-C(12)	109.4(7)
N(2)-Fe-N(6)	91.9(3)	N(3)-Fe-N(4)	86.3(4)	C(11)-N(5)-C(12)	111.7(9)	Fe-N(6)-C(13)	107.8(6)
N(3)-Fe-N(5)	90.1(4)	N(3)-Fe-N(6)	95.4(3)	Fe-N(6)-C(14)	117.7(6)	C(13)-N(6)-C(14)	111.8(8)
N(4)-Fe-N(5)	171.2(4)	N(4)-Fe-N(6)	88.8(3)	C(2)-C(1)-C(7)	111.0(9)	C(2)-C(1)-C(11)	108.6(9)
N(5)-Fe-N(6)	83.6(4)	O(5)-Cl(1)-O(6)	109.8(9)	C(2)-C(1)-C(15)	108.8(9)	C(7)-C(1)-C(11)	110.9(9)
O(5)-Cl(1)-O(7)	109.2(7)	O(5)-Cl(1)-O(8)	110.1(7)	C(7)-C(1)-C(15)	106.5(9)	C(11)-C(1)-C(15)	111.0(9)
O(6)-Cl(1)-O(7)	110(1)	O(6)-Cl(1)-O(8)	105.8(8)	O(1)-C(2)-N(1)	125(1)	O(1)-C(2)-C(1)	120(1)
O(7)-Cl(1)-O(8)	112(1)	O(9)-Cl(21)-O(10)	106(1)	N(1)-C(2)-C(1)	114.8(9)	N(1)-C(3)-C(4)	108.1(8)
O(9)-Cl(21)-O(11)	127(1)	O(9)-Cl(21)-O(121)	113(1)	N()-C(4)-C(3)	111.1(9)	N(2)-C(5)-C(6)	113.1(9)
O(10)-Cl(21)-O(11)	113(1)	O(10)-Cl(21)-O(121)	81(1)	C(5)-C(6)-C(10)	111(1)	C(5)-C(6)-C(14)	111(1)
O(11)-Cl(121)-O(121)	108(1)	O(9)-Cl(22)-O(10)	111(2)	C(5)-C(6)-C(1)	107.2(9)	C(10)-C(6)-C(14)	110(1)
O(9)-Cl(22)-O(11)	104(1)	O(9)-Cl(22)-O(122)	113(1)	C(10)-C(6)-C(16)	109(1)	C(14)-C(6)-C(16)	109.1(9)
O(10)-Cl(22)-O(11)	124(2)	O(10)-Cl(22)-O(122)	105(2)	N(3)-C(7)-C(1)	115.3(9)	N(3)-C(8)-C(9)	109(1)
O(11)-Cl(22)-O(122)	99(1)	Cl(21)-O(9)-Cl(22)	28.9(5)	N(4)-C(9)-C(8)	108(1)	N(4)-C(10)-C(6)	114(1)
Cl(21)-O(10)-Cl(22)	29.4(8)	Cl(21)-O(11)-C(22)	30.4(5)	N(5)-C(11)-C(1)	114.0(9)	C(5)-C(12)-C(13)	107.5(9)
Fe-N(1)-C(2)	124.2(7)	Fe-N(1)-C(3)	117.6(6)	N(6)-C(13)-C(12)	106.1(9)	N(6)-C(14)-C(6)	114.6(9)
C(2)-N(1)-C(3)	115.8(9)	Fe-N(2)-C(4)	106.4(7)	O(2)-C(15)-O(3)	123(1)	O(2)-C(15)-C(1)	113(1)
Fe-N(2)-C(5)	117.9(7)	C(4)-N(2)-C(5)	111.1(9)	O(3)-C(15)-C(1)	124(1)		

The N-Fe-N bond angles of [Fe^{III}(Me,CO_2H-2-oxosar-H)](ClO_4)$_2$.0.5H_2O deviate slightly from the ideal angles expected for octahedral symmetry of the FeN_6 core; the angles vary by 2° to 10° from the ideal values. The average twist angle between the two sets of N_3 planes, perpendicular to the long axis through the metal, is 48.2°; the two N_3 planes also occur at an angle to one another (1.43°) which indicates the metal possesses a pseudo-octahedral character due to all of these small displacements. The introduction of an amide moiety has caused some change in the conformation of the basic cage structure. In this instance the five membered chelate ring, N(1)-C(3)-C(4)-C(2) containing the amide group, has a torsion angle of -25(1)° while the two remaining amide free chelate rings, namely N(3)-C(8)-C(9)-C(4) and N(5)-C(12)-C(13)-C(6), have torsion angles of -51(1)° and -55(1)° respectively.

Clearly, the structural data shows that the Fe(III) amido complex is a low spin d^5 ion with basically an octahedral configuration. It can therefore be expected to be kinetically inert to ligand loss and possibly able to sustain the Fe(IV) oxidation state.

3.3.3.5 Electrochemistry

The cyclic voltammograms of the Co(III), Fe(III), Mn(III), Cu(II), Ni(II), Fe(II) and Mn(II) amide cage complexes at 20 mVs^{-1} appear in Figure 37 and essentially they show that the systems display reversible behaviour. The reduction potentials (vs SCE) for the complexes are listed in Table 17.

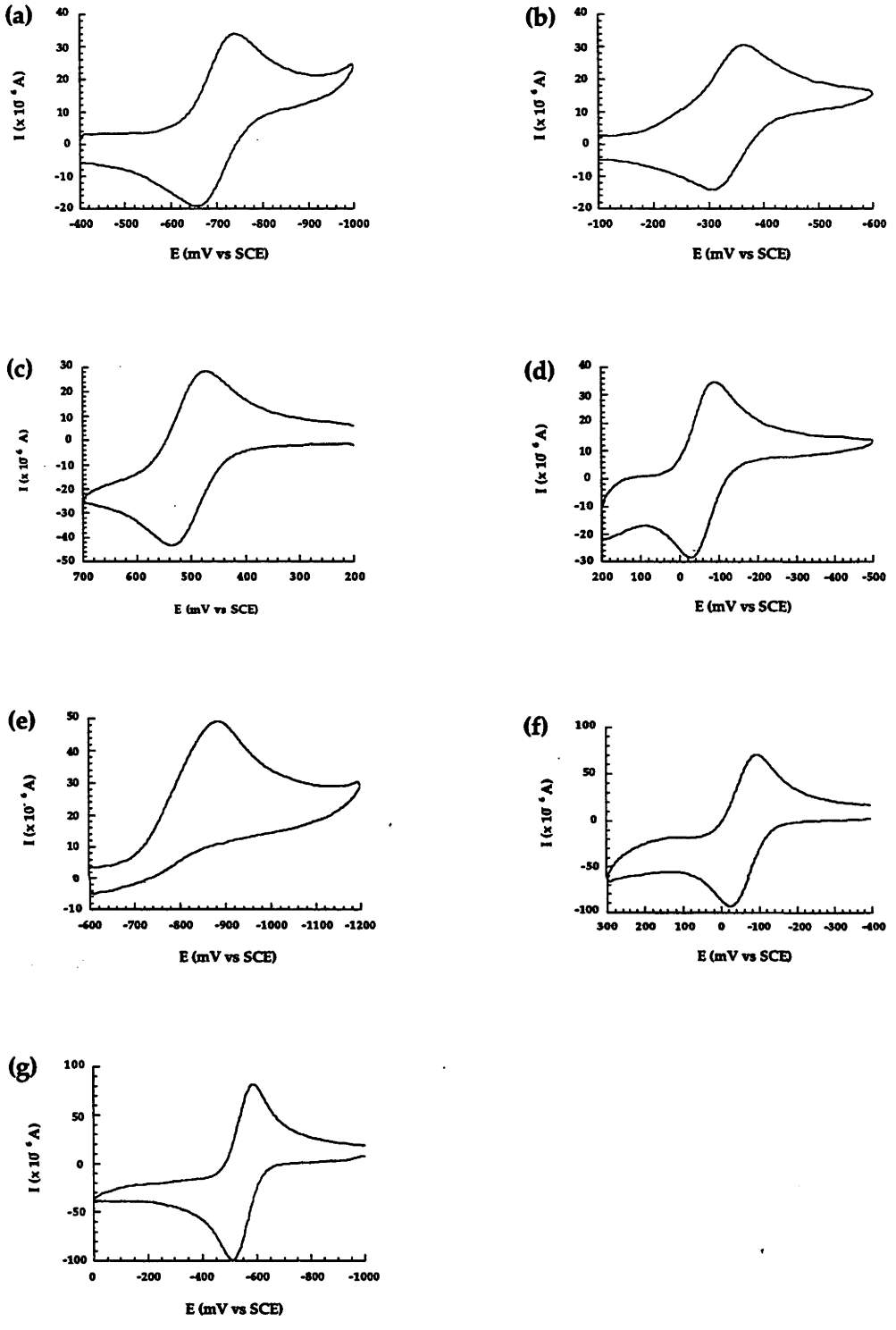

Figure 37. Cyclic voltammograms for (a) $[Co^{III}(Me,CO_2H\text{-}2\text{-}oxosar\text{-}H)]^{2+}$, (b) $[Fe^{III}(Me,CO_2H\text{-}2\text{-}oxosar\text{-}H)]^{2+}$ and (c) $[Ni^{II}(Me,CO_2^-\text{-}2\text{-}oxosar)]^{+}$ recorded in 0.05 M $KH_3(C_2O_4)_2.2H_2O$ and for (d) $[Mn^{III}(Me,CO_2^-\text{-}2\text{-}oxosar\text{-}H)]^{+}$, (e) $[Cu^{II}(Me\text{-}2\text{-}oxosar)]^{2+}$, (f) $[Mn^{II}(Me,CO_2^-\text{-}2\text{-}oxosar\text{-}H)]^{0}$ and (g) $[Fe^{II}(Me,CO_2^-\text{-}2\text{-}oxosar\text{-}H)]^{0}$ recorded in 0.1 M $NaClO_4$. All measurements were performed at 20° C with an EPG electrode and a scan rate of 20 mV s^{-1}.

Table 17. Electrochemical data for Co(III)/(II), Fe(III)/(II), Mn(III)/(II), Cr(III)/(II) and Cu(II)/(I) couples of monoamide and saturated cage complexes (vs SCE). (EPG electrode; 1 mM solutions of complex in 0.05 M $KH_3(C_2O_4)_2.2H_2O$, 0.1 M $NaClO_4$ and 0.05 M Na_3PO_4 at 20° C with a scan rate of 20 mVs^{-1}).

Complex	pH	$E_{1/2}$ vs SCE (V)	E_{pc} vs SCE (mV)	E_{pa} vs SCE (mV)	i_{pc}/i_{pa}	ΔE_p (mV)
$[Co^{III}(Me,CO_2H\text{-}2\text{-}oxosar\text{-}H)]^{2+}$	1.68 [a]	-0.70	-741	-659	1.00	82
$[Co^{III}(Me,CO_2H\text{-}2\text{-}oxosar\text{-}H)]^{2+}$	~6	-0.72[32]	-	-	-	-
$[Co^{III}(Me,CO_2^-\text{-}2\text{-}oxosar\text{-}H)]^{+}$	12.04 [c]	-0.91	-940	-872	0.92	68
$[Co^{III}(sar)]^{3+}$	~6 [b]	-0.66	-698	-634	0.85	64
$[Fe^{III}(Me,CO_2H\text{-}2\text{-}oxosar\text{-}H)]^{2+}$	1.68 [a]	-0.34	-365	-305	0.62	60
$[Fe^{III}(Me,CO_2H\text{-}2\text{-}oxosar\text{-}H)]^{2+}$	~6 [b]	-0.38	-414	-350	0.87	64
$[Fe^{III}(Me,CO_2^-\text{-}2\text{-}oxosar\text{-}H)]^{+}$	12.04 [c]	-0.56	-593	-534	0.81	59
$[Fe^{III}(sar)]^{3+}$ [51]	~6	-0.17	-	-	1.10	60
$[Mn^{III}(Me,CO_2^-\text{-}2\text{-}oxosar\text{-}H)]^{+}$	~8 [b]	-0.061	-91	-30	1.26	61
$[Cu^{II}(Me\text{-}2\text{-}oxosar)]^{2+}$	1.68 [a]	-	-676	-	-	-
$[Cu^{II}(Me\text{-}2\text{-}oxosar)]^{2+}$	~6 [b]	-	-886	-	-	-
$[Cu^{II}(Me\text{-}2\text{-}oxosar)]^{2+}$	12.04 [c]	-	-978	-	-	-
$[Cu^{II}(sar)]^{2+}$ [52]	6	-	-800	-	-	-
$[Ni^{II}(Me,CO_2H\text{-}2\text{-}oxosar)]^{2+}$	1.68 [a]	0.50	471	534	1.02	63
$[Ni^{II}(Me,CO_2^-\text{-}2\text{-}oxosar)]^{+}$	~6 [b]	0.44	394	477	0.94	83
$[Ni^{II}(Me,CO_2^-\text{-}2\text{-}oxosar\text{-}H)]^{0}$	12.04 [c]	0.29	250	320	0.98	70
$[Ni^{II}(sar)]^{2+}$ [38]	- [d]	0.65	-	-	1.10	61
$[Fe^{II}(Me,CO_2^-\text{-}2\text{-}oxosar\text{-}H)]^{0}$	~8 [b]	-0.55	-587	-511	1.32	76
$[Mn^{II}(Me,CO_2^-\text{-}2\text{-}oxosar\text{-}H)]^{0}$	~8 [b]	-0.062	-98	-25	1.17	73
$[Mn^{II}(sar)]^{2+}$ [53]	~7	0.29	-	-	-	-

[a] 0.05 M $KH_3(C_2O_4)_2.2H_2O$, [b] 0.1 M $NaClO_4$, [c] 0.05 M Na_3PO_4, [d] 0.1 M $NaCF_3SO_3$/0.1 M CF_3SO_3H.

In the various solutions employed most of the amide cage complexes exhibited either a reversible or quasireversible M(III)/(II) couple with $i_p \propto$ (scan rate)$^{1/2}$, and peak to peak separation increasing with scan rate. For most coordination complexes, quasireversible behaviour is related to a moderate homogeneous or heterogeneous electron transfer.[32] Repeated cycling of the various complexes, at 100 mV/s, under all the conditions employed produced no changes in the observed waves and the systems were clearly at least chemically reversible. The position of the redox couple of the different metal amide complexes depended on the pH of the solution. In some instances the potentials become more negative when moving from acidic to basic conditions. The position of the redox couple depends partly on whether the apical carboxyl group is protonated or not. If it is protonated it functions as an electron withdrawing group which removes some charge from the metal and the potential moves to more positive values. Under conditions where the carboxyl group is deprotonated the overall positive charge is lowered and a more negative potential results. The six coordinate amido complexes also display a negative shift in their potentials compared with their hexaamine $[M(sar)]^{x+}$ analogues.

From the crystallographic evidence obtained for the $[Ni^{II}(Me,CO_2^-\text{-}2\text{-}oxosar)]^+$ complex the amide nitrogen is both bound to the metal and protonated. The same situation probably exists in solution especially in acidic media because the crystallographic sample was obtained from acidified (pH 3) aqueous solution. In more acidic conditions, the carboxylate group would also be protonated. In basic solution though, the results indicate that the complex has lost the proton from the amido nitrogen atom. On moving from neutral to basic media a shift of -150 mV is observed in the Ni(II)/(III) potential. As the apical carboxyl group is already deprotonated in neutral solution the observed shift must then arise from loss of the proton from the coordinated and protonated amide N atom. The complex is then the same as the other deprotonated amido cage systems where the Ni(II)/(III) potential is less positive than that of $[Ni^{II}(sar)]^{2+}$.

The redox chemistry of the pentacoordinate Cu(II) amide is the same as that of the six coordinate $[Cu^{II}(sar)]^{2+}$ ion in that both systems are irreversible although the reduction potential of the $[Cu^{II}(Me\text{-}2\text{-}oxosar)]^{2+}$ ion is slightly more negative than that of $[Cu^{II}(sar)]^{2+}$ in neutral and basic conditions. However, some caution must be expressed here as

comparisons between five and six coordinate complexes are tenuous at best. The redox potential of the $[Cu^{II}(sar)]^{2+}$ ion is reported in Table 16 only to highlight the differences in the redox chemistry of the two complexes. Also, out of this set of amido complexes the Cu(II) monoamide is the only system to display irreversible behaviour. It is anticipated that $Cu^{II} + e^- \rightarrow Cu^{I}$ leads to loss of Cu^+ from the cage rapidly as it does for $[Cu^{II}(sar)]^{2+}$ and therefore the system is irreversible. Cu^+ is clearly too large for these cages and with Cu^+ out of the cage the oxidation wave is not observed.

Despite the fact that a range of different metal monoamide complexes exist with the Me,COOH-2-oxosar ligand Ni(III) was the only higher oxidation state stabilised by this ligand. Other oxidation states such as Co(IV), Fe(IV), Mn(IV), Cr(IV) and Cu(III) were not observed. One way to possibly overcome this problem is to choose appropriate apical substituents to aid the stabilisation process. However, it appears that more than one amide moiety is required to effect stabilisation of these ions. These aspects will be examined with the Co(III), Cr(III) and Ni(II) complexes in the following chapter. Again peripheral charge was less effective compared to that of an anionic binding site.

3.3.3.6 Electronic Absorption Spectroscopy

The electronic absorption spectra of the various metal amide cage systems appear in Figure 38. In addition, the UV/visible spectral maxima of these complexes appear in Table 18.

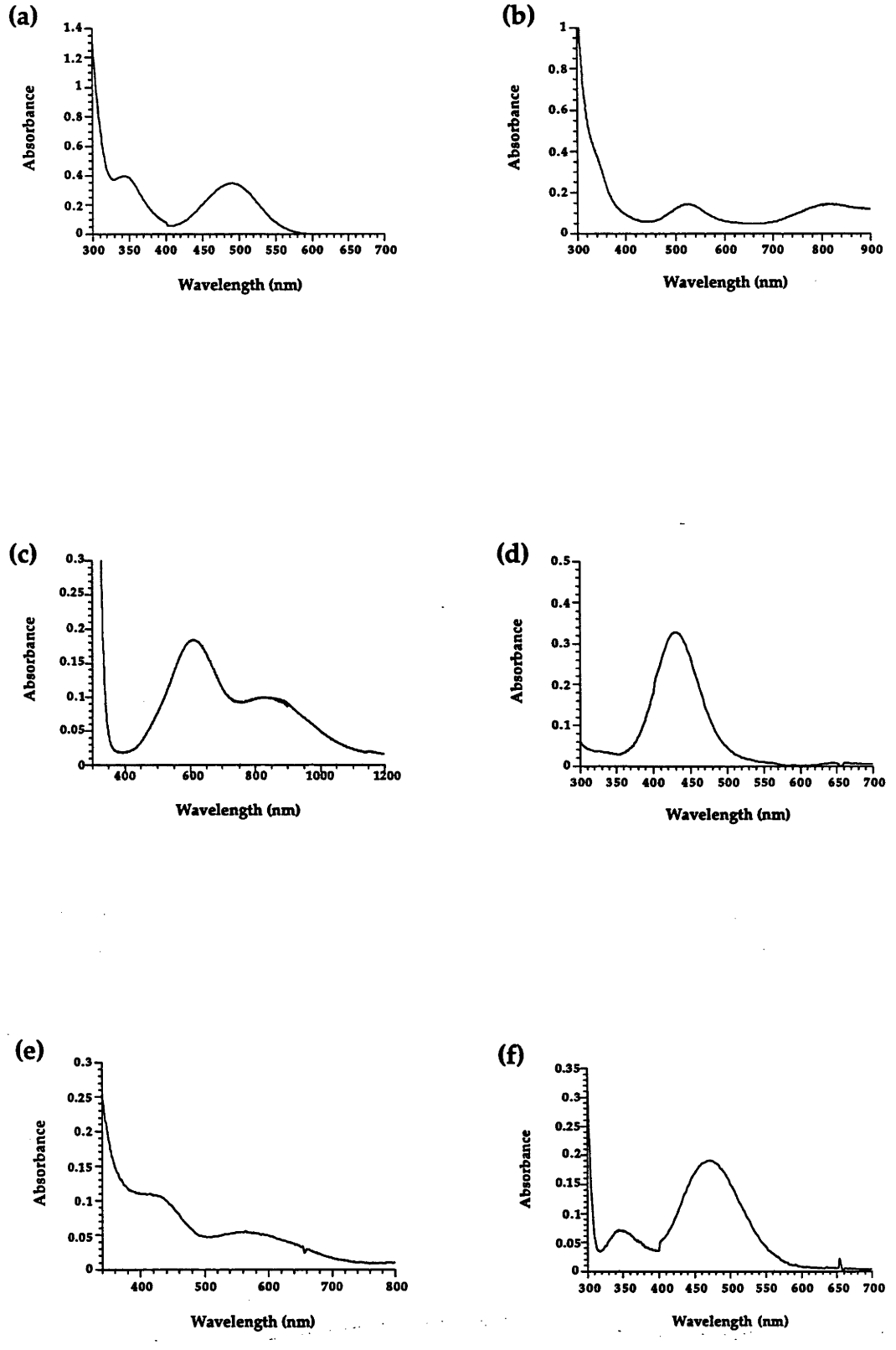

Figure 38. Electronic spectra of (a) $[Co^{III}(Me,CO_2H\text{-}2\text{-}oxosar\text{-}H)]^{2+}$, (b) $[Ni^{II}(Me,CO_2^{-}\text{-}2\text{-}oxosar)]^{+}$, (c) $[Cu^{II}(Me\text{-}2\text{-}oxosar)]^{2+}$, (d) $[Fe^{III}(Me,CO_2H\text{-}2\text{-}oxosar\text{-}H)]^{2+}$, (e) $[Mn^{III}(Me,CO_2^{-}\text{-}2\text{-}oxosar\text{-}H)]^{+}$ and (f) $[Cr^{III}(Me,CO_2H\text{-}2\text{-}oxosar\text{-}H)]^{2+}$ in water at 20° C.

Table 18. Electronic absorption data on some transition metal monoamide and saturated cage complexes (1mM solutions of complex in water at 20° C unless otherwise stated).

Complex	Band Origin Transition	λ_{max} nm (ε_{max} $M^{-1}cm^{-1}$)
$[Co(Me,CO_2H\text{-}2\text{-}oxosar\text{-}H)]^{2+}$	$^1T_{2g}\leftarrow{}^1A_{1g}$	346 (363)
	$^1T_{1g}\leftarrow{}^1A_{1g}$	490 (314)
$[Co(sar)]^{3+}$ [33] a	$^1T_{2g}\leftarrow{}^1A_{1g}$	343 (108)
	$^1T_{1g}\leftarrow{}^1A_{1g}$	471 (135)
$[Ni(Me,CO_2H\text{-}2\text{-}oxosar)]^{2+}$ a	$^3T_{1g}\leftarrow{}^3A_{2g}$ (P)	340 sh (35)
	$^3T_{1g}\leftarrow{}^3A_{2g}$ (F)	524 (14)
	$^3T_{2g}\leftarrow{}^3A_{2g}$	818 (15)
$[Ni(Me,CO_2^-\text{-}2\text{-}oxosar)]^{+}$	$^3T_{1g}\leftarrow{}^3A_{2g}$ (P)	340 sh (38)
	$^3T_{1g}\leftarrow{}^3A_{2g}$ (F)	524 (14)
	$^3T_{2g}\leftarrow{}^3A_{2g}$	818 (14)
$[Ni(Me,CO_2^-\text{-}2\text{-}oxosar\text{-}H)]^{0}$ b	$^3T_{1g}\leftarrow{}^3A_{2g}$ (P)	330 sh (21)
	$^3T_{1g}\leftarrow{}^3A_{2g}$ (F)	512 (14)
	$^3T_{2g}\leftarrow{}^3A_{2g}$	812 (25)
$[Ni(sar)]^{2+}$ [38] c	$^3T_{1g}\leftarrow{}^3A_{2g}$ (P)	329 (9)
	$^3T_{1g}\leftarrow{}^3A_{2g}$ (F)	506 (8)
	$^3T_{2g}\leftarrow{}^3A_{2g}$	805 (15)
$[Cu(Me\text{-}2\text{-}oxosar)]^{2+}$ a		605 (150)
		820 (59)
$[Cu(Me\text{-}2\text{-}oxosar)]^{2+}$		613 (182)
		820 (95)
$[Cu(Me\text{-}2\text{-}oxosar)]^{2+}$ b		552 (111)
		700 sh (73)
$[Cu(sar)]^{2+}$ [51]	$^2A,{}^2B,{}^2A\leftarrow{}^2B_{1g}$	653 (114)
	$^2A_{1g}\leftarrow{}^2B_{1g}$	1189 (48)

a 0.1 M HCl, b 0.05 M Na_3PO_4, c 0.1 M CF_3SO_3H

Table 18 cont. Electronic absorption data on some transition metal monoamide and saturated cage complexes (1mM solutions of complex in water at 20° C unless otherwise stated).

Complex	Band Origin Transition	λ_{max} nm (ε_{max} $M^{-1}cm^{-1}$)
$[Fe(Me,CO_2H\text{-}2\text{-}oxosar\text{-}H)]^{2+}$ [d]	$^2A_{1g}$,$^2T_{2g}$,$^2T_{1g}$, ^2E_g,$^2T_{2g}$←$^2T_{2g}$	430 (2705)
$[Fe(sar)]^{3+}$ [51]	$^2A_{1g}$←$^2T_{2g}$	366 (924)
	^2E_g←$^2T_{2g}$	438 (333)
	$^2T_{2g}$←$^2T_{2g}$	529 sh (108)
$[Mn(Me,CO_2^-\text{-}2\text{-}oxosar\text{-}H)]^{+}$	^5E_g←$^5B_{1g}$	410 sh (431)
	$^5B_{2g}$←$^5B_{1g}$	562 (231)
$[Mn(sar)]^{3+}$ [53 c]	^5E_g←$^5B_{1g}$	277 (7510)
	$^5B_{2g}$←$^5B_{1g}$	420 (1400)
$[Cr(Me,CO_2H\text{-}2\text{-}oxosar\text{-}H)]^{2+}$	$^4T_{2g}$←$^4A_{2g}$	347 (63)
	$^4T_{1g}$←$^4A_{2g}$	470 (168)
$[Cr(sar)]^{3+}$ [54]	$^4T_{2g}$←$^4A_{2g}$	347 (91)
	$^4T_{1g}$←$^4A_{2g}$	450 (156)

[a] 0.1 M HCl, [b] 0.05 M Na_3PO_4, [c] 0.1 M CF_3SO_3H, [d] 1 x 10^{-4} M

In all instances, the observed maxima and their intensities correspond to those expected for the respective high or low spin metal ions. Each six coordinate amide complex also displays a small red shift in all or some of their d-d bands when compared to the relevant six coordinate $[M(sar)]^{x+}$ complex. This is consistent with the trend observed for the $[Co^{III}(Me,CN\text{-}2\text{-}oxosar\text{-}H)]^{2+}$ ion. A similar result occurs for the $[Co^{III}(\{NO_2\}_2\text{-}sar)]^{3+}$ complex after it loses a proton from a coordinated nitrogen in basic solution.[33] It appears then that a deprotonated nitrogen within a cage complex results in a red shift in the absorption bands regardless of the type of metal present within the cage amide complex. There is also an increase in the molar absorption coefficients of the d-d bands of the six coordinate amide complexes when compared to the corresponding hexacoordinated $[M(sar)]^{x+}$ complexes. Again, based on the

electrochemical data, in acidic and neutral conditions the $[Ni^{II}(Me,CO_2^-\text{-}2\text{-}oxosar)]^+$ complex is expected to have the amide nitrogen atom protonated and bound while in basic solution the complex becomes a $NiN_{5(amine)}N_{(amido)}$ complex.

Even at pH ~14 the electronic spectroscopy indicates the Cu(II) amide complex is still five coordinate. In $Cu^{II}N_6$ compounds a d-d transition appearing at approximately 1185 nm in the electronic spectrum is indicative of hexadentate metal binding. This has certainly been observed for the known six coordinate Cu(II) complexes of $[Cu^{II}(sar)]^{2+}$ (653 (114) and 1189 (48)) and $[Cu^{II}(\{NH_3^+)_2\text{-}sar)]^{4+}$ (662 (139) and 1182 (58)). Under all pH conditions the transition at ~1185 nm is absent for the $[Cu^{II}(Me\text{-}2\text{-}oxosar)]^{2+}$ ion. Therefore, in aqueous media the Cu(II) amide remains as a pentadentate complex independent of pH. Again direct comparison between the five coordinate $[Cu^{II}(Me\text{-}2\text{-}oxosar)]^{2+}$ and six coordinate $[Cu^{II}(sar)]^{2+}$ is tenuous at best. The two complexes appear in Table 13 simply to highlight the electronic differences between five and six coordinate Cu(II) cage systems.

A preliminary investigation into the Ni(III) electronic spectroscopy of $[Ni^{III}(Me,CO_2H\text{-}2\text{-}oxosar\text{-}H)]^{2+}$ was undertaken. The olive green Ni(III) complex was obtained by electrochemical oxidation of $[Ni^{II}(Me,CO_2^-\text{-}2\text{-}oxosar)]^+$ in acidic aqueous solution while the generation of the Ni(III) species was monitored electronically (Appendix Figure 3.1.9). The absorption spectrum shows that the $[Ni^{III}(Me,CO_2H\text{-}2\text{-}oxosar\text{-}H)]^{2+}$ ion possesses two d-d bands present at 631 nm and 1455 nm. Also, an ill-defined shoulder is evident at ~400 nm and another at ~320 nm. In addition like the situation observed for the Ni(II) species, the higher energy maximum of $[Ni^{III}(Me,CO_2H\text{-}2\text{-}oxosar\text{-}H)]^{2+}$ (631 nm) is red shifted when compared to the corresponding transition of the $[Ni^{III}(sar)]^{3+}$ ion (570 nm).

For the Fe(III) amido complex, both the structural study (Fe^{III}-N ~2.0 Å) and the relatively intense visible absorption spectrum are clear indications of the low spin state. High spin ions of this type would be expected to have bond lengths of Fe^{III}-N ~2.2 Å and relatively low intensities for the d-d bands.

3.4 Discussion

3.4.1 Syntheses

Reactions of $NCCH_2COOEt$

A condensation reaction mechanism for the formation of the $[Co^{III}(Me,CN\text{-}2\text{-}oxosar\text{-}H)]^{2+}$ complex is depicted in Scheme 1. The reaction requires the initial formation of a monoimine at one of the primary amines of $[Co^{III}(sen)]^{3+}$. The carbon base then attacks this species producing a pendant [(ethyl cyanocarbonyl)ethyl]amine derivative. After formation of an adjacent imine, ring closure occurs by attack by the carbon base arm. This new species has the ester and cyano groups exo to the newly formed six-membered ring. This process leads to two isomers depending on the relative position of the -CN and -COOR groups Schemes 1 and 2. For the amido cage formation the last step involves attack by the remaining deprotonated amine on the carbonyl group of the ester, forming an amide group and the completed macrobicyclic cage.

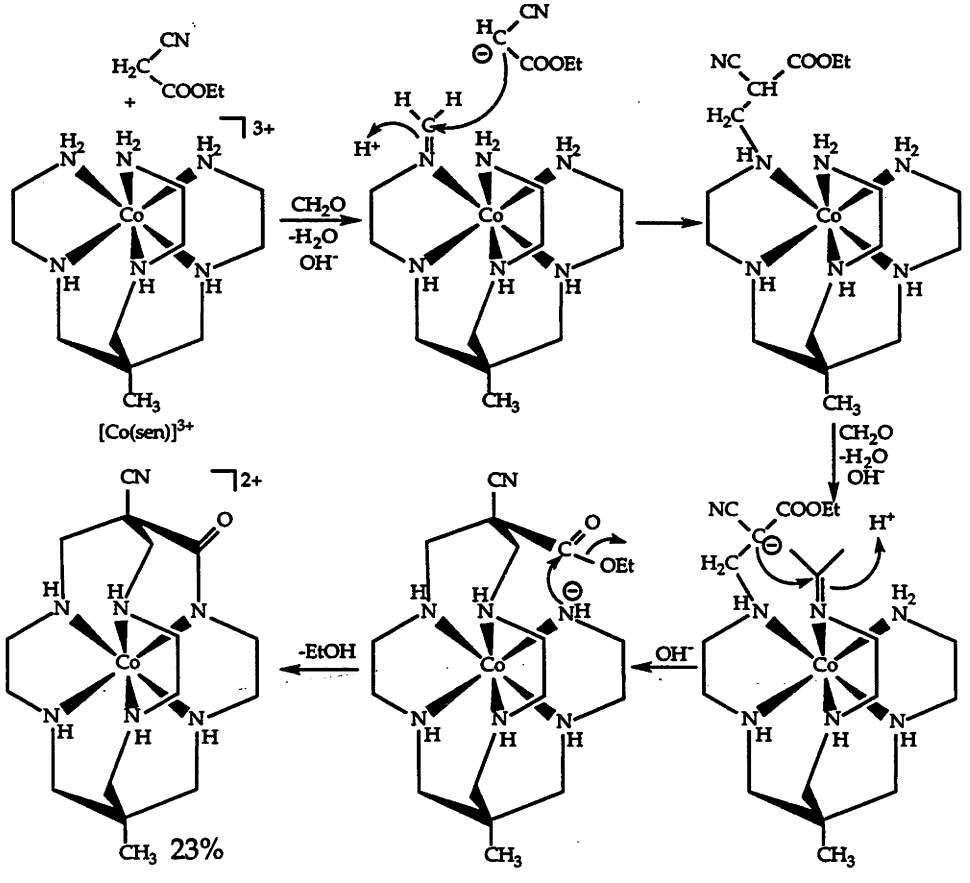

Scheme 1.

A mechanism for the production of the Co(III) amidine cages appears in Scheme 2. It is envisaged that the formation of the amidine cage follows a similar path to that of the cyano amido complex, except that, the final step involves attack of the deprotonated amine on the adjacent nitrile group. Once formed the amidine cage then undergoes hydrolysis at the apical ester group and decarboxylation producing the two observed cages.

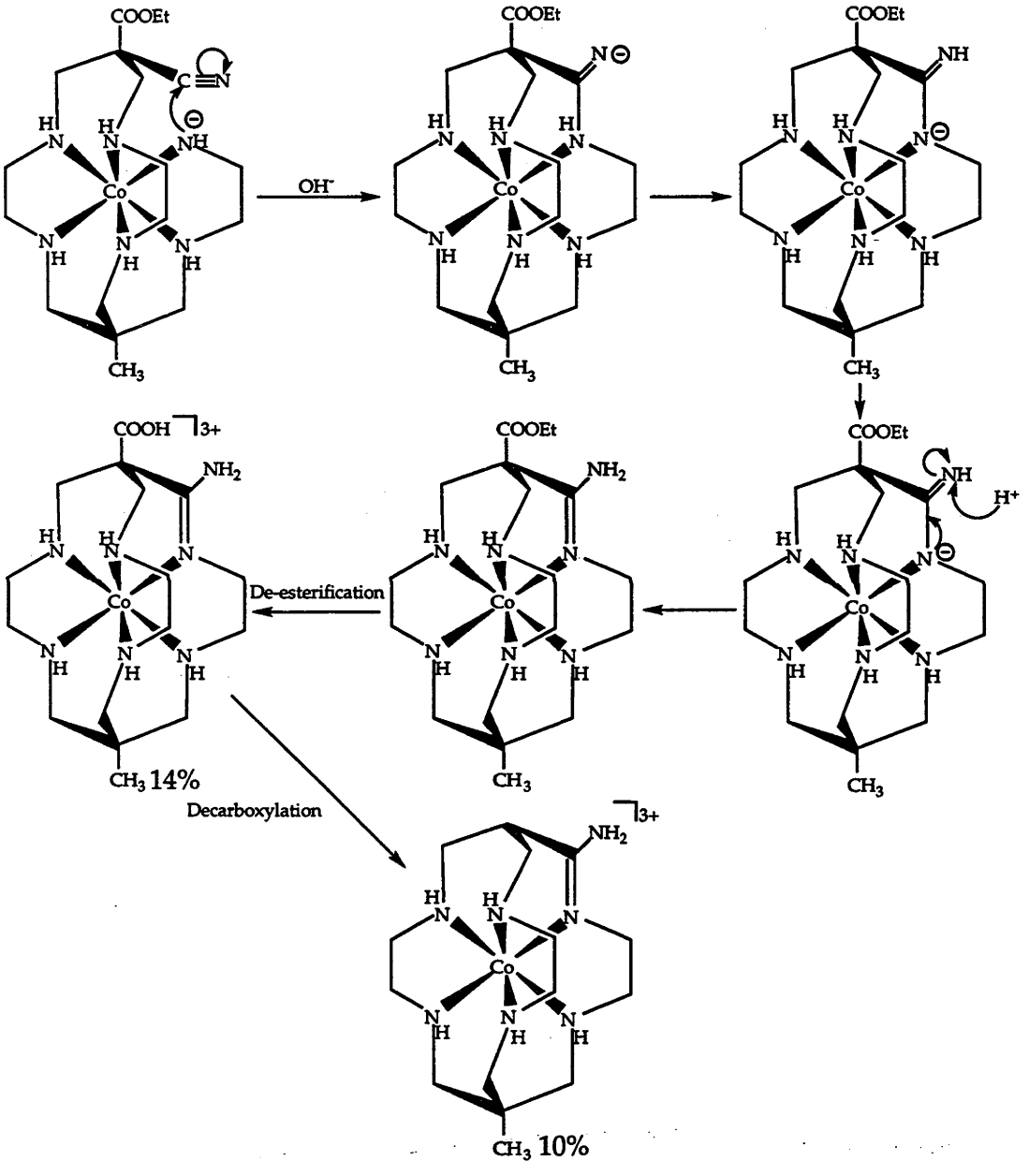

Scheme 2. Proposed mechanism for the formation of the amidine cage complexes from the reaction of $[Co^{III}(sen)]^{3+}$ with ethyl cyanoacetate and formaldehyde in basic aqueous solution.

Hydrolysis of ethyl cyanoacetate to ethyl malonamate also occurs on or off the metal during the reaction (Scheme 3). Subsequent hydrolysis of this species to the half-ester ethyl malonate follows, releasing ammonia, which then adventitiously reacts with $[Co^{III}(sen)]^{3+}$ and formaldehyde forming some $[Co^{III}(Meazasar)]^{3+}$. In addition, during this reaction the methanimine produced from the condensation of a formaldehyde with $[Co^{III}(sen)]^{3+}$ also undergoes a Cannizzaro type reaction with excess CH_2O that results in the formation of $[Co^{III}(N\text{-}Me\text{-}sen)]^{3+}$ (Scheme 3).

It was also envisaged that a cage complex with both amido and amidine functional groups situated in the one cap could form in this reaction. Once the [(ethyl cyanocarbonyl)ethyl] derivative is formed both the -CN and COOEt groups then have a chance to condense with $[Co^{III}(sen)]^{3+}$ to produce such a bifunctional capped cage complex. However, a Co(III) amide amidine cage was either not produced at all or formed in such a small amount it may be part of the unidentified small fractions. A possible explanation for this observation is deprotonation of the second proton, from the carbon acid to form a NC-C$^-$-COOEt group, would force the nitrile and ester groups to become planar to one another. As a result of this planarity, it is then only possible to place one functional group within the cage of the cage complex. Once one group condenses with a deprotonated amine the remaining group would then be forced away from the last available amine making it difficult for it to close off the complex and form the bifunctional cage. Instead the remaining group forms the apical substituent of the amido or amidine cage. Another possible reason could be that the carbanion reacts faster with the adjacent imine, forming the new six-membered ring, thus preventing the ester and nitrile groups forming the bifunctional cage.

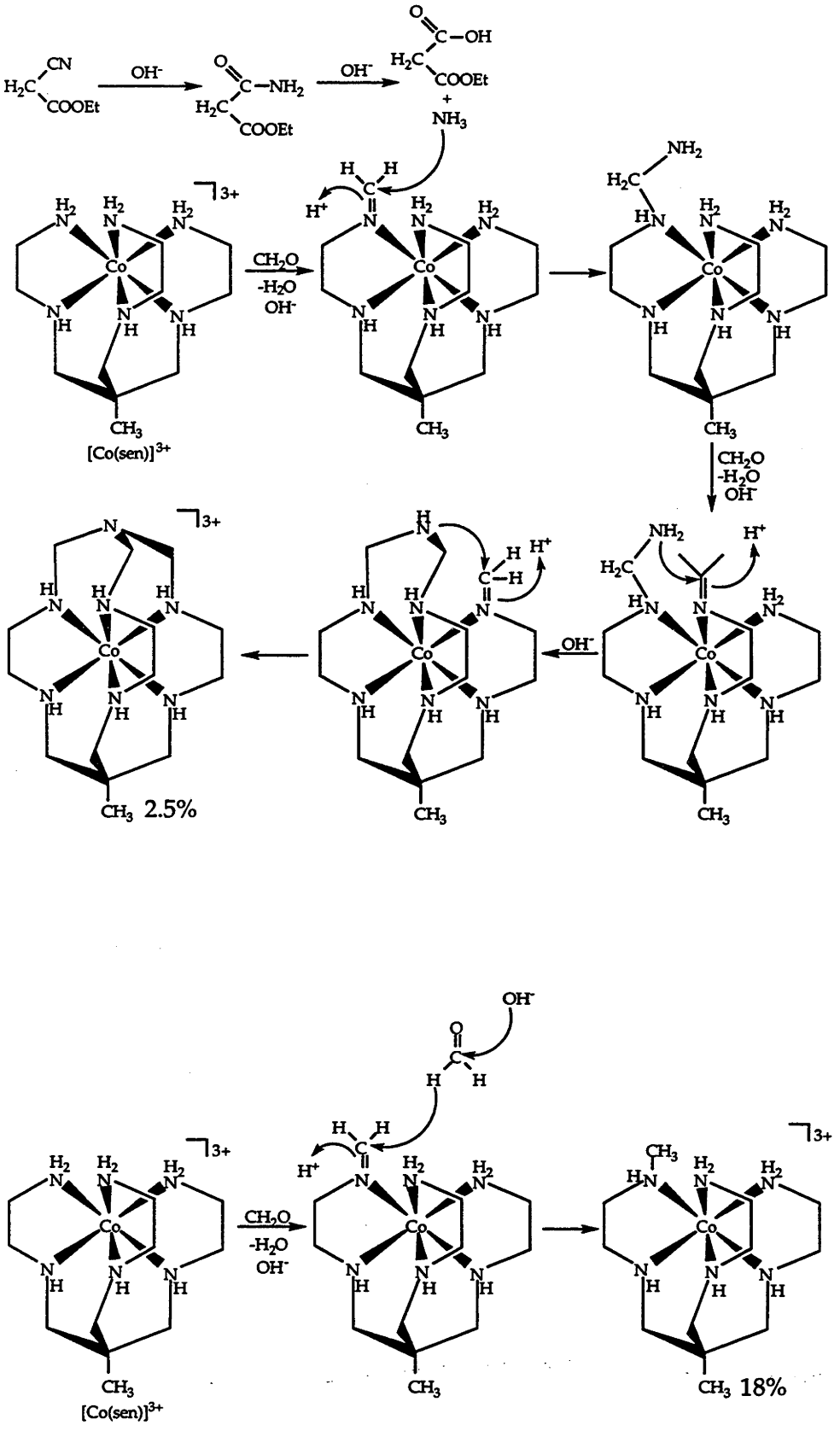

Scheme 3. Proposed mechanism for the formation of the by-products $[Co^{III}(Meazasar)]^{3+}$ and $[Co(N\text{-}Me\text{-}sen)]^{3+}$ from the reaction of $[Co^{III}(sen)]^{3+}$ with ethyl cyanoacetate and formaldehyde in basic aqueous solution.

A proposed mechanism for the condensation reaction of $[Co^{III}(sen)]^{3+}$ with ethyl acetoacetate and formaldehyde, in basic conditions, appears in Scheme 4. Initially the reaction is similar to that observed for $[Co^{III}(Me,CN\text{-}2\text{-}oxosar\text{-}H)]^{2+}$. After initial formation of an imine, at one of the primary amines of $[Co^{III}(sen)]^{3+}$, the carbon base then condenses with the imine resulting in a pendant [(ethyl acetocarbonyl)ethyl] amine species. Following this, intramolecular ring closure occurs after the carbon base arm attacks a newly formed imine on an adjacent primary amine. This results in the formation of a new six-membered ring with the ester and ketone substituents. However, unlike the ethyl cyanoacetate condensation this reaction only appears to produce one isomer. By examination of the products of the reaction it appears that this species has the ketone adjacent to the remaining primary amine of $[Co^{III}(sen)]^{3+}$ as depicted in Scheme 4. This species then appears to lose acetic acid after attack by a hydroxide ion. This accounts for the fact that an imine cage is not a product of this condensation reaction. After this, the newly created carbanion can then react either with an adjacent imine or with excess CH_2O. In the first instance, $[Co^{III}(Me,COOEt\text{-}sar)]^{3+}$ arises which then undergoes ester hydrolysis to produce the $[Co^{III}(Me,COOH\text{-}sar)]^{3+}$ ion. For the latter case, the formaldehyde condenses directly with the carbanion to form a hydroxy methyl pendant and a macrocyclic pendant complex. This latter species undergoes ester hydrolysis to produce the $[Co^{III}(\{CO_2H,CH_2OH\}\text{-}Medesar)]^{3+}$ species and both complexes are present at the end of the reaction. Some $[Co^{III}(N\text{-}Me\text{-}sen)]^{3+}$ ion is also formed in this reaction by the same type of Cannizzaro reaction as described previously.

Another possible product from this condensation reaction is the $[Co^{III}(Me,C(=O)CH_2COOEt\text{-}sar)]^{3+}$ species although the complex itself was not identified. To form this complex, the methyl group of the ketone would need to condense with the formaldehyde and $[Co(sen)]^{3+}$ directly, in the basic conditions, as depicted in Scheme 5. The final product would arise from OH^- hydrolysis of the $C(O)CH_2COOEt$ substituent to produce the apical carboxylate group and acetate ion (Scheme 5). It is therefore possible that the $[Co^{III}(Me,COOH\text{-}sar)]^{3+}$ complex is formed concurrently by two different paths as shown in Schemes 4 and 5 but it is more likely that the methylene group being more acidic is the effective path.

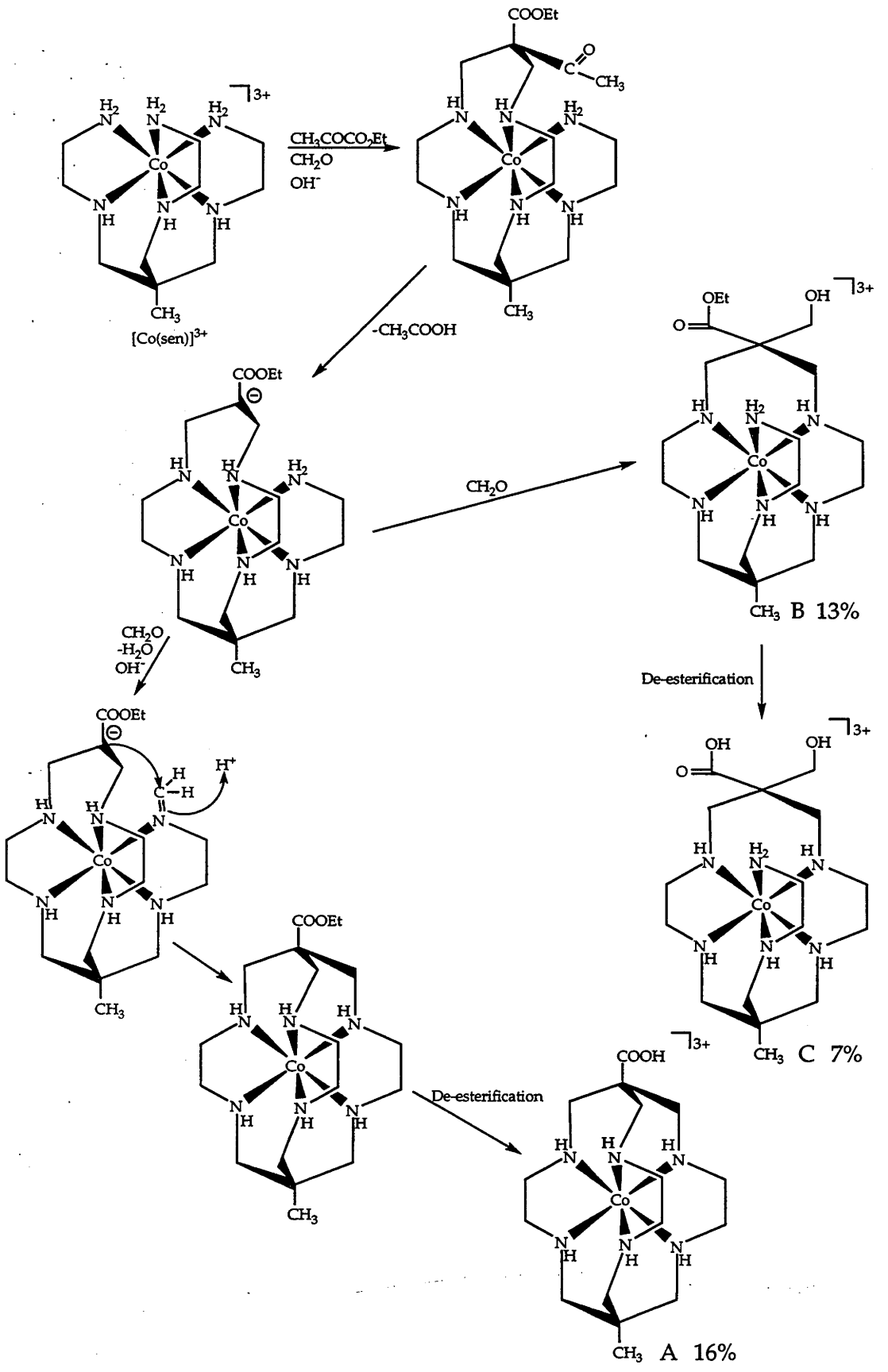

Scheme 4. Preferred mechanism for the formation of the products from the reaction of $[Co^{III}(sen)]^{3+}$ with ethyl acetoacetate and formaldehyde in basic aqueous solution.

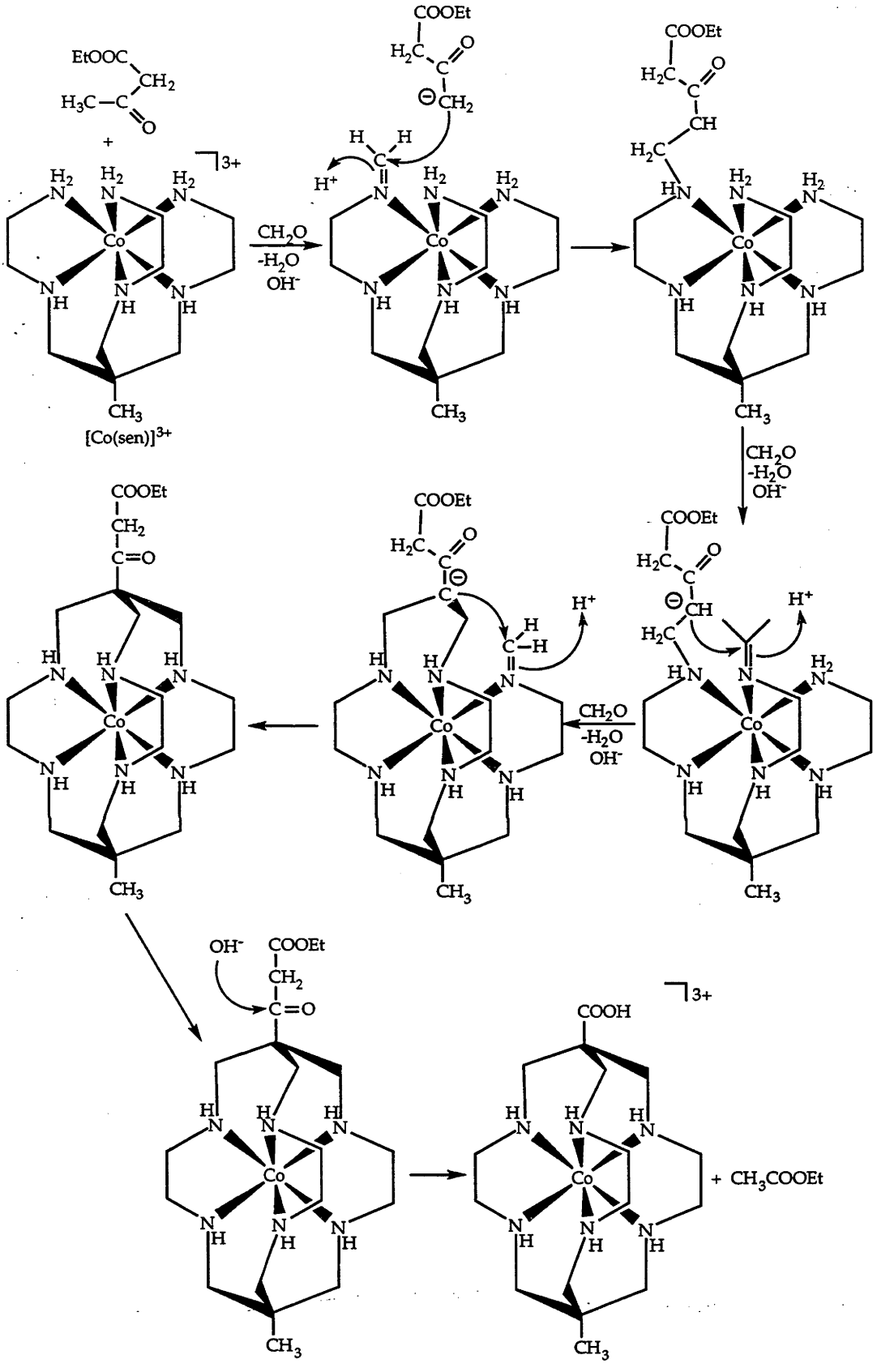

Scheme 5. Alternative mechanism for the possible formation and subsequent hydrolysis of the $[Co^{III}(Me,C(O)CH_2COOEt\text{-}sar)]^{3+}$ ion from the reaction of $[Co^{III}(sen)]^{3+}$ with ethyl acetoacetate and formaldehyde in basic aqueous solution.

Like the ethyl cyanoacetate condensation reaction, it was envisaged that other products could arise from this particular reaction. However, the expected bifunctional amido imine and separate amido and imine cages were not found although they may be part of unidentified small fractions. For the bifunctional complex, as outlined previously, the planarity of the $H_3CC(O)$-C^--COOEt group would more than likely inhibit such a species being formed. The absence of an amide cage may be due to the fact that only one isomer (Scheme 4) is apparently produced in this reaction where the ketone group is located adjacent to the remaining template primary amine. As a result the deprotonated amine cannot condense with the ester group to form an amide cage. Even after loss of acetic acid the anionic site and finally the methylene hydroxy pendant would also prevent amide formation by not allowing the ester to approach the last deprotonated amine. It is also thought that an imine cage is not formed in this reaction because acetic acid is cleaved faster than the ketone group condenses to form the imine. Clearly, the use of ethyl acetoactate as a capping reagent is not a feasible route to the production of amide and imine cage complexes

3.4.2 Infra-red Spectroscopy

Theoretically, it should be possible to distinguish between unbound and bound amide groups since the bond order of the amide carbonyl linkage is reduced by coordination with the metal ion and simultaneous displacement of a proton. Consequently, the infra-red amide carbonyl band will shift to lower frequency. The amide cage compounds generally displayed amide carbonyl stretching frequencies that were lower than that of the free amide cage ligand, Me,COOK-2-oxosar (amide stretch = 1630 cm^{-1}). This provides some evidence that the metal is bound to the amido nitrogen atom. Certainly, in some instances it was confirmed crystallographically and from the charge on the cation. Conversly, non-bonded amide groups within cage ligands, such as that displayed in the structure of the Cu(II) monoamide complex, possess an amide absorption frequency about 1630 cm^{-1} - 1660 cm^{-1}. Certainly the amide carbonyl absorption frequencies of the amide complexes in this chapter appear to comply with the above theoretical analysis. Further support for this analysis also comes about from the crystallographic evidence. It follows that IR spectroscopy is a useful tool to help evaluate the type of bonding displayed by these complexes.

It was also found that the IR spectroscopy may be able to distinguish between a metal-N bound amido group or a metal-N bound protonated

amide group. For $[Ni^{II}(Me,COO^{-}\text{-}2\text{-}oxosar)]^{+}$ the amide carbonyl stretching vibration occurs at 1709 cm^{-1} and 1691 cm^{-1} while for $[Co^{III}(Me,COOH\text{-}2\text{-}oxosar\text{-}H)]^{2+}$ the amido carbonyl frequency appears at a value of 1599 cm^{-1}. Clearly, a higher carbonyl absorption frequency would be expected for the nickel complex because in the metal-N bound protonated form the amide can basically be seen as a coordinated distorted tetrahedral configuration about the N atom. As a result the usual delocalisation of charge between the anionic nitrogen and oxygen atoms is limited and the $C\text{-}O_{(amide)}$ group gains more ketonic character. Therefore, the bond order of the carbonyl linkage is increased in this instance and the IR absorption moves to a higher frequency. The absence of the usual amido resonance was also consistent with the crystal data obtained on the $[Ni^{II}(Me,COO^{-}\text{-}2\text{-}oxosar)]^{+}$ ion where the C=O bond distances of both ions (1.20 Å (Figure 33, Table 10) and 1.22Å (Figure 34, Table 10) respectively) are shorter than that expected for an amido C=O group (1.27 Å). The normal distance anticipated for a ketone group is (1.20 Å)[24] and an IR stretching frequency of ~1700 cm^{-1} is also expected. In addition, for the coordinated tertiary amide in, $[Co^{III}(treneone)Cl]^{2+}$, the $C\text{-}O_{(amide)}$ group displays a stretching frequency (1706 cm^{-1}) much closer to that of a saturated ketone than that of an unbound tertiary amide (~1650 cm^{-1}).[15] This is additional evidence of the value of IR spectroscopy as a tool to help evaluate the type of bonding which occurs within amide cage complexes.

Some interesting results also arose from the deuterated IR studies on the Ni(II) and Cu(II) monoamide complexes. Firstly, the IR spectroscopy indicated that the Ni(II) monoamide becomes a non-electrolyte when placed in basic conditions. A freeze-dried sample of the Ni(II) complex, obtained from basic D_2O, showed that the amide carbonyl stretching vibration moved from 1709 cm^{-1} and 1691 cm^{-1} to 1577 cm^{-1} (Figure 26a and c) which is consistent with the loss of the proton from the amide nitrogen atom to produce a $Ni\text{-}N_{(amido)}$ bond. For the Cu(II) complex though, the IR spectroscopy revealed that the Cu(II) ion binds the monoamide ligand as a pentadentate, leaving the amide nitrogen unbound, even in basic conditions (Figure 25a, b and c). Therefore, the IR analysis of the $[Cu^{II}(Me\text{-}2\text{-}oxosar)]^{2+}$ ion indicates that the Cu(II) ion has distinctly different binding characteristics to those of the Co(III) and Cr(III) ions for the amide group at least.

3.4.3 Electrochemistry

A number of interesting properties can be seen for the complexes here, and it is instructive to look at some of the trends that are present. For the Co(III)/(II) potentials of the Co(III) monoamido cages, a shift of approximately -0.2 V is observed when compared to that of the saturated parent, $[Co^{III}(Mesar)]^{3+}$. This arises from the amide anion fragment present within the ligand structure which reduces the overall charge to 2+ thereby making the Co(III) ion more difficult to reduce. It is not a surprising result since a reduction in charge of the overall complex 3+ → 2+ → 1+ should lead to stabilisation of the high oxidation state. The effect is also significant if strong electron-withdrawing or donating groups are attached to the periphery of the cage. In essence, there is a two fold effect, the reduction in net charge and an increase in donation of charge from the anionic ligand directly to the metal ion. Both effects influence the redox potential. With each amide complex possessing these properties, the polarographic window becomes shifted to more negative values, hence it is easier to oxidise the metal to a higher oxidation state. However, the type of apical substituent also modulates the potentials. For the Co(III) amide cages at least, some substituents counter the stabilising effect of the amido group for the higher oxidation state and thus there is a "trade-off" between the two effects. For the Co(III) amide cages described here the substituents possess mainly electron withdrawing properties. Therefore, the potentials move to slightly more positive values as a result (Figure 39). The variation also shows that it is possible to fine tune the redox properties of the complexes with the appropriate choice of apical substituent and number of amide groups. However, the desired Co(IV) state with these monoamido ligand systems was unattainable in water. Simply the d^6 Co(III) state is an extremely stable oxidation state with these ligands.

The two amidine complexes show a shift to more negative values when compared to that of the hexamine parents $[Co^{III}(Me,COOH\text{-}sar)]^{3+}$ and $[Co^{III}(Mesar)]^{3+}$ (Figure 39) despite the fact that the amidine group is a neutral ligand. However, the shift here probably arises from a substituent effect in that the amidine group acts as a better electron-donating group than the secondary amine. The *exo*-nitrogen of the amidine group may donate charge to the metal leading to a slight stabilisation of the Co(III) state. In addition, the amidine moiety may also reduce the cavity size of the cage complex which would lead to a slight stabilisation of the Co(III)

state. The Co(IV) was not observed with the amidine cage systems either and this was not surprising given its neutral character.

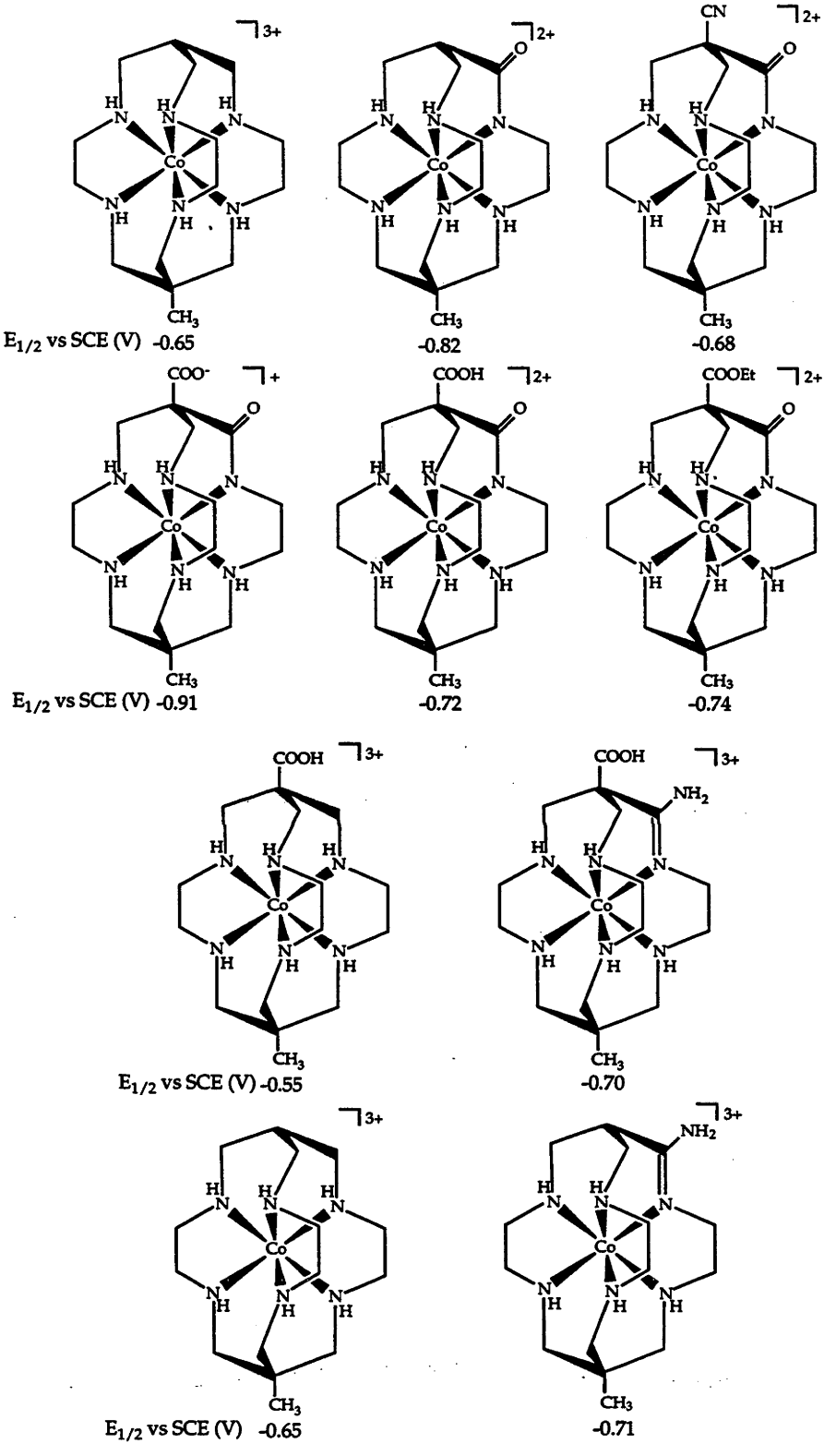

Figure 39. Diagram showing the effect that an amido and amidine moieties and various apical substituents have on cage Co(III)/(II) electrochemical properties.

In general, the substituent effects on the cage periphery are larger than expected from more normal organic chemistry but this influence has also been observed previously with these small cages and their redox phenomena.[34]

The Ni(II), Fe(III), Mn(III) and Cr(III) amide complexes show a negative shift in their reduction potentials compared to those of the respective $[M(sar)]^{x+}$ complexes (Table 17). In some instances, namely for the Fe(III), Mn(III) and Cr(III) amido complexes as well as the $[Ni^{II}(Me,CO_2H\text{-}2\text{-}oxosar\text{-}H)]^{+}$ ion obtained in basic solution, the shift arises for the same reasons as those outlined for the earlier Co(III) compounds. Even the copper amide complex displays a negative shift in its reduction potential when compared to $[Cu(sar)]^{2+}$. However, comparison between five and six coordinate complexes is not really valid.

For both the amide complexes of Ni(II) in acidic and neutral media and Cu(II) though the negative shift occurs as a result of some other factor. The exact reason for this is not known but perhaps the small reduction in the cavity size of the complex from the incorporation of the amide group within the ligand is playing a part. It would not be the sole reason for the observed shift though and other factors would more than likely be involved. Nevertheless, as observed from the results the shift is great enough for the Ni(II) complex that Ni(III) is now readily accessible in water with this ligand. Also, the Ni(III) species was found to be more stable in acidic conditions. This is because in more basic solution the complex loses a proton from a coordinated nitrogen which leads to the eventual breakdown of the complex via disproportionation to Ni(IV) and oxidation of the ligand.[38] Acidic conditions prevent this from occurring. Again higher oxidation states of the other metals were not observed. Perhaps for the same reason as described for the Co(III) ion earlier.

For the two species $[Co^{III}(\{CO_2H,CH_2OH\}\text{-}Me\text{-}desar)]^{3+}$ and $[Co^{III}(\{CO_2Et,CH_2OH\}\text{-}Me\text{-}desar)]^{3+}$ potentials are more positive than that found for $[Co^{III}(Me\text{-}sar)]^{3+}$ (Table 7) but these systems are not really comparable since one is a hexadentate cage and the other two pendant-macrocyclic complexes. They are essentially reversible in neutral solution but not so in acidic conditions and this is not surprising since the Co(II) ions could dissociate at least part of the ligand in aqueous acid.

3.4.4 Comparison of the Electrochemical Properties of the Me,COOH-2-oxosar Ligand with Different Metal Ions

A number of monoamide first row transition metal complexes now exist with the Me,COOH-2-oxosar ligand where the electrochemical potential is an important characteristic of their chemistry. The variation in the electrochemical potential in a related series of elements reflect the variation in ionisation potential and the chemical properties in that series. Plotted in Figure 40 are the electrochemical potentials in water (vs SCE) for the $[M(H_2O)_6]^{x+}$, $[M(sar)]^{x+}$ and $[M(Me,COOH\text{-}2\text{-}oxosar\text{-}H)]^{x+}$ systems compared to the ionisation potential in this transition metal series.

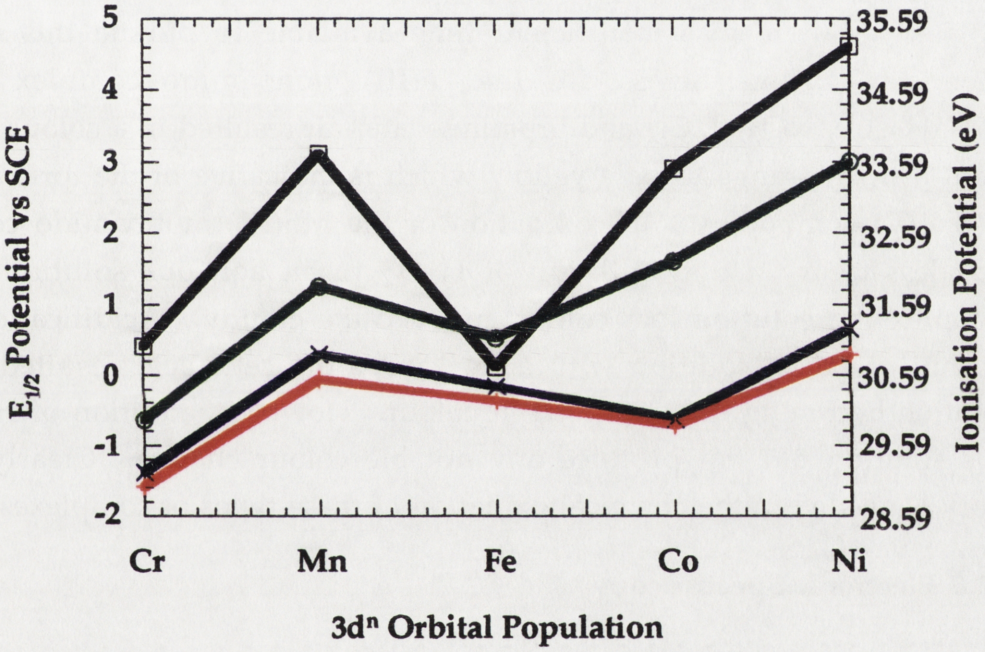

Figure 40. Variation of M(III)/(II) redox potentials with 3d electron configuration for $[M(H_2O)_6]^{3+/2+}$ (O), $[M(sar)]^{3+/2+}$ (X) and $[M(Me,COOH\text{-}2\text{-}oxosar\text{-}H)]^{2+/+}$ (+) in aqueous solution along with the $M^{2+} \rightarrow M^{3+}$ ionisation potentials (❑) of these ions in the gaseous state.

Firstly, the graph shows that the third ionisation potentials of the three systems, $[M(H_2O)_6]^{x+}$, $[M(sar)]^{x+}$ and $[M(Me,COOH\text{-}2\text{-}oxosar\text{-}H)]^{x+}$, are below that of the free ions with the exception of the $[Fe(H_2O)_6]^{3+/2+}$ complex. Also, relative to $[M(H_2O)_6]^{3+/2+}$ the M(III) ions are significantly stabilised by the N_6-amine ligands. Furthermore, replacement of one amine ligand by an amido moiety results in a slightly greater stabilisation of these ions than that observed for the N_6-amine systems. A large

deviation at Co in the graph is also observed for the N_6 complexes. This distortion arises because Co(III) possesses a low spin configuration and therefore becomes significantly stabilised when complexed to the N_6 ligands. For $[Co(H_2O)_6]^{3+}$ however, the Co(III) ion is very close to the spin crossover point because of H_2O being a weaker ligand than that of N and hence the potential for this complex appears at a more positive value. Also, low spin Ni(III) like that of Co(III) is significantly stabilised by N_6 ligands and even more so by the amido system.

3.4.5 Chemical Oxidations of the Fe(III) and Mn(III) Systems

Preliminary chemical oxidations on the Fe(III) and Mn(III) monoamido complexes were also carried out with a number of different oxidants. However the products from the various reactions were not isolated as there was insufficient time available to pursue this area of chemistry. Nevertheless, for the Fe(III) monoamido complex H_2O_2, $[NH_4]_2[Ce^{IV}(NO_3)_6]$, Cl_2 and bromine water all resulted in a colour change from brown/orange to pale yellow which is indicative of the formation of an Fe(IV) compound. The oxidation of the Mn(III) monoamido complex was less clear. Upon addition of H_2O_2 to an aqueous solution of the complex the solution lost colour and became cloudy. Acidification of a freshly prepared solution with a few drops of acetic acid resulted in the solution becoming brown/green in colour. However, addition of H_2O_2 to this solution did not produce any notable colour change. Clearly more work is needed in the chemical oxidation of these types of complexes.

3.4.6 Electronic Spectroscopy

All the complexes display maxima that are either similar to, or, red shifted with respect to the parent $[M(X,Y\text{-sar})]^{x+}$ (X,Y = H, H; H, Me; Me, COOH) species. A red shift corresponds to a weaker ligand field for that particular compound compared to the parent hexamine complex. The shift is greatest for the amido complexes and is similar to that found for the $[Co^{III}(\{NO_2\}_2\text{-sar})]^{3+}$ complex after loss of a proton from a coordinated nitrogen in strongly basic solution.[33] This red shift in the ligand field for the octahedral amide complexes results from the deprotonated amido nitrogen possessing a lone pair of electrons which undergo a π interaction with the occupied metal based t_{2g} electrons.[55] Consequently, the t_{2g} orbitals rise in energy and move closer to the e_g^* set the net result is a decrease in the ligand field strength of each amide as observed spectroscopically. At the same time the deprotonated ligand can be expected to be a better ligating

centre in a σ sense but this is not detected in the Δ value which is the difference between e_g^* and t_{2g} energy levels. The σ and π effects in these systems are too complicated to unravel in this study and a precise understanding would require single crystal studies on uniaxial crystals in order to evaluate the splittings in the lower symmetry. Such an analysis may be relevant in these and similar cases because intuitively it would be expected that the amido ion is a better ligand than NH_3 for example. To ascertain if this were true would require some knowledge of the e_g and e_g^* energy separations as well as the t_{2g}, e_g^* energy separations and the splittings of the states involved.

For the $[Ni^{II}(COO^-\text{-}2\text{-}oxosar)]^+$ ion, in both acidic and neutral media, the above explanation does not apply. The reason being the amide nitrogen is not deprotonated so the anionic influence is absent in this instance. However, a red shift is still observed in its electronic spectrum. This presumably results from the coordination properties of the protonated amide group which could be expected to be a rather weak donor. The crystal structures obtained on the two $[Ni^{II}(COO^-\text{-}2\text{-}oxosar)]^+$ ions confirmed this by displaying $Ni\text{-}N_{(amide)}$ distances that were marginally longer than the remaining $Ni\text{-}N_{(amine)}$ bond lengths within each complex.

The visible absorption spectrum of $[Ni^{III}(Me,CO_2H\text{-}2\text{-}oxosar\text{-}H)]^{2+}$ (Appendix Figure 3.1.9) is indicative of that expected for a Ni(III) cage ion and is similar to the spectrum observed for $[Ni^{III}(sar)]^{3+}$ (~400 nm, 570 nm and 1734 nm). However, the Ni(III) monoamide complex (~320 nm, ~400 nm, 631 nm and 1455 nm) displays a weaker ligand field in the higher energy band to that of the $[Ni^{III}(sar)]^{3+}$ ion and this probably results from the possible presence of a bound deprotonated amido group within the complex. It is expected, on going from Ni(II) to Ni(III), that the monoamide complex will have the amide nitrogen atom deprotonated since the higher oxidation state should have a lower pK_a for the amide proton. Therefore, a red shift in the electronic spectroscopy would be expected on going from $[Ni^{III}(sar)]^{3+}$ to $[Ni^{III}(Me,CO_2H\text{-}2\text{-}oxosar\text{-}H)]^{2+}$. This has been observed for the band present as 631 nm of the $[Ni^{III}(Me,CO_2H\text{-}2\text{-}oxosar\text{-}H)]^{2+}$ ion.

For low spin Ni(III)-N_6 systems a number of characteristic bands are expected however it is rare to see some of these in the spectrum. Firstly the $[Ni^{III}(Me,CO_2H\text{-}2\text{-}oxosar\text{-}H)]^{2+}$ ion displays a near-infra-red peak at 1455 nm which has been assigned to a $^2B_{1g} \leftarrow {}^2A_{1g}$ transition. This band, until now, has never been seen spectroscopically for a nickel complex in the unusual oxidation state of +III. The near-infra-red peak arises as a result of

strong Jahn-Teller splitting of the ^2E_g ground state. Furthermore, the bands at 631 nm, ~400 nm and ~320 nm have been assigned to $^2T_{1g(a)} \leftarrow {}^2A_{1g}$, $^2T_{2g} \leftarrow {}^2A_{1g}$ and $^2T_{1g(b)} \leftarrow {}^2A_{1g}$ transitions respectively.

[Since this thesis was examined the X-ray crystallographic analysis of $[Ni^{III}(Me,CO_2H\text{-}2\text{-}oxosar\text{-}H)](ClO_4)_2.H_2O$ has established the Ni(III) oxidation state and detailed structure. This is now given in an additional Appendix to the thesis].

The spectra of the amidine complexes are somewhat surprising. The ligand is neutral and partly delocalised. If anything it might have been expected to provide a somewhat greater ligand field. The only obvious possibility is that the amidine has some charge transfer character which influences the spectroscopy at the ligand field (LF) level. This would also be consistent with the higher intensities of the spectral bands compared with those of $[Co^{III}(sar)]^{3+}$.

Most of the complexes here also display intensities greater than that of their respective parent hexamines. This could be due to the presence of ligating functional groups that affect the metal by distorting its environment, making it less octahedral in character. These distortions assist the transitions to become more allowed because the symmetry diminishes and the selection rules become less rigid. In addition, the delocalised nature of the amide and amidine groups may introduce some charge transfer character in the LF bands as described above and both mechanisms would contribute to the LF band intensities.

3.4.7 Properties of the Amido/Amide Group within a Cage Ligand

The comparison between the monoamido and saturated amine cage complexes allows a direct evaluation of the stabilising effect and some properties exerted by the deprotonated amido group compared to that of the amino group. Clearly, the addition of just one amido group immediately affects both the electrochemical and electronic properties of the sar cage. Generally, the redox results showed that the M(III)/(II) couples were more negative for the amido complexes than for the equivalent sar cages indicating that the amido group is more effective at stabilising the M(III) state. This is not a surprising result since stabilisation of the trivalent M(III) state results from the quenching of the tripositive charge of the metal due to the complexation of the negatively charged ligand. In addition, the electronic spectra of the six coordinate amido cages are red shifted due to

the presence of the deprotonated nitrogen atom compared to that of the saturated six coordinate parents. For amido cage systems it appears that a red shift generally occurs regardless of the type of metal atom within the complex.

These are not the only two unique properties that the amide cage systems display which are different to those observed for the saturated analogues. For instance, the crystallographic data, on the six coordinate amido cage systems, show that the trigonal C-N^- distances (approximately 1.30 Å) are shorter than the tetrahedral C-N bond lengths (1.45 Å). The reason is that the amide group is delocalised over the carbon, nitrogen and oxygen atoms and as a result so is the charge of the anionic amido nitrogen atom. Therefore, the cavity size of the amide cage is expected to be somewhat smaller than that for the saturated parent. The amide cage crystal structures also revealed that when compared to a free peptide ligand, complexation of the amide nitrogen shortens the amide C-N (from ~1.325 Å to ~1.30 Å) and lengthens the C-O bond (from ~1.24 Å to ~1.27 Å)[20] resulting in more double-bond character in the C-N bond and less double-bond character in the C=O bond. In addition, the crystallography revealed that the planarity of the amide group, within the cage ligand, is generally maintained when the deprotonated trigonal amide nitrogen is coordinated to a metal ion. Therefore, it is assumed that the same applies to all amide cage systems which display coordination to the amido nitrogen atom.

It is also possible within the amide cage ligand systems, as outlined earlier, for the metal not to bind the amide nitrogen and produce pentadentate species. This is different to the binding properties of amine cage systems where the metal is always bound to the six nitrogens. It was hoped that by combining the well known encapsulating properties of the cage ligand and amide moieties that six coordinate amide species would arise with all first row transition metal ions. Nevertheless, the crystal structure of the $[Cu(Me\text{-}2\text{-}oxosar)]^{2+}$ ion shows that the metal is five coordinate with the amide unbound and protonated. This may indicate that the Cu(II) ion possesses different binding characteristics to that of the Co(III) ion, for instance, with the amide cage ligand. In the protonated form (-CONH-) the amide group is a poor ligand[56] because it does not have an orbital readily available for metal binding. To produce a $M\text{-}N_{(amido)}$ bond the metal must displace the hydrogen from the amide nitrogen atom. However, amide groups generally possess high pK_a values (> 15) and so act as very weak acids for proton loss from the trigonal nitrogen to give a

negatively charged species.[24] In essence, log K of the metal for binding needs to be greater than the pK_a of the amide nitrogen atom. Therefore, it may be more difficult for some transition metal ions, in the cage amide systems, to substitute for the nitrogen bound amide hydrogen. For this reason the Cu(II) ion may not possess a sufficiently high enough log K to bind the amide nitrogen atom, within the cage, and hence remains unbound resulting in the observed pentadentate Cu(II) complex.

The monoamide ligand, $Me,CO_2^-K^+$-2-oxosar, was also observed to have little interaction with Zn^{2+} and to date a zinc complex with this ligand has not been characterised. This is contrary to the binding properties observed in the crystal structure for the $[Zn(sar)]^{2+}$ ion. The lability of the zinc ion may be one of the factors in the failure of the monoamide ligand to produce a complex. However, another reason may be that a $ZnOH^-$ species, once complexed to the ligand, may act as a nucleophile for the hydrolysis of the amide unit. A similar reaction has been proposed to occur in macrocyclic amides when the ligand is complexed to Zn^{2+}.[57] This could result in the decomposition of the amide ligand and explain why less than sixteen signals were observed in the ^{13}C NMR of the product at the completion of the reaction. Despite the failure to produce a zinc monoamide complex, it does show that the amide cage ligands may display some selectivity towards certain transition metal ions. This then raises the possibility of potentially using the properties of the amide cage to preferentially remove certain metal ions from the body for example.

3.5 Conclusions and Future Directions

In this chapter a number of Co(III) monoamide cage complexes have been produced from the capping reaction of $[Co^{III}(sen)]^{3+}$ with formaldehyde and an appropriate bifunctional methylene compound. However, it was also shown that amide complexes were not the only products formed from the various reactions. This led to the discovery that the carbon acid can and does undergo reaction itself during the condensation reaction. Consequently, amidine and saturated cages and macrocyclic Co(III) complexes also arose from the various reactions undertaken. It was also shown that it is possible to demetallate certain Co(III) amide cage complexes and then complex the free ligand to different metal ions to give a range of different metal amide cage complexes.

Most of the complexes produced in this work were found to be extraordinarily stable with respect to ligand stability and dissociation, which is a function of the encapsulation. In fact, the new complexes both amides and amidines provide stable new cages and ligands for manipulating the transition metal ion chemistry. This stability was highlighted by the amidine cage systems which proved to be essentially unreactive in the presence of acid, base, HNO_3 and NO^+ when bound to the Co(III) ion. All attempts to cleave the amidine or oxidise or reduce it have failed dismally. This contrasts remarkably with the ease of decomposition of such functional groups in regular organic chemistry. Removing the ligand from the metal ion therefore is not likely to produce a stable free cage and so this process was not attempted for the amidines.

The amide complexes also display a red shift in their electronic and a negative shift in their redox properties when compared to that of the saturated cage parents. The strong electron donating and withdrawing groups clearly also have an influence on the redox potentials along with that of the ligand itself. For all the metal ions involved, Cr(III), Mn(III), Fe(III), Co(III), Ni(III), it was found that the amido ligand [M(Me,COOH-2-oxosar-H)]$^{2+}$ stabilises the high oxidation state by about 0.2 V relative to the equivalent [M(sar)]$^{3+/2+}$ ions. However, in the cyclic voltammetry the Cr(IV), Mn(IV), Fe(IV), Co(IV) and Ni(IV) states were not observed in aqueous media. Nor was Cr(II) or Cu(I) observed. The former is too negative a potential and the latter irreversible because Cu^+ comes out of the cage rapidly. So while the amido ligand served a good purpose in stabilising the higher oxidation state, it was not sufficient to readily access

all the M(IV) states. Nevertheless, the monoamide cages themselves as well as the other complexes in this chapter display interesting properties that warrant further investigation. For example, it would be of interest to tie other organic fragments to the COOH, COOR and CN substituents so that these cage and partial cage complexes can act as building blocks for larger macromolecular assemblies. It would be expected that the new substituents would alter the properties, such as the redox potentials, of the complexes further.

3.6 References

(1) Buckingham, D. A.; Foster, D. M.; Sargeson, A. M. *J. Am. Chem. Soc* **1969**, *91*, 3451.

(2) Geue, R. J.; Petri, W. R.; Sargeson, A. M.; Snow, M. R. *Aust. J. Chem.* **1992**, *45*, 1681.

(3) Lawrance, G. A.; Maeder, M.; Wilkes, E. N. *Reviews in Inorganic Chemistry* **1993**, *13*, 199.

(4) Tomioka, K.; Sakaguchi, U.; Yoneda, H. *Inorg. Chem.* **1984**, *23*, 2863.

(5) Sarneski, J. E.; Urbach, F. L. *J. Am. Chem. Soc.* **1971**, *93*, 884.

(6) Green, R. W.; Catchpole, K. W.; Phillip, A. T.; Lions, F. *Inorg. Chem.* **1963**, *2*, 597.

(7) Sheldrick, G. M. In *Crystallographic Computing 3*; G. M. Sheldrick, C. Krüger and R. Goddard, Eds.; Oxford University Press: 1985; p 175.

(8) Beurskens, P. T.; Admiraal, G.; Beurskens, G.; Bosman, W. P.; Garcia-Granda, S.; Gould, R. O.; Smits, J. M. M.; Smykalla, C. *DIRDIF92 In The DIRDIF program system, Technical Report of the Crystallography Laboratory*; University of Nijimegen: The Netherlands, 1992.

(9) Cromer, D. T.; Waber, J. T. In *International Tables of X-ray Crystallography*; The Kynoch Press: Birmingham, England, 1974; Vol. IV.

(10) Ibers, J. A.; Hamilton, W. C. *Acta Crystallogr.* **1964**, *17*, 781.

(11) Creagh, D. C.; McAuley, W. J. In *International Tables for Crystallography*; A. J. C. Wilson, Ed.; Kluwer Academic Publishers: Boston, 1992; Vol. C; p 219.

(12) Creagh, D. C.; Hubbel, J. H. In *International Tables for Crystallography*; A. J. C. Wilson, Ed.; Kluwer Academic Publishers: Boston, 1992; Vol. C; p 200.

(13) *teXsan: Crystal Structure Analysis Package*; Molecular Structure Corporation: 1985 & 1992.

(14) Geue, R. J.; West, M. L. M. *Personal communication*

(15) Gainsford, A. R.; Pizer, R. D.; Sargeson, A. M.; Whimp, P. O. *J. Am. Chem. Soc.* **1981**, *103*, 792.

(15a) *SIR92:* Altomare, A.; Casarano, M.; Giacovazzo, C.; Guagliardi, A. *J. Appl. Cryst.* **1993**, *26*, 343.

(16) Spek, A. L. *PLATON-94 In Program for the Automated Analysis of Molecular Geometry*; Utrecht University: The Netherlands, 1994.

(17) Beurskens, P. T.; Admiraal, G.; Beurskens, G.; Bosman, W. P.; de Gelder, R.; Israel, R.; Smits, J. M. M. *DIRDIF94 In The DIRDIF-94 program system, Technical Report of the Crystallography Laboratory*; University of Nijimegen: The Netherlands, 1994.

(18) *Xtal 3.2*; S. R. Hall, H. D. Flack, J. M. Stewart, Ed.; Universities of Western Australia, Geneva and Maryland: 1992.

(19) Angus, P. M. *Personal communication*

(20) Sargeson, A. M. *Pure & Appl. Chem.* **1984**, *56*, 1603.

(21) Fenn, J. B.; Mann, M.; Meng, C. K.; Wong, S. F.; Whitehouse, C. M. *Science* **1989**, *246*, 64.

(22) Schneider, M. L.; Ferguson, G.; Balahura, R. J. *Can. J. Chem.* **1973**, *51*, 2180.

(23) Barnet, M. T.; Buckingham, D. A.; Freeman, H. C.; Hsu, I.-N.; van der Helm, D. *J. Chem. Soc. Chem. Commun.* **1970**, 367.

(24) Martin, R. B.; Sigel, H. *Chem. Rev.* **1982**, *82*, 385.

(25) Höhn, A.; Geue, R. J.; Sargeson, A. M.; Willis, A. C. *J. Chem. Soc., Chem. Commun.* **1989**, 1644.

(26) Balahura, R. J.; Ferguson, G.; Ruhl, B. L.; Wilkins, R. J. *Inorg. Chem.* **1983**, *22*, 3990.

(27) Bernhardt, P. V.; Bygott, A. M. T.; Geue, R. J.; Hendry, A. J.; Korybut-Daszkiewicz, B. R.; Sargeson, A. M.; Willis, A. C. *Inorg. Chem.* **1994**, *33*, 4553.

(28) Clark, I. J.; Geue, R. J.; Engelhardt, L. M.; Harrowfield, J. M.; Sargeson, A. M.; White, A. H. *Aust. J. Chem.* **1993**, *46*, 1585.

(29) Creaser, I. I.; Lydon, J. D.; Sargeson, A. M.; Horn, E.; Snow, M. R. *J. Am. Chem. Soc.* **1984**, *106*, 5729.

(30) Creaser, I. I.; Geue, R. J.; Harrowfield, J. M.; Herlt, A. J.; Sargeson, A. M.; Snow, M. R.; Springborg, J. *J. Am. Chem. Soc.* **1982**, *104*, 6016.

(31) Buckingham, D. A.; Clark, C. R.; Foxman, B. M.; Gainsford, G. J.; Sargeson, A. M.; Wein, M.; Zanella, A. *Inorg. Chem.* **1982**, *21*, 1986.

(32) Bond, A. M.; Lawrance, G. A.; Lay, P. A.; Sargeson, A. M. *Inorg. Chem.* **1983**, *22*, 2010.

(33) Geue, R. J.; Hambley, T. W.; Harrowfield, J. M.; Sargeson, A. M.; Snow, M. R. *J. Am. Chem. Soc.* **1984**, *106*, 5478.

(34) Lawrance, G. A.; Lay, P. A.; Sargeson, A. M. *Inorg. Chem.* **1990**, *29*, 4808.

(35) Osvath, P.; Sargeson, A. M. *Unpublished Data*

(36) Poon, C. K.; Tobe, M. L. *J. Chem. Soc. (A)* **1968**, 1549.

(37) Williams, D. H.; Fleming, I. In *Spectroscopic Methods in Organic Chemistry*; 4th ed.; McGraw-Hill Book Company (UK) Limited: London, 1987; Chapter 2, p 29.

(38) Clark, I. J.; Creaser, I. I.; Engelhardt, L. M.; Harrowfield, J. M.; Krausz, E. R.; Moran, G. M.; Sargeson, A. M.; White, A. H. *Aust. J. Chem.* **1993**, *46*, 111.

(39) Bernhardt, P. V.; Bramley, R.; Engelhardt, L. M.; Harrowfield, J. M.; Hockless, D. C. R.; Korybut-Daskiewicz, B. R.; Krausz, E. R.; Morgan, T.; Sargeson, A. M.; Skelton, B. W.; White, A. H. *Inorg. Chem.* **1995**, *34*, 3589.

(40) Comba, P.; Sargeson, A. M.; Engelhardt, L. M.; Harrowfield, J. M.; White, A. H.; Horn, E.; Snow, M. R. *Inorg. Chem.* **1985**, *24*, 2325.

(41) Bernhardt, P. V.; Harrowfield, J. M.; Hockless, D. C. R.; Sargeson, A. M. *Inorg. Chem.* **1994**, *33*, 5659.

(42) Lim, M. C.; Sinn, E.; Martin, R. B. *Inorg. Chem.* **1976**, *15*, 807.

(43) Simmons, C. J.; Lundeen, M.; Seff, K. *Inorg. Chem.* **1978**, *17*, 1429.

(44) Ray, N. J.; Hathaway, B. J. *Acta Crystallogr., Sect. B* **1978**, *B34*, 3224.

(45) Nardin, G.; Randaccio, L.; Bonomo, R. P.; Rizzarelli, E. J. *J. Chem. Soc., Dalton Trans.* **1980**, 369.

(46) Neitzel, C. J.; Desiderato, R. *Cryst. Struct. Commun.* **1975**, *4*, 333.

(47) Comba, P.; Horn, E.; Sargeson, A. M.; Snow, M. R. *Unpublished work*

(48) Wieghardt, K.; Schmidt, W.; Herrmann, W.; Küppers, H.-J. *Inorg. Chem.* **1983**, *22*, 2953.

(49) Marsh, R. E. *Acta Crystallogr., Sect. B* **1987**, *B34*, 174.

(50) Kostka, K. L.; Fox, B. G.; Hendrich, M. P.; Collins, T. J.; Rickard, C. E. F.; Wright, L. J.; Münck, E. *J. Am. Chem. Soc.* **1993**, *115*, 6746.

(51) Martin, L. L. Ph.D. Thesis, Australian National University, 1986.

(52) Gainsford, G. J.; Jackson, W. G.; Sargeson, A. M. *J. Am. Chem. Soc.* **1977**, *99*, 2383.

(53) Anderson, P. A.; Creaser, I. I.; Dean, C.; Harrowfield, J. M.; Horn, E.; Martin, L. L.; Sargeson, A. M.; Snow, M. R.; Tiekink, E. R. T. *Aust. J. Chem.* **1993**, *46*, 449.

(54) Comba, P.; Creaser, I. I.; Gahan, L. R.; Harrowfield, J. M.; Lawrance, G. A.; Martin, L. L.; Mau, A. W. H.; Sargeson, A. M.; Sasse, W. H. F.; Snow, M. R. *Inorg. Chem.* **1986**, *25*, 384.

(55) Bull, D. J.; Creaser, I. I.; Sargeson, A. M.; Skelton, B. W.; White, A. H. *Inorg. Chem.* **1987**, *26*, 3040.

(56) Margerum, D. W.; Dukes, G. R. In *Metal Ions in Biological Systems*; H. Sigel, Ed.; Marcel Dekker: New York, 1974; Vol. 1; Chapter 5, p 157.

(57) Kimura, E.; Koike, T.; Shiota, T.; Iitaka, Y. *Inorg. Chem.* **1990**, *29*, 4621.

CHAPTER 4.

Oxidation of Co(III) Encapsulated Ligands with Mercuric Acetate.

4.1 Introduction

The most general way to introduce an amide moiety into the cage skeleton is via template condensation with formaldehyde and an appropriate carbon acid such as malonic acid diester. However, oxidation of the saturated cage is also an obvious route to such derivatives.

Generally, oxidation of coordinated amine ligands can be achieved with or without involvement of the metal, with the most common result being the formation of an imine bond within the ligand.[1] However, other unsaturated groups can and do arise depending on the particular oxidative method employed. One such method of oxidising the ligand involves dehydrogenation triggered by a high oxidation state of the metal. An illustration of this path is intramolecular redox reaction of the $[Os^{IV}(en)_2(en\text{-}2H)]^{2+}$ ion (Figure 1).[2] Under N_2, the Os(IV) ethylenediamine complex was observed to undergo spontaneous oxidative dehydrogenation of the ligand to form an Os(II) imine species. In the presence of more O_2, the $[Os^{II}(en)_2(im)]^{2+}$ complex was oxidised further to $[Os^{II}(en)_2(diim)]^{2+}$ and finally to $[Os^{II}(en)(diim)_2]Cl_2.HCl.H_2O$. Such chemistry is not uncommon for Fe and Ru amines where the M^{IV} state is accessible and a reasonable oxidant.

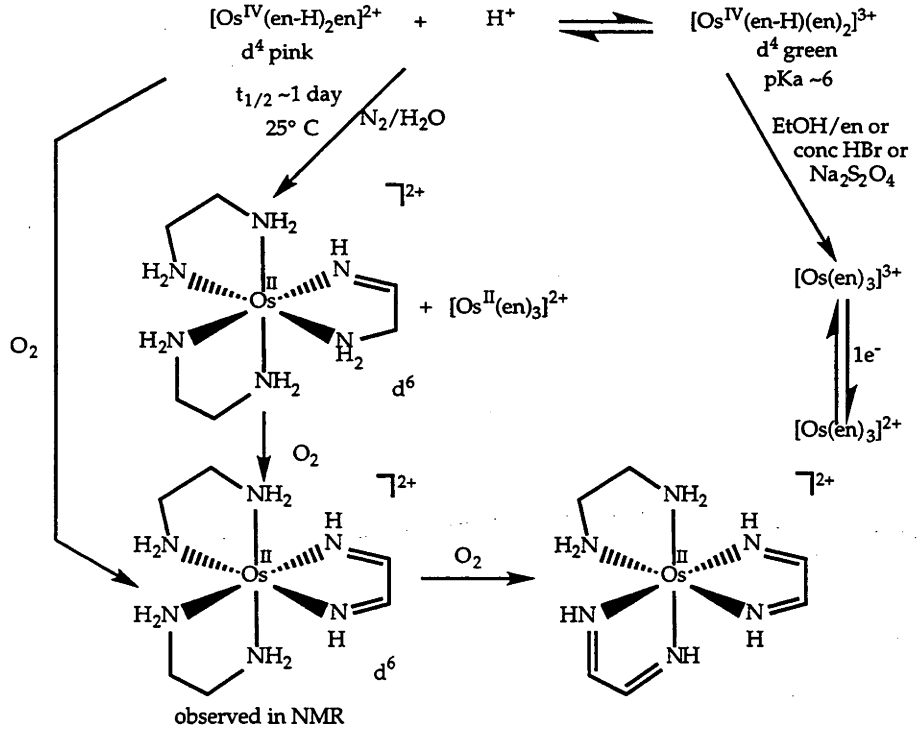

Figure 1

The above strategy should be less effective for the inert Co(III) cage systems where the higher oxidation states of cobalt are not readily accessible. The Co(III) ion is not a good oxidant bound to amine groups and would also protect the ligand from oxidative dehydrogenation so an external oxidant must be used to effect oxidation of the ligand. While the metal ion can protect the coordinated amine from attack at one pair of electrons, it can also activate the loss of a proton at the amine site so oxidation is not precluded but is restricted by these facets. For this particular oxidative method, which will be the focus of the work in this chapter, only the ligand appears to be oxidised. This type of ligand oxidation reaction, via an external oxidant, is not so prevalent in the literature; however, some examples follow to illustrate the potential pathways for an intermolecular oxidant.

Protection of the amine in oxidising circumstances is displayed by coordinated amino alcohols, $[Co^{III}(NH_3)_5NH_2CH_2CH(OH)CH_3]^{3+}$ and $[Co^{III}(NH_3)_5NH_2CH_2CH(OH)C_6H_5]^{3+}$, which can be easily oxidised with acid-dichromate solutions to the amino ketone with little or no oxidation of the amine centre (Figures 2 and 3).[3] Treatment of these ketone complexes with base then allows the formation of imines. For example, the amino ketone complexes undergo an intramolecular capture of the carbonyl group by a deprotonated <u>cis</u> ammine centre to give the bidentate aminocarbinol chelate. A subsequent base-catalysed reaction produces the imine complexes quantitatively.

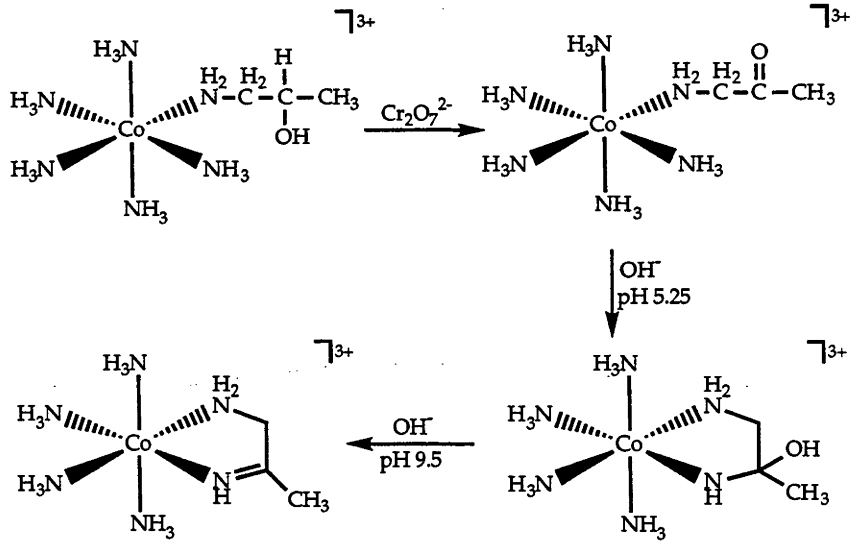

Figure 2

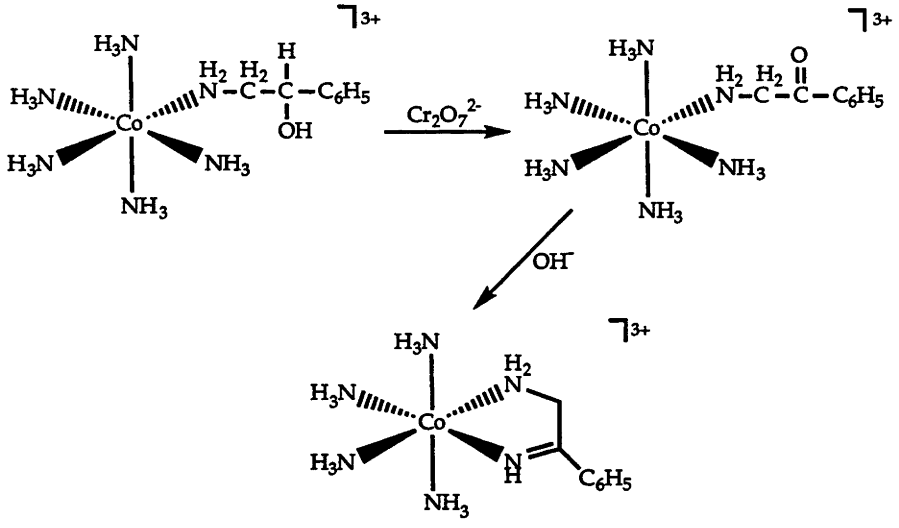

Figure 3

It is also possible to produce amide groups directly from these types of oxidative reactions as well. The carbinolamine complex, (RRR,SSS)-t-[Co^{III}(treneol)Cl](Br)(ClO_4), can be oxidised with the $Cr_2O_7^{2-}$ ion leading to the formation of a tertiary amide while the Cl^- ion remains coordinated (Figure 4).[3] In this example, the coordinated tertiary amide N atom clearly restricts the delocalisation of charge over the amido moiety since it is not possible to lose a proton from the amide N atom. This is reflected in the amide C=O IR stretching frequency (1706 cm^{-1}) which is closer to that of saturated ketones (~1700 cm^{-1}) than that of tertiary amides (~1650 cm^{-1}) and therefore more ketonic in character.

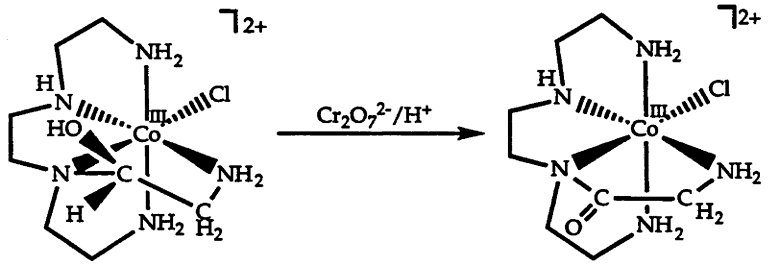

Figure 4

Some preliminary work on the oxidation of cage ligands using an external oxidant has been undertaken. This work has revealed that not only are imine groups obtained but amide moieties are produced as well, at least with some oxidants. For example, $[Co^{III}(\{NO_2\}_2\text{-sar})]^{3+}$ was oxidised by

MnO_4^{2-} or OH^-/Br_2 to give a range of products although a monoimine cage complex was isolated as a major species.[4] Similarly, $[Co^{III}(sep)]^{3+}$ reacts with $Hg^{II}(OAc)_2$ to yield a range of different products containing amide and/or imine moieties.[5] The major product from this reaction has been identified by X-ray crystallography (Figure 5a) although complete characterisation of the other minor products obtained has yet to be carried out. Further, oxidations with $Hg^{II}(OAc)_2$ were performed on $[Co^{III}(\{NH_3^+\}_2\text{-sar})]^{5+}$ and after 25 hrs reaction the major product was $[Co^{III}(\{NH_3^+\}_2\text{-2-oxosar-H})]^{4+}$ (Figure 5b).[6] Moreover, it has been shown that $[Co^{III}(\{NH_3^+\}_2\text{-sar})]^{5+}$ can be oxidised with a $Co^{II}Cl_2$-charcoal mixture and O_2 under basic conditions.[6] From this reaction a diamido cage complex arose where the two amido moieties are located in the one ethylenediamine ring (Figure 5c). To date however, the extent of long term oxidation of $[Co^{III}(\{NH_3^+\}_2\text{-sar})]^{5+}$ with $Hg^{II}(OAc)_2$ to produce polyamide species has not been investigated. Also the role of the Co(III) ion in these processes needs to be evaluated.

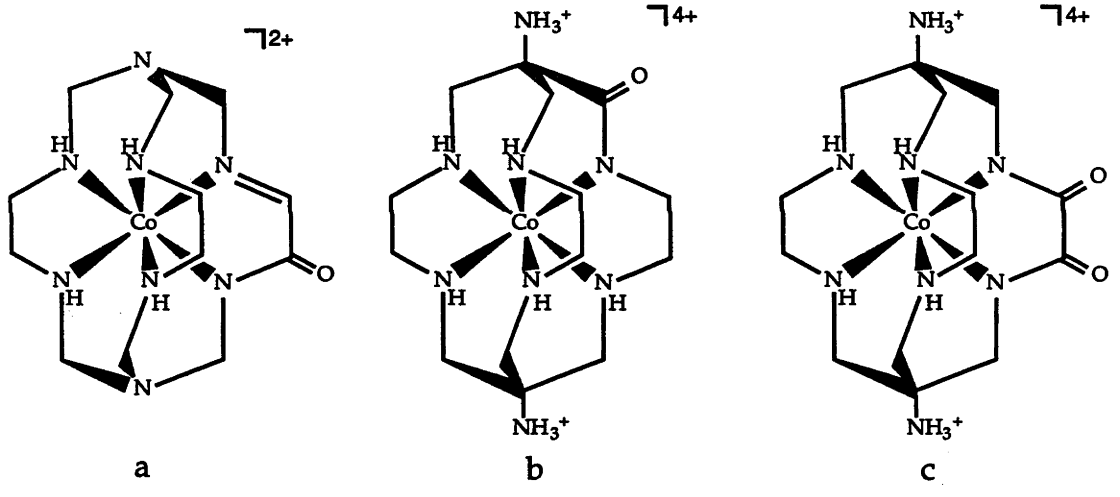

a b c

Figure 5

Therefore, the work in this chapter covers a number of areas. Firstly, the Co(III) amido cage complex (Figure 5b) has been demetallated to obtain the free ligand, (NH_2)-2-oxosar, which was then recomplexed to other metal ions. Furthermore, $[Co^{III}(\{NH_3^+\}_2\text{-sar})]^{5+}$ has been oxidised with $Hg^{II}(OAc)_2$, over a much longer time to explore the product evolution. The synthesis of this series of compounds is important for several reasons. It now allows comparison between three types of cage compounds, the hexamine, monoamido and polyamido metal cage complexes. This permits the progressive effects that the amide moiety has upon the properties of the (NH_2)-sar ligand to be assessed.

4.2 Experimental

4.2.1 Syntheses

All chemicals (AR grade) were used as received unless otherwise specified. $[Co^{III}(\{NH_3^+\}_2\text{-sar})]Cl_5.H_2O$ was prepared from a published method.[7]

[1,8-diammonio-2-oxo-3,6,10,13,16,19-hexaazabicyclo[6.6.6]icosanato]-cobalt(III)]chloride.5H_2O, $[Co^{III}(\{NH_3^+\}_2\text{-2-oxosar-H})]Cl_4.5H_2O$

This compound has been prepared previously but is reported in detail here.[8] $[Co^{III}(\{NH_3^+\}_2\text{-sar})]Cl_5.H_2O$ (200 g; 0.350 mol) was dissolved in dilute acetic acid (5% v/v; 2L) in a large robust flask (10 L). $Hg^{II}(OAc)_2$ (1020 g, 3.201 mol) was then added and the solution (pH ~2) stirred until most of the solid had dissolved. The solution was then refluxed (oil bath at ca. 120° C) and stirred for 48 hr. Over several hours the initially orange solution changed to a reddish colour while foaming vigorously, and a white precipitate of (Hg_2Cl_2) (containing some Hg metal) was formed. After 48 hr the mixture was cooled to 20° C, the solid (Hg_2Cl_2), Hg residues (ca. 350 g recovered) filtered off, washed thoroughly with water and air dried. The filtrate was sorbed onto Dowex 50Wx2 resin (60 cm x 6.5 cm) and washed copiously with water and then with 1 M $NaNO_3$/0.1 M HNO_3 solution to remove Co(II) and remaining Hg(II) ions. The nitrate eluate was concentrated, cooled (< 10° C) and much of the Hg(II) recovered as $HgCl_2$ by addition of 6 M HCl (ca. 400 g dried $HgCl_2$ recovered). The column was then washed with water and 1 M HCl to remove NO_3^-, Na^+ ions, and the complex reaction products were eluted with 3.5 M HCl. The 3.5 M HCl eluate was evaporated to dryness, redissolved in water and sorbed onto two columns of SP-Sephadex C-25 cation exchange resin (100 cm x 10 cm). The columns were washed with water and 0.1 M HCl to remove some minor low charged species. Chromatography of the main complexes was then commenced using 0.5 M HCl to yield four main band groups B1 - B4, with some intermediate material between B2 (red) and B3 (red/orange) and B3 containing the main reddish/orange reaction product $[Co^{III}(\{NH_3^+\}_2\text{-2-oxosar-H})]^{4+}$.

Subsequent chromatography of B1 (very intense red/orange) and B2 (red) indicated that B1 contained four main trioxosar (triamide) derivatives. B1 and B2 totalled less than 10% of the reaction yield with B2 containing the bulk of this (7 - 8%). After desalting the orange B4 band

effluent by using Dowex 50Wx2 resin with water, 1 M HCl washing and eluting with 3 M HCl, the orange product was crystallised from 6 M HCl using ethanol (ca. 20 mL). It was shown to contain mainly $[Co^{III}(\{NH_3^+\}_2\text{-sar})]^{5+}$ starting material (ca. 10% as the chloride salt) by ^{13}C NMR spectroscopy.

The main band B3 (red/orange) was rechromatographed on SP-Sephadex C-25 cation exchange resin using 0.05 M K_2SO_4 (pH 3, H_2SO_4) eluent, but was found to contain mainly one product B3/1 (red/orange). This band was collected and desalted using Dowex 50Wx2 resin with water, 1 M HCl washing and then eluted with 3 M HCl. The eluate was evaporated to dryness and crystallised from 8 M HCl by the careful addition of MeOH to the turbidity point, standing and then slow addition of EtOH until crystallisation was completed. The reddish product was filtered off, washed with ethanol and diethyl ether and air dried. Yield = 80 g (39%). pKa's (I = 0.1 M): pKa_1 (NH_3) 3.38; pKa_2 (NH_3) 5.15.[8] Anal. Calc. for $C_{14}H_{33}N_8Cl_4CoO.5H_2O$: C, 27.1; H, 7.0; N, 18.1; Cl, 22.9. Found C, 27.3; H, 7.3; N, 18.5; Cl, 23.1. ^1H NMR (δ, D_2O): 2.16 - 2.68 (complex pattern, 10H, NCH_2); 2.80 - 3.06 (complex pattern, 8H, NCH_2); 3.18 (m, 2H, CH_2); 3.36 (m, 1H, CH_2); 3.46 (m, 1H, CH_2). ^{13}C NMR (δ, D_2O): 56.6 ($\underline{C}qNH_3^+$); 60.7 ($\underline{C}qC=O$); 47.1, 54.5, 54.7, 54.9, 55.3, 55.4, 55.5, 55.8, 55.9, 56.3, 56.9 ($N\underline{C}H_2$); 178.1 ($\underline{C}=O$). IR in KBr ($\nu\text{-}_{max}/cm^{-1}$): 3408, 3061 (NH stretch); 2868 (C-H stretch); 2569, 2000 (NH_3^+ overtone band); 1627 (C=O amide stretch); 1520 (NH_3^+ symmetric bending); 1465, 1440 (C-H deformation); 1360, 1329, 1273, 1209, 1166 (C-H twisting); 1089 (C-N-C); 1050, 951, 923, 882, 845, 760 (CH_2 rock). IR in D_2O ($\nu\text{-}_{max}/cm^{-1}$): 3465, 3426 (NH stretch); 2960 (C-H stretch); 1625 (C=O amide stretch); 1474 (C-H deformation). IR of the deuterated complex in KBr ($\nu\text{-}_{max}/cm^{-1}$): 3391 (NH stretch); 2923 (C-H stretch); 2537 (ND stretch); 2252 (ND_3^+ asym and sym stretch); 1621 (C=O amide stretch); 1459 (C-H deformation); 1260, 1216 (C-H twisting); 1137 (C-N-C); 1064, 1034, 955, 901, 835, 756 (CH_2 rock). Low resolution ESMS (50 V) [m/z, obs (calc) (%) assignment where cage = $[^{12}C_{14}{}^1H_{33}{}^{14}N_8{}^{59}Co^{16}O]^{4+}$]: 384.9 (385) (100%) $[Cocage^{4+} - 3H^+]^+$; 420.8 (421) (10%) $[Cocage^{4+} - 2H^+ + {}^{35}Cl^-]^+$.

1,8-diamino-2-oxo-3,6,10,13,19-hexaazabicyclo[6.6.6]icosane, $(NH_2)_2$-2-oxosar

$[Co^{III}(\{NH_3^+\}_2\text{-2-oxosar-H})]Cl_4.5H_2O$ (17.3 g; 0.03 mol) was dissolved in 150 mL of H_2O and to this was added a solution of $CoCl_2.6H_2O$ (7.1 g; 0.03 mol) in 100 mL of H_2O. A second solution of KCN (38.8 g; 0.60 mol) in 150 mL of H_2O was added dropwise, over a period of ten minutes, after both solutions had been deaerated with N_2 for approximately one hour. The

resultant solution was stirred at ~20° C for a period of one week and over this time the colour changed from red to pale yellow. Separation of the ligand from the cyanide consisted of precipitating out the KCN with ethanol (2 L), filtering the solution and removing the solvent under vacuum. The residue was then redissolved in ethanol (200 mL), refiltered to remove more KCN and once again the ethanol was removed under vacuum to yield a thick yellow oil. This procedure was repeated until no more KCN could be observed. Yield = 7.43 g (78%). ^{1}H NMR (δ, D_2O): 2.65 - 3.25 (complex pattern, 22H, NCH_2). ^{13}C NMR (δ, D_2O) 40.3 ($\underline{C}qNH_2$); 58.6 ($\underline{C}qC=O$); 48.8, 49.3, 50.1,50.4, 53.4, 57.7, 58.3 ($N\underline{C}H_2$); 177.7 ($\underline{C}=O$).

[(1-ammonio-8-amino-2-oxo-3,6,10,13,19-hexaazabicyclo[6.6.6]icosanato)-nickel(II)]perchlorate.4.5H_2O, [Ni^{II}({NH_3^+}$_2$-2-oxosar-H)](ClO_4)$_3$.4.5H_2O

To a solution of $Ni^{II}Cl_2.6H_2O$ (7.4 g; 0.03 mol) and triethylamine (2.3 g; 0.02 mol) in 100 mL of H_2O was added (NH_2)-2-oxosar (7.43 g; 0.02 mol) in 100 mL of H_2O with stirring after both solutions had been deaerated, with N_2, for approximately one hour. The resultant solution was initially light blue in colour and a precipitate was formed. However over time the solution changed from blue to pink indicating that complex formation had occurred and the precipitate was eventually taken back up into solution. After several days the pink solution was diluted to two litres and sorbed onto a SP-Sephadex C-25 column (40 cm x 5 cm). Elution with 0.25 M $NaClO_4$ produced a single pink band which was collected and reduced in volume. This was acidified with a few drops of concentrated perchloric acid and after standing a few days in the air a pink solid crystallised. This was collected by filtration, washed with ethanol and ether and air dried. Further crops were obtained by allowing the filtrate to continually evaporate in air. Yield = 7.0 g (53%). Anal. Calc. for $C_{14}H_{33}N_8Cl_3NiO_{13}.4.5H_2O$: C, 25.2; H, 6.2; N, 16.8; Cl, 10.6. Found C, 25.0; H, 5.7; N, 16.6; Cl, 11.0. IR in KBr (ν-$_{max}$/cm^{-1}): 3300, 3200 (NH stretch); 2925, 2878 (C-H stretch); 1589 (C=O amide stretch); 1453, 1420 (C-H deformation); 1330, 1315 (C-H twisting); 1092 (ClO_4^-), 1030, 965, 941, 928, 834, 759 (CH_2 rock); 625 (ClO_4^-). IR in D_2O (ν-$_{max}$/cm^{-1}): 3418 (NH stretch); 2942 (C-H stretch); 2444 (ND stretch); 2024 (ND_3^+ asym and sym stretch); 1597 (C=O amide stretch); 1454 (C-H deformation). IR of the deuterated complex in KBr (ν-$_{max}$/cm^{-1}): 3298 (NH stretch); 2927 (C-H stretch); 1596 (C=O amide stretch); 1467 (C-H deformation); 1323 (C-H twisting); 1089 (ClO_4^-); 929. 870, 744 (CH_2 rock); 625 (ClO_4^-). Low resolution ESMS (25 V) [m/z, obs (calc) (%)

assignment where cage = $[^{12}C_{14}{}^{1}H_{32}{}^{14}N_8{}^{59}Ni^{16}O]^{2+}$]: 384.8 (385) (100%) [Nicage^{3+} - 2H$^+$]$^+$; 484.9 (485) (11%) [Nicage^{3+} - H$^+$ + $^{35}ClO_4^-$]$^+$.

[(1,8-diammonio-2-oxo-3,6,10,13,19-hexaazabicyclo[6.6.6]icosanato)nickel-(II)]chloride.hydrochloride.5H$_2$O, [Ni^{II}({NH$_3^+$}$_2$-2-oxosar-H)]Cl$_3$.HCl.5H$_2$O

[Ni^{II}({NH$_2$}$_2$-2-oxosar-H)](ClO$_4$)$_2$.5H$_2$O (1 g; 1.5 x 10^{-3} mol) was sorbed onto a Dowex 50Wx2 column (10 cm x 2 cm). This was then washed with water and 1 M HCl to remove perchlorate ions and elution with 3 M HCl produced a single pink band which was collected and reduced to a very small volume. The chloride complex was then precipitated by adding ethanol and ether to the aqueous solution; the light pink solid was collected by filtration, washed with ether and air dried. Yield = 0.67 g (71%). Anal. Calc. for $C_{14}H_{33}N_8Cl_3NiO.HCl.5H_2O$: C, 27.8; H, 7.3; N, 18.5; Cl, 23.4. Found C, 28.4; H, 7.2; N, 18.5; Cl, 23.9. IR in KBr (ν-$_{max}$/cm^{-1}): 3407, 3180 (NH stretch); 2923, 2880 (C-H stretch); 2500, 2053 (NH$_3^+$ overtone band); 1615 (C=O amide stretch); 1524 (NH$_3^+$ symmetric bending); 1455, 1415 (C-H deformation); 1327, 1293, 1257, 1217 (C-H twisting); 1100 (C-N-C); 1059, 1025, 980, 931, 899, 874, 848, 781 (CH$_2$ rock). IR in D$_2$O (ν-$_{max}$/cm^{-1}): 3415 (NH stretch); 2948 (C-H stretch); 1612 (C=O amide stretch); 1470 (C-H deformation). IR of the deuterated complex in KBr (ν-$_{max}$/cm^{-1}): 3409 (NH stretch); 2925, 2877 (C-H stretch); 2562, 2360 (ND stretch); 2100 (ND$_3^+$ asym and sym stretch); 1607 (C=O amide stretch); 1457 (C-H deformation); 1352, 1323, 1244, 1190, 1154 (C-H twisting); 1120 (C-N-C); 1018, 932, 872, 759, 714 (CH$_2$ rock). Low resolution ESMS (80 V) [m/z, obs (calc) (%) assignment where cage = $[^{12}C_{14}{}^{1}H_{33}{}^{14}N_8{}^{59}Ni^{16}O]^{3+}$]: 384.8 (385) (25%) [Nicage^{3+} - 2H$^+$]$^+$; 420.9 (421) (0.3%) [Nicage^{3+} - H$^+$ + $^{35}Cl^-$]$^+$.

[1,8-diammonio-2-oxo-3,6,10,13,16,19-hexaazabicyclo[6.6.6]icosanato]-chromium(III)]chloride.4H$_2$O, [Cr^{III}({NH$_3^+$}$_2$-2-oxosar-H)]Cl$_4$.4H$_2$O

The crude complex has been prepared previously but is reported in detail here.[8] Dry ethanol (150 mL; 24 hr over freshly prepared 3 Å sieves) was degassed (Ar purged, using Schlenk-type apparatus) and placed in a glove compartment under O$_2$-free argon. Crude (ca. 90% w/w) (NH$_2$)$_2$-2-oxosar ligand (3.56 g, 1.08 x 10^{-2} mol) and the chromium complexes [Cr^{III}Cl$_3$pyridine$_3$][9] (2.66 g; 6.72 x 10^{-3} mol) and [Cr^{II}(CH$_3$CO$_2$)$_2$.H$_2$O]$_2$ (0.60 g, 1.60 x 10^{-3} mol, 3.19 x 10^{-3} mol in Cr^{III}) were also introduced into the glove box (under Ar). The ligand was first dissolved in the dry ethanol. Then the [Cr^{II}(CH$_3$CO$_2$)$_2$.H$_2$O]$_2$ dimer was added, followed by the [Cr^{III}Cl$_3$pyridine$_3$] complex and the mixture stirred under Ar at 20° C. The reaction mixture

quickly changed to a dark brownish-red colour. It was removed from the glove box after 3 hr, quickly poured into water (600 mL), filtered and the filtrate sorbed onto Dowex 50Wx2 cation exchange resin (10 cm x 2.5 cm). The column was washed with water, 1 M HCl and then eluted off with 3 M HCl. The 3 M HCl eluant was evaporated to dryness, redissolved in water and chromatographed on a SP-Sephadex C-25 cation exchange column (40 cm x 5 cm) using 0.1 M K_2SO_4 as the eluant. The main red/orange band was collected, desalted using Dowex 50Wx2 cation exchange resin with water, 1 M HCl eluants, and finally eluted of with 3 M HCl. The 3 M HCl eluent was reduced in volume and the complex crystallised/precipitiated by the slow addition of ethanol and diethyl ether. The orange solid was collected by filtration, washed with EtOH and ether and air dried. Yield = 3.24 g (49% based on Cr). pKa's (I = 0.1 M): pKa_1 (HNC=O) 2.06; pKa_2 (NH_3) 4.61; pKa_3 (NH_3) 6.54.[8]

Purification of the compound consisted of absorbing the complex (3 g) on a SP-Sephadex C-25 column (30 cm x 5 cm) and eluting with 0.25 M $NaClO_4$. Three bands were eluted and the first two minor bands were not isolated while the third, the largest band, was collected and desalted on Dowex 50Wx2. The orange product after it had been washed with 1M HCl and eluted with 3 M HCl, was collected reduced to a small volume and the complex precipitated with ethanol. This was collected by filtration, washed with ether and dried under vacuum. Yield = 2.6 g. Anal. Calc. for $C_{14}H_{33}N_8Cl_4CrO.4H_2O$: C, 28.2; H, 6.9; N, 18.8; Cl, 23.8. Found C, 28.0; H, 7.1; N, 18.4; Cl, 23.5. IR in KBr ($\nu\tilde{}_{max}/cm^{-1}$): 3417, 3038 (NH stretch); 2849 (C-H stretch); 2500, 2000 (NH_3^+ overtone band); 1625 (C=O amide stretch); 1517 (NH_3^+ symmetric bending); 1450 (C-H deformation); 1356, 1330, 1270, 1216 (C-H twist); 1055, 1030, 920, 875, 836, 761 (CH_2 rock). IR in D_2O ($\nu\tilde{}_{max}/cm^{-1}$): 3417 (NH stretch); 2953 (C-H stretch); 1619 (C=O amide stretch); 1470 (C-H deformation). IR of the deuterated complex in KBr ($\nu\tilde{}_{max}/cm^{-1}$): 3424 (NH stretch); 2952, 2853 (C-H stretch); 2552 (ND stretch); 2245 (ND_3^+ asym and sym stretch); 1618 (C=O amide stretch); 1456 (C-H deformation); 1325, 1265, 1182 (C-H twisting); 1182 (C-N-C); 1059, 1030, 952, 882, 829, 756 (CH_2 rock). Low resolution ESMS (80 V) [m/z, obs (calc) (%) assignment where cage = $[^{12}C_{14}{}^{1}H_{33}{}^{14}N_8{}^{52}Cr^{16}O]^{4+}$]: 377.8 (378) (100%) [Crcage^{4+} - $3H^+$]$^+$; 413.7 (414) (90%) [Crcage^{4+} - $2H^+$ + $^{35}Cl^-$]$^+$.

[1,8-Diammonio-2,7-dioxo-3,6,10,13,16,19-hexaazabicyclo[6.6.6]icosanato]-cobalt(III)]chloride.4.5H_2O, [Co^{III}({NH_3^+}$_2$-2,7-dioxosar-2H)]Cl_3.4.5H_2O, [1,8-Diammonio-2,9-dioxo-3,6,10,13,16,19-hexaazabicyclo[6.6.6]icosanato]cobalt-(III)]chloride.4H_2O, [Co^{III}({NH_3^+}$_2$-2,9-dioxosar-2H)]Cl_3.4H_2O, [(6-Amino-methyl-13-carboxamide-6,13-diammonio-1,4,8,11-tetraazacyclotetradecane)-cobalt(III)]chloride.2.75H_2O, [Co^{III}(6-{NH_3^+,C(O)NH}-13-{NH_3^+,CH_2NH_2}-cyclam)]Cl_4.2.75H_2O and [1,8-Diammonio-2-oxo-3,6,10,13,16,19-hexaazabi-cyclo[6.6.6]icosanato]cobalt(III)]chloride.3H_2O, [Co^{III}({NH_3^+}$_2$-2-oxosar-H)]-Cl_4.3H_2O.

[Co^{III}({NH_3^+}$_2$-sar)]Cl_5.H_2O (40 g; 0.07 mol) was dissolved in a 5% acetic acid solution (2 L) and treated with $Hg^{II}(OAc)_2$ (1 kg; 3 mol). The orange mixture was then refluxed, with stirring, over a period of forty-eight hours and during this time the mixture changed to a red colour. At the completion of the reaction, filtration removed the Hg_2Cl_2 and elemental mercury that had precipitated out of the mixture. The filtrate was loaded onto a column of Dowex 50Wx2 cation exchange resin (25 cm x 10 cm) and the column was washed successively with water then 2 M $NaNO_3$/0.1 M HNO_3 solution to remove free Co^{2+} and Hg^{2+} ions. Elution with 1 M HCl removed a diffuse orange band (not isolated), a red-orange band (A) and after increasing the eluant strength to 3 M HCl, a second red-orange band (B). Some orange material was removed from the column with 6 M HCl, but this was shown by NMR spectra to contain none of the desired diamide products. After evaporating all fractions, each was diluted to 1 L with water and loaded onto separate columns of SP-Sephadex C-25 cation exchange resin and eluted with 0.05 M Na_2HPO_4 solution. For the red-orange band (A) an initial red band (A1) was collected then a crimson orange band (A2) while two other minor orange fractions were not isolated. Chromatography of the red orange-band (B) produced two separate bands, a minor orange band (not isolated) and a substantial red orange band (B1). All of the collected fractions were then desalted on Dowex and reloaded onto Sephadex and eluted again with 0.05 M Na_2HPO_4. Chromatography of the red band (A1) revealed that it comprised mainly a red fraction (A1a) followed by a small orange band (not isolated). The crimson-orange band (A2) gave essentially three different fractions composed of an orange band (not recovered) a crimson red band (A2a) and a second orange band (not recovered). Lastly, the large red orange band (B1) split into three separate fractions, a minor orange band (not collected) a substantial orange band (B1a), and a major red band (B1b). The recovery of the isolated fractions consisted of desalting them separately on Dowex, reducing the eluate to a

very small volume and then precipitating out the complexes as chloride salts by the addition of ethanol and ether. The NMR spectra of A1a and A2a indicated that these corresponded to two of the number of possible isomers of $[Co^{III}(\{NH_3^+\}_2$-dioxosar-2H)]Cl_3 while B1a was a Co(III) amide complex that had lost two carbon atoms during the reaction and the last fraction B1b was $[Co^{III}(\{NH_3^+\}_2$-2-oxosar-H)]Cl_4. The yields of the four species were 2.5 g (6%), 0.2 g (0.5%), 4.5 g (13.5%) and 1.8 g (4.5%) respectively.

Anal. Calc. for A1a $C_{14}H_{30}N_8Cl_3CoO_2.4.5H_2O$: C, 28.6; H, 6.7; N, 19.0; Cl, 18.1. Found C, 28,4; H, 6.2; N, 19.3; Cl, 18.4. ^1H NMR (**δ**, 500 MHz, D_2O): 2.52, 2.62, 2.96, 3.26 (ABCD spin system, 8H, CH_2 en); 2.35, 2.74, 2.60, 3.26 (AA'BB' coupling pattern, 4H, CH_2 en); 2.78, 3.82 (AB doublet of doublets, 4H, CH_2 caps). ^{13}C NMR (**δ**, D_2O) 56.9 (CqC=O); 51.3, 54.8, 55.6, 55.7, 60.6 (NCH$_2$); 177.4 (C=O). IR in KBr (ν-$_{max}$/cm^{-1}): 3382, 3087 (NH stretch); 2958, 2923, 2875 (C-H stretch); 2500 (NH_3^+ overtone band); 1620 (C=O amide stretch); 1601, 1582 (NH_3^+ assymmetric bending); 1519 (NH_3^+ symmetric bending); 1457, 1423 (C-H deformation); 1327, 1290, 1274, 1233, 1204, 1158 (C-H twisting); 1133, 1117 (C-N-C); 1076, 1039, 1017, 1001, 974, 938, 924, 893, 870, 856, 843, 829, 789, 759, 734, 721, 708 (CH_2 rock). IR in D_2O (ν-$_{max}$/cm^{-1}): 3417 (NH stretch); 2953 (C-H stretch); 1619 (C=O amide stretch); 1470 (C-H deformation). IR of the deuterated complex in KBr (ν-$_{max}$/cm^{-1}): 3400 (NH stretch); 2951 (C-H stretch); 2500 (ND stretch); 2322, 2269 (ND_3^+ asym and sym stretch); 1618 (C=O amide stretch); 1457, 1427 (C-H deformation); 1329, 1197 (C-H twisting); 1110 (C-N-C); 1068, 1035, 944, 912, 892, 836, 800, 753 (CH_2 rock). Low resolution ESMS (50 V) [m/z, obs (calc) (%) assignment where cage = $[^{12}C_{14}{}^1H_{30}{}^{14}N_8{}^{59}Co^{16}O_2]^{3+}$]: 398.8 (399) (100%) [Cocage^{3+} - 2H$^+$]$^+$; 434.8 (435) (10%) [Cocage^{3+} - H$^+$ + $^{35}Cl^-$]$^+$.

Anal. Calc. for A2a $C_{14}H_{30}N_8Cl_3CoO_2.4H_2O$: C, 29.0; H, 6.6; N, 19.3; Cl, 18.3. Found C, 29.0; H, 6.1; N, 19.3; Cl, 18.3. ^1H NMR (**δ**, 500 MHz, D_2O): 2.37, 2.71, 2.97, 3.83 (ABCD spin system, 4H, CH_2 en); 2.59, 3.02, 2.64, 2.98 (AA'BB' coupling pattern, 4H, CH_2 caps); 2.85, 3.34 (AB doublet of doublets, 4H, CH_2 caps). ^{13}C NMR (**δ**, D_2O) 56.8 (CqC=O); 46.4, 55.7, 56.2, 57.9, 59.9 (NCH$_2$); 176.7 (C=O). IR in KBr (ν-$_{max}$/cm^{-1}): 3948, 3365, 3083 (NH stretch); 2925, 2860 (C-H stretch); 2592, 2022 (NH_3^+ overtone band); 1636 (C=O amide stretch); 1555 (NH_3^+ assymmetric bending); 1521 (NH_3^+ symmetric bending); 1460, 1430 (C-H deformation); 1050, 765 (CH_2 rock). IR in D_2O (ν-$_{max}$/cm^{-1}): 3416 (NH stretch); 2950 (C-H stretch); 1622 (C=O amide stretch); 1471 (C-H deformation). IR of the deuterated complex in KBr

(ν-$_{max}$/cm^{-1}): 3416 (NH stretch); 2924, 2854 (C-H stretch); 2500 (ND stretch); 2258 (ND_3^+ asym and sym stretch); 1625 (C=O amide stretch); 1427 (C-H deformation); 1334, 1260, 1215 (C-H twisting); 1136 (C-N-C); 1090, 1067, 1035, 952, 923, 891, 823, 757 (CH_2 rock). Low resolution ESMS (50 V) [m/z, obs (calc) (%) assignment where cage = $[^{12}C_{14}{}^{1}H_{30}{}^{14}N_8{}^{59}Co^{16}O_2]^{3+}$]: 398.8 (399) (100%) [Cocage^{3+} - 2H$^+$]$^+$.

Anal. Calc. for B1a $C_{12}H_{31}N_8Cl_4CoO.3H_2O$: C, 25.8; H, 6.7; N, 20.1; Cl, 25.4. Found C, 25.9; H, 7.0 N, 19.8; Cl, 25.2. ^{1}H NMR (δ, D_2O): 2.00 - 3.20 (complex pattern, 18H, NCH_2). ^{13}C NMR (δ, D_2O) 63.0 ($\underline{C}qNH_3^+$); 66.4 ($\underline{C}qC=O$); 54.9, 62.4, 63.5, 64.0, 64.3, 64.4, 64.9, 65.7, 68.5 ($N\underline{C}H_2$); 188.2 ($\underline{C}$=O). IR in KBr (ν-$_{max}$/cm^{-1}): 3538, 3465, 3349, 3240, 3170, 3079 (NH stretch); 2923, 2871 (C-H stretch); 2588, 2026 (NH_3^+ overtone band); 1631 (C=O amide stretch); 1605 (NH_2 in plane bending); 1590 (NH_3^+ assymmetric bending); 1525 (NH_3^+ symmetric bending); 1455, 1427 (C-H deformation); 1305, 1280 (C-H twisting); 1081, 1052, 1022, 790 (CH_2 rock). IR in D_2O (ν-$_{max}$/cm^{-1}): 3494, 3454, 3411, 3364, 3324 (NH stretch); 2952 (C-H stretch); 1626 (C=O amide stretch); 1472 (C-H deformation). IR of the deuterated complex in KBr (ν-$_{max}$/cm^{-1}): 3462, 3337 (NH stretch); 2924, 2854 (C-H stretch); 2402, 2356, 2314, 2259, 2191 (ND stretch and ND_3^+ asym and sym stretch); 1611 (C=O amide stretch); 1464, 1434 (C-H deformation); 1325, 1255, 1180 (C-H twisting); 1119 (C-N-C); 1030, 897,835, 762, 731 (CH_2 rock). Low resolution ESMS (50 V) [m/z, obs (calc) (%) assignment where cage = $[^{12}C_{12}{}^{1}H_{31}{}^{14}N_8{}^{59}Co^{16}O]^{4+}$]: 358.9 (359) (100%) [Cocage^{4+} - 3H$^+$]$^+$; 376.8 (377) (10%) [Cocage^{4+} - 3H$^+$ + H_2O]$^+$.

Anal. Calc. for B1b $C_{14}H_{33}N_8Cl_4CoO.3H_2O$: C, 28.8; H, 6.7; N, 19.2; Cl, 24.3. Found C, 28.4; H, 7.1 N, 18.7; Cl, 24.2. ^{1}H NMR (δ, D_2O): 2.16 - 2.68 (complex pattern, 10H, NCH_2); 2.80 - 3.06 (complex pattern, 8H, NCH_2); 3.18 (d, 2H, CH_2); 3.36 (m, 1H, CH_2); 3.46 (m, 1H, CH_2). ^{13}C NMR (δ, D_2O): 56.6 ($\underline{C}qNH_3^+$); 60.7 ($\underline{C}qC=O$); 47.1, 54.5, 54.7, 54.9, 55.3, 55.4, 55.5, 55.8, 55.9, 56.3, 56.9 ($N\underline{C}H_2$); 178.1 ($\underline{C}$=O). IR in KBr (ν-$_{max}$/cm^{-1}): 3408, 3061 (NH stretch); 2868 (C-H stretch); 2569, 2000 (NH_3^+ overtone band); 1627 (C=O amide stretch); 1520 (NH_3^+ symmetric bending); 1465, 1440 (C-H deformation); 1360, 1329, 1273, 1209, 1166 (C-H twisting); 1089 (C-N-C); 1050, 951, 923, 882, 845, 760 (CH_2 rock). IR in D_2O (ν-$_{max}$/cm^{-1}): 3465, 3426 (NH stretch); 2960 (C-H stretch); 1625 (C=O amide stretch); 1474 (C-H deformation). IR of the deuterated complex in KBr (ν-$_{max}$/cm^{-1}): 3391 (NH stretch); 2923 (C-H stretch); 2537 (ND stretch); 2252 (ND_3^+ asym and sym stretch); 1621 (C=O amide stretch); 1459 (C-H deformation); 1260, 1216 (C-H twisting); 1137 (C-

N-C); 1064, 1034, 955, 901, 835, 756 (CH_2 rock). Low resolution ESMS (50 V) [m/z, obs (calc) (%) assignment where cage = $[^{12}C_{14}{}^{1}H_{33}{}^{14}N_8{}^{59}Co^{16}O]^{4+}$]: 384.9 (385) (100%) [Cocage^{4+} - $3H^+$]$^+$; 420.8 (421) (10%) [Cocage^{4+} - $2H^+$ + $^{35}Cl^-$]$^+$.

Demetallation of [1,8-Diammonio-2,7-dioxo-3,6,10,13,16,19-hexaazabicyclo-[6.6.6]icosanato]cobalt(III)]chloride.4.5H_2O, [Co^{III}({NH_3^+}$_2$-2,7-dioxosar-2H)]-Cl_3.4.5H_2O

[Co^{III}({NH_3^+}$_2$-2,7-dioxosar-2H)]Cl_3.4.5H_2O (5 g; 8.5 x 10^{-3} mol) was dissolved in 250 mL of H_2O and $Co^{II}Cl_2$.6H_2O (2.02 g; 8.5 x 10^{-3} mol) in 100 mL of H_2O added. The resultant solution was deaerated with N_2 over a period of ten minutes and reduced with Zn powder (0.56 g; 8.5 x 10^{-3} mol) addition. A second solution of KCN (11.07 g; 0.17 mol) in 250 mL of H_2O was added dropwise, over a period of ten minutes, after both solutions had been deoxygenated with N_2 for a further hour. The mixture was stirred at ~20° C for a period of one week and over this time the colour changed from red to pale orange yellow. Separation of the ligand from the cyanide salt was effected with ethanol (2 L). KCN precipitated preferentially and was removed by filtering the solution and evaporating the solvent under vacuum. The residue was then dissolved in ethanol (200 mL), refiltered to remove more cyanide and once again taken to dryness. This procedure was repeated until no more KCN could be detected. The NMR spectra of the product obtained showed that the ligand was rather impure, indicating that some decomposition of the ligand occurred during the process. Purification was effected by making the Ni(II) complex from the crude product.

[1,8-Diammonio-2,7-dioxo-3,6,10,13,16,19-hexaazabicyclo[6.6.6]icosanato]-nickel(II)]perchlorate.3.5H_2O, [Ni^{II}({NH_3^+}$_2$-2,7-dioxosar-2H)](ClO_4)$_2$.3.5H_2O

The crude ligand was dissolved in water (250 mL) and triethylamine was added to make the solution basic. A solution of $Ni^{II}Cl_2$.6H_2O in water (250 mL) was added and the mixture stirred over night at ~20° C. The resultant pink solution was then diluted to 1 L with water and acidified with acetic acid; it was then loaded onto a column of SP-Sephadex C-25 cation exchange resin (30 cm x 4 cm) and the column was washed with water. Elution with 0.1 M $NaClO_4$ (adjusted to pH ~3-4 with conc $HClO_4$) removed a fast moving green band (not isolated) followed by a single diffuse pink band while some orange-red material remained at the top of the column. The isolated pink fraction was then concentrated by rotary

evaporation. The mixture was allowed to stand at ~20° C for several days whereupon a pink product precipitated; this was collected, washed with ethanol and ether and air-dried. Yield = 0.9 g. Anal. Calc. for $C_{14}H_{30}N_8Cl_2NiO_{10}.3.5H_2O$: C, 25.4; H, 5.6; N, 16.9; Cl, 10.7. Found C, 25.5; H, 5.1 N, 16.6; Cl, 10.3. IR in KBr (ν-$_{max}$/cm^{-1}): 3399, 2300 (N-H stretch); 2925, 2868 (C-H stretch); 1594 (C=O amide stretch); 1453 (C-H deformation); 1323, 1305 (C-H bending); 1090 (ClO_4^-); 1026, 956, 925, 889, 837 (C-H rock); 626 (ClO_4^-). IR in D_2O (ν-$_{max}$/cm^{-1}): 3410 (NH stretch); 2960 (C-H stretch); 1602 (C=O amide stretch); 1472 (C-H deformation). IR of the deuterated complex in KBr (ν-$_{max}$/cm^{-1}): 3408, 3299 (NH stretch); 2929, 2872 (C-H stretch); 2443 (ND stretch); 1594 (C=O amide stretch); 1453, 1409 (C-H deformation); 1360, 1322, 1305 (C-H twisting); 1088 (ClO_4^-); 1029, 923, 725 (CH_2 rock); 626 (ClO_4^-). Low resolution ESMS (50 V) [m/z, obs (calc) (%) assignment where cage = $[^{12}C_{14}{}^{1}H_{30}{}^{14}N_8{}^{59}Ni{}^{16}O_2]^{2+}$]: 398.8 (399) (100%) [Nicage^{2+} - H$^+$]; 498.7 (499) (40%) [Nicage^{2+} + $^{35}ClO_4^-$]$^+$.

4.2.2 X-ray Crystallography

X-ray Crystal Analysis of $[Co^{III}(\{NH_3^+\}_2\text{-2-oxosar-H})](NO_3)_4.H_2O$

Data Collection

A red block of the Co(III) complex having approximate dimensions of 0.14 x 0.25 x 0.40 mm was mounted in a quartz fibre. All measurements were made on a Rigaku AFC6S diffractometer with graphite monochromated Mo-Kα radiation. Cell constants and an orientation matrix for data collection, obtained from a least squares refinement using the setting angles of 25 carefully centered reflections in the range $36.67 < 2\theta < 45.53°$ corresponded to a primitive orthorhombic cell with dimensions a = 8.352(4) Å, b = 16.075(3) Å, c = 18.782(6) Å and V = 2522(2) Å^3. For Z = 4 and F.W. = 654.44, the calculated density is 1.72 g/cm^3. Based on the systematic absences of h00: h ≠ 2n, 0k0: k ≠ 2n and 00l: l ≠ 2n uniquely determine the space group to be $P2_12_12_1$ (# 19). The data were collected at a temperature of 23 ± 1° C using the ω-2θ scan technique to a maximum 2θ value of 55.1°. Omega scans of several intense reflections, made prior to data collection, had an average width at half height of 0.48° with a take-off angle of 6.0°. Scans of (1.60 + 0.34 tan θ)° were made at a speed of 8.0°/min (in omega). The weak reflections ($I < 10.0\sigma(I)$) were rescanned (maximum of four scans) and the counts were accumulated to ensure good counting

statistics. Stationary background counts were recorded on each side of the reflection. The ratio of peak counting time to background counting time was 2:1. The diameter of the incident beam collimator was 1.0 mm, the crystal to detector distance was 200 mm, and the detector aperture was 8.0 x 4.0 mm (horizontal x vertical).

Data Reduction

A total of 3311 reflections was collected. The intensities of three representative reflections were measured after every 150 reflections. No decay correction was required. The linear absorption coefficient, μ, for Mo-Kα radiation is 7.7 cm^{-1}. An analytical absorption correction was applied which resulted in transmission factors ranging from 0.81 to 0.88. The data were corrected for Lorentz and polarization effects.

Structure Solution and Refinement

The structure was solved by direct methods[10] and expanded using Fourier techniques[11]. All non-hydrogen atoms were located. One nitrate anion was found to be disorded about one of its N-O bonds, and this was modelled by assuming that there are two orientations for the group, one population q and one of population 1-q, and q was refined in the least squares process. Bond lengths and angles within this anion are not reliable. Non-hydrogen atoms with occupancy > 0.7 were refined anisotropically, while O(15) and O(16) were refined isotropically (B values constrained to be equal). Hydrogen atoms attached to carbon and nitrogen atoms were included at calculated positions but not refined; hydrogen atoms of the water molecule were located in a difference electron-density map. The final cycle of full-matrix least-squares refinement was based on 2296 observed reflections ($I > 3.00s(I)$) and 378 variable parameters and converged (largest parameter shift was 0.01 times its esd) with unweighted and weighted agreement factors of $R = \Sigma||Fo| - |Fc||/\Sigma|Fo| = 0.042$ and $R_\omega = \sqrt{(\Sigma\omega(|Fo| - |Fc|)^2/\Sigma\omega Fo^2)} = 0.043$. The standard deviation of an observation of unit weight was 1.82. The weighting scheme was based on counting statistics and included a factor ($p = 0.020$) to downweight the intense reflections. Plots of $\Sigma w(|Fo| - |Fc|)^2$ verses $|Fo|$, reflection order in data collection, $\sin\theta/\lambda$ and various classes of indices showed no unusual trends. The maximum and minimum peaks on the final difference Fourier map corresponded to 0.54 and -0.45 $e^-/Å^3$, respectively. The absolute structure was established by also refining a model with coordinates transformed by (-x, -y, -z) which yielded a higher R-factor of 5.04 and R_ω of

5.14 and thereby showed that the original model was correct. Neutral atom scattering factors were taken from Cromer and Waber[12]. Anomalous dispersion effects were included in Fcalc[13]; the values for Δf' and Δf'' were those of Creagh and McAuley[14]. The values for the mass attenuation coefficients are those of Creagh and Hubbel[15]. All calculations were performed using the texsan[16] crystallographic software package of the Molecular Structure Corporation.

X-ray Crystal Analysis of $[Co^{III}(\{NH_3^+\}_2\text{-}2,7\text{-dioxosar-}2H)]ClZnCl_4.H_2O$

Crystal Structure Solution and Refinement

For the Co(III) diamide a red prismatic crystal was attached to a quartz fibre and mounted on a Rigaku AFC6S diffractometer equipped with a graphite monochromator. Using Mo-Kα radiation, lattice parameters were determined by least-squares refinement of the setting angles of 25 reflections in the range of $47.49° < 2\theta < 54.13°$. The data were collected at a temperature of 23(1)° C using the ω-2θ scan technique to a maximum value of 55.1°. Scans of $(1.20 + 0.34 \tan \theta)°$ in ω were made at a speed of 4.0°/min in ω. The weak reflections were rescanned (maximum of four scans) and the counts were accumulated to ensure good counting statistics. Stationary background counts were recorded on each side of the reflection. Three representative reflections measured at intervals of 150 reflections showed a decrease of 0.5% in the standards during the course of data collection. A linear correction factor was applied to the data to account for this phenomenon. The data set was reduced, an analytical absorption correction applied and Lorentz and polarisation effects were accounted for.

The structure was solved by heavy-atom Patterson methods[17] and expanded using Fourier techniques.[18] The non-hydrogen atoms were refined with anisotropic displacement factors. All hydrogen atoms were located and their coordinates refined, but their isotropic B values were held fixed.

Least-squares refinement was performed using full-matrix methods minimising the function $\Sigma\omega(|F_o| - |F_c|)^2$ where the weighting scheme was based on counting statistics and included a factor (p = 0.005) to downweight the intense reflections. Data reduction and refinement computations were performed with texsan.[16] Neutral atom scattering factors were taken from Cromer and Waber.[12] Anomalous dispersion effects were included in Fcalc[13]; the values of Δf' and Δf'' were those of Creagh and McAuley.[14] The

values of the mass attenuation coefficients were those of Creagh and Hubbel.[15]

X-ray Crystal Analysis of $[Co^{III}(\{NH_3^+\}_2\text{-}2,9\text{-dioxosar-}2H)](S_2O_6)_{1.5}.3H_2O$

Crystal Structure Solution and Refinement

For the second Co(III) diamide complex an orange rod-shaped crystal was attached to a glass fibre and mounted on a Rigaku AFC6S diffractometer equipped with a graphite monochromator. Using Cu-Kα radiation and a 12 kW rotating anode generator, lattice parameters were determined by least-squares refinement of the setting angles of 25 reflections in the range of $84.80° < 2\theta < 103.05°$. The data were collected at a temperature of -60(1)° C using the ω-2θ scan technique to a maximum value of 120.2°. Scans of $(1.20 + 0.30 \tan \theta)°$ in ω were made at a speed of 32.0°/min in ω. The weak reflections were rescanned (maximum of four scans) and the counts were accumulated to ensure good counting statistics. Stationary background counts were recorded on each side of the reflection. Three representative reflections were measured at intervals of 150 reflections and no decay correction was required. The data set was reduced, an analytical absorption correction applied and Lorentz and polarisation effects were accounted for.

The structure was solved by direct methods[10] and expanded using Fourier techniques.[11] The non-hydrogen atoms were refined anisotropically. Hydrogen atoms attached to carbon and nitrogen atoms of the cation were included at calculated positions. Those bonded to N(2), N(3), N(4) and N(5) were refined positionally using the least-squares procedure; the remainder were not refined but were recalculated periodically. The hydrogen atoms of the water molecules were located in difference electron-density maps or by analysis of the hydrogen-bonding network, and then were refined with tight restraints imposed upon the O-H distances and H-O-H angles.

Least-squares refinement was performed using full-matrix methods minimising the function $\Sigma\omega(|F_o| - |F_c|)^2$ where the weighting scheme was based on counting statistics and included a factor ($p = 0.02$) to downweight the intense reflections. Data reduction and refinement computations were performed with texsan[16] with the exception of the hydrogen-bonding network which was calculated with the Platon computing programme.[19] Neutral atom scattering factors were taken from Cromer and Waber.[12]

Anomalous dispersion effects were included in Fcalc[13]; the values of Δf' and Δf'' were those of Creagh and McAuley.[14] The values of the mass attenuation coefficients were those of Creagh and Hubbel.[15]

X-ray Crystal Analysis of $[Co^{III}(6\text{-}\{NH_3^+,C(O)NH\}\text{-}13\text{-}\{NH_3^+,CH_2NH_2\}\text{-cyclam})]Cl_4.2.75H_2O$

Crystal Structure Solution and Refinement

For the Co(III) monoamido macrocyclic complex an orange cuboid crystal was attached to a quartz fibre and mounted on a Rigaku AFC6S diffractometer equipped with a graphite monochromator. Using Mo-Kα radiation, lattice parameters were determined by least-squares refinement of the setting angles of 25 reflections in the range of $31.69° < 2\theta < 42.97°$. The data were collected at a temperature of 23(1)° C using the ω-2θ scan technique to a maximum value of 55.0°. Scans of $(1.20 + 0.34 \tan \theta)°$ in ω were made at a speed of 4.0°/min in ω. The weak reflections were rescanned (maximum of four scans) and the counts were accumulated to ensure good counting statistics. Stationary background counts were recorded on each side of the reflection. Three representative reflections measured at intervals of 150 reflections showed a decrease of 1% in the standards during the course of data collection. A linear correction factor was applied to the data to account for this phenomenon. The data set was reduced, an analytical absorption correction applied and Lorentz and polarisation effects were accounted for. A correction for secondary extinction was also applied to the data (coefficient = 5.22×10^{-8}).

The structure was solved by heavy-atom Patterson methods[17] and expanded using Fourier techniques.[18] The non-hydrogen atoms were refined anisotropically. Water molecule O(3) has an occupancy estimated to be 0.75. All hydrogen atoms of the cation and those on O(1) and O(2) were observed in a difference electron density map. Hydrogen atoms attached to nitrogen and oxygen atoms were refined positionally with fixed B_{iso} values, while those on carbon atoms were held fixed at calculated positions.

Least-squares refinement was performed using full-matrix methods minimising the function $\Sigma\omega(|F_o| - |F_c|)^2$ where the weighting scheme was based on counting statistics and included a factor (p = 0.002) to downweight the intense reflections. Data reduction and refinement computations were performed with texsan.[16] Neutral atom scattering factors were taken from

Cromer and Waber.[12] Anomalous dispersion effects were included in Fcalc[13]; the values of $\Delta f'$ and $\Delta f''$ were those of Creagh and McAuley.[14] The values of the mass attenuation coefficients were those of Creagh and Hubbel.[15]

4.3 Results

4.3.1 Synthesis

Refluxing $[Co^{III}(\{NH_3^+\}_2sar)]^{5+}$ and $Hg^{II}(OAc)_2$ in 5% aqueous acetic acid for a period of 25 hours led to the previously prepared $[Co^{III}(\{NH_3^+\}_2$-2-oxosar-H)$]^{4+}$ ion as a major product of the reaction which was separated out from the other minor components by cation exchange chromatography. The monoamide was produced in reasonable yield (39%) and although dioxo and trioxo species seemed to be present they were not characterised. It was also discovered that prolonged reaction (48 hr) of $[Co^{III}(\{NH_3^+\}_2$-sar)$]^{5+}$ with $Hg^{II}(OAc)_2$ in 5% acetic acid produced two isomeric diamido cage complexes in addition to a macrocyclic Co(III) monoamido complex derived from the cage by loss of a $-CH_2-CH_2-$ fragment as well as some $[Co^{III}(\{NH_3^+\}_2$-2-oxosar-H)$]^{4+}$ (Figure 6) as the major components. These were separated from minor fractions by ion exchange chromatography. As these four fractions represented the main bulk of the material, characterisation of the other small products was not pursued.

The $[Co^{III}(\{NH_3^+\}_2$-2-oxosar-H)$]^{4+}$ complex was then reacted further with KCN and $Co^{II}Cl_2.6H_2O$, to demetallate the complex, producing the free monoamide ligand and $[Co^{III}(CN)_6]^{3-}$ ion. Extraction of the free ligand with ethanol led finally to a thick yellow oil. Complexation of the free ligand to Ni(II) and Cr(III) was then achieved. Firstly, the Ni^{2+} ion and the monoamide ligand were reacted in aqueous solution in the presence of base over some hours to give a pink Ni(II) complex $[Ni^{II}(\{NH_3^+\}_2$-2-oxosar-H)$]^{3+}$ (Figure 7) isolated as a perchlorate salt. The Cr(III) monoamide complex $[Cr^{III}(\{NH_3^+\}_2$-2-oxosar-H)$]^{4+}$ (Figure 7) was synthesised by mixing the ligand with $[Cr^{III}Cl_3pyridine_3]$ and $[Cr^{II}(CH_3CO_2)_2.H_2O]_2$ in water. In addition the first diamido isomer isolated (6%), $[Co^{III}(\{NH_3^+\}_2$-2,7-dioxosar-2H)$]^{3+}$, was also demetallated in a similar way to the Co(III) monoamido ion, with KCN, $Co^{II}Cl_2.6H_2O$ and Zn powder. The recovered ligand was impure but it was complexed directly to Ni(II) in aqueous solution at ~20° C to yield finally a pure Ni(II) diamido complex $[Ni^{II}(\{NH_3^+\}_2$-2,7-dioxosar-2H)$]^{2+}$ (Figure 7).

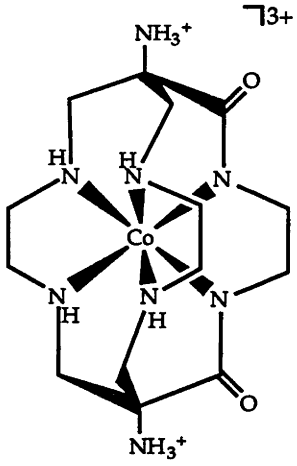

$[Co(\{NH_3^+\}_2\text{-}2,7\text{-dioxosar-2H})]^{3+}$

Fraction A1a

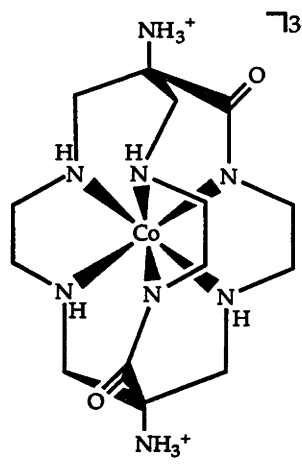

$[Co(\{NH_3^+\}_2\text{-}2,9\text{-dioxosar-2H})]^{3+}$

Fraction A2a

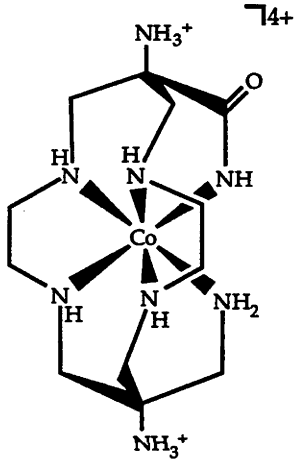

$[Co(6\text{-}\{NH_3^+,C(O)NH\}\text{-}13\{NH_3^+,CH_2NH_2\}\text{-cyclam})]^{4+}$

Fraction B1a

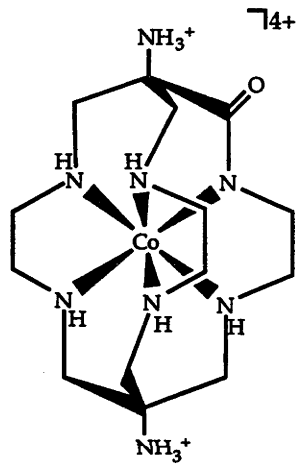

$[Co(\{NH_3^+\}_2\text{-}2\text{-oxosar-H})]^{4+}$

Fraction B1b

Figure 6

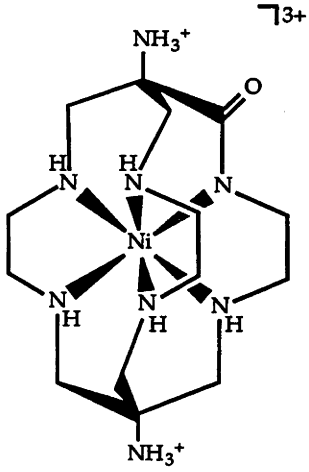

$[Ni(\{NH_3^+\}_2\text{-}2\text{-oxosar-H})]^{3+}$

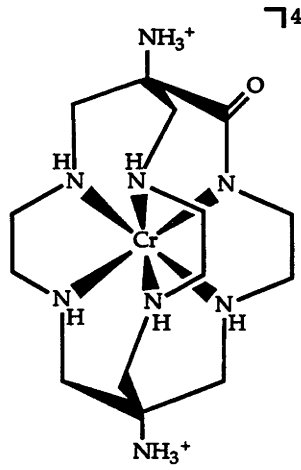

$[Cr(\{NH_3^+\}_2\text{-}2\text{-oxosar-H})]^{4+}$

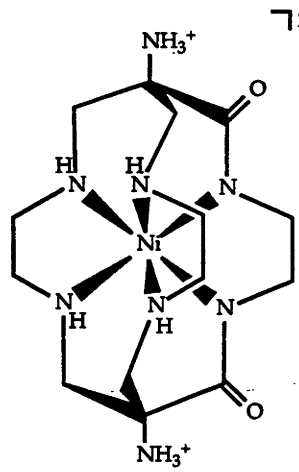

$[Ni(\{NH_3^+\}_2\text{-}2,7\text{-dioxosar-2H})]^{2+}$

Figure 7

All of the Co(III) products isolated from the various reactions have been structurally analysed and their connectivity is displayed in Figure 6 while the anticipated structures for the Ni(II) and Cr(III) derivatives appear in Figure 7. For the two isomeric diamido complexes X-ray crystallography was the only technique that could determine the positions of the two amide groups within each cage ligand. Otherwise there would be no way of telling with certainty which isomer is which. It should be pointed out that the Ni(II) ion is likely to be bound to the deprotonated amido nitrogen atoms in the monoamido and diamido cages. This binding mode is different to that observed for the $[Ni^{II}(Me,COO^{-}\text{-}2\text{-oxosar})]^{+}$ ion described earlier. Although by no means conclusive the physical data provide good evidence that the above assertion is correct. This evidence will be elaborated upon in the following sections.

4.3.2 NMR Spectroscopy

The $[Co^{III}(\{NH_3^{+}\}_2\text{-}2\text{-oxosar-H})]^{4+}$ ion

The proton decoupled ^{13}C NMR and ^{1}H NMR spectra of the N-deuterated $[Co^{III}(\{NH_3^{+}\}_2\text{-}2\text{-oxosar-H})]^{4+}$ ion are displayed in Figure 8. The spectra reflect the lack of symmetry that the molecule possesses. In the ^{13}C NMR spectrum all of the carbon atoms are inequivalent and a separate signal is present for each. These signals are attributed to eleven CH_2 groups, two quaternary carbon atoms in the apical positions and the remaining amide carbon. These spectral features are similar to those observed for the Co(III) monoamido complexes described in earlier. Thus the quaternary carbons adjacent to the primary amine and directly connected to the amide carbon appear at chemical shift values of 56.6 and 60.7 ppm respectively while the remaining methylene resonances appear at 47.1, 54.3, 54.7, 54.9, 55.3, 55.4, 55.5, 55.8, 55.9, 56.5 and 56.9 ppm respectively and lastly the amide carbon appears at 178.1 ppm.

Turning to the ^{1}H NMR spectrum (Figure 8) it can be observed that this is not as informative as the ^{13}C NMR spectrum due to the complexity in the region attributed to the methylene protons (2.16 - 3.18 ppm). As already mentioned with the Co(III) complexes in Chapter 3 the observed complexity, seen with $[Co^{III}(\{NH_3^{+}\}_2\text{-}2\text{-oxosar-H})]^{4+}$ is due to the overlap of the methylene proton signals and the extensive spin-spin splitting. One noticeable feature though, apart from the overlapping CH_2 resonances, is the pair of multiplets at about 3.5 ppm and this feature is also present in the oxo capped N_6 species in Chapter 3 (at 3.98 ppm) although only one

multiplet is displayed in this case.[20] Again integration indicated that these resonances resulted from one single proton in each case and as they are shifted further downfield they are assigned to each of the protons attached to the CH_2 directly bonded to the coordinated deprotonated amide. It is also known that axial and equatorial protons of the methylene protons have quite distinct chemical shifts for cage complexes[21] and the above observation is consistent with this type of assignment.

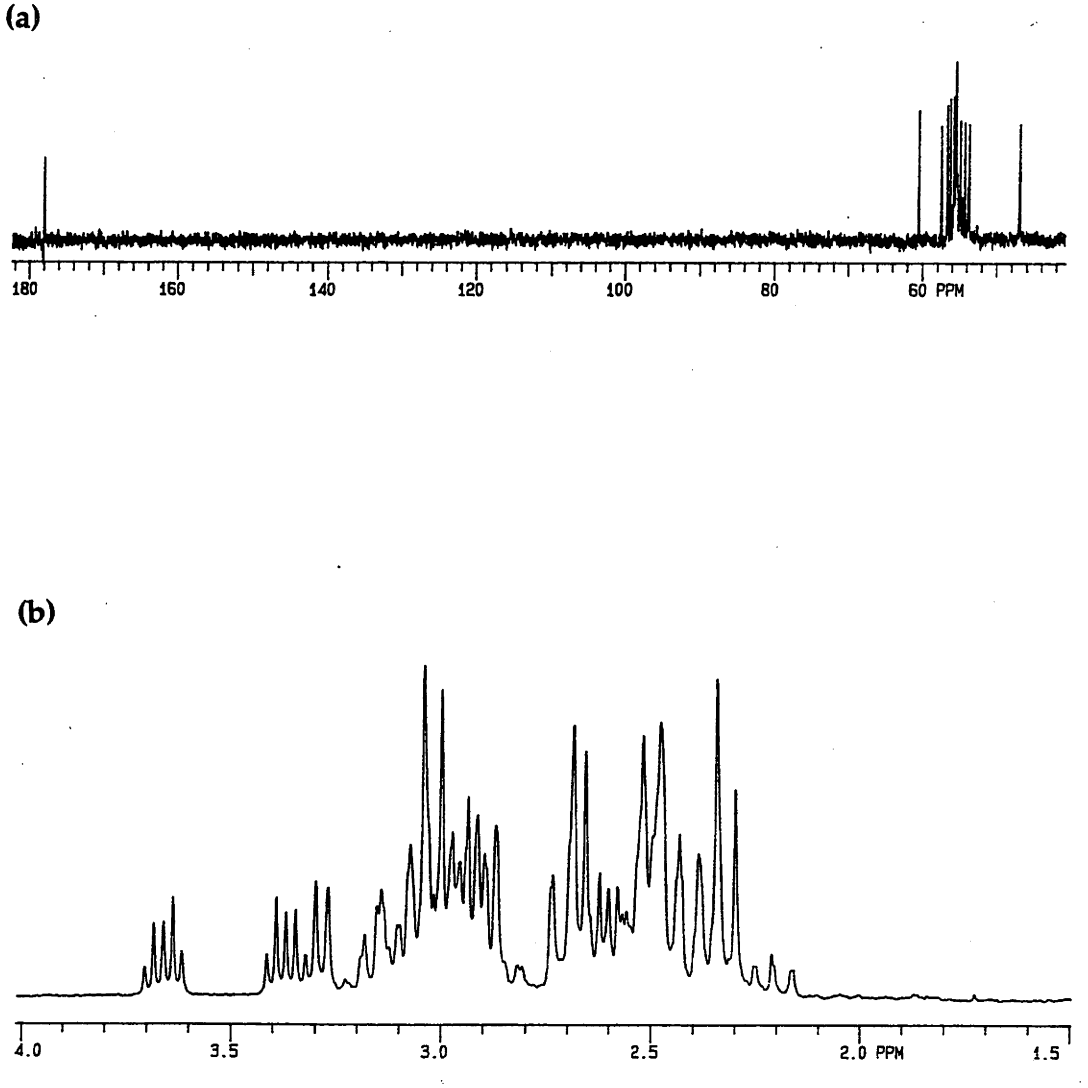

Figure 8. ^{13}C (a) and ^{1}H (b) NMR spectra of $[Co^{III}(\{NH_3^+\}_2\text{-2-oxosar-H})]^{4+}$ (Chloride salts in D_2O).

The $[Co^{III}(\{NH_3^+\}_2\text{-}2,7\text{-dioxosar-}2H)]^{3+}$ and $[Co^{III}(\{NH_3^+\}_2\text{-}2,9\text{-dioxosar-}2H)]^{3+}$ ions

The ^{13}C NMR spectra of the two diamido isomers (Figure 9) display only seven signals but these appear at different chemical shift values in each case. Each isomer has some symmetry, namely C_2 axes through the five membered chelate rings. The carbon atoms that generate these signals arise from quaternary, amide and five inequivalent pairs of methylene groups. For $[Co^{III}(\{NH_3^+\}_2\text{-}2,7\text{-dioxosar-}2H)]^{3+}$, where the amide moieties occur on the same strap, these signals appear at 56.9, 177.4, 51.3, 54.8, 55.6, 55.7 and 60.6 ppm respectively. For the second isomer, $[Co^{III}(\{NH_3^+\}_2\text{-}2,9\text{-dioxosar-}2H)]^{3+}$, with the amides located on different straps and different caps, the signals appear at 56.8, 176.7, 46.4, 55.7, 56.2, 57.9 and 59.9 ppm respectively.

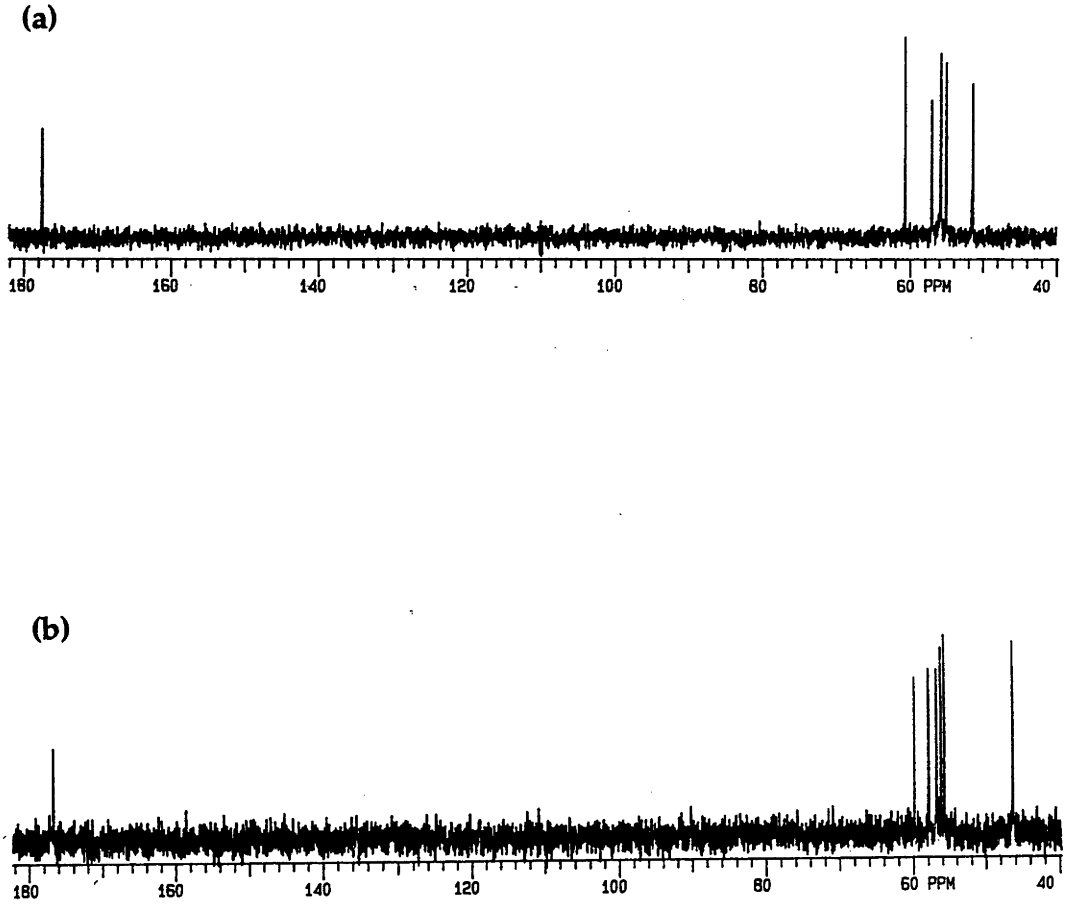

Figure 9. ^{13}C NMR spectrum of (a) $[Co^{III}(\{NH_3^+\}_2\text{-}2,7\text{-dioxosar-}2H)]^{3+}$ and (b) $[Co^{III}(\{NH_3^+\}_2\text{-}2,9\text{-dioxosar-}2H)]^{3+}$ (chloride salts in D_2O).

The ^1H NMR spectra of the two Co(III) diamide isomers (Figure 10) display a number of characteristic features present in both cases. Examination of Dreiding models indicate that for the ^1H NMR spectroscopy each isomer should display certain characteristic signals. Firstly, the models show that each diamido isomer possesses an *ob$_2$lel* configuration. Therefore, both systems are expected to display one ABCD spin system for the two *ob* five membered chelate rings, two AB doublets of doublets arising from the methylene protons in the caps and finally an AA'BB' coupling pattern for the remaining *lel* ethylene link. Only one ABCD system is expected to arise in the ^1H NMR spectra because the C_2 axis, of each isomer, makes the corresponding hydrogens on the two *ob* five membered chelate rings magnetically equivalent. Likewise, as a result of the symmetry in both isomers, the corresponding methylene protons of the opposite caps within each complex are equivalent and so only one set of signals will arise for each pair. Therefore, two AB doublets of doublets should occur within each spectrum. All of the above features are observed in both the Co(III) diamido isomers which confirms that the above assessment and the *ob$_2$lel* conformation for each isomer is correct. For $[Co^{III}(\{NH_3^+\}_2\text{-}2,7\text{-dioxosar-}2H)]^{3+}$ these signals appear at 2.78, 3.82 ppm (AB doublet of doublets), 2.35, 2.74, 2.60, 3.26 ppm (AA'BB' coupling pattern), 2.52, 2.62, 2.96 and 3.26 ppm (ABCD spin system) respectively. However the last multiplet of the ABCD system appears under the AB doublet at 3.26 ppm. This multiplet was visible in the 300 MHz ^1H NMR of the product, being present at the side of the AB doublet. Nevertheless upon moving to a higher frequency the last multiplet of the ABCD system was found to shift underneath and become obscured by the other system. For the second isomer, $[Co^{III}(\{NH_3^+\}_2\text{-}2,9\text{-dioxosar-}2H)]^{3+}$, with the amides located <u>*cis*</u> to each other, the same signals appear at 2.59, 3.02 ppm (AB doublet of doublets), 2.85, 3.34, 2.64, 2.98 ppm (AA'BB' coupling pattern), 2.37, 2.71, 2.97 and 3.83 ppm (ABCD spin system) respectively. Further conformation of the above couplings between the various systems, within each isomer, was also established from absolute COSY (^1H - ^1H correlation) experiments (Figures 11 and 12) which were also used to aid in the assignments of the two spectra.

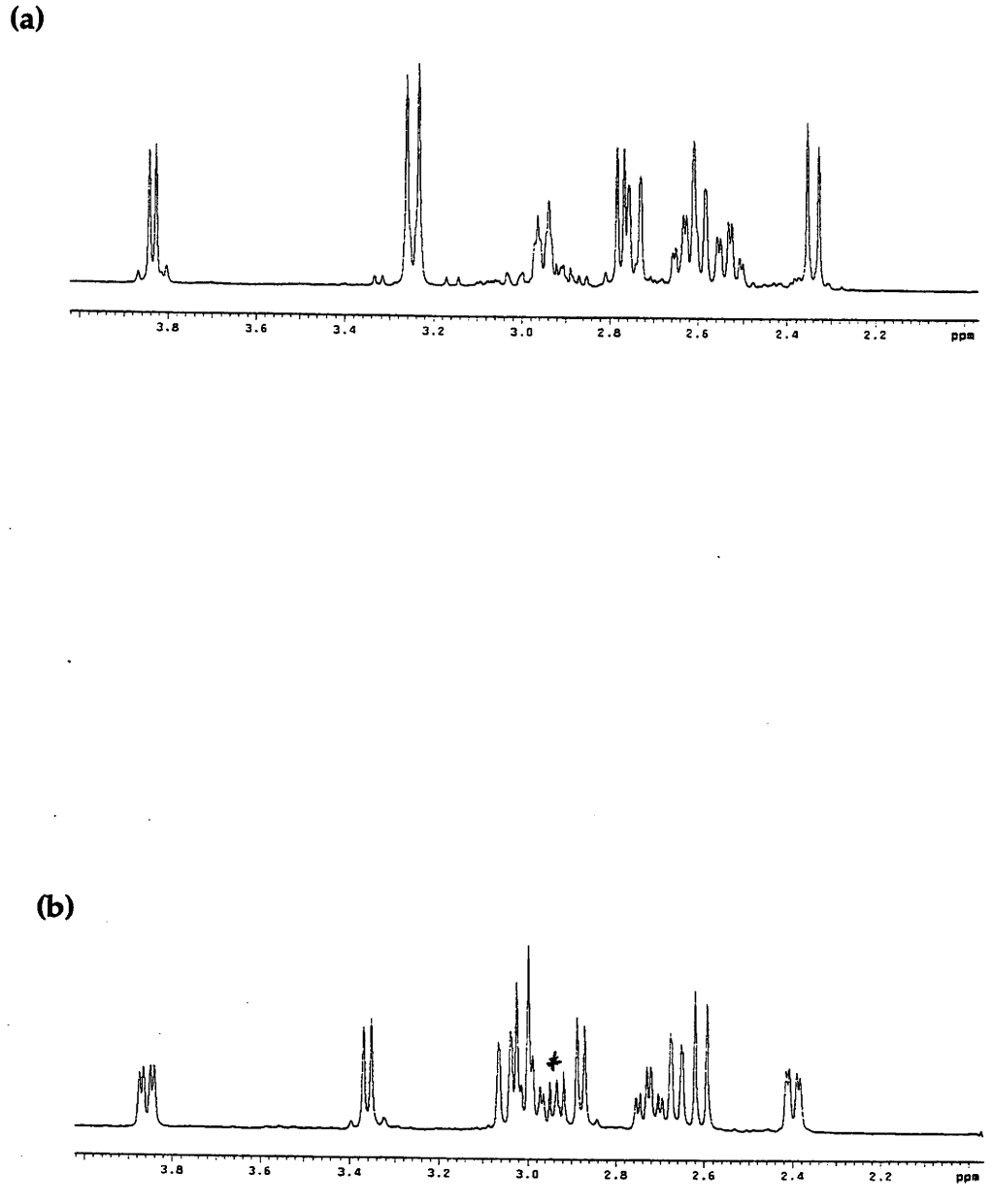

Figure 10. 500 MHz ^1H NMR spectrum of (a) $[Co^{III}(\{NH_3^+\}_2\text{-}2,7\text{-dioxosar-}2H)]^{3+}$ and (b) $[Co^{III}(\{NH_3^+\}_2\text{-}2,9\text{-dioxosar-}2H)]^{3+}$ (Chloride salts in D_2O, * = NaTSP (sodium(trimethylsilyl)propanesulfonate)).

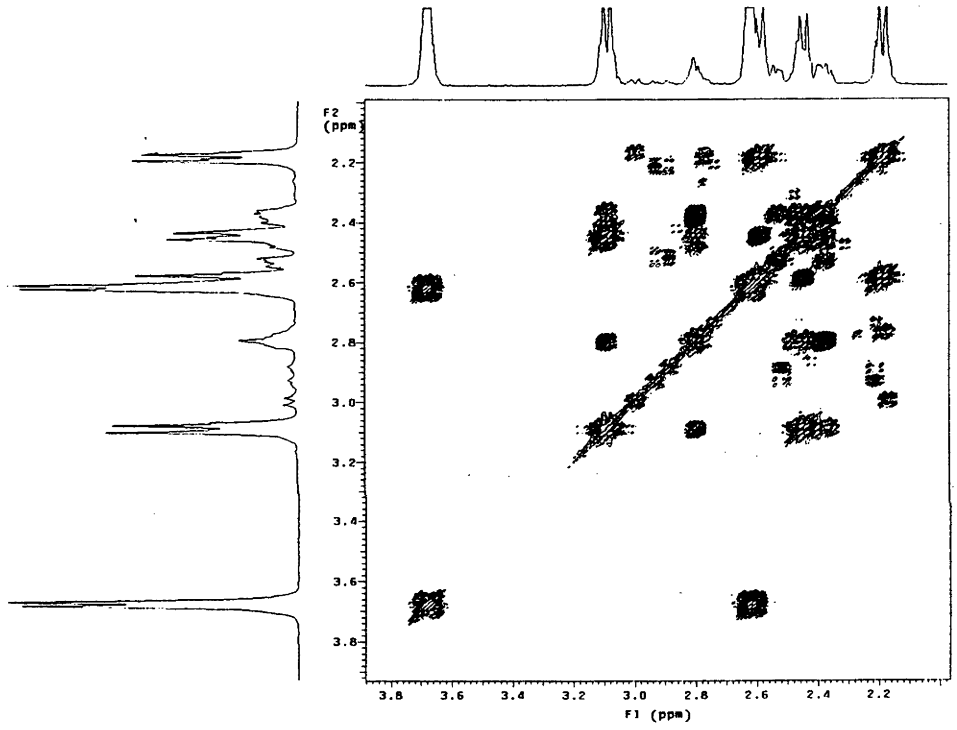

Figure 11. The ^{1}H - ^{1}H COSY results for $[Co^{III}(\{NH_3^+\}_2\text{-}2,7\text{-dioxosar-}2H)]^{3+}$.

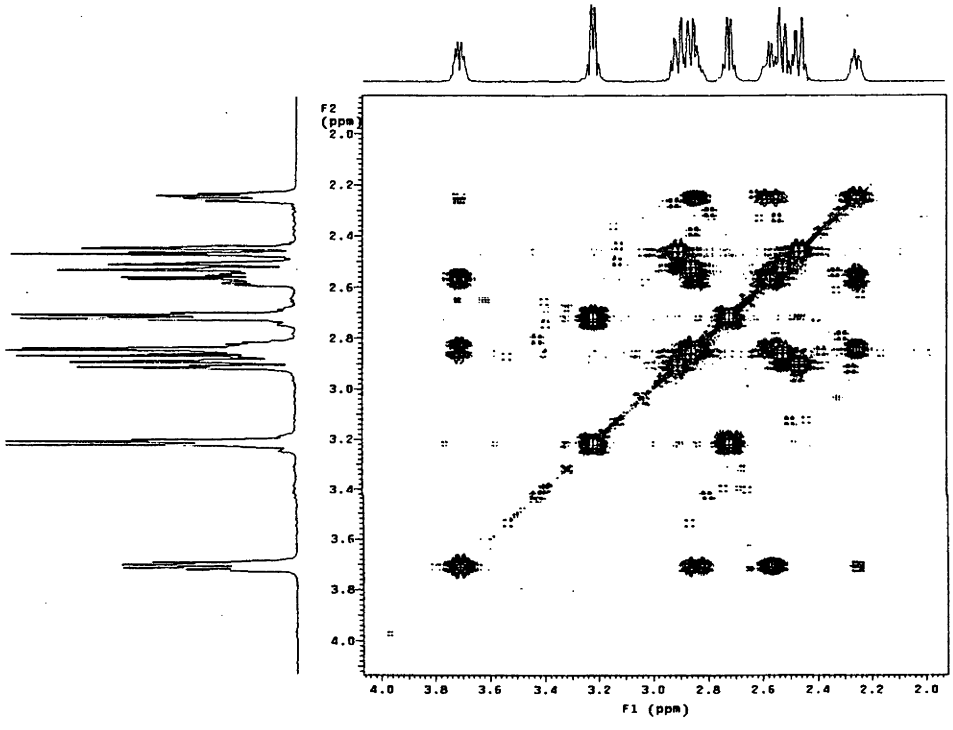

Figure 12. The ^{1}H - ^{1}H COSY results for $[Co^{III}(\{NH_3^+\}_2\text{-}2,9\text{-dioxosar-}2H)]^{3+}$.

The $[Co^{III}(6\text{-}\{NH_3^+,C(O)NH\}\text{-}13\text{-}\{NH_3^+,CH_2NH_2\}\text{-cyclam})]^{4+}$ ion

The ^{13}C NMR spectrum of the Co(III) monoamido macrocyclic complex (Figure 13a) highlights the general lack of symmetry within the molecule; all the carbon atoms are inequivalent and a separate signal occurs for each. These comprise two quaternary, an amide and nine methylene signals. Thus the quaternary signals, next to the primary amine and directly connected to the amide carbon atom, have chemical shift values of 63.0 and 66.4 ppm respectively. The remaining methylene resonances have shifts at 54.9, 62.4, 63.5, 64.0, 64.3, 64.4, 64.9, 65.7 and 68.5 ppm respectively. Lastly the amide carbon signal appears at 188.2 ppm.

In the ^1H NMR spectrum of the fragmented cage complex (Figure 13b), a series of overlapping methylene resonances occur between 2.0 and 3.2 ppm. The complexity within this spectrum arises because of the overlap of the methylene proton signals and the extensive spin-spin splitting. Assignments of the signals therefore are more difficult and are not especially revealing.

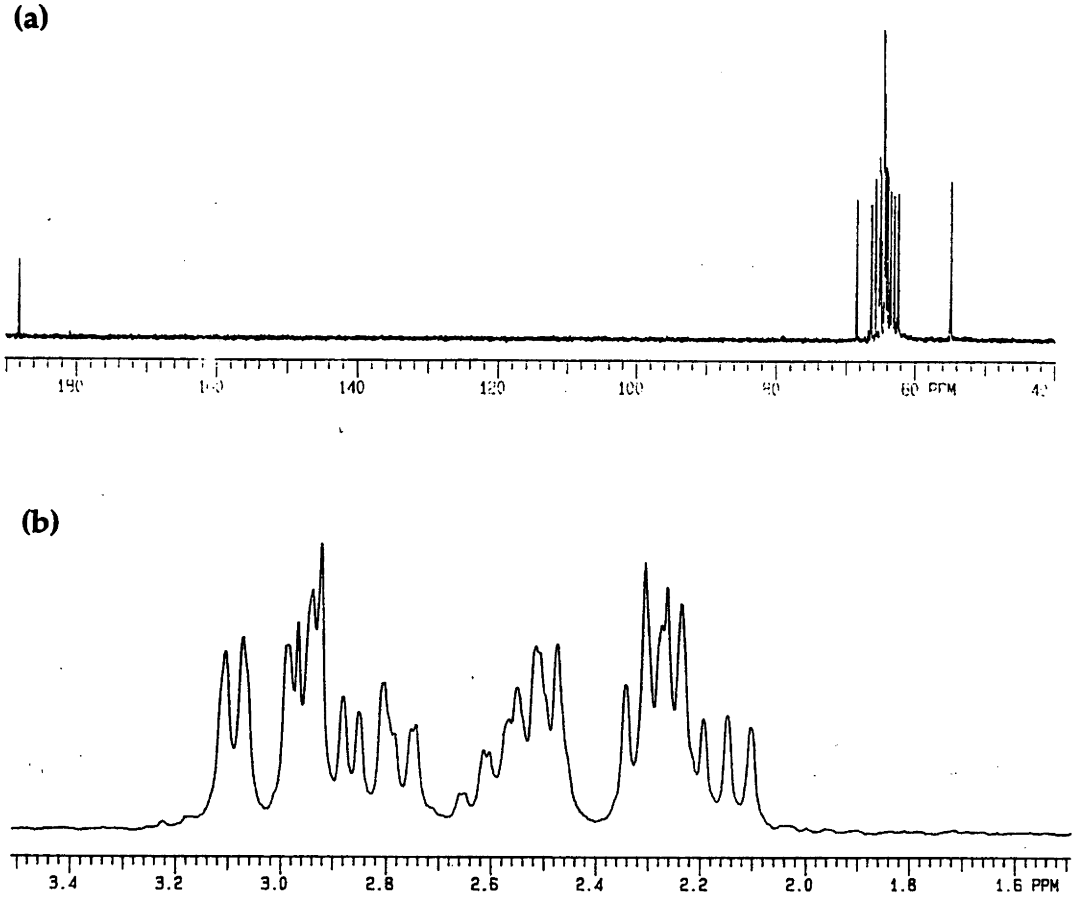

Figure 13. ^{13}C (a) and ^1H (b) NMR spectra of $[Co^{III}(6\text{-}\{NH_3^+,C(O)NH\}\text{-}13\text{-}\{NH_3^+,CH_2NH_2\}\text{-cyclam})]^{4+}$ (Chloride salts in D_2O).

4.3.3 Infra-red Spectroscopy

Co(III), Cr(III) and Ni(II) Monoamido Cage Systems

The infra-red spectroscopy assisted with the characterisation of the functionalised cage systems by providing some evidence of the presence of the amido groups within each complex. Selected functional group absorption bands for the undeuterated complexes are tabulated in Table 1. For $[Co^{III}(\{NH_3^+\}_2\text{-2-oxosar-H})]^{4+}$ a broad absorption band, appearing at 1627 cm^{-1}, arises from the deprotonated coordinated amido carbonyl group. The crystallography of this compound also confirms that the metal is six coordinate and bound to the deprotonated amido N atom. Turning to $[Cr^{III}(\{NH_3^+\}_2\text{-2-oxosar-H})]^{4+}$ an amido absorption band appears at 1625 cm^{-1} while for $[Ni^{II}(\{NH_3^+\}_2\text{-2-oxosar-H})]^{3+}$ the amido band occurs at a slightly lower value of 1615 cm^{-1} for the chloride salt and the value for the perchlorate salt of $[Ni^{II}(\{NH_2\}_2\text{-2-oxosar-H})]^{+}$ appears at an even lower frequency of 1589 cm^{-1}.

Table 1. Selected functional group infra-red absorption frequencies of the Co(III), Ni(II) and Cr(III) monoamido cage systems.

Complex	ν~, cm^{-1}	Assignment
$[Co^{III}(\{NH_3^+\}_2\text{-2-oxosar-H})]^{4+}$	1627	$C{=}O_{(amido)}$ stretch
	1520	NH_3^+ symm bend
$[Ni^{II}(\{NH_2\}_2\text{-2-oxosar-H})]^{+}$ [a]	1589	$C{=}O_{(amido)}$ stretch
$[Ni^{II}(\{NH_3^+\}_2\text{-2-oxosar-H})]^{3+}$ [b]	1615	$C{=}O_{(amido)}$ stretch
	1524	NH_3^+ symm bend
$[Cr^{III}(\{NH_3^+\}_2\text{-2-oxosar-H})]^{4+}$	1625	$C{=}O_{(amido)}$ stretch
	1517	NH_3^+ symm bend

[a] Perchlorate salt, [b] Chloride salt.

The above systems were also examined, by IR spectrosopy, in D_2O solution and as deuterated complexes in KBr. Selected absorption bands for these compounds appear in Table 2. Essentially, the results show that the amido absorption bands occur at values similar to those of the earlier corresponding undeuterated complexes.

Table 2. Selected functional group infra-red absorption frequencies of the deuterated Co(III), Ni(II) and Cr(III) monoamido cage systems in D_2O and KBr.

Complex	ν~, cm^{-1}	Assignment
$[Co^{III}(\{ND_3^+\}_2\text{-2-oxosar-H})]^{4+}$ [a]	1625	$C{=}O_{(amido)}$ stretch
$[Co^{III}(\{ND_3^+\}_2\text{-2-oxosar-H})]^{4+}$ [b]	1621	$C{=}O_{(amido)}$ stretch
$[Ni^{II}(\{ND_2\}_2\text{-2-oxosar-H})]^{+}$ [a, c]	1597	$C{=}O_{(amido)}$ stretch
$[Ni^{II}(\{ND_2\}_2\text{-2-oxosar-H})]^{+}$ [b, c]	1596	$C{=}O_{(amido)}$ stretch
$[Ni^{II}(\{ND_3^+\}_2\text{-2-oxosar-H})]^{3+}$ [a, d]	1615	$C{=}O_{(amido)}$ stretch
$[Ni^{II}(\{ND_3^+\}_2\text{-2-oxosar-H})]^{3+}$ [b, d]	1607	$C{=}O_{(amido)}$ stretch
$[Cr^{III}(\{ND_3^+\}_2\text{-2-oxosar-H})]^{4+}$ [a]	1619	$C{=}O_{(amido)}$ stretch
$[Cr^{III}(\{ND_3^+\}_2\text{-2-oxosar-H})]^{4+}$ [b]	1618	$C{=}O_{(amido)}$ stretch

[a] D_2O, [b] KBr, [c] Perchlorate salt, [d] Chloride salt.

Co(III) and Ni(II) Diamido Cage and Co(III) Monoamido Macrocyclic Systems

Selected undeuterated infra-red absorption frequencies of these functionalised complexes appear in Table 3. For the two diamide isomers, $[Co^{III}(\{NH_3^+\}_2\text{-2,7-dioxosar-2H})]^{3+}$ and $[Co^{III}(\{NH_3^+\}_2\text{-2,9-dioxosar-2H})]^{3+}$, amido C=O stretching absorption bands appear at 1619 cm^{-1} and 1636 cm^{-1} respectively and these values are similar to the frequency of 1627 cm^{-1} observed for the related amido bound $[Co^{III}(\{NH_3^+\}_2\text{-2-oxosar-H})]^{4+}$ species. Also the crystallographic evidence obtained on both diamido isomers shows the Co(III) centre is bound to both amido nitrogens in each case so the coherence of the values is not surprising. In the infrared spectrum of $[Ni^{II}(\{NH_3^+\}_2\text{-2,7-dioxosar-2H})]^{2+}$, a characteristic C=O stretching vibration band for the bound amido groups appears at 1594 cm^{-1}. In addition, these amido carbonyl frequencies are generally lower than that observed for the $(NH_2)_2$-2,7-dioxosar free ligand (1629 cm^{-1}). It would also be expected that the monoamide free ligand, $(NH_2)_2$-2,-oxosar, would display a similar amide carbonyl frequency. For the $[Co^{III}(6\text{-}\{NH_3^+,C(O)NH\}\text{-}13\text{-}\{NH_3^+,CH_2NH_2\}\text{-cyclam})]^{4+}$ complex an amido stretching band appears at 1631 cm^{-1}. Again the crystallographic evidence for this complex shows that the metal is bound to the amido nitrogen.

Table 3. Functional group infra-red absorption frequencies of the Co(III) and Ni(II) Diamido Cage, Diamide Cage Free Ligand and Co(III) Monoamido Macrocyclic Systems.

Complex	ν~, cm^{-1}	Assignment
$[Co^{III}(\{NH_3^+\}_2$-2,7-dioxosar-2H)$]^{3+}$	1619	$C{=}O_{(amido)}$ stretch
	1582	NH_3^+ asymm bend
	1519	NH_3^+ symm bend
$[Co^{III}(\{NH_3^+\}_2$-2,9-dioxosar-2H)$]^{3+}$	1636	$C{=}O_{(amido)}$ stretch
	1555	NH_3^+ asymm bend
	1521	NH_3^+ symm bend
$(NH_2)_2$-2,7-dioxosar	1629	$C{=}O_{(amide)}$ stretch
	1597	NH_2 in-plane bending
	1563	NH_2 in-plane bending
$[Co^{III}$(6-$\{NH_3^+$,C(O)NH$\}$-13-	1631	$C{=}O_{(amido)}$ stretch
$\{NH_3^+,CH_2NH_2\}$-cyclam)$]^{4+}$	1605	NH_2 in-plane bending
	1590	NH_3^+ asymm bend
	1525	NH_3^+ symm bend
$[Ni^{II}(\{NH_3^+\}_2$-2,7-dioxosar-2H)$]^{2+}$	1594	$C{=}O_{(amido)}$ stretch

Likewise the deuterated systems were examined both in D_2O and KBr respectively and selected absorption bands for these complexes appear in Table 4. Again the amido carbonyl bands were found to occur at similar values to those of the undeuterated systems.

Table 4. Amide carbonyl group infra-red absorption frequencies of the deuterated Co(III) and Ni(II) Diamido Cage, Diamide Cage Free Ligand and Co(III) Monoamido Macrocyclic Systems in D_2O and KBr.

Complex	ν~, cm^{-1}	Assignment
$[Co^{III}(\{ND_3^+\}_2$-2,7-dioxosar-2H)$]^{3+}$ [a]	1619	$C{=}O_{(amido)}$ stretch
$[Co^{III}(\{ND_3^+\}_2$-2,7-dioxosar-2H)$]^{3+}$ [b]	1618	$C{=}O_{(amido)}$ stretch
$[Co^{III}(\{ND_3^+\}_2$-2,9-dioxosar-2H)$]^{3+}$ [a]	1622	$C{=}O_{(amido)}$ stretch
$[Co^{III}(\{ND_3^+\}_2$-2,9-dioxosar-2H)$]^{3+}$ [b]	1625	$C{=}O_{(amido)}$ stretch
$[Co^{III}$(6-{ND_3^+,C(O)NH}-13-{ND_3^+,CH_2NH_2}-cyclam)$]^{4+}$ [a]	1626	$C{=}O_{(amido)}$ stretch
$[Co^{III}$(6-{ND_3^+,C(O)NH}-13-{ND_3^+,CH_2NH_2}-cyclam)$]^{4+}$ [b]	1611	$C{=}O_{(amido)}$ stretch
$[Ni^{II}(\{ND_3^+\}_2$-2,7-dioxosar-2H)$]^{2+}$ [a]	1602	$C{=}O_{(amido)}$ stretch
$[Ni^{II}(\{ND_3^+\}_2$-2,7-dioxosar-2H)$]^{2+}$ [b]	1594	$C{=}O_{(amido)}$ stretch

[a] D_2O, [b] KBr

4.3.4 Electrospray Mass Spectrometry

Co(III), Cr(III) and Ni(II) Monoamido Cage Systems

The Electrospray Mass Spectra (ESMS) of the three monoamido complexes within this series are displayed in Figures 14, 15 and 16 respectively. Firstly, the $[Co^{III}(\{NH_3^+\}_2$-2-oxosar-H)$]^{4+}$ ion possesses a base signal at m/z 384.8 which has been attributed to a $[Cocage^{4+} - 3H^+]^+$ species. Also, a second series of signals located at m/z 420.8 arise from a $[Cocage^{4+} - 2H^+ + {}^{35}Cl^-]^+$ species. For the Ni(II) amido cage complex, $[Ni^{II}(\{NH_3^+\}_2$-2-oxosar-H)$]^{3+}$, both the perchlorate and chloride compounds display signals at an m/z value of 385.0 which corresponds to a $[Nicage^{3+} - 2H^+]^+$ species. In addition, the perchlorate salt also displays a series of signals centred on m/z 484.9 which arise from an $[Nicage^{3+} - H^+ + {}^{35}ClO_4^-]^+$ ion. Turning to the Cr(III) amide complex, $[Cr^{III}(\{NH_3^+\}_2$-2-oxosar-H)$]^{4+}$, the base signal, appearing at an m/z value of 377.8, arises from a $[Crcage^{4+} - 3H^+]^+$ species. A second series of signals present at m/z 413.7 correspond to a mono charged ion pair species, $[Crcage^{4+} - 2H^+ + {}^{35}Cl^-]^+$. This species in both the Co(III) and Cr(III) cases arises presumably by hydrogen bonding between the charged cage and a chloride ion. For all of these complexes the loss of H^+ is

likely to originate from the protonated apical amines (~pK_a 2 - 6) and to a lesser extent the secondary amine sites ($pK_a \geq 12$). A number of lesser signals appear around those of the observed ions. These signals arise from the contributions of the isotopes of the various elements present within each complex, especially ^{13}C, ^{35}Cl and ^{36}Cl. Also the various spectra fit the simulated patterns for the observed ions and are consistent with the microanalytical data.

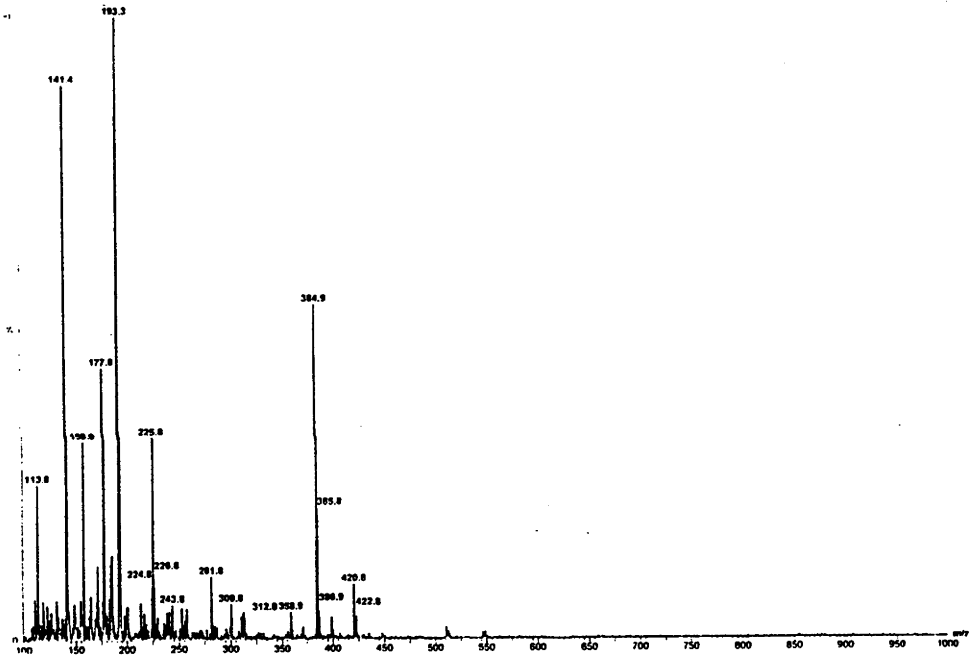

Figure 14. ESM spectrum of aqueous $[Co^{III}(\{NH_3^+\}_2\text{-2-oxosar-H})]^{4+}$ (Cone Voltage = 50 V).

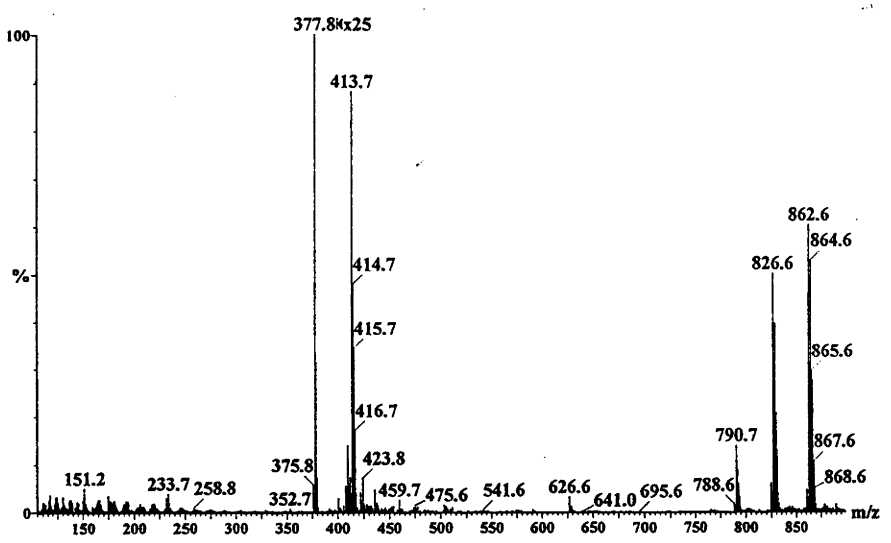

Figure 15. ESM spectrum of aqueous $[Cr^{III}(\{NH_3^+\}_2\text{-2-oxosar-H})]^{4+}$ (Cone Voltage = 80 V).

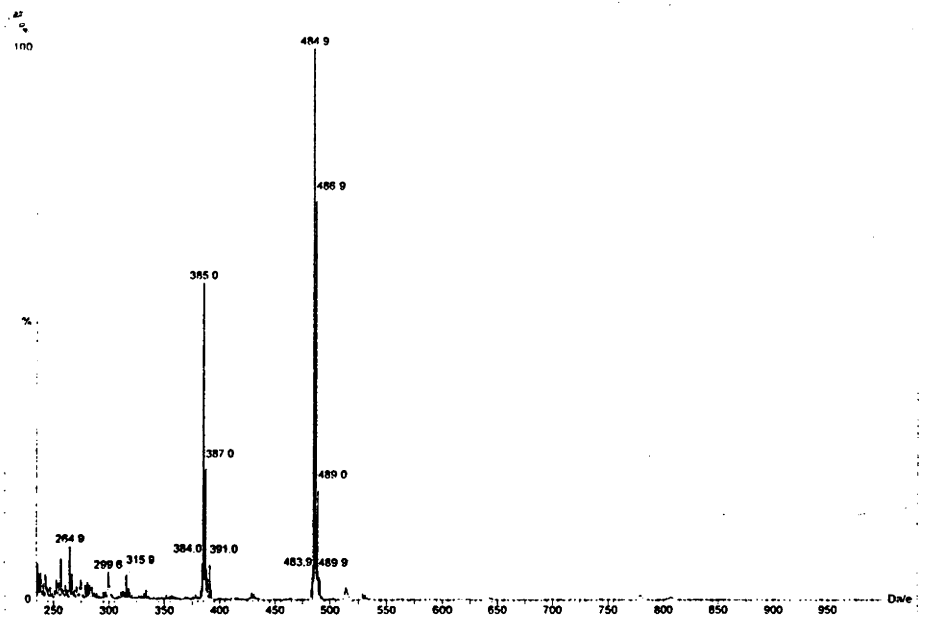

Figure 16. ESM spectrum of aqueous $[Ni^{II}(\{NH_3^+\}_2\text{-2-oxosar-H})]^{3+}$ (Cone Voltage = 25 V).

Co(III) and Ni(II) Diamido Cage and Co(III) Monoamido Macrocyclic Systems

The ESM spectra of the Co(III) diamido cage isomers and macrocyclic monoamido complexes appear in Figures 17, 18 and 19. For the two diamido compounds, $[Co^{III}(\{NH_3^+\}_2\text{-}2,7\text{-dioxosar-}2H)]^{3+}$ and $[Co^{III}(\{NH_3^+\}_2\text{-}2,9\text{-dioxosar-}2H)]^{3+}$, a signal appearing at an m/z value of 398.8, corresponding to a $[Cocage^{3+} - 2H^+]^+$ species, is the most abundant peak in each spectrum. In addition, the first isomer, $[Co^{III}(\{NH_3^+\}_2\text{-}2,7\text{-dioxosar-}2H)]^{3+}$, displays an extra signal attributed to a $[Cocage^{3+} - H^+ + {}^{35}Cl^-]^+$ species at m/z = 435.8. In the spectrum of the macrocyclic amido complex, $[Co^{III}(6\text{-}\{NH_3^+,C(O)NH\}\text{-}13\text{-}\{NH_3^+,CH_2NH_2\}\text{-cyclam})]^{4+}$, the most abundant signal appears at m/z = 358.9 which corresponds to a $[Cocage^{4+} - 3H^+]^+$ species. The ESM spectrum of $[Ni^{II}(\{NH_3^+\}_2\text{-}2,7\text{-dioxosar-}2H)]^{2+}$, in water with a cone voltage of 50 V, appears in Figure 20. The parent ion with the highest intensity appears at an m/z value of 398.8 which corresponds to a $[Nicage^{2+} - H^+]^+$ species. A second series of signals centred on an m/z value of 499 arise from the ion-pair $[Nicage^{2+} - {}^{35}ClO_4^-]^+$ where a cage molecule and a single perchlorate ion are linked probably through hydrogen bonding. Again for this series of complexes loss of the H^+ ion is likely to originate from the protonated apical amines. These data are consistent with the formulations proposed from the analytical data and the crystallography. The technique is not so good for observing the parent forms since H^+ is readily lost in these experiments. It is the most common and substantial fragmentation process observed. As usual, several isotope satellite signals were observed arising largely from ^{35}Cl, ^{36}Cl, and ^{13}C. Also the various spectra fit the simulated patterns of the observed ions and are consistent with the microanalytical data.

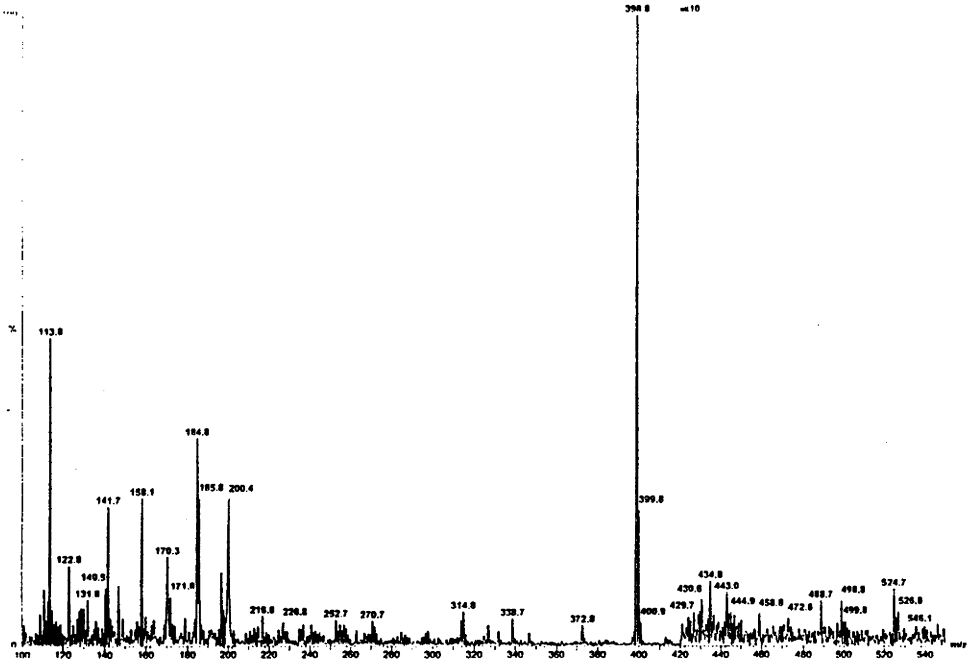

Figure 17. ESM spectrum of aqueous $[Co^{III}(\{NH_3^+\}_2\text{-}2,7\text{-dioxosar-}2H)]^{3+}$ (Cone Voltage = 50 V).

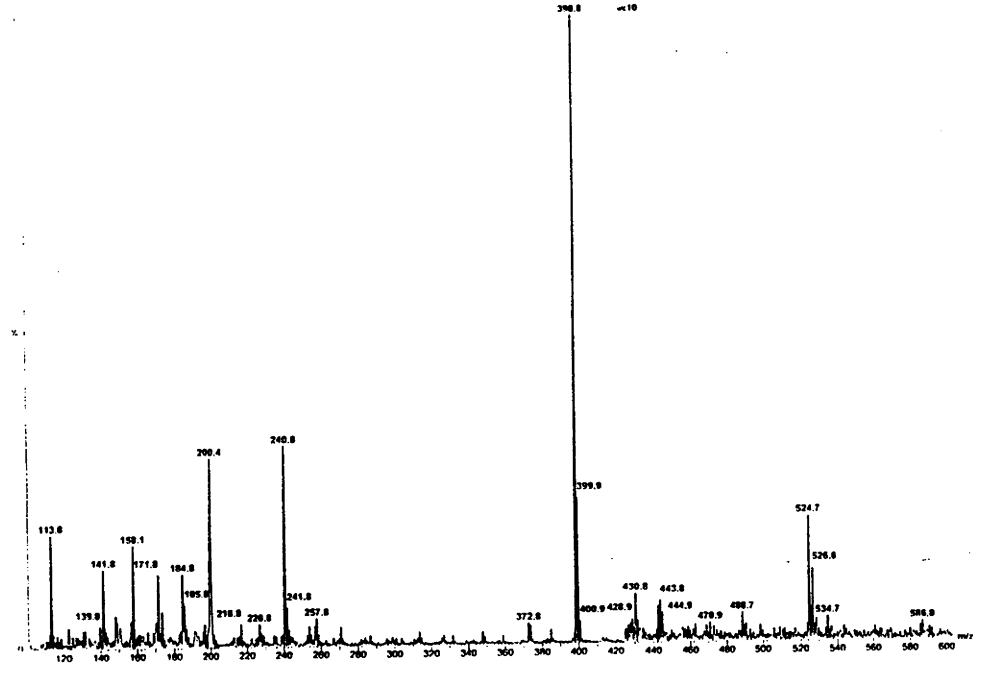

Figure 18. ESM spectrum of aqueous $[Co^{III}(\{NH_3^+\}_2\text{-}2,9\text{-dioxosar-}2H)]^{3+}$ (Cone Voltage = 50 V).

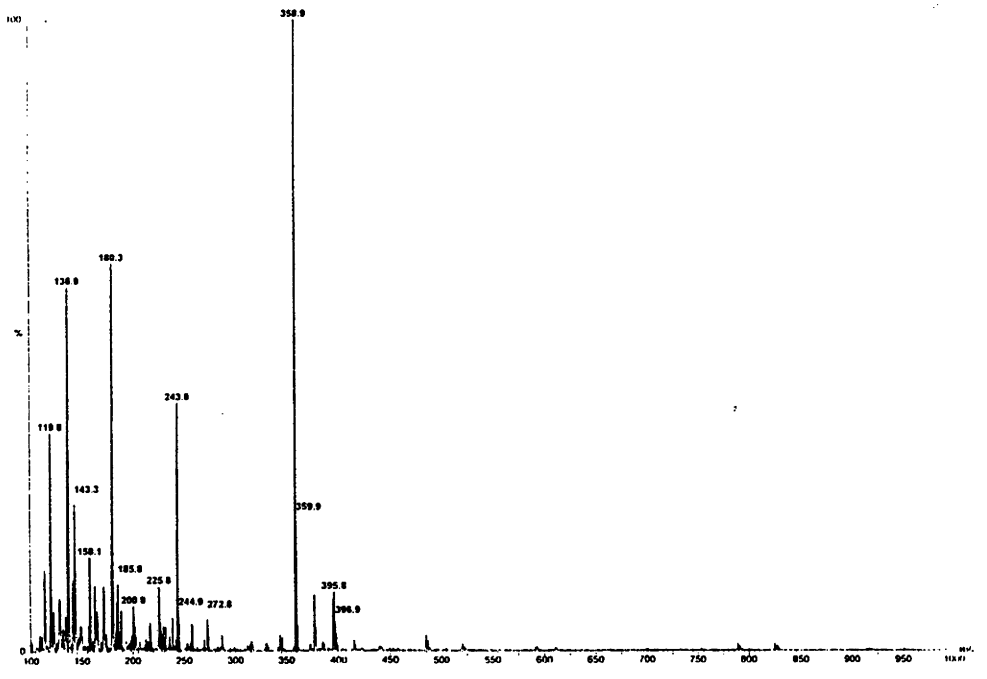

Figure 19. ESM spectrum of aqueous $[Co^{III}(6\text{-}\{NH_3^+,C(O)NH\}\text{-}13\text{-}\{NH_3^+,CH_2NH_2\}\text{-cyclam})]^{4+}$ (Cone Voltage = 50 V).

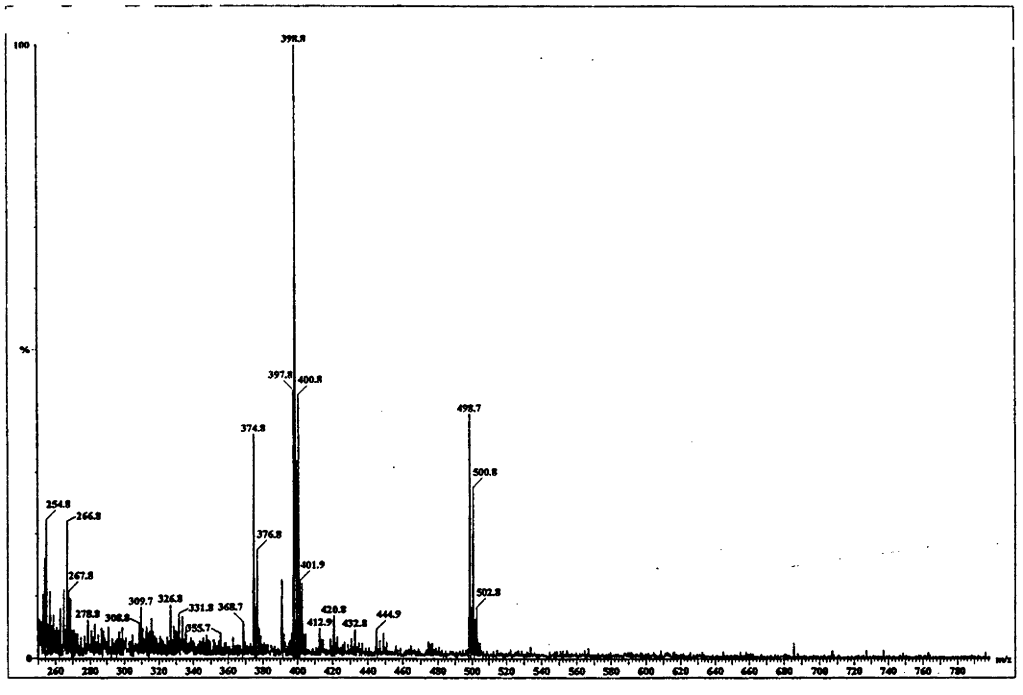

Figure 20. ESM spectrum of aqueous $[Ni^{II}(\{NH_3^+\}_2\text{-}2,7\text{-dioxosar-}2H)]^{2+}$ (Cone Voltage = 50 V).

4.3.5 X-ray Crystallography

X-ray Crystallographic Analysis of $[Co^{III}(\{NH_3^+\}_2\text{-2-oxosar-H})](NO_3)_4.H_2O$

The structure of the Co(III) monoamido complex and selected interatomic distances and bond angles are displayed in Figure 21 and Tables 5 and 6 respectively. The ORTEP diagram shows that the Co(III) ion is fully encapsulated and is also bonded to the amido nitrogen atom which has lost a proton. For the Co(III) complex the net charge is therefore a 4+ ion provided the two exo amine groups are protonated. Another feature of this complex is that for the two sectors free of the amide group the five membered chelate rings have adopted a *lel* configuration while in the remaining strap containing the amido group, the five membered chelate ring possesses an *ob* conformation with respect to the pseudo C_3 axis through the metal giving the complex an overall conformation of lel_2ob. This structure is similar to those observed for the $[Co^{III}$(Me,CN-2-oxosar-H)$]^{2+}$ (Chapter 3) and $[Co^{III}$(Me,COOH-2-oxosar-H)$]^{2+}$ [20] ions.

The $Co\text{-}N_{(amine)}$ bond distances are similar to those reported for other amine and amido sar-type Co(III) complexes[7,20,22-24] and as observed previously two of the $Co\text{-}N_{(amine)}$ bonds, namely Co-N(2) and Co-N(6), were found to be slightly shorter than the remaining $Co\text{-}N_{(amine)}$ bonds (Table 5). The $Co\text{-}N_{(amido)}$ distance however, 1.905(5) Å, is much shorter than those observed for the $Co\text{-}N_{(amine)}$ bonds. This value is similar to that obtained for other amido Co(III) cage complexes[20] and the $[CH_3CONHCo^{III}(NH_3)_5]^{2+}$ ion (1.911(8) Å)[25] but is longer than that observed for some other Co(III) amido compounds, for instance, the bis(glycylglycinato)cobalt(III) anion has a $Co\text{-}N_{(amido)}$ bond distance of 1.87 Å.[26] The N(1)-C(2) amido bond length (1.300(8) Å) is similar to other amido Co(III) cage complexes and is identical to the expected $C\text{-}N_{(peptide)}$ distance of 1.30 Å[27] while the other saturated C-N bonds, completing the caps, have distances that are similar to other sar type cages. In addition the amido carbon-oxygen distance was found to be 1.242(7) Å which is slightly shorter than the expected $C\text{-}O_{(peptide)}$ bond length of 1.27 Å.[27]

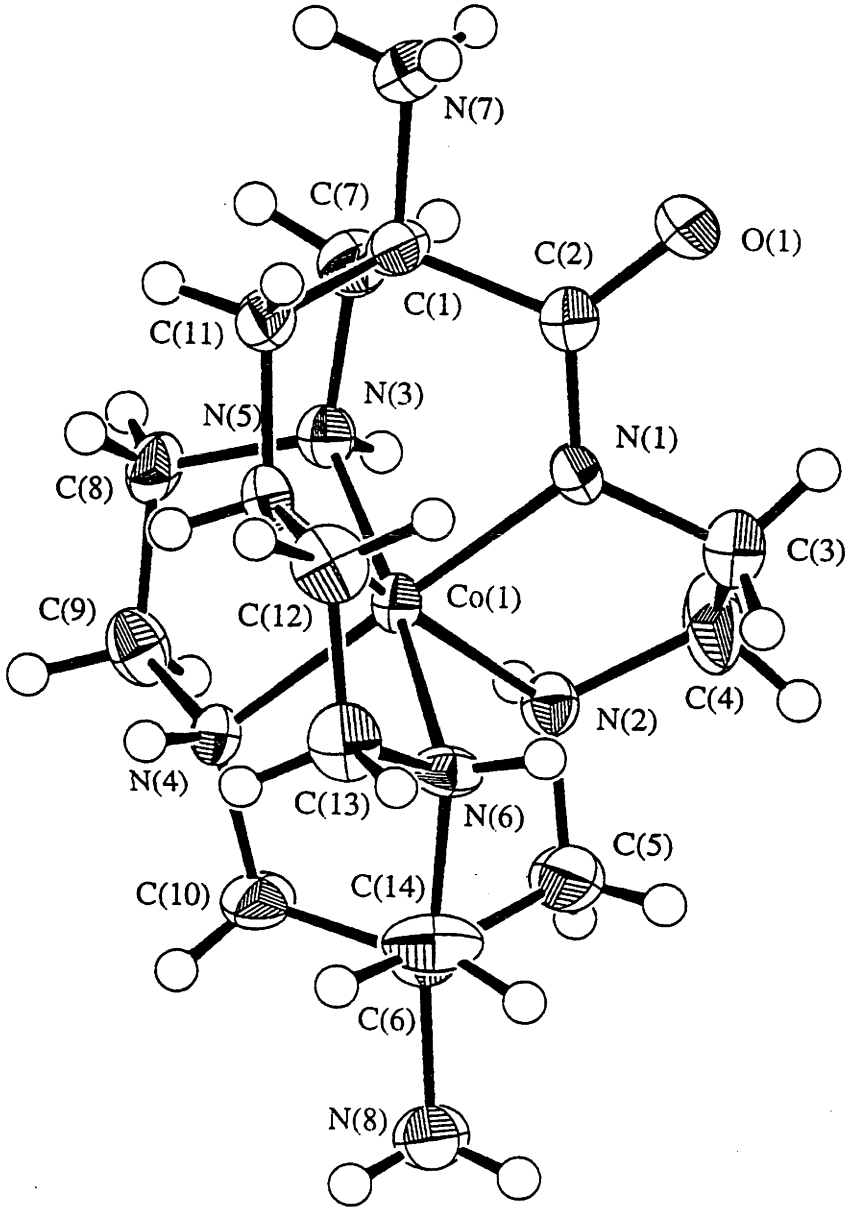

Figure 21. Thermal ellipsoid diagram of $[Co^{III}(\{NH_3^+\}_2\text{-2-oxosar-H})](NO_3)_4.H_2O$ showing atomic labelling. Ellipsoids show 50% probability levels, except the hydrogen atoms which are drawn as circles of arbitrary small radius.

Table 5. Bond distances (Å) for $[Co^{III}(\{NH_3^+\}_2\text{-2-oxosar-H})](NO_3)_4.H_2O$.

Atom	Distance (Å)	Atom	Distance (Å)
Co-N(1)	1.905(5)	Co-N(2)	1.933(4)
Co-N(3)	1.970(5)	Co-N(4)	1.981(4)
Co-N(5)	1.975(5)	Co-N(6)	1.955(5)
O(1)-C(2)	1.242(7)	O(3)-N(9)	1.238(7)
O(4)-N(9)	1.254(7)	O(5)-N(9)	1.231(7)
O(6)-N(10)	1.323(8)	O(7)-N(10)	1.248(8)
O(8)-N(10)	1.242(7)	O(9)-N(11)	1.229(7)
O(10)-N(11)	1.241(7)	O(11)-N(11)	1.229(7)
O(12)-N(12)	1.181(9)	O(13)-O(15)	1.31(4)
O(13)-O(16)	1.43(4)	O(13)-N(12)	1.22(1)
O(14)-O(16)	1.22(4)	O(14)-N(12)	1.16(1)
O(15)-N(12)	1.33(4)	O(16)-N(12)	1.14(4)
N(1)-C(2)	1.300(8)	N(1)-C(3)	1.455(8)
N(2)-C(4)	1.494(8)	N(2)-C(5)	1.466(8)
N(3)-C(7)	1.496(8)	N(3)-C(8)	1.482(8)
N(4)-C(9)	1.497(7)	N(4)-C(10)	1.483(7)
N(5)-C(11)	1.480(7)	N(5)-C(12)	1.490(7)
N(6)-C(13)	1.483(8)	N(6)-C(14)	1.501(7)
N(7)-C(1)	1.489(8)	N(8)-C(6)	1.518(7)
C(1)-C(2)	1.537(8)	C(1)-C(7)	1.529(9)
C(1)-C(11)	1.515(8)	C(3)-C(4)	1.47(1)
C(5)-C(6)	1.515(9)	C(6)-C(10)	1.532(8)
C(6)-C(14)	1.499(9)	C(8)-C(9)	1.507(8)
C(12)-C(13)	1.496(9)		

Table 6. Bond angles (°) for $[Co^{III}(\{NH_3^+\}_2\text{-2-oxosar-H})](NO_3)_4.H_2O$.

Atom	Angle	Atom	Angle	Atom	Angle	Atom	Angle
N(1)-Co-N(2)	85.3(2)	N(1)-Co-N(3)	90.2(2)	O(6)-N(10)-O(7)	121.6(7)	O(6)-N(10)-O(8)	119.1(8)
N(1)-Co-N(4)	174.8(2)	N(1)-Co-N(5)	88.5(2)	O(7)-N(10)-O(8)	119.2(7)	O(9)-N(11)-O(10)	118.7(6)
N(1)-Co-N(6)	93.3(2)	N(2)-Co-N(3)	93.3(3)	O(9)-N(11)-O(11)	120.1(6)	O(10)-N(11)-O(11)	121.1(6)
N(2)-Co-N(4)	90.6(2)	N(2)-Co-N(5)	172.7(2)	O(12)-N(12)-O(13)	125(1)	O(12)-N(12)-O(14)	116(1)
N(2)-Co-N(6)	90.8(2)	N(3)-Co-N(4)	86.8(2)	O(12)-N(12)-O(15)	119(2)	O(12)-N(12)-O(16)	131(2)
N(3)-Co-N(5)	90.5(2)	N(3)-Co-N(6)	174.8(2)	O(13)-N(12)-O(14)	119(1)	O(13)-N(12)-O(15)	62(2)
N(4)-Co-N(5)	95.9(2)	N(4)-Co-N(6)	89.9(2)	O(13)-N(12)-O(16)	74(2)	O(14)-N(12)-O(15)	92(2)
N(5)-Co-N(6)	85.7(2)	O(15)-O(13)-O(16)	95(3)	O(14)-N(12)-O(16)	64(2)	O(15)-N(12)-O(16)	110(3)
O(15)-O(13)-N(12)	63(2)	O(16)-O(13)-N(12)	50(2)	N(7)-C(1)-C(2)	107.1(5)	N(7)-C(1)-C(7)	107.9(5)
O(16)-O(14)-N(12)	57(2)	O(13)-O(15)-N(12)	55(2)	N(7)-C(1)-C(11)	107.9(5)	C(2)-C(1)-C(7)	106.3(5)
O(13)-O(16)-O(14)	101(3)	O(13)-O(16)-N(12)	55(2)	C(2)-C(1)-C(11)	116.6(5)	C(7)-C(1)-C(11)	110.7(6)
O(14)-O(16)-N(12)	59(2)	Co-N(1)-C(2)	124.5(4)	O(1)-C(2)-N(1)	126.8(6)	O(1)-C(2)-C(1)	119.3(5)
Co-N(1)-C(3)	112.1(4)	C(2)-N(1)-C(3)	119.8(5)	N(1)-C(2)-C(1)	113.7(5)	N(1)-C(3)-C(4)	106.9(5)
Co-N(2)-C(4)	108.2(4)	Co-N(2)-C(5)	116.5(4)	N(2)-C(4)-C(3)	112.0(5)	N(2)-C(5)-C(6)	113.2(5)
C(4)-N(2)-C(5)	112.0(5)	Co-N(3)-C(7)	117.9(4)	N(8)-C(6)-C(5)	107.4(5)	N(8)-C(6)-C(10)	104.6(5)
Co-N(3)-C(8)	107.7(4)	C(7)-N(3)-C(8)	112.0(5)	N(8)-C(6)-C(14)	107.9(5)	C(5)-C(6)-C(10)	113.2(5)
Co-N(4)-C(9)	108.3(3)	Co-N(4)-C(10)	116.7(4)	C(5)-C(6)-C(14)	111.7(6)	C(10)-C(6)-C(14)	111.6(5)
C(9)-N(4)-C(10)	110.5(5)	Co-N(5)-C(11)	116.8(4)	N(3)-C(7)-C(1)	111.0(5)	N(3)-C(8)-C(9)	107.4(5)
Co-N(5)-C(12)	106.9(3)	C(11)-N(5)-C(12)	111.0(5)	N(4)-C(9)-C(8)	110.1(5)	N(4)-C(10)-C(6)	113.2(5)
Co-N(6)-C(13)	108.4(4)	Co-N(6)-C(14)	117.7(4)	N(5)-C(11)-C(1)	112.5(5)	N(5)-C(12)-C(13)	106.8(5)
C(13)-N(6)-C(14)	109.7(5)	O(3)-N(9)-O(4)	118.8(7)	N(6)-C(13)-C(12)	107.6(5)	N(6)-C(14)-C(6)	111.4(5)
O(3)-N(9)-O(5)	119.5(6)	O(4)-N(9)-O(5)	121.7(7)				

Most of the N-Co-N bond angles are within 3 - 7° of the values required for octahedral symmetry of the CoN_6 core. Also of interest is the twist angle between the two sets of N_3-planes perpendicular to the long axis of the molecule; the average value has been determined to be 53° i.e. not far from the octahedral value of 60°. In addition, the tilt angle between the two N_3 planes, 2.3°, indicates that they are near parallel to one another although the coordination geometry can be viewed as a slightly distorted octahedron as a result of all these displacements. As a consequence of incorporating an amide moiety within the cage structure the five membered chelate ring attached to the amide fragment has a torsion angle of -41.1(8)° for N(1)-C(3)-C(4)-N(2) while the two remaining chelate rings, namely N(3)-C(8)-C(9)-N(4) and N(5)-C(12)-C(13)-N(6), have torsion angles of 47.9(6)° and 53.9(6)° to give the *lel*$_2$*ob* conformation.

Although microcrystals of the Ni(II) and Cr(III) monoamido complexes were obtained analytically pure, crystals suitable for x-ray analysis were elusive.

X-ray Crystallographic Analyses of $[Co^{III}(\{NH_3^+\}_2$-2,7-dioxosar-2H)]Cl-$ZnCl_4.H_2O$ and $[Co^{III}(\{NH_3^+\}_2$-2,9-dioxosar-2H)]$(S_2O_6)_{3/2}.3H_2O$

The structures of the two isomeric diamides, along with the bond distances and angles, are displayed in Figure 22 and Tables 7 and 8 for $[Co^{III}(\{NH_3^+\}_2$-2,7-dioxosar-2H)]$ClZnCl_4.H_2O$ and Figure 23 and Tables 9 and 10 for $[Co^{III}(\{NH_3^+\}_2$-2,9-dioxosar-2H)]$(S_2O_6)_{3/2}.3H_2O$ respectively. The crystallography shows that the cobalt(III) ion is still encapsulated and is bonded to both deprotonated amido nitrogen atoms. Moreover, the six N atoms bonded to the Co(III) occupy basically octahedral sites. Incorporating two amide moieties into the caps of the sar structure has resulted in two of the five membered chelate rings in the ligand strands adopting an *ob* conformation while the remaining strap is *lel* so that each isomer has the overall configuration *ob*$_2$*lel*.

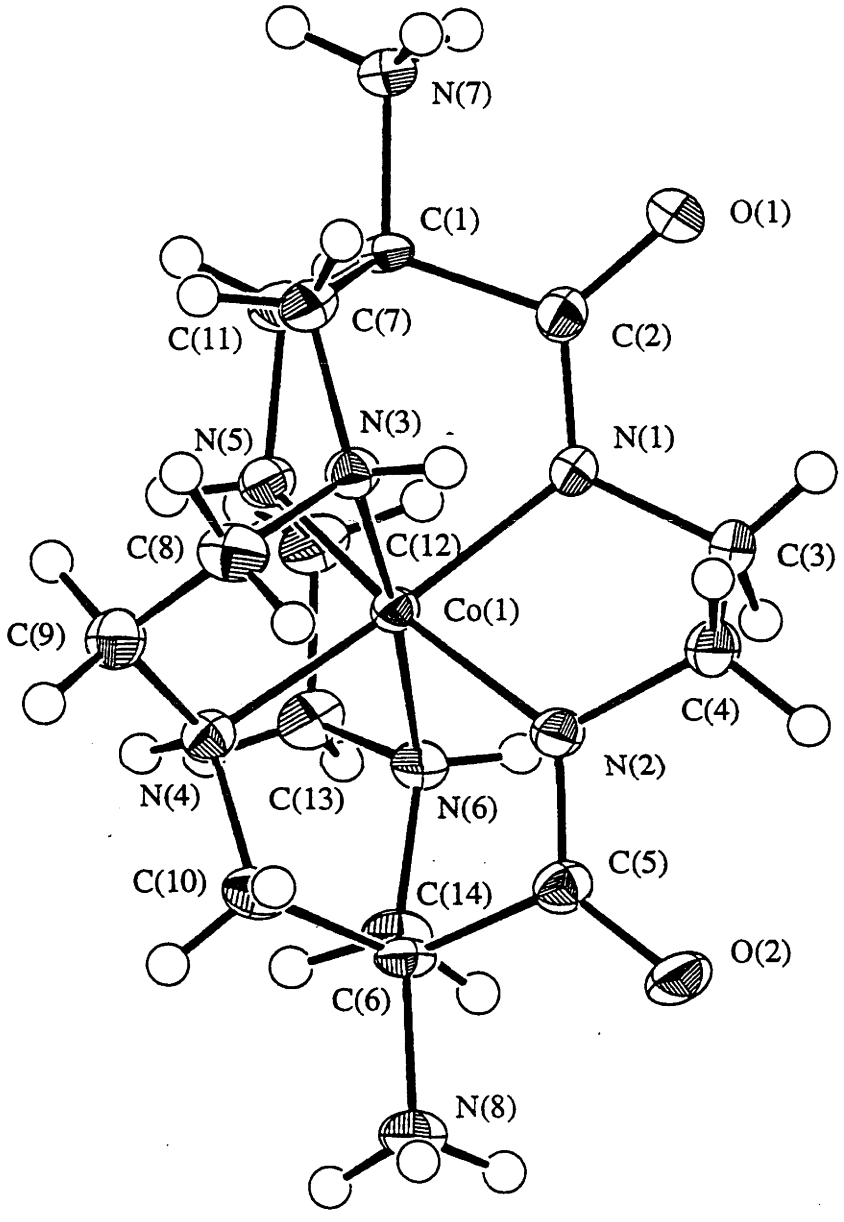

Figure 22. Thermal ellipsoid diagram of $[Co^{III}(\{NH_3^+\}_2\text{-}2,7\text{-dioxosar-}2H)]Cl\text{-}ZnCl_4.H_2O$ showing atomic labelling. Ellipsoids show 50% probability levels, except the hydrogen atoms which are drawn as circles of arbitrary small radius.

Table 7. Bond Distances (Å) for $[Co^{III}(\{NH_3^+\}_2\text{-}2,7\text{-dioxosar-}2H)]ClZnCl_4.H_2O$.

Atom	Distance (Å)	Atom	Distance (Å)
Zn-Cl(1)	2.2676(8)	Zn-Cl(2)	2.2616(8)
Zn-Cl(3)	2.2731(8)	Zn-Cl(4)	2.2749(7)
Co-N(1)	1.918(2)	Co-N(2)	1.940(2)
Co-N(3)	1.957(2)	Co-N(4)	1.972(2)
Co-N(5)	1.995(2)	Co-N(6)	1.985(2)
O(1)-C(2)	1.253(3)	O(2)-C(5)	1.251(3)
N(1)-C(2)	1.320(3)	N(1)-C(3)	1.474(3)
N(2)-C(4)	1.475(3)	N(2)-C(5)	1.317(3)
N(3)-C(7)	1.488(3)	N(3)-C(8)	1.494(3)
N(4)-C(9)	1.500(3)	N(4)-C(10)	1.487(3)
N5)-C(11)	1.481(3)	N(5)-C(12)	1.502(3)
N(6)-C(13)	1.487(3)	N(6)-C(14)	1.491(3)
N(7)-C(1)	1.500(3)	N(8)-C(6)	1.496(3)
C(1)-C(2)	1.541(3)	C(1)-C(7)	1.534(4)
C(1)-C(11)	1.525(3)	C(3)-C(4)	1.510(4)
C(5)-C(6)	1.528(3)	C(6)-C(10)	1.525(4)
C(6)-C(14)	1.524(3)	C(8)-C(9)	1.493(4)
C(12)-C(13)	1.481(4)		

Table 8. Bond angles (°) for $[Co^{III}(\{NH_3^+\}_2\text{-}2,7\text{-dioxosar-}2H)]ClZnCl_4.H_2O$.

Atom	Angle	Atom	Angle	Atom	Angle	Atom	Angle
Cl(1)-Zn-Cl(2)	109.68(3)	Cl(1)-Zn-Cl(3)	106.83(3)	Co-N(5)-C(12)	106.1(2)	C(11)-N(5)-C(12)	109.8(2)
Cl(1)-Zn-Cl(4)	110.62(3)	Cl(2)-Zn-Cl(3)	111.48(3)	Co-N(6)-C(13)	109.2(2)	Co-N(6)-C(14)	116.0(2)
Cl(2)-Zn-Cl(4)	107.91(3)	Cl(3)-Zn-Cl(4)	110.34(3)	C(13)-N(6)-C(14)	110.0(2)	N(7)-C(1)-C(2)	108.4(2)
N(1)-Co-N(2)	83.23(8)	N(1)-Co-N(3)	85.38(9)	N(7)-C(1)-C(7)	107.8(2)	N(7)-C(1)-C(11)	107.1(2)
N(1)-Co-N(4)	171.98(9)	N(1)-Co-N(5)	87.8(9)	C(2)-C(1)-C(7)	110.8(2)	C(2)-C(1)-C(11)	112.0(2)
N(1)-Co-N(6)	101.39(9)	N(2)-Co-N(3)	92.33(8)	C(7)-C(1)-C(11)	110.5(2)	O(1)-C(2)-N(1)	127.5(2)
N(2)-Co-N(4)	95.91(9)	N(2)-Co-N(5)	166.69(9)	O(1)-C(2)-C(1)	118.9(2)	N(1)-C(2)-C(1)	113.7(3)
N(2)-Co-N(6)	86.98(8)	N(3)-Co-N(4)	86.68(9)	N(1)-C(3)-C(4)	105.7(2)	N(2)-C(4)-C(3)	105.9(2)
N(3)-Co-N(5)	96.74(9)	N(3)-Co-N(6)	173.05(9)	O(2)-C(5)-N(2)	128.4(2)	O(2)-C(5)-C(6)	119.0(2)
N(4)-Co-N(5)	94.32(9)	N(4)-Co-N(6)	86.51(9)	N(2)-C(5)-C(6)	112.5(2)	N(8)-C(6)-C(5)	107.3(2)
N(5)-Co-N(6)	85.17(8)	Co-N(1)-C(2)	122.3(2)	N(8)-C(6)-C(10)	107.7(2)	N(8)-C(6)-C(14)	106.9(2)
Co-N(1)-C(3)	112.7(2)	C(2)-N(1)-C(3)	118.8(2)	C(5)-C(6)-C(10)	112.8(2)	C(5)-C(6)-C(14)	109.0(2)
Co-N(2)-C(4)	113.3(2)	Co-N(2)-C(5)	122.3(2)	C(10)-C(6)-C(14)	112.8(2)	N(3)-C(7)-C(1)	111.1(2)
C(4)-N(2)-C(5)	118.0(2)	Co-N(3)-C(7)	114.9(2)	N(3)-C(8)-C(9)	108.2(2)	N(4)-C(9)-C(8)	107.7(2)
Co-N(3)-C(8)	109.0(2)	C(7)-N(3)-C(8)	113.4(2)	N(4)-C(10)-C(6)	110.4(2)	N(5)-C(11)-C(1)	111.5(2)
Co-N(4)-C(9)	107.8(2)	Co-N(4)-C(10)	113.6(2)	N(5)-C(12)-C(13)	106.8(2)	N(6)-C(13)-C(12)	106.6(2)
C(9)-N(4)-C(10)	112.5(2)	Co-N(5)-C(11)	117.8(2)	N(6)-C(14)-C(6)	111.5(2)		

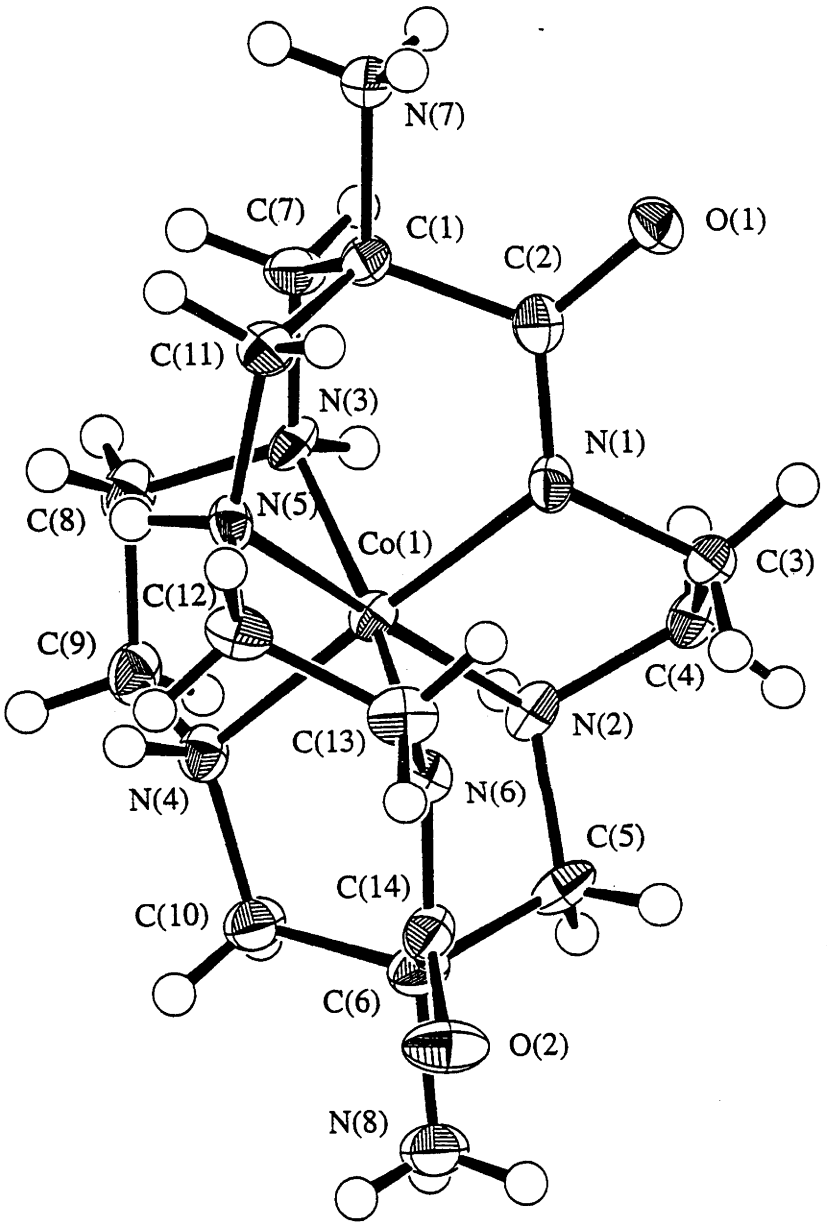

Figure 23. Thermal ellipsoid diagram of $[Co^{III}(\{NH_3^+\}_2\text{-}2,9\text{-dioxosar-}2H)](S_2O_6)_{3/2}.3H_2O$ showing atomic labelling. Ellipsoids show 50% probability levels, except the hydrogen atoms which are drawn as circles of arbitrary small radius.

Table 9. Bond Distances (Å) for $[Co^{III}(\{NH_3^+\}_2\text{-}2,9\text{-dioxosar-}2H)](S_2O_6)_{3/2}\cdot 3H_2O$.

Atom	Distance (Å)	Atom	Distance (Å)
Co-N(1)	1.906(5)	Co-N(2)	1.985(5)
Co-N(3)	1.982(5)	Co-N(4)	1.967(5)
Co-N(5)	1.992(5)	Co-N(6)	1.901(5)
S(1)-S(2)	2.128(2)	S(1)-O(3)	1.437(5)
S(1)-O(4)	1.431(5)	S(1)-O(5)	1.435(5)
S(2)-O(6)	1.440(5)	S(2)-O(7)	1.456(5)
S(2)-O(8)	1.455(5)	S(3)-S(3)[a]	2.129(4)
S(3)-O(9)	1.470(4)	S(3)-O(10)	1.444(5)
S(3)-O(11)	1.438(5)	O(1)-C(2)	1.271(7)
O(2)-C(14)	1.247(8)	N(1)-C(2)	1.314(8)
N(1)-C(3)	1.463(8)	N(2)-C(4)	1.512(8)
N(2)-C(5)	1.493(8)	N(3)-C(7)	1.502(7)
N(3)-C(8)	1.493(8)	N(4)-C(9)	1.495(8)
N(4)-C(10)	1.499(8)	N(5)-C(11)	1.496(7)
N(5)-C(12)	1.507(8)	N(6)-C(13)	1.464(7)
N(6)-C(14)	1.316(7)	N(7)-C(1)	1.491(7)
N(8)-C(6)	1.496(8)	C(1)-C(2)	1.508(8)
C(1)-C(7)	1.540(9)	C(1)-C(11)	1.537(8)
C(3)-C(4)	1.508(9)	C(5)-C(6)	1.538(8)
C(6)-C(10)	1.522(9)	C(6)-C(14)	1.529(9)
C(8)-C(9)	1.493(9)	C(12)-C(13)	1.513(9)

[a]Atom generated by the symmetry operation (1/2-x, 1/2-y, -z)

Table 10. Bond angles (°) for $[Co^{III}(\{NH_3^+\}_2\text{-}2,9\text{-dioxosar-}2H)](S_2O_6)_{3/2}.3H_2O$.

Atom	Angle	Atom	Angle	Atom	Angle	Atom	Angle
N(1)-Co-N(2)	84.4(2)	N(1)-Co-N(3)	91.5(2)	Co-N(3)-C(8)	107.7(4)	C(7)-N(3)-C(8)	112.8(5)
N(1)-Co-N(4)	173.2(2)	N(1)-Co-N(5)	91.8(2)	Co-N(4)-C(9)	109.0(4)	Co-N(4)-C(10)	115.2(4)
N(1)-Co-N(6)	92.4(2)	N(2)-Co-N(3)	95.5(2)	C(9)-N(4)-C(10)	111.8(5)	Co-N(5)-C(11)	114.5(4)
N92)-Co-N(4)	89.5(2)	N(2)-Co-N(5)	174.1(2)	Co-N(5)-C(12)	109.1(4)	C(11)-N(5)-C(12)	111.6(5)
N(2)-Co-N(6)	91.1(2)	N(3)-Co-N(4)	86.2(2)	Co-N(6)-C(13)	111.5(4)	Co-N(6)-C(14)	125.1(5)
N(3)-Co-N(5)	89.0(2)	N(3)-Co-N(6)	172.7(2)	C(13)-N(6)-C(14)	120.1(5)	N(7)-C(1)-C(2)	108.6(5)
N(4)-Co-N(5)	94.5(2)	N(4)-Co-N(6)	90.7(2)	N(7)-C(1)-C(7)	106.5(5)	N(7)-C(1)-C(11)	107.2(5)
N(5)-Co-N(6)	84.6(2)	S(2)-S(1)-O(3)	105.5(2)	C(2)-C(1)-C(7)	111.1(5)	C(2)-C(1)-C(11)	109.0(5)
S(2)-S(1)-O(4)	103.8(2)	S(2)-S(1)-O(5)	103.9(2)	C(7)-C(1)-C(11)	114.1(5)	O(1)-C(2)-N(1)	126.4(6)
O(3)-S(1)-O(4)	113.9(4)	O(3)-S(1)-O(5)	114.4(3)	O(1)-C(2)-C(1)	119.6(6)	N(1)-C(2)-C(1)	114.0(5)
O(4)-S(1)-O(5)	113.9(3)	S(1)-S(2)-O(6)	103.8(2)	N(1)-C(3)-C(4)	104.1(5)	N(2)-C(4)-C(3)	107.5(5)
S(1)-S(2)-O(7)	104.2(2)	S(1)-S(2)-O(8)	105.0(2)	N(2)-C(5)-C(6)	110.9(5)	N(8)-C(6)-C(5)	108.1(5)
O(6)-S(2)-O(7)	114.8(3)	O(6)-S(2)-O(8)	114.9(3)	N(8)-C(6)-C(10)	105.0(5)	N(8)-C(6)-C(14)	108.7(6)
O(7)-S(2)-O(8)	112.6(3)	S(3)[a]-S(3)-O(9)	104.2(2)	C(5)-C(6)-C(10)	113.3(6)	C(5)-C(6)-C(14)	10.5(5)
S(3)[a]-S(3)-O(10)	104.7(3)	S(3)[a]-S(3)-O(11)	105.7(2)	C(10)-C(6)-C(14)	113.0(6)	N(3)-C(7)-C(1)	112.5(5)
O(9)-S(3)-O(10)	111.5(3)	O(9)-S(3)-O(11)	113.9(3)	N(3)-C(8)-C(9)	107.8(5)	N(4)-C(9)-C(8)	107.7(5)
O(10)-S(3)-O(11)	115.5(3)	Co-N(1)-C(2)	123.4(5)	N(4)-C(10)-C(6)	113.3(5)	N(5)-C(11)-C(1)	113.1(5)
Co-N(1)-C(3)	111.6(4)	C(2)-N(1)-C(3)	121.6(5)	N(5)-C(12)-C(13)	108.4(5)	N(6)-C(13)-C(12)	104.7(5)
Co-N(2)-C(4)	109.0(4)	Co-N(2)-C(5)	115.3(4)	O(2)-C(14)-N(6)	128.5(6)	O(2)-C(14)-C(6)	120.2(6)
C(4)-N(2)-C(5)	111.0(5)	Co-N(3)-C(7)	116.3(4)	N(6)-C(14)-C(6)	111.2(6)		

[a]Atom generated by the symmetry operation (1/2-x, 1/2-y, -z)

The four Co-$N_{(amine)}$ bond distances in each diamide isomer are all rather similar to each other and similar to those in other amide sar-type Co(III) cage complexes.[20] In both instances, the Co-$N_{(amido)}$ distances are significantly shorter than the remaining amine bonds; for the first isomer the reported distances are 1.918(2) Å and 1.940(2) Å for Co-N(1) and Co-N(2) respectively, in the second isomer the amide distances, 1.906(5) Å and 1.901(5) Å for Co-N(1) and Co-N(6) respectively, are slightly shorter. The values obtained here are comparable with those observed for $[Co^{III}(Me,COOH\text{-}2\text{-}oxosar\text{-}H)]^{2+}$ (1.917(4) Å)[20] and $[CH_3CONHCo^{III}(NH_3)_5]^{2+}$ (1.911(8) Å)[25] but longer than those reported for other Co(III) amido bonds (eg 1.87 Å[26] and 1.89 Å[28]).

The amide bonds within these complexes are short for two reasons. Firstly, the sp^2 orbital radius of the nitrogen is necessarily shorter than that for an sp^3 configuration while the N^- ligand is probably a better ligand than the neutral one. The C-$N_{(amido)}$ bond lengths for the two isomeric diamides (Tables 7 and 9) are also similar to those of other amido Co(III) cage complexes[20] as well as the expected C-$N_{(peptide)}$ distance of 1.30 Å[27]. The remaining saturated C-C and C-N bonds, completing the cage, have distances that are close to those in other sar type cages.[22,28] In addition the C-$O_{(amido)}$ distances vary only slightly from the expected C-$O_{(peptide)}$ bond length of 1.27 Å.[27]

Most of the N-Co-N bond angles for $[Co^{III}(\{NH_3^+\}_2\text{-}2,7\text{-}dioxosar\text{-}2H)]^{3+}$ are within ~4° to 9° of their ideal values for octahedral symmetry of the CoN_6 core with two exceptions. The angles subtended by the atoms N(1)-Co-N(6) and N(2)-Co-N(5) are approximately 11° and 14° respectively from the ideal value of 180°. For the second isomer, $[Co^{III}(\{NH_3^+\}_2\text{-}2,9\text{-}dioxosar\text{-}2H)]^{3+}$, the N-Co-N bond angles are approximately 1° to 8° from the expected ideal octahedral values. Also of interest is the twist angle between the two sets of N_3-planes, for each isomer, perpendicular to the pseudo C_3 axis; the average value has been determined to be 53° for $[Co^{III}(\{NH_3^+\}_2\text{-}2,7\text{-}dioxosar\text{-}2H)]^{3+}$ and 52° for $[Co^{III}(\{NH_3^+\}_2\text{-}2,9\text{-}dioxosar\text{-}2H)]^{3+}$. This plus the angle between the two N_3 planes, for each isomer (6° and 4° respectively) indicates that the bound atom orientations about the metal are near octahedral in character in both instances The introduction of amide moieties has caused some change in the conformation of the basic cage structure. For the first diamido isomer this has resulted in the ligand strand containing the five membered chelate ring, N(1)-C(3)-C(4)-N(2) and both amide functions, possessing an *ob* torsion angle of 46°; the two

remining amide-free straps, namely N(3)-C(8)-C(9)-N(4) and N(5)-C(12)-C(13)-N(6), display *ob* and *lel* torsion angles of -50° and -55° respectively. A similar situation also exists for $[Co^{III}(\{NH_3^+\}_2\text{-}2,9\text{-dioxosar-}2H)]^{3+}$ but in this case the amide moieties are on different straps resulting in these two sectors possessing *ob* torsion angles of -50° for N(1)-C(3)-C(4)-N(2) and -48° for N(5)-C(12)-C(13)-N(6); the remaining strand containing the chelate ring (N(3)-C(8)-C(9)-N(4)) and no amide group displays a *lel* conformation that has a torsion angle of 51°.

X-ray Crystallographic Analysis of $[Co^{III}(6\text{-}\{NH_3^+,C(O)NH\}\text{-}13\text{-}\{NH_3^+,CH_2NH_2\}\text{-cyclam})]Cl_4.2.75H_2O$

The crystallography of the Co(III) monoamido macrocyclic structure in this series (Figure 24, Tables 11 and 12) shows that during the oxidation reaction two carbon atoms are lost from the original starting cage complex. A Co(III) macrocyclic complex with amido and amine pendant arms is thereby produced. The structure confirms that the ligand is hexadentate; four of the coordination sites come from a cyclam core and the two pendant substituents complete the octahedron. In addition, the macrocycle possesses a boat conformation where the two six membered chelate rings fold inwards enabling the co-ordination of the two pendants; the remaining four co-ordination sites, as a result of bonding to the metal, has also produced a slight twisting of the cyclam ligand.

The $Co\text{-}N_{(amine)}$ bond distances in this particular case are comparable to the values obtained for Co(III) *cis* and *trans* cyclam complexes (1.986(7) Å to 2.016(6) Å)[29,30], as well as, other reported Co(III) sar amido cage compounds[20]. However, they are slightly longer than the average distances reported for $[Co^{III}(en)_3]^{3+}$ and $[Co^{III}(NH_3)_6]^{3+}$ which are 1.964(7) Å[31] and 1.961 Å[32] respectively. Again the $Co\text{-}N_{(amido)}$ bond, 1.902(4) Å, is shorter than the other Co-N saturated amine distances and while similar to other cage $Co\text{-}N_{(amido)}$ bond ranges[20], and that of the $[CH_3CONHCo^{III}(NH_3)_5]^{2+}$ (1.911(8) Å)[25] ion, the value is still longer than that observed for the bis(glycylglycinato)cobalt(III) ion (1.87 Å).[26] The atoms completing the amide bond, namely N(32)-C(31) and C(31)-O(31), have distances that are also comparable to the expected $C\text{-}N_{(peptide)}$ and $C\text{-}O_{(peptide)}$ bond lengths.[27]

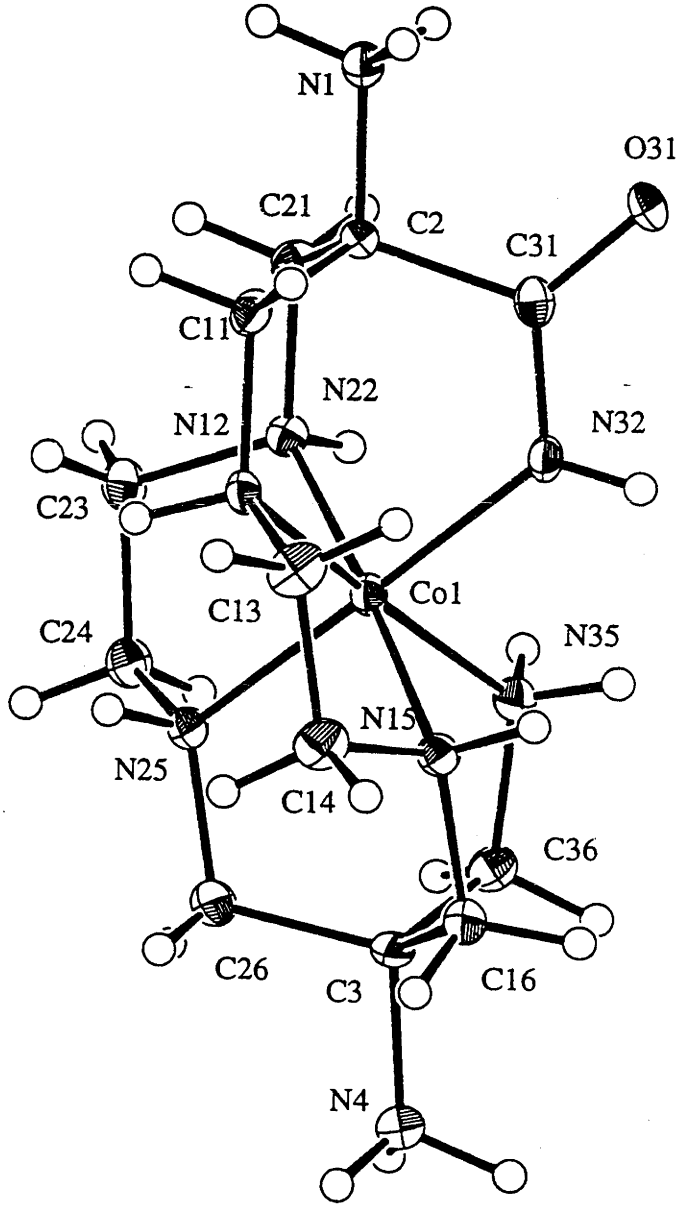

Figure 24. Thermal ellipsoid diagram of $[Co^{III}(6\text{-}\{NH_3^+,C(O)NH\}\text{-}13\text{-}\{NH_3^+,CH_2NH_2\}\text{-cyclam})]Cl_4.2.75H_2O$ showing atomic labelling. Ellipsoids show 50% probability levels, except the hydrogen atoms which are drawn as circles of arbitrary small radius.

Table 11. Bond Distances (Å) for $[Co^{III}(6\text{-}\{NH_3^+,C(O)NH\}\text{-}13\text{-}\{NH_3^+,CH_2NH_2\}\text{-cyclam})]Cl_4.2.75H_2O$.

Atom	Distance (Å)	Atom	Distance (Å)
Co-N(12)	1.991(3)	Co-N(15)	1.963(4)
Co-N(22)	1.976(4)	Co-N(25)	1.974(3)
Co-N(32)	1.902(4)	Co-N(35)	1.966(4)
O(31)-C(31)	1.245(4)	N(1)-C(2)	1.486(5)
N(4)-C(3)	1.505(5)	N(12)-C(11)	1.503(5)
N(12)-C(13)	1.486(5)	N(15)-C(14)	1.488(5)
N(15)-C(16)	1.494(5)	N(22)-C(21)	1.484(5)
N(22)-C(23)	1.496(5)	N(25)-C(24)	1.487(5)
N(25)-C(26)	1.485(5)	N(32)-C(31)	1.314(5)
N(35)-C(36)	1.477(5)	C(2)-C(11)	1.529(5)
C(2)-C(21)	1.523(5)	C(2)-C(31)	1.525(5)
C(3)-C(16)	1.529(6)	C(93)-C(26)	1.532(6)
C(3)-C(36)	1.522(6)	C(13)-C(14)	1.506(6)
C(23)-C(24)	1.501(6)		

Table 12. Bond Angles (°) for $[Co^{III}(6\text{-}\{NH_3^+,C(O)NH\}\text{-}13\text{-}\{NH_3^+,CH_2NH_2\}\text{-cyclam})]Cl_4.2.75H_2O$.

Atom	Angle (°)	Atom	Angle(°)
N(12)-Co-N(15)	87.0(1)	N(12)-Co-N(22)	91.0(1)
N(12)-Co-N(25)	94.0(1)	N(12)-Co-N(32)	87.9(1)
N(12)-Co-N(35)	173.6(1)	N(15)-Co-N(22)	176.7(1)
N(15)-Co-N(25)	91.9(1)	N(15)-Co-N(32)	92.0(1)
N(15)-Co-N(35)	88.2(2)	N(22)-Co-N(25)	85.7(1)
N(22)-Co-N(32)	90.6(1)	N(22)-Co-N(35)	94.0(1)
N(25)-Co-N(32)	175.9(2)	N(25)-Co-N(35)	90.4(2)
N(32)-Co-N(35)	88.0(2)	Co-N(12)-C(11)	116.5(3)
Co-N(12)-C(13)	106.6(3)	C(11)-N(12)-C(13)	111.8(3)
Co-N(15)-C(14)	106.8(3)	Co-N(15)-C(16)	117.5(3)
C(14)-N(15)-C(16)	112.8(3)	Co-N(22)-C(21)	118.0(2)
Co-N(22)-C(23)	108.4(3)	C(21)-N(22)-C(23)	112.7(3)
Co-N(25)-C(24)	108.0(3)	Co-N(25)-C(26)	118.1(3)
C(24)-N(25)-C(26)	112.7(3)	Co-N(32)-C(31)	125.0(3)
Co-N(35)-C(36)	120.0(3)	N(1)-C(2)-C(11)	107.3(3)
N(1)-C(2)-C(21)	106.9(3)	N(1)-C(2)-C(31)	107.7(3)
C(11)-C(2)-C(21)	112.3(3)	C(11)-C(2)-C(31)	111.2(3)
C(21)-C(2)-C(31)	111.2(3)	N(4)-C(3)-C(16)	107.2(3)
N(4)-C(3)-C(26)	105.7(3)	N(4)-C(3)-C(36)	107.1(3)
C(16)-C(3)-C(26)	112.5(4)	C(16)-C(3)-C(36)	111.7(3)
C(26)-C(3)-C(36)	112.2(4)	N(12)-C(11)-C(2)	112.9(3)
N(12)-C(13)-C(14)	107.7(3)	N(15)-C(14)-C(13)	106.3(4)
N(15)-C(16)-C(3)	112.6(3)	N(22)-C(21)-C(2)	112.3(3)
N(22)-C(23)-C(24)	106.7(3)	N(25)-C(24)-C(23)	106.4(4)
N(25)-C(26)-C(3)	111.8(3)	O(31)-C(31)-N(32)	127.3(4)
O(31)-C(31)-C(2)	119.6(4)	N(32)-C(31)-C(2)	113.1(4)
N(35)-C(36)-C(3)	109.7(3)		

The bond angles within the complex indicate that the ligand possesses no substantial strain; all N-Co-N angles are within ~1° to 7° of the ideal octahedral value while the saturated carbon tetrahedral angles are close to 109.5°. In addition, the two remaining five membered chelate rings have *lel* torsion angles of 55.7(4)° for N(12)-C(13)-C(14)-N(15) and 54.2(4)° for N(22)-C(23)-C(24)-N(25) respectively.

4.3.6 Electrochemistry

Co(III), Cr(III) and Ni(II) Monoamido Complexes

The redox waves recorded at 20 mVs^{-1} of the Co(III) and Ni(II) monoamido complexes appear in Figure 25 and the CV's show that these systems are essentially reversible. The electrochemical data obtained for the Co(III), Cr(III) and Ni(II) monoamido complexes in aqueous solutions are displayed in Table 13.

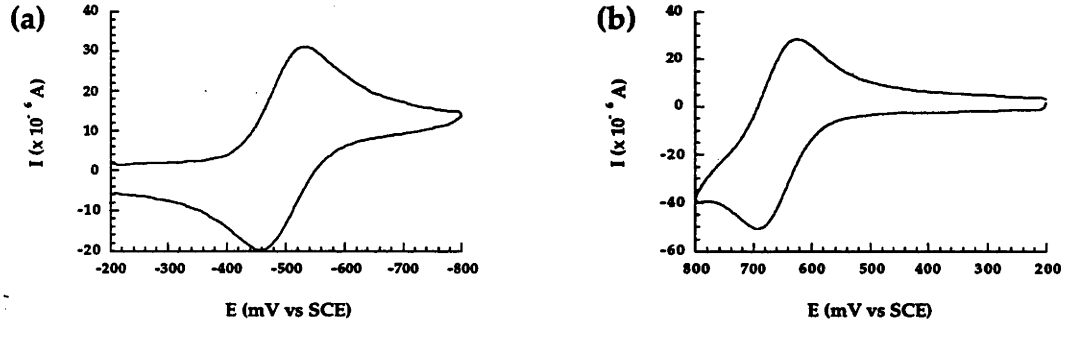

Figure 25. Cyclic voltammetry for (a) $[Co^{III}(\{NH_3^+\}_2\text{-2-oxosar-H})]^{4+}$ and (b) $[Ni^{II}(\{NH_3^+\}_2\text{-2-oxosar-H})]^{3+}$ recorded in 0.1 M $NaClO_4$ at 20° C with an EPG electrode at a scan rate of 20 mV s^{-1}.

Table 13. Electrochemical data for Co(III)/(II), Cr(III)/(II) and Ni(II)/(III) couples of monoamido and saturated cage complexes with diammonio and diamino apical substituents (vs SCE). (EPG electrode or HMDE; 1 mM solutions of complex in 0.05 M $KH_3(C_2O_4)_2.2H_2O$, 0.1 M $NaClO_4$ and 0.05 M Na_3PO_4 at 20° C with a scan rate of 20 mVs^{-1}.)

Complex	pH	$E_{1/2}$ vs SCE (V)	E_{pc} vs SCE (mV)	E_{pa} vs SCE (mV)	i_{pc}/i_{pa}	ΔE_p
$[Co^{III}(\{NH_3^+\}_2\text{-2-oxosar-H})]^{4+}$	1.68 [a]	-0.52	-540	-463	0.86	77
$[Co^{III}(\{NH_3^+\}_2\text{-2-oxosar-H})]^{4+}$	~5 [b]	-0.50	-532	-458	0.91	74
$[Co^{III}(\{NH_2\}_2\text{-2-oxosar-H})]^{2+}$	7 [c]	-0.79	-823	-758	0.97	65
$[Co^{III}(\{NH_2\}_2\text{-2-oxosar-H})]^{2+}$	8 [d]	-0.79	-823	-757	0.94	66
$[Co^{III}(\{NH_2\}_2\text{-2-oxosar-H})]^{2+}$	12.04 [e]	-0.82	-855	-789	1.01	66
$[Co^{III}(\{NH_3^+\}_2\text{-sar})]^{5+}$	-	-0.18[33]	-	-	-	-
$[Co^{III}(\{NH_2\}_2\text{-sar})]^{3+}$	-	-0.54[33]	-	-	-	-
$[Cr^{III}(\{NH_3^+\}_2\text{-2-oxosar-H})]^{4+}$	-	- [f]	-	-	-	-
$[Cr^{III}(\{NH_3^+\}_2\text{-sar})]^{5+}$	-	-1.04[34]	-	-	-	-
$[Cr^{III}(\{NH_2\}_2\text{-sar})]^{3+}$	-	-1.35[34]	-	-	1	-70
$[Ni^{II}(\{NH_3^+\}_2\text{-2-oxosar-H})]^{3+}$	1.68 [a]	0.64	608	670	1.01	62
$[Ni^{II}(\{NH_3^+\}_2\text{-2-oxosar-H})]^{3+}$	~5 [b]	0.66	624	692	1.00	68
$[Ni^{II}(\{NH_3^+\}_2\text{-2-oxosar-H})]^{3+}$	12.04 [e]	- [g]	-	-	-	-
$[Ni^{II}(\{NH_3^+\}_2\text{sar})]^{4+}$	-	~1.3[35]	-	-	-	-

[a] 0.05 M $KH_3(C_2O_4)_2.2H_2O$, [b] 0.1 M $NaClO_4$, [c] pH adjusted to 7 after dissolution of complex in 0.1 M $NaClO_4$, [d] pH adjusted to 8 after dissolution of complex in 0.1 M $NaClO_4$, [e] 0.05 M Na_3PO_4, [f] Not observable even by HMDE, [g] Ni(II)/(III) oxidation wave not observed.

For the Co(III) complex, the CV is quasireversible under the conditions employed and an $E_{1/2}$ value of -0.79 V (vs SCE) is obtained in essentially neutral conditions. An $E_{1/2}$ value could not be obtained for the Cr(III) monoamide complex, even with use of a hanging mercury drop electrode (HMDE), because the Cr(III)/(II) couple had moved out of the range of the HMDE. In both cases, higher oxidation states were not observed. In addition, the Ni(II)/(III) potential is readily accessible in water and is reversible. It has an $E_{1/2}$ value of 0.66 V (vs SCE) (Table 13) in 0.1 M $NaClO_4$. When moving to basic media however, a Ni(II)/(III) wave was not observed or recorded but in acidic solution the potential occurs at $E_{1/2}$ = 0.64 V (vs SCE) almost the same as the neutral pH value.

The fact that the Ni(II)/(III) potential of the $[Ni^{II}(\{NH_3^+\}_2$-2-oxosar-H)$]^{3+}$ ion is significantly less positive than that of the $[Ni^{II}(\{NH_3^+\}_2$-sar$)]^{4+}$ ion (~1.3 V vs SCE) in acid conditions implies that the Ni(II) ion is bound to an amide nitrogen anion. This type of shift would not be expected if the proton was attached to the amide nitrogen while bonded to the Ni(II) because the neutral amide group is expected to be a weaker ligand than its deprotonated counterpart[27,36] and the positive charge on the complex ion would be greater.

Co(III) and Ni(II) Diamido and Co(III) Monoamido Macrocyclic Complexes

The cyclic voltammograms, at a scan rate of 20 mVs^{-1}, of the diamido cage and monoamido macrocyclic complexes are displayed in Figure 26. Observation of the CV's revealed that the $[Co^{III}(\{NH_3^+\}_2$-2,7-dioxosar-2H)$]^{3+}$ and $[Co^{III}$(6-$\{NH_3^+$,C(O)NH$\}$-13-$\{NH_3^+$,$CH_2NH_2\}$-cyclam)$]^{4+}$ ions display essentially reversible behaviour while the reduction of $[Co^{III}(\{NH_3^+\}_2$-2,9-dioxosar-2H)$]^{3+}$ complex was found to be less reversible than that of the first isomer. In acidic conditions the Ni(II) CV (Figure 26d) shows basically quasireversible behaviour. The electrochemical data for these complexes appears in Table 14.

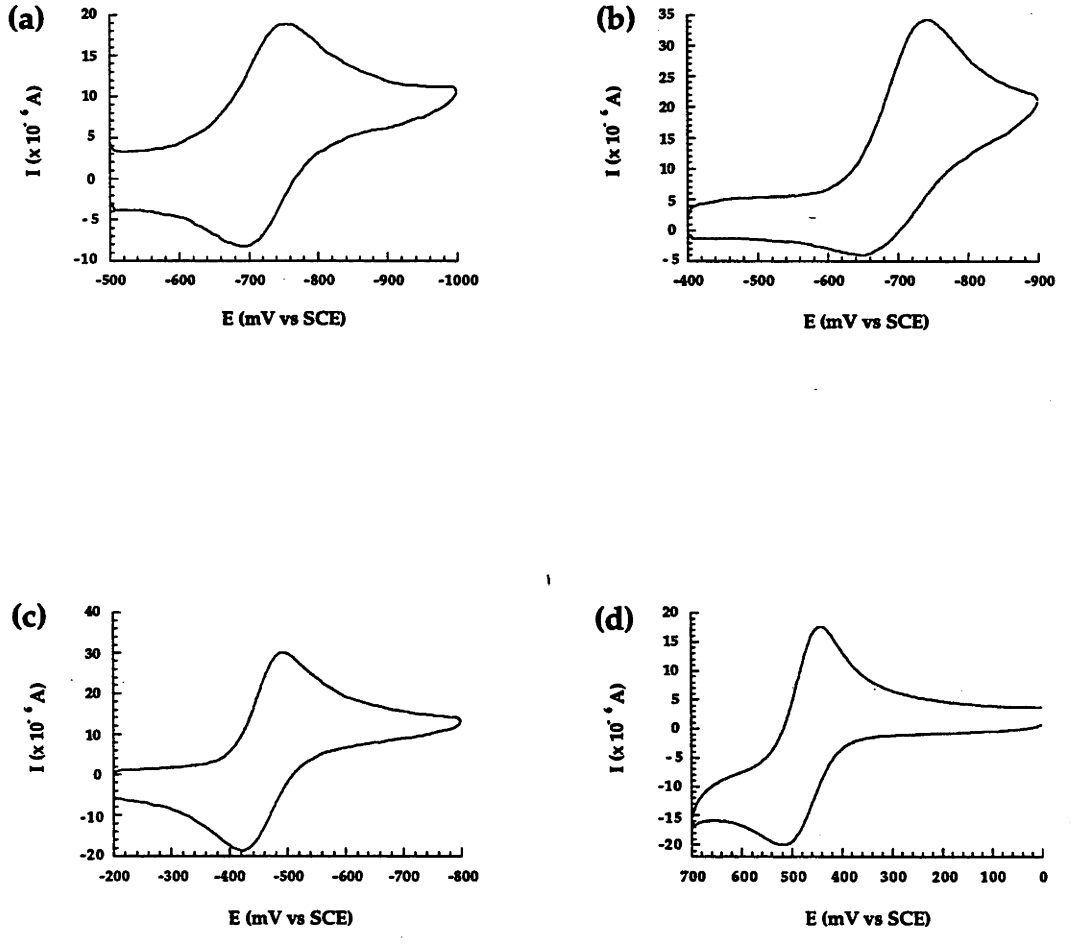

Figure 26. Cyclic voltammograms for (a) $[Co^{III}(\{NH_3^+\}_2\text{-}2,7\text{-dioxosar-}2H)]^{3+}$, (b) $[Co^{III}(\{NH_3^+\}_2\text{-}2,9\text{-dioxosar-}2H)]^{3+}$, (c) $[Co^{III}(6\text{-}\{NH_3^+,C(O)NH\}\text{-}13\text{-}\{NH_3^+,CH_2NH_2\}\text{-cyclam})]^{4+}$ recorded in 0.1 M $NaClO_4$ and (d) $[Ni^{II}(\{NH_3^+\}_2\text{-}2,7\text{-dioxosar-}2H)]^{2+}$ recorded in 0.05 M $KH_3(C_2O_4)_2.2H_2O$. All measurements were performed at 20° C with an EPG electrode and a scan rate of 20 mVs^{-1}.

Table 14. Electrochemical data for Co(III)/(II) and Ni(II)/(III) couples of diamido, monoamido and saturated cage complexes with diammonio and diamino apical substituents (vs SCE). (EPG electrode; 1 mM solutions of complex in 0.05 M $KH_3(C_2O_4)_2.2H_2O$, 0.1 M $NaClO_4$ and 0.05 M Na_3PO_4 at 20° C with a scan rate of 20 mVs^{-1}).

Complex	pH	$E_{1/2}$ vs SCE (V)	E_{pc} vs SCE (mV)	E_{pa} vs SCE (mV)	i_{pc}/i_{pa}	ΔE_p
$[Co^{III}(\{NH_3^+\}_2$-2,7-dioxosar-2H)$]^{3+}$	1.68 [a]	-0.64	-704	-566	0.70	138
$[Co^{III}(\{NH_3^+\}_2$-2,7-dioxosar-2H)$]^{3+}$	~5 [b]	-0.73	-756	-696	0.79	60
$[Co^{III}(\{NH_2\}_2$-2,7-dioxosar-2H)$]^{+}$	7 [c]	-1.02	-1053	-987	0.95	66
$[Co^{III}(\{NH_2\}_2$-2,7-dioxosar-2H)$]^{+}$	8 [d]	-1.02	-1054	-987	0.88	67
$[Co^{III}(\{NH^+\}_2$-2,7-dioxosar-2H)$]^{+}$	12.04 [e]	-1.04	-1072	-1007	0.94	65
$[Co^{III}(\{NH_3^+\}_2$-2,9-dioxosar-2H)$]^{3+}$	1.68 [a]	-0.70	-739	-656	0.54	83
$[Co^{III}(\{NH_3^+\}_2$-2,9-dioxosar-2H)$]^{3+}$	~5 [b]	-0.70	-743	-652	0.87	91
$[Co^{III}(\{NH_2\}_2$-2,9-dioxosar-2H)$]^{+}$	7 [c]	-1.00	-1029	-961	0.87	68
$[Co^{III}(\{NH_2\}_2$-2,9-dioxosar-2H)$]^{+}$	8 [d]	-0.99	-1030	-958	0.88	72
$[Co^{III}(\{NH_2\}_2$-2,9-dioxosar-2H)$]^{+}$	12.04 [e]	-1.01	-1040	-974	0.84	66
$[Co^{III}(\{NH_3^+\}_2$-2-oxosar-H)$]^{4+}$	1.68 [a]	-0.52	-540	-463	0.86	77
$[Co^{III}(\{NH_3^+\}_2$-2-oxosar-H)$]^{4+}$	~5 [b]	-0.50	-532	-458	0.91	74
$[Co^{III}(\{NH_2\}_2$-2-oxosar-H)$]^{2+}$	7 [c]	-0.79	-823	-758	0.97	65
$[Co^{III}(\{NH_2\}_2$-2-oxosar-H)$]^{2+}$	8 [d]	-0.79	-823	-757	0.94	66
$[Co^{III}(\{NH_2\}_2$-2-oxosar-H)$]^{2+}$	12.04 [e]	-0.82	-855	-789	1.01	66
$[Co^{III}(\{NH_3^+\}_2$-sar)$]^{5+}$ [f]	-	0.18[33]	-	-	-	-
$[Co^{III}(\{NH_2\}_2$-sar)$]^{3+}$	-	-0.54[33]	-	-	-	-
$[Co^{III}$(6-$\{NH_3^+$,C(O)NH}-13-$\{NH_3^+$,$CH_2NH_2\}$-cyclam)$]^{4+}$	1.68 [a]	-	-520	-	-	-

Table 14 cont. Electrochemical data for Co(III)/(II) and Ni(II)/(III) couples of diamido, monoamido and saturated cage complexes with diammonio and diamino apical substituents (vs SCE). (EPG electrode; 1 mM solutions of complex in 0.05 M $KH_3(C_2O_4)_2.2H_2O$, 0.1 M $NaClO_4$ and 0.05 M Na_3PO_4 at 20° C with a scan rate of 20 mVs^{-1}).

Complex	pH	$E_{1/2}$ vs SCE (V)	E_{pc} vs SCE (mV)	E_{pa} vs SCE (mV)	i_{pc}/i_{pa}	ΔE_p
$[Co^{III}$(6-{NH_3^+,C(O)NH}-13-{NH_3^+,CH_2NH_2}-cyclam)$]^{4+}$	~5 [b]	-0.46	-495	-424	0.90	71
$[Co^{III}$(6-{NH_2,C(O)NH}-13-{NH_2,CH_2NH_2}-cyclam)$]^{2+}$	7 [c]	-	-822	-	-	-
		-	-	-529 [g]	-	-
$[Co^{III}$(6-{NH_2,C(O)NH}-13-{NH_2,CH_2NH_2}-cyclam)$]^{2+}$	8 [d]	-	-824	-	-	-
		-	-	-535 [g]	-	-
$[Co^{III}$(6-{NH_2,C(O)NH}-13-{NH_2,CH_2NH_2}-cyclam)$]^{2+}$	12.04 [e]	-	-813	-	-	-
		-	-	-621 [g]	-	-
$[Ni^{II}$({NH_3^+}$_2$-2,7-dioxosar-2H)$]^{2+}$	1.68 [a]	0.48	517	442	1.34	75
$[Ni^{II}$({NH_3^+}$_2$-2,7-dioxosar-2H)$]^{2+}$	~5 [b]	0.26	346	220	0.90	126
$[Ni^{II}$({NH_2}$_2$-2,7-dioxosar-2H)$]^{0}$	12.04 [e]	0.19	264	116	1.12	148
$[Ni^{II}$({NH_3^+}$_2$-2-oxosar-H)$]^{3+}$	1.68 [a]	0.64	608	670	1.01	62
$[Ni^{II}$({NH_3^+}$_2$-2-oxosar-H)$]^{3+}$	~5 [b]	0.66	624	692	1.00	68
$[Ni^{II}$({NH_2}$_2$-2-oxosar-H)$]^{+}$	12.04 [e]	- [h]				
$[Ni^{II}$({NH_3^+}$_2$sar)$]^{4+}$	-	~1.3[35]	-	-	-	-
$[Ni^{II}$(sar)$]^{2+}$	- [i]	0.65[37]	-	-	1.1	61

[a] 0.05 M $KH_3(C_2O_4)_2.2H_2O$, [b] 0.1 M $NaClO_4$, [c] pH adjusted to 7 after dissolution of complex in 0.1 M $NaClO_4$, [d] pH adjusted to 8 after dissolution of complex in 0.1 M $NaClO_4$, [e] 0.05 M Na_3PO_4, , [f] 0.05 M $HClO_4$/0.5M $NaClO_4$, [g] Co(II)/Co(III) oxidation wave belonging to a second species generated from the reduction of the parent compound, [h] Ni(II)/(III) oxidation wave not observed, [i] 0.1 M CF_3SO_3H/0.1 M CF_3SO_3Na.

For the two diamido complexes Co(III)/Co(II) waves occur about $E_{1/2}$ = -0.73 V for $[Co^{III}(\{NH_3^+\}_2\text{-}2,7\text{-dioxosar-2H})]^{3+}$ and $E_{1/2}$ = -0.70 V for $[Co^{III}(\{NH_3^+\}_2\text{-}2,9\text{-dioxosar-2H})]^{3+}$ respectively in near neutral conditions. However these values varied under the different pH conditions employed. In acidic solution, the $E_{1/2}$ values shifted to less negative potentials and a greater movement occurred for $[Co^{III}(\{NH_3^+\}_2\text{-}2,7\text{-dioxosar-2H})]^{3+}$. The first isomer became less reversible as the scan rate increased while for $[Co^{III}(\{NH_3^+\}_2\text{-}2,9\text{-dioxosar-2H})]^{3+}$ the CV remained essentially quasireversible. In low pH conditions, the $[Co^{III}(\{NH_3^+\}_2\text{-}2,7\text{-dioxosar-2H})]^{3+}$ ion possesses a ΔE_p value of 138 mV indicating that the system is not reversible. This results from H^+ coupling, i.e., the Co^{II}-N bonds rupture allowing protonation to occur at the amine leading to a less reversible system. Simply increasing the pH of both diamide complexes makes each system more reversible (Table 14) by preventing this process. Therefore, the Co(III) and Co(II) compounds both remain intact during the electrochemical experiment. In addition, changing the pH from five to seven for the diamide complexes also resulted in a shift of the reduction potentials of approximately -0.3 V (Table 14). A similar type shift has also been observed for the $[Co^{III}(\{NH_3^+\}_2\text{-}2\text{-oxosar-H})]^{4+}$ ion (Tables 13 and 14). Obviously, the protonation/deprotonation of the apical amines of these systems is influencing the redox potentials somewhat. Also, it appears that the apical amines are not protonated above pH 6. In basic media, the potentials occur at approximately $E_{1/2}$ = -1 V. It is therefore harder to stabilise the Co(II) ion in each instance. Despite the negative shift in potential in all cases higher oxidation states of cobalt, such as Co(IV), appear to be inaccessible in water with these diamido ligand systems.

The cyclic voltammetry of the monoamido macrocyclic complex displayed a quasireversible Co(III)/Co(II) wave at $E_{1/2}$ = -0.46 V in 0.1 M $NaClO_4$ while in acidic and basic solution an irreversible wave appears at E_{pc} = -0.52 V and -0.81 V respectively. At pH 7 and above the $[Co^{III}(6\text{-}\{NH_3^+,C(O)NH\}\text{-}13\text{-}\{NH_3^+,CH_2NH_2\}\text{-cyclam})]^{4+}$ ions displays a Co(II)/(III) oxidation wave of a new species generated from the reduction of the parent macrocyclic amide. Clearly this species is not as robust as the cage systems. Continuous cycling of the macrocyclic amide in both neutral and basic conditions revealed that after initial reduction two different species existed in solution. The original macrocyclic complex possesses an irreversible wave around -0.82 V while the new species displays a Co(III)/(II) $E_{1/2}$ couple at -0.66 V with a ΔE_p = 79 mV.

Turning to the Ni(II) diamido complex (Figure 26d) a quasireversible Ni(III)/Ni(II) redox couple is present at $E_{1/2}$ = 0.26 V in 0.1 M $NaClO_4$ (Table 14). In both acidic and basic media, Ni(II)/Ni(III) redox waves occurred and the values appear in Table 14. Again it can be observed that different potentials arise in the three different media with the potential becoming less positive when moving from acid to basic conditions. Like the Co(III) systems earlier, the protonated/deprotonated apical amines have some influence on the observed potential. The observed waves of the Ni(II) diamide also become less reversible when moving away from acidic media as evidenced by the ΔE_P values (Table 14). However, this system seems more robust electrochemically than that of the $[Ni^{II}(\{NH_3^+\}_2\text{-2-oxosar-H})]^{3+}$ ion. For the latter complex when in basic media the compound completely breaks down and an oxidation wave is not observed. The $[Ni^{II}(\{NH_3^+\}_2\text{-2,7-dioxosar-2H})]^{2+}$ ion on the other hand displays an oxidation wave in the same basic conditions albeit not very reversibly. However, this implies that the Ni(II) diamide to some extent resists the same type of breakdown process observed earlier for the $[Ni^{II}(\{NH_3^+\}_2\text{-2-oxosar-H})]^{3+}$ ion.

The oxidation potential of the Ni(II) diamide is also the least positive displayed by a Ni(II) sar-type cage. This is again further evidence that Ni(II) is bonded to both deprotonated amido nitrogen atoms of the diamide ligand even in acidic conditions. As the Ni(II)/(III) potential of the diamide is even less positive, in acid conditions, than that of the $[Ni^{II}(\{NH_3^+\}_2\text{-2-oxosar-H})]^{3+}$ ion the Ni(II) must be bonded to two deprotonated amido nitrogens to effect this shift. Also, as outlined earlier, if the amide nitrogen atoms and the apical substituents were protonated a shift of this nature is not expected.

General Properties

Generally, the redox potentials were dependant on the pH of the solutions and, as expected, the monoamido and diamido cage complexes have significantly more negative redox potentials than their saturated counterparts. The position of the redox potential depends largely on whether the apical amine groups are protonated or not. If they are both protonated some charge is removed from the metal and the potential moves to more positive values. Under conditions where they are deprotonated extra charge flows to the metal which results in a more negative value. In the situation where one apical amine is protonated and the other not, the potential should be intermediate between the two extremes. The complexes also displayed quasireversible waves, as indicated

by the cyclic voltammetry, where the separations of the anodic and cathodic peak potentials increased with increasing scan rates while repeated cycling of each complex at 100 mV/s did not produce any change in the observed waves.

4.3.7 Electronic Absorption Spectroscopy

Co(III), Cr(III) and Ni(II) Monoamido Cage Systems

The electronic spectra for this series of monoamido cage systems appear in Figure 27 and their absorption data are tabulated in Table 15.

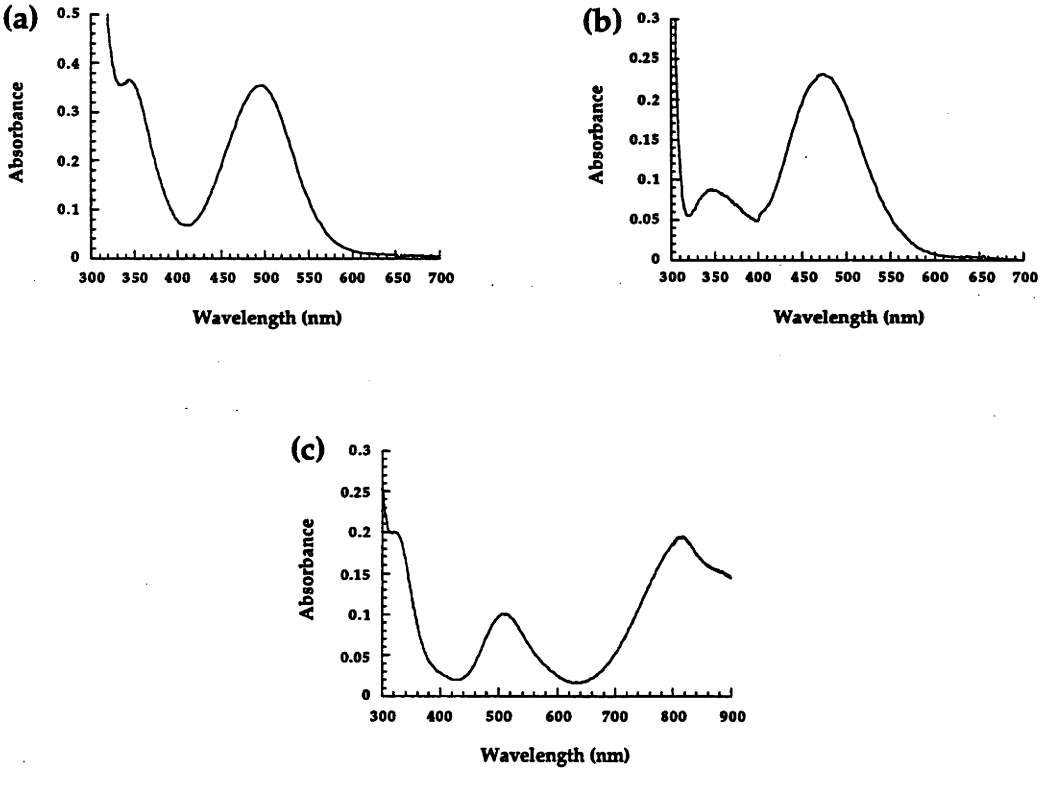

Figure 27. Electronic spectrum of (a) $[Co^{III}(\{NH_3^+\}_2\text{-2-oxosar-H})]^{4+}$, (b) $[Cr^{III}(\{NH_3^+\}_2\text{-2-oxosar-H})]^{4+}$ and (c) $[Ni^{II}(\{NH_3^+\}_2\text{-2-oxosar-H})]^{3+}$ in water at 20° C.

Table 15. Electronic absorption data on some Co(III), Cr(III) and Ni(II) monoamido and saturated cage complexes. (1mM solutions of complex in water at 20° C unless otherwise stated).

Complex	Transition	λ_{max} nm (ε_{max} $M^{-1}cm^{-1}$)
$[Co^{III}(\{NH_3^+\}_2\text{-2-oxosar-H})]^{4+}$	$^1T_{2g} \leftarrow {}^1A_{1g}$	344 (372)
	$^1T_{1g} \leftarrow {}^1A_{1g}$	496 (361)
$[Co^{III}(\{NH_3^+\}_2\text{-sar})]^{5+}$ [7]	$^1T_{2g} \leftarrow {}^1A_{1g}$	344.5 (150)
	$^1T_{1g} \leftarrow {}^1A_{1g}$	475 (150)
$[Co^{III}(\{NH_2\}_2\text{-sar})]^{3+}$ [22]	$^1T_{2g} \leftarrow {}^1A_{1g}$	343 (130)
	$^1T_{1g} \leftarrow {}^1A_{1g}$	475 (150)
$[Cr^{III}(\{NH_3^+\}_2\text{-2-oxosar-H})]^{4+}$	$^4T_{1g} \leftarrow {}^4A_{2g}$	348 (58)
	$^4T_{2g} \leftarrow {}^4A_{2g}$	476 (153)
$[Cr^{III}(\{NH_3^+\}_2\text{-sar})]^{5+}$ [34]	$^4T_{1g} \leftarrow {}^4A_{2g}$	345 (109)
	$^4T_{2g} \leftarrow {}^4A_{2g}$	447 (208)
$[Ni^{II}(\{NH_3^+\}_2\text{-2-oxosar-H})]^{3+}$ [a]	$^3T_{1g} \leftarrow {}^3A_{2g}$ (P)	Not observed [c]
	$^3T_{1g} \leftarrow {}^3A_{2g}$ (F)	508 (10)
	$^3T_{2g} \leftarrow {}^3A_{2g}$	811 (19)
$[Ni^{II}(\{NH_3^+\}_2\text{-2-oxosar-H})]^{3+}$	$^3T_{1g} \leftarrow {}^3A_{2g}$ (P)	322 (20)
	$^3T_{1g} \leftarrow {}^3A_{2g}$ (F)	508 (10)
	$^3T_{2g} \leftarrow {}^3A_{2g}$	817 (20)
$[Ni^{II}(\{NH_3^+\}_2\text{-2-oxosar-H})]^{3+}$ [b]	$^3T_{1g} \leftarrow {}^3A_{2g}$ (P)	319 (16)
	$^3T_{1g} \leftarrow {}^3A_{2g}$ (F)	511 (10)
	$^3T_{2g} \leftarrow {}^3A_{2g}$	813 (20)
$[Ni^{II}(\{NH_3^+\}_2\text{-sar})]^{4+}$ [37]	$^3T_{1g} \leftarrow {}^3A_{2g}$ (P)	328 (13)
	$^3T_{1g} \leftarrow {}^3A_{2g}$ (F)	504 (10)
	$^3T_{2g} \leftarrow {}^3A_{2g}$	805 (15)
$[Ni^{II}(sar)]^{2+}$ [37]	$^3T_{1g} \leftarrow {}^3A_{2g}$ (P)	329 (9)
	$^3T_{1g} \leftarrow {}^3A_{2g}$ (F)	506 (8)
	$^3T_{2g} \leftarrow {}^3A_{2g}$	805 (15)

[a] 0.1 M HCl, [b] 0.05 M Na_3PO_4, [c] $^3T_{1g} \leftarrow {}^3A_{2g}$ (P) transition obscured by charge transfer band.

The introduction of a bonded amido functional group into $[Co^{III}(\{NH_3^+\}_2\text{-sar})]^{5+}$ brings about a change in the solution electonic spectrum. A red or bathochromic shift is observed in the lower energy d-d band of $[Co^{III}(\{NH_3^+\}_2\text{-2-oxosar-H})]^{4+}$ (Figure 27a, Table 15). In fact the change is large enough so that the monoamido complex is now red in colour compared to the parent yellow-orange. In addition, it was found that the two d-d absorption bands, arising from the $^1T_{1g} \leftarrow {}^1A_{1g}$ and $^1T_{2g} \leftarrow {}^1A_{1g}$ (O_h) parent transitions for low spin Co(III), were significantly more intense than the corresponding transitions of the saturated hexamine (Table 15). When cobalt(III) was replaced by chromium(III) a similar trend was observed on going from the saturated hexamine to the monoamido complex (Figure 27b, Table 15). The monoamide is orange in colour instead of yellow. In this instance, the absorption bands arise from the $^4T_{2g} \leftarrow {}^4A_{2g}$ and $^4T_{1g} \leftarrow {}^4A_{2g}$ (O_h) parent transitions for high spin chromium(III). When Ni(II) is placed in the monoamide cage ligand (Figure 27c, Table 15) the effects are not as significant as those observed for the Co(III) and Cr(III) systems. The absorption maxima for this complex in water, at 322 (20) ($^3T_{1g} \leftarrow {}^3A_{2g}$ (P)), 508 (10) ($^3T_{1g} \leftarrow {}^3A_{2g}$ (F)) and 817 nm (20) ($^3T_{2g} \leftarrow {}^3A_{2g}$), again are slightly different to those of other Ni(II) hexamine cage complexes (Table 15) and at longer wavelengths for the ligand field bands.[37] In addition, compared to the Co(III) system the Ni(II) monoamido complex displays transitions that are weaker than that of Co(III).

The olive green Ni(III) species, $[Ni^{III}(\{NH_3^+\}_2\text{-2-oxosar-H})]^{4+}$, has also been produced electrochemically and the result of which appears in Appendix Figure 4.1.9. From this preliminary investigation it has been shown that over time in acidic aqueous media above 500 nm two d-d absorption bands arise at 625 nm and 1454 nm for the Ni(III) ion. Below 500 nm two shoulders appear at ~400 nm and ~300 nm but these are less well defined than the long wavelength bands. The higher energy transition (625 nm) is also red shifted when compared to the corresponding maximum of $[Ni^{III}(sar)]^{3+}$ ((570 nm) as expected (Chapter 3).

Co(III) and Ni(II) Diamido Cage and Co(III) Monoamido Macrocyclic Complexes

The electronic spectra for the diamido cage and monoamido macrocyclic complexes appear in Figure 28 and the absorption data for the complexes is displayed in Table 16.

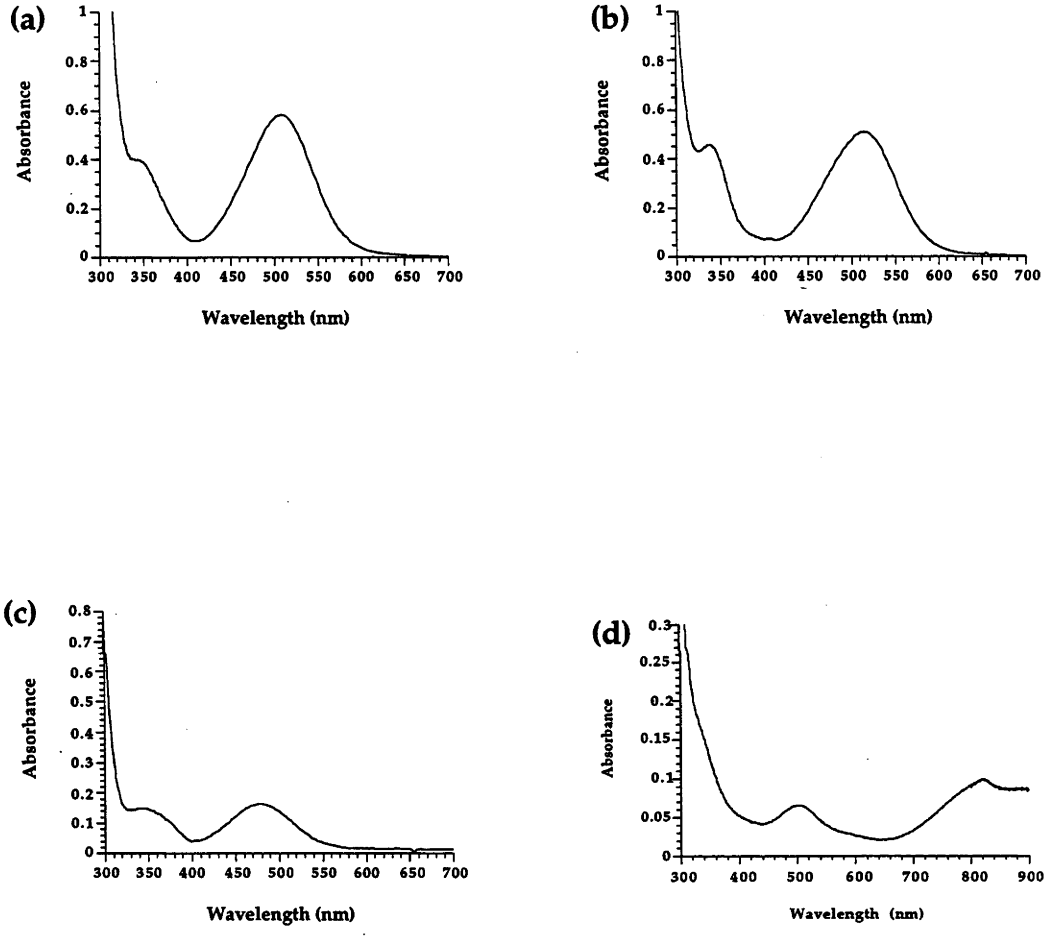

Figure 28. Electronic spectrum of (a) $[Co^{III}(\{NH_3^+\}_2\text{-}2,7\text{-dioxosar-}2H)]^{3+}$, (b) $[Co^{III}(\{NH_3^+\}_2\text{-}2,9\text{-dioxosar-}2H)]^{3+}$, (c) $[Co^{III}(6\text{-}\{NH_3^+,C(O)NH\}\text{-}13\text{-}\{NH_3^+,CH_2NH_2\}\text{-cyclam})]^{4+}$ and (d) $[Ni^{II}(\{NH_3^+\}_2\text{-}2,7\text{-dioxosar-}2H)]^{2+}$ in water at 20° C.

Table 16. Electronic absorption data on some Co(III) and Ni(II) diamido, monoamido and saturated cage and macrocyclic amido complexes. (1mM solutions of complex in water at 20° C unless otherwise stated).

Complex	Band Origin Transition	λ_{max} nm (ε_{max} $M^{-1}cm^{-1}$)
$[Co^{III}(\{NH_3^+\}_2\text{-}2,7\text{-dioxosar-2H})]^{3+}$	$^1T_{2g}\leftarrow{}^1A_{1g}$	342 (329)
	$^1T_{1g}\leftarrow{}^1A_{1g}$	510 (482)
$[Co^{III}(\{NH_3^+\}_2\text{-}2,9\text{-dioxosar-2H})]^{3+}$	$^1T_{2g}\leftarrow{}^1A_{1g}$	339 (440)
	$^1T_{1g}\leftarrow{}^1A_{1g}$	514 (491)
$[Co^{III}(6\text{-}\{NH_3^+,C(O)NH\}\text{-}13\text{-}$	$^1T_{2g}\leftarrow{}^1A_{1g}$	343 (120)
$\{NH_3^+,CH_2NH_2\}\text{-cyclam})]^{4+}$	$^1T_{1g}\leftarrow{}^1A_{1g}$	476 (128)
cis-$[Co^{III}cyclam(OH_2)_2]^{3+}$ [38]	$^1T_{2g}\leftarrow{}^1A_{1g}$	367 (99)
	$^1T_{1g}\leftarrow{}^1A_{1g}$	506 (110)
$[Co^{III}(\{NH_3^+\}_2\text{-sar})]^{5+}$ [7 a]	$^1T_{2g}\leftarrow{}^1A_{1g}$	344.5 (130)
	$^1T_{1g}\leftarrow{}^1A_{1g}$	475 (149)
$[Co^{III}(\{NH_2\}_2\text{-sar})]^{3+}$ [22]	$^1T_{2g}\leftarrow{}^1A_{1g}$	343 (130)
	$^1T_{1g}\leftarrow{}^1A_{1g}$	475 (150)
$[Ni^{II}(\{NH_3^+\}_2\text{-}2,7\text{-dioxosar-2H})]^{2+}$ [a]		442 (34)
$[Ni^{II}(\{NH_3^+\}_2\text{-}2,7\text{-dioxosar-2H})]^{2+}$	$^3T_{1g}\leftarrow{}^3A_{2g}$ (P)	330 sh (37)
	$^3T_{1g}\leftarrow{}^3A_{2g}$ (F)	507 (17)
	$^3T_{2g}\leftarrow{}^3A_{2g}$	821 (23)
$[Ni^{II}(\{NH_2\}_2\text{-}2,7\text{-dioxosar-2H})]^{0}$ [b]	$^3T_{1g}\leftarrow{}^3A_{2g}$ (P)	330 sh (61)
	$^3T_{1g}\leftarrow{}^3A_{2g}$ (F)	512 (15)
	$^3T_{2g}\leftarrow{}^3A_{2g}$	821 (23)
$[Ni^{II}(\{NH_3^+\}_2\text{-}2\text{-oxosar-H})]^{3+}$	$^3T_{1g}\leftarrow{}^3A_{2g}$ (P)	322 (20)
	$^3T_{1g}\leftarrow{}^3A_{2g}$ (F)	508 (10)
	$^3T_{2g}\leftarrow{}^3A_{2g}$	817 (20)
$[Ni^{II}(\{NH_3^+\}_2\text{-sar})]^{4+}$ [37]	$^3T_{1g}\leftarrow{}^3A_{2g}$ (P)	328 (13)
	$^3T_{1g}\leftarrow{}^3A_{2g}$ (F)	504 (10)
	$^3T_{2g}\leftarrow{}^3A_{2g}$	805 (15)

[a] 0.1 M HCl, [b] 0.05 M Na_3PO_4

The UV/Visible spectra of the Co(III) diamido complexes (Figures 28a and b) are slightly different to those of the $[Co^{III}(\{NH_3^+\}_2\text{-2-oxosar-H})]^{4+}$ and $[Co^{III}(\{NH_3^+\}_2\text{-sar})]^{5+}$. The d-d transitions are further red shifted to ca. 340 nm and 512 nm and each pseudo-octahedral ion displays the two expected absorption envelopes derived from the $^1T_{1g}\leftarrow{}^1A_{1g}$ and $^1T_{2g}\leftarrow{}^1A_{1g}$ (O_h) parent transitions for low spin Co(III)-N_6. The absorptions are also more intense than the usual Co-N_6^{3+} and Co-$N_5N_{(amido)}^{2+}$ d-d transitions.

The absorption spectrum (Figure 28c) of the Co(III) monoamido macrocyclic compound is different and the complex is orange rather than the characteristic red colour associated with other Co^{III}-$N_5N_{(amide)}^{2+}$ species. In this instance, as shown in Figure 28c and Table 16, the transitions appear at 343 nm and 476 nm. These d-d bands occur at higher energy when the macrocyclic complex is compared with <u>*cis*</u>-$[Co^{III}cyclam(OH_2)_2]^{3+}$ (367 (99) and 506 (110))[38] for example. Comparison with cage systems is not so valid.

In the electronic spectrum of $[Ni^{II}(\{NH_3^+\}_2\text{-2,7-dioxosar-2H})]^{2+}$ in water (Figure 28d) the d-d absorption maxima occur at 821 nm, 507 nm and as a shoulder at 330 nm. They correspond to the three expected transitions of ($^3T_{2g}\leftarrow{}^3A_{2g}$), ($^3T_{1g}\leftarrow{}^3A_{2g}$ (F)) and ($^3T_{1g}\leftarrow{}^3A_{2g}$ (P)) (O_h) parentage for high spin d^8 Ni(II). In base, the Ni(II) diamido ion becomes a nonelectrolyte and the three transitions barely alter (821 nm, 512 nm and as the shoulder at 330 nm Table (16)). The d-d bands of $[Ni^{II}(\{NH_3^+\}_2\text{-2,7-dioxosar-2H})]^{2+}$ and $[Ni^{II}(\{NH_2\}_2\text{-2,7-dioxosar-2H})]^0$ show a slight shift to lower energy compared to $[Ni^{II}(\{NH_3^+\}_2\text{-sar})]^{4+}$, and the magnitude of the shift is practically identical to that observed for the $[Ni^{II}(\{NH_3^+\}_2\text{-2-oxosar-H})]^{3+}$ ion.

The molar absorption coefficients of $[Ni^{II}(\{NH_3^+\}_2\text{-2,7-dioxosar-2H})]^{2+}$ and $[Ni^{II}(\{NH_2\}_2\text{-2,7-dioxosar-2H})]^0$ are also slightly greater than that of the parent hexamine, $[Ni^{II}(\{NH_3^+\}_2\text{-sar})]^{4+}$, as well as that displayed for the $[Ni^{II}(\{NH_3^+\}_2\text{-2-oxosar-H})]^{3+}$ ion. The increase in intensity is not as great for this amide series as that observed for the analogous Co(III) amide cage complexes. This is to be expected since, in relative terms, Ni(II) should be less intense than Co(III). There is approximately a four fold difference between the intensities of the $[Co^{III}(NH_3)_6]^{3+}$ and $[Ni^{II}(NH_3)_6]^{2+}$ ions. When these metal ions are placed respectively into the same cage type ligand the intensity difference increases.

However, in strong acid the $[Ni^{II}(\{NH_3^+\}_2\text{-}2,7\text{-dioxosar-2H})]^{2+}$ ion becomes yellow in colour and a single transition at 442 nm appears in the spectrum. It is likely that rupture of two bonds occurs, probably the two Ni-$N_{(amido)}$ bonds, and the Ni(II) diamide becomes a diamagnetic square planar complex with a protonated uncoordinated ligand diamide strand. This molecule was not isolated but $[Cu^{II}(sar)]^{2+}$ shows a similar process when it is placed in strong acid.[39] The addition of base to the yellow acidified Ni(II) diamide square planar complex restored the pale pink colour expected for hexadentate Ni(II) diamido complex. In neutral and basic media the electronic spectra indicate that the Ni(II) ion is six-coordinate in these conditions. Like the $[Ni^{II}(\{NH_3^+\}_2\text{-}2\text{-oxosar-H})]^{3+}$ ion described earlier, the other physical data on the Ni(II) diamido complex imply the Ni(II) ion is bound to both amido nitrogen atoms under these conditions.

Generation of the olive green Ni(III) species of $[Ni^{III}(\{NH_3^+\}_2\text{-}2,7\text{-dioxosar-2H})]^{3+}$ resulted in a somewhat different spectrum (Appendix Figure 4.1.10) to that observed for $[Ni^{III}(\{NH_3^+\}_2\text{-}2\text{-oxosar-H})]^{4+}$ (Appendix Figure 4.1.9). In this instance, over time, three well defined absorption peaks occur above 500 nm (532 nm, 633 nm and 1261 nm) instead of the two peaks which were observed for the other two Ni(III) cage ions, $[Ni^{III}(\{NH_3^+\}_2\text{-}2\text{-oxosar-H})]^{4+}$ (~ 300 nm, ~400 nm, 625 nm and 1454 nm) and $[Ni^{III}(sar)]^{3+}$ (~400 nm, 570 nm and 1734 nm), in the same region. An ill defined shoulder also exists at ~300 nm for the $[Ni^{III}(\{NH_3^+\}_2\text{-}2,7\text{-dioxosar-2H})]^{3+}$ ion.

4.4 Discussion

4.4.1 Syntheses

Co(III) Monoamido and Diamido Cage Systems

Generally, in the oxidation of organic amines with $Hg^{II}(OAc)_2$, an imine results. However even though macrocyclic amine complexes readily undergo oxidation to produce macrocyclic imines, $Hg^{II}(OAc)_2$ has not been widely used, if at all, in these cases. Even though imine bonds are the expected result from a $Hg^{II}(OAc)_2$ oxidation, this is not the case for the Co(III) cage complexes where the oxidation carries through to the amide. In addition, compared to the reaction between $[Co^{III}(sen)]^{3+}$, CH_2O and diethylmalonate, the oxidation of $[Co^{III}(\{NH_3^+\}_2\text{-sar})]^{5+}$ with $Hg^{II}(OAc)_2$ is about as efficient a way to introduce a bound amido group but the condensation of course does not produce the diamine derivative. So both methods are valuable for different functionalities

On the basis of literature about $Hg^{II}(OAc)_2$ oxidations[40] a possible mechanism for the formation of the amide bond in the $[Co^{III}(\{NH_3^+\}_2\text{-2-oxosar-H})]^{4+}$ ion is given below (Scheme 1). The initial step requires loss of a proton from a coordinated amine followed by attack of the oxidant. An hydroxide ion or water molecule may then convert the resultant imine into a carbinolamine which reacts further with the oxidant to produce the amide complex. In this case, the oxidant attacks the cap carbon preferentially rather than the ethylenediamine ring as observed in the oxidation of $[Co^{III}(\{NH_3^+\}_2\text{-sar})]^{5+}$ with charcoal and O_2 under basic conditions. So far it is one of the few ways the cage carbon skeleton can be manipulated once it is formed.

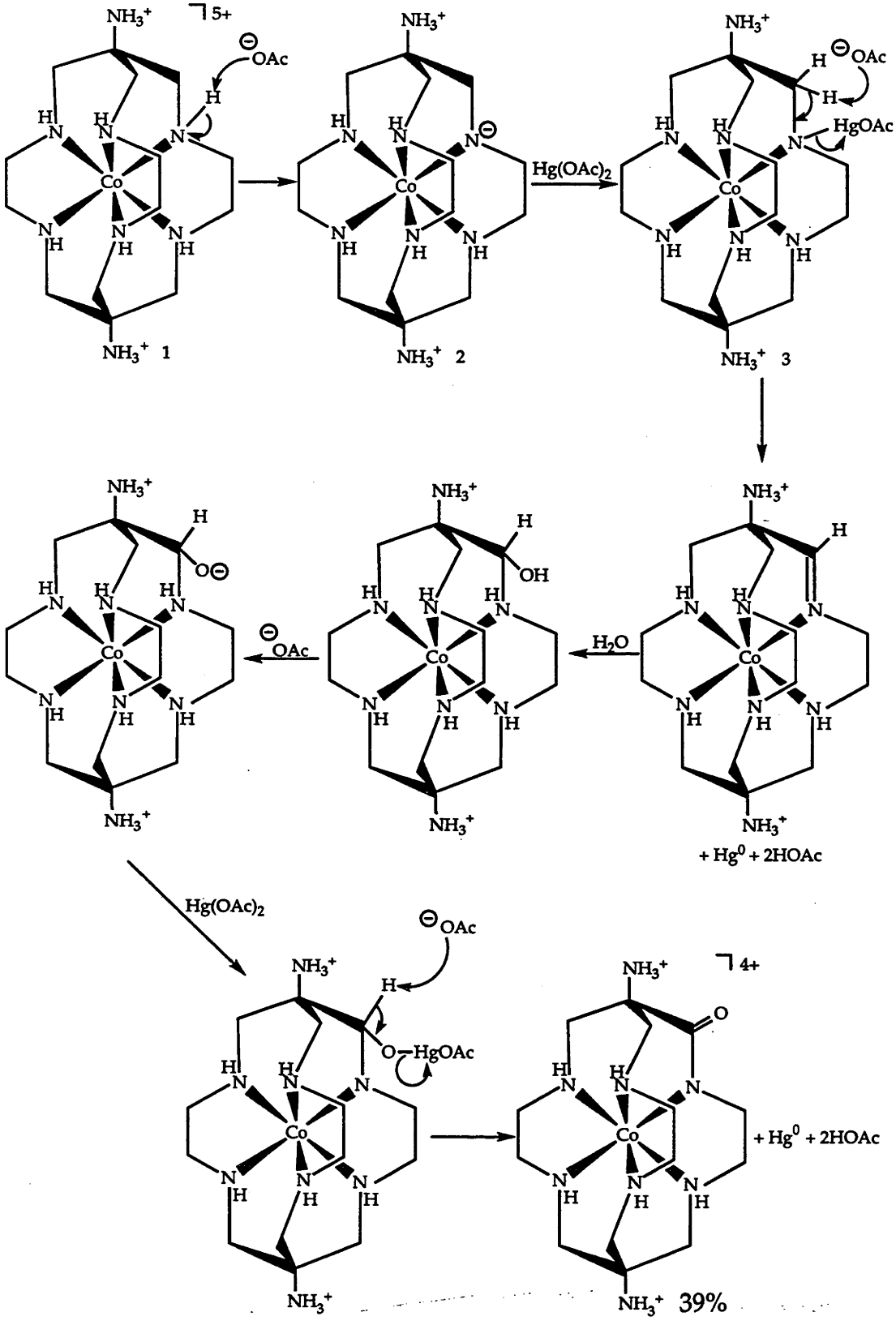

Scheme 1. Proposed mechanism for the formation of $[Co^{III}(\{NH_3^+\}_2\text{-}2\text{-oxosar-H})]^{4+}$ from the oxidation of $[Co^{III}(\{NH_3^+\}_2\text{-sar})]^{5+}$ by $Hg^{II}(OAc)_2$ in 5% acetic acid.

The oxidation of $[Co^{III}(\{NH_3^+)_2\text{-sar})]^{5+}$ with excess $Hg^{II}(OAc)_2$ in aqueous acetic acid for forty-eight hours, at reflux temperatures, resulted in a different set of products from those arising under the conditions described earlier. Besides the $[Co^{III}(\{NH_3^+)_2\text{-2-oxosar-H})]^{4+}$ ion two isomeric diamido complexes as well as a monoamido macrocyclic compound emerged as major products from the reaction (Figure 5). Although only two diamide isomers (Figure 29) were significant products from this particular reaction many more were possible. Either the others are not formed during the oxidation of $[Co^{III}(\{NH_3^+)_2\text{-sar})]^{5+}$ with $Hg^{II}(OAc)_2$ or have formed in such small quantities that they were not identified.

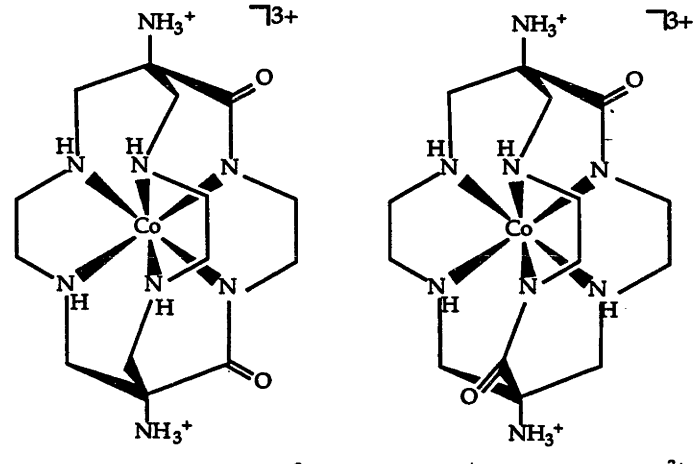

$[Co(\{NH_3^+\}_2\text{-2,7-dioxosar-2H})]^{3+}$ 6%

$[Co(\{NH_3^+\}_2\text{-2,9-dioxosar-2H})]^{3+}$ 0.5%

Figure 29

Presumably the same type of mechanism occurs here as for the synthesis of the $[Co^{III}(\{NH_3^+)_2\text{-2-oxosar-H})]^{4+}$ ion except that oxidation occurs not only on one strand but also on two strands of the cage and in both caps. Once the first amide is established the oxidant can then attack at one of five cap sites however it seems to place amides preferentially in two different sites on the opposite cap resulting in the formation of the two isomeric complexes. Not surprisingly the diamides form late in the reaction and only small amounts of each arise over shorter reaction times. The formation of the first amide probably increases the pK_a of the nitrogen centres all over the molecule because of the lower overall charge. It then becomes more difficult to deprotonate these secondary nitrogen centres, which is presumably the initial step in the overall oxidation reaction (Scheme 1). Moreover, the initial amido cap is likely to be more basic than its partner and it may be for this reason that the diamides are formed in the two caps rather than one.

In addition, the formation of the monoamido macrocyclic complex needs to be accounted for and it is very likely that this derives from the first apical oxosar product, $[Co^{III}(\{NH_3^+)_2$-2-oxosar-H)$]^{4+}$. Since, this is the highest yielding product in the milder conditions. Afterwards the reaction then probably continues down two paths resulting in the isomeric diamides (Figure 29) on one hand and the macrocyclic complex on the other. For the formation of the monoamido macrocyclic complex, the loss of the ethylene fragment is most likely to occur as shown in Scheme 2. In addition to the formation of the amide in the cap, the ethylenediamine chelate ring, of the same strap, probably undergoes oxidation leading to a further two amide groups being placed in the strand by the paths described in Scheme 2. Afterwards hydrolysis of the oxidised ring ensues to give the monoamido macrocyclic amido amine hexadentate complex and oxalic acid. The formation of this macrocyclic compound is strong evidence for a triamido intermediate and that the proposed mechanism is correct. It also implies that the adjacent amides assisted in further oxidation to a substantial degree in the same strand since the macrocyclic complex is the most abundant product (~14%) recovered from the reaction.

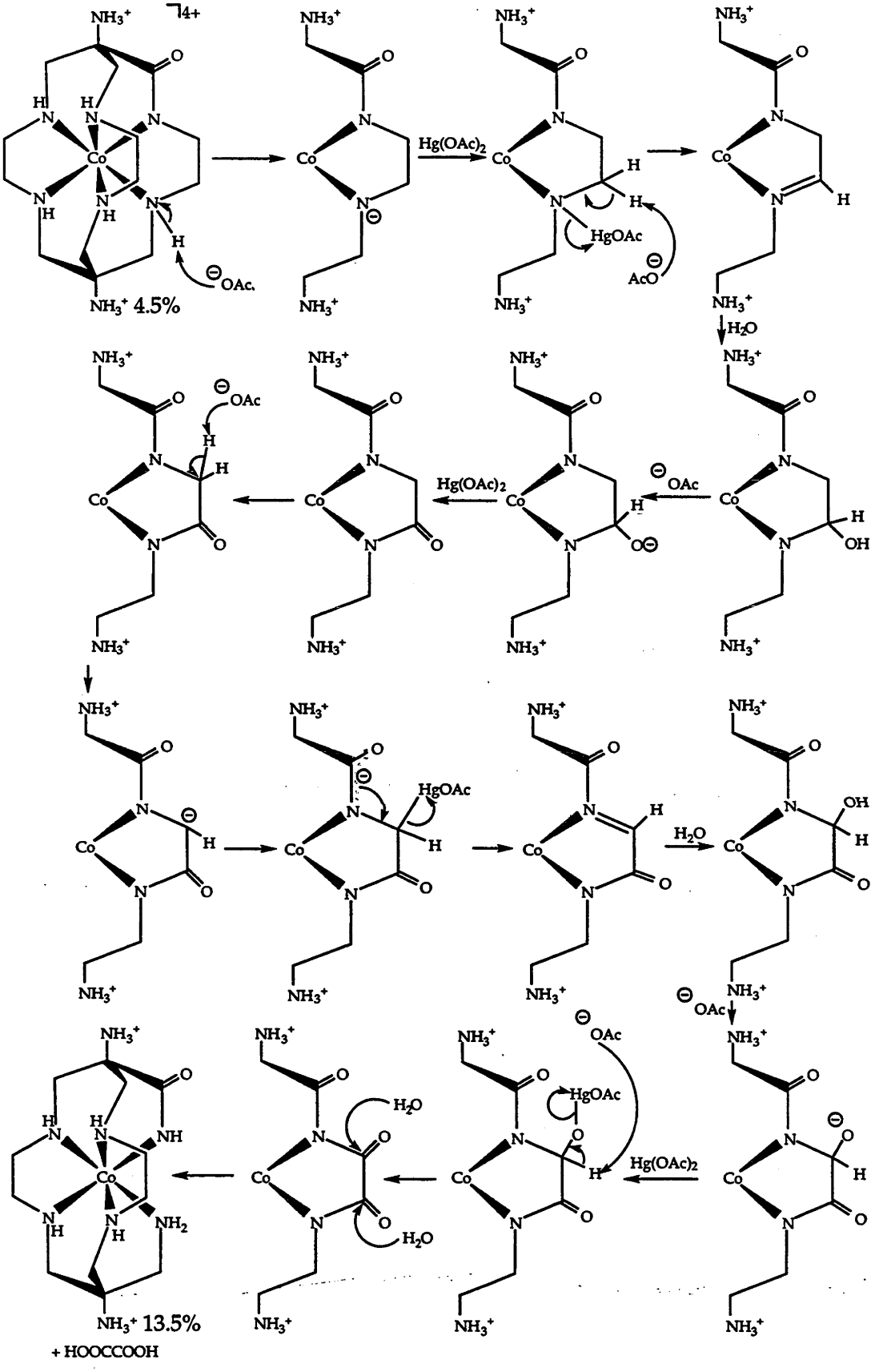

Scheme 2. Proposed mechanism for the formation of $[Co^{III}(6\text{-}\{NH_3^+,C(O)NH\}\text{-}13\text{-}\{NH_3^+,CH_2NH_2\}\text{-cyclam})]^{4+}$ from the oxidation of $[Co^{III}(\{NH_3^+\}_2\text{-sar})]^{5+}$ by $Hg^{II}(OAc)_2$ in 5% acetic acid over 48 hours.

An important aspect of the formation of this monoamido macrocyclic compound is that it implies that the Co(III) oxidation state is retained during its formation. Evidence for this assertion comes in two forms. Firstly, a less stable cyclam conformation is produced and retained. Also, the two pendant arms are still *cis* to each other. If the oxidation state of the cobalt had changed from Co(III) to Co(II) even transiently during the macrocycle's formation then it would have been provided with the opportunity to attain a more stable ligand configuration. Since this has obviously not occurred, it is very likely the cobalt has remained in the 3+ state throughout the reaction.

From the products obtained it appears that oxidation in the same strap is heavily favoured over oxidation in different strands overall. The reason for this specificity is unknown. Perhaps after formation of the initial amido fragment the remaining part of this strand is then placed in an orientation that predisposes it to further oxidation. Whatever the cause the oxidation reaction produces the monoamido ion in abundance which then undergoes further oxidation. This leads to the 2,7- diamido and the 2,4,5- derivatives preferentially. Clearly the 2,7 and 2,9 isomers do not lead to macrocycles in any abundance. So it seems the 2-oxosar ion assists oxidation first at the 5-position and then probably at the 4-position. At which point the oxamido derivative hydrolyses more readily than further oxidation occurs.

It also seems that in the $Hg^{II}(OAc)_2$ oxidation of $[Co^{III}(\{NH_3^+\}_2$-sar$)]^{5+}$ oxidation preferentially occurs in the cap rather than in the en fragment. This may arise from the stereochemistry of the methylene fragment in intermediate 3 Scheme 1. If one proton is orientated largely vertical to the chelate pseudo plane then it should be removed preferentially by a base such as acetate ion as shown. Once the imine is formed, the amide should follow at the same site. For the diamide complexes the same process is repeated in the oxidation of the other cap. For the ethanediamine fragment once the $[Co^{III}(\{NH_3^+\}_2$-2-oxosar-H$)]^{4+}$ ion is produced, the *ob* conformer of the ethanediamine fragment may be more suitably orientated for oxidation and the 5-position could be oxidised followed by the 4-position.

Co(III) Monoamido and Diamido Cage Demetallation and Complexation Reactions

The reaction of the $[Co^{III}(\{NH_3^+\}_2\text{-2-oxosar-H})]^{4+}$ ion with $Co^{II}Cl_2$ and excess CN^- extruded the Co(III) from the complex to yield the free ligand. In the extraction of the cobalt, the $[Co^{II}(CN)_5]^{3-}$ ion initially reduces the Co(III) to Co(II) which is more labile. The superior ligand, cyanide ion, is finally able to bind to the Co(II) ion and progressively assist in unravelling the cage from the Co(II) ion. Finally, the Co is extruded from the cage as $[Co^{II}(CN)_6]^{4-}$, oxidised by O_2 and trapped as $[Co^{III}(CN)_6]^{3-}$. The formation of this very stable low spin hexacyano Co(III) complex then prevents the cobalt being recomplexed by the cage ligand. This is a complicated process and the details are not yet fully dissected. Although this synthetic route involves the use of cyanide ion it is still the method of choice here because acidic processes lead to more ready hydrolysis of the amide bond. Isolation of the free ligand thus allowed the direct synthesis of Ni(II) and Cr(III) monoamide cage complexes.

The free ligand of the first diamide isomer, $[Co^{III}(\{NH_3^+\}_2\text{-2,7-dioxosar-2H})]^{4+}$, arose from the complex's reaction with $Co^{II}Cl_2$, Zn and excess CN^-. Again the same process occurs here as it did for the $[Co^{III}(\{NH_3^+\}_2\text{-2-oxosar-H})]^{4+}$ ion however as the $[Co^{II}(CN)_5]^{3-}$ ion was not a strong enough reductant to reduce the Co(III) to Co(II) in the diamido case, Zn was added to effect the reduction. The complexation of this ligand to Ni(II) then followed to produce a Ni(II) diamido complex with the two amide groups located on the same strap.

Both $[Ni^{II}(\{NH_3^+\}_2\text{-2-oxosar-H})]^{3+}$ and $[Ni^{II}(\{NH_3^+\}_2\text{-2,7-dioxosar-2H})]^{2+}$ were isolated and although crystal structures were not obtained, the physical data provides evidence that both complexes display bonding to the deprotonated amido nitrogen atoms in each case. Firstly, the microanalytical data acquired on the two Ni(II) amido cages support the constitution and charge assignment for each complex. Furthermore, the electrochemical data shows that the Ni(II)/(III) potential becomes less positive upon going from the saturated amine to monoamido and diamido forms of the diamsar ligand. This shift also occurs in acidic conditions. Under these circumstances, if the amide fragments were in the protonated form (-CONH-) while bound to the Ni(II) the amide would be expected to become a weaker donor than its deprotonated counterpart. Therefore, the observed shift in the electrochemical potentials for the two complexes would not be anticipated. In fact, the inverse shift should occur since in

acidic media the apical amines of both complexes would be protonated and the charge more positive. As mentioned previously this has the effect of withdrawing charge from the metal and making the potential more positive. Then it should be more difficult to attain Ni(III).

4.4.2 Infra-red Spectroscopy

As outlined previously, when a metal ion is coordinated to an amido nitrogen atom the amide carbonyl stretching frequency should fall below that of an unbound amide group. This was found to be consistent with the amido compounds produced in the previous chapter. The same would be expected to occur for the amide complexes in this chapter when the metal is bound to the amido nitrogen atom. A comparison is now made between the amide complexes described in this chapter with the monoamide compounds of Chapter 3 to establish if this correlation holds for all the amide cage complexes. The amide carbonyl stretching frequencies of the monoamide compounds of Chapter 3 and an average amide stretching vibration for each of the amide complexes in this chapter are collected in Tables 17 and 18 respectively.

Table 17. Functional Group IR Absorption Frequencies of the Monoamido and Monoamide Cage Systems of Chapter 3.

	$C{=}O_{(amide)}$	COOH	COO^-	COOH	COO^-
$[Co^{III}(Me,CO_2H\text{-}2\text{-}oxosar\text{-}H)]^{2+}$	1599	1727	-	1272	-
$[Fe^{III}(Me,CO_2H\text{-}2\text{-}oxosar\text{-}H)]^{2+}$	1557	1743	-	1213	-
$[Ni^{II}(Me,CO_2^-\text{-}2\text{-}oxosar)]^{+}$	1709, 1691	-	1602	-	1354
$[Cu^{II}(Me\text{-}2\text{-}oxosar)]^{2+}$	1656	-	-	-	-
$[Mn^{III}(Me,CO_2^-\text{-}2\text{-}oxosar\text{-}H)]^{+}$	1595	-	1610	-	1310
$[Cr^{III}(Me,CO_2H\text{-}2\text{-}oxosar\text{-}H)]^{2+}$	1597	1725	-	1250	-
$Me,CO_2K\text{-}2\text{-}oxosar$	1630	-	1591	-	1349
$[Co^{III}(Me,CN\text{-}2\text{-}oxosar\text{-}H)]^{2+}$	1621, 1605	-	-	-	-

Table 18. Functional Group IR Absorption Frequencies of the Monoamido and Diamido Cage Systems in this Chapter (Average values derived from the protonated and deuterated complex see pgs 161 - 169).

	$C{=}O_{(amide)}$
$[Co^{III}(\{NH_3^+\}_2\text{-2-oxosar-H})]^{4+}$	1625
$[Ni^{II}(\{NH_3^+\}_2\text{-2-oxosar-H})]^{3+}$ [a]	1596
$[Ni^{II}(\{NH_3^+\}_2\text{-2-oxosar-H})]^{3+}$ [b]	1612
$[Cr^{III}(\{NH_3^+\}_2\text{-2-oxosar-H})]^{4+}$	1619
$[Co^{III}(\{NH_3^+\}_2\text{-2,7-dioxosar-2H})]^{3+}$	1618
$[Co^{III}(\{NH_3^+\}_2\text{-2,9-dioxosar-2H})]^{3+}$	1623
$[Ni^{II}(\{NH_3^+\}_2\text{-2,7-dioxosar-2H})]^{2+}$	1598
$(NH_2)_2$-2,7-dioxosar	1629

[a] Perchlorate salt, [b] Chloride salt.

The results show that the amide carbonyl stretching vibrations of the amido complexes in Table 18 occur at slightly higher but similar frequencies to those observed in the previous chapter. However, they all fall below the free diamide ligand, $(NH_2)_2$-2,7-dioxosar, value of 1629 cm^{-1} and the range expected for an unbound secondary amide (1680 cm^{-1} - 1630 cm^{-1}).[41] Based on these IR results and the theoretical rationale on the effect of a metal ion and a proton on the IR stretching frequency, all of the complexes of Table 18 should display metal coordination to the respective amido nitrogen atoms. For the Co(III) complexes at least this was confirmed crystallographically. Consequently, from the findings in this work and the previous chapter, it appears that IR spectroscopy can be used to predict the type of amide bonding present within the possible coordination modes. Therefore, for the Ni(II) and Cr(III) of Table 18, for which structures were not obtained, the respective carbonyl stretching frequencies indicate that these systems possess the same type of bonding as that observed for the Co(III) amido cage compounds. If the Ni(II) and Cr(III) complexes had a similar bonding mode to that of $[Ni^{II}(Me,CO_2^-\text{-2-oxosar})]^+$, where the metal is bound to the protonated amide nitrogen atom, then a value of ~1700 cm^{-1} would have been expected. In addition, if both metals remained unbound to the amide nitrogen atoms then a value between 1680 cm^{-1} and 1630 cm^{-1} would have been anticipated because the previously crystallographically characterised unbound Cu(II) monoamide, $[Cu^{II}(Me\text{-2-oxosar})]^{2+}$, displays an amide carbonyl stretching frequency at 1656 cm^{-1}.

A complication associated with these particular amido complexes is that the apical NH_3^+ bending modes (near 1600 cm^{-1} and 1500cm^{-1})[41] may overlap with the amido carbonyl stretching vibration. Therefore, it may then become more difficult to properly assign the amido absorption frequency. To alleviate this problem each complex was dissolved in D_2O to deuterate the apical amine atoms. This resulted in a shifting of the apical amine absorptions to lower frequencies thus exposing the amido carbonyl stretch. Examination of the deuterated complexes both in D_2O and in KBr disks revealed that the amido stretching frequencies occurred at similar values to those of the corresponding undeuterated complexes. In most of these spectra, secondary N-H stretching vibration frequencies are also evident indicating that complete exchange had not taken place. This was not totally unexpected since some of these complexes do not readily exchange these protons. Although the bending frequencies of these amines do appear in a similar region (1580 cm^{-1} - 1490 cm^{-1})[41] to that of the amido carbonyl stretching frequency, they are also weak and do not cause any problem with the assignment of the amide group absorption bands.

4.4.3 Electrochemistry

Co(III) and Cr(III) Monoamido and Co(III) Diamido Cage Complexes

The presence of the amido ion as one of the ligating groups within the diamsar ligand has shifted the redox potentials of the Co(III) and Cr(III) monoamido complexes, compared with the parent saturated Co(III) and Cr(III) complexes, to more negative values. The shift of the redox window for the two metals arises from the amido anion reducing the overall charge on each of the metals. It is then more difficult to reduce the complexes and the higher oxidation state becomes more stable. However, the higher oxidation states of Co(IV) and Cr(IV) were not evident in aqueous solution and are therefore still too positive to be accessed in water electrochemically. This is because both metals are extremely stable in the M(III) state (d^3 and low spin d^6) with these ligands and a single amide moiety does not surmount this stability. Clearly more than a single amido ion is required to attain the Co(IV) and Cr(IV) ions readily and this is one of the reasons the diamido chemistry was pursued.

The cyclic voltammetry of the two Co(III) diamido complexes shows that their reduction potentials are more negative than that of the $[Co^{III}(\{NH_3^+)_2$-2-oxosar-H$)]^{4+}$ ion in water as expected. This arises from the second amide anion fragment present within the ligand structure thereby

reducing the overall charge to 1+ and making the Co(III) ion even more difficult to reduce. However as for the earlier Co(III) monoamido case, the Co(IV) species with these diamido ligand systems in water is not observed electrochemically. Simply, two amido ions are not sufficient to lower the Co(IV)-Co(III) potential to the accessible region and it seems three amido groups or more will be required to access the Co(IV) ion readily.

Ni(II) Monoamido and Diamido Cage Complexes

For the nickel(II) monoamido complex, $[Ni^{II}(\{NH_3^+\}_2\text{-2-oxosar-H})]^{3+}$, the addition of one amide group to the diamsar ligand allows Ni(III) to become readily accessible in water (E 0.66 V vs SCE). This represents a significant stabilisation of Ni(III) since the Ni(III)/Ni(II) couple of the $[Ni^{II}(\{NH_3^+\}_2\text{-sar})]^{4+}$ ion is barely accessible in water (E ~1.3 V vs SCE) and was only isolated through oxidation of the Ni(II) complex with concentrated nitric acid. With the incorporation of the second amide fragment into the basic diamsar ligand ($[Ni^{II}(\{NH_3^+\}_2\text{-2,7-dioxosar-2H})]^{2+}$) Ni(III) is even easier to attain in water compared to $[Ni^{II}(\{NH_3^+\}_2\text{-2-oxosar-H})]^{3+}$ and $[Ni^{II}(\{NH_3^+\}_2\text{-sar})]^{4+}$. The potential for the $[Ni^{II}(\{NH_3^+\}_2\text{-2,7-dioxosar-2H})]^{2+}$ ion appears at 0.48 V vs SCE in water at acidic pH some 160 mV less positive than that observed for the $[Ni^{II}(\{NH_3^+\}_2\text{-2-oxosar-H})]^{3+}$ (0.64 V vs SCE) species. Again donation of charge onto the metal from the amide anion as well as the reduction of overall charge influences the observed shift and allows easier access to Ni(III).

The production of all the Ni(III) cage species with these amide ligands occurred best in acidic solution although redox waves were observed for both complexes in neutral conditions and only for the Ni(II) diamide in basic media. The lower pH appears to minimise the decomposition of the Ni(III) complex that commonly occurs with these types of compounds at higher pH values. Again the breakdown probably occurs via the loss of a proton from a coordinated secondary nitrogen centre at the higher pH[37] followed by disproportionation to Ni(II) and Ni(IV) and then intramolecular oxidation of the ligand by Ni(IV) to a Ni(II) imine complex (yet to be characterised). This type of pathway has been established for the ligand oxidation of analogous Fe(III) and Ru(III) amine complexes.

4.4.4 Electronic Spectroscopy

Monoamido, Diamido Cage and Macrocyclic Monoamido Complexes

All the monoamide complexes here show a red shift in their spectra, especially in the lower energy ligand field bands, compared to those of the respective parent saturated hexaamines (Table 15). The shift to lower energy indicates that a weaker ligand field exists in these complexes than that of the saturated parents. The electronic absorption band maxima of the two diamido complexes are red shifted compared to that of the $[Co^{III}(\{NH_3^+)_2$-2-oxosar-H$]^{4+}$ ion (Table 16). Here the shift to lower energy again indicates a weaker ligand field for the Co(III) diamides compared to that of the parent hexamine $[Co^{III}(\{NH_3^+\}_2$-sar$]^{5+}$. Also the two diamides are red and more intense in colour than the Co(III) monoamide ion, $[Co^{III}(\{NH_3^+)_2$-2-oxosar-H$]^{4+}$. Similarly, a red shift occurs for the $[Co^{III}(\{NO_2\}_2$-sar)$]^{3+}$ complex after loss of a proton from a coordinated nitrogen in strongly basic solution. In addition, the $[Ni^{II}(\{NH_3^+)_2$-2,7-dioxosar-2H$]^{2+}$ ion shows a much weaker red shift in its electronic spectrum compared to that of $[Ni^{II}(\{NH_3^+)_2$-sar$]^{4+}$. As mentioned previously the red shift in the ligand field for the octahedral amide complexes results from the deprotonated amide nitrogen possessing a lone pair of electrons which undergo a π interaction with the occupied metal based t_{2g} electrons.[42] Therefore, as a result the electronic spectra of these amido cage systems are affected in the same way as that outlined for the amido complexes in the preceding chapter. Obviously, the Δ value will decrease with multiple amido groups within the skeleton of the cage ligand even though the anion probably provides a higher bond strength.

For the monoamido macrocyclic complex the electronic maxima are blue shifted when compared to those of the *cis*-$[Co^{III}$cyclam$(OH_2)_2]^{3+}$ ion. The substitution of the two extra N donor atoms, which would be inherently stronger ligands than OH_2, is the cause of the observed shift. The blue shift is opposite to that observed in the amide cage systems. The exact reason of this is not entirely clear but it could be that the cage ligands influence the spectra more than the macrocyclic ligand. For example, when the spectra of the Co(III) cage complexes is compared to $[Co^{III}(NH_3)_6]^{3+}$ the cages display a weaker ligand field than the hexaammine. A similar type of situation is expected to exist between the amido cage and macrocyclic ligand here.

The electronic spectroscopy of the Ni(III) amido complexes, $[Ni^{III}(\{NH_3^+\}_2\text{-2-oxosar-H})]^{4+}$ and $[Ni^{III}(\{NH_3^+\}_2\text{-2,7-dioxosar-2H})]^{3+}$, display some interesting features. Firstly, both spectra are indicative of the spectroscopic properties expected for a Ni(III)-N_6 ion. For both complexes the near-infra-red band present at 1454 nm for $[Ni^{III}(\{NH_3^+\}_2\text{-2-oxosar-H})]^{4+}$ and 1261 nm for $[Ni^{III}(\{NH_3^+\}_2\text{-2,7-dioxosar-2H})]^{3+}$ is a low intensity band expected for Ni(III) and is attributed to a $^2B_{1g} \leftarrow {}^2A_{1g}$ symmetry transition arising from a strong Jahn-Teller splitting of the ^2E_g ground state. Until now this band has only been estimated to occur at approximately 1540 nm for $[Ni^{III}([9]aneN_3)_2]^{3+}$ [43] and has apparently never been observed spectroscopically for other Ni(III)-N_6 systems. Another unusual feature observed with the Ni(III) amido systems is that the $^2B_{1g} \leftarrow {}^2A_{1g}$ bands become increasingly blue shifted and more intense as more amido groups are incorporated into the sar cage ligand. The exact reason for this is unclear, however, perhaps this indicates a stronger Jahn-Teller interaction with the presence of more amido groups within the sar ligand.

In the spectrum of $[Ni^{III}(\{NH_3^+\}_2\text{-2-oxosar-H})]^{4+}$ the transitions appearing at 625 nm, ~400 nm and ~300 nm have been assigned to transitions from the $^2A_{1g}$ ground state to the split levels of the excited octahedral parent states $^2T_{1g(a)}$, $^2T_{2g}$ and $^2T_{1g(b)}$. These same transitions also occur for the $[Ni^{III}(\{NH_3^+\}_2\text{-2,7-dioxosar-2H})]^{3+}$ ion however they appear as two separate bands at 633 nm and 532 nm and a shoulder at ~300 nm respectively. Also, when compared to saturated Ni(III)-N_6 systems, such as $[Ni^{III}(sar)]^{3+}$ (~400 nm, 570 nm and 1734 nm) and $[Ni^{III}([9]aneN_3)_2]^{3+}$ (350 nm, 416 nm, 555 nm and 1540 nm (estimated)), the $^2A_{1g} \rightarrow {}^2T_{1g}$ and $^2A_{1g} \rightarrow {}^2T_{2g}$ transitions are red shifted for both the Ni(III) mono and diamido cage systems with the greatest movement occurring for the $[Ni^{III}(\{NH_3^+\}_2\text{-2,7-dioxosar-2H})]^{3+}$ ion. In fact, for this last complex the two transition now occur as distinct bands in the visible region. Presumably the same type of rationale for the shifts exists for these amido complexes as that described for the Co(III) amido compounds earlier.

Again, like the amide compounds in Chapter 3 all the amide complexes here display spectral intensities that are greater than those observed for the respective parent hexaamines of $[Co^{III}(\{NH_3^+)_2\text{-sar})]^{5+}$, $[Cr^{III}(\{NH_3^+)_2\text{-sar})]^{5+}$ and $[Ni^{II}(\{NH_3^+)_2\text{-sar})]^{4+}$. Therefore, the increase in intensity is ascribed to the same reasons as previously outlined. Recapitulating, if the complexes were strictly octahedral in character then the absorption bands would be rather weak like those of $[Co^{III}(NH_3)_6]^{3+}$ for

example. However in lower symmetry fields the transitions become more allowed because the selection rules become less rigid. There maybe some charge transfer component in the bands as well arising from the anionic ligands and their delocalised character. Also the amide fragment destroys the symmetry and distorts the complex from an octahedral environment more than the parent D_3 complex hence the intensities become greater than those of the parents.

4.4.5 Properties of the Amido Group within a Cage Ligand

Although amide cages can be viewed as hybrids of polyamine cages and oligopeptides they display properties which are not observed with either of the parent compounds. Therefore, it is of interest to review some of these properties of the amide cage complexes compared to those observed for the amine cage systems. Firstly, the synthesis of diamido cage complexes, from $[Co^{III}(\{NH_3^+\}_2\text{-sar})]^{5+}$, now allows an assessment of the effects of replacing not one but two amine groups of the diamsar cage ligand with deprotonated amido units. In addition it also highlights the progressive differences in properties when the amino, monoamido and diamido cages are compared across this common ligand series with the metal ions of Co(III) and Ni(II). Two of the more significant differences that arise, when going from amine to amide cage, occur in the electrochemical and electronic properties. Firstly, the electrochemistry shows that the electrochemical window is negatively shifted for the amide cages compared to that of the amine systems, and the effect becomes more pronounced with an increased number of amido groups within the cage. Therefore, these results show that replacement of an amine donor with an amido group aids in the stabilisation of the higher oxidation state. This was adequately demonstrated in the Ni(II) series while the same effect was also observed in the Co(III)/(II) reduction couples of the cobalt amido complexes. It is not a surprising result since, as previously stated, stabilisation of the higher valent metal ion results from the quenching of the higher positive charge of the metal due to the complexation of the (-) or the (2-) ligand.

Across both the Co(III) and Ni(II) series the lower d-d absorption bands are also affected, by being red shifted compared to those of the $[Co^{III}(\{NH_3^+\}_2\text{-sar})]^{5+}$ and $[Ni^{II}(\{NH_3^+\}_2\text{-sar})]^{4+}$ ions respectively, by the presence of the amido groups. Again, the effect becomes more pronounced with the more amide groups within the cage however successive replacement of the amine donors with amido groups does not additively

lower the d-d band transtions by a fixed amount when moving from polyamine to monoamido or from monoamido to diamido complexes. Also, upon changing the metal ion but keeping the ligand sequence the same it was found that the size of the red shift between the polyamine, monoamido and diamido complexes varied for different metal ions. This could arise simply from the fact that the cobalt ion carries a 3+ charge while the nickel ion is a 2+ species.

Some general structural properties also arise for the Co(III) amido and diamido cages. Regardless of whether one or two amido groups are present within the cage ligand Co(III) is found to always bind the amido nitrogen atom or atoms. To date no Co(III) amido cage complex has been structurally characterised where an amide nitrogen atom is both bound to the Co(III) and protonated. In addition, the amido cages distort the octahedral environment of the Co(III) ion. This gives rise to a small pseudo-trigonal twist angle of ~50° - 53° for both the monoamido and diamido complexes. These trigonal twist angles are slightly smaller than that observed for other $[Co^{III}(sar)]^{3+}$ type cages. As mentioned previously, the Co^{III}-$N_{(amido)}$ bond distance (~1.91 Å - 1.94 Å) is always shorter than that of a Co^{III}-$N_{(amine)}$ bond (~1.97 Å - 1.98 Å). Also, the trigonal C-N^- bond lengths for the monoamido and diamido Co(III) cages are the same or slightly larger than that expected for a coordinated peptide group for instance. However, they are shorter than the distance expected for a C-$N_{(amine)}$ group (~1.45 Å). Lastly, with an amido group present within the cap of the cage complex this usually results in an *ob* conformation for the NCH_2CH_2N fragment of that strand. Generally, the monoamido cage systems possess a *lel*$_2$*ob* conformation while the diamido complexes display an *ob*$_2$*lel* conformation. Also, on the assumption that the Ni(II) monoamido and diamido complexes contain coordinated amido nitrogens then it is expected that these systems would display structural behaviour similar to that of the Co(III) compounds.

The crystal data obtained for the Co(III) amide complexes, $[Co^{III}(\{NH_3^+)_2$-2-oxosar-H$]^{4+}$, $[Co^{III}(\{NH_3^+)_2$-2,7-dioxosar-2H$]^{3+}$ and $[Co^{III}(\{NH_3^+)_2$-2,9-dioxosar-2H$]^{3+}$, indicates that the cavity size of the amide cages become somewhat smaller as more amido groups are added to the cage ligand compared to that of the normal amine cage systems. Like that observed for the amido complexes within the previous chapter the trigonal C-N^- distances (~1.32 Å) are shorter than those of the tetrahedral C-N bond lengths (1.45 Å)[27]. This is a result of the delocalisation of negative charge

over the C, N and O atoms and to a degree with the metal ion. Therefore with the progressive reduction in the cavity size on going from saturated to monoamido to diamido complexes the cage ligand becomes more *ob* in nature as mentioned above. This process will also be assisted by incorporation of amido groups within the cage ligand. The more amido groups within the cage ligand the more *ob* in nature the cage ligand becomes. As formerly mentioned the cavity size of the amide cage is significant for a number of reasons. For instance, it has implications for the properties of the resultant complex including the stability of the complex, the rate of replacement of different metal ions, redox reaction rates, etc.

The Co(III), Cr(III) and Ni(II) monoamido and Co(III) diamido cage ligands of this series have also shown that they are able to resist attack of both acid and base at the amide group. This arises because the coordinated amides are protected by the metal ion from both acid and base hydrolysis hence the cage amides are resistant to ring opening.[20] On one hand, the metal is not as able as a proton to activate the amide to nucleophilic attack and therefore leads to a net stabilisation of the amido group. On the other hand, the negatively charged deprotonated amide resists attack of an electron rich reagent such as OH^-. The positively charged metal ion also inhibits addition of a proton at the oxygen and the kinetic inertness of the metal-$N_{(amido)}$ bonds along with the delocalisation in the amide group inhibits addition at the amido nitrogen atom. This was clearly demonstrated by the $[Ni(\{NH_3^+\}_2\text{-2-oxosar-H})]^{3+}$ ion with its ability to be precipitated from 6 M HCl without any sign of decomposition of the cage amide ligand.

The Ni(II) diamide complex shows somewhat different behaviour in acidic conditions. The Ni(II) ion becomes square planar, as indicated by a colour change from pink to yellow, as a result of the rupture of two Ni-N bonds. This observation may indicate that the Ni(II) diamide complex behaves more like a peptide complex in that acid attacks the coordinated amide bond leading to bond rupture.[36] This is contary to the behaviour observed for the other Ni(II), Co(III) and Cr(III) amido cage systems. Perhaps the reduction in cavity size, as a result of the presence of the two amido groups within the cage skeleton, destabilises the larger Ni(II) ion in the cavity and makes it more susceptible to amido-N-Ni bond rupture. Obviously, more work is needed to understand the differing properties between the Ni(II) monoamido and diamido complexes.

4.5 Conclusions and Future Directions

This chapter has shown firstly that the monoamide ligand, NH_2-2-oxosar, readily coordinates the metal ions of Ni(II) and Cr(III). The properties of the resultant complexes, as well as that of Co(III), were examined by a number of techniques including crystallography, IR spectroscopy and ESM spectrometry. All three monoamido compounds were found to be stable under a variety of different conditions which has been attributed to the fully encapsulating hexadentate amide ligand.

Secondly oxidation of $[Co^{III}(\{NH_3^+\}_2\text{-sar})]^{5+}$ with $Hg(OAc)_2$ in 5% acetic acid for forty-eight hours led to the production of two isomeric Co(III) diamido cage complexes as well as a Co(III) monoamido cage and a Co(III) macrocyclic monoamido compound. This approach appears to be an effective route to oxidise the metallated saturated cage. All of the major compounds obtained from this reaction were characterised by crystallography and it was shown that the Co(III) ion displays hexadentate coordination with each of the amide ligands. The complexes also show remarkable stability which augers well for them to be useful in other areas. For example, they may find use as low charged or nonelectrolyte imaging agents both in a NMR and radionuclide sense. These complexes are also capable of further derivatisation to build larger macromolecules. It would be of interest to tie photosensitisers to the complexes to evaluate their use in photocyclic reactions to produce H_2. In addition, the production of the Ni(II) complex from NH_2-2,7-dioxosar was also achieved but it would be of interest to determine the properties of other metals, such as Cu(III)/(II) and Fe(IV)/(III), with these types of ligands.

Some understanding has been gained of how amide ligands alter the electronic and redox properties of the encapsulated metals of Co(III), Cr(III) and Ni(II). Compared to those of the saturated parent ligands, the d-d absorption bands become red shifted while the redox couples occur at more negative values. The greatest shifts were observed for the diamido complexes and the higher oxidation states. One of the aims of this work was to assess the viability of obtaining higher oxidation states of metals with these ligands, especially with the diamido cages. This was realised for both the $[Ni^{III}(\{NH_3^+\}_2\text{-2-oxosar-H})]^{4+}$ and $[Ni^{III}(\{NH_3^+\}_2\text{-2,7-dioxosar-2H})]^{3+}$ ions, but higher oxidation states such as nickel(IV), cobalt(IV) and chromium(IV) were elusive. The stability of the Co(III) and Cr(III) ions appear too great for one and two amido ions respectively to surmount.

More than two amido ions within the cage ligand structure are required to diminish the three plus oxidation state of cobalt and chromium. Nevertheless, other metal ions, such as Cu(III) and Fe(IV), should be readily stabilised with the diamido ligands and need to be investigated in the future. Further work is also required to produce Ni(III) complexes from the $[Ni^{II}(\{NH_3^+)_2$-2-oxosar-H$)]^{3+}$ and $[Ni^{II}(\{NH_3^+)_2$-2,7-dioxosar-2H$)]^{2+}$ ions and to characterise their properties.

4.6 References

(1) *Coordination Chemistry of Macrocyclic Complexes*; Melson, G. A., Ed.; Plenum: New York, 1982.

(2) Lay, P. A.; Sargeson, A. M.; Skelton, B. W.; White, A. H. *J. Am. Chem. Soc.* **1982**, *104*, 6161.

(3) Gainsford, A. R.; Pizer, R. D.; Sargeson, A. M.; Whimp, P. O. *J. Am. Chem. Soc.* **1981**, *103*, 792.

(4) Harrowfield, J. M. *Unpublished Results*

(5) Gainsford, G.; Geue, R. J. *Unpublished Results*

(6) McCarthy, M. G. Ph.D. Thesis, Australian National University, 1984.

(7) Geue, R. J.; Hambley, T. W.; Harrowfield, J. M.; Sargeson, A. M.; Snow, M. R. *J. Am. Chem. Soc.* **1984**, *106*, 5478.

(8) Geue, R. J.; West, M. L. M. *Personal communication*

(9) Taft, J. C.; Jones, M. M. *J. Am. Chem. Soc.* **1960**, *82*, 4196.

(10) Sheldrick, G. M. In *Crystallographic Computing 3*; G. M. Sheldrick, C. Krüger and R. Goddard, Eds.; Oxford University Press: 1985; p 175.

(11) Beurskens, P. T.; Admiraal, G.; Beurskens, G.; Bosman, W. P.; de Gelder, R.; Israel, R.; Smits, J. M. M. *DIRDIF94 In The DIRDIF-94 program system, Technical Report of the Crystallography Laboratory*; University of Nijimegen: The Netherlands, 1994.

(12) Cromer, D. T.; Waber, J. T. In *International Tables of X-ray Crystallography*; The Kynoch Press: Birmingham, England, 1974; Vol. IV.

(13) Ibers, J. A.; Hamilton, W. C. *Acta Crystallogr.* **1964**, *17*, 781.

(14) Creagh, D. C.; McAuley, W. J. In *International Tables for Crystallography*; A. J. C. Wilson, Ed.; Kluwer Academic Publishers: Boston, 1992; Vol. C; p 219.

(15) Creagh, D. C.; Hubbel, J. H. In *International Tables for Crystallography*; A. J. C. Wilson, Ed.; Kluwer Academic Publishers: Boston, 1992; Vol. C; p 200.

(16) *teXsan: Crystal Structure Analysis Package;* Molecular Structure Corporation: 1985 & 1992.

(17) Beurskens, P. T.; Admiraal, G.; Beurskens, G.; Bosman, W. P.; Garcia-Granda, S.; Gould, R. O.; Smits, J. M. M.; Smykalla, C. *PATTY In The DIRDIF program system, Technical Report of the Crystallography Laboratory;* University of Nijimegen: The Netherlands, 1992.

(18) Beurskens, P. T.; Admiraàl, G.; Beurskens, G.; Bosman, W. P.; Garcia-Granda, S.; Gould, R. O.; Smits, J. M. M.; Smykalla, C. *DIRDIF92 In The DIRDIF program system, Technical Report of the Crystallography Laboratory;* University of Nijimegen: The Netherlands, 1992.

(19) Spek, A. L. *PLATON-94 In Program for the Automated Analysis of Molecular Geometry;* Utrecht University: The Netherlands, 1994.

(20) Geue, R. J.; Petri, W. R.; Sargeson, A. M.; Snow, M. R. *Aust. J. Chem.* **1992**, *45*, 1681.

(21) Sargeson, A. M. *Pure & Appl. Chem.* **1984**, *56*, 1603.

(22) Bernhardt, P. V.; Bygott, A. M. T.; Geue, R. J.; Hendry, A. J.; Korybut-Daszkiewicz, B. R.; Sargeson, A. M.; Willis, A. C. *Inorg. Chem.* **1994**, *33*, 4553.

(23) Clark, I. J.; Geue, R. J.; Engelhardt, L. M.; Harrowfield, J. M.; Sargeson, A. M.; White, A. H. *Aust. J. Chem.* **1993**, *46*, 1585.

(24) Creaser, I. I.; Lydon, J. D.; Sargeson, A. M.; Horn, E.; Snow, M. R. *J. Am. Chem. Soc.* **1984**, *106*, 5729.

(25) Schneider, M. L.; Ferguson, G.; Balahura, R. J. *Can. J. Chem.* **1973**, *51*, 2180.

(26) Barnet, M. T.; Buckingham, D. A.; Freeman, H. C.; Hsu, I.-N.; van der Helm, D. *J. Chem. Soc. Chem. Commun.* **1970**, 367.

(27) Martin, R. B.; Sigel, H. *Chem. Rev.* **1982**, *82*, 385.

(28) Collins, T. J.; Powell, R. D.; Slebodnick, C.; Uffelman, E. S. *J. Am. Chem. Soc.* **1991**, *113*, 8419.

(29) Restivo, R. J.; Ferguson, G.; Hay, R. W.; Piplani, D. P. *J. Chem. Soc., Dalton Trans.* **1978**, 1131.

(30) Lai, T. F.; Poon, C. K. *Inorg. Chem.* **1976**, *15*, 1562.

(31) Bernhardt, P. V.; Lawrance, G. A.; Hambley, T. W. *J. Chem. Soc., Dalton Trans.* **1989**, 1059.

(32) Figgis, B. N.; Skelton, B. W.; White, A. H. *Aust. J. Chem.* **1979**, *32*, 417.

(33) Bond, A. M.; Lawrance, G. A.; Lay, P. A.; Sargeson, A. M. *Inorg. Chem.* **1983**, *22*, 2010.

(34) Comba, P.; Creaser, I. I.; Gahan, L. R.; Harrowfield, J. M.; Lawrance, G. A.; Martin, L. L.; Mau, A. W. H.; Sargeson, A. M.; Sasse, W. H. F.; Snow, M. R. *Inorg. Chem.* **1986**, *25*, 384.

(35) Martin, L. L. Ph.D. Thesis, Australian National University, 1986.

(36) Margerum, D. W.; Dukes, G. R. In *Metal Ions in Biological Systems*; H. Sigel, Ed.; Marcel Dekker: New York, 1974; Vol. 1; Chapter 5, p 157.

(37) Clark, I. J.; Creaser, I. I.; Engelhardt, L. M.; Harrowfield, J. M.; Krausz, E. R.; Moran, G. M.; Sargeson, A. M.; White, A. H. *Aust. J. Chem.* **1993**, *46*, 111.

(38) Poon, C. K.; Tobe, M. L. *J. Chem. Soc. (A)* **1968**, 1549.

(39) Sargeson, A. M. *Pure & Appl. Chem.* **1986**, *58*, 1511.

(40) Dayagi, S.; Degani, Y. In *The Chemistry of the Carbon-Nitrogen Double Bond*; S. Patai, Ed.; Interscience: London, 1970; Chapter 2.

(41) Williams, D. H.; Fleming, I. In *Spectroscopic Methods in Organic Chemistry*; 4th ed.; McGraw-Hill Book Company (UK) Limited: London, 1987; Chapter 2, p 29.

(42) Bull, D. J.; Creaser, I. I.; Sargeson, A. M.; Skelton, B. W.; White, A. H. *Inorg. Chem.* **1987**, *26*, 3040.

(43) Wieghardt, K.; Walz, W.; Nuber, B.; Weiss, J.; Ozarowski, A.; Stratemeier, H.; Reinen, D. *Inorg. Chem.* **1986**, *25*, 1650.

CHAPTER 5.

Synthesis, Complexation and Properties of Two Triamido Tripodal Ligands with Cobalt(III).

5.1 Introduction

The strategy of condensing an ester with a primary amine, leading to an amide linkage, is not new chemistry. A large number of acyclic and macrocyclic amido ligands has stemmed from this procedure perhaps one of the most interesting being dioxo[14]ane N_4 (Figure 1).[1] Other methods also exist such as condensations between acid chlorides, mixed anhydrides and amines etc. that also allow the production of this type of ligand.[2] The complexes produced from these molecules display a number of useful characteristics. One of these is the ability to stabilise non-traditional high oxidation states of transition metal ions, such as Cu(III) and Ni(IV). It is therefore instructive to look at some of the developments that have recently occurred within this area of chemistry.

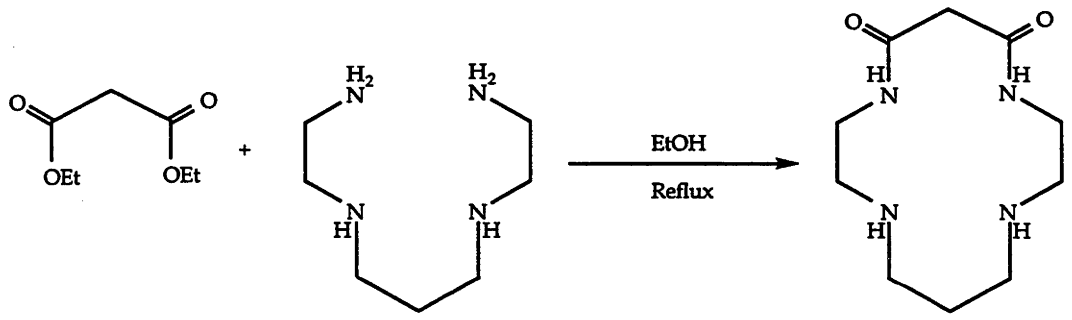

Figure 1

The addition of pendant groups on the macrocyclic ring also allows the properties of the ligands to be fine tuned (Figure 2). The nature of the pendant group influences the stability, redox, electronic, kinetic and structural properties of the metal ion complexes. Generally, the pendant is part of one of the starting materials[3] although addition of pendant arms can be made at a later stage (Figure 3).[4] Apart from being able to stabilise metals in higher oxidation states these ligands also act generally as efficient sequestering agents since they have high affinities for metal ions such as Cu(II), Ni(II), Pd(II), Pt(II) and Co(II).[5]

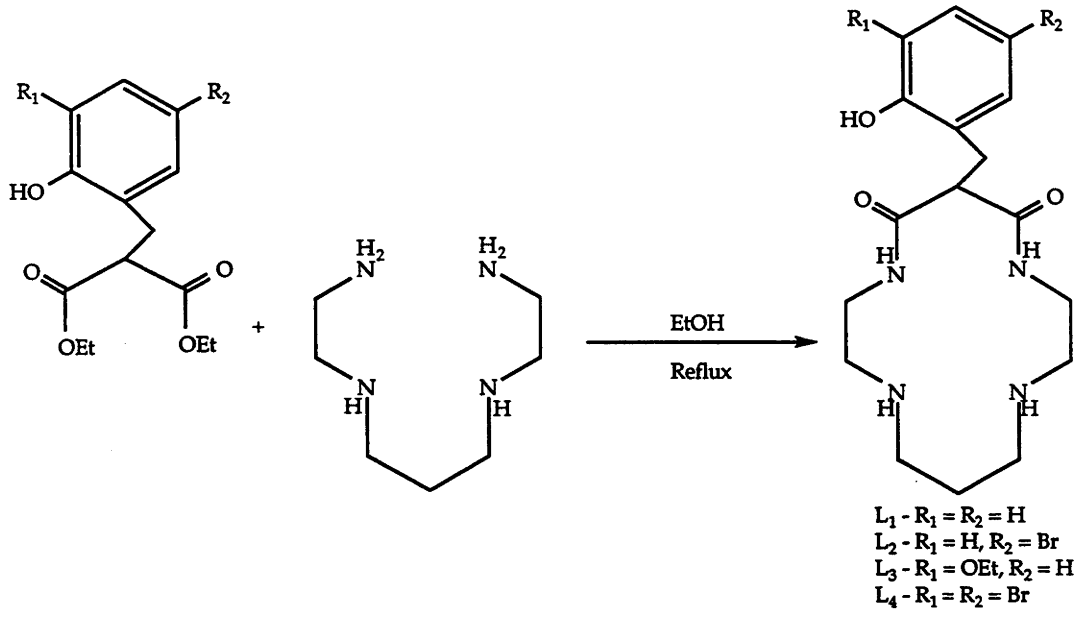

Figure 2

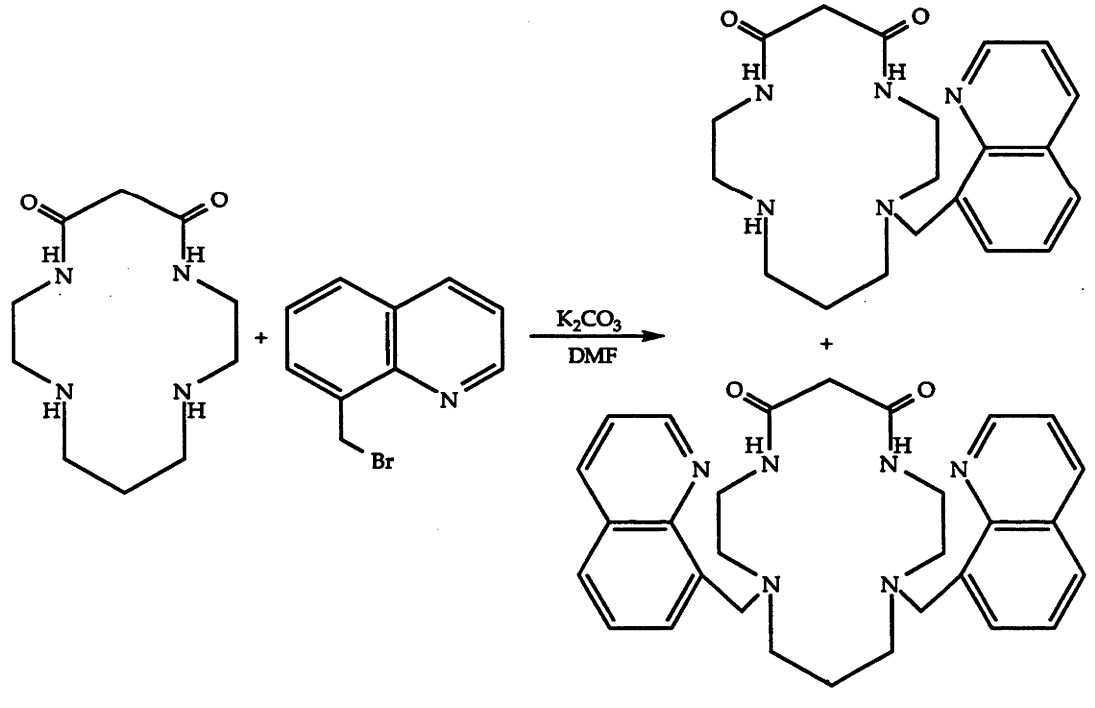

Figure 3

In addition to the large amount of research on the synthesis of macrocyclic dioxotetraamines, the complexes of many linear-chain amide ligands have also advanced our knowledge. The synthesis of a series of diamidate-diphenolate ligands, complexed to oxovanadium(IV), for

example has led to the stabilisation of the vanadium(IV) centre in each case.[6] The route to the overall synthesis of these complexes appears in Figure 4. Treatment of the appropriate methoxyaniline with diethylmalonyl dichloride afforded the dimethyl protected ligand in high yield. Reaction with BBr_3 in methylene chloride then produced the diamide-diphenol ligands cleanly. Finally the production of the oxovanadium(IV) complexes involved the reaction of a methanolic solution of the ligand with $V^{IV}O(acac)_2$.

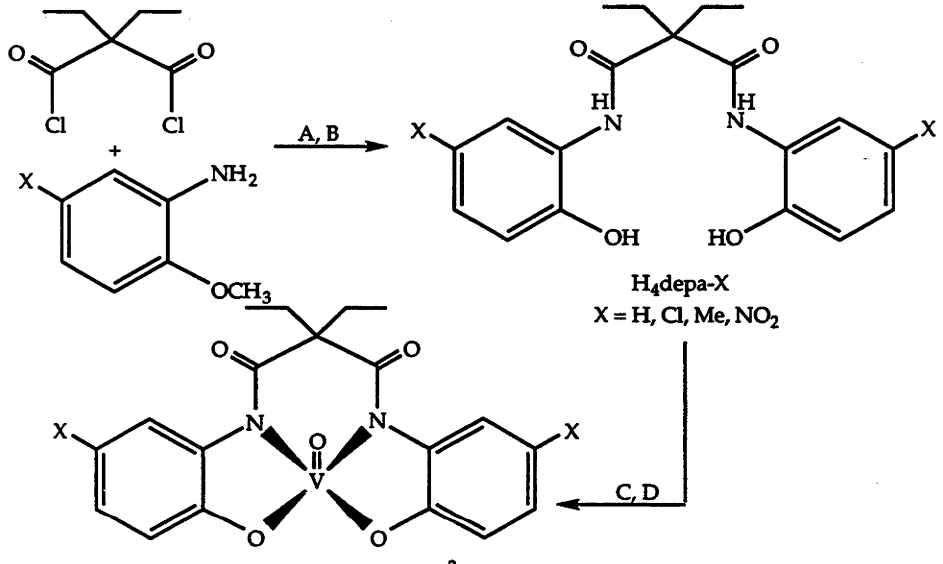

(A) Triethylamine/THF/0° C; (B) BBr_3/CH_2Cl_2; (C) $Bu_4NOH/MeOH$; (D) $VO(acac)_2$

Figure 4

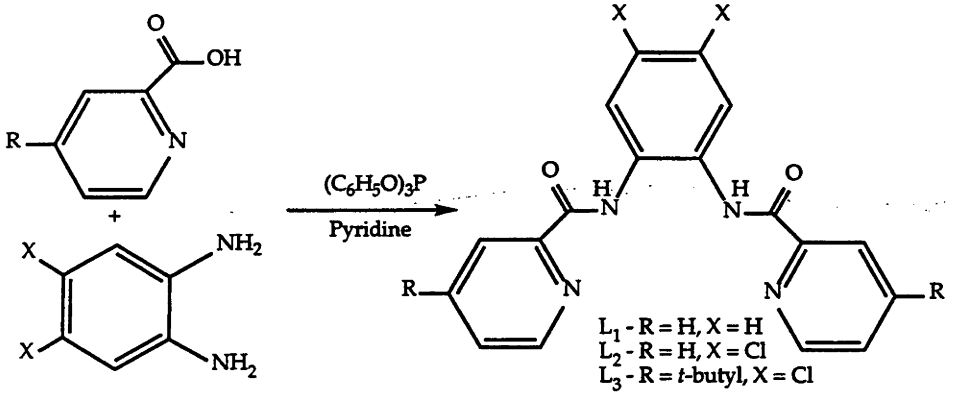

Figure 5

It is also possible to use these types of ligands in other areas such as metal catalysis and nuclear medicine. Previous work revealed that the Mn(III)[7], Cr(III)[8] and Ru(III)[9] complexes of a series of 1,2-bis(pyridine-2-carboxamido)benzene ligands are active catalysts in the oxidation of alkenes and alkanes. An example of the typical preparation of these ligands is the reaction of 4-t-butylpyridine-2-carboxylic acid with 1,2-diamino-4,5-dichlorobenzene. In the presence of triphenyl phosphite, this reaction readily produces the diamide ligand 1,2-bis(4-t-butylpyridine-2-carboxamido)-4,5-dichlorobenzene (H_2bbpc) (Figure 5).

In another example, the triamido radiopharmaceutical $^{99m}Tc^{V}$-oxo(2-thioacetyltriglycine) ($[^{99m}Tc^{V}O(MAG_3)]^-$) acts as a renal function imaging agent providing an alternative to the less favoured ^{131}I-labelled *o*-iodohippurate that imparts high radiation doses to the patient.[10] The synthesis of the ligand involves a number of steps as outlined in Figure 6 and the complexation reaction occurs readily.

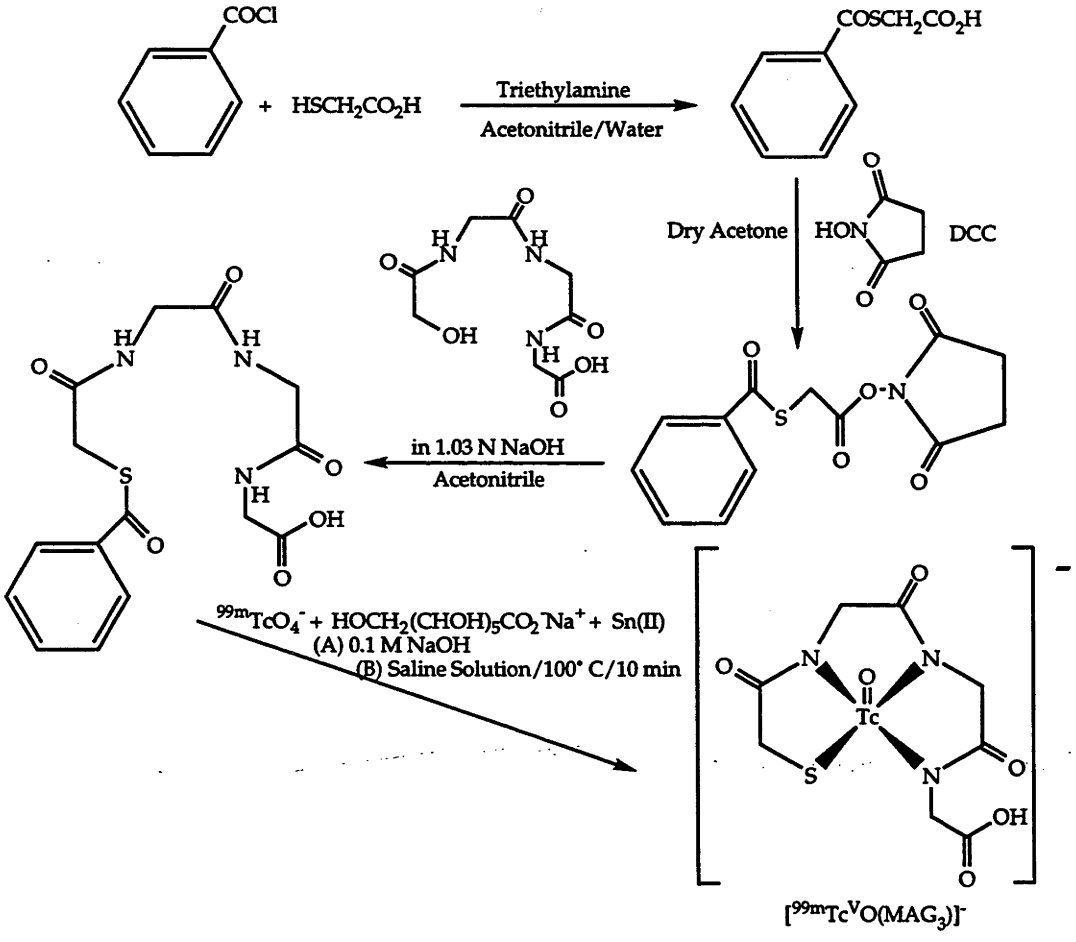

Figure 6

Clearly, various multidentate amide ligands have been synthesised which give stable complexes in high oxidation states. Therefore the production of two different triamide sen-like ligands, by regular organic syntheses are the subject of research described in this chapter (Figure 7). The introduction of amide moieties into sen may generate ligands that have different attributes to those of the saturated parent. Therefore, it was the initial aim of this investigation to produce Co(III) complexes with the two triamide tripodal ligands and then establish whether it was possible to obtain new Co(III) triamide cage compounds with these ligands. Secondly, a study of the spectral and redox characteristics of the synthesised compounds would establish if higher oxidation states were accessible in these cases.

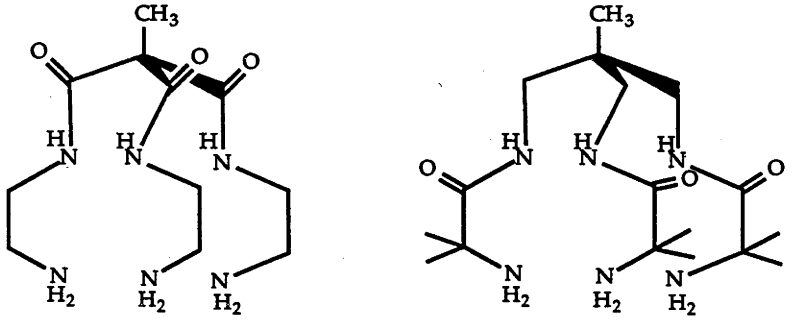

Figure 7

5.2 Experimental

5.2.1 Syntheses

Methanetricarboxylic acid triethylester

A reported method was employed.[11] In a 1 litre round-bottomed flask provided with an efficient and not too narrow reflux condenser, were placed magnesium turnings (25 g, 1.03 moles), absolute alcohol (25 mL), carbon tetrachloride (1 mL) and 30 mL of a diethyl malonate absolute alcohol mixture (151 mL of the ester in 80 mL of the alcohol). Provision was made for cooling the flask when necessary and the mixture was gently heated until hydrogen evolved. The remaining diethyl malonate mixture was added drop-wise through the condenser at such a rate that the reaction proceeded vigorously but not beyond control. After the reaction moderated, the flask was cooled and 300 mL of ether, dried for twenty-four hours over calcium chloride, was added through the condenser. On gentle heating, the crystals which had separated, were once again dissolved, and more hydrogen was evolved for some time without further heating. The reaction mixture was heated in an oil bath to bring the reaction to completion. The flask was then removed from the oil bath, and a mixture of ethyl chloroformate (100 mL) and dry ether (100 mL) was added through the condenser from a dropping funnel at such a rate that vigorous boiling was maintained throughout the addition. The reaction was completed after heating in an oil bath.

The viscous magnesium compound formed was cautiously decomposed with dilute acetic acid (75 mL in 300 mL of water). Two different layers formed and, after separation, the aqueous layer was extracted with ether. The combined ethereal extracts were washed with water, dried with sodium sulphate, and the ether was removed by rotary evaporation. The residue was distilled under reduced pressure. After some distillation the temperature rose rapidly to 160°C at 18 mm of Hg where the pure tricarbethoxymethane began to distil. The yield of material collected over a five degree interval was 215.3 g (93%). ^{1}H NMR (δ, $CDCl_3$): 1.30 (t, 9H, CH_3 ester); 4.27 (q, 6H, CH_2 ester); 4.41 (s, 1H, CH tail). ^{13}C NMR (δ, $CDCl_3$): 13.4 ($\underline{C}H_3CH_2$); 58.5 ($\underline{C}qC=O$); 61.8 ($CH_3\underline{C}H_2$); 163.5 ($\underline{C}=O$).

Sodium-methanetricarboxylic acid triethylester

A reported method was employed.[12] Sodium (25 g, 1.08 mol), cut into small pieces, was refluxed under nitrogen in absolute dioxane (1000 mL). Drop-wise addition of a solution of the triester (215.31 g, 0.93 mol) in absolute dioxane (250 mL) led, after a short while, to hydrogen evolution. When the addition was completed the mixture was refluxed overnight, allowed to cool and the sodium salt was then collected by filtration. This was washed with ether and air dried to yield a light brown solid. Yield 203.6 g (86%). ^{1}H NMR (**δ**, D_2O): 1.19 (t, 9H, CH_3 ester); 4.04 (q, 6H, CH_2 ester). ^{13}C NMR (**δ**, D_2O): 14.7 ($\underline{C}H_3CH_2$); 58.3 ($\underline{C}q^-C{=}O$); 60.7 ($CH_3\underline{C}H_2$); 172.7 ($\underline{C}{=}O$).

1,1,1-Ethanetricarboxylic acid triethyl ester

A reported method was employed.[13] The sodium salt of the triester (101.8 g; 0.41 mol) was dissolved in absolute dioxane (1000 mL) and to this solution was added methyl iodide (87 g; 0.61 mol). The mixture was then refluxed, while being protected from the light, overnight. After cooling the mixture was filtered to remove the sodium iodide produced and the filtrate was then reduced in volume to yield a light brown liquid. Yield 83.4 g (84.5%). ^{1}H NMR (**δ**, $CDCl_3$): 1.29 (t, 9H, CH_3 ester); 1.71 (s, 3H, CH_3 tail); 4.26 (q, 6H, CH_2 ester). ^{13}C NMR (**δ**, $CDCl_3$): 13.3 ($\underline{C}H_3CH_2$); 18.2 ($\underline{C}H_3Cq$); 61.5 ($CH_3\underline{C}q$); 61.6 ($CH_3\underline{C}H_2$); 167.2 ($\underline{C}{=}O$).

1,1,1-Tris(4-amino-1-oxo-2-azabutyl)ethane

The ethyl tricarboxylate triethylester (60 g; 0.24 mol) in ethanol was added drop-wise to a refluxing solution of 1,2-ethanediamine (600 mL; 9.0 mol) under nitrogen. After the addition was complete the solution was refluxed for 72 hr and at the completion of the reaction the mixture was cooled and the excess 1,2-ethane diamine was removed by evaporation yielding a dark brown oil (74.4g). Both the total yield and NMR studies indicated that the ligand was impure. The isolation of a small amount of pure ligand involved absorbing the crude ligand (3 g) on silica gel and elution with $CHCl_3$: CH_3OH: 28% aqueous ammonia (8:3:1) afforded 1 g of the desired ligand; ethane-1,2-diamine comprised the major impurity while the remainder of the reaction mixture consisted of several other species which were not recovered. ^{1}H NMR (**δ**, D_2O): 1.27 (s, 3H, CH_3 tail); 2.69 (t, 6H, CH_2 en); 3.21 (t, 6H, CH_2 en). ^{13}C NMR (**δ**, D_2O): 14.7 ($\underline{C}H_3Cq$); 40.5 ($H_2N\underline{C}H_2$); 42.1 ($\underline{C}H_2NHC{=}O$); 48.6 ($CH_3\underline{C}q$); 174.3 ($\underline{C}{=}O$).

[(1,1,1-Tris(4-amino-1-oxo-2-azabutyl)ethane)cobalt(III)].3H_2O, [Co^{III}(2,2′,2″-trioxosen-3H)].3H_2O

The crude ligand (6 g) was dissolved in water (100 mL) and a solution of $Co^{II}Cl_2.6H_2O$ (6 g; 0.025 mol) in water (100 mL) was added; charcoal (10 g) was stirred in and the solution was then aerated for 12 hr. After filtration, the orange solution was diluted to 4 L and sorbed onto a column (20 cm x 5 cm) of SP Sephadex C-25 resin where an orange band eluted straight from the column. This was reduced to 20 mL in volume and allowed to evaporate in the air which resulted in dark red orange crystals. Yield 1 g. Anal. Calc. for $C_{11}H_{21}N_6CoO_3.3H_2O$: C, 33.2; H, 6.8; N, 21.1; Co, 14.8. Found: C, 32.7; H, 6.8; N, 20.7; Co, 14.4. ^1H NMR (**δ**, D_2O): 1.17 (s, 3H, CH_3 tail); 2.20, 2.60, 2.71, 3.60 (abcd spin system, 12H, CH_2 en). ^{13}C NMR (**δ**, D_2O): 16.2 ($\underline{C}H_3Cq$); 44.8 ($H_2N\underline{C}H_2$); 47.8 ($\underline{C}H_2NC=O$); 67.1 ($CH_3\underline{C}q$); 178.5 ($\underline{C}=O$). IR in KBr (ν_{max}/cm^{-1}): 3341, 3275, 3155, 3000 (NH stretch); 2960, 2944, 2874 (C-H stretch); 1610 (C=O amide stretch); 1560 (NH_2 in-plane bending); 1455 (C-H deformation); 1360 (C-CH_3); 1264, 1249, 1216, 1198, 1165 (C-H twist); 1128 (C-N stretch); 1040, 939, 924, 908, 898, 770, 699 (CH_2 rock).

Attempted Cage Syntheses of [Co^{III}(2,2′,2″-trioxosen-3H)].3H_2O

In acetonitrile/water.

[Co^{III}(2,2′,2″-trioxosen-3H)].3H_2O (0.5 g; 1.45 x 10^{-3} mol) was dissolved in an acetonitrile (30 mL)/water (25 mL) solution containing 36% aqueous formaldehyde (5 mL; 0.06 mol), nitromethane (5 mL; 0.09 mol) and triethylamine (3 mL; 0.022 mol). The mixture was stirred for four days and during this time formaldehyde (0.5 mL) and nitromethane (0.5 mL) were added at four hourly intervals. After this time the reaction was quenched with acetic acid, diluted to 1 L with water and placed on a 50Wx2 Dowex column (10 cm x 5 cm). As the column was being washed with water a single red-orange band was collected and taken to dryness. Investigation of the solid by ^{13}C NMR indicated none of the desired C_3 symmetric cage product was present.

In methanol.

[Co^{III}(2,2′,2″-trioxosen-3H)].3H_2O (1.0 g; 2.9 x 10^{-3} mol) in methanol 50 mL was added to a solution containing nitromethane (0.2 g; 3.3 x 10^{-3} mol), paraformaldehyde (0.8 g; 0.027 mol) and triethylamine (0.2 mL; 1.45 x 10^{-3} mol) with stirring. The mixture was refluxed for four days and the solution remained cloudy during this time. After cooling a red solid was

collected and the red-orange filtrate was quenched with acetic acid, diluted to 1 L with water and placed on a 50Wx2 Dowex column (10 cm x 5 cm). As the column was being washed with water a single red-orange band was collected and taken to dryness. Analysis of the final products, by NMR, indicated that the solid material was unreacted starting material while the filtrate consisted of unreacted starting material and unidentified decomposition products.

In water.

$[Co^{III}(2,2',2''\text{-trioxosen-3H})].3H_2O$ (0.5 g; 1.45×10^{-3} mol) was dissolved in 100 mL of water. To this was added, with stirring, 36% aqueous formaldehyde (2.35 g; 0.08 mol), nitromethane (1.25 g; 0.02 mol) and sodium carbonate (0.4 g; 3.8×10^{-3} mol). The reaction mixture was stirred for three days with little change in the colour of the solution. NaOH was added at this point to raise the pH of the solution to approximately 12 and this resulted in the solution becoming darker in colour after a further two days of stirring. After this time the reaction was quenched with acetic acid, diluted to 1 L with water and placed on a 50Wx2 Dowex column (10 cm x 5 cm). As the column was being washed with water a single red-orange band was collected and taken to dryness. Investigation of the solid by ^{13}C NMR indicated none of the desired C_3 symmetric cage product was present.

In acetonitrile with paraformaldhyde.

$[Co^{III}(2,2',2''\text{-trioxosen-3H})].3H_2O$ (0.2 g; 5×10^{-4} mol) was suspended in acetonitrile (30 mL) and to this was added paraformaldehyde (1.74 g; 0.058 mol) and triethylamine (2 mL; 0.014 mol). The resultant reaction mixture was then stirred for one week after which it was quenched with concentrated hydrochloric acid, diluted to 1 L and placed on a 50Wx2 Dowex column (10 cm x 5 cm) where it was eluted with water. One red-orange band was collected and taken to dryness on a rotary evaporator; NMR analysis indicated that the band was unreacted starting material. The above reaction was repeated except that the mixture was refluxed for one week. Again one red-orange band was collected off the Dowex column however the ^{13}C NMR showed that other decomposition products were present with the unreacted starting material.

1,1,1-Tris(4-bromo-4-methyl-3-oxo-2-azapentyl)ethane

A variation on a reported method was employed.[14] 1,1,1-tris(aminomethyl)ethane (tame) (3 g; 0.026 mol) and Et_3N (12.5 mL; 0.09 mol) were added to CH_2Cl_2 (200 mL). The mixture was dried over Na_2SO_4 (1 hr) and then filtered into a three-neck round-bottomed flask (1 L) equipped with a reflux condenser and a pressure-equalising addition funnel. Under a N_2 atmosphere, 2-bromo-2-methylpropionyl bromide (9.5 mL; 0.077 mol) was carefully added to the solution from the addition funnel to avoid boiling the solvent (The reaction was VERY exothermic.). The solution became cloudy upon production of $[Et_3NH]Br$. After being stirred (1 hr), the reaction mixture was washed twice with dilute aqueous HCl and twice with dilute aqueous Na_2CO_3. The resultant CH_2Cl_2 solution was dried over Na_2SO_4 to give a clear, pale yellow solution. The CH_2Cl_2 was removed under reduced pressure to leave a yellow oil. Yield = 13.6 g (97%). ^1H NMR (**δ**, $CDCl_3$): 0.90 (s, 3H, CH_3 tail); 1.95 (s, 18H, CH_3 $H_2NC(C\underline{H}_3)_2$); 2.99 (s, 3H, CH_2 cap); 3.02 (s, 3H, CH_2 cap); 7.72 (s, 3H amide NH). ^{13}C NMR (**δ**, $CDCl_3$): 19.2 ($\underline{C}H_3Cq$); 31.9 ($H_2NC(\underline{C}H_3)_2$); 41.8 ($CH_3\underline{C}q$); 42.0 ($CH_3Cq\underline{C}H_2$); 60.4 ($H_2N\underline{C}(CH_3)_2$); 172.8 ($\underline{C}$=O).

1,1,1-Tris(4-amino-4-methyl-3-oxo-2-azapentyl)ethane

The above product (13.6 g; 0.025 mol) was dissolved in ethanol (250 mL), an aqueous solution of NaN_3 (5.85 g; 0.09 mol) (CAUTION!) was added and the mixture was heated under reflux (12 hr). Solvent was removed under reduced pressure until precipitation was initiated. The aqueous solution was extracted twice with CH_2Cl_2 and the extract was dried over anhydrous Na_2SO_4. It is important to execute this procedure to remove the NaN_3, since the product is exposed to Pd/C in the next step and care should be taken to avoid the formation of a heavy metal azide. The CH_2Cl_2 was again removed under reduced pressure until precipitation was initiated. Ethanol (ca. 500 mL) was added and the solution was again concentrated under reduced pressure. CAUTION! A small sample (ca. 5 mg) was isolated as a solid for spectroscopic analysis; the bulk triazide product was not isolated. ^1H NMR (**δ**, $CDCl_3$): 0.74 (s, 3H, CH_3 tail); 1.49 (s, 18H, CH_3 $H_2NC(C\underline{H}_3)_2$); 2.86 (s, 3H, CH_2 cap); 2.88 (s, 3H, CH_2 cap); 7.67 (s, 3H amide NH). ^{13}C NMR (**δ**, $CDCl_3$): 18.6 ($\underline{C}H_3Cq$); 24.5 ($H_2NC(\underline{C}H_3)_2$); 41.3 ($CH_3\underline{C}q$); 42.3 ($CH_3Cq\underline{C}H_2$); 64.2 ($H_2N\underline{C}(CH_3)_2$); 173.8 ($\underline{C}$=O). This solution was reduced in portions with H_2 in a bomb (50 psi) with 10% Pd/C. Because the reaction evolves one N_2 molecule for every H_2 molecule absorbed, frequent evacuation of the bomb and refilling with H_2 is advantageous (i.e.,

H_2 from the high pressure reservoir is not efficiently consumed). The mixture was filtered to remove the catalyst, the filtrate was stripped to dryness yielding a resultant grey-white solid. Yield = 7.4 g (79%). ^{1}H NMR (**δ**, D_2O): 0.72 (s, 3H, CH_3 tail); 1.36 (s, 18H, CH_3 $H_2NC(C\underline{H}_3)_2$); 3.01 (s, 6H, CH_2 cap). ^{13}C NMR (**δ**, D_2O): 19.8 ($\underline{C}H_3Cq$); 28.2 ($H_2NC(\underline{C}H_3)_2$); 41.9 ($CH_3\underline{C}q$); 42.9 ($CH_3Cq\underline{C}H_2$); 55.8 ($H_2N\underline{C}(CH_3)_2$); 181.7 ($\underline{C}$=O).

[(1,1,1-Tris(4-amino-4-methyl-3-oxo-2-azapentyl)ethane)cobalt(III)].8H_2O.-0.5C_2H_5OH, [Co^{III}(5,5′,5″-tri(Me_2)-4,4′,4″-trioxosen-3H)].8H_2O.0.5C_2H_5OH

1,1,1-Tris(4-amino-4-methyl-3-oxo-2-azapentyl)ethane (1 g; 2.68 x 10^{-3} mol) was dissolved in water (200 mL) and a solution of $Co^{II}Cl_2.6H_2O$ (0.65 g; 2.68 x 10^{-3} mol) in water (200 mL) was added; charcoal was stirred in and the solution aerated for 12 hr. The Co(III) complex was isolated after a workup similar to that used for [Co(2,2′,2″-trioxosen-3H)].3H_2O except the complex was stripped to dryness and then recrystallised from aqueous ethanol in this case to yield a dark red solid. Yield = 1.1 g (68%). Anal. Calc. for $C_{17}H_{33}N_6CoO_3$.8H_2O.0.5C_2H_5OH: C, 35.8; H, 8.8; N, 13.9. Found: C, 35.7; H, 8.1; N, 13.9. ^{1}H NMR (**δ**, D_2O): 1.02 (s, 3H, CH_3 tail); 1.40 (s, 18H, CH_3 $H_2NC(C\underline{H}_3)_2$); 2.47, 3.13 (AB doublets of doublets, 6H, CH_2 cap). ^{13}C NMR (**δ**, D_2O): 21.7 ($\underline{C}H_3Cq$); 27.1 ($H_2NC(\underline{C}H_3)_2$); 30.2 ($H_2NC(\underline{C}H_3)_2$); 44.6 ($CH_3\underline{C}q$); 51.9 ($CH_3Cq\underline{C}H_2$); 61.5 ($H_2N\underline{C}(CH_3)_2$); 184.0 ($\underline{C}$=O). IR in KBr ($\nu$-$_{max}$/$cm^{-1}$): 3400, 3241, 3137 (NH stretch); 2930, 2852 (C-H stretch); 1568 (C=O amide stretch); 1473, 1460, 1410 (C-H deformation); 1377 (C-CH_3); 1284, 1242, 1193, 1172 (C-H twist); 1108 (C-NH2); 1015, 945, 894, 758 (CH_2 rock).

5.2.2 X-ray Crystal Structure Analysis of [Co^{III}(2,2′,2″-trioxosen-3H)].3H_2O

Data Collection

An orange-red hexagonal prismatic crystal of the Co(III) triamide complex having approximate dimensions of 0.18 x 0.18 x 0.28 mm was mounted on a quartz fibre. All reflections were collected using a Rigaku AFC6R diffractometer with graphite monochromated Cu-Kα radiation and a 12 kW rotating anode generator. Cell constants and an orientation matrix for data collection, obtained from a least squares refinement using the setting angles of 25 carefully centered reflections in the range 93.85 < 2θ < 98.46° corresponded to a primative hexagonal cell (laue class: 6/m) with dimensions a = 8.040(3) Å, c = 43.730(4) Å and V = 2447.8(5) $Å^3$. For Z = 6 and F.W. = 398.30, the calculated density is 1.62 g/cm^3. Based on the

systematic absences of: 0001: $l \neq 6n$ and the successful solution and refinement of the structure, the space group was determined to be: $P6_5$ (# 170). The data were collected at a temperature of 23 ± 1° C using the ω scan technique to a maximum 2θ value of 120.0°. Omega scans of several intense reflections, made prior to data collection, had an average width at half height of 0.31° with a take-off angle of 6.0°. Scans of (1.30 + 0.30 tan θ)° were made at a speed of 16.0°/min (in omega). The weak reflections ($I < 10.0\sigma(I)$) were rescanned (maximum of four scans) and the counts were accumulated to ensure good counting statistics. Stationary background counts were recorded on each side of the reflection. The ratio of peak counting time to background counting time was 2:1. The diameter of the incident beam collimator was 0.5 mm, the crystal to detector distance was 400 mm, and the detector aperture was 9.0 x 9.0 mm (horizontal x vertical).

Data Reduction

Of the 3956 reflections which were collected, ±h, +k, +l, 1259 were unique (R_{int} = 0.050). The intensities of three representative reflections were measured after every 150 reflections. Over the course of data collection, the standards decrease by 1.7%. A linear correction factor was applied to the data to account for this phenomenon. The linear absorption coefficient, μ, for Cu-Kα radiation is 86.5 cm^{-1}. An analytical absorption correction was applied which resulted in transmission factors ranging from 0.24 to 0.34. The data were corrected for Lorentz and polarisation effects.

Structure Solution and Refinement

The structure was solved by direct methods[15] and expanded using Fourier techniques.[16] The non-hydrogen atoms were refined anisotropically. Hydrogen atoms attached to carbon and nitrogen atoms were generated geometrically and recalculated periodically as refinement proceeded. Hydrogen atoms of the water molecules were located in an inner-data difference map. An attempt to refine the positional parameters of these atoms was not successful, so they were held fixed at the observed positions. Some of the O-H distances and H-O-H angles do not agree well with expected values, but they do give indications of the general hydrogen-bonding network within the unit cell and so have been retained. Refinement in the space group $P6_1$ with inverted coordinates gave a much higher R-factor, indicating that the absolute configuration of the molecule is as shown in the Figure 12. The final cycle of full-matrix least-squares refinement was based on 1090 observed reflections ($I > 3.00\sigma(I)$) and 216

variable parameters and converged (largest parameter shift was 0.01 times its esd) with unweighted and weighted agreement of: $R = \Sigma | |Fo| - |Fc| | / \Sigma |Fo| = 0.027$ and $R_w = \sqrt{(\Sigma\omega(|Fo| - |Fc|)^2/\Sigma\omega Fo^2)} = 0.029$. The standard deviation of an observation of unit weight was 1.72. The weighting scheme was based on counting statistics and included a factor (p = 0.006) to downweight the intense reflections. Plots of $Sw(|Fo| - |Fc|)^2$ verses $|Fo|$, reflection order in data collection, $\sin\theta/\lambda$ and various classes of indices showed no unusual trends. The maximum and minimum peaks on the final difference Fourier map corresponded to 0.30 and -0.31 $e^-/Å^3$, respectively. Neutral atom scattering factors were taken from Cromer and Waber.[17] Anomalous dispersion effects were included in Fcalc[18]; the values for $\Delta f'$ and $\Delta f''$ were those of Creagh and McAuley.[19] The values for the mass attenuation coefficients are those of Creagh and Hubbel.[20] All calculations were performed using the texsan[21] crystallographic software package of the Molecular Structure Corporation.

5.3 Results

5.3.1 Syntheses

Synthesis of $[Co^{III}(2,2',2''\text{-trioxosen-3H})].3H_2O$ was achieved through a six step procedure and Figure 8 outlines the synthetic approach used. Firstly, diethyl malonate was reacted with ethyl chloroformate to replace one of the backbone hydrogen atoms with a third ester to produce a tripod with an apical hydrogen. This was subsequently converted into the sodium salt by reacting the tripod with sodium metal to eliminate dihydrogen. Methylation was ultimately achieved by reacting the sodium salt with methyl iodide. The methylated ester was then treated with excess ethylenediamine to produce the triamide ligand and purification was achieved through complexation with Co(III). An excess of the amine reagent helps to steer the synthesis towards the tripodal ligand and limits, to a degree, two ester groups reacting with one diamine either inter or intra molecularly. However, the yield of the triester was not high and converting the desired tripod to the Co(III) triamido complex using Co^{2+} and O_2 in the presence of charcoal was the easiest method of purification. Isolation of the complex from the ion exchange resin and crystallisation of the product plus microanalysis indicated that the product was a non-electrolyte. The hexadentate appears to bind as the trianion.

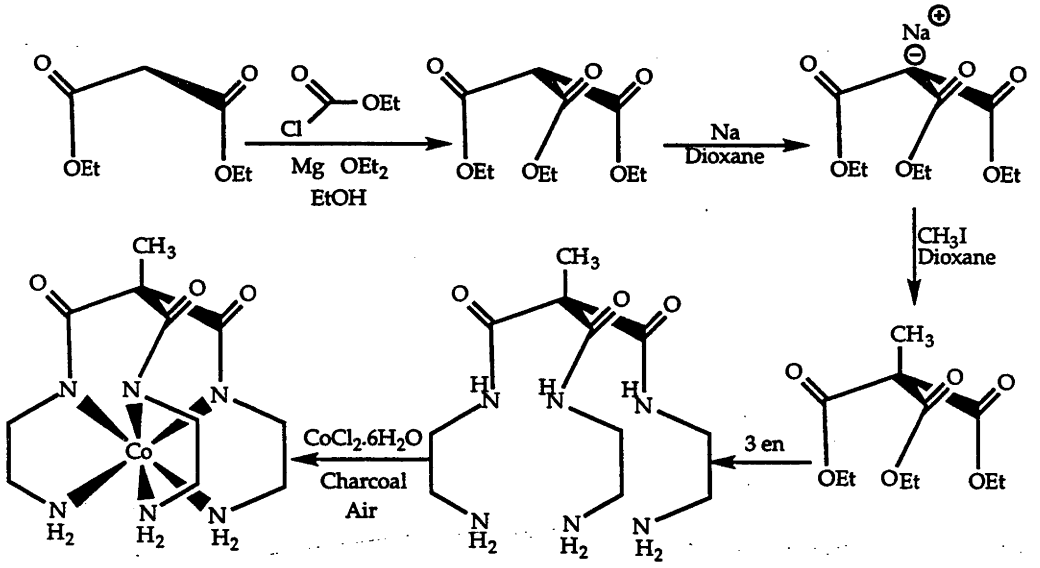

Figure 8

The attempts undertaken to produce a cage complex from the triamido species, $[Co^{III}(2,2',2''\text{-trioxosen-3H})]^0$ with formaldehyde and nitromethane, were unsuccessful. Various changes in solvents and

reaction conditions produced none of the desired product. In all instances, either starting material or decomposition products, or a combination of both arose from the respective reactions. Although the complex possesses three primary amines on one octahedral face, which should, in principle, be susceptible to the capping process, the results indicate that it is difficult for formaldehyde to form an imine with these amines under the conditions usually successful for the condensation reaction. Since the complex is a nonelectrolyte and the ligand a trianion, the N-protons are not as acidic as those in the $[Co^{III}(en)_3]^{3+}$ or $[Co^{III}(sen)]^{3+}$ ions for example. This property would limit the encapsulation process but whether it is the only factor is not so clear.

The synthesis of $[Co^{III}(5,5',5''\text{-tri}(Me_2)\text{-}4,4',4''\text{-trioxosen-}3H)]^0$ followed the procedures summarised in Figure 9. Initially, 1,1,1-tris(aminoethyl)ethane was reacted with 2-bromo-2-methylpropionyl bromide producing the triamidetribromide tripod. The next step involved converting the tribromide to the triazide with sodium azide. Reduction of the triazide in ethanolic $Pd/C/H_2$ then afforded the triamidetriamine tripod in high yield. Production of the Co(III) complex followed using Co^{2+}, the ligand, oxygen as the oxidant and charcoal as the catalyst. Isolation of this complex from the ion exchange column and the microanalytical data indicated that the amide ligand was binding as a trianion.

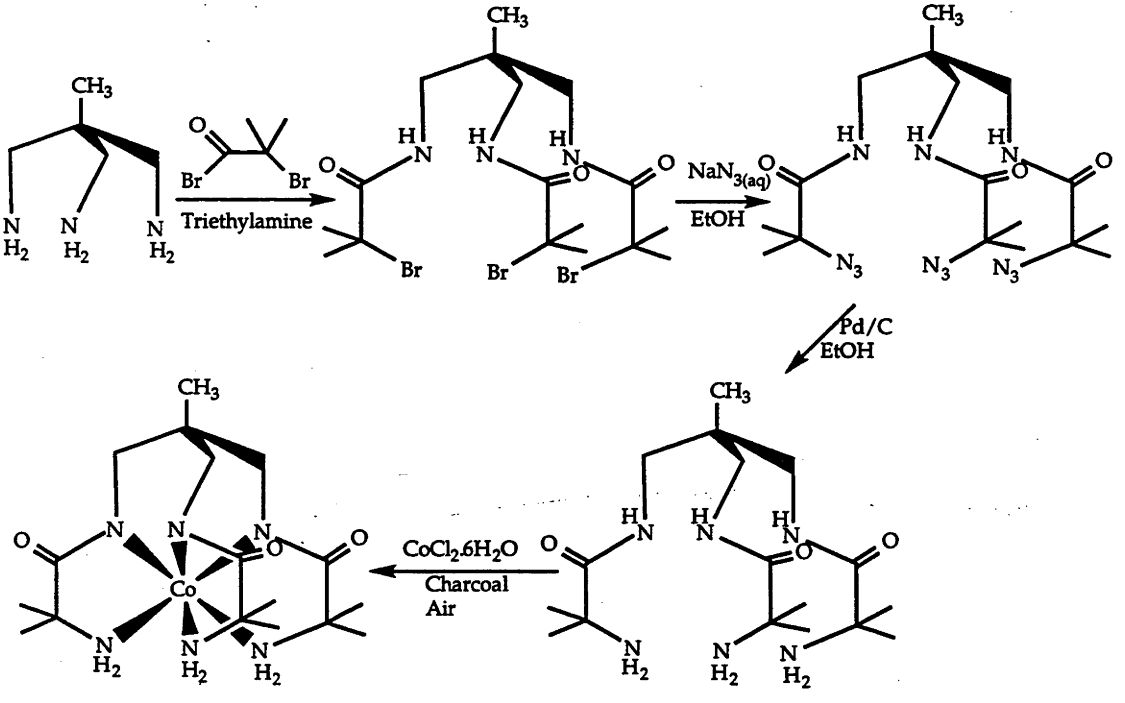

Figure 9

5.3.2 NMR Spectroscopy

The fully deuterated, proton-decoupled ^{13}C NMR spectra of both triamide complexes are given in Figure 10. Each complex is highly symmetric, possessing a C_3 axis. The carbon atoms within each arm of the tripods are inequivalent to each other but equivalent to the corresponding carbons on the other arms. As a result five signals appear in the spectrum of $[Co^{III}(2,2',2''\text{-trioxosen-3H})]^0$ while seven signals occur for the second triamide complex, $[Co^{III}(5,5',5''\text{-tri}(Me_2)\text{-}4,4',4''\text{-trioxosen-3H})]^0$. In the first case, the amides are in the cap of the complex and the observed peaks are assigned to a methyl, a quaternary, an amide and two methylene carbon atoms that have the respective chemical shift values of 16.2, 67.1, 178.5, 44.8, and 47.8 ppm. For the second compound, where the amides are situated in the five-membered chelate rings, the seven carbon atoms comprise three methyl, a methylene, two quaternary and an amide. Here the corresponding seven signals are assigned 21.7, 27.1, 30.2, 44.6, 51.9, 61.5 and 184.0 ppm accordingly.

The ^1H NMR spectra of the two triamides are distinctly different (Figure 11). For the first triamide a singlet arises from the methyl group in the apical position of the complex (1.17 ppm) while a complex ABCD spin system arises from the methylene protons over 2.20 - 3.60 ppm. In the second triamide complex, a singlet occurs at 1.2 ppm for the apical methyl protons while a distorted AB doublet pair arises for the remaining gem-methylene hydrogens. Although the protons of each methyl group, located on the five membered chelate rings, are equivalent to each other in each case, the two groups are chemically different hence one signal occurs for each type of methyl group; coupling also exists between the two methyl groups and hence two AB spin patterns should arise. However, as the coupling between the two methyl groups is small the peak intensities become distorted and deviate from the classical AB pattern; the two expected AB doublet pairs merge and appear as a broad multiplet at 1.40 ppm in the ^1H NMR spectrum. The two methylene protons, within the cap of this complex, are also different and coupled to each other and these generate two AB doublets centred on 2.47 and 3.13 ppm respectively.

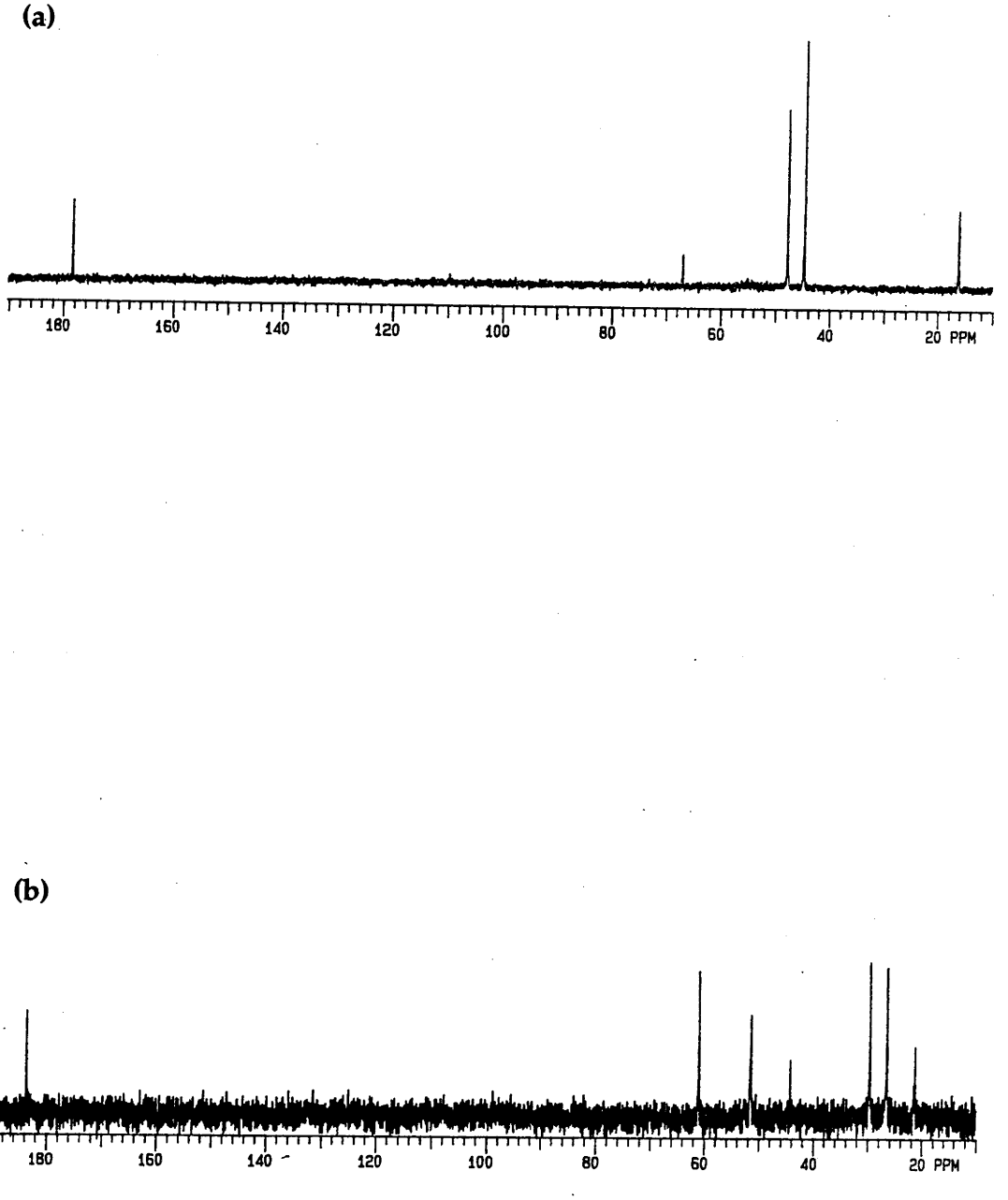

Figure 10. ^{13}C NMR spectrum of (a) $[Co^{III}(2,2',2''\text{-trioxosen-3H})]^0$ and (b) $[Co^{III}(5,5',5''\text{-tri}(Me_2)\text{-}4,4',4''\text{-trioxosen-3H})]^0$ in D_2O.

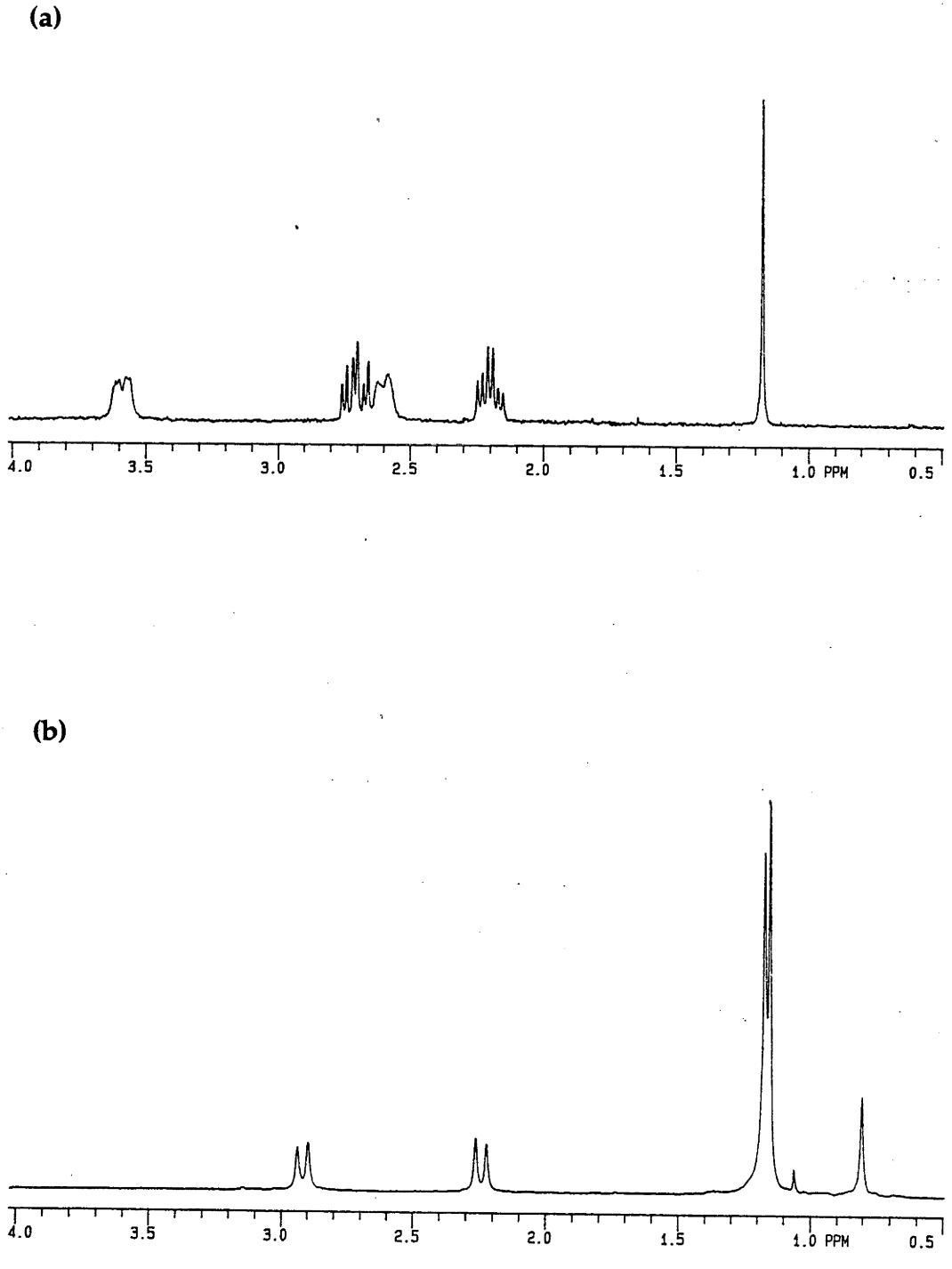

Figure 11. ^{1}H NMR spectrum of (a) $[Co^{III}(2,2',2''\text{-trioxosen-3H})]^{0}$ and (b) $[Co^{III}(5,5',5''\text{-tri}(Me_2)\text{-}4,4',4''\text{-trioxosen-3H})]^{0}$ in D_2O.

5.3.3 Infra-red Spectroscopy

The functional group absorption frequencies for the two triamide complexes are tabulated in Table 1. For both triamide complexes, a strong absorption band, attributed to the C=O stretching vibration of the deprotonated coordinated amide, is displayed at 1609 cm^{-1} for $[Co^{III}(2,2',2''$-trioxosen-3H)$]^0$ while the same band for $[Co^{III}(5,5',5''$-tri(Me_2)-4,4',4''-trioxosen-3H)$]^0$ occurs at 1568 cm^{-1}. Also, from the crystallography obtained on $[Co^{III}(2,2',2''$-trioxosen-3H)$]^0$ the ORTEP diagram confirms that this complex is six coordinate. On the other hand, for $[Co^{III}(5,5',5''$-tri(Me_2)-4,4',4''-trioxosen-3H)$]^0$ a crystal structure was not obtained. However, the analysis, ^{13}C NMR spectrum and single C=O observed absorption vibration similar to that found for $[Co^{III}(2,2',2''$-trioxosen-3H)$]^0$ all indicate hexadentate coordination of the ligand as a trianion to give a C_3 symmetric complex. It is then reasonable to conclude that the Co(III) ion in $[Co^{III}(5,5',5''$-tri(Me_2)-4,4',4''-trioxosen-3H)$]^0$ is also bound to three amido nitrogen atoms. This is consistent with the C_3 symmetry deduced from the NMR spectroscopy.

Table 1. Functional group infrared absorption vibrations of the Co(III) triamido triamine tripodal complexes.

Complex	$\tilde{\nu}$, cm^{-1}	Assignment
$[Co^{III}(2,2',2''$-trioxosen-3H)$]^0$	1609	$C=O_{(amido)}$ stretch
	1560	NH_2 in-plane bending
$[Co^{III}(5,5',5''$-tri(Me_2)-4,4',4''-trioxosen-3H)$]^0$	1568	$C=O_{(amido)}$ stretch

5.3.4 X-ray Crystallography

The structure of the neutral complex $[Co^{III}(2,2',2''$-trioxosen-3H)$].3H_2O$ along with its bond distances and angles are given in Figure 12 and Tables 2 and 3 respectively. The crystallography confirms that the ligand binds as a hexadentate. Three coordination sites are occupied by three deprotonated amide nitrogen atoms and the other three by the three remaining primary amine groups. Each of the five membered chelate rings

has adopted an *ob* conformation about the C_3 axis through the metal. The triamide cap conformation also fixes the orientation of the opposite open trigonal primary amine face giving the complex an overall conformation of C_3ob_3. This structure is different to that observed for $[Co^{III}(sen)]^{3+}$.[22] The sen ligand of the complex cation is in the lel_3 conformation. This difference between the two tripod complexes could be significant in relation to their ability to form the cage readily along with the difference in charge.

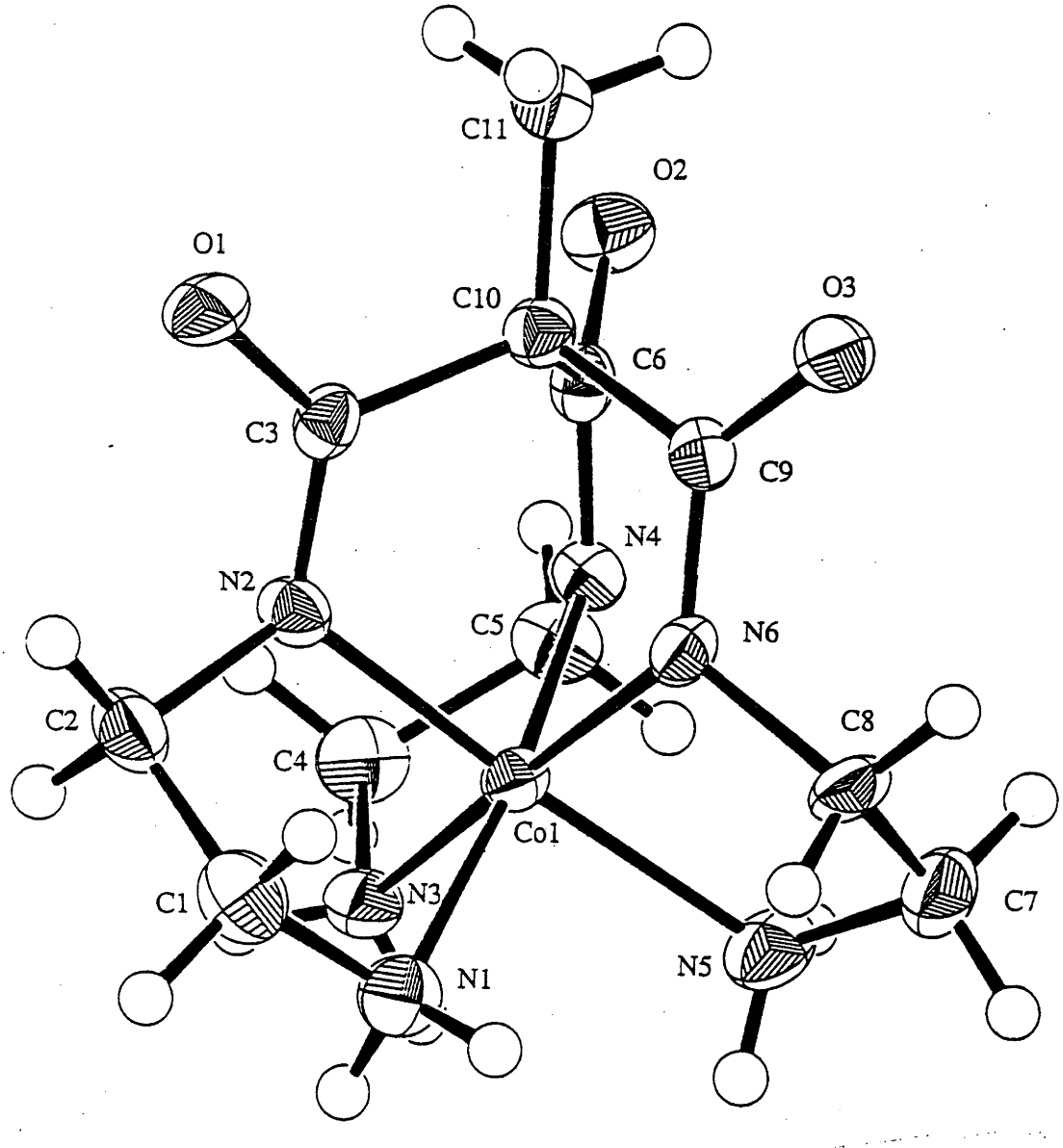

Figure 12. Thermal ellipsoid diagram of $[Co^{III}(2,2',2''\text{-trioxosen-3H})].3H_2O$ showing atomic labelling. Ellipsoids show 50% probability levels, except the hydrogen atoms which are drawn as circles of arbitary radius.

Table 2. Bond Distances (Å) for $[Co^{III}(2,2',2''\text{-trioxosen-3H})].3H_2O$.

Atoms	Distance (Å)	Atoms	Distance (Å)
Co-N(1)	1.989(4)	Co-N(2)	1.895(4)
Co-N(2)	2.003(4)	Co-N(4)	1.902(4)
Co-N(5)	1.995(4)	Co-N(6)	1.895(4)
O(1)-C(3)	1.260(6)	O(2)-C(6)	1.267(6)
O(3)-C(9)	1.254(6)	N(1)-C(1)	1.491(7)
N(2)-C(2)	1.480(7)	N(2)-C(3)	1.312(6)
N(3)-C(4)	1.457(7)	N(4)-C(5)	1.469(6)
N(4)-C(6)	1.291(6)	N(5)-C(7)	1.466(7)
N(6)-C(8)	1.480(6)	N(6)-C(9)	1.296(6)
C(1)-C(2)	1.522(8)	C(3)-C(10)	1.561(7)
C(4)-C(5)	1.487(8)	C(6)-C(10)	1.575(7)
C(7)-C(8)	1.514(9)	C(9)-C(10)	1.564(7)
C(10)-C(11)	1.505(7)		

The three $Co\text{-}N_{(amine)}$ distances (1.989(4) Å, 2.003(4) Å and 1.995(4) Å respectively) are somewhat longer than the average $Co\text{-}N_{(amine)}$ bond length observed for $[Co^{III}(sen)]^{3+}$, which is 1.971(3) Å[22], and that of other ob_3 sar type cages such as $[Co^{III}(\{NMe_3)_2\text{-sar}\}]^{5+}$ which has an average identified $Co\text{-}N_{(amine)}$ distance of 1.961(6) Å.[23] This is not unexpected however as N^- binding of the Co(III) ion leads to a lengthening of the bond *trans* to it as a result of the N^- donor being a stronger σ-donor than NH_2. The structure displays this factor in the $Co\text{-}N_{(amido)}$ bond lengths (1.895(4) Å, 1.902(4) Å and 1.895(4) Å respectively) are significantly shorter than the three $Co\text{-}N_{(amine)}$ bonds and are comparable to those observed for other amido Co(III) cage complexes.[24] Compared to other types of Co(III) amido complexes the $Co\text{-}N_{(amido)}$ bond lengths of the triamide compound are shorter than the $Co\text{-}N_{(amido)}$ distance (1.911(8) Å)[25] observed for the $[CH_3CONHCo^{III}(NH_3)_5]^{2+}$ cation but longer than that quoted for the simple N-bound amide in the bis(glycylglycinato)cobalt(III) ion (1.87 Å).[26] In addition the $N\text{-}C_{(amido)}$ bonds (Table 2) are similar to the expected $N\text{-}C_{(peptide)}$ (1.30 Å) bond length[27] and the $C\text{-}O_{(amide)}$ bonds, namely C(3)-O(1), C(9)-O(3) and C(6)-O(2) (Table 2), correlate with the anticipated $C\text{-}O_{(peptide)}$ distance of 1.27 Å[27] (within 3σ).

Table 3. Bond Angles (°) for $[Co^{III}(2,2',2''\text{-trioxosen-3H})].3H_2O$.

Atom	Angle (°)	Atom	Angle (°)
N(1)-Co-N(2)	86.0(2)	N(1)-Co-N(3)	89.4(2)
N(1)-Co-N(4)	171.5(2)	N(1)-Co-N(5)	91.7(2)
N(1)-Co-N(6)	96.6(2)	N(2)-Co-N(3)	94.5(2)
N(2)-Co-N(4)	89.8(2)	N(2)-Co-N(5)	171.2(2)
N(2)-Co-N(6)	88.6(2)	N(3)-Co-N(4)	83.6(2)
N(3)-Co-N(5)	93.9(2)	N(3)-Co-N(6)	173.2(2)
N(4)-Co-N(5)	93.5(2)	N(4)-Co-N(6)	90.6(2)
N(5)-Co-N(6)	83.3(2)	Co-N(1)-C(1)	108.4(3)
Co-N(2)-C(2)	112.7(3)	Co-N(2)-C(3)	119.7(3)
C(2)-N(2)-C(3)	118.9(4)	Co-N(3)-C(4)	110.0(3)
Co-N(4)-C(5)	113.0(3)	Co-N(4)-C(6)	121.6(3)
C(5)-N(4)-C(6)	119.6(4)	Co-N(5)-C(7)	111.9(3)
Co-N(6)-C(8)	112.5(3)	Co-N(6)-C(9)	122.2(3)
C(8)-N(6)-C(9)	120.5(4)	N(1)-C(1)-C(2)	108.1(4)
N(2)-C(2)-C(1)	106.3(4)	O(1)-C(3)-N(2)	126.1(5)
O(1)-C(3)-C(10)	118.2(5)	N(2)-C(3)-C(10)	115.6(4)
N(3)-C(4)-C(5)	108.8(4)	N(4)-C(5)-C(4)	106.2(4)
O(2)-C(6)-N(4)	127.0(5)	O(2)-C(6)-C(10)	118.2(4)
N(4)-C(6)-C(10)	114.8(4)	N(5)-C(7)-C(8)	109.4(4)
N(6)-C(8)-C(7)	105.2(4)	O(3)-C(9)-N(6)	127.9(5)
O(3)-C(9)-C(10)	118.4(4)	N(6)-C(9)-C(10)	113.7(4)
C(3)-C(10)-C(6)	109.4(4)	C(3)-C(10)-C(9)	105.6(4)
C(3)-C(10)-C(11)	111.6(4)	C(6)-C(10)-C(9)	107.5(4)
C(6)-C(10)-C(11)	111.0(4)	C(9)-C(10)-C(11)	111.6(4)

The N-Co-N bond angles of $[Co^{III}(2,2',2''\text{-trioxosen-3H})].3H_2O$ deviate slightly from the typical angles observed for octahedral symmetry of the CoN_6 core; in this case the angles vary by ~2° to 7° from the ideal values. In addition, the average twist angle between the two sets of N_3 planes, perpendicular to the C_3 axis, is 51°; the two N_3 planes also are not exactly parallel (tipped ~3°), which indicates the metal possesses a pseudo-octahedral character resulting largely from the rotation of the two N_3 planes. Lastly, the torsion angles of the three five membered rings of the

triamide are -46.4(5) for N(1)-C(1)-C(2)-N(2), -45.9(6) for N(3)-C(4)-C(5)-N(4) and -41.2(6) for N(5)-C(7)-C(8)-N(6) respectively. The slight non parallel N_3 planes and variations in the torsional angles are probably crystallographic influences rather than electronic effects within the molecule which would be expected to be C_3 symmetric with this ligand and a low spin d^6 electronic configuration.

[Co^{III}(5,5′,5″-tri(Me_2)-4,4′,4″-trioxosen-3H)].8H_2O.1/2C_2H_5OH

Although a structure has not been determined for [Co^{III}(5,5′,5″-tri(Me_2)-4,4′,4″-trioxosen-3H)].8H_2O.1/2C_2H_5OH it is expected that the three -NH_2-C($Me)_2$-C(O)-N$^-$- chelate rings will be either planar or near planar. This expected geometry should arise as a result of the rigidity of the amido fragment. As a result of this the planar rings should produce a pseudo ob_3 type complex and a predicted structure appears in Figure 13. In addition, the Co-$N_{(amide)}$ bonds are expected to have a bond length around 1.91 Å i.e., close to the value observed for the related [$CH_3CONHCo^{III}(NH_3)_5]^{2+}$ cation.[25] Further the N-$C_{(amide)}$ and C-$O_{(amide)}$ bonds are expected to be similar to the average bond distances observed for the fragments of N-$C_{(peptide)}$ (1.30 Å)[27] and C-$O_{(peptide)}$ (1.27 Å)[27] respectively.

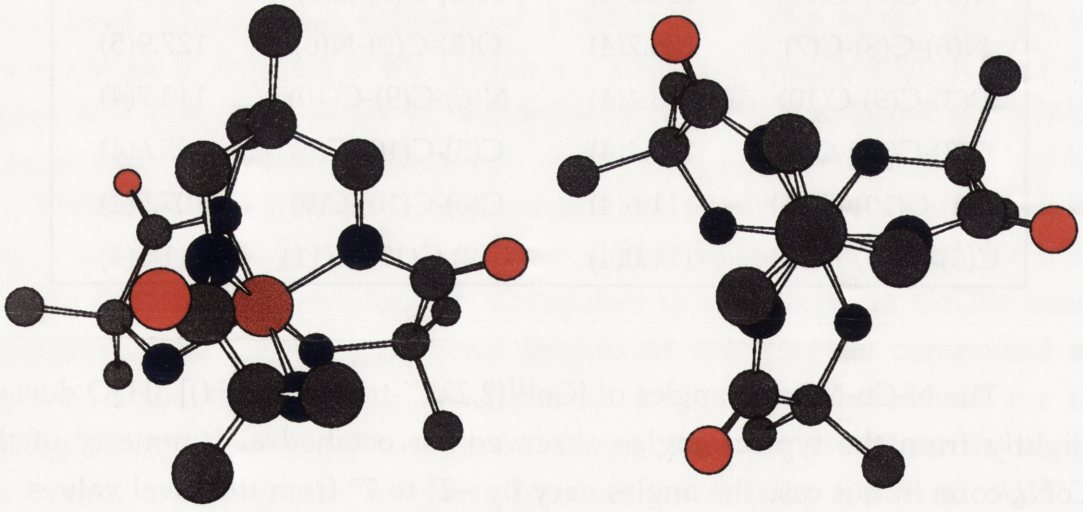

Figure 13

5.3.5 Electrochemistry

The cyclic voltammetry (CV), measured with a hanging mercury drop electrode (HMDE), of the two triamide complexes in aqueous solution appears in Figure 14 and Table 4.

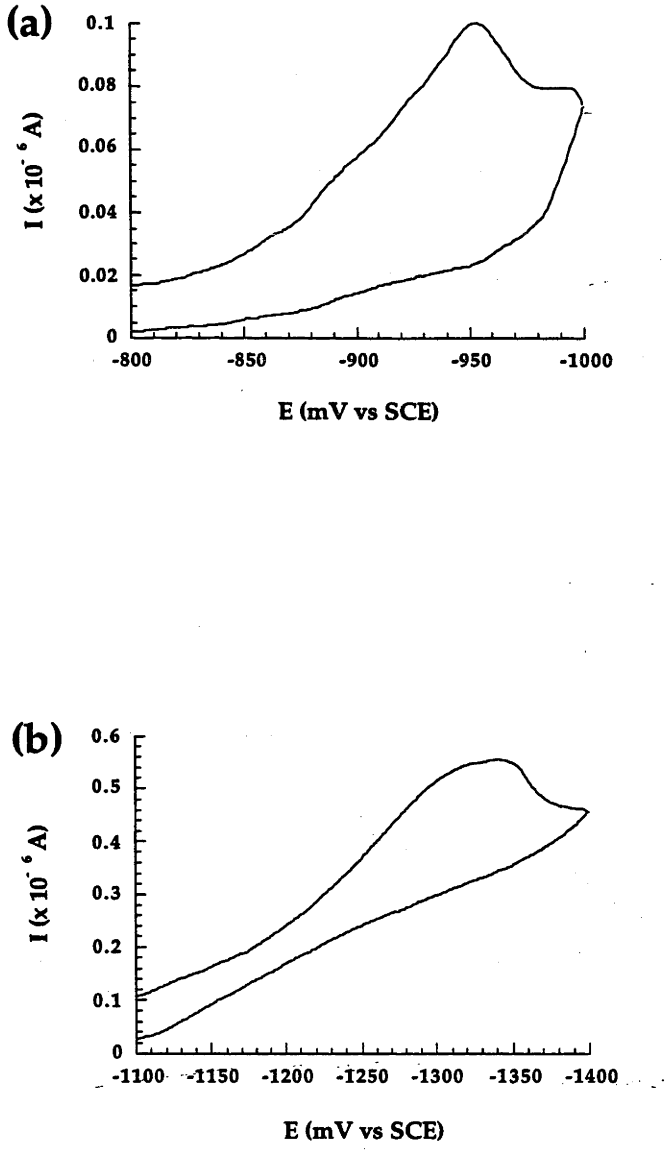

Figure 14. Cyclic voltammetry for (a) $[Co^{III}(2,2',2''\text{-trioxosen-3H})]^0$ and (b) $[Co^{III}(5,5',5''\text{-tri}(Me_2)\text{-}4,4',4''\text{-trioxosen-3H})]^0$ recorded in 0.1 M $NaClO_4$ at 20° C with an HMDE electrode at a scan rate of 20 mV s^{-1}.

Table 4. Electrochemical data for Co(III)/(II) couples of triamido, monoamido and saturated tripodal complexes (vs SCE). HMDE electrode; 1mM solutions of complex in 0.05 M $KH_3(C_2O_4)_2.2H_2O$, 0.1 M $NaClO_4$ and 0.05 M Na_3PO_4 at 20° C with a scan rate of 20 mVs^{-1}.

Complex	pH	$E_{1/2}$ vs SCE (V)	E_{pc} vs SCE (mV)	E_{pa} vs SCE (mV)	i_{pc}/i_{pa}	ΔE_p
$[Co^{III}$(2,2′,2″-trioxosen-3H)$]^0$	1.68 [a]	-	-565	-	-	-
$[Co^{III}$(2,2′,2″-trioxosen-3H)$]^0$	~7 [b]	-	-954	-	-	-
$[Co^{III}$(2,2′,2″-trioxosen-3H)$]^0$	12.04 [c]	-	-1104	-	-	-
$[Co^{III}$(5,5′,5″-tri(Me_2)-4,4′,4″-trioxosen-3H)$]^0$	1.68 [a]	-	-782	-	-	-
$[Co^{III}$(5,5′,5″-tri(Me_2)-4,4′,4″-trioxosen-3H)$]^0$	~7 [b]	-	-1332	-	-	-
$[Co^{III}$(5,5′,5″-tri(Me_2)-4,4′,4″-trioxosen-3H)$]^0$	12.04 [c]	- [d]	-	-	-	-
$[Co^{III}(CO_2Et$-2-oxosen-H$)]^{2+}$	1.68 [a]	-	-462	-	-	-
$[Co^{III}(CO_2Et$-2-oxosen-H$)]^{2+}$	~7 [b]	-	-500	-	-	-
$[Co^{III}(CO_2Et$-2-oxosen-H$)]^{2+}$	12.04 [c]	-0.76	-795	-720	0.98	75
$[Co^{III}$(sen)$]^{3+}$ [28]	7.0	-0.5	-	-	-	-

[a] 0.05 M $KH_3(C_2O_4)_2.2H_2O$, [b] 0.1 M $NaClO_4$, [c] 0.05 M Na_3PO_4, [d] Not observable by HMDE.

The Co(III)/(II) reduction potential differs for the two triamide compounds. For $[Co^{III}(2,2',2''\text{-trioxosen-3H})]^0$ the reduction wave occurs at E_{pc} = -0.95 V at pH ~7 while for the second triamide, $[Co^{III}(5,5',5''\text{-tri}(Me_2)\text{-}4,4',4''\text{-trioxosen-3H})]^0$, the Co(III)/(II) potential appears at E_{pc} = -1.33 V in neutral pH. Both complexes displayed irreversible behaviour in all media at scan rates of 20 mVs^{-1} and higher. These results indicate that the potentials of both triamide complexes are more negative and much less reversible than that of the parent hexamine, $[Co^{III}(sen)]^{3+}$. Under the same conditions (neutral pH and and a scan rate of 20 mVs^{-1}) the reversible Co(III)/(II) reduction potential of this species occurs at $E_{1/2}$ = -0.5 V vs SCE. The potential of the Co(III)/(II) reduction wave depended largely on the pH of the medium employed in each triamide case. As the solutions were made more basic, the redox couples shifted to more negative values. The irreversible behaviour in acidic, neutral and basic solutions indicates that both protonation and deprotonation of the Co(III) moiety is involved and that rapid partial ligand dissociation is likely in the Co(II) state of each triamide under these conditions.

On the oxidation scan, Co(IV) appears to be inaccessible in water with these triamide ligand systems. No oxidation waves were observed for either triamide complex when scanned to 1.4 V with an EPG electrode. This was disappointing since it was hoped that by exchanging the three secondary amines of $[Co^{III}(sen)]^{3+}$ for three amido anionic nitrogen ligands, Co(IV) would have been attainable.

The $[Co^{III}(oxosen\text{-}H)]^{2+}$ molecule has a reduction potential 0.2 - 0.3 V more negative than that for $[Co^{III}(sen)]^{3+}$. The expected change for the triamido complex therefore could be 0.6 - 0.9 V more negative and the results appear to sustain this estimate.

5.3.6 Electronic Absorption Spectroscopy

Small differences exist in the absorption spectra of the two triamide complexes and these can be observed in Figure 15 while their electronic data compared to other Co(III) tripodal complexes are tabulated in Table 5.

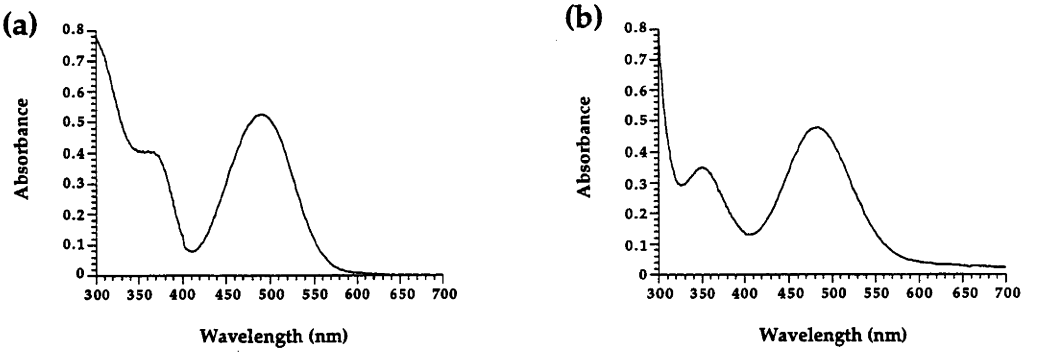

Figure 15. Electronic spectrum of (a) $[Co^{III}(2,2',2''\text{-trioxosen-3H})]^0$ and (b) $[Co^{III}(5,5',5''\text{-tri}(Me_2)\text{-}4,4',4''\text{-trioxosen-3H})]^0$ in water at 20° C.

Table 5. Electronic absorption data on some Co(III) triamide, monoamide and saturated tripodal complexes (1mM solutions in water at 20° C).

Complex	λ_{max} nm (ε_{max} $M^{-1}cm^{-1}$)	
	$^1T_{2g} \leftarrow {}^1A_{1g}$	$^1T_{1g} \leftarrow {}^1A_{1g}$
	Band Origin	Band Origin
	Transition	Transition
$[Co^{III}(2,2',2''\text{-trioxosen-3H})]^0$	358 (323)	490 (398)
$[Co^{III}(5,5',5''\text{-tri}(Me_2)\text{-}4,4',4''\text{-trioxosen-3H})]^0$	350 (214)	482 (292)
$[Co^{III}(CO_2Et\text{-}2\text{-oxosen-H})]^{2+}$	342 sh (163)	492 (159)
$[Co^{III}(sen)]^{3+}$	339 (117)	466 (118)

For $[Co^{III}(2,2',2''\text{-trioxosen-3H})]^0$ the two d-d absorptions occur at 358 nm and 490 nm while for the second triamide, $[Co^{III}(5,5',5''\text{-tri}(Me_2)\text{-}4,4',4''\text{-trioxosen-3H})]^0$, they appear at 350 nm and 482 nm respectively. The spectra are not much different from that of the $[Co^{III}(CO_2Et\text{-}2\text{-oxosen-H})]^{2+}$ ion.[24] Comparison between the two systems is valid here because the nature of the apical substituent has only a small influence on the position of the d-d bands.[29] In each instance, relatively weak absorption bands arise from the Laporte forbidden transitions of origin $^1T_{1g} \leftarrow {}^1A_{1g}$ and $^1T_{2g} \leftarrow {}^1A_{1g}$ (O_h parentage) for low spin Co(III) and a red shift occurs in the lower energy d-d transition of both complexes compared to the parent hexamine $[Co^{III}(sen)]^{3+}$. Consequently the two triamide compounds are red in colour

compared to that of the orange-yellow observed for the $[Co^{III}(sen)]^{3+}$ ion. In addition the band intensities of the two triamides are significantly greater than those of the saturated parent complex.

5.4 Discussion

5.4.1 Syntheses

Multi-step organic syntheses, employed in both cases, yielded the two triamide precursor ligands that were then complexed to cobalt. For the 2,2′,2″-trioxosen impure ligand mixture, the formation of the Co(III) complex allowed it to be purified from the other unwanted organic material. Methylation of the tri-ester precursor to this ligand was also essential since the apical proton is very acidic as a result of the three ester groups. Due to the delocalisation of charge over the three carbonyl groups, it would be difficult to get such an anion to function as a tripodal tridentate ligand. On the other hand for $[Co^{III}(5,5',5''\text{-tri}(Me_2)\text{-}4,4',4''\text{-trioxosen-}3H)]^0$ although its synthesis involved the use of a potentially hazardous azide intermediate, it was the method of choice since it produced the ligand with much less impurity.

The synthesis of the Co(III) complexes from Co(II), ligand, O_2 and charcoal were straightforward except for the ligand impurities. These Co(III) complexes were purified by ion exchange chromatography and well characterised by microanalysis, NMR, structural analysis, as neutral basically octahedral complexes.

5.4.2 Infra-red Spectroscopy

For the two triamide complexes, $[Co^{III}(2,2',2''\text{-trioxosen-}3H)]^0$ (amide carbonyl stretch = 1609 cm^{-1}) and $[Co^{III}(5,5',5''\text{-tri}(Me_2)\text{-}4,4',4''\text{-trioxosen-}3H)]^0$ (amide carbonyl stretch = 1568 cm^{-1}), the amide carbonyl stretching vibrations fall bellow that expected for an unbound secondary amide (1680 cm^{-1} to 1630 cm^{-1}). On the basis of what should occur theoretically, as described previously, the conclusion would be that both systems have the Co(III) ion bound to the amide nitrogen atoms which are all deprotonated. The crystallography on the $[Co^{III}(2,2',2''\text{-trioxosen-}3H)]^0$ complex does confirm that the Co(III) ion is bound to all three amido nitrogen atoms. Therefore, based on this evidence the IR theory can be also applied to the triamide tripodal compounds in the same way as the amide cage systems. Consequently, it can now be predicted with some confidence that the second triamide complex, $[Co^{III}(5,5',5''\text{-tri}(Me_2)\text{-}4,4',4''\text{-trioxosen-}3H)]^0$, displays the same type of binding as that of the $[Co^{III}(2,2',2''\text{-trioxosen-}3H)]^0$ complex. Overall, from the conclusions drawn from the cage and tripodal amide systems it has been demonstrated that IR spectroscopy can be a

useful tool to at least give some indication of the bonding characteristics within these types of compounds.

5.4.3 Electrochemistry

The Co(III)/(II) reduction waves of the two triamide complexes in water appear to be the most negative of all the Co(III) amide complexes reported to date. This arises from the presence of the three amido ions within the tripodal ligand which reduce the formal charge of the complex to zero. Consequently, the Co(III) ion becomes more difficult to reduce as a result of the exact same factors outlined earlier. Therefore, these factors result in a substantial shift of the Co(III)/(II) potential to more negative values.

It follows that the effects should make the neutral complex much easier to oxidise to Co(IV). However in aqueous solution the desired Co(IV) systems are not accessible with either of the triamide tripodal complexes, $[Co^{III}(2,2',2''\text{-trioxosen-3H})]^0$ and $[Co^{III}(5,5',5''\text{-tri}(Me_2)\text{-}4,4',4''\text{-trioxosen-3H})]^0$. This was somewhat surprising and disappointing since Cu(III), Ni(III) and Ni(IV) are readily accessible in water with related macrocyclic triamide ligands. At this stage there does not appear to be an authentic example of an octahedral Co(IV) triamide complex in water although Co(IV) probably exists as a four coordinate d^5 tetraamide macrocyclic complex.[30] All these results to date indicate how difficult it is to oxidise Co(III) to Co(IV) even when the net positive charge is substantially reduced and the negative charge on the Co(III) centre is increased.

5.4.4 Electronic Spectroscopy

With the incorporation of three amido groups into the ligand framework a red shift occurs in each triamide spectrum compared to the saturated $[Co^{III}(sen)]^{3+}$ ion (Table 5). Both triamide complexes are red and more intense in colour than the yellow hexamine parent. A similar red shift also occurs for the $[Co^{III}(\{NO_2\}_2\text{-sar})]^{3+}$ complex after it loses a proton from one of the coordinated secondary nitrogen centres (pK_a ~10). The absorption shift to lower energy also indicates that both triamides possess weaker ligand fields than that of $[Co^{III}(sen)]^{3+}$. As mentioned previously this weakening of the ligand field for the octahedral amide complexes here results from the deprotonated amide nitrogen atoms possessing a lone pair of electrons which interact via a π interaction with the occupied metal

based t_{2g} electrons.[31] Therefore, again the positioning of the d-d bands is influenced by the same factors which affected the earlier amido cage systems.

Again, like the amido cage systems in Chapters 3 and 4 both of the triamide tripodal complexes also display intensities that are greater than that of the parent hexamine $[Co^{III}(sen)]^{3+}$. For the triamide complexes this is also ascribed to the presence of the three amido fragments within each ligand which affect the metal by distorting its environment making it less octahedral and also more charge transfer in character. As described previously this arises because the symmetry restrictions are somewhat diminished and as a consequence the observed transitions become more allowed and therefore more intense. This effect would be expected to increase with an increasing number of amide groups present within a ligand.

Simplistically, the absorption bands of $[Co^{III}(2,2',2''\text{-trioxosen-3H})]^0$ might be expected to occur at higher energy than that of $[Co(sen)]^{3+}$ because the *ob*$_3$ conformation of the triamide complex plays a part in the positioning of the two observed absorption envelopes. In going from a *lel*$_3$ to an *ob*$_3$ conformation there is an increased interaction between the ligand and metal orbitals induced by the somewhat smaller *ob*$_3$ cavity. In the simple saturated amine cage systems, a shift of about 30 nm to higher energies is observed in the change from *lel*$_3$ to *ob*$_3$ for the Co(III) complexes. Not only do the two ligand field bands move to lower wavelengths but their intensities decrease at the same time as the Co(III) complex becomes more octahedral in character. However, opposing this shift is the effect of the increased negative charge on the ligand itself which inherently shifts the absorptions to longer wavelengths. Therefore a trade-off exists between the shift to higher energy in going from *lel*$_3$ to *ob*$_3$ and the movement to lower energy forced upon the complex by the anionic ligand. This property is less evident for $[Co^{III}(5,5',5''\text{-tri}(Me_2)\text{-}4,4',4''\text{-trioxosen-3H})]^0$ where the *ob*$_3$ character is probably not so pronounced simply because the -NH_2-$C(Me)_2$-C(O)-N^-- chelate is maybe near planar for each ring.

5.4.5 Attempted Capping Reactions on $[Co^{III}(2,2',2''\text{-trioxosen-3H})]^0$

Despite many different capping reactions being attempted with $[Co^{III}(2,2',2''\text{-trioxosen-3H})]^0$, none of them produced the desired cage complex. Changing reaction conditions and solvents did not cause much change in the observed results. Clearly with the incorporation of the amide

fragments it is now more difficult for the three primary amines to partake in the capping reactions. A possible explanation for this is that the pK of the three primary amines in this case has increased as a result of the coordinated amides reducing the net charge of the complex and an increased electon density at the metal. Also it is known that an *ob*$_3$ tripodal complex is difficult to cap and in fact there has not been a successful encapsulation of a complex of this type to date. Despite the failure to make the cages, these tripodal ligands have interesting aspects. The Ni(IV) and Fe(IV) chemistry with such ligands could be especially interesting.

5.4.6 Comparison of the Methods used for the Synthesis of Amido Cage Complexes

Throughout this work three different approaches have been made to produce amide cage complexes. The first two methods proved to be useful in this regard and amido cage complexes were synthesised. In the template condensation reactions, a series of monoamido cage complexes with different apical substituents arose. The oxidation of $[Co^{III}(\{NH_3^+\}_2\text{-sar})]^{5+}$ with $Hg^{II}(OAc)_2$ further extended this area by producing diamido cage systems. However, although organic syntheses can readily produce triamido tripod ligands and finally Co(III) compounds, the formation of cage complexes from these templates has not yet been achieved. It is not clear why this is the case but several possible reasons are outlined above. Obviously, compared to the first two methods this route is not as feasible for the production of polyamide amide cage systems. Either more work is required to effect encapsulation or alternative methods for the production of a Co(III) triamido cage complex will have to be found.

5.4.7 Bonding Modes of the Amide Ligand

Different modes of bonding are possible with an amide ligand and it is interesting to describe some examples to highlight these variations and then compare them with those observed in cage and tripodal systems in this work. In principle, transition metal ions can coordinate to the amide moiety either via the oxygen or nitrogen atoms. As a result several different amide complexes have arisen with various transition metal ions. For instance, it has been shown that Co(III) has the ability to coordinate with the amide oxygen. However, relatively few Co(III) monodentate O-bound amide systems exist in the literature. Nevertheless a series of pentaamminecobalt(III) amide complexes, of the form shown in Figure 16a, have been characterised as CoN_5O chromophores by UV/visible, ^{13}C and

^1H NMR spectroscopy.[32] The ^{13}C NMR in particular showed that the chemical shift for the C=O resonance is increased on coordination and is higher than that found in related N-bonded amide complexes. These data are also evidence that the carbonyl group becomes polarised by direct coordination to the metal. Further evidence of the existence of O-bonded amide systems comes from X-ray crystallography. Analysis of the crystals of the racemic β-(triethylenetetramine-O-ethylglycylglycine)cobalt(III) perchlorate hydrate (β-[Co^{III}(trien)(Gly-Gly-OEt)]$ClO_4.H_2O$)[33] complex confirmed that the amide carbonyl oxygen is coordinated to the Co(III) (Figure 16b). Like in other metal amide complexes, the carbonyl oxygen atom in this example is preferred to the amide nitrogen atom as the metal binding site at pH's where the amide proton is not dissociated.

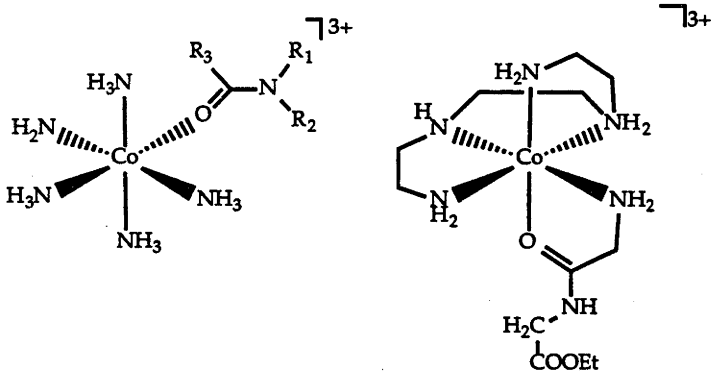

Figure 16

In another example, the structure of the bidentate complex [$Co^{III}(en)_2$(S-AlaenH)]$(NO_3)_2(ClO_4)_2$ [34] (Figure 17a) containing protonated ethylenediamine attached to the acyl function of the chelated (S)-alanine also showed that the Co(III) ion is bonded to the amide oxygen. It is also possible for other metal ions to form O-bonded amides. When Zn(II) and a urea-carrying pyridine ligand are mixed a zinc complex is formed (Figure 17b).[35] X-ray crystallography of the resultant complex showed the zinc had complexed the amide oxygen atom. In this and the previous example the $M\text{-}O_{(amide)}$ bond is shorter than the remaining metal-ligand distances.

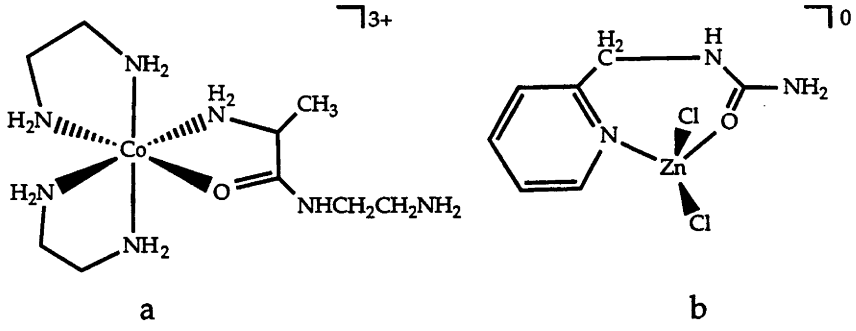

Figure 17

Complexation of transition metal ions by the amide nitrogen atom would be by far the most common type of metal-amide bonding observed. It has also been shown on numerous occasions that metal ions readily substitute for a nitrogen-bound amide hydrogen in solution. A strong metal-$N_{(amide)}$ bond results. Perhaps one of the most simple examples of an N-bonded amide is the acetamidopentaamminecobalt(III) ion[25] (Figure 18a). The X-ray crystallography of this complex clearly established that the acetamide was nitrogen bound to the cobalt atom. As observed earlier bidentate N-bonded amido complexes are also possible (Figure 18b). In this instance a crystal structure was not obtained however the physical data confirm the existance of the Co^{III}-$N_{(amido)}$ bond.

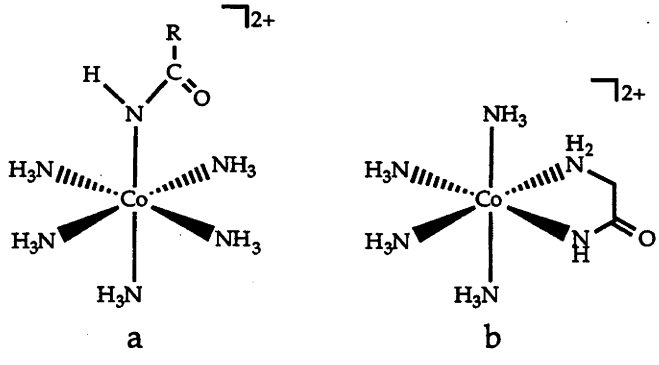

Figure 18

Other metal-N amide complexes also exist which display the same type of bonding. For example, the crystal structure of the bis(glycylglycinato)cobalt(III) ion[26] (Figure 19a) has been determined to be an N-bonded amide. This complex is also interesting in that when placed in acidic conditions it takes up two protons per complex ion and

protonation occurs at the $O_{(amide)}$ atoms (Figure 19b) which was also confimed by X-ray crystallography.[26] Although evidence exists that protonation occurs at the amide oxygen while the nitrogen atom is bound to a metal ion, crystal structures are rare.

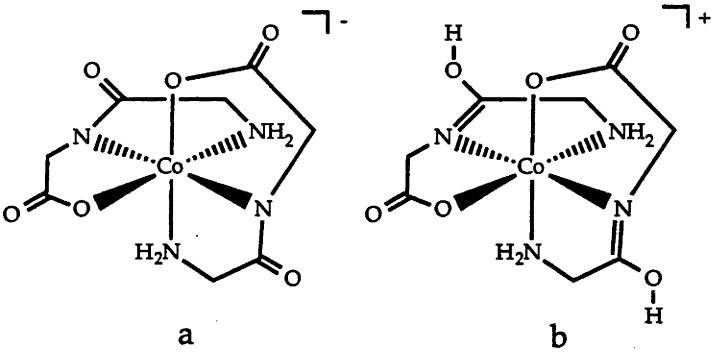

Figure 19

Another mode of amide bonding possible is that the metal may complex the amide nitrogen while it is still protonated. This is certainly rare but it has been shown to exist crystallographically with a Cu(II) substituted urea complex (Figure 20). In this form the amide moiety displays different properties to it's usual amido counterpart. Although the urea functionality (N-C-O-NH-R) is still planar, the $N\text{-}C_{(amide)}$ bond is significantly longer (1.45 Å) than that expected for a $N\text{-}C_{(amido)}$ distance (1.30 Å). Furthermore, the $C\text{-}O_{(amide)}$ distance (1.22 Å) is shorter than the anticipated $C\text{-}O_{(amido)}$ length of 1.27 Å. These results provide firm evidence that the amide resonance usually associated with the coordinated amido group is absent when the coordinated amide nitrogen atom remains protonated. Consequently, the amide when in this form is expected to be a weaker σ-donor than that of its amido counterpart. Therefore, the metal-$N_{(amide)}$ distance is expected to be slightly longer than that observed in the more common amido complexes.

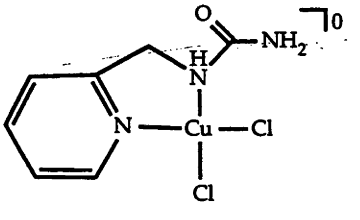

Figure 20

Many other X-ray crystallographic structures have been determined for a range of transition metal N-bound amido complexes and a selection of these appear in Figure 21.[36-40] Again these types of systems display short metal-amide N bonds, compared to the other metal ligand distances, while the amide nitrogen binds the metal with the nitrogen deprotonated.

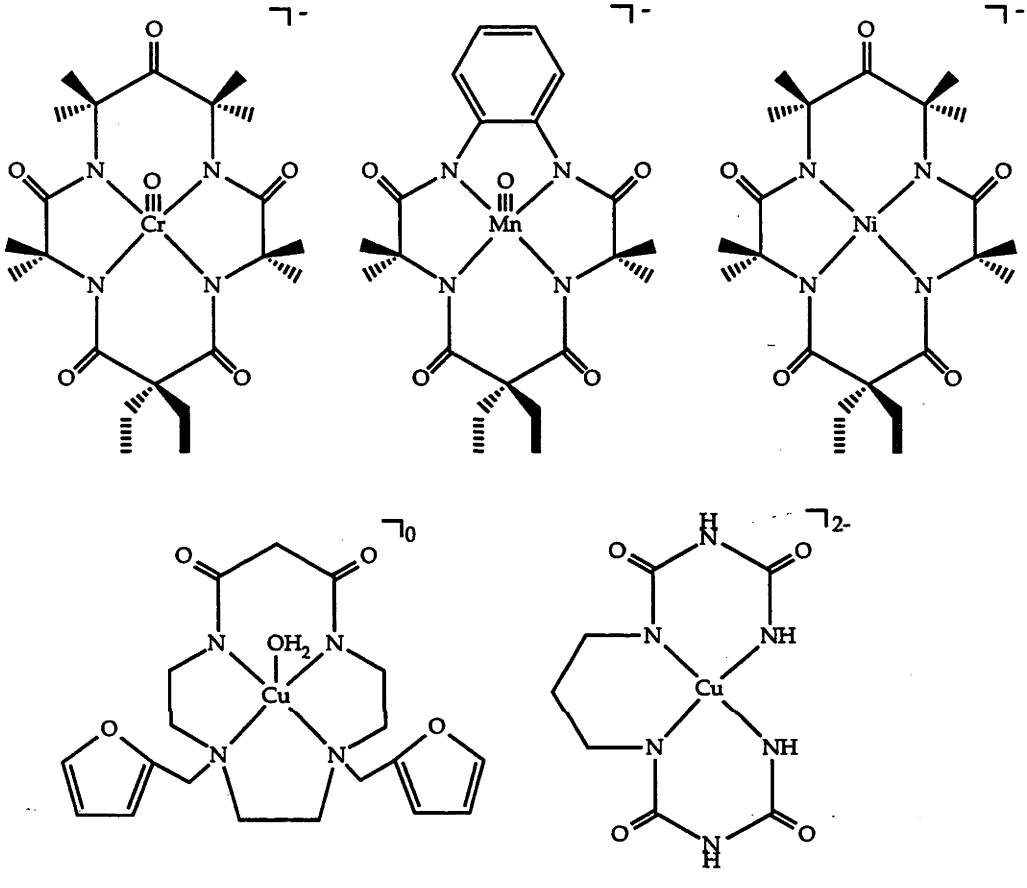

Figure 21

Throughout this work it has been shown that the metal ion generally coordinates to the cage and tripodal amido nitrogen atom which is deprotonated. Therefore, the cage and tripodal amide systems in this work display the most common type of bonding expected for a metal-amide bond. However, absolute confirmation of this type of binding, within the cage and tripodal amido systems, came from the X-ray crystallography on the $[Co^{III}(Me,CN\text{-}2\text{-}oxosar\text{-}H)]^{2+}$, $[Fe^{III}(Me,COOH\text{-}2\text{-}oxosar\text{-}H)]^{2+}$ and $[Co^{III}(2,2',2''\text{-}trioxosen\text{-}3H)]^{0}$ complexes. For the other cage and tripodal amido complexes, for which structures were not obtained, the physical data suggested metal-$N_{(amide)}$ bonding within these systems as well.

It is also not possible for the cage amido ligand to undergo a rearrangement of the amide from N to O bonding. Dreiding models indicate that this would create considerable strain in the cage system which would be extremely unfavourable. Therefore, O-bonded amido cage systems would not be expected to arise. Also, amido cage systems protonated at the oxygen while the deprotonated nitrogen atom is bonded to a metal have not yet been observed. It is also envisaged that such systems would be rare as the metal ion inhibits protonation at the oxygen atom in these cases.

A type of bonding that the amide cage systems are capable of and one which is not usually observed crystallographically is that displayed by the $[Ni^{II}(COO^{-}\text{-}2\text{-}oxosar)]_2^{2+}$ ion. This system has the Ni(II) ion of each complex bonded to the amide nitrogen atom which is still protonated. For this type of bonding arrangement to occur the metal probably coordinated the amide nitrogen atom through a π-type interaction. Certainly this is an interesting result and one which is rare for any amide complex to adopt.

The metal can also choose not bond to the amide group which remains protonated. This is different from the situation observed for most other amide complexes where the metal ion shows some form of bonding to the amide moiety either O or N. The X-ray crystallography on the Cu(II) complex confirmed the metal ion was non-bonded and about 3 Å away from the amide nitrogen.

Clearly, different metal-amide bonding modes are possible within the cage and tripodal amide systems. Generally they display metal-$N_{(amido)}$ bonding which is the most common type of bonding observed for most amide complexes. However, O- or N-amide and non-bonded amide forms remain feasible for amide cage and tripodal systems. Determination of the crystal structure is currently the only way to conclusively prove the type of bonding present within the amide complex.

5.4.8 Replacing Cage Amine Nitrogen Atoms with Deprotonated Amido Groups

The properties observed for the two Co(III) tripodal triamido complexes within this work have shown that they are different to those of the saturated parent $[Co^{III}(sen)]^{3+}$. Although they show a similar trend to

that of the amido cage complexes described earlier. Quite obviously, it is the deprotonated amido group that has caused this change. Therefore, a comparison between the two types of complex, triamido triamine and hexaamine, will allow an evaluation of the effects of the deprotonated amido group within these tripodal systems compared to that of the amine group. One of the most notable changes occurs in the electrochemical data where the Co(III)/(II) couples for the triamides are more negative than that of $[Co^{III}(sen)]^{3+}$. This shows that the deprotonated amido group is more likely to be effective at stabilising metal ions into higher oxidation states than the amino group, the reasons for which were outlined in the earlier chapters. At the same time the electronic spectra of the Co(III) triamide complexes are red shifted compared to that of the saturated parent. Again this is due to the presence of the deprotonated amides within the ligand structure and an explanation on how they effect the observed red shift also appears earlier.

The crystallography of $[Co^{III}(2,2',2''\text{-trioxosen-3H})]^{0}$ also shows that the amide functions have some influence on the conformation of the complex. In this instance, the ethylenediamine chelates all display an *ob* configuration while the parent hexaamine, $[Co^{III}(sen)]^{3+}$, posesses a lel_3 conformation. The reason this occurs is that the trigonal C-N^{-} distances, of the amide functions, are shorter than those of the tetrahedral C-N bond length. This comes about as a result of the delocalisation of charge between the nitrogen and oxygen atoms of the amide group because of the presence of the deprotonated anionic amido nitrogen. Therefore, it follows that the cavity sizes of both triamide tripods are expected to be smaller than that observed for the saturated parent, $[Co^{III}(sen)]^{3+}$. Two other properties that the crystallography reveals are the Co-$N_{(amido)}$ distances are shorter than those observed for a normal Co-$N_{(amine)}$ distance and the Co(III) ion binds to the amide N atom only when it is deprotonated. Furthermore, the planarity of the amide group is maintained when the deprotonated trigonal peptide nitrogen is complexed to Co(III). The crystallography also revealed that when compared to a free peptide ligand, substitution of an amide proton by a metal ion leads to bond length changes in the direction of more double bond character in the C-N bond (from ~1.325 Å to ~1.30 Å) and less double bond character in the C-O bond (from ~1.24 Å to ~1.27 Å).[27,41]

One common property that is shared between $[Co^{III}(sen)]^{3+}$ and the triamide complexes is their stability over a wide pH range. For the triamides this property arises because the metal protects the amido unit

from both acid and base hydrolysis.[24] Therefore, the Co(III) ion makes the amide functions resistant to ring opening reactions. This comes about for two reasons; firstly the negatively charged deprotonated amide resists attack of an electron rich reagent. In the second instance, the positively charged metal ion inhibits addition of a proton at the oxygen, and the kinetic inertness of the metal-$N_{(amido)}$ bonds along with the delocalisation in the amide group inhibits addition at the amido nitrogen atom. However, one distinction between the triamide complexes compared to $[Co^{III}(sen)]^{3+}$ is that the three amido functions affect the reactivity of the remaining amine groups. It has now become very difficult to cap the remaining amine face of the triamide complexes, which is contrary to the situation observed for the saturated parent $[Co^{III}(sen)]^{3+}$. As mentioned previously, one of the possible causes is the pK_a of the three primary amines has increased as a result of the coordinated amides reducing the overall charge at the complex and thus the ease of forming imines to effect encapsulation.

5.5 Conclusions and Future Directions

Two new interesting tripodal triamide ligands have been synthesised, which form octahedral complexes with Co(III) although triamido cage complexes from these templates were not obtained. Clearly, the presence of the three amido ions within the tripodal ligand affects the ability of the template to form a cage. Therefore, further work is required to discover a way in which to produce cage ligands from these triamide tripods. However, the tripodal triamido complexes display some interesting properties that will require more investigation in the future especially as Fe, Cu and Ni complexes.

5.6 References

(1) Tabushi, I.; Taniguchi, Y.; Kato, H. *Tetrahedron Lett.* **1977**, *12*, 1049.

(2) Sandler, S. R.; Karo, W. In *Organic Functional Group Preparations.*; Academic Press: New York, 1968.

(3) Zhu, S.; Lin, H.; Lin, C.; Kou, F.; Chen, Y. T. *Inorg. Chim. Acta* **1995**, *59*, 147.

(4) Bu, X. H.; An, D. L.; Chen, Y. T.; Shionoya, M.; Kimura, E. *J. Chem. Soc. Dalton Trans.* **1995**, 2289.

(5) Krakowiak, K. E.; Bradshaw, J. S.; Izatt, R. M. *J. Heterocyclic Chem.* **1990**, *27*, 1585.

(6) Borovik, A. S.; Dewey, T. M.; Raymond, K. N. *Inorg. Chem.* **1993**, *32*, 413.

(7) Che, C. M.; Cheng, W. K. *J. Chem. Soc. Chem. Commun.* **1986**, 1443.

(8) Leung, W. H.; Ma, J. X.; Yam, V. W. W.; Che, C. M.; Poon, C. K. *J. Chem. Soc. Dalton Trans.* **1991**, 1071.

(9) Ko, P.-H.; Chen, T.-Y.; Zhu, J.; Cheng, K.-F.; Peng, S.-M.; Che, C.-M. *J. Chem. Soc. Dalton Trans.* **1995**, 2215.

(10) Grummon, G.; Rajagopalan, R.; Palenik, G. J.; Koziol, A. E.; Nosco, D. L. *Inorg. Chem.* **1995**, *34*, 1764.

(11) Lund, H.; Voigt, A. In *Organic Syntheses Collective Volume 2.*; 5th ed.; John Wiley and Sons: New York, 1948; Vol. 2; p 594.

(12) Böhme, H.; Häfer, L. *Chem. Ber.* **1966**, *99*, 281.

(13) Böhme, H.; Häfner, L. *Chem. Ber.* **1966**, *99*, 879.

(14) Collins, T. J.; Kostka, K. L.; Uffelman, E. S.; Weinberger, T. L. *Inorg. Chem.* **1991**, *30*, 4204.

(15) Sheldrick, G. M. In *Crystallographic Computing 3*; G. M. Sheldrick, C. Krüger and R. Goddard, Eds.; Oxford University Press: 1985; p 175.

(16) Beurskens, P. T.; Admiraal, G.; Beurskens, G.; Bosman, W. P.; Garcia-Granda, S.; Gould, R. O.; Smits, J. M. M.; Smykalla, C. *DIRDIF92 In The*

DIRDIF program system, Technical Report of the Crystallography Laboratory; University of Nijimegen: The Netherlands, 1992.

(17) Cromer, D. T.; Waber, J. T. In *International Tables of X-ray Crystallography*; The Kynoch Press: Birmingham, England, 1974; Vol. IV.

(18) Ibers, J. A.; Hamilton, W. C. *Acta Crystallogr.* **1964**, *17*, 781.

(19) Creagh, D. C.; McAuley, W. J. In *International Tables for Crystallography*; A. J. C. Wilson, Ed.; Kluwer Academic Publishers: Boston, 1992; Vol. C; p 219.

(20) Creagh, D. C.; Hubbel, J. H. In *International Tables for Crystallography*; A. J. C. Wilson, Ed.; Kluwer Academic Publishers: Boston, 1992; Vol. C; p 200.

(21) *teXsan: Crystal Structure Analysis Package*; Molecular Structure Corporation: 1985 & 1992.

(22) Okazaki, H.; Sakaguchi, U.; Yoneda, H. *Inorg. Chem.* **1983**, *22*, 1539.

(23) Bernhardt, P. V.; Bygott, A. M. T.; Geue, R. J.; Hendry, A. J.; Korybut-Daszkiewicz, B. R.; Sargeson, A. M.; Willis, A. C. *Inorg. Chem.* **1994**, *33*, 4553.

(24) Geue, R. J.; Petri, W. R.; Sargeson, A. M.; Snow, M. R. *Aust. J. Chem.* **1992**, *45*, 1681.

(25) Schneider, M. L.; Ferguson, G.; Balahura, R. J. *Can. J. Chem.* **1973**, *51*, 2180.

(26) Barnet, M. T.; Buckingham, D. A.; Freeman, H. C.; Hsu, I.-N.; van der Helm, D. *J. Chem. Soc. Chem. Commun.* **1970**, 367.

(27) Martin, R. B.; Sigel, H. *Chem. Rev.* **1982**, *82*, 385.

(28) Bond, A. M.; Lawrance, G. A.; Lay, P. A.; Sargeson, A. M. *Inorg. Chem.* **1983**, *22*, 2010.

(29) Lawrance, G. A.; Lay, P. A.; Sargeson, A. M. *Inorg. Chem.* **1990**, *29*, 4808.

(30) Collins, T. J.; Powell, R. D.; Slebodnick, C.; Uffelman, E. S. *J. Am. Chem. Soc.* **1991**, *113*, 8419.

(31) Bull, D. J.; Creaser, I. I.; Sargeson, A. M.; Skelton, B. W.; White, A. H. *Inorg. Chem.* **1987**, *26*, 3040.

(32) Angus, P. M.; Fairlie, D. P.; Jackson, W. G. *Inorg. Chem.* **1993**, *32*, 450.

(33) Buckingham, D. A.; Marzilli, P. A.; Maxwell, I. E.; Sargeson, A. M.; M., F.; Freeman, H. C. *J. Chem. Soc., Chem. Commun.* **1968**, 488.

(34) Buckingham, D. A.; Binney, G. S.; Clark, C. R.; Garnham, B.; Simpson, J. *Inorg. Chem.* **1985**, *24*, 135.

(35) Maslak, P.; Sczepanski, J. J.; Parvez, M. *J. Am. Chem. Soc.* **1991**, *113*, 1062.

(36) Collins, T. J.; Slebodnick, C.; Uffelman, E. S. *Inorg. Chem.* **1990**, *29*, 3433.

(37) Collins, T. J.; Powell, R. D.; Slebodnick, C.; Uffelman, E. S. *J. Am. Chem. Soc.* **1990**, *112*, 899.

(38) Collins, T. J.; Nichols, T. R.; Uffelman, E. S. *J. Am. Chem. Soc.* **1991**, *113*, 4708.

(39) Bu, X. H.; Zhang, Z. H.; Cao, X. C.; Ma, S. Y.; Chen, Y. T. *Polyhedron* **1997**, *16*, 3525.

(40) Barbier, J.-P.; Biyyadh, A. E.; Kappenstein, C.; Mabiala, N.; Hugel, R. P. *Inorg. Chem.* **1985**, *24*, 3615.

(41) Margerum, D. W.; Dukes, G. R. In *Metal Ions in Biological Systems*; H. Sigel, Ed.; Marcel Dekker: New York, 1974; Vol. 1; Chapter 5, p 157.

CHAPTER 6.

Metal-Directed Synthesis, Reactivity and Biological Activity of Cage Complexes with Ethyl and Propyl Substituents.

6.1 Introduction

The formation of coordinated imines in inorganic chemistry, by the template condensation reaction between aldehydes or ketones with amines in the presence of metal ions, has led to an extensive array of acyclic and cyclic ligands. These template type studies highlight the importance of coordinated imines.[1-3] They can also be generated by oxidative dehydrogenation of coordinated amines, as briefly outlined earlier, and by high dilution techniques[4] but this will not be discussed further as it is not directly relevant to the work of this chapter.

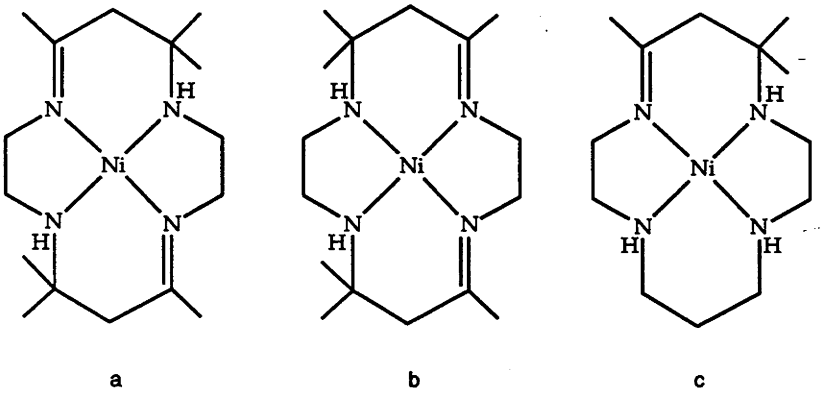

Figure 1

A number of excellent reviews of macrocyclic imine formation exist within the literature[5-7] and it is instructive to look at the specific types of template reactions that have been developed within the area. Perhaps the first and foremost reaction is that between acetone and Ni(II) ethylenediamine complexes[8] leading to the Curtis macrocyclic diimine ligand complexes (Figure 1a and b). This type of reaction was then extended further by reaction of acetone or a similar ketone with multidentate amine complexes to produce a series of macrocyclic imine compounds and one of these is displayed in Figure 1c. In all of the reactions, it has been proposed that a nucleophilic attack of a ketonyl carbanion on the carbon of a coordinated imine occurs.[8] Another way of producing coordinated imine complexes is to react complexed multidentate amines with bifunctional aldehydes or ketones (Figure 2a) or inversely to react complexed multidentate aldehydes or ketones with diamines (Figure 2b).[9-11] Series of pentadentate and larger ring system macrocyclic schiff base ligands have

been produced by condensation of 2,6-diacetylpyridine and various amines in the presence of a suitable metal ion template (Figure 2c).[12,13] In all these instances it is not clear if the condensation occurs between the amine and the C=O group while the former is bound to the metal ion. In fact it is most likely that the amine group reacts while dissociated and then recoordinates as the imine.

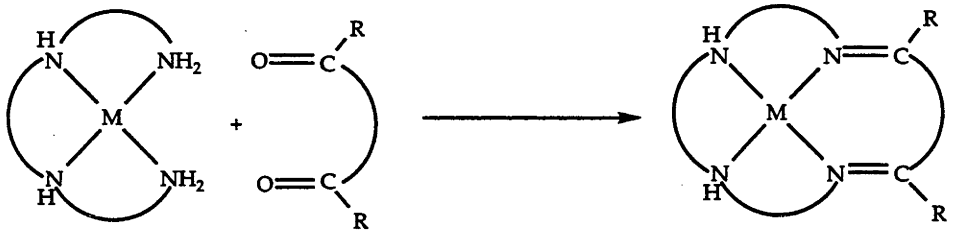

Figure 2a

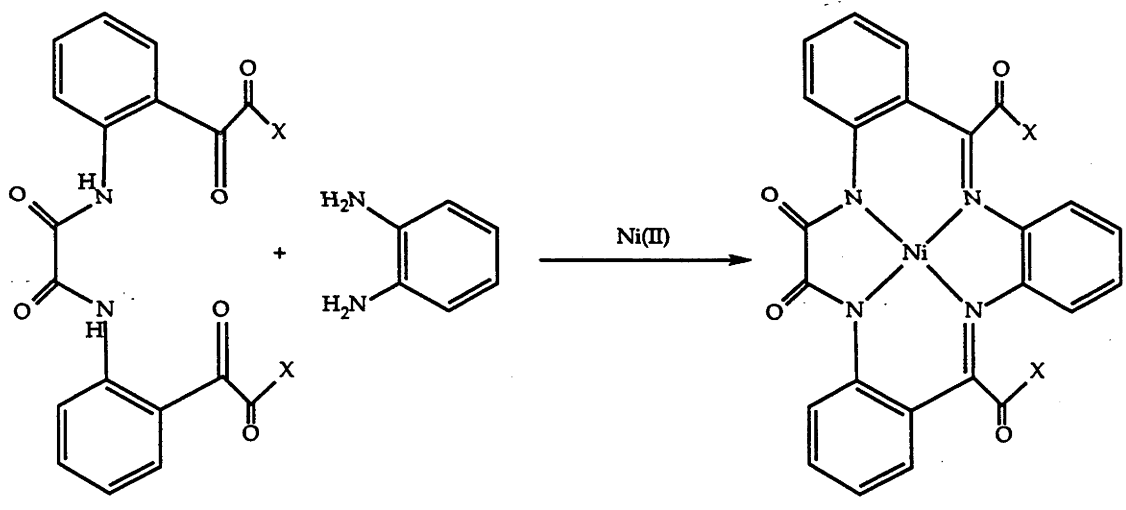

Figure 2b

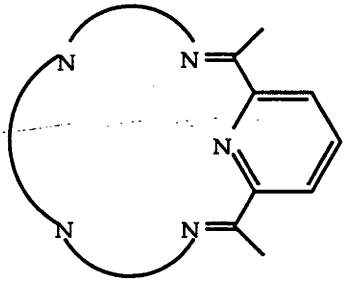

Figure 2c

Often Cu(II) and Ni(II) ions seem to be the metals of choice in template synthesis, at least for macrocyclic systems, although other metals have been used, such as Mg(II), Sr(II), Fe(II), Fe(III), Co(II), Pb(II) etc.[5] It is also possible, though rare, to use labile metal ions in the synthesis of macrobicyclic systems. An example is the production of $[Ni^{II}(sep)]^{2+}$ in very low yield.[14] However inert metal ion complexes of Co(III), Pt(IV), Ir(IV) and Rh(III) offer a more effective route to bicyclic systems.[15] These systems do not decompose like the labile systems generally do during encapsulating reactions. Two examples of macrobicyclisation about an inert metal centre are shown below. In these cases $[Co^{III}(sen)]^{3+}$ was treated with an aldehyde and formaldehyde in non-aqueous basic media to give monoimine cage complexes (Figure 3).[16,17] This type of reaction has the potential for adding various substituents to the cage and one aspect is explored in this chapter.

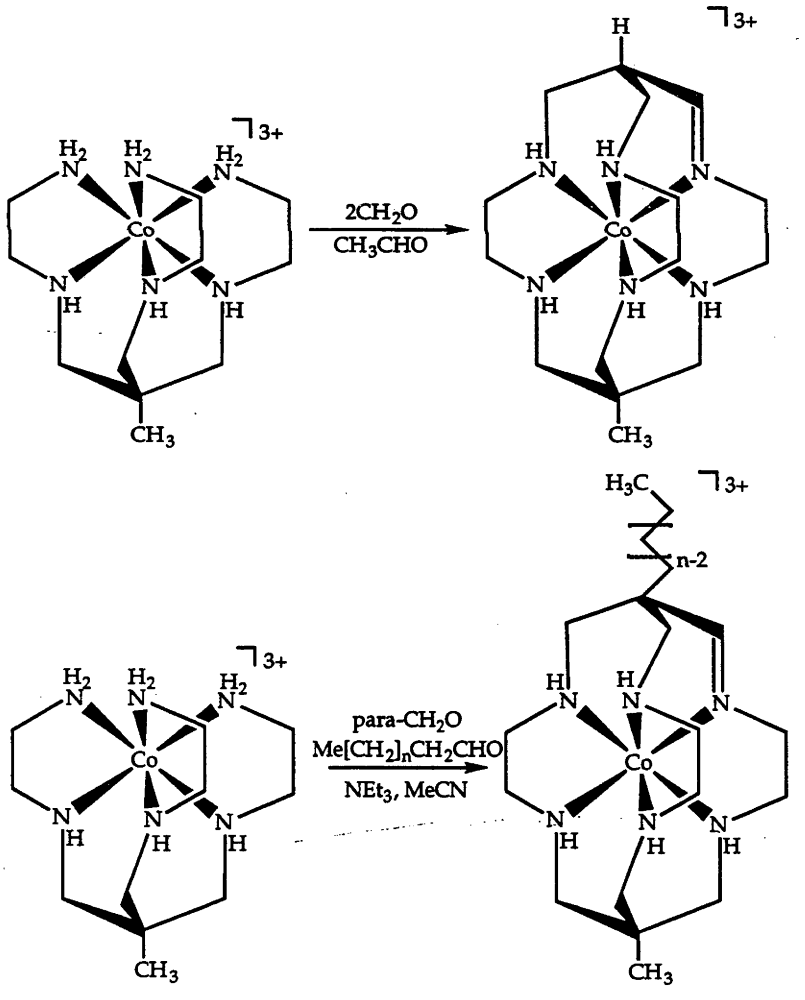

Figure 3

In addition further reactions of the coordinated imine complexes are possible. Reduction with borohydride leads to the fully saturated amine. A second route is to add a carbon acid to the imine. The coordinated imine is generally susceptible to attack by a variety of nucleophiles at the imine carbon centres and this factor makes them very useful reagents.[18,19] For example, it was found that when two forms of the Curtis macrocycles were reacted with nitromethane, in the presence of base, the less hindered form added nitromethyl pendant arms to the imine double bonds (Figure 4a)[20]. However for the chelated α diimine (1, Figure 4b) when reacted with nitromethane in the presence of base, the result was two different products (2 and 3, Figure 4b).[21] The major product (2, Figure 4b) is produced in 60% yield from a multistep process consisting of nitromethane addition to the C=N double bonds followed by HNO_2 elimination. Complex 3 (Figure 4b), in 3% yield, is probably formed from a 2 + 2 dinitro-adduct, which after oxidation by the nitric oxides present in the reaction mixture, eliminates one molecule of HNO_2.

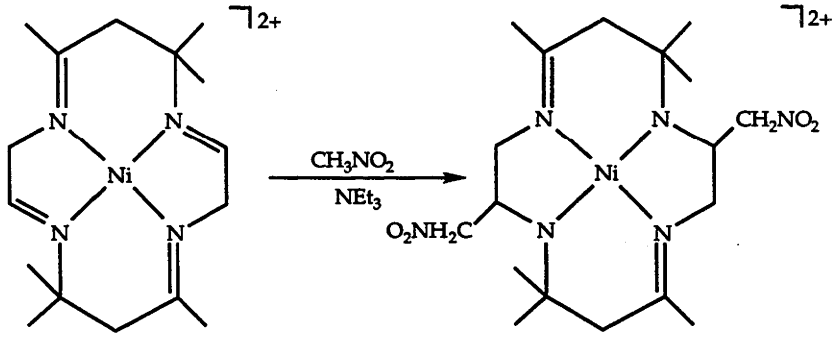

Figure 4a

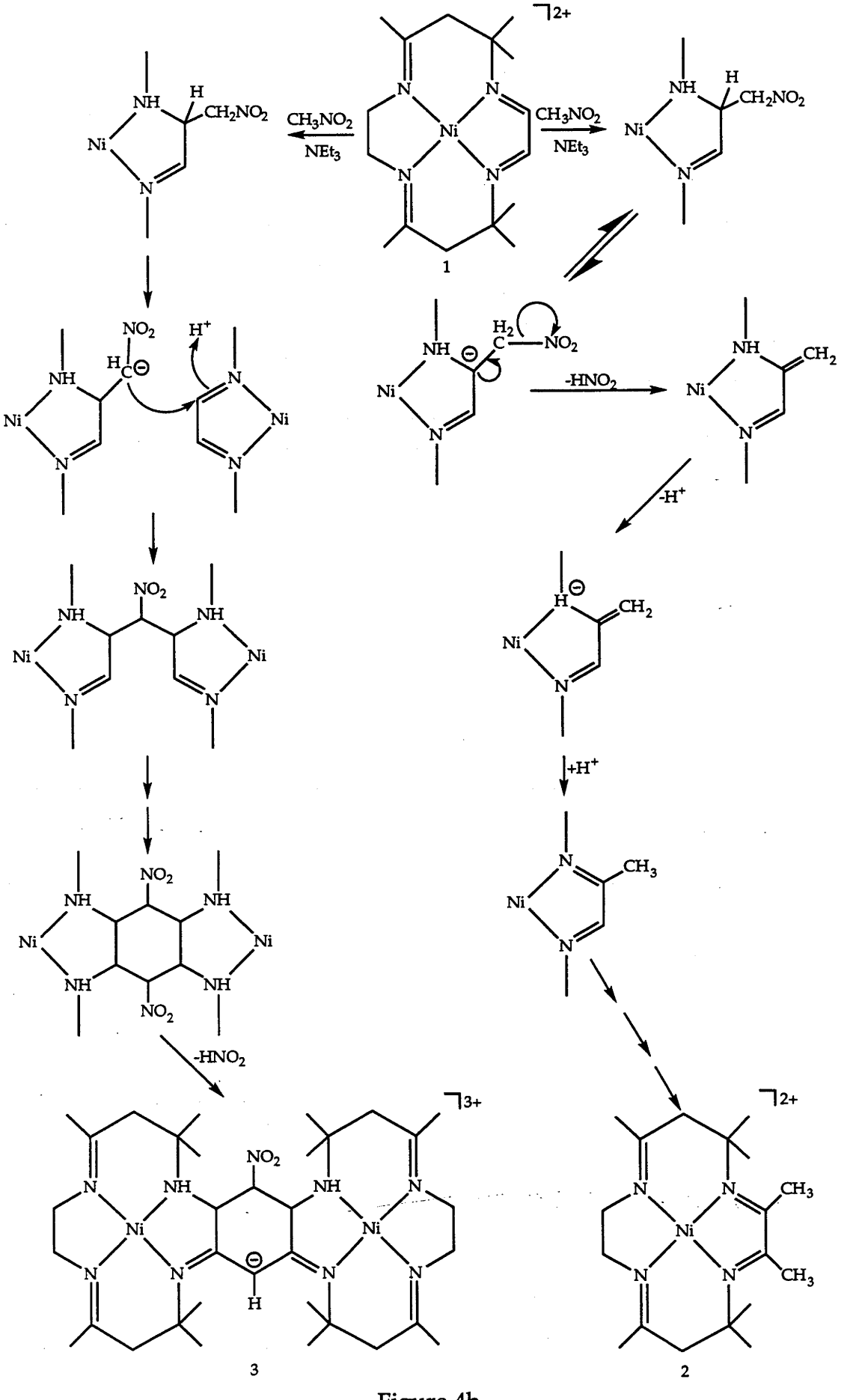

Figure 4b

Further work in this area showed that the nitromethyl pendant arms can be reduced to the corresponding amine (Figure 5).[22] The formation of the pendant amines then allows further chemistry to be pursued. In some cases, in these macrocyclic systems, the pendant amine can coordinate to the metal centre altering the complex properties,[23] while in other instances it is possible to tie extra groups, such as photosensitisers, to the pendant amines.[24] Other carbon acids, like acetylacetone and diethyl malonate, can be used in these reactions.[18] Preliminary work with Co(III) cage imine systems indicates that nitromethane possibly adds at the imine carbon under basic aqueous conditions.[25]

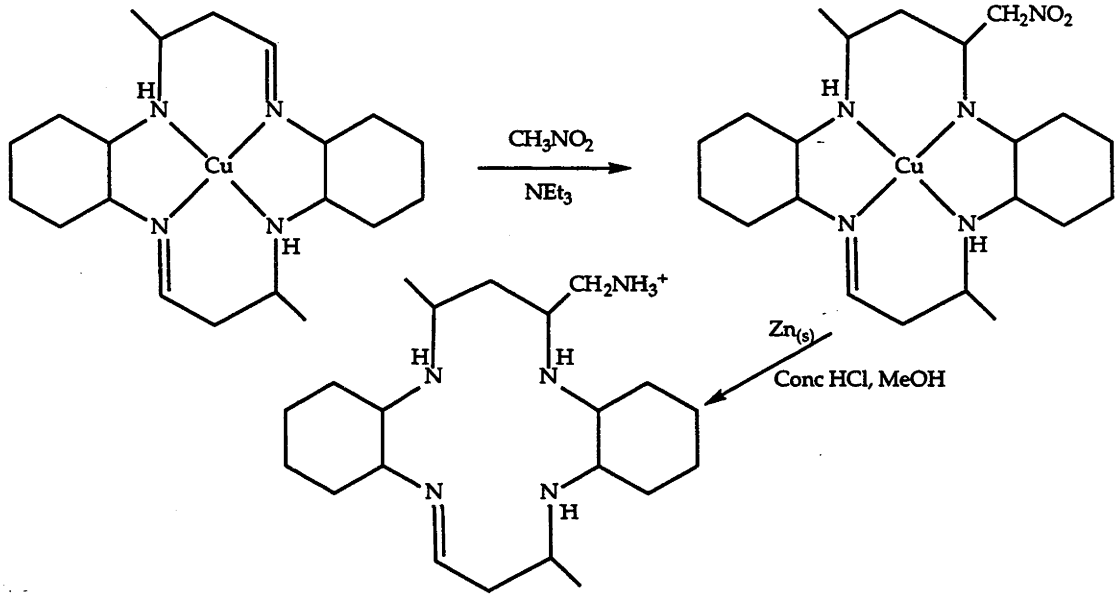

Figure 5

Many cyclic metal complexes, such as cage complexes, have uses in biology and one potential application is in the treatment of disease. For example, free cage ligands have the ability to remove Cu^{2+} from the liver and prevent it from entering cells. They also remove Zn^{2+} *in vivo*. After complexation, and detoxification of the system, the stable complex is eliminated from the cells by normal routes. The problem is to get selectivity for the metal ion and Cu^{2+} is favoured by diamsar. Moreover, the free ligands do not affect the Na^{+}, K^{+} or Ca^{2+} metabolism. Also, various cage complexes have been shown to be extremely stable and inert within animals. It has also been reported that Co(III) cage complexes with long alkyl chain tails have the power to disrupt biological membranes and may be useful as anthelmintics.

A number of synthetic routes exist to produce cage complexes that target areas of biology. One such synthesis involves firstly the template

production of alkyl tail imine cage complexes which are then reduced to the saturated analogue. This route allows the introduction of a variety of tails to the cage complex. Therefore, by using this strategy it may be possible to tailor the cage for use in various clinical areas. One such area is as control agents for viral infections since some macrocyclic amines[26] and cage reagents have been shown already to have the ability to inhibit the Human Immunodeficiency Virus (HIV) and the Hepatitis B Virus (HBV). Alkylated and imine cages are one such series of complexes. To date the antiviral properties of the alkyl tailed cages are largely unexplored so it is interesting to look at their characteristics in this regard. Few antiviral drugs are currently in widespread clinical use because of the difficulty of inhibiting viruses while leaving the non-infected cells unimpaired. This is especially true of the viruses within the families retroviridae, hepadnaviridae and flaviviridae. The cage complexes seem to be rather innocuous towards normal cells and display only a weak anticholinesterase activity. A selection of the alkyl tail cage systems developed in this work are therefore being tested against the above three viral families and will be the main thrust of this part of the thesis. Some background on these viral families follows.

The causative agent for Acquired Immune Deficiency Syndrome (AIDS), the Human Immunodeficiency Virus (HIV), which is also known as Human T-cell Lymphotropic Virus III (HLTV-III) is a member of the family Retroviridae. Infection with HIV is associated with depletion of T4 lymphocytes, brain disease and several types of cancer including Karposis Sarcoma. Patients infected with the virus have a high incidence of opportunistic infections and a significantly reduced life span. Another virus within the same family is the Human T-cell Lymphotropic Virus Type 1 (HLTV-1) the causative agent of Adult T-cell leukaemia, another infection with high mortality.

All members of the family retroviridae possess a unique enzyme, reverse transcriptase (RT), that is necessary for their replication. As this enzyme is not normally present in uninfected cells, it is considered a target for antiviral drugs. Another virus utilising reverse transcriptase during replication is the Hepatitis B Virus (HBV) which is a member of the family Hepadnaviridae. HBV causes widespread morbidty and mortality and is the main source of primary hepatocellular carcinoma in individuals who are chronic carriers of the virus. It is also the cause of canine arthritis/encephalitis, feline arthritis and duck hepatitis.

Flaviviruses are known to be the causative agents in a number of human diseases including the most important arthropod-borne viral afflictions of mankind - dengue and yellow fever, and Japanese encephalitis. In addition, eight flaviviruses cause disease in domestic or wild animals of ecomonic importance. Yellow fever and dengue fever are widespread and well known as mosquito borne diseases in tropical countries. There are between thirty to sixty million flavivirus infections per year including one million Japanese encephalitis infections. The extent of Hepatitis C is not known with any degree of certainty yet because an infection can exist for many years in a patient without any obvious symptoms. Hepatitis C produces a much higher rate of chronic liver infection than Hepatitis B, which is a recognised hazard in many countries. About fifty percent of patients develop chronic infections, compared to five to ten percent of those infected with Hepatitis B. Chronic infection causes cirrhosis of the liver, impairs liver function and twenty to thirty years later causes liver failure. It has been estimated that the rate of infection approaches and may exceed one percent of the population of Australia. There is no proven cure or vaccine of Hepatitis C. Therefore this is an important target area.

Effective vaccines are available for some flaviviruses. For example, yellow fever, Japanese encephalitis and tick-borne encephalitis. Treatment of dengue fever and Australian encephalitis relies on the patient's own defences; infections can be fatal. An antiviral drug to control infections of flaviviruses is thus highly desirable.

One chelating agent of a similar kind to those outlined has been found to be active in the inhibition of HIV. It is therefore relevant to give some background to this result and indicate how it might be effective and what the projection for similar reagents could be. These examples also point the way to elaboration of the cage with apical alkyl substituents.

In the fight against HIV many of the compounds tested target or interfere with the virus associated reverse transcriptase (RT). However, other potential targets are the inhibition of the entry of the virus and of the uncoating of the virus. Either could block the release of functional RNA inside the cells thus interrupting the HIV replicative cycle before it proceeds to the RT step. Few compounds exist that act at the uncoating of HIV or retroviruses in general. A possible example of compounds of this type is a series of bicyclam ligands which appear to be selective HIV inhibitors that target the viral uncoating event.[26] Since these reagents are

such good metal ion chelating reagents, metal ions and probably Zn^{2+} are presumed to be involved and the active agent appears to be effective early in the replicative process, i.e. it blocks the entry of the virus into the cell or interferes with the uncoating process. However these systems do not hold a metal and the lability of such systems *in vivo* reduces the molecules' effectiveness. Therefore, inert systems, like cage complexes, are worth exploration in this context.

The Co(III) cage compounds are kinetically inert and stable[15,27] and so offer better prospects for acting as HIV inhibitors; possibly at the uncoating stage. To this end the dimeric cage complex (Figure 6a) was first tried against HIV, however, although it was effective it was found to be far too toxic towards healthy cells.[28] Better results were obtained with the $[Co^{III}(\{NH_3^+\}_2\text{-sar})]^{5+}$ ion, but the Co(III) dimethyl cage complexes were more potent towards HIV. The alkyl tailed cage complexes were also found to be much less toxic towards healthy cells. Therefore a study of various Co(III) alkyl tail cage complexes is desirable so as to determine what tail length best affects the virus. Also, resolution of the best inhibitor into its enantiomers, may show that one enantiomer is more active than the other.

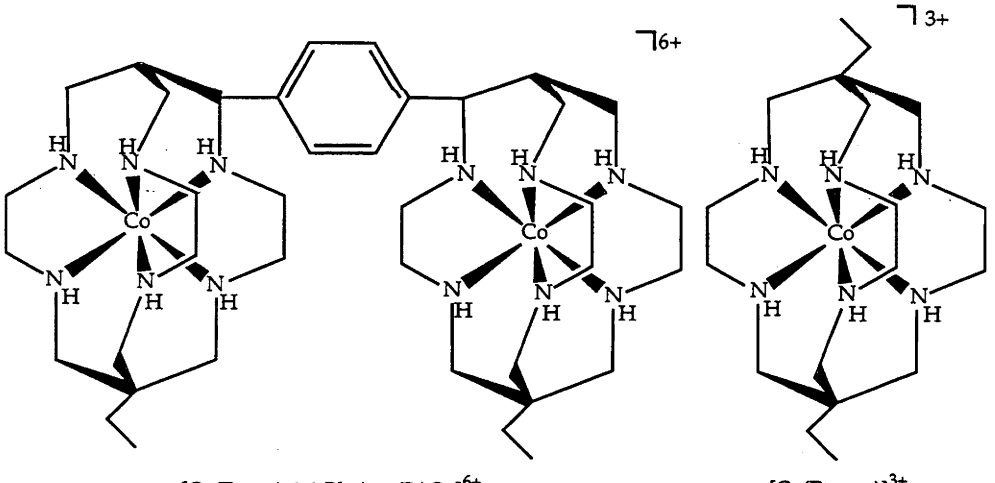

Figure 6

One aim of this study was to look at the antiviral properties of several dialkyl tailed Co(III) cage systems (Figure 6b) towards the AIDS virus and certain other viruses since the molecules shown in Figure 6b have already displayed activity in this area.

6.2 Experimental

6.2.1 Syntheses

All chemicals (AR grade) were used as received unless otherwise specified. [Tris(ethane-1,2-diamine)cobalt(III)]chloride.H_2O ($[Co^{III}(en)_3]Cl_3.H_2O$) and [1,1,1-Tris(4-amino-2-azabutyl)ethane)cobalt(III)]chloride.H_2O ($[Co^{III}(sen)]Cl_3.H_2O$) were prepared according to literature methods.[29-32]

<u>*cis*</u>-[(1,8-Diethyl-3,6,10,13,16,19-hexaazabicyclo[6.6.6]icosa-2,9-diene)cobalt-(III)]chloride.2.5H_2O, <u>*cis*</u>-$[Co^{III}(Et_2\text{-sar-2,9-diene})]Cl_3.2.5H_2O$, [(1,8-Diethyl-3,6,10,13,-16,19-hexaazabicyclo[6.6.6]icosa-2,6-diene)cobalt(III)]chloride.-$CH_3OH.2H_2O$, $[Co^{III}(Et_2\text{-sar-2,6-diene})]Cl_3.CH_3OH.2H_2O$, and <u>*trans*</u>-[(1,8-Diethyl-3,6,10,13,16,19-hexa-azabicyclo-[6.6.6]icosa-2,9-diene)cobalt(III)]-chloride.4H_2O, <u>*trans*</u>-$[Co^{III}(Et_2\text{-sar-2,9-diene})]Cl_3.4H_2O$.

$[Co^{III}(en)_3]Cl_3.H_2O$ (36.4 g; 0.1 mol) and $NaClO_4.H_2O$ (120 g; 0.85 mol) were added to acetonitrile (600 mL) and the solution stirred for 30 minutes, during which time some of the complex dissolved. To the stirred suspension was added paraformaldehyde (15 g; 0.5 mol) and 1-butyraldehyde (36 mL; 0.4 mol). After the mixture was stirred for a further 5 minutes, triethylamine (80 mL; 0.6 mol) was added. The mixture rapidly turned brown in colour. After stirring for a further 30 minutes, the reaction was quenched with glacial acetic acid (50 mL), diluted to approx 2 L and sorbed onto a column of Dowex 50Wx2 cation exchange resin (20 cm x 10 cm). The column was washed successively with water and 1 M HCl and the sorbed complexes were removed as a single band with 3 M HCl. Some material was removed from the column with concentrated HCl but this was shown by NMR to contain none of the desired product. The 3 M eluate was taken to dryness, diluted to 5 L with water, loaded onto a column of SP Sephadex C-25 resin (100 cm x 10 cm) and eluted with 0.1 M K_2SO_4. An initial fast moving green band was discarded. This was followed successively by a red band, a yellow band, a pale yellow band, a yellow band, a pale yellow band and finally a yellow band. Each band was desalted on Dowex, using HCl and taken to dryness. Each compound was then redissolved in methanol and then again taken to dryness to remove the last traces of HCl. The red and pale yellow bands were minor fractions and their NMR spectra indicated that each contained a number of different compounds, whose separation and characterisation was not pursued further. The NMR spectra of the other three yellow bands indicated that they corresponded to the three isomers of $[Co^{III}(Et_2\text{-diim-sar})]Cl_3$. The yield

of the three isomers was 0.57 g (1.1%), 1.93 g (3.4%) and 0.48 g (0.9%) respectively.

Anal. Calc. for isomer 1 $C_{18}H_{36}N_6Cl_3Co.2.5H_2O$: C, 39.5; H, 7.6; N, 15.4; Cl, 19.5. Found C, 39.6; H, 7.4; N, 15.2; Cl, 19.7. ^1H NMR (**δ**, 500 MHz, D_2O): 1.05 (t, 6H, CH_3, tail); 1.83 (m, 4H, CH_2 tail); 2.63 (m, 4H, CH_2); 2.82 (m, 1H, CH_2); 3.01 (m, 4H, CH_2); 3.06 - 3.21 (complex pattern, 6H, CH_2); 3.50 (m, 4H, CH_2); 4.11 (m, 1H, CH_2); 8.53 (s, 2H, H imine hydrogens). ^{13}C NMR (**δ**, D_2O): 8.4 ($\underline{C}H_3CH_2$); 26.4 ($CH_3\underline{C}H_2$); 53.1 ($\underline{C}qC=N$); 53.0, 54.4, 55.8, 56.3 ($N\underline{C}H_2$); 62.1 ($C=N-\underline{C}H_2$); 185.9 ($\underline{C}=N$). IR in KBr (ν-$_{max}$/cm^{-1}): 3100 (NH stretch); 2960, 2870 (C-H stretch); 1670 (C=N); 1460 (C-H deformation); 1045 (CH_2 rock). Low resolution ESMS (25 V) [m/z obs (calc) assignment where cage = $[^{59}Co^{14}N_6{}^{12}C_{18}{}^1H_{36}]^{3+}$]: 392.7 (393) (100%) [Cocage^{3+} - $2H^+$]$^+$; 428.7 (429) (68%) [Cocage^{3+} - H^+ + $^{35}Cl^-$]$^+$; 464.6 (465) (5%) [Cocage^{3+} + 2($^{35}Cl^-$)]$^+$.

Anal. Calc. for isomer 2 $C_{18}H_{36}N_6Cl_3Co.CH_3OH.2H_2O$: C, 40.0; H, 7.9; N, 14.8; Cl, 18.7. Found C, 39.9; H, 8.6; N, 14.6; Cl, 18.3. ^1H NMR (**δ**, 500 MHz, D_2O): 1.05 (t, 6H, CH_3, tail); 1.85 (m, 4H, CH_2 tail); 2.57 (m, 8H, CH_2); 2.78 (m, 1H, CH_2); 2.83 (m, 4H, CH_2); 3.15 (m, 1H, CH_2); 3.22 (m, 4H, CH_2); 3.38 (m, 1H, CH_2); 4.30 (m, 1H, CH_2); 8.50 (s, 2H, H imine hydrogens). ^{13}C NMR (**δ**, D_2O): 8.6 ($\underline{C}H_3CH_2$); 26.4 ($CH_3\underline{C}H_2$); 53.7 ($\underline{C}qC=N$); 51.8, 51.9, 54.4, 56.0 ($N\underline{C}H_2$); 65.3 ($C=N-\underline{C}H_2$); 187.2 ($\underline{C}=N$). IR in KBr (ν-$_{max}$/cm^{-1}): 3090 (NH stretch); 2970, 2860 (C-H stretch); 1660 (C=N); 1450 (C-H deformation); 1050 (CH_2 rock). Low resolution ESMS (50 V) [m/z obs (calc) assignment where cage = $[^{59}Co^{14}N_6{}^{12}C_{18}{}^1H_{36}]^{3+}$]: 392.7 (393) (100%) [Cocage^{3+} - $2H^+$]$^+$; 428.7 (429) (32%) [Cocage^{3+} - H^+ + $^{35}Cl^-$]$^+$; 464.6 (465) (18%) [Cocage^{3+} - 2($^{35}Cl^-$)]$^+$.

Anal. Calc. for isomer 3 $C_{18}H_{36}N_6Cl_3Co.4H_2O$: C, 37.7; H, 7.7; N, 14.6; Cl, 18.5. Found C, 37.9; H, 7.2 N, 14.9; Cl, 18.4. ^1H NMR (**δ**, 500 MHz, D_2O): 1.05 (t, 6H, CH_3, tail); 1.90 (m, 4H, CH_2 tail); 2.59 (m, 2H, CH_2); 2.69 (m, 4H, CH_2); 2.81 - 2.92 (m, 5H, CH_2); 2.99 (m, 2H, CH_2); 3.09 (m, 4H, CH_2); 3.13 (m, 1H, CH_2); 3.38 (m, 1H, CH_2); 4.28 (m, 1H, CH_2); 8.65 (s, 2H, H imine hydrogens). ^{13}C NMR (**δ**, D_2O): 8.3 ($\underline{C}H_3CH_2$); 26.7 ($CH_3\underline{C}H_2$); 52.7 ($\underline{C}qC=N$); 50.6, 51.5, 52.6, 56.3 ($N\underline{C}H_2$); 62.4 ($C=N-\underline{C}H_2$); 187.7 ($\underline{C}=N$). IR in KBr (ν-$_{max}$/cm^{-1}): 3100 (NH stretch); 2950, 2890 (C-H stretch); 1670 (C=N); 1465 (C-H deformation); 1045 (CH_2 rock). Low resolution ESMS (50 V) [m/z obs (calc) assignment where cage = $[^{59}Co^{14}N_6{}^{12}C_{18}{}^1H_{36}]^{3+}$]: 392.7 (393) (100%) [Cocage^{3+} - $2H^+$]$^+$; 428.7 (429) (40%) [Cocage^{3+} - H^+ - $^{35}Cl^-$]$^+$.

<u>cis</u>-[(1,8-Dipropyl-3,6,10,13,16,19-hexaazabicyclo[6.6.6]icosa-2,9-diene)cobalt-(III)]chloride.2H_2O, <u>cis</u>-[Co^{III}(Pr_2-sar-2,9-diene)]Cl_3.2H_2O, [(1,8-Dipropyl-3,6,-10,13,16,-19-hexaazabicyclo[6.6.6]icosa-2,6-diene)cobalt(III)]chloride.-2CH_3OH.4H_2O, [Co^{III}(Pr_2-sar-2,6-diene)]Cl_3.2CH_3OH.4H_2O, and <u>trans</u>-[(1,8-Dipropyl-3,6,10,13,16,19-hexaazabicyclo-[6.6.6]icosa-2,9-diene)cobalt(III)]-chloride.3H_2O, <u>trans</u>-[Co^{III}(Pr_2-sar-2,9-diene)]Cl_3.3H_2O.

The same procedure was employed as above except that 1-valeraldehyde was substitiuted for the 1-butyraldehyde. The yield of the three isomers in this particular case was 0.92 g (1.6%), 0.70 g (1.1%) and 0.86 g (1.5%) respectively.

Anal. Calc. for isomer 1 $C_{20}H_{40}N_6Cl_3Co.2H_2O$: C, 42.5; H, 7.8; N, 14.9; Cl, 18.9. Found C, 42.5; H, 7.6; N, 14.2; Cl, 18.5. ^1H NMR (**δ**, 500 MHz, D_2O): 0.97 (t, 6H, CH_3, tail); 1.45 (m, 4H, CH_2 tail); 1.75 (m, 4H, CH_2 tail); 2.63 (m, 4H, CH_2); 2.81 (m, 1H, CH_2); 3.01 (m, 4H, CH_2); 3.06 - 3.21 (complex pattern, 6H, CH_2); 3.49 (m, 4H, CH_2); 4.10 (m, 1H, CH_2); 8.53 (s, 2H, H imine hydrogens). ^{13}C NMR (**δ**, D_2O): 8.4 ($\underline{C}H_3CH_2$); 26.3 ($CH_3\underline{C}H_2$); 53.1 ($\underline{C}qC=N$); 53.0, 54.4, 55.8, 56.3 ($N\underline{C}H_2$); 62.1 ($C=N-\underline{C}H_2$); 185.7 ($\underline{C}=N$). IR in KBr (ν-$_{max}$/cm^{-1}): 3100 (NH stretch); 2960, 2870 (C-H stretch); 1670 (C=N); 1460 (C-H deformation); 1045 (CH_2 rock). Low resolution ESMS (50 V) [m/z obs (calc) assignment where cage = $[^{59}Co^{14}N_6{}^{12}C_{20}{}^1H_{40}]^{3+}$]: 420.7 (421) (100%) [Cocage^{3+} - 2H^+]$^+$; 456.7 (457) (45%) [Cocage^{3+} - H^+ - $^{35}Cl^-$]$^+$.

Anal. Calc. for isomer 2 $C_{20}H_{40}N_6Cl_3Co.2CH_3OH.4H_2O$: C, 40.8; H, 8.4; N, 13.0; Cl, 16.4. Found C, 40.6; H, 8.1; N, 13.3; Cl, 16.7. ^1H NMR (**δ**, 500 MHz, D_2O): 0.97 (t, 6H, CH_3, tail); 1.45 (m, 4H, CH_2 tail); 1.77 (m, 4H, CH_2 tail); 2.57 (m, 8H, CH_2); 2.78 (m, 1H, CH_2); 2.85 (m, 4H, CH_2); 3.14 (m, 1H, CH_2); 3.22 (m, 4H, CH_2); 3.36 (m, 1H, CH_2); 4.27 (m, 1H, CH_2); 8.50 (s, 2H, H imine hydrogens). ^{13}C NMR (**δ**, D_2O): 8.6 ($\underline{C}H_3CH_2$); 26.4 ($CH_3\underline{C}H_2$); 53.7 ($\underline{C}qC=N$); 51.8, 51.9, 54.4, 56.0 ($N\underline{C}H_2$); 65.3 ($C=N-\underline{C}H_2$); 187.2 ($\underline{C}=N$). IR in KBr (ν-$_{max}$/cm^{-1}): 3090 (NH stretch); 2970, 2880 (C-H stretch); 1660 (C=N); 1450 (C-H deformation); 1050 (CH_2 rock). Low resolution ESMS (50 V) [m/z obs (calc) assignment where cage = $[^{59}Co^{14}N_6{}^{12}C_{20}{}^1H_{40}]^{3+}$]: 420.7 (421) (100%) [Cocage^{3+} - 2H^+]$^+$; 456.7 (457) (20%) [Cocage^{3+} - H^+ - $^{35}Cl^-$]$^+$.

Anal. Calc. for isomer 3 $C_{20}H_{40}N_6Cl_3Co.3H_2O$: C, 41.1; H, 7.9; N, 14.4; Cl, 18.2. Found C, 41.7; H, 7.8; N, 14.2; Cl, 18.3. ^1H NMR (**δ**, 500 MHz, D_2O): 0.98 (t, 6H, CH_3, tail); 1.44 (m, 4H, CH_2 tail); 1.81 (m, 4H, CH_2 tail); 2.59 (m, 2H, CH_2); 2.68 (m, 4H, CH_2); 2.85 - 2.92 (m, 5H, CH_2); 3.00 (m, 2H, CH_2); 3.06 (m, 4H, CH_2); 3.11 (m, 1H, CH_2); 3.38 (m, 1H, CH_2); 4.26 (m, 1H, CH_2); 8.65 (s, 2H,

H imine hydrogens). ^{13}C NMR (δ, D_2O): 8.3 ($\underline{C}H_3CH_2$); 26.7 ($CH_3\underline{C}H_2$); 52.7 ($\underline{C}qC=N$); 50.6, 51.5, 52.6, 56.3 ($N\underline{C}H_2$); 62.4 ($C=N-\underline{C}H_2$); 187.7 ($\underline{C}=N$). IR in KBr ($\nu\tilde{}_{max}/cm^{-1}$): 3100 (NH stretch); 2970, 2880 (C-H stretch); 1670 (C=N); 1465 (C-H deformation); 1050 (CH_2 rock). Low resolution ESMS (50 V) [m/z obs (calc) assignment where cage = $[^{59}Co^{14}N_6{}^{12}C_{20}{}^{1}H_{40}]^{3+}$]: 420.7 (421) (100%) [$Cocage^{3+}$ - $2H^+$]$^+$; 456.7 (457) (38%) [$Cocage^{3+}$ - H^+ - $^{35}Cl^-$]$^+$.

Λ-(-)$_D$-[(1,8-Diethyl-3,6,10,13,16,19-hexaazabicyclo[6.6.6]icosane)cobalt(III)]-chloride.3H_2O, Λ-(-)$_D$-[$Co^{III}(Et_2$-sar)]$Cl_3.3H_2O$ and Δ-(+)$_D$-[(1,8-Diethyl-3,6,10,13,16,19-hexaazabicyclo[6.6.6]icosane)cobalt(III)]chloride.2H_2O, Δ-(+)$_D$-[$Co^{III}(Et_2$-sar)]$Cl_3.2H_2O$.

[$Co^{III}(Et_2$-sar-2,6-diene)]$Cl_3.CH_3OH.2H_2O$ (1 g; 2.01 x 10^{-3} mol) was dissolved in 50 mL of a carbonate buffer solution (pH 10), to this was added solid $NaBH_4$ (1 g; 0.03 mol) and the resultant mixture was stirred for a further 60 minutes. The reaction mixture was quenched with excess acetic acid, diluted to 4 litres and sorbed onto a column of Dowex 50Wx2 cation exchange resin (10 cm x 5 cm) in the H^+ form. The column was washed sequentially with water, 0.5 M HCl and the complex eluted with 3 M HCl. An orange/yellow band separated from some red polymeric material which remained at the top of the column. The collected orange band was taken to dryness, dissolved in water and resorbed onto SP Sephadex C-25 cation exchange resin (100 cm x 2 cm). Elution with 0.15 M $Na_2[Sb_2((+)tartrate)_2]$ resolved the complex into its respective enantiomers. These were collected separately, desalted on Dowex and elution with 3 M HCl produced a single yellow band in each case which were subsequently stripped to dryness. The Λ enantiomer was the first off the column and the yields of Λ and Δ enantiomers were 0.43 g and 0.41 g respectively.

Anal. Calc. for Λ-$C_{18}H_{40}N_6Cl_3Co.3H_2O$: C, 38.6; H, 8.3; N, 15.0; Cl, 19.0. Found C, 39.2; H, 8.9; N, 14.6; Cl, 19.0. ^1H NMR (δ, D_2O): 0.69 (t, 6H, CH_3 tail); 1.15 (m, 4H, CH_2 tail); 2.13, 2.76 (AB doublet of doublets, 12H, CH_2 caps); 2.42, 2.91 (AA'BB' coupling pattern, 12H, CH_2 en). ^{13}C NMR (δ, D_2O): 7.5 ($\underline{C}H_3CH_2$); 28.1 ($CH_3\underline{C}H_2$); 46.2 ($\underline{C}q$); 53.6, 55.1 ($N\underline{C}H_2$). IR in KBr ($\nu\tilde{}_{max}/cm^{-1}$): 3050 (NH stretch); 2960, 2870 (C-H stretch); 1450, 1400 (C-H deformation); 1065 (CH_2 rock). Low resolution ESMS (80 V) [m/z obs (calc) assignment where cage = $[^{59}Co^{14}N_6{}^{12}C_{18}{}^{1}H_{40}]^{3+}$]: 396.8 (397) (100%) [$Cocage^{3+}$ - $2H^+$]$^+$; 199.4 (199.5) (75%) [$Cocage^{3+}$ - H^+]$^{2+}$; 432.8 (433) (9%) [$Cocage^{3+}$ - H^+ - $^{35}Cl^-$]$^+$. $[M]_{510}$ = -640° $M^{-1}m^{-1}$, $[M]_{435}$ = +1150° $M^{-1}m^{-1}$ and $[M]_{360}$ = +730° $M^{-1}m^{-1}$. $\Delta\varepsilon_{469}$ = -4.65 $M^{-1}cm^{-1}$.

Anal. Calc. for Δ-$C_{18}H_{40}N_6Cl_3Co.2H_2O$: C, 39.9; H, 8.2; N, 15.5; Cl, 19.6. Found C, 40.0; H, 9.2; N, 15.5; Cl, 19.3. ^1H NMR (δ, D_2O): 0.67 (t, 6H, CH_3 tail); 1.12 (m, 4H, CH_2 tail); 2.10, 2.72 (AB doublet of doublets, 12H, CH_2 caps); 2.39, 2.88 (AA'BB' coupling pattern, 12H, CH_2 en). ^{13}C NMR (δ, D_2O): 7.6 ($\underline{C}H_3CH_2$); 28.1 ($CH_3\underline{C}H_2$); 46.2 ($\underline{C}q$); 53.6, 55.1 ($N\underline{C}H_2$). IR in KBr (ν^-_{max}/cm^{-1}): 3050 (NH stretch); 2960, 2870 (C-H stretch); 1450, 1400 (C-H deformation); 1065 (CH_2 rock). Low resolution ESMS (100 V) [m/z obs (calc) assignment where cage = $[^{59}Co^{14}N_6{}^{12}C_{18}{}^1H_{40}]^{3+}$]: 396.8 (397) (100%) [Cocage^{3+} - $2H^+$]$^+$; 199.4 (199.5) (50%) [Cocage^{3+} - H^+]$^{2+}$; 432.8 (433) (6%) [Cocage^{3+} - H^+ - $^{35}Cl^-$]$^+$. $[M]_{510}$ = +640° $M^{-1}m^{-1}$, $[M]_{435}$ = -1151° $M^{-1}m^{-1}$ and $[M]_{360}$ = -729° $M^{-1}m^{-1}$. $\Delta\varepsilon_{469}$ = +4.66 $M^{-1}cm^{-1}$.

[(1,8-Dimethyl-3,6,10,13,16,19-hexaazabicyclo[6.6.6]icosa-2-ene)cobalt(III)]-triflate.$CF_3SO_3H.2H_2O$, [Co^{III}(Me_2-sar-2-ene)](CF_3SO_3)$_3$.$CF_3SO_3H.2H_2O$.

This compound has been prepared previously.[16] [Co^{III}(sen)]Cl_3 (10 g; 0.02 mol) and $NaClO_4.H_2O$ (40.5 g; 0.29 mol) were added to acetonitrile (250 mL) and the solution stirred for 30 minutes, during which time some of the complex dissolved. To the stirred suspension was added paraformaldehyde (1.8 g; 0.06 mol) and propionaldehyde (3.6 mL; 0.05 mol). After the mixture was stirred for a further 5 minutes, triethylamine (3.3 mL; 0.02 mol) was added. The mixture rapidly turned dark brown. After stirring for 30 minutes, the reaction mixture was quenched with excess glacial acetic acid, diluted to 2 L and loaded onto a column of Dowex 50Wx2 cation exchange resin (8 cm x 4 cm). The column was washed successively with water and 1 M HCl and the adsorbed complexes were removed as a single band with 3 M HCl, while the polymeric material remained on the column. The eluate was taken to dryness, diluted to 2 L with water, loaded onto a column of SP Sephadex C-25 cation exchange resin (30 cm x 4 cm) and eluted with 0.1 M K_2SO_4. The leading half of the single yellow band that eluted contained the desired product. This material was desalted by treatment with Dowex-HCl, and re-chromatographed on SP Sephadex C-25, using 0.05 M trisodium citrate as eluant. Two minor yellow bands were eluted first and discarded. These were followed by a single yellow band which was collected, desalted on Dowex and dried. The complex was then dissolved in trifluoromethanesulfonic acid (150 mL) and the HCl evolved was removed completely by blowing N_2 through the stirred solution overnight. After cooling the mixture, diethylether (400 mL) was added cautiously to the solution. The resulting yellow precipitate was filtered, washed with ether, and air dried. Yield 8.6 g (75%).

Anal. Calc. for $C_{20}H_{35}N_6CoF_{12}S_4O_{12}.2H_2O$: C, 24.0; H, 3.9; N, 8.4. Found C, 23.9; H, 4.2; N, 8.1. ^{13}C NMR (δ, D_2O): 19.1 ($\underline{C}H_3Cq$); 21.2 ($\underline{C}H_3CqC=N$); 41.9 ($CH_3\underline{C}q$); 49.4 ($\underline{C}qC=N$); 52.6, 53.0, 53.3, 54.0, 55.2, 55.3, 55.4, 56.1, 56.9, 59.0 ($N\underline{C}H_2$); 61.6 ($C=N-\underline{C}H_2$); 188.3 ($\underline{C}=N$). IR in KBr (ν_{max}/cm^{-1}): 3190 (NH stretch); 2970, 2890 (C-H stretch); 1670 (C=N); 1470, 1450 (C-H deformation); 1260, 1170, 1085, 1030, 765, 580, 520 ($CF_3SO_3^-$).

Attempted Reactions at the Imine Carbon.

(a) Reaction of $[Co^{III}(Me_2\text{-sar-2-ene})]^{3+}$ with acetylacetone in carbonate buffer

$[Co^{III}(Me_2\text{-sar-2-ene})]^{3+}$ (1 g; $2.1x10^{-3}$ mol) was dissolved in a carbonate buffered (pH 10) aqueous solution. To this was added acetylacetone (1.05 g; 0.01 mol). The mixture was stirred for two hours and then quenched with acetic acid. Adsorption on SP Sephadex C-25 cation exchange resin and elution with 0.05 M trisodium citrate produced one orange band. This material was desalted on Dowex 50Wx2 cation exchange resin and dried. NMR data indicated that the starting material was returned quantitatively.

(b) Reaction of $[Co^{III}(Me_2\text{-sar-2-ene})]^{3+}$ with 4-nitroacetophenone in acetonitrile

$[Co^{III}(Me_2\text{-sar-2-ene})]^{3+}$ (1 g; $2.1x10^{-3}$ mol) was dissolved in acetonitrile (50 mL). To this was added 4-nitroacetophenone (1.73 g; 0.01 mol) and triethylamine (1.5 mL; 0.01 mol). After stirring for two hours the reaction was quenched with acetic acid, diluted with water (1 L) and loaded onto a column of Dowex 50Wx2 cation exchange resin to remove the complex from the polymeric material. The column was washed with water and 1 M HCl, and then eluted with 5 M HCL to yield one orange band which was dried. This was then redissolved in water (500 mL) and reloaded onto a column of SP Sephadex C-25 cation exchange resin. Elution with 0.05 M Na_3citrate produced a single orange band which was collected, desalted on Dowex and taken to dryness. NMR studies revealed that only starting material was present and no reaction had taken place.

(c) Reaction of $[Co^{III}(Pr_2\text{-sar-2,6-diene})]^{3+}$ with nitromethane in water

$[Co^{III}(Pr_2\text{-sar-2,6-diene})]^{3+}$ (0.3 g; $6.3x10^{-4}$ mol) was dissolved in water (30 mL). To this was added nitromethane (0.20 g; $3.2x10^{-3}$ mol) and triethylamine (0.3 mL; $1.9x10^{-3}$ mol). The red mixture was stirred for

approximately 5 - 10 min and then quenched with acetic acid. It was then diluted to 500 mL with water, loaded onto a column of SP Sephadex C-25 cation exchange resin, and eluted with 0.05 M trisodium citrate to yield a single yellow band. This was collected, desalted on Dowex and taken to dryness. NMR data again revealed that the starting material was quantitatively returned.

(d) Reaction of $[Co^{III}(Pr_2\text{-sar-2,6-diene})]^{3+}$ with nitromethane in acetonitrile

$[Co^{III}(Pr_2\text{-sar-2,6-diene})]^{3+}$ (0.3 g; $6.3x10^{-4}$ mol) was suspended in acetonitrile (50 mL) containing $NaClO_4.H_2O$ (0.35 g; $2.5x10^{-3}$ mol) and this mixture was allowed to stir for thirty minutes. Nitromethane (0.20 g; $3.2x10^{-3}$ mol) and triethylamine (0.3 mL; $1.9x10^{-3}$ mol) were added and stirring of the brown mixture was continued for two hours. The reaction was quenched with acetic acid diluted to 500 mL with water and loaded onto a column of SP Sephadex C-25 cation exchange resin. Elution with 0.05 M Na_3citrate yielded a single yellow band that was collected, desalted on Dowex and taken to dryness. NMR data again revealed that the starting material was quantitatively returned.

6.2.2 X-ray Crystal Structure Analysis of *trans*-$[Co^{III}(Et_2\text{-sar-2,9-diene})]Cl_3.3H_2O$

Data Collection

A yellow block crystal of the Co(III) diimine complex having approximate dimensions of 0.12 x 0.14 x 0.27 mm was mounted on a quartz fibre. All measurements were made using a Rigaku AFC6S diffractometer with graphite monochromated Mo-Kα radiation. Cell constants and an orientation matrix for data collection, obtained from a least squares refinement using the setting angles of 23 carefully centered reflections in the range $18.90 < 2\theta < 29.59°$ corresponded to a C-centered monoclinic cell with dimensions a = 8.863(3) Å, b = 16.369 Å, c = 18.025 Å and V = 2598(1) $Å^3$. For Z = 4 and F.W. = 573.88, the calculated density is 1.47 g/cm^3. Based on the systematic absences of hkl: $h+k \neq 2n$ and h0l: $l \neq 2n$ packing considerations, a statistical analysis of intensity distribution, and the successful solution and refinement of the structure, the space group was determined to be C2/c (# 15). The data were collected at a temperature of 23 ± 1° C using the ω-2θ scan technique to a maximum 2θ value of 55.1°. Omega scans of several intense reflections, made prior to data collection, had an average width at half height of 0.35° with a take-off angle of 6.0°.

Scans of (1.31 + 0.34 tan θ)° were made at a speed of 4.0°/min (in omega). The weak reflections ($I < 10.0\sigma(I)$) were rescanned (maximum of four scans) and the counts were accumulated to ensure good counting statistics. Stationary background counts were recorded on each side of the reflection. The ratio of peak counting time to background counting time was 2:1. The diameter of the incident beam collimator was 0.5 mm, the crystal to detector distance was 200 mm, and the detector aperture was 4.0 x 4.0 mm (horizontal x vertical).

Data Reduction

Of the 3314 reflections collected, 3113 were unique ($R_{int} = 0.017$). The intensities of three representative reflections were measured every 150 reflections. No decay correction was required. The linear absorption coefficient, μ, for Mo-Kα radiation is 10.0 cm^{-1}. An analytical absorption correction was applied which resulted in transmission factors ranging from 0.87 to 0.89. The data were corrected for Lorentz and polarization effects.

Structure Solution and Refinement

The structure was solved by Patterson heavy atom methods[33] and expanded using Fourier techniques.[34] The non-hydrogen atoms were refined anisotropically. The hydrogen atom coordinates were refined but their isotropic B values were held fixed. The final cycle of full-matrix least-squares refinement was based on 2157 observed reflections ($I > 3.00\sigma(I)$), 212 variable parameters and it converged (largest parameter which was 0.03 times its esd) with unweighted and weighted agreement of $R = \Sigma | |Fo| - |Fc| | / \Sigma |Fo| = 0.029$ and $R_w = \sqrt{(\Sigma\omega(|Fo| - |Fc|)^2 / \Sigma\omega Fo^2)} = 0.025$. The standard deviation of an observation of unit weight was 1.65. The weighting scheme was based on counting statistics and included a factor ($p = 0.005$) to downweight the intense reflections. Plots of $\Sigma\omega(|Fo| - |Fc|)^2$ verses $|Fo|$, reflection order in data collection, $\sin\theta/\lambda$ and various classes of indices showed no unusual trends. The maximum and minimum peaks on the final difference Fourier map corresponded to 0.26 and -0.35 $e^-/Å^3$, respectively. Neutral atom scattering factors were taken from Cromer and Waber.[35] Anomalous dispersion effects were included in Fcalc;[36] the values for Δf' and Δf'' were those of Creagh and McAuley.[37] The values for the mass attenuation coefficients are those of Creagh and Hubbel.[38] All calculations were performed using the texsan crystallographic software package of the Molecular Structure Corporation.[39]

6.2.3 Antiviral Activity

The antiviral testing of some of the alkyl tail complexes presented in this work was performed by Dr. S. Marcuccio and his team at the Division of Molecular Science, CSIRO, Clayton, Victoria.

Anti-HIV Testing

The diimine and saturated cage complexes described in this chapter were tested against a HIV screen by the MTT method. MT-4 cells (2.5 x 10^4/well) were challenged with HIV-1 (HTLV-IIIB) or HIV-2 (LAV-2 ROD) at a concentration of 100 CCID50, and incubated in the presence of various concentrations of the test compounds, added immediately after the virus. After five days at 37° C in a CO_2 incubator, the number of viable cells was assessed by the MTT (tetrazolium) method. A control test was performed using the known anti-HIV reagent AZT, and a number of comparison compounds were also run.

Mouse Test for Mammalian Toxicity

All tests were caried out on fully-grown male white mice (*Mus musculus*) strain BALB/c, weighing 20 to 25 g per mouse, and supplied by the Animal Breeding Unit of the University of N.S.W. The mice were obtained at least one day prior to the test day and acclimatised in the test room (Temp 25° C), where they were held, five to a box and given commercial rat pellets and water *ad lib.*

On the day of the test, the compound to be tested was weighed and dissolved in either olive oil or DMSO to give a stock solution which when injected at the level of 100 µL per mouse gave a dose of 100 mg/kg. Two further doses of 10 mg/kg and 1.0 mg/kg were prepared from this solution.

Up to 100 µL of solution was injected intraperitoneally into each mouse. Five of ten mice were dosed at each concentration i.e. 100 mg/kg, 50 mg/kg, 10 mg/kg and 1 mg/kg, with five control mice dosed with solvent.

For those compounds tested for multiple dosing, the injections were repeated, as above, each day at the same time of day, for the number of days required. The mice were observed at half-hourly intervals and symptoms recorded. Further readings were taken for the next seven days.

Anti Hepatitis Testing

Tests of antiviral activity in human cells infected with Hepatitis B were performed according to a published procedure.[40]

Antiviral Testing

The compounds were tested for their ability to inhibit RNA synthesis in an *in vitro* polymerase assay.[41-43] In this assay, flavivirus RNA comprising the genomic 44S RNA, a double-stranded replicative form (RF) and a partially-double stranded replicative intermediate (RI) were detected by the incorporation of [a-^{32}P]GTP.

(a) Preparation of Virus-infected Vero Cell Extracts

Vero cells were infected at a multiplicity of infection of 7 for Type 2 dengue (DEN-2) virus (New Guinea C strain)[44] of Kunjin (KUN) virus (strain MRM61C)[45]. Extracts containing RNA-dependant RNA polymerase (RDRP) activity derived from DEN-2 virus-infected cells were prepared at 30 and 36 h.p.i., when polymerase activity was at a maximum. Similarly, extracts of KUN virus-infected cells were prepared at the time of maximum polymerase activity at 24 h.p.i..[41]

The cells were pelleted by centrifugation and resuspended in 10mM sodium acetate at a concentration of 2 x 10^7 cells/mL. They were then disrupted by passing 20 times through a 21 gauge needle followed by 20 time through a 26 gauge needle. The disrupted cells were centrifuged at 800 G for 7 min to obtain a supernatant fraction and a pellet of the nuclear-associated material. All RDRP assays were performed using the supernatant fraction, hereafter referred to as the cell extract, which was stored at -70° C and used after only one cycle of freeze/thawing.

(b) RNA-dependant RNA polymerase assay

The RDRP activity in the cell extract was assayed as previously described with the following modifications.[41] In each RDRP assay the virus-infected cell extract contained 4.5 - 6 mg/mL of protein. The compound to be tested was dissolved in double distilled water and RNasin (0.5 units/mL, Promaga). This was added to the cell extract 10 min prior to the addition of the other components of the RDRP assay. The final reaction mixture (total volume of 50 ml) contained 50 mM Tris-HCl pH 8, 10mM magnesium acetate, 7.5 mM potassium acetate, 10 mM 2-mercaptoethanol,

6 mg actinomycin D (AMD), 5 mM phosphoenolpyruvate, 3 units/mL pyruvate kinase, 0.5 mM ATP, 0.5 mM CTP, 0.5 mM UTP, 25 mM GTP, 5 mCi [a-^{32}P]GTP (Amersham, specific activity 410 Ci/mmol), 0.5 units/mL RNasin, 30 ml of infected cell extract and the test compound (from 0.5 to 100 mM). The reaction was stopped after 30 min at 37° C by the addition of EDTA to a final concentration of 10 mM. An equal volume of TNE-SDS (50 mM Tris-acetate pH 7.6, 0.1 M sodium acetate, 1 mM EDTA and 2% SDS) was added to disrupt the membranes. The RNA was then extracted with phenol and precipitated by the addition of ethanol.

(c) Electrophoresis of RNA

RNA samples were mixed with an equal volume of sample buffer contining 7 M urea in TBE (89 mM Tris-HCl, 89mM boric acid, 2.5 mM EDTA) and 0.5% bromophenol blue, and were separated by electrophoresis through 3% polyacrylamide gels containing 7 M urea in TBE. The gels were fixed in 10% acetic acid, dried and radiolabelled bands were detected by autoradiography.

6.3 Results

6.3.1 Nomenclature of the Di-imine Cage Isomers

Examination of the structures of the Co(III) isomeric di-imine cage complexes obtained in this thesis show that within each set the complexes there are diastereomers. Distinction between each of the three isomers in each set is therefore necessary. Firstly, the isomer that has the imine groups situated in the same strand is different from the remaining two isomers. The locants of the imine groups in this complex are the 2 and 6 positions of the ligand (Figures 7b and 8) and the imine moiety takes precedence over a secondary amine. For the remaining two isomers, although they are different from each other, the ligand imine groups are in the 2 and 9 positions for both. However, the relative locations of the imine groups within each complex are *cis* to each other in one case and *trans* in the other (Figures 7b and 8). Therefore the isomers can be named by a combination of their locants and stereochemical relationship of the two imines. The chirality about the metal ion also needs to be specified. For the cage complex the ligand strands about the metal ion can trace out a left- or right-handed three strand helix. Cage ligands having a right-handed helicity are labelled Δ and those with a left-handed helicity are labelled Λ[46] in conformity with the configurations of the Λ- and Δ-$[Co^{III}(en)_3]^{3+}$ templates as prescribed by the IUPAC convention[46] and depicted in Figure 7a. Figure 7b illustrates the helical structure and the diastereomeric relationships of the diimine.

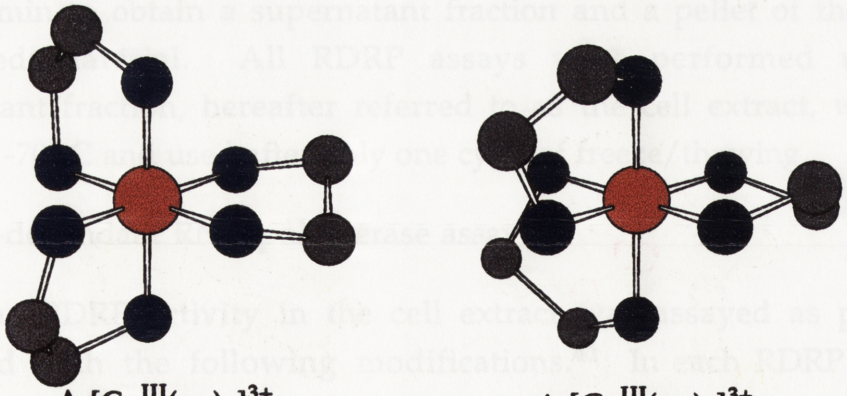

Λ-$[Co^{III}(en)_3]^{3+}$ Δ-$[Co^{III}(en)_3]^{3+}$

Figure 7a

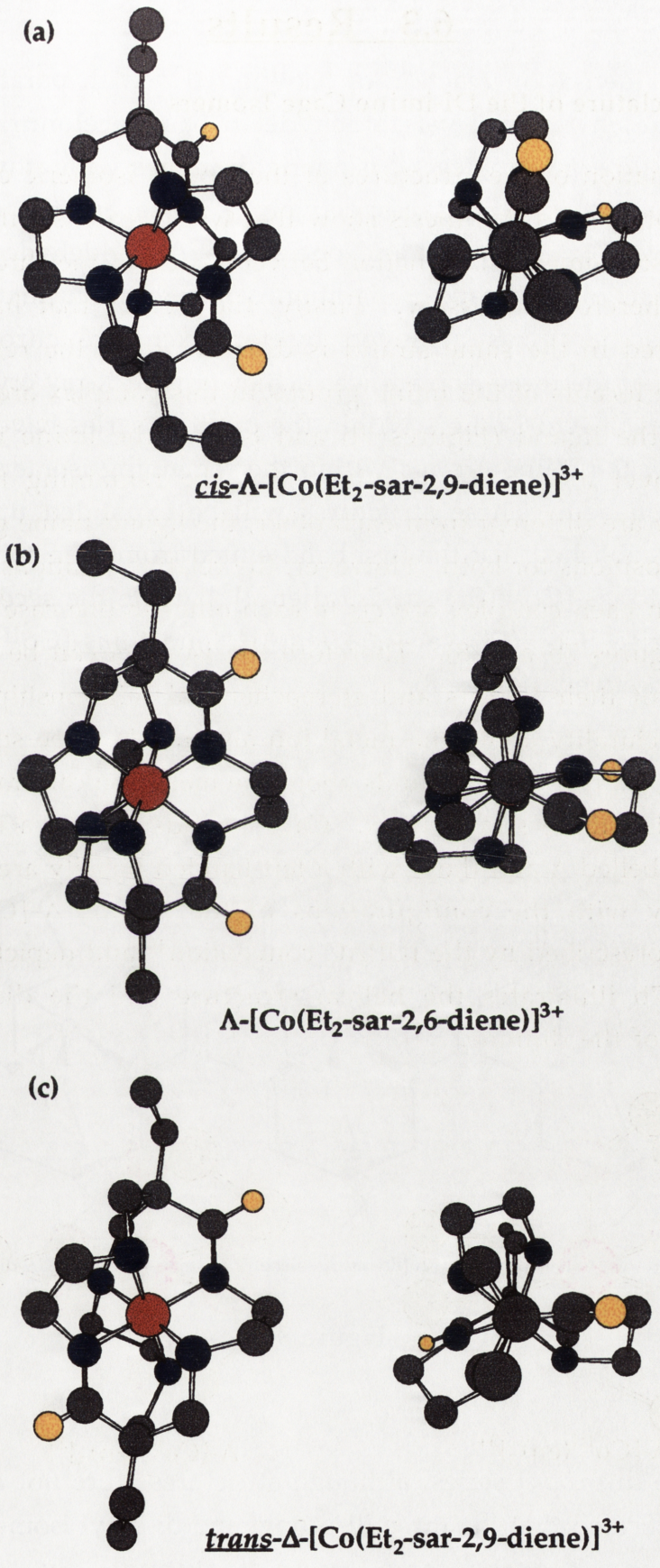

Figure 7b. Diagram displaying ligand and imine C-H configurations of the three Co(III) di-imine cage diasteromers viewed both along and down the long axis. All hydrogens, except imine C-H's, have been omitted for clarity.

6.3.2 Syntheses

The condensation reaction of $[Co^{III}(en)_3]^{3+}$ with paraformaldehyde and 1-butyraldehyde or 1-valeraldehyde in basic acetonitrile led to the formation of three macrobicyclic isomeric di-imines with ethyl and propyl tails in the apical positions respectively. These are the only isomers possible if two formaldehydes and one substituted aldehyde are involved in the synthesis of each cap. Separation of the reaction mixtures into the individual isomers was achieved by ion exchange chromatography. Identification of the three isomers was achieved with X-ray crystallography. The structures of two isomers within the di-ethyl series have been solved so the sites of the imine groups within the remaining isomeric complex is thereby established. These structures will be expanded upon later but clearly it is established that the first band eluted from the Sephadex column corresponds to *cis*-$[Co^{III}(Et_2\text{-sar-2,9-diene})]^{3+}$ while the second and third bands comprise $[Co^{III}(Et_2\text{-sar-2,6-diene})]^{3+}$ and *trans*-$[Co^{III}(Et_2\text{-sar-2,9-diene})]^{3+}$ respectively (Figure 8).

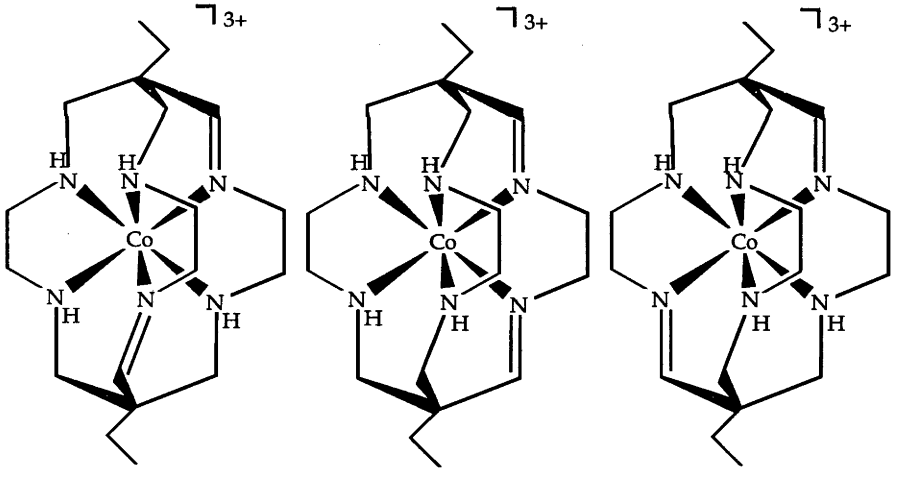

cis-$[Co(Et_2\text{-sar-2,9-diene})]^{3+}$ $[Co(Et_2\text{-sar-2,6-diene})]^{3+}$ *trans*-$[Co(Et_2\text{-sar-2,9-diene})]^{3+}$

Figure 8

For the di-propyl series, although structures were not obtained, the NMR data indicated that the three di-propyl and di-ethyl isomers correlated (see ahead) and had the same order of elution. By coupling this information with the crystallographic evidence of the other di-imine set

the di-propyl isomer configurations can be assigned in exactly the same way.

$[Co^{III}(Et_2\text{-sar-2,6-diene})]^{3+}$ was then treated with $NaBH_4$ in a carbonate buffered solution at pH 10 to produce the fully saturated cage which was resolved into its respective enantiomers (Figure 9a).

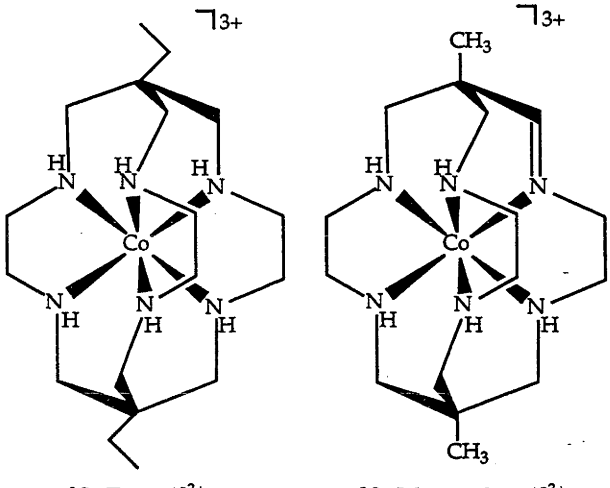

Figure 9

Production of the di-methyl derivative, $[Co^{III}(Me_2\text{-sar-2-ene})]^{3+}$, (Figure 9b) was achieved by reaction of $[Co^{III}(sen)]^{3+}$ paraformaldehyde and propionaldehyde in basic acetonitrile and was isolated, in a similar manner to that used for the di-imine complexes except that it was finally converted to a triflate salt by reacting the chloride with trifluoromethanesulfonic acid. It has been reduced to the saturated $[Co^{III}(Me_2\text{-sar})]^{3+}$ ion with BH_4^- as outlined previously.[16]

Attempts to add a number of carbon acids to the imine carbon centres of these cages were unsuccessful. Reaction of $[Co^{III}(Me_2\text{-sar-2-ene})]^{3+}$ and $[Co^{III}(Pr_2\text{-sar-2,6-diene})]^{3+}$, with various carbon acids under basic conditions did not produce any saturated cages with new substituents at the former imine carbon site. The various reaction mixtures, after quenching with acid, were chromatographed on ion exchange resins and gave the starting material either quantitatively or near quantitatively. Changing reaction conditions and solvents did not influence the results.

This lack of reactivity was surprising since it has been claimed that $NO_2CH_2^-$ can be reacted effectively with the mono imine $[Co^{III}(Me_2\text{-sar-2-ene})]^{3+}$.[47]

6.3.3 NMR Spectroscopy

The ^{13}C NMR spectra show that each isomer has two-fold symmetry with a different rotation axis for each isomer. This yields nine and ten signals instead of eighteen and twenty respectively for the di-ethyl and di-propyl isomers. The ^{13}C NMR spectra of the three dipropyl isomers are depicted in Figure 10. Using the first di-propyl isomer as an example, the resonances at 53.0, 54.4, 55.8, 56.3 and 62.1 ppm are assigned to methylene carbon atoms attached to the secondary coordinated nitrogen atoms. In addition resonances at 53.1, 8.4 and 26.3 ppm are assigned to the quaternary carbon, the methylene carbon and the methyl carbon atoms in the cap and tail of the complex respectively. Lastly the equivalent imine carbon atoms possess a shift value of 185.7 ppm. These features are present within each isomer but at slightly different chemical shift values. Also for the di-ethyl isomers one less carbon was observed within this set of ^{13}C NMR spectra.

The ^1H NMR spectrum of each di-imine isomer shows some characteristic features although they were less informative than the ^{13}C NMR spectra. As an example the di-propyl isomers are displayed in Figure 11. All spectra display matching resonances for the tail and imine protons respectively, the only difference between each set of isomers being that the di-ethyl isomers display fewer signals because of the shorter apical tail. The spectra are complicated by extensive spin-spin splitting and coupling except for the imine and terminal tail signals. Even at 500 MHz the signals appear as complex and overlapping multiplets between the shift values of 2.5 ppm and 4.5 ppm. However, by coupling the earlier crystallographic evidence with the analogous NMR spectra, obtained for both sets of isomers, it is possible to assign the imine moieties within the three individual isomeric di-propyl complexes and the analogy is precise. It follows the assignment of the structures is also compelling.

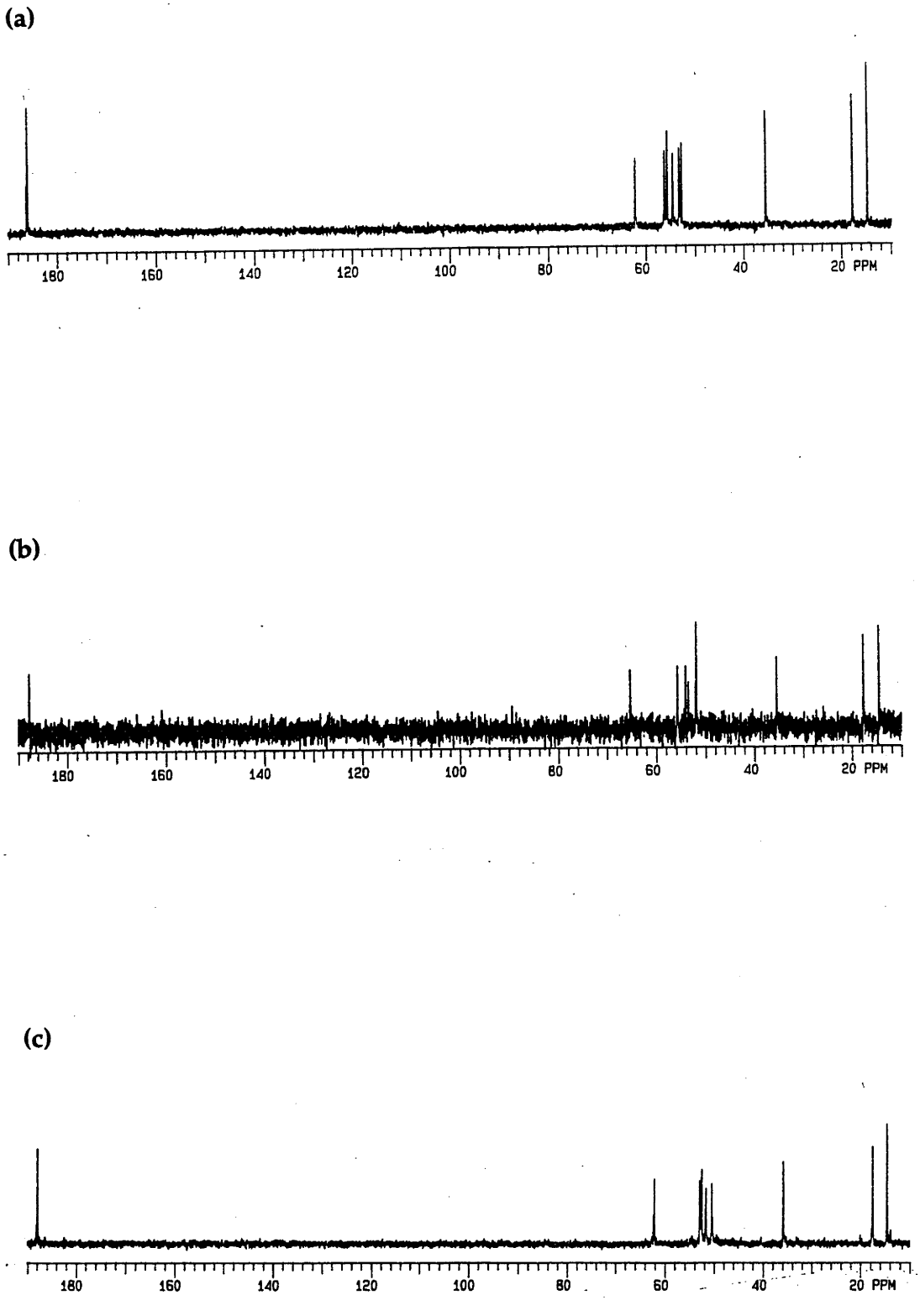

Figure 10. ^{13}C NMR spectrum of (a) *cis*-[$Co^{III}(Pr_2$-sar-2,9-diene)]$^{3+}$, (b) [$Co^{III}(Pr_2$-sar-2,6-diene)]$^{3+}$, (c) *trans*-[$Co^{III}(Pr_2$-sar-2,9-diene)]$^{3+}$ (Chloride salts in D_2O).

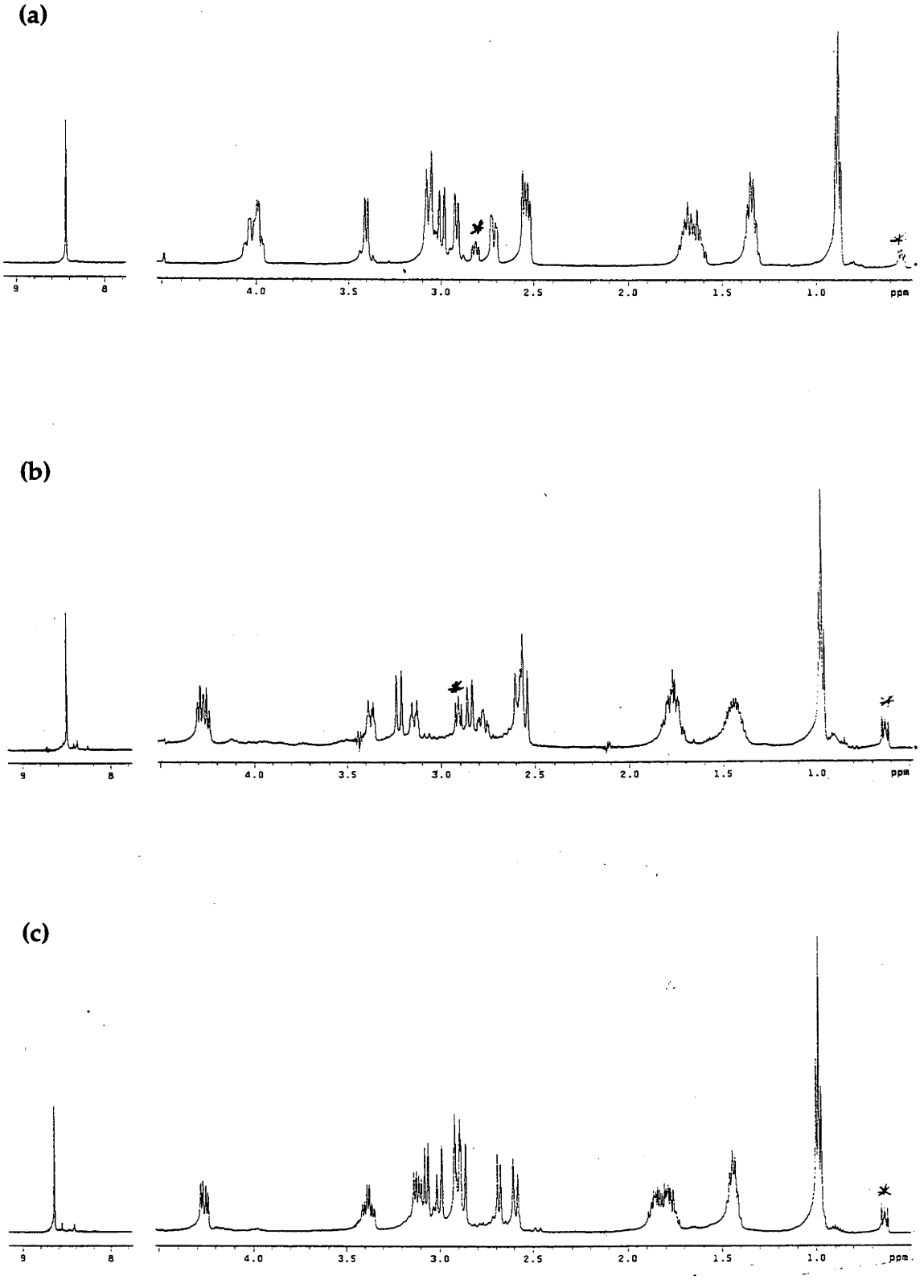

Figure 11. ^1H NMR spectrum of (a) *cis*-$[Co^{III}(Pr_2\text{-sar-2,9-diene})]^{3+}$, (b) $[Co^{III}(Pr_2\text{-sar-2,6-diene})]^{3+}$, (c) *trans*-$[Co^{III}(Pr_2\text{-sar-2,9-diene})]^{3+}$ (Chloride salts in D_2O, * = NaTSP (sodium(trimethylsilyl)propanesulfonate)).

Reduction of the di-ethyl isomer to the saturated complex, $[Co^{III}(Et_2\text{-sar})]^{3+}$, led to a simplification of both the ^{13}C and ^{1}H NMR spectra since the compound changes from C_2 to D_3 symmetry. In the ^{13}C NMR spectrum only five signals were observed. The resonances at 7.5 ppm and 28.1 ppm are attributed to the methyl and methylene carbons respectively of the tail. The remaining chemical shifts at 46.2, 53.6 and 55.1 ppm are assigned to the quaternary carbon and the methylene groups adjacent to the secondary nitrogens. In the ^{1}H NMR spectrum the methyl and methylene tail protons generate a triplet and mutiplet at 0.67 and 1.12 ppm respectively, while an AB doublet of doublets occurs at 2.10 and 2.72 ppm for the cap methylene protons. An AA'BB' spin system, at 2.39 and 2.88 ppm, is observed for the protons of the ethylenediamine moiety.

6.3.4 Infra-red Spectroscopy

The infra-red spectroscopy proved to be of limited value in evaluating the functionality of the di-imine isomers and saturated Co(III) cage complexes. Apart from absorptions resulting from N-H and C-H stretches only weak stretching vibrations were observed for the C=N groups at either 1660 cm^{-1} or 1670 cm^{-1}. Generally C=N absorptions are expected between 1690 cm^{-1} and 1640 cm^{-1} but they are usually weak and therefore more difficult to identify. In addition, identification of the C=N group is further complicated by the fact that they overlap with the N-H bending mode (1650 cm^{-1} - 1550 cm^{-1}).

6.3.5 Electrospray Mass Spectrometry

The ESM spectra of the two sets of diimine Co(III) cage isomers with di-ethyl and di-propyl tails in water appear in Figures 12 to 17. The ESM spectra for the two enantiomers of the $[Co^{III}(Et_2\text{-sar})]^{3+}$ ion are also given in Figures 18 and 19 and they are not different as expected. Firstly, the ESM spectra highlight the fact that this technique is sensitive enough to detect H_2 missing from each di-imine isomer. For the three di-ethyl isomers (*cis*-$[Co^{III}(Et_2\text{-sar-2,9-diene})]^{3+}$, $[Co^{III}(Et_2\text{-sar-2,6-diene})]^{3+}$ and *trans*-$[Co^{III}(Et_2\text{-sar-2,9-diene})]^{3+}$) all the spectra display a base peak centred on an m/z value of 393 that corresponds to a $[Cocage^{3+} - 2H^+]^+$ species. Also in all three spectra another peak centred on m/z 429 shows that the deprotonated doubly charged cage species combines with a chloride ion resulting in a mono charged ion, $[Cocage^{3+} - H^+ + {}^{35}Cl^-]^+$.

With the di-propyl isomers (*cis*-$[Co^{III}(Pr_2\text{-sar-2,9-diene})]^{3+}$, $[Co^{III}(Pr_2\text{-sar-2,6-diene})]^{3+}$ and *trans*-$[Co^{III}(Pr_2\text{-sar-2,9-diene})]^{3+}$) the same types of ions arise, however, the $[Cocage^{3+} - 2H^+]^+$ and $[Cocage^{3+} - H^+ + {}^{35}Cl^-]^+$ ion pair species are centred on m/z values of 421 and 457 respectively.

For the $[Co^{III}(Et_2\text{-sar})]^{3+}$ a $[Cocage^{3+} - 2H^+]^+$ species appears at an m/z value of 397 in both cases while the peak at m/z 199 corresponds to a $[Cocage^{3+} - H^+]^{2+}$ species. Also the peak occurring at an m/z value of 432.8 is due to the mono charged species, $[Cocage^{3+} - H^+ + {}^{35}Cl^-]^+$. The $[Cocage^{3+} - H^+ + {}^{35}Cl^-]^+$ ion pair appears in each spectrum. It is likely that Cl^- is H-bonded to the cation in the ion pair since these anions often appear in the crystal structures H-bonded in this manner to the secondary-N protons. A number of other peaks appear around those of the observed ions. These peaks are due to the isotopic contributions of the various elements present within each complex particularly ^{35}Cl, ^{36}Cl and ^{13}C. Again the various spectra fit the simulated patterns of the observed ions and the supporting the microanalytical data.

The combination of ESMS, microanalysis and NMR spectrometry is a powerful strategy for characterising such molecules in the absence of an X-ray crystallographic analysis.

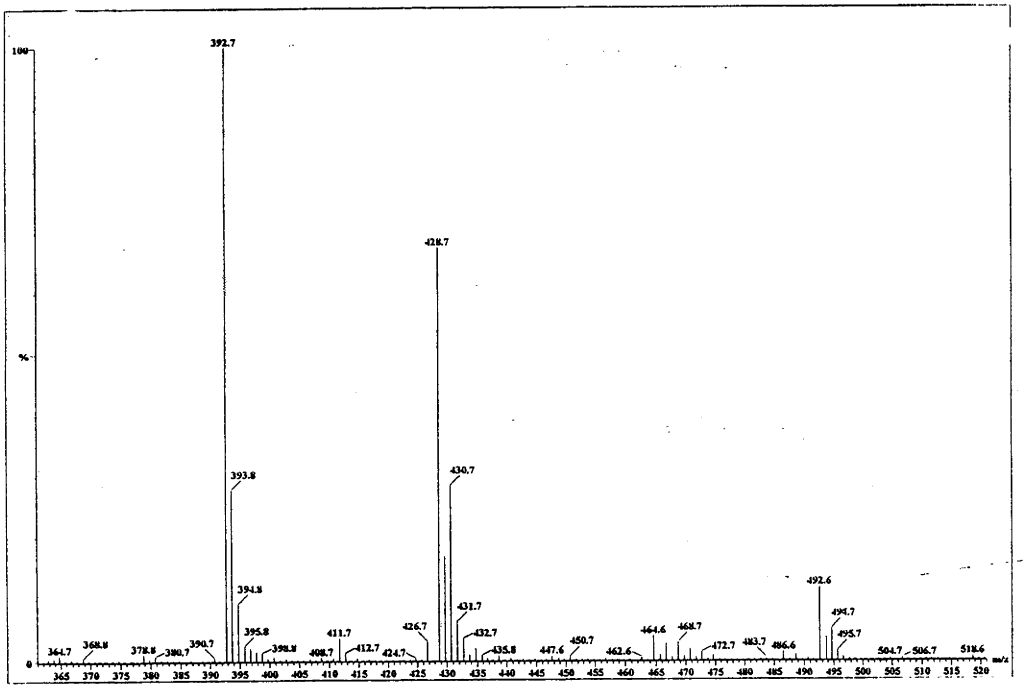

Figure 12. ESM spectrum of aqueous *cis*-$[Co^{III}(Et_2\text{-sar-2,9-diene})]^{3+}$ (Cone Voltage = 80 V).

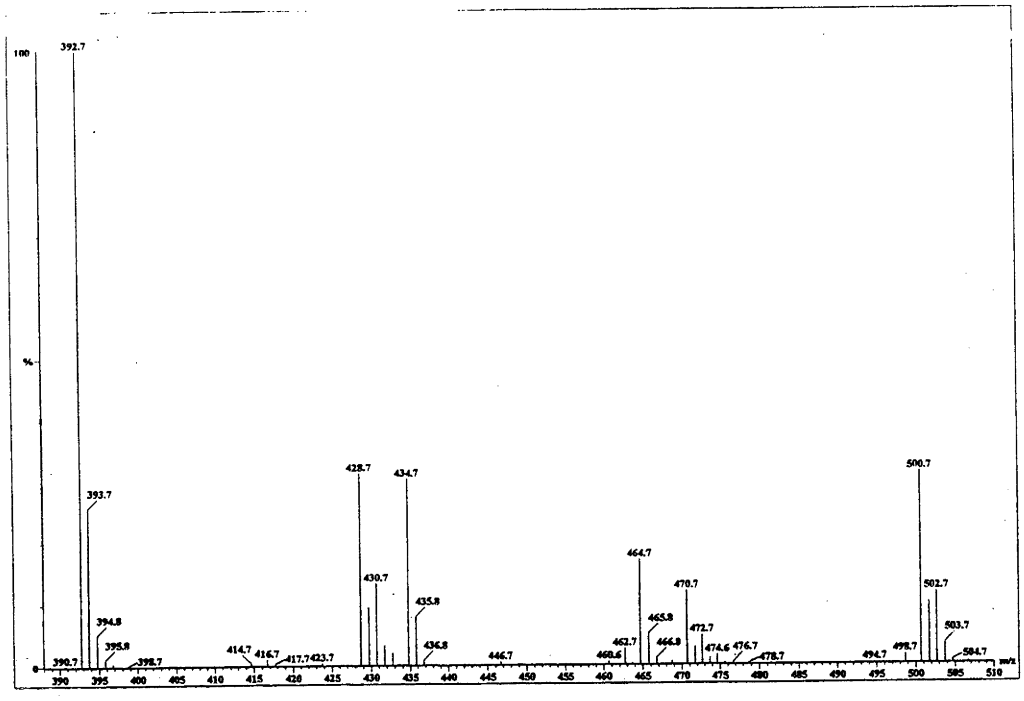

Figure 13. ESM spectrum of aqueous $[Co^{III}(Et_2\text{-sar-2,6-diene})]^{3+}$ (Cone Voltage = 80 V).

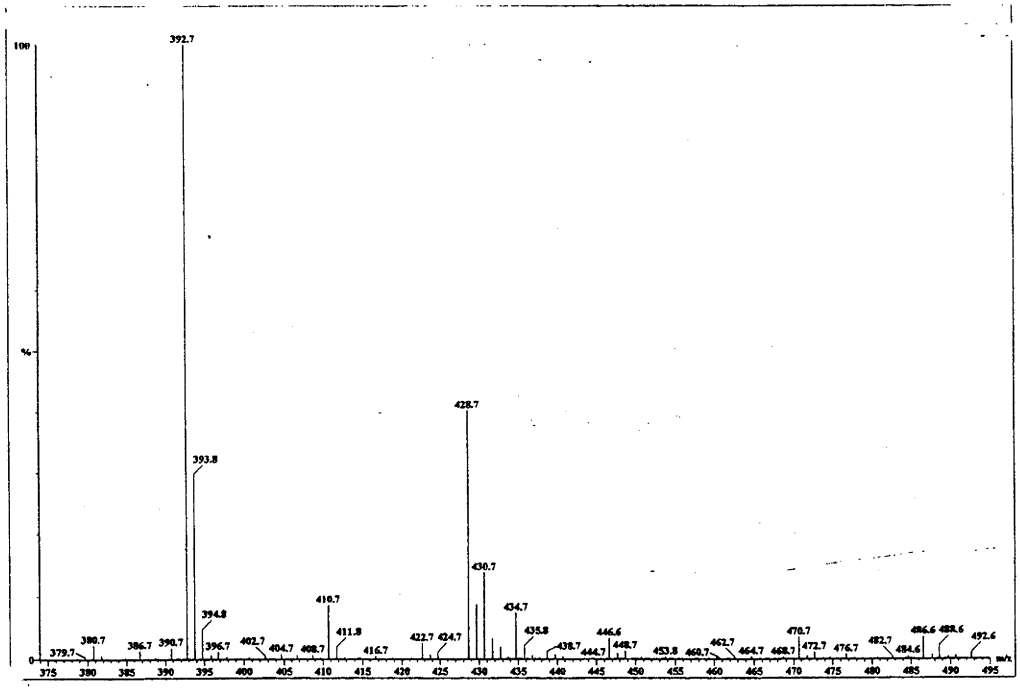

Figure 14. ESM spectrum of aqueous *trans*-$[Co^{III}(Et_2\text{-sar-2,9-diene})]^{3+}$ (Cone Voltage = 80 V).

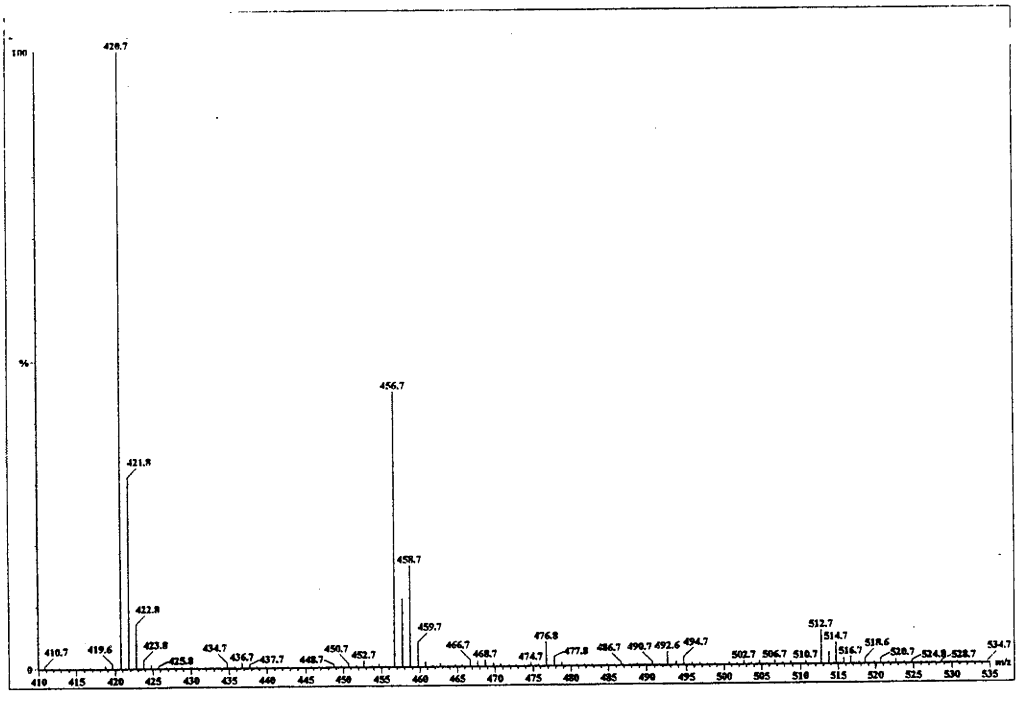

Figure 15. ESM spectrum of aqueous <u>*cis*</u>-$[Co^{III}(Pr_2\text{-sar-2,9-diene})]^{3+}$ (Cone Voltage = 80 V).

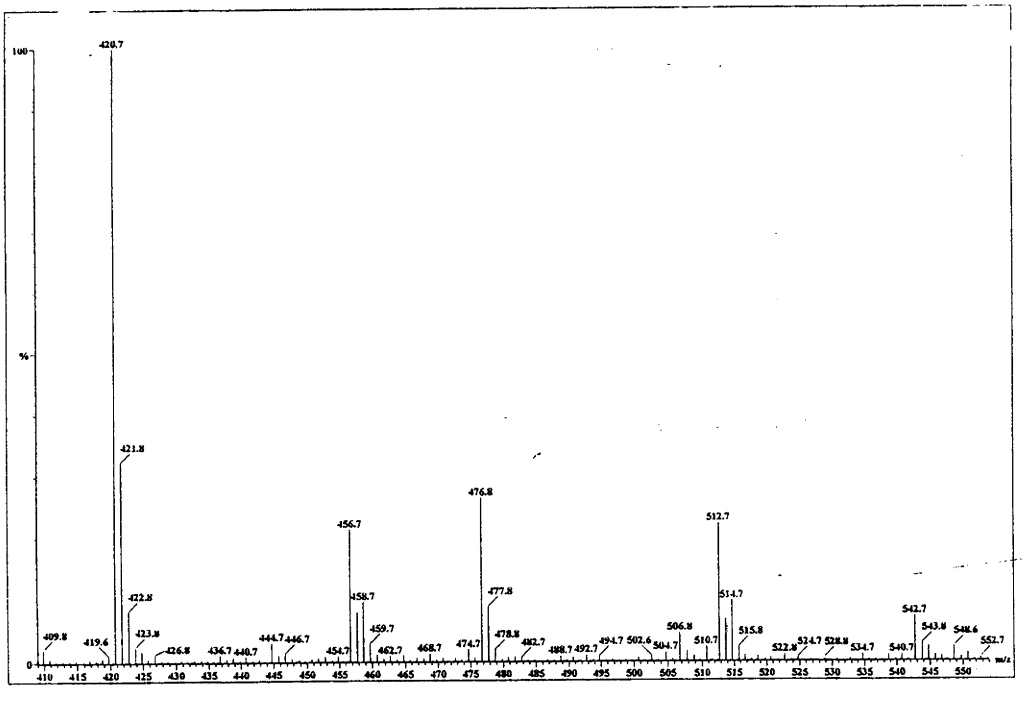

Figure 16. ESM spectrum of aqueous $[Co^{III}(Pr_2\text{-sar-2,6-diene})]^{3+}$ (Cone Voltage = 80 V).

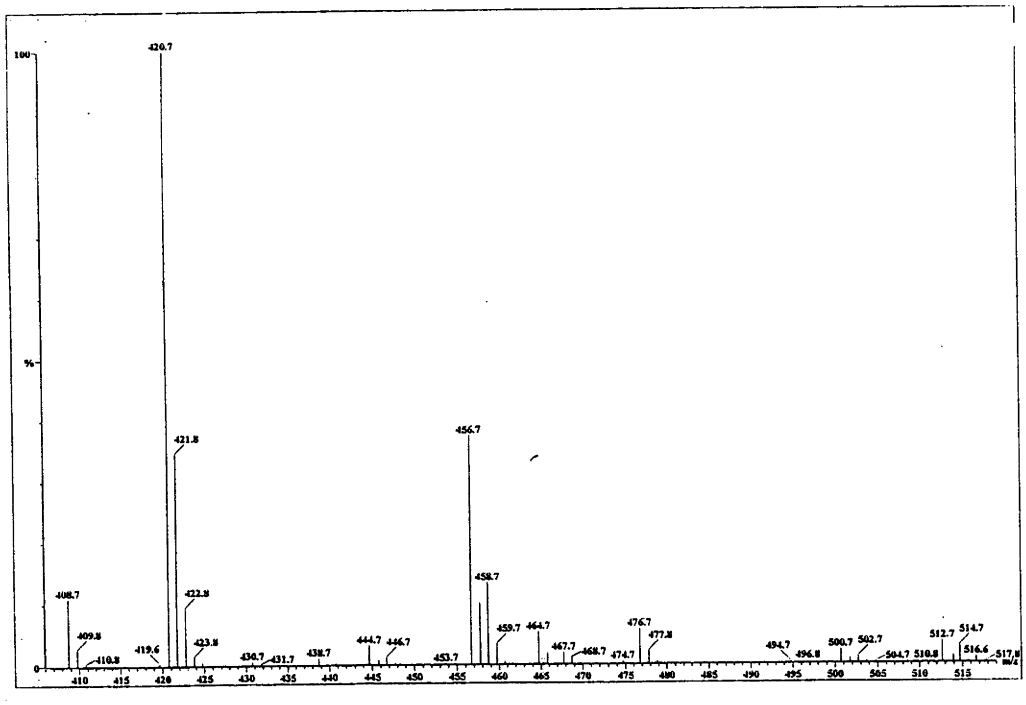

Figure 17. ESM spectrum of aqueous *trans*-[$Co^{III}(Pr_2$-sar-2,9-diene)]$^{3+}$ (Cone Voltage = 80 V).

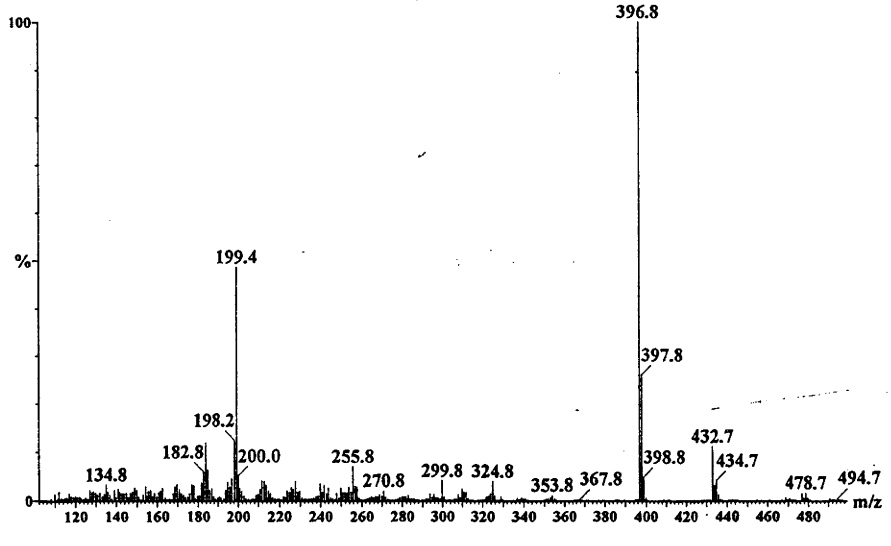

Figure 18. ESM spectrum of aqueous Λ-[$Co^{III}(Et_2$-sar)]$^{3+}$ (Cone Voltage = 80 V).

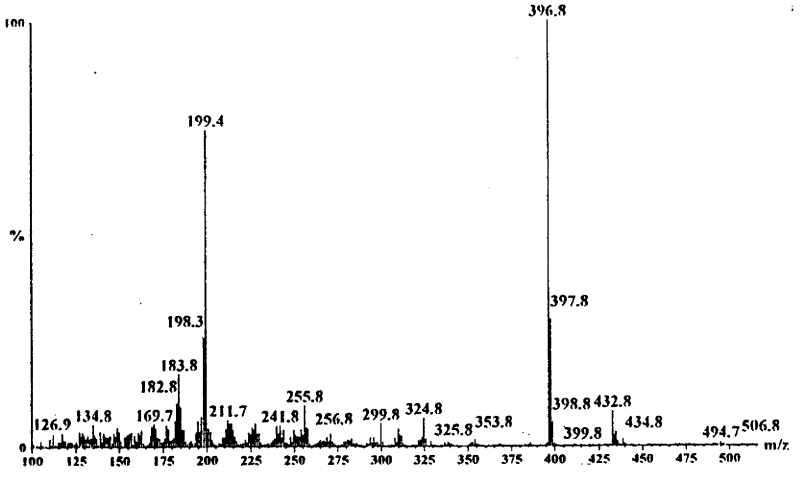

Figure 19. ESM spectrum of aqueous Δ-$[Co^{III}(Et_2\text{-sar})]^{3+}$ (Cone Voltage = 80 V).

6.3.6 X-ray Crystallography

X-ray Crystallographic Analysis of *trans*-$[Co^{III}(Et_2\text{-sar-2,9-diene})]Cl_3.3H_2O$

The structure of the Co(III) di-imine complex with bond distances and angles is displayed in Figure 20, and, Tables 1 and 2 respectively. The structure shows that the Co(III) ion is fully encapsulated with the two imine bonds trans to one another. A notable feature of this complex is that the five membered chelate rings have adopted an *ob* conformation with respect to the long axis through the metal giving the complex an overall conformation of ob_3.

The $Co\text{-}N_{(amine)}$ bond distances (1.966 Å and 1.970 Å respectively) are similar to those reported for other ob_3 sar-type Co(III) complexes[48-51] while the $Co\text{-}N_{(imine)}$ bond lengths, 1.900 Å, are significantly shorter than their saturated counterparts. This value is practically identical to that obtained for a comparable di-imine cage Co(III) complex, $[Co^{III}(Me_2\text{-sar-2,9-diene})]^{3+}$ [28], and is within the range expected for a typical $Co\text{-}N_{(imine)}$ bond. The N(1)-C(4) imine bond lengths (1.265 Å) are almost identical to the same types of bonds in $[Co^{III}(Me_2\text{-sar-2,9-diene})]^{3+}$ but are somewhat shorter than the expected C=N bond length of 1.30 Å[52]. The other saturated C-N bonds, completing the cap, have distances that are similar to other sar type structures.[48,50]

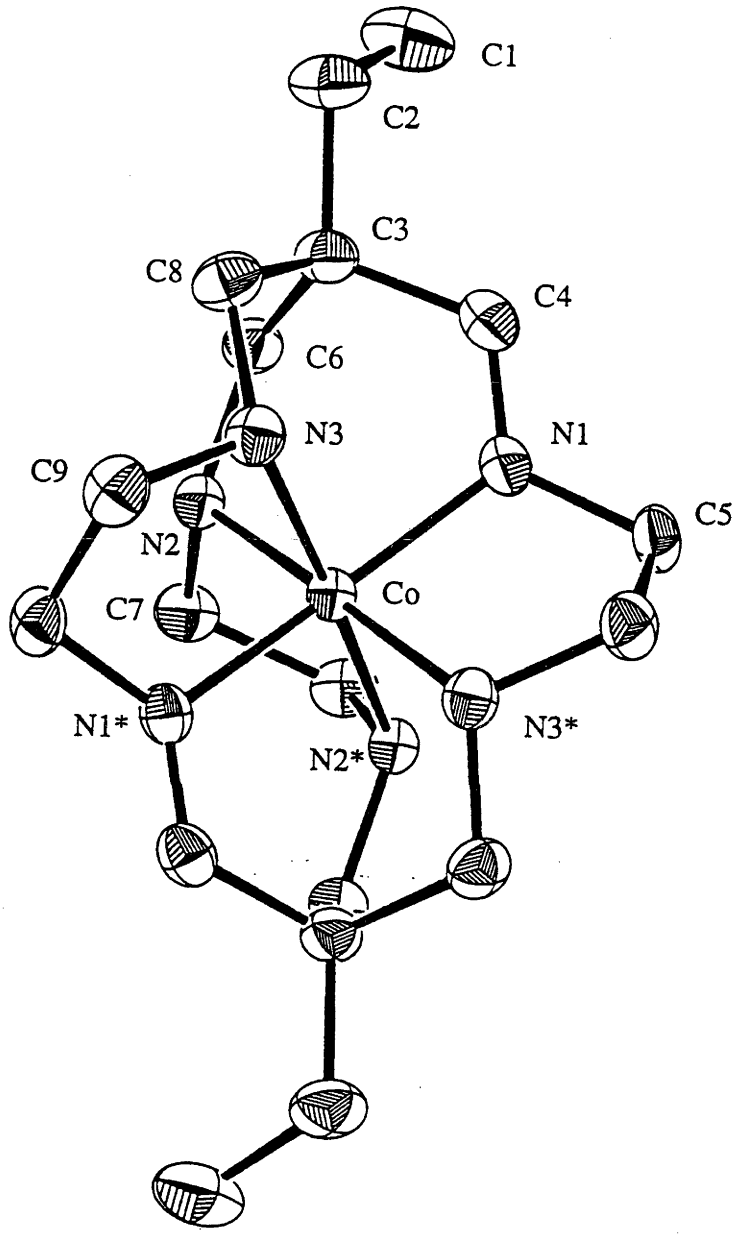

Figure 20. Thermal ellipsoid diagram of the *trans*-[Co^{III}(Et_2-sar-2,9-diene)]$Cl_3.3H_2O$ cation with labelling of selected atoms. Ellipsoids show 50% probability levels, except for hydrogen atoms which have been deleted for clarity.

Table 1. Bond distances (Å) for *trans*-[Co^{III}(Et_2-sar-2,9-diene)]$Cl_3.3H_2O$.

Atoms	Distance (Å)	Atoms	Distance (Å)
Co-N(1)	1.900(2)		
Co-N(2)	1.966(2)	Co-N(3)	1.970(2)
N(1)-C(4)	1.265(3)	N(1)-C(5)	1.474(3)
N(2)-C(6)	1.492(3)	N(2)-C(7)	1.490(3)
N(3)-C(8)	1.497(3)	N(3)-C(9)	1.503(3)
C(1)-C(2)	1.518(4)	C(2)-C(3)	1.539(3)
C(3)-C(4)	1.508(3)	C(3)-C(6)	1.534(3)
C(3)-C(8)	1.545(3)	C(5)-C(9)*	1.518(4)
C(7)-C(7)*	1.498(5)		

*Atom generated by the symmetry operation (1-x, y, 1/2-z)

Table 2. Band angles (°) for *trans*-[Co^{III}(Et_2-sar-2,9-diene)]$Cl_3.3H_2O$.

Atoms	Angle (°)	Atoms	Angle (°)
N(1)-Co-N(1)*	166.8(1)	N(1)-Co-N(2)	95.20(8)
N(1)-Co-N(2)*	94.39(8)	N(1)-Co-N(3)	86.68(8)
N(1)-Co-N(3)*	84.52(8)	N(2)-Co-N(2)*	86.3(1)
N(2)-Co-N(3)	88.94(8)	N(2)-Co-N(3)*	175.17(8)
N(3)-Co-N(3)*	95.9(1)	Co-N(1)-C(4)	121.4(2)
Co-N(1)-C(5)	113.4(2)	C(4)-N(1)C(5)	122.8(2)
Co-N(2)-C(6)	113.9(1)	Co-N(2)-C(7)	108.5(1)
C(6)-N(2)-C(7)	112.7(2)	Co-N(3)-C(8)	113.2(2)
Co-N(3)-C(9)	111.4(2)	C(8)-N(3)-C(9)	113.3(2)
C(1)-C(2)-C(3)	114.5(2)	C(2)-C(3)-C(4)	111.4(2)
C(2)-C(3)-C(6)	110.6(2)	C(2)-C(3)-C(8)	108.0(2)
C(4)-C(3)-C(6)	108.3(2)	C(4)-C(3)-C(8)	109.3(2)
C(6)-C(3)-C(8)	109.2(2)	N(1)-C(4)-C(3)	118.2(2)
N(1)-C(5)-C(9)*	105.9(2)	N(2)-C(6)-C(3)	111.0(2)
N(2)-C(7)-C(7)*	107.5(2)	N(3)-C(8)-C(3)	113.5(2)
N(3)-C(9)-C(5)*	109.6(2)		

*Atom generated by the symmetry operation (1-x, y, 1/2-z)

Most of the N-Co-N bond angles are within ~4° to 6° of their ideal values for octahedral symmetry of the CoN_6 core with two exceptions. The angle subtended by the atoms N(2)-Co-N(3) is close to 90° while for N(1)-Co-N(1)* the angle is 166.8(1)°, some 14° from the ideal value of 180°. As a consequence of incorporating imine moieties within the cage structure the five membered chelate rings attached to the imine fragments possess a torsion angle of 38.9(3)° for N(1)-C(5)-C(9)*-N(3)* and N(3)-C(9)-C(3)*-N(1)* while the remaining ring, N(2)-C(7)-C(7)*-N(2)*, has a torsion angle of 50.9(4)°.

$[Co^{III}(Et_2\text{-}2,7\text{-dimethoxysar})]^{3+}$

The structure of the second eluted di-ethyl di-imine isomer, in this series, has also been determined and is shown below (Figure 21).[53] It shows that the complex is a saturated molecule with two methoxy groups located on the same strap. For this to occur, two molecules of methanol must have condensed with the original di-imine to form the methoxy pendants during the recrystallisation of the di-imine from methanol. However, from the determined structure it is clear that the two imine groups were originally located on the same strap of the molecule. Also it is clear from the NMR spectroscopy that in aqueous solution, the methanol is readily lost and the isomer exists in the di-imine form. The other structure from this series displays the two imine bonds *trans* to one another. This complex was the last to elute from the Sephadex column. Therefore, the first isomer eluted must have the imine groups located on adjacent straps *cis* to each other. It follows that the order of elution from the Sephadex column and hence the respective assignments of the isomers are: the *cis* isomer, the isomer with the imines on the same strap and then the *trans* isomer.

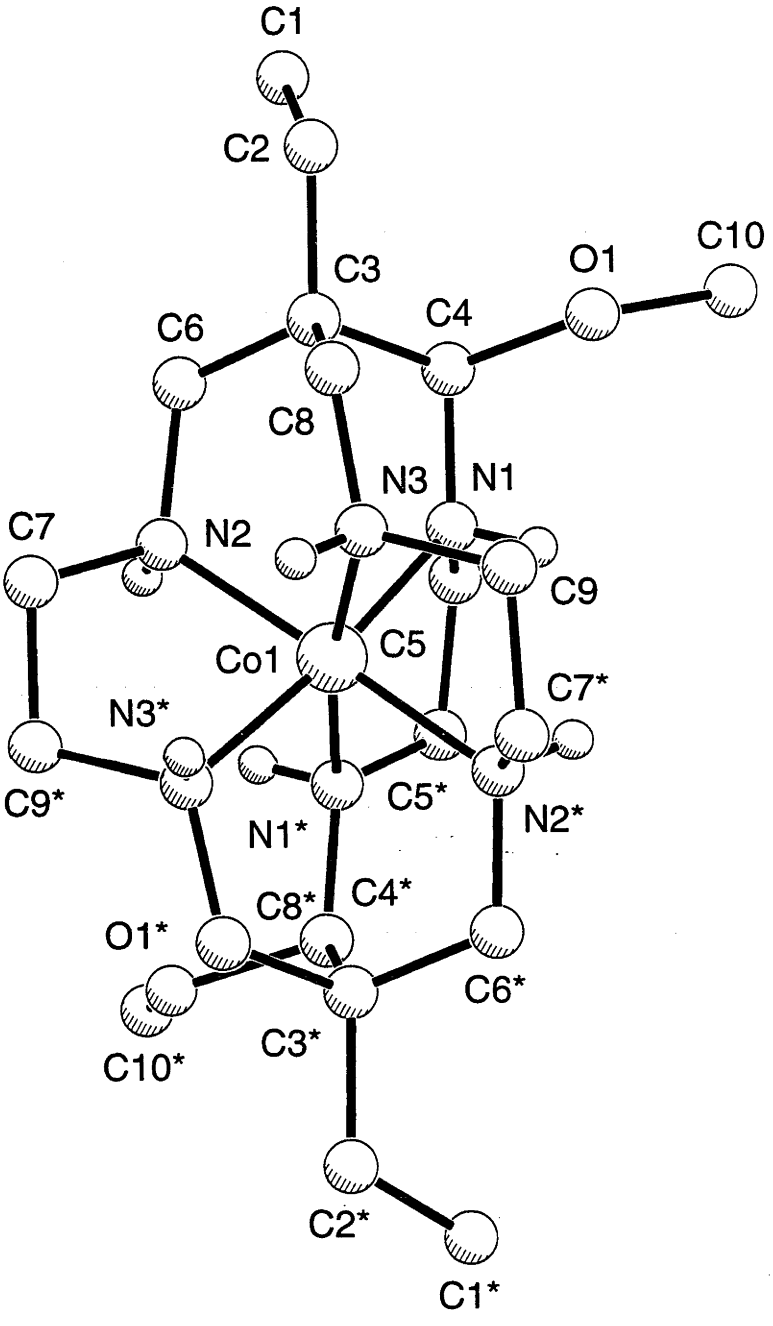

Figure 21. Ortep diagram of the partially solved structure of the $[Co^{III}(Et_2\text{-}2,7\text{-dimethoxysar})]^{3+}$ cation.

6.3.7 Electrochemistry

The cyclic voltammograms, at a scan rate of 20 mVs^{-1}, for the three di-ethyl di-imine isomers appear in Figure 22. These CV's show near reversible behaviour for each complex however they are all certainly chemically reversible. Quasireversible behaviour was also indicated by the cyclic voltammetry where the separations of the anodic and cathodic peak potentials increased with increasing scan rates. Repeated cycling of each complex at 100 mVs^{-1} did not produce any change in the observed waves. The di-propyl isomers showed the same type of behaviour. The Co(III)/Co(II) reduction potentials (vs SCE) for the various amine cage complexes are displayed in Table 3.

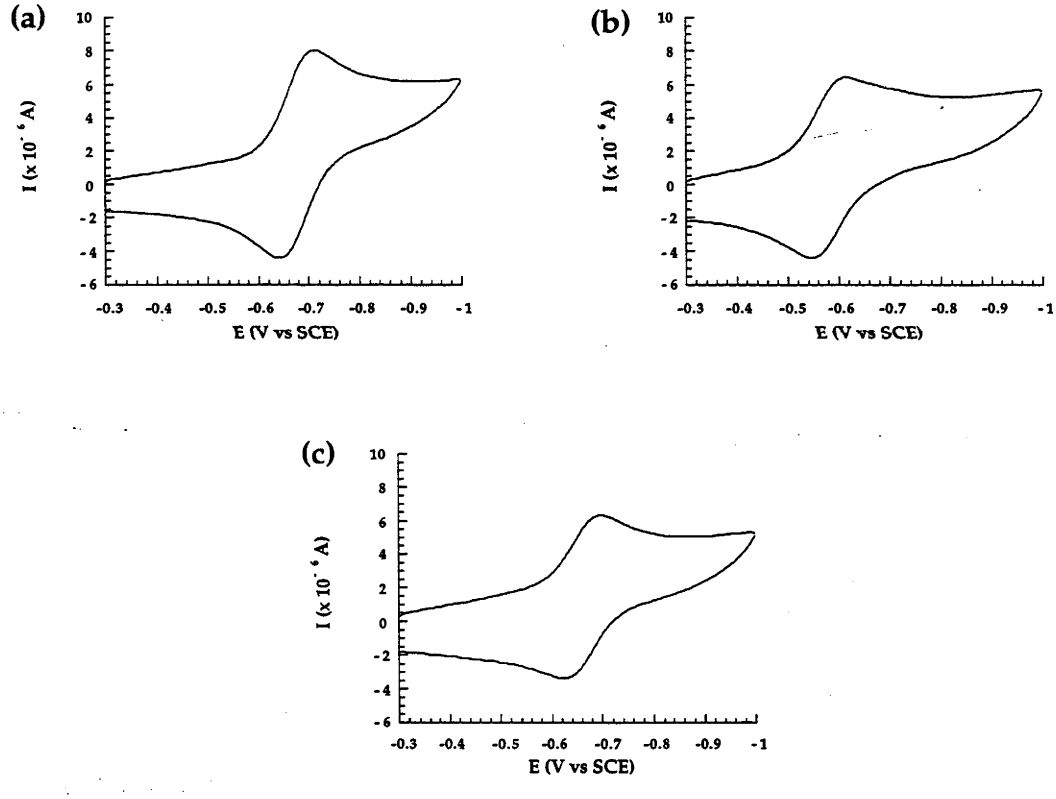

Figure 22. Co(III)/(II) cyclic voltammograms for (a) *cis*-$[Co^{III}(Et_2\text{-sar-2,9-diene})]^{3+}$, (b) $[Co^{III}(Et_2\text{-sar-2,6-diene})]^{3+}$ and (c) *trans*-$[Co^{III}(Et_2\text{-sar-2,9-diene})]^{3+}$ recorded in 0.1 M $NaClO_4$ at 20° C with an EPG electrode and a scan rate of 20 mVs^{-1}.

Table 3. Electrochemical data for cobalt(III)/(II) couple of cage complexes with apical alkyl and hydrogen substituents (vs SCE). (EPG electrode; 1 mM solutions of complex in 0.1 M $NaClO_4$ at 20° C with a scan rate of 20 mVs^{-1}).

Complex	$E_{1/2}$ vs SCE (V)	E_{pc} vs SCE (mV)	E_{pa} vs SCE (mV)	i_{pc}/i_{pa}	ΔE_p (mV)
cis-$[Co^{III}(Et_2\text{-sar-2,9-diene})]^{3+}$	-0.68	-715	-642	0.97	73
$[Co^{III}(Et_2\text{-sar-2,6-diene})]^{3+}$	-0.58	-617	-547	1.2	70
trans-$[Co^{III}(Et_2\text{-sar-2,9-diene})]^{3+}$	-0.66	-699	-623	1.01	76
cis-$[Co^{III}(Pr_2\text{-sar-2,9-diene})]^{3+}$	-0.68	-716	-648	1.06	68
$[Co^{III}(Pr_2\text{-sar-2,6-diene})]^{3+}$	-0.59	-624	-551	1.16	73
trans-$[Co^{III}(Pr_2\text{-sar-2,9-diene})]^{3+}$	-0.67	-703	-629	1.01	74
$[Co^{III}(Me_2\text{-sar-2-ene})]^{3+}$	-0.68	-708	-645	0.92	63
Λ-$[Co^{III}(Et_2\text{-sar})]^{3+}$	-0.68	-714	-649	0.97	65
Δ-$[Co^{III}(Et_2\text{-sar})]^{3+}$	-0.68	-715	-648	1.24	67
$[Co^{III}(sar)]^{3+}$ [54]	-0.66	-698	-634	0.96	64
$[Co^{III}(Me_2\text{-sar})]^{3+}$	-0.69	-720	-656	0.94	64

Two sets of di-imine isomers show similar patterns of redox behaviour which indicates that the different alkane apical substituents have a little effect on each Co(III)/Co(II) potential which is not really surprising. The potential, however, varies from isomer to isomer with the values ranging from -580 mV to -680 mV which is a surprising large variation and should be compared to those of the $[Co^{III}(Et_2\text{-sar})]^{3+/2+}$ (-680 mV) and $[Co^{III}(sar)]^{3+/2+}$ (-666 mV) potentials. The di-methyl monoimine potential occurs at -688 mV while that for the saturated hexamine, $[Co^{III}(Me_2\text{-sar})]^{3+}$, appears at -680 mV. It is clear therefore that alkyl groups at the apical sites make the Co(III)/(II) potential more negative than that of $[Co^{III}(sar)]^{3+}$ by about 40 - 50 mV which is consistent with their electron donating capacity. The potentials do not vary much from the saturated to the unsaturated systems except for the di-imine isomer with the imines located in the same strap which is significantly (100 mV) more positive than the other isomers. Some effect from the imine could have been

expected for the stabilisation of the low oxidation state relative to the fully saturated system. Also some strain is introduced by the imine formation but there is no obvious rationalisation to account of the 100 mV variation in potential. Presumably the strain induced by the unsaturation only in one strand balances the effect expected from the imine formation. The increases in ΔE_p with scan rate for these systems imply moderate electron transfer rates between Co(III) and Co(II) i.e. not greatly different from that of $[Co^{III}(sar)]^{3+/2+}$.

6.3.8 Electronic Spectroscopy

The electronic absorption spectra for the di-ethyl di-imine cage isomers are displayed in Figures 23a, b and c and the di-propyl isomers showed similar behaviour. The electronic spectra are characteristic of low spin octahedral cobalt(III) (Table 4). As Co(III) is a d^6 metal ion in basically an octahedral field, two absorption bands arising from the transitions of $^1T_{1g} \leftarrow {}^1A_{1g}$ and $^1T_{2g} \leftarrow {}^1A_{1g}$ (O_h) origin are expected.

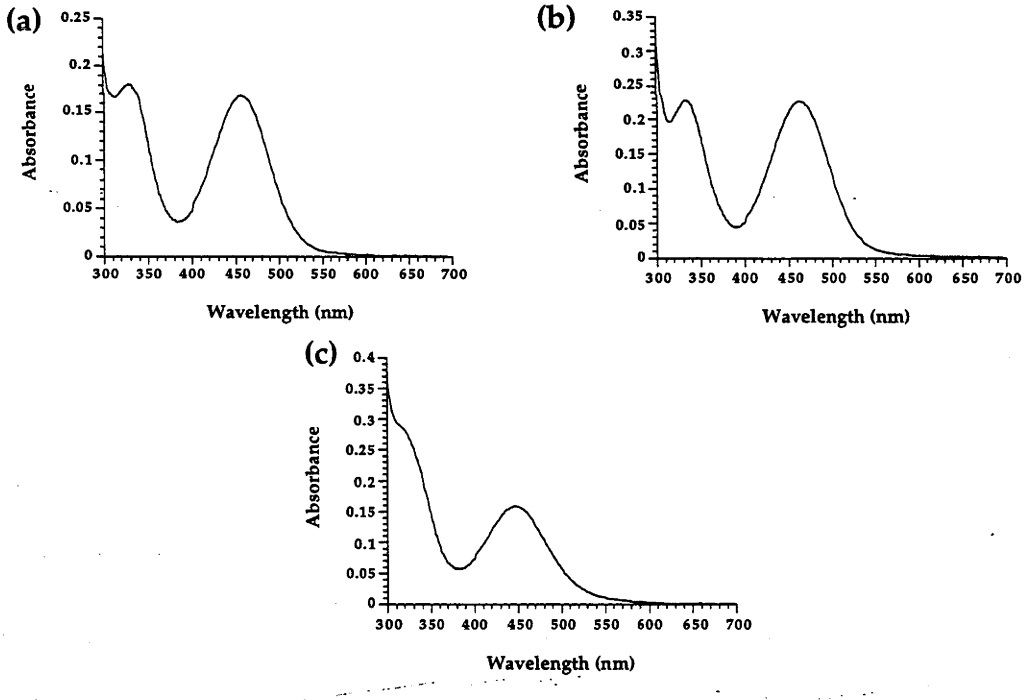

Figure 23. Electronic spectrum of (a) *cis*-$[Co^{III}(Et_2\text{-sar-2,9-diene})]^{3+}$, (b) $[Co^{III}(Et_2\text{-sar-2,6-diene})]^{3+}$ and (c) *trans*-$[Co^{III}(Et_2\text{-sar-2,9-diene})]^{3+}$ in water at 20° C.

Table 4. Electronic absorption data on some Co(III) cage and hexamine complexes. (1mM solutions of complex in water at 20° C).

Complex	λ_{max} nm (ε_{max} $M^{-1}cm^{-1}$)	
	$^1T_{2g} \leftarrow {}^1A_{1g}$ (O_h) Origin	$^1T_{1g} \leftarrow {}^1A_{1g}$ (O_h) Origin
cis-[$Co^{III}(Et_2$-sar-2,9-diene)]$^{3+}$	318 (333)	456 (279)
[$Co^{III}(Et_2$-sar-2,6-diene)]$^{3+}$	332 (350)	464 (295)
trans-[$Co^{III}(Et_2$-sar-2,9-diene)]$^{3+}$	322 sh (456)	444 (295)
cis-[$Co^{III}(Pr_2$-sar-2,9-diene)]$^{3+}$	325 sh (442)	456 (328)
[$Co^{III}(Pr_2$-sar-2,6-diene)]$^{3+}$	326 (462)	464 (387)
trans-[$Co^{III}(Pr_2$-sar-2,9-diene)]$^{3+}$	327 (384)	444 (290)
[$Co^{III}(Me_2$-sar-3-ene)]$^{3+}$	343 (227)	464 (215)
Λ-[$Co^{III}(Et_2$-sar)]$^{3+}$	340 (117)	468 (136)
Δ-[$Co^{III}(Et_2$-sar)]$^{3+}$	340 (117)	468 (136)
[Co^{III}(sar)]$^{3+}$ [49, a]	343 (108)	471 (135)
[$Co^{III}(NH_3)_6]^{3+}$ [23]	339 (46)	475 (75)

a 0.1 M HCl

For all of the di-imines the lower energy d-d band maximum appears between the values of 440 nm and 465 nm, while the higher energy band appears as either a distinct band or shoulder around 330 nm near the base of the more intense allowed charge transfer band (maximum at ~220 nm). These absorptions occur at somewhat higher energy and are significantly more intense (~2 fold) than the usual saturated Co-N_6^{3+} absorptions (Table 4) indicating that they possess a somewhat stronger ligand field, and are more readily allowed than the equivalent transitions for [$Co^{III}(NH_3)_6]^{3+}$ ion for example. For the monoimine complex, the electronic maxima shift to 343 nm and 464 nm, while for the saturated hexamine, [$Co^{III}(Et_2$-sar)]$^{3+}$, the positions of the d-d bands are similar to those observed for [Co^{III}(sar)]$^{3+}$. The absorption maxima of the *trans*-[$Co^{III}(Et_2$-sar-2,9-diene)]$^{3+}$ isomer however also shows a significantly stronger ligand field than those for the other isomers.

The imines *trans* to each other supply the largest variation to the ligand field if the field is viewed as the sum of the three components

mutually trans to each other (i.e. holohedrised) and this may be the origin of the spectral shift.

6.3.9 Resolution of $[Co(Et_2\text{-sar})]^{3+}$

The saturated hexamine complex, $[Co^{III}(Et_2\text{-sar})]^{3+}$, was resolved into its respective enantiomers by ion exchange chromatography. $[Co^{III}(Et_2\text{-sar-2,6-diene})]^{3+}$ was firstly reduced with $NaBH_4$ in an aqueous solution buffered at pH 10 and the chloride salt, obtained from desalting $[Co^{III}(Et_2\text{-sar})]^{3+}$ on Dowex, sorbed on SP Sephadex C-25 cation exchange resin was eluted with 0.15 M $[Sb_2((+)_D\text{tartrato})_2]^{2-}$ ion to yield the two enantiomers. The circular dichroism and optical rotary dispersion spectra of Λ-$(-)_D$-$[Co^{III}(Et_2\text{-sar})]^{3+}$ are shown in Figure 24. The molecular rotations in H_2O for the Co(III) complex were $[M]_{510}$ = -640° $M^{-1}m^{-1}$, $[M]_{435}$ = +1150° $M^{-1}m^{-1}$ and $[M]_{360}$ = +730° $M^{-1}m^{-1}$, while the CD spectrum displayed a maximum in H_2O of $\Delta\varepsilon_{469}$ = -4.65 $M^{-1}cm^{-1}$. The values obtained for the Δ enantiomer were essentially equal, but opposite in sign, to those of the Λ enantiomer within 1% as required for enantiomers.

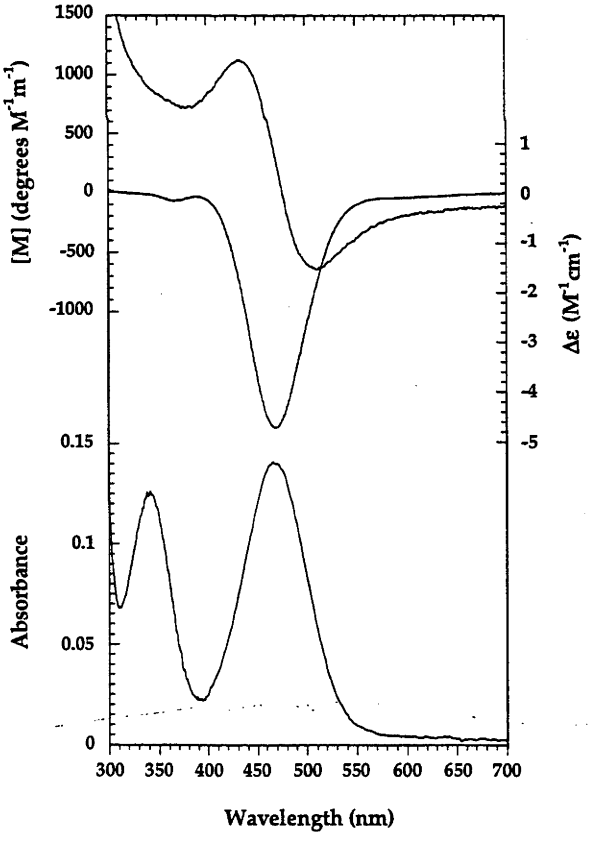

Figure 24 Optical Rotary Dispersion, Circular Dichroism and Electronic Spectrum of Λ-$(-)_D$-$[Co^{III}(Et_2\text{-sar})]^{3+}$ in water at 20° C.

6.3.10 Antiviral Activity

The inhibitory properties of some of the complexes described in this chapter for a series of viruses have been examined. The complexes used include the set of di-ethyl imine isomers and $[Co^{III}(Et_2\text{-sar})]^{3+}$ (Figure 6b). In addition $[Co^{III}(\{NH_3^+\}_2\text{-sar})]^{5+}$ and two other dimeric cage complexes (Figure 25) were also chosen. The complexes were tested against HIV, Hepatitis B and the flavivirus that induces dengue fever in order to establish whether these compounds could offer an effective treatment or prophylaxis of these viral infections.

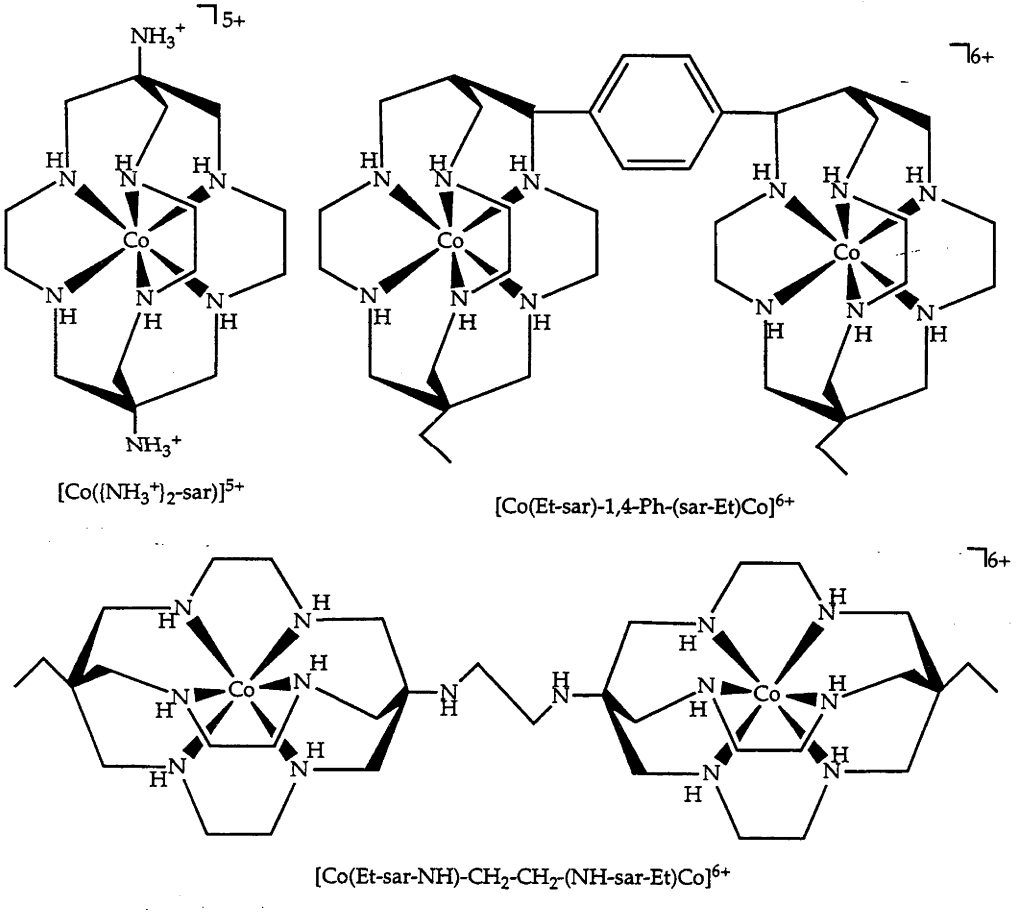

Figure 25

The results obtained for the various tests performed are shown Tables 5 and 6 while Table 7 shows the results obtained from the mouse test for mammalian toxicity to gauge crudely the effects the different compounds have upon living cells.

Table 5. Antiviral activity of some Co(III) cage compounds against the AIDS virus.

Compound	HIV - Rega HIV 1 CC_{50} µM	IC_{50} µM	SI_{50}
$[Co^{III}(Et_2\text{-sar})]Cl_3$	>494	2	>248
	>494	1.7	>295
	>494	1.7	>285
	>494	1.9	>264
	>494	2	>244
$[Co^{III}(Me,Et\text{-sar})]Cl_3$	>125	1.6	>79
	>125	0.39	>317
$[Co^{III}(Et,Bu\text{-sar})]Cl_3$	>129	0.89	>144
	>129	0.32	>407
$[Co^{III}(Et,Pr\text{-sar})]Cl_3$	>130	0.73	>177
	>130	0.33	>393
$[Co^{III}(Et\text{-sar})\text{-}1,4\text{-Ph-}(sar\text{-}Et)Co^{III}]Cl_6$	>243	0.74	>328
	>234	1.3	>191
	>243	0.59	>410
$[Co^{III}(Et\text{-sar-NH})\text{-}CH_2CH_2\text{-}(NH\text{-sar-}Et)Co^{III}]Cl_6$	80	0.39	205
	>100	0.3	>336
	90	-	-
$[Co^{III}(\{NH_3^+\}_2\text{-sar})]Cl_5$	>125	4.2	>30
	>125	5.3	>24

Table 6. Antiviral activity of some Co(III) cage complexes against hepatitis B and the flavivirus.

Compound	HBV - NIAID			FLAVI		
	CC_{50} µM	IC_{50} µM	SI_{50}	CC_{50} µM	IC_{50} µM	SI_{50}
$[Co^{III}(Et_2\text{-diimsar})]Cl_3$	587	25	6.5	-	-	-
$[Co^{III}(Et_2\text{-sar})]Cl_3$	144	0.11	1309	>200	NA	I
$[Co^{III}(Et\text{-sar})\text{-}1,4\text{-Ph-}(sar\text{-}Et)Co^{III}]Cl_6$	1485	1.5	990	>600	<12.5	>16
$[Co^{III}(Et\text{-sar-NH})\text{-}CH_2CH_2\text{-}(NH\text{-sar-}Et)Co^{III}]Cl_6$	334	2.1	159	190	NA	I
$[Co^{III}(\{NH_3^+\}_2\text{-sar})]Cl_5$	1236	1.6	773	>200	NA	I

Table 7. Results of some Co(III) cage complexes tested on mice for mammalian toxicity.

Compound	Mouse Toxicity			
	100 mg/kg	50 mg/kg	10 mg/kg	1 mg/kg
$[Co^{III}(Et_2\text{-sar})]Cl_3$	0/10	0/10	0/10	-
$[Co^{III}(Et\text{-sar})\text{-}1,4\text{-Ph-}(sar\text{-}Et)Co^{III}]Cl_6$	5/5	-	2/5	0/5
$[Co^{III}(\{NH_3^+\}_2\text{-sar})]Cl_5$	0/5	0/5	0/5	-

The effectiveness of a compound, towards a particular virus, is measured by a number of factors. CC_{50} is a measure of the cell toxicity, i.e. fifty per cent of the cells die at the stated concentration. IC_{50} and IC_{90} are the inhibitory concentrations sufficient to stop viral replication, by 50% and 90% respectively while SI, the selectivity index, is the ratio between the cell toxicity index CC_{50} and the inhibitory concentration IC_{50}. Generally for a complex to be adjudged an effective inhibitor towards a certain virus the selectivity index must be high while the inhibitory concentration remains low. Other terms used within the tables include NA and I which mean the compound was "not active" or "inaffective" for that particular virus.

Also, for each separate complex a set number of mice were tested at different concentrations over a specified period (Table 7). The number of mice that died during the test period were then recorded as a fraction of the original starting number. For example, a number of 0/10 means that none of the ten mice, tested at that particular concentration, died during the test for that particular compound. Consequently, a number of 2/5 highlights the toxic nature of a compound because two of the original five test mice died during the test at the set concentration.

Of all the compounds tested in this series $[Co^{III}(Et_2\text{-sar})]Cl_3$ was found to offer the best non toxic inhibitory properties against the Hepatitis B virus (Table 6) with a selectivity index of 1309 and an IC_{50} of 0.11 μM. The next best inhibitor was the dimeric complex $[Co^{III}(Et\text{-sar})\text{-}1,4\text{-}Ph\text{-}(sar\text{-}Et)Co]Cl_6$ with a SI of 990 and an IC_{50} of 1.5 μM, while $[Co^{III}(\{NH_3^+\}_2\text{-}sar)]Cl_5$ and $[Co^{III}(Et\text{-}sar\text{-}NH)\text{-}CH_2CH_2\text{-}(NH\text{-}sar\text{-}Et)Co]Cl_6$ returned SI's and IC_{50}'s of 773 and 1.6 μM and 159 and 2.1 μM respectively. Lastly, the three di-ethyl di-imine isomers were also tested, however, the results indicated that these compounds, along with $[Co^{III}(\{NH_3^+\}_2\text{-}sar)]Cl_5$ and $[Co^{III}(Et\text{-}sar\text{-}NH)\text{-}CH_2CH_2\text{-}(NH\text{-}sar\text{-}Et)Co^{III}]Cl_6$, were not as active as $[Co^{III}(Et_2\text{-}sar)]Cl_3$ towards this particular virus. The di-propyl isomers have not been tested yet. Although the results for $[Co^{III}(Et\text{-}sar)\text{-}1,4\text{-}Ph\text{-}(sar\text{-}Et)Co^{III}]Cl_6$ were more encouraging it turns out that this compound is also much more toxic than $[Co^{III}(Et_2\text{-}sar)]Cl_3$ in the mouse toxicity tests and hence due to this toxicity the complex was ruled out as an effective treatment of the Hepatitis B virus.

The results of the AIDS tests were less encouraging than those of the HBV tests (Table 5) . However, the complexes, including $[Co^{III}(Et_2\text{-}sar)]Cl_3$, did display some activity towards the HIV virus. In most instances the SI values ranged between 20 and 410 while the IC_{50} values were between 0.3

and 5.3 μM. Again the values obtained for $[Co^{III}(Et\text{-}sar)\text{-}1,4\text{-}Ph\text{-}(sar\text{-}Et)Co^{III}]Cl_6$ were encouraging but once more the toxicity of this complex towards healthy cells prevents it from being used as an antiviral agent. The di-ethyl and di-propyl di-imine complexes have not been tested with HIV yet. Finally, tests of the various complexes on the flavivirus (Table 6) indicated they were not significantly active and hence a selectivity index was not obtained. The dimeric complex $[Co^{III}(Et\text{-}sar)\text{-}1,4\text{-}Ph\text{-}(sar\text{-}Et)Co^{III}]Cl_6$ was found to be slightly active but not enough to warrant further investigation. The three di-imine isomers have not been tested separately and nor have the enantiomers of $[Co^{III}(Et_2\text{-}sar)]Cl_3$ at this stage.

6.4 Discussion

6.4.1 Synthesis

The production of the three isomeric imine complexes can be rationalised by the path outlined in Scheme 1. The mechanism is similar to that proposed for the $[Co^{III}(Me_2\text{-sar-2-ene})]^{3+}$ ion[16] except that capping occurs at both trigonal faces instead of on just one amine face. The reaction, like that for the amide complexes involves the initial formation of a monoimine at one of the primary amines of $[Co^{III}(en)_3]^{3+}$. The carbon base then attacks this species producing a pendant aldehyde amine derivative. Following the formation of a second adjacent imine, ring closure occurs by attack of the carbon base at the imine. The new species now has the alkyl and aldehyde groups *exo* to the newly formed six-membered ring. The last step involves capture of the carbonyl group of the aldehyde by the remaining deprotonated amine forming an imine group and the completed cap. Once the first cap forms the remaining face then undergoes the same condensation process and another imine cap forms to produce a Co(III) cage di-imine complex. However, for the second capping reaction the carbanion can now attack any one of the three remaining imine sites, leading to the three observed isomeric imine complexes. Finally the $[Co^{III}(Et_2\text{-sar-2,6-diene})]^{3+}$ ion was reduced with BH_4^- ion to give the the same fully saturated hexamine cage complex.

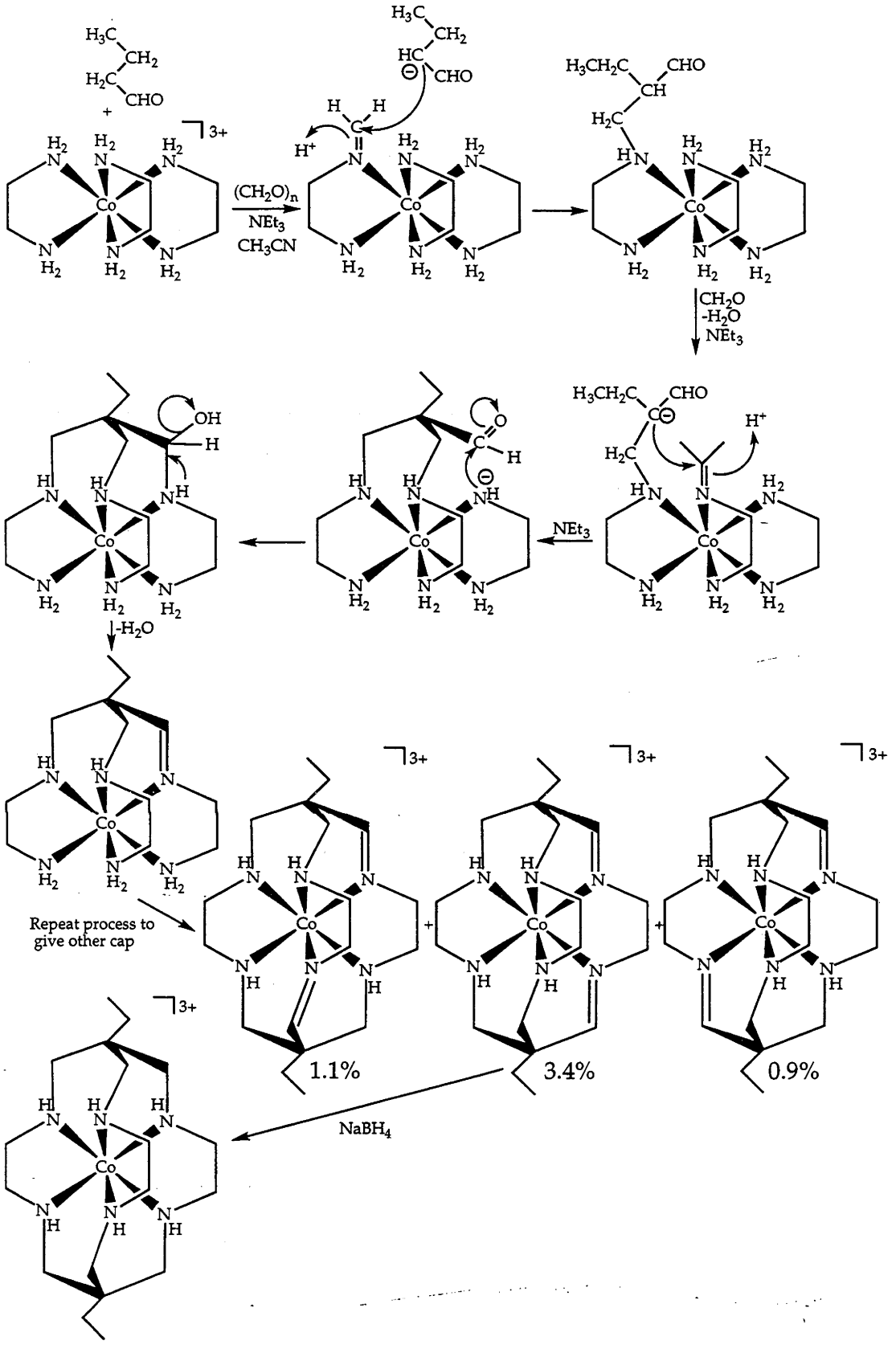

Scheme 1. Mechanism for the formation of *cis*-$[Co^{III}(Et_2\text{-sar-2,9-diene})]^{3+}$, $[Co^{III}(Et_2\text{-sar-2,6-diene})]^{3+}$ and *trans*-$[Co^{III}(Et_2\text{-sar-2,9-diene})]^{3+}$ from $[Co^{III}(en)_3]^{3+}$ and reduction of $[Co^{III}(Et_2\text{-sar-2,6-diene})]^{3+}$ to $[Co^{III}(Et_2\text{-sar})]^{3+}$.

6.4.2 Electronic Spectroscopy

With the incorporation of two imine groups into the basic sar ligand the two observed d-d bands become somewhat blue shifted when compared to that of the parent hexamine $[Co^{III}(sar)]^{3+}$. This indicates that these compounds possess a somewhat stronger ligand field than that of the parent $[Co^{III}(sar)]^{3+}$. This arises from the three isomers in each set possessing an ob_3 instead of a lel_3 conformation as a result of the two imine fragments within each ligand. This leads inherently to a tighter cavity and an increased interaction between the ligand and metal orbitals within each di-imine complex. This shifts the two observed bands in each case to higher energy. Also, the imine itself provides a stronger ligand field than the saturated amine. The combination of both probably contribute to the higher ligand field strength. A way to dissect these effects has not yet been devised. The intensities of the two bands also decrease at the same time since as a result of the *lel* to *ob* conformation change the CoN_6 core becomes more octahedral in character. Therefore the bands become less allowed and less intense as a result.

It should also be noted that both the *trans*-$[Co^{III}(Et_2\text{-sar-2,9-diene})]^{3+}$ and *trans*-$[Co^{III}(Pr_2\text{-sar-2,9-diene})]^{3+}$ isomers possess slightly stronger ligand fields than the remaining two respective isomers (Table 4). This arises mainly as a result of the *trans* positioning of the two imine groups within the cage ligand. As a result, the imine ligands interact with the metal orbitals of the Co(III) in such a way that it leads to a strengthening of the ligand field which is reflected in the electronic spectroscopy.

The absolute configurations of the $[Co^{III}(Et_2\text{-sar})]^{3+}$ isomers have been assigned by analogy with those of the $[Co^{III}(sep)]^{3+}$ ion.[55] Both of these complexes, which have been derived from $[Co^{III}(en)_3]^{3+}$, display CD and ORD spectra that are essentially opposite to that of the $[Co^{III}(en)_3]^{3+}$ parent ion of the same configuration. Generally, in the solution CD of Co(III) hexamine type complexes, the first ligand field band of $^1T_{1g} \leftarrow {}^1A_{1g}$ origin, in a reduced D_3 symmetry ligand field, is split into $^1E_1 \leftarrow {}^1A_1$ and $^1A_2 \leftarrow {}^1A_1$ components which are CD active and of opposite sign. Taking the Λ configuration as an example the $^1E_1 \leftarrow {}^1A_1$ component is large and positive and that of the $^1A_2 \leftarrow {}^1A_1$ component is large and negative for both $[Co^{III}(en)_3]^{3+}$ and $[Co^{III}(sep)]^{3+}$ ions and of similar magnitude.[56-58] Presumably the same holds for the Λ-$[Co^{III}(Et_2\text{-sar})]^{3+}$ ion from this work. In solution, both CD components are observed simultaneously and therefore largely cancel. For Λ-$[Co^{III}(en)_3]^{3+}$ the positive $^1E_1 \leftarrow {}^1A_1$

component dominates the solution dichroism whereas for Λ-$[Co^{III}(sep)]^{3+}$ the negative $^1A_2 \leftarrow {}^1A_1$ component dominates.[56-58] This gives rise to a net small positive CD band at 490 nm for Λ-$[Co^{III}(en)_3]^{3+}$ and a net small negative CD band at 461 nm for Λ-$[Co^{III}(sep)]^{3+}$. The hazard in assigning absolute configurations from solution CD is therefore substantial but in this instance both the $[Co^{III}(sep)]^{3+}$ ion the $[Co^{III}(Et_2\text{-sar})]^{3+}$ have largely *lel* comfigurations in solution and would therefore be expected to have very similar CD spectra for the same configuration. Based on this analysis and the known absolute configuration of the $[Co^{III}(sep)]^{3+}$ ion the $(-)_{468}$-$[Co^{III}(Et_2\text{-sar})]^{3+}$ enantiomer has been assigned the Λ configuration while the $(+)_{468}$-$[Co^{III}(Et_2\text{-sar})]^{3+}$ enantiomer the Δ configuration.

6.4.3 Anti-Viral Testing

Early studies show that the $[Co^{III}(Et_2\text{-sar})]Cl_3$ complex offers good inhibitory properties towards HBV while it also targets the AIDS virus, somewhat less effectively. However, it was found to be virtually ineffective against flaviviruses. To date the anti viral properties of cage complexes, with alkyl tails, have largely been unexplored but early studies show that they have the potential to target certain retroviruses, which is encouraging. Clearly from these results, it is possible to cheaply and effectively design Co(III) cage complexes that target areas of biology. Also, the $[Co^{III}(Et_2\text{-sar})]^{3+}$ system has been shown to be relatively non-toxic to rats and mice, is quantitatively eliminated from the body and is active at the 0.1 μM level. It still remains to be seen if the two chiral forms of $[Co^{III}(Et_2\text{-sar})]^{3+}$ offer different inhibitory properties. Although these early results are encouraging further work is required to determine the point at which the $[Co^{III}(Et_2\text{-sar})]^{3+}$ ion is effective in the retroviral process. Studies to determine this issue are currently underway. However, the mechanism of the AIDS virus will now be examined as an example, to highlight the possible areas that the $[Co^{III}(Et_2\text{-sar})]Cl_3$ complex may interfere with the retroviral process. HBV, being a retrovirus as well, presumably behaves similarly and so the complex may affect the HBV in a similar way to HIV.

The search for an effective treatment against HIV is on going and a more complete knowledge of the virus itself is needed; what follows is some explanation of the known virus processes. HIV and other viruses contain RNA instead of DNA and as explained earlier HIV belongs to a family of viruses named the retroviruses. Retroviruses are so-called because the virus causes the host cell to convert viral RNA back into DNA, contrary to a cell's normal mode of operation, which involves making

RNA from a DNA template. When HIV infects a cell, its outer envelope fuses with the membrane of the cell (Figure 26). This releases viral RNA into the cell, along with an enzyme which tells the cell to make DNA from the RNA template. This enzyme is called reverse transcriptase. It is unique to the virus and does not occur in healthy human cells. This individuality is an important factor in the design of drugs to combat the HIV virus, as it is a good target to disrupt without damaging healthy human cells.

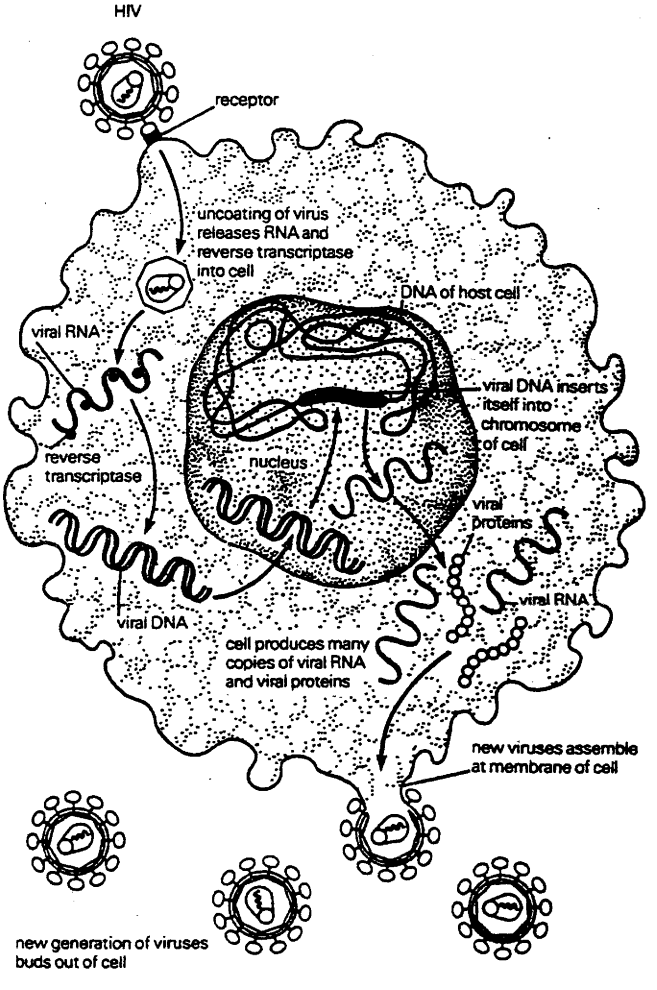

Figure 26. The life cycle of the human immunodeficiency virus.[59] It takes over the cell's machinery for making proteins, channelling the activity of the cell into the manufacture of many new viruses.

The viral DNA enters the nucleus and integrates itself into the DNA of the cell. Once there, the viral DNA lies dormant. This is the latent stage of infection, the incubation period. It can last for months or years. Eventually, when some trigger activates the cell, the viral DNA starts to direct the production of viral components. There are many theories about what the trigger might be. For example, there is some evidence that

subsequent infections with other viruses, such as herpes viruses, can activate infected cells. Whatever the trigger, the result is the manufacture of viral protein and viral RNA - the two main components of HIV. The viral proteins migrate to the surface of the host cell, where they stick out through its outer membrane. The remaining elements of the virus, including the RNA also assemble themselves beneath the cell membrane. Then by a process known as budding, multitudes of new viruses detach themselves from the host cell, borne away in the bloodstream to attack other cells.

From the preliminary work completed with the $[Co^{III}(Et_2\text{-sar})]Cl_3$ complex on the AIDS and Hepatitis B viruses it is clear that it attacks relatively early in the viral process. As previously mentioned it is not known exactly how and at what point the Co(III) compound has an effect but work is currently continuing to determine this. It is at present, thought that it either binds at the entry site and inhibits the entry of the virus or that it inhibits the viral uncoating or reverse transcriptase stages by electrostatically disrupting or altering these steps and slowing or preventing the spread of the virus. Though this point still remains unclear and more work is needed, the early experiments show that the $[Co^{III}(Et_2\text{-sar})]Cl_3$ complex does affect certain retroviruses and may point the way to the design of molecules which are benign yet inhibit diseases like AIDS and Hepatitis B.

6.5 Conclusions and Future Directions

In this chapter it has been demonstrated that a series of di-imine di-alkyl tail Co(III) cage complexes can be prepared from template capping reactions. This strategy proved useful in that it introduced two types of functionalisation to the cage, that is, the imine moiety within the actual cage ligand and various apical alkyl tails. Attempts to add a variety of carbon acids to the imine groups were also undertaken but proved to be unsuccessful. However, reactions of this kind should be possible with these complexes as they have been observed to be successful with other imine compounds and further work is required to explore this problem. The saturated complex, $[Co^{III}(Et_2\text{-sar})]Cl_3$, was then produced from the corresponding di-imine cage complexes via a $NaBH_4$ reduction. In addition, all the complexes were found to be extraordinarily stable with respect to ligand dissociation and association, which is a function of the cage structure and the expected kinetic inertness of Co(III) hexaamine complexes.

The stability of the $[Co^{III}(Et_2\text{-sar})]^{3+}$ ion allowed it to be examined for its anti viral properties, an area in which cage complexes have not been looked at before. Early studies show that the $[Co^{III}(Et_2\text{-sar})]^{3+}$ ion appears to offer good inhibitory properties towards the hepatitis B virus but is somewhat less effective for the AIDS virus. At this time it is not known at what stage the Co(III) cage complex targets hepatitis B other than it seems to be early in the process of replication. Nor is it known yet if one enantiomer of $[Co^{III}(Et_2\text{-sar})]^{3+}$ is more effective than the other as a viral agent. These two areas form the focus for the work that is currently ongoing with these complexes.

6.6 References

(1) Busch, D. H.; Farmery, K.; Goedken, V.; Katovic, A. C.; Sperati, C. R. S.; Tokel, N. *Adv. Chem. Ser.* **1971**, *No. 100*, 44.

(2) Martin, J. W. L.; Curtis, N. F. *J. Chem.Soc. Dalton Trans.* **1975**, 87.

(3) Pietraszkiewicz, M. *J. Coord. Chem.* **1992**, *27*, 151.

(4) Owston, P. G.; Peters, R.; Ramsamy, E.; Tasker, P. A.; Trotter, J. *J. Chem. Soc., Chem. Commun.* **1980**, 1218.

(5) Lindoy, L. F. *The Chemistry of Macrocyclic Ligand Complexes*; Cambridge University Press: Cambridge, 1989.

(6) Chaudhuri, P.; Wieghardt, K. *Progr. Inorg. Chem.* **1987**, *35*, 329.

(7) Black, D. S. C.; Hartshorn, A. J. *Coord. Chem. Rev.* **1972**, *9*, 219.

(8) Curtis, N. F. *Coord. Chem. Rev.* **1968**, *3*, 3.

(9) Black, D. S. C.; Moss, G. I. *Aust. J. Chem.* **1987**, *40*, 129.

(10) Lindoy, L. F.; Busch, D. H. *Prep. Inorg. Chem.* **1971**, *6*, 1.

(11) Healy, M. d. S.; Rest, A. J. *Adv. Inorg. Chem. Radiochem.* **1978**, *21*, 1.

(12) Drew, M. G. B.; McFall, S. G.; Nelson, S. M. *J. Chem. Soc. Dalton Trans.* **1979**, 575.

(13) Bhula, R.; Osvath, P.; Weatherburn, D. C. *Coord. Chem. Rev.* **1988**, *91*, 89.

(14) Shu, M. P.; Shin, W.; Kim, S. *Inorg. Chem.* **1984**, *23*, 618.

(15) Sargeson, A. M. *Pure & Appl. Chem.* **1984**, *56*, 1603.

(16) Höhn, A.; Geue, R. J.; Sargeson, A. M. *J. Chem. Soc., Chem. Commun.* **1990**, 1473.

(17) Behm, C. A.; Creaser, I. I.; Korybut-Daszkiewicz, B.; Geue, R. J.; Sargeson, A. M.; Walker, G. W. *J. Chem. Soc., Chem. Commun.* **1993**, 1844.

(18) Golding, B. T.; Harrowfield, J. M.; Robertson, G. B.; Sargeson, A. M.; Whimp, P. O. *J. Am. Chem. Soc.* **1974**, *96*, 3691.

(19) Harrowfield, J. M.; Sargeson, A. M. *J. Am. Chem. Soc.* **1979**, *101*, 1514.

(20) Korybut-Daszkiewicz, B. *J. Chem. Soc. Dalton Trans.* **1992**, 1673.

(21) Korybut-Daszkiewicz, B. *J. Coord Chem* **1992**, *27*, 219.

(22) Kang, S.-G.; Kim, M.-S.; Kim, S.-J.; Ryu, K. *Polyhedron* **1996**, *15*, 1835.

(23) Bernhardt, P. V.; Lawrance, G. A.; Hambley, T. W. *J. Chem. Soc., Dalton Trans.* **1989**, 1059.

(24) Sargeson, A. M. *Chemistry in Australia* **1991**, 176.

(25) Walker, G. W. *Personal communication*

(26) De Clercq, E.; Yamamoto, N.; Pauwels, R.; Baba, M.; Schols, D.; Nakashima, H.; Balzarini, J.; Debyser, Z.; Murrer, B. A.; Schwartz, D.; Thornton, D.; Bridger, G.; Fricker, S.; Henson, G.; Abrams, M.; Picker, D. *Proc. Natl. Acad. Sci. USA* **1992**, *89*, 5286.

(27) Sargeson, A. M. *Pure & Appl. Chem.* **1986**, *58*, 1511.

(28) Sargeson, A. M. *Personal Communication*

(29) Broomhead, J. A.; Dwyer, F. P.; Hogarth, J. W. *Inorg. Synth.* **1960**, *6*, 183.

(30) Tomioka, K.; Sakaguchi, U.; Yoneda, H. *Inorg. Chem.* **1984**, *23*, 2863.

(31) Sarneski, J. E.; Urbach, F. L. *J. Am. Chem. Soc.* **1971**, *93*, 884.

(32) Green, R. W.; Catchpole, K. W.; Phillip, A. T.; Lions, F. *Inorg. Chem.* **1963**, *2*, 597.

(33) Beurskens, P. T.; Admiraal, G.; Beurskens, G.; Bosman, W. P.; Garcia-Granda, S.; Gould, R. O.; Smits, J. M. M.; Smykalla, C. *PATTY In The DIRDIF program system, Technical Report of the Crystallography Laboratory*; University of Nijimegen: The Netherlands, 1992.

(34) Beurskens, P. T.; Admiraal, G.; Beurskens, G.; Bosman, W. P.; Garcia-Granda, S.; Gould, R. O.; Smits, J. M. M.; Smykalla, C. *DIRDIF92 In The DIRDIF program system, Technical Report of the Crystallography Laboratory*; University of Nijimegen: The Netherlands, 1992.

(35) Cromer, D. T.; Waber, J. T. In *International Tables of X-ray Crystallography*; The Kynoch Press: Birmingham, England, 1974; Vol. IV.

(36) Ibers, J. A.; Hamilton, W. C. *Acta Crystallogr.* **1964**, *17*, 781.

(37) Creagh, D. C.; McAuley, W. J. In *International Tables for Crystallography*; A. J. C. Wilson, Ed.; Kluwer Academic Publishers: Boston, 1992; Vol. C; pp 219.

(38) Creagh, D. C.; Hubbel, J. H. In *International Tables for Crystallography*; A. J. C. Wilson, Ed.; Kluwer Academic Publishers: Boston, 1992; Vol. C; pp 200.

(39) *teXsan: Crystal Structure Analysis Package*; Molecular Structure Corporation: 1985 & 1992.

(40) Korba; Gerin *Antiviral Research* **1992**, *19*, 55.

(41) Chu, P. W. G.; Westaway, E. G. *Virology* **1985**, *140*, 68.

(42) Chu, P. W. G.; Westaway, E. G. *Virology* **1987**, *157*, 330.

(43) Grun, J. B.; Brinton, M. A. *Journal of Virology* **1986**, *60*, 1113.

(44) Sabin, A. B.; Schlesinger, R. W. *Science* **1945**, *101*, 640.

(45) Boulton, R. W.; Westaway, E. G. *Virology* **1972**, *49*, 283.

(46) Leigh, G. J. *Nomenclature of Inorganic Chemistry - Recommendations 1990. International Union of Pure and Applied Chemistry*; Blackwell: Oxford, 1990.

(47) Walker, G. W. Ph.D Thesis, Australian National University, 1997.

(48) Bernhardt, P. V.; Bygott, A. M. T.; Geue, R. J.; Hendry, A. J.; Korybut-Daszkiewicz, B. R.; Sargeson, A. M.; Willis, A. C. *Inorg. Chem.* **1994**, *33*, 4553.

(49) Geue, R. J.; Hambley, T. W.; Harrowfield, J. M.; Sargeson, A. M.; Snow, M. R. *J. Am. Chem. Soc.* **1984**, *106*, 5478.

(50) Balahura, R. J.; Ferguson, G.; Ruhl, B. L.; Wilkins, R. J. *Inorg. Chem.* **1983**, *22*, 3990.

(51) Höhn, A.; Geue, R. J.; Sargeson, A. M.; Willis, A. C. *J. Chem. Soc., Chem. Commun.* **1989**, 1648.

(52) *Coordination Chemistry of Macrocyclic Complexes;* Melson, G. A., Ed.; Plenum: New York, 1982.

(53) Osvath, P. *Personal communication*

(54) Bond, A. M.; Lawrance, G. A.; Lay, P. A.; Sargeson, A. M. *Inorg. Chem.* **1983**, *22*, 2010.

(55) Creaser, I. I.; Geue, R. J.; Harrowfield, J. M.; Herlt, A. J.; Sargeson, A. M.; Snow, M. R.; Springborg, J. *J. Am. Chem. Soc.* **1982**, *104*, 6016.

(56) Mason, S. F. *Q. Rev., Chem. Soc.* **1963**, *17*, 20.

(57) Mason, S. F.; Norman, B. J. *J. Chem. Soc. (A)* **1966**, 307.

(58) Dubicki, L.; Ferguson, J.; Geue, R. J.; Sargeson, A. M. *Chem. Phys. Lett.* **1980**, *74*, 393.

(59) Conner, S.; Kingman, S. *The Search for the Virus. The Scientific Discovery of AIDS and the Quest for a Cure.;* Penguin Books: London, 1988.

APPENDICES.

Appendix 3.1

Table A3.1.1: Crystallographic Data for $[Co^{III}(Me,CN\text{-}2\text{-}oxosar\text{-}H)](ClO_4)_{3/2}Cl_{1/2}.H_2O$

Empirical formula	$C_{16}H_{32}Cl_2CoN_7O_8$
Formula weight	580.31
Crystal colour, habit	orange, block
Crystal Dimensions	0.17 x 0.09 x 0.07 mm
Crystal system	monoclinic
Lattice Type	C-centred
w Scan PWHH	0.33°
Lattice parameters	a = 26.143(1) Å
	b = 10.794(2) Å
	c = 17.061(2) Å
	β = 108.522(6)°
V	4564.9(9) Å^3
Space group	C2/c (#15)
Z Value	8
D_{calc} g/cm^3	1.689 g cm^{-3}
F_{000}	2416.00
m(CuKα)	85.88 cm^{-1}
X-radiation	Cu-Kα
λ, Å	1.5478
T, °C	-60.0
No of Data Collected	3734
No of Unique Data	3598
No Obs, (I>3.00s(I))	2284
R	0.033
R_w	0.026
Goodness of Fit	1.64

Table A3.1.2: Atomic Coordinates (non-Hydrogen atoms) for $[Co^{III}(Me,CN\text{-}2\text{-}oxosar\text{-}H)](ClO_4)_{3/2}Cl_{1/2}.H_2O$

	x/a	y/b	z/c
Co(1)	0.36008(3)	0.24600(7)	0.32275(4)
Cl(1)	0.0000	0.2946(2)	0.2500
Cl(2)	0.12091(5)	0.2995(1)	0.04847(8)
Cl(3)	0.5000	0.3139(1)	0.2500
O(11)	0.0325(1)	0.3709(3)	0.3159(2)
O(12)	0.0347(1)	0.2206(4)	0.2206(3)
O(21)	0.1148(2)	0.4205(3)	0.0138(2)
O(22)	0.1449(2)	0.2223(3)	0.0032(2)
O(23)	0.0703(1)	0.2529(4)	0.0472(2)
O(24)	0.1553(1)	0.3067(4)	0.1320(2)
O(31)	0.2458(1)	-0.0061(3)	0.2091(2)
O(50)	0.1530(2)	0.2780(4)	0.3060(3)
N(1)	0.2564(1)	0.0120(3)	0.0190(2)
N(12)	0.3986(1)	0.1521(3)	0.2590(2)
N(15)	0.4071(1)	0.1599(3)	0.4212(2)
N(22)	0.3184(1)	0.3358(3)	0.2211(2)
N(25)	0.4121(1)	0.3845(3)	0.3434(2)
N(32)	0.3051(1)	0.1237(3)	0.2987(2)
N(35)	0.3200(1)	0.3137(3)	0.3933(2)
C(1)	0.2776(2)	0.0580(4)	0.0801(3)
C(2)	0.3054(2)	0.1216(4)	0.1589(2)
C(3)	0.4121(2)	0.3682(4)	0.4915(3)
C(4)	0.4368(2)	0.4310(5)	0.5751(3)
C(11)	0.3662(2)	0.1019(4)	0.1766(3)
C(13)	0.4300(2)	0.0532(4)	0.3139(3)
C(14)	0.4532(2)	0.1070(4)	0.3983(3)
C(16)	0.4250(2)	0.2299(5)	0.5015(3)
C(21)	0.2904(2)	0.2605(4)	0.1465(3)
C(23)	0.3556(2)	0.4307(4)	0.2050(3)
C(24)	0.3854(2)	0.4877(4)	0.2868(3)
C(26)	0.4377(2)	0.4241(4)	0.4310(3)
C(31)	0.2839(2)	0.0709(4)	0.2273(3)
C(33)	0.2755(2)	0.1092(4)	0.3582(3)
C(34)	0.2948(2)	0.2074(4)	0.4242(3)
C(36)	0.3515(2)	0.3939(4)	0.4632(3)

Table A3.1.3: Crystallographic Data for [Ni^{II}(Me,COO$^-$-2-oxosar)]$(ClO_4)_2.2H_2O$

Empirical formula	$C_{32}H_{72}Cl_2N_{12}Ni_2O_{19}$
Formula weight	1117.30
Crystal colour, habit	mauve, rhomboid
Crystal Dimensions	0.32 x 0.16 x 0.11 mm
Crystal system	triclinic
Lattice Type	Primitive
ω Scan PWHH	0.34°
Lattice parameters	a = 8.996(5) Å
	b = 15.939(5) Å
	c = 17.701(6) Å
	α = 69.65(2)°
	β = 108.522(6)°
	γ = 81.27(4)°
V	2351(2) Å^3
Space group	P1 (#2)
Z Value	2
D_{calc} g/cm^3	1.578 g/cm^{-3}
F_{000}	1180.00
μ(CuKα)	27.90 cm^{-1}
X-radiation	Cu-Kα
λ, Å	1.54178
T, °C	-60.0
No of Data Collected	7488
No of Unique Data	6972
No Obs, (I>3.00s(I))	5940
R	0.040
R_w	0.053
Goodness of Fit	2.69

Table A3.1.4: Atomic Coordinates (non-Hydrogen atoms) for $[Ni^{II}(Me,COO^{-}\text{-}2\text{-}oxosar)](ClO_4)_2.2H_2O$

	x/a	y/b	z/c
Ni(1)	0.30244(3)	0.74116(2)	0.74108(2)
Ni(2)	0.24529(3)	0.81378(2)	0.23065(2)
Cl(1)	0.19107(6)	0.37575(4)	0.40630(3)
Cl(2)	0.17767(7)	0.39255(4)	0.90631(4)
O(1)	-0.0986(2)	0.7910(1)	0.77720(9)
O(2)	-0.1942(2)	0.95962(9)	0.57459(8)
O(3)	-0.1476(2)	1.0067(1)	0.67441(8)
O(4)	-0.1694(2)	0.8261(1)	0.23441(9)
O(5)	-0.2503(2)	0.9975(1)	0.04400(8)
O(6)	-0.2392(2)	1.0478(1)	0.14689(9)
O(7)	0.1069(3)	0.3436(2)	0.4744(1)
O(7a)	0.142(2)	0.3066(8)	0.4737(8)
O(8)	0.1026(3)	0.3981(2)	0.3330(1)
O(8a)	0.161(2)	0.366(1)	0.3364(6)
O(9)	0.2592(3)	0.4520(2)	0.4007(1)
O(9a)	0.132(2)	0.4589(6)	0.4149(8)
O(10)	0.3097(3)	0.3049(2)	0.4074(2)
O(10a)	0.3500(8)	0.366(1)	0.4202(8)
O(11)	0.1444(3)	0.3155(1)	0.8929(2)
O(12)	0.0791(3)	0.4153(2)	0.9588(2)
O(13)	0.1664(3)	0.4642(2)	0.8304(1)
O(14)	0.3236(2)	0.3800(2)	0.9366(2)
O(15)	0.3087(2)	0.1222(1)	0.5229(1)
O(16)	0.6228(2)	0.1257(1)	0.51230(9)
O(17)	0.5383(2)	0.1905(1)	0.0711(1)
O(18)	0.9640(3)	0.3986(1)	0.7324(1)
O(19)	0.3796(3)	0.1610(2)	0.9452(2)
O(20)	0.4825(4)	0.0955(2)	0.9624(2)
N(1)	0.1346(2)	0.8148(1)	0.80216(9)
N(2)	0.2775(2)	0.6338(1)	0.84601(9)
N(3)	0.3040(2)	0.8716(1)	0.65364(9)
N(4)	0.5018(2)	0.7662(1)	0.7819(1)
N(5)	0.1332(2)	0.7271(1)	0.66512(9)
N(6)	0.4349(2)	0.6445(1)	0.70196(9)
N(7)	0.0321(2)	0.8624(1)	0.2854(1)
N(8)	0.2316(2)	0.6997(1)	0.3316(1)
N(9)	0.2350(2)	0.9451(1)	0.1470(1)

Table A3.1.4 cont: Atomic Coordinates (non-Hydrogen atoms) for $[Ni^{II}(Me,COO^{-}\text{-}2\text{-}oxosar)](ClO_4)_2.2H_2O$

	x/a	y/b	z/c
N(10)	0.4004(2)	0.8549(1)	0.2909(1)
N(11)	0.1122(2)	0.7880(1)	0.14540(9)
N(12)	0.4208(2)	0.7470(1)	0.1853(1)
C(1)	0.0209(2)	0.8812(1)	0.6632(1)
C(2)	0.0079(2)	0.8286(1)	0.7528(1)
C(3)	0.1300(2)	0.7545(1)	0.8872(1)
C(4)	0.1469(2)	0.6569(1)	0.8926(1)
C(5)	0.4218(2)	0.5997(1)	0.8936(1)
C(6)	0.5604(2)	0.5965(1)	0.8407(1)
C(7)	0.1563(2)	0.9323(1)	0.6412(1)
C(8)	0.4232(2)	0.9121(1)	0.6784(1)
C(9)	0.5543(2)	0.8398(1)	0.7143(1)
C(10)	0.6214(2)	0.6864(1)	0.8125(1)
C(11)	0.0273(2)	0.8105(1)	0.6216(1)
C(12)	0.2192(2)	0.6878(1)	0.6091(1)
C(13)	0.3373(2)	0.6112(1)	0.6568(1)
C(14)	0.5230(2)	0.5694(1)	0.7691(1)
C(15)	-0.1203(2)	0.9547(1)	0.6349(1)
C(16)	0.6860(2)	0.5242(1)	0.8913(1)
C(17)	-0.0404(2)	0.9342(1)	0.1404(1)
C(18)	-0.0706(2)	0.8729(1)	0.2251(1)
C(19)	0.0.164(3)	0.7939(2)	0.3655(1)
C(20a)	0.075(1)	0.7072(7)	0.3734(6)
C(20)	0.1600(3)	0.7331(2)	0.3946(1)
C(21)	0.3809(3)	0.6452(2)	0.3623(1)
C(22)	0.5171(2)	0.6891(1)	0.3321(1)
C(23)	0.0795(2)	0.9953(1)	0.1346(1)
C(24)	0.3439(2)	0.9923(1)	0.1727(1)
C(25)	0.4675(2)	0.9234(1)	0.2252(1)
C(26)	0.5140(2)	0.7806(1)	0.3423(1)
C(27)	0.0074(2)	0.8680(1)	0.0945(1)
C(28)	0.2187(2)	0.7478(1)	0.0974(1)
C(29)	0.3514(2)	0.6899(1)	0.1503(1)
C(30)	0.5472(3)	0.6970(2)	0.2432(1)
C(31)	-0.1911(2)	0.9984(1)	0.1069(1)
C(32)	0.6537(3)	0.6265(2)	0.3821(2)

Table A3.1.5: Crystallographic Data for $[Cu^{II}(Me\text{-}2\text{-}oxosar)](Cl0_4)_2.1.3H_2O$

Empirical formula	$C_{15}H_{34.6}N_6Cl_2CuO_{10.3}$
Formula weight	598.32
Crystal colour, habit	dark-blue, block
Crystal Dimensions	0.31x0.28x0.11
Crystal system	monoclinic
Lattice Type	Primitive
ω Scan PWHH	-
Lattice parameters	a = 9.076(3) (Å)
	b = 13.696(4) (Å)
	c = 19.609(6) (Å)
	β = 101.77(3) °
V	2433(1)
Space group	$P2_1/n$ (#14)
Z Value	4
D_{calc} g/cm^3	1.633
F_{000}	1248
μ(CuKα)	11.80
X-radiation	Mo-Kα
λ, Å	0.71069
T, °C	23(1)
No of Data Collected	4641
No of Unique Data	4506
No Obs, (I>3.00s(I))	2929
R	0.063
R_w	0.068
Goodness of Fit	3.16

Table A3.1.6: Atomic Coordinates (non-Hydrogen atoms) for $[Cu^{II}(Me\text{-}2\text{-}oxosar)](Cl0_4)_2.1.3H_2O$

	x/a	y/b	z/c
Cu(1)	0.23418(5)	0.23105(3)	0.18034(2)
Cl(1)	0.3382(2)	0.1530(1)	-0.07604(6)
Cl(2)	0.6420(2)	0.01186(9)	0.33857(7)
O(1)	0.3475(3)	0.4967(2)	0.2403(2)
O(2a)	0.4155(8)	0.2511(4)	-0.0727(4)
O(2b)	0.2974(10)	0.2361(5)	-0.1208(4)
O(3a)	0.1953(5)	0.1670(5)	-0.0648(4)
O(3b)	0.1888(7)	0.1064(6)	-0.0740(4)
O(4a)	0.3501(8)	0.1214(5)	-0.1440(3)
O(4b)	0.4115(9)	0.0877(5)	-0.1131(4)
O(5a)	0.4359(7)	0.0995(5)	-0.0229(3)
O(5b)	0.4060(9)	0.1766(7)	-0.0090(3)
O(6)	0.5542(5)	0.0917(3)	0.3455(2)
O(7)	0.7576(5)	0.0368(3)	0.3051(2)
O(8)	0.6875(6)	-0.0264(4)	0.4052(2)
O(9)	0.5456(6)	-0.0535(4)	0.2974(3)
O(10)	0.5707(5)	0.3383(3)	0.0556(2)
O(11)	0.4760(2)	0.3800(1)	-0.0708(8)
N(1)	0.3848(4)	0.4171(2)	0.1459(2)
N(2)	0.0987(4)	0.3238(2)	0.0942(2)
N(3)	0.4571(3)	0.1968(2)	0.2067(2)
N(4)	0.2295(3)	0.1365(2)	0.1037(2)
N(5)	0.2497(3)	0.3029(2)	0.2716(2)
N(6)	0.0378(3)	0.1783(2)	0.2030(2)
C(1)	0.5043(4)	0.3951(3)	0.2613(2)
C(2)	0.4100(5)	0.4323(3)	0.2135(2)
C(3)	0.2673(6)	0.4648(3)	0.0975(3)
C(4)	0.1677(5)	0.3926(3)	0.0527(2)
C(5)	-0.0084(4)	0.2621(3)	0.0545(2)
C(6)	-0.0482(4)	0.1654(3)	0.0736(2)
C(7)	-0.1848(5)	0.1273(3)	0.0223(2)
C(8)	0.5701(4)	0.2748(3)	0.2268(2)
C(9)	0.9435(4)	0.1289(3)	0.1544(2)
C(10)	0.3544(4)	0.0688(3)	0.1272(2)
C(11)	0.0815(4)	0.0931(3)	0.0777(2)
C(12)	0.4040(5)	0.3248(3)	0.3107(2)

Table A3.1.6 cont: Atomic Coordinates (non-Hydrogen atoms) for $[Cu^{II}(Me\text{-}2\text{-}oxosar)](Cl0_4)_2.1.3H_2O$

	x/a	y/b	z/c
C(13)	0.1584(5)	0.2487(3)	0.3122(2)
C(14)	0.0096(4)	0.2251(3)	0.2669(2)
C(15)	-0.0919(4)	0.1760(3)	0.1449(2)

Table A3.1.7: Crystallographic Data for $[Fe^{III}(Me,CO_2H\text{-}2\text{-}oxosar\text{-}H)](Cl0_4)_2.\text{-}0.5H_2O$

Empirical formula	$C_{16}H_{32}N_6Cl_2FeO_{11.5}$
Formula weight	619.22
Crystal colour, habit	red, prism
Crystal Dimensions	0.20x0.20x0.10
Crystal system	orthorhombic
Lattice Type	Primitive
ω Scan PWHH	0.44°
Lattice parameters	a = 33.493(4) (Å)
	b = 10.280(2) (Å)
	c = 13.803(2) (Å)
	β = - °
V	4752(3)
Space group	Pbcn (#60)
Z Value	8
D_{calc} g/cm^3	1.731
F_{000}	2576
μ(CuKα)	78.27
X-radiation	Cu-Kα
l, Å	1.54178
T, °C	-60(1)
No of Data Collected	4025
No of Unique Data	-
No Obs, (I>3.00s(I))	1709

Table A3.1.7 cont: Crystallographic Data for $[Fe^{III}(Me,CO_2H\text{-}2\text{-}oxosar\text{-}H)](Cl0_4)_2.0.5H_2O$

R	0.064
R_w	0.067
Goodness of Fit	2.27

Table A3.1.8: Atomic Coordinates (non-Hydrogen atoms) for $[Fe^{III}(Me,CO_2H\text{-}2\text{-}oxosar\text{-}H)](Cl0_4)_2.0.5H_2O$

	x/a	y/b	z/c
Fe(1)	0.37429(5)	0.6782(2)	0.5692(1)
Fe(2)	0.3743	0.8218	0.5692
Cl(1)	0.4606(1)	-0.2004(4)	0.8736
Cl(21)	0.2377(3)	0.6600(1)	0.7381(5)
Cl(22)	0.2259(4)	0.7140(1)	0.7270(7)
O(1)	0.3884(2)	0.4594(3)	0.8103(5)
O(2)	0.4617(3)	0.2809(8)	0.6884(7)
O(3)	0.4006(2)	0.2073(7)	0.7085(6)
O(4)	0.5000	0.0729(9)	0.7500
O(5)	0.4976(4)	-0.1380(1)	0.8887(7)
O(6)	0.4343(5)	-0.1680(1)	0.9480(1)
O(7)	0.4448(3)	-0.1610(3)	0.7840(1)
O(8)	0.4652(3)	-0.3300(1)	0.8785(8)
O(9)	0.2554(4)	0.7230(2)	0.8030(1)
O(10)	0.2391(7)	0.7380(3)	0.6550(2)
O(11)	0.2057(4)	0.6000(2)	0.7470(1)
O(121)	0.2621(8)	0.5880(3)	0.6840(2)
O(122)	0.1972(7)	0.7940(2)	0.7380(2)
N(1)	0.3699(3)	0.6093(8)	0.6954(6)
N(2)	0.3770(3)	0.8469(8)	0.6422(6)
N(3)	0.3629(2)	0.5036(9)	0.5096(6)
N(4)	0.3177(3)	0.7184(9)	0.5449(6)
N(5)	0.4327(3)	0.6366(8)	0.5717(7)
N(6)	0.3881(2)	0.7667(8)	0.4431(6)
C(1)	0.4083(3)	0.4210(1)	0.6434(8)
C(2)	0.3873(3)	0.4990(1)	0.7245(8)
C(3)	0.3566(4)	0.6970(1)	0.7728(7)

Table A3.1.8 cont: Atomic Coordinates (non-Hydrogen atoms) for $[Fe^{III}(Me,CO_2H\text{-}2\text{-}oxosar\text{-}H)](Cl0_4)_2.0.5H_2O$

	x/a	y/b	z/c
C(4)	0.3515(4)	0.8300(1)	0.7302(8)
C(5)	0.3663(4)	0.9690(1)	0.5889(9)
C(6)	0.3405(4)	0.9450(1)	0.4990(8)
C(7)	0.3796(3)	0.3890(1)	0.5626(9)
C(8)	0.3185(3)	0.4930(1)	0.4991(9)
C(9)	0.3020(3)	0.6220(1)	0.4740(1)
C(10)	0.3055(4)	0.8540(1)	0.5225(9)
C(11)	0.4439(3)	0.5020(1)	0.6053(9)
C(12)	0.4503(3)	0.6670(1)	0.4773(8)
C(13)	0.4316(3)	0.7900(1)	0.4423(8)
C(14)	0.3652(3)	0.8870(1)	0.4168(8)
C(15)	0.4224(4)	0.2920(1)	0.6850(8)
C(16)	0.3240(4)	1.0740(1)	0.4676(9)

Figure A3.1.9: Electronic spectrum of $[Ni^{III}(Me,COOH\text{-}2\text{-}oxosar\text{-}H)]^{2+}$ in 0.1 M $NaClO_4$ at pH ~ 1 - 1.5 at 20° C.

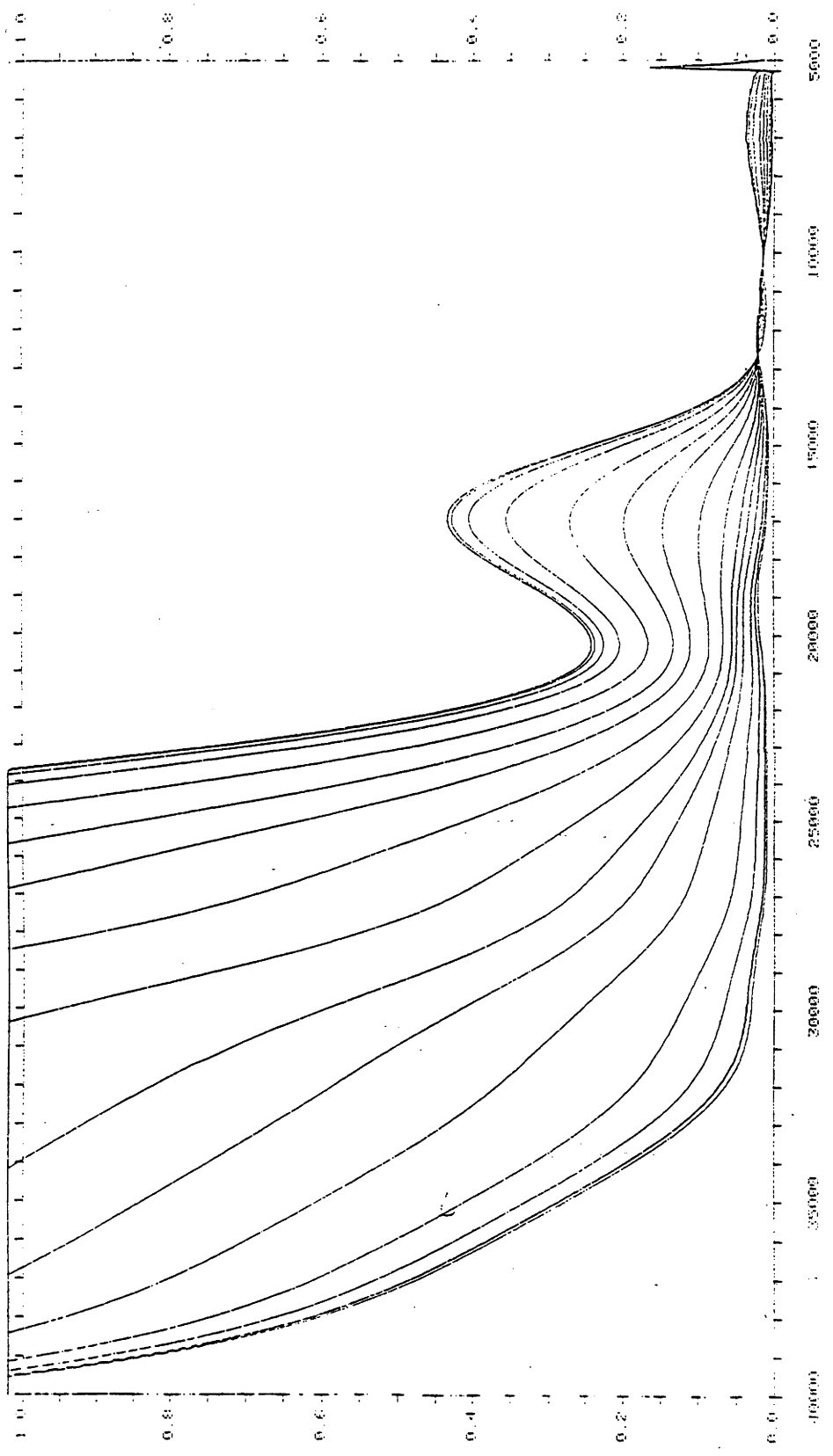

Appendix 4.1

Table A4.1.1: Crystallographic Data for $[Co^{III}(\{NH_3^+\}_2\text{-2-oxosar-H})](NO_3)_4.H_2O$

Empirical formula	$C_{14}H_{35}CoN_{12}O_{14}$
Formula weight	654.44
Crystal colour, habit	red, block
Crystal Dimensions	0.14 x 0.25 x 0.40 mm
Crystal system	orthorhombic
Lattice Type	Primitive
ω Scan PWHH	0.48°
Lattice parameters	a = 8.352(4) Å
	b = 16.075(3) Å
	c = 18.782(6) Å
V	2252(2) Å^3
Space group	$P2_12_12_1$ (#19)
Z Value	4
D_{calc} g/cm^3	1.724 g cm^{-3}
F_{000}	1368.00
μ(MoKα)	7.75 cm^{-1}
X-radiation	Mo-Kα
λ, Å	0.71069
T, °C	23.0
No of Data Collected	3311
No Obs, (I>3.00s(I))	2296
R	0.042
R_w	0.043
Goodness of Fit	1.82

Table A4.1.2: Atomic Coordinates (non-Hydrogen atoms) for $[Co^{III}(\{NH_3^+\}_2\text{-2-oxosar-H})](NO_3)_4.H_2O$

	x/a	y/b	z/c
Co(1)	0.33652(9)	0.34185(5)	0.20941(4)
O(1)	0.5488(6)	0.5502(3)	0.1355(2)
O(2)	0.2460(7)	0.4786(3)	-0.1086(3)
O(3)	0.0457(7)	0.7277(4)	0.0279(3)
O(4)	0.2624(6)	0.6561(4)	0.0296(3)
O(5)	0.0570(8)	0.6192(4)	0.0930(3)
O(6)	0.8506(8)	0.2242(3)	0.2798(4)
O(7)	0.9267(6)	0.1225(4)	0.2123(3)
O(8)	0.6768(6)	0.1466(4)	0.2297(3)
O(9)	-0.1889(7)	0.3149(4)	0.1377(3)
O(10)	-0.0076(6)	0.2477(4)	0.0830(3)
O(11)	-0.2553(6)	0.2144(3)	0.0699(3)
O(12)	0.957(1)	0.5248(7)	-0.0566(4)
O(13)	0.723(1)	0.5717(8)	-0.0340(7)
O(14)	0.791(2)	0.4515(7)	-0.0138(9)
O(15)	0.706(4)	0.515(2)	-0.083(2)
O(16)	0.773(4)	0.515(3)	0.021(2)
N(1)	0.4445(5)	0.4459(3)	0.2027(3)
N(2)	0.5157(5)	0.3089(3)	0.2736(2)
N(3)	0.4478(6)	0.3026(4)	0.1233(3)
N(4)	0.2437(5)	0.2287(3)	0.2164(3)
N(5)	0.1630(6)	0.3891(3)	0.1505(2)
N(6)	0.2054(5)	0.3778(3)	0.2927(3)
N(7)	0.4180(7)	0.5010(3)	0.0165(3)
N(8)	0.2833(7)	0.1940(3)	0.4142(3)
N(9)	0.1217(7)	0.6674(4)	0.0509(3)
N(10)	0.8191(8)	0.1653(4)	0.2403(3)
N(11)	-0.1516(7)	0.2591(4)	0.0962(3)
N(12)	0.824(1)	0.5165(6)	-0.0360(4)
C(1)	0.3888(7)	0.4453(4)	0.0785(3)
C(2)	0.4657(8)	0.4869(4)	0.1438(3)
C(3)	0.5509(9)	0.4603(5)	0.2628(4)
C(4)	0.6295(8)	0.3803(5)	0.2786(4)
C(5)	0.4707(9)	0.2769(5)	0.3439(4)
C(6)	0.2994(7)	0.2461(4)	0.3472(3)
C(7)	0.4815(8)	0.3634(4)	0.0659(3)

Table A4.1.2 cont: Atomic Coordinates (non-Hydrogen atoms) for $[Co^{III}(\{NH_3^+\}_2\text{-2-oxosar-H})](NO_3)_4.H_2O$

	x/a	y/b	z/c
C(8)	0.3594(8)	0.2293(4)	0.0960(3)
C(9)	0.3157(8)	0.1761(4)	0.1591(3)
C(10)	0.2564(8)	0.1866(4)	0.2864(3)
C(11)	0.2105(7)	0.4285(4)	0.0825(3)
C(12)	0.736(7)	0.4486(4)	0.1964(4)
C(13)	0.0472(8)	0.4062(4)	0.2663(4)
C(14)	0.1826(9)	0.3167(4)	0.3523(3)

Table A4.1.3: Crystallographic Data for $[Co^{III}(\{NH_3^+\}_2\text{-2,7-dioxosar-2H})]Cl\text{-}ZnCl_4.H_2O$

Empirical formula	$C_{14}H_{32}Cl_5Co\text{-}N_8O_3Zn$
Formula weight	662.04
Crystal colour, habit	red, prism
Crystal Dimensions	0.21x0.24x0.31
Crystal system	monoclinic
Lattice Type	Primitive
ω Scan PWHH	0.36
Lattice parameters	a = 9.965(1) (Å)
	b = 15.528(2) (Å)
	c = 15.667(2) (Å)
	β = 93.40(1)°
V	2419.9(6)
Space group	$P2_1/c$ (#14)
Z Value	4
D_{calc} g/cm^3	1.817
F_{000}	1352
μ(MoKα)	22.64
X-radiation	MoKα
λ, Å	0.71069
T, °C	23(1)

Table A4.1.3 cont: Crystallographic Data for $[Co^{III}(\{NH_3^+\}_2\text{-}2,7\text{-dioxosar-}2H)]ClZnCl_4.H_2O$

No of Data Collected	5987
Unique Data	5788
No Obs, (I>3.00s(I))	4159
R	0.026
R_w	0.022
Goodness of Fit	1.76

Table A4.1.4: Atomic Coordinates (non-Hydrogen atoms) for $[Co^{III}(\{NH_3^+\}_2\text{-}2,7\text{-dioxosar-}2H)]ClZnCl_4.H_2O$

	x/a	y/b	z/c
Zn(1)	0.70645(3)	0.16015(2)	0.56792(2)
Co(1)	0.26903(3)	0.12917(2)	0.22600(2)
Cl(1)	0.81793(8)	0.08995(5)	0.46678(5)
Cl(2)	0.51726(7)	0.08700(4)	0.58474(4)
Cl(3)	0.65854(9)	0.29398(5)	0.51580(5)
Cl(4)	0.83566(7)	0.16915(5)	0.69227(4)
Cl(5)	0.26042(8)	0.36306(5)	0.42423(4)
O(1)	0.0831(2)	-0.0561(1)	0.0811(1)
O(2)	0.6720(2)	0.1024(1)	0.2080(1)
O(3)	0.9683(3)	0.2585(2)	0.3767(2)
N(1)	0.2248(2)	0.0194(1)	0.1758(1)
N(2)	0.4418(2)	0.1081(1)	0.1791(1)
N(3)	0.1938(2)	0.1775(1)	0.1181(1)
N(4)	0.3078(2)	0.2488(1)	0.2616(1)
N(5)	0.0966(2)	0.1230(1)	0.2843(1)
N(6)	0.3543(2)	0.0943(1)	0.3384(1)
N(7)	-0.1245(2)	0.0481(2)	0.0955(2)
N(8)	0.6730(2)	0.2222(2)	0.3255(1)
C(1)	0.0048(2)	0.0764(2)	0.1408(2)
C(2)	0.1110(2)	0.0056(2)	0.1304(2)
C(3)	0.3446(3)	-0.0308(2)	0.1560(2)
C(4)	0.4413(3)	0.0333(2)	0.1210(2)
C(5)	0.5563(2)	0.1293(2)	0.2201(2)
C(6)	0.5367(2)	0.1914(2)	0.2940(1)

Table A4.1.4 cont: Atomic Coordinates (non-Hydrogen atoms) for $[Co^{III}(\{NH_3^+\}_2\text{-}2,7\text{-dioxosar-2H})]ClZnCl_4.H_2O$

C(7)	0.0478(3)	0.1610(2)	0.0998(2)
C(8)	0.2305(3)	0.2706(2)	0.1141(2)
C(9)	0.2275(3)	0.3074(2)	0.2020(2)
C(10)	0.4535(3)	0.2702(2)	0.2669(2)
C(11)	-0.0238(3)	0.0908(2)	0.2343(2)
C(12)	0.1242(3)	0.0675(2)	0.3619(2)
C(13)	0.2525(3)	0.0979(2)	0.4040(2)
C(14)	0.4785(3)	0.1421(2)	0.3674(2)

Table A4.1.5: Crystallographic Data for $[Co^{III}(\{NH_3^+\}_2\text{-}2,9\text{-dioxosar-2H})]\text{-}(S_2O_6)_{1.5}.3H_2O$

Empirical formula	$C_{14}H_{36}CoN_8\text{-}O_{14}S_3$
Formula weight	1391.19
Crystal colour, habit	orange, rod
Crystal Dimensions	0.19x0.06x0.06
Crystal system	monoclinic
Lattice Type	C-centred
ω Scan PWHH	0.4
Lattice parameters	a = 33.612(6) (Å)
	b = 8.536(5) (Å)
	c = 18.420(3) (Å)
	β = 93.00(2)°
V	5277(3)
Space group	C2/c (#15)
Z Value	4
D_{calc} g/cm^3	1.751
F_{000}	2904
μ(CuKα)	80.72
X-radiation	CuKα

Table A4.1.5 cont: Crystallographic Data for $[Co^{III}(\{NH_3^+\}_2\text{-}2,9\text{-dioxosar-}2H)](S_2O_6)_{1.5}.3H_2O$

λ, Å	1.54178
T, °C	-60(1)
No of Data Collected	4333
Unique Data	4248
No Obs, (I>3.00s(I))	2316
R	0.043
R_w	0.05
Goodness of Fit	1.48

Table A4.1.6: Atomic Coordinates (non-Hydrogen atoms) for $[Co^{III}(\{NH_3^+\}_2\text{-}2,9\text{-dioxosar-}2H)](S_2O_6)_{1.5}.3H_2O$

	x/a	y/b	z/c
Co(1)	0.38774(2)	0.3846(1)	0.14721(4)
S(1)	0.40581(4)	0.1247(2)	0.41810(7)
S(2)	0.43941(4)	0.0003(2)	0.34208(7)
S(3)	0.26485(4)	0.1530(2)	0.02566(8)
O(1)	0.50033(10)	0.4952(5)	0.0956(2)
O(2)	0.3056(1)	0.7280(5)	0.1707(2)
O(3)	0.4338(1)	0.2260(6)	0.4564(2)
O(4)	0.3764(1)	0.2062(1)	0.3735(2)
O(5)	0.3897(1)	0.0037(5)	0.4620(2)
O(6)	0.4120(1)	-0.1161(5)	0.3129(2)
O(7)	0.4732(1)	-0.0619(5)	0.3856(2)
O(8)	0.4511(1)	0.1181(5)	0.2902(2)
O(9)	0.3070(1)	0.1770(5)	0.0112(2)
O(10)	0.2580(1)	0.1710(5)	0.1019(2)
O(11)	0.2476(1)	0.0157(5)	-0.0085(2)
O(12)	0.3295(1)	0.8243(6)	0.3649(2)
O(13)	0.2694(2)	0.3228(7)	0.3836(3)
O(14)	0.2272(2)	0.5414(6)	0.1939(3)
N(1)	0.4370(1)	0.4915(5)	0.1383(2)
N(2)	0.3979(1)	0.4222(5)	0.2529(2)
N(3)	0.4147(1)	0.1781(5)	0.1465(2)

Table A4.1.6 cont: Atomic Coordinates (non-Hydrogen atoms) for $[Co^{III}(\{NH_3^+\}_2\text{-}2,9\text{-dioxosar-}2H)](S_2O_6)_{3/2}.3H_2O$

	x/a	y/b	z/c
N(4)	0.3393(1)	0.2676(6)	0.1681(2)
N(5)	0.3788(1)	0.3701(6)	0.0397(2)
N(6)	0.3580(1)	0.5734(5)	0.1374(2)
N(7)	0.4853(1)	0.2729(5)	-0.0013(2)
N(8)	0.2948(1)	0.5656(6)	0.2911(3)
C(1)	0.4525(1)	0.3077(7)	0.0476(3)
C(2)	0.4650(1)	0.4428(6)	0.0964(3)
C(3)	0.4460(1)	0.5958(7)	0.2000(3)
C(4)	0.4385(2)	0.4965(7)	0.2656(3)
C(5)	0.3667(2)	0.5152(7)	0.2885(3)
C(6)	0.3267(2)	0.5066(7)	0.2443(3)
C(7)	0.4461(1)	0.1579(6)	0.0921(3)
C(8)	0.3832(2)	0.0550(6)	0.1400(3)
C(9)	0.3504(2)	0.1024(7)	0.1871(3)
C(10)	0.3142(2)	0.3401(7)	0.2241(3)
C(11)	0.4160(1)	0.3570(7)	-0.0009(3)
C(12)	0.3535(1)	0.5064(7)	0.0131(3)
C(13)	0.3609(2)	0.6420(7)	0.0650(3)
C(14)	0.3287(2)	0.6143(7)	0.1782(3)

Table A4.1.7: Crystallographic Data for $[Co^{III}(6\text{-}\{NH_3^+,C(O)NH\}\text{-}13\text{-}\{NH_3^+,CH_2NH_2\}\text{-cyclam})]Cl_4.2.75H_2O$

Empirical formula	$C_{12}H_{36.5}Cl_4\text{-}CoN_8O_{3.75}$
Formula weight	553.72
Crystal colour, habit	orange, cuboid
Crystal Dimensions	0.18x0.23x0.18
Crystal system	orthorhombic
Lattice Type	Primitive

Table A4.1.7 cont: Crystallographic Data for [Co(6-{NH_3^+,C(O)NH}-13-{NH_3^+,CH_2NH_2}-cyclam)]Cl_4.2.75H_2O

ω Scan PWHH	0.35
Lattice parameters	a = 12.513(2) (Å)
	b = 16.847(3) (Å)
	c = 22.244(3) (Å)
	β = - °
V	4688(1)
Space group	Pbca (#61)
Z Value	8
D_{calc} g/cm^3	1.569
F_{000}	2316
μ(MoKα)	12.22
X-radiation	MoKα
λ, Å	0.71069
T, °C	23(1)
No of Data Collected	6005
Unique Data	-
No Obs, (I>3.00s(I))	2785
R	0.038
R_w	0.025
Goodness of Fit	1.61

Table A4.1.8: Atomic Coordinates (non-Hydrogen atoms) for [Co^{III}(6-{NH_3^+,C(O)NH}-13-{NH_3^+,CH_2NH_2}-cyclam)]Cl_4.2.75H_2O

	x/a	y/b	z/c
Co(1)	0.13701(4)	0.19536(3)	0.13996(4)
Cl(1)	0.81713(10)	0.12466(8)	0.09612(6)
Cl(2)	0.96040(9)	0.24735(9)	0.40040(6)
Cl(3)	0.8715(1)	0.04447(7)	0.47040(6)
Cl(4)	0.7349(1)	0.12807(8)	0.74469(6)
O(1)	0.9813(3)	0.0044(2)	0.3479(2)
O(2)	0.5686(4)	0.0895(3)	0.6379(2)

Table A4.1.8 cont: Atomic Coordinates (non-Hydrogen atoms) for $[Co^{III}(6\text{-}\{NH_3^+,C(O)NH\}\text{-}13\text{-}\{NH_3^+,CH_2NH_2\}\text{-cyclam})]Cl_4.2.75H_2O$

	x/a	y/b	z/c
O(3)	0.7871(5)	0.0830(4)	0.5964(3)
O(31)	0.3534(2)	0.0737(2)	0.2400(1)
N(1)	0.1810(3)	0.0349(2)	0.2995(2)
N(4)	0.1078(3)	0.3620(2)	-0.0194(2)
N(12)	0.0668(3)	0.0897(2)	0.1471(2)
N(15)	0.1709(3)	0.1662(2)	0.0567(2)
N(22)	0.0942(3)	0.2232(2)	0.2228(2)
N(25)	0.0047(3)	0.2500(2)	0.1149(2)
N(32)	0.2645(3)	0.1475(2)	0.1691(2)
N(35)	0.2191(3)	0.2936(2)	0.1279(2)
C(2)	0.1630(3)	0.0877(2)	0.2470(2)
C(3)	0.1190(3)	0.3072(3)	0.0337(2)
C(11)	0.0874(3)	0.0443(3)	0.2041(2)
C(13)	0.0982(4)	0.0436(3)	0.0930(2)
C(14)	0.0982(4)	0.0997(3)	0.0402(2)
C(16)	0.1718(3)	0.2310(3)	0.0109(2)
C(21)	0.1147(3)	0.1643(2)	0.2711(2)
C(23)	-0.0194(3)	0.2509(3)	0.2216(2)
C(24)	-0.0319(2)	0.3002(3)	0.1659(2)
C(26)	0.0052(3)	0.2932(3)	0.0567(2)
C(31)	0.2711(3)	0.1030(2)	0.2175(2)
C(36)	0.1885(4)	0.3496(3)	0.0798(2)

Figure A4.1.9: Electronic spectrum of $[Ni^{III}(\{NH_3^+\}_2\text{-2-oxosar-H})]^{4+}$ in 0.1 M $NaClO_4$ at pH ~ 1 - 1.5 at 20° C.

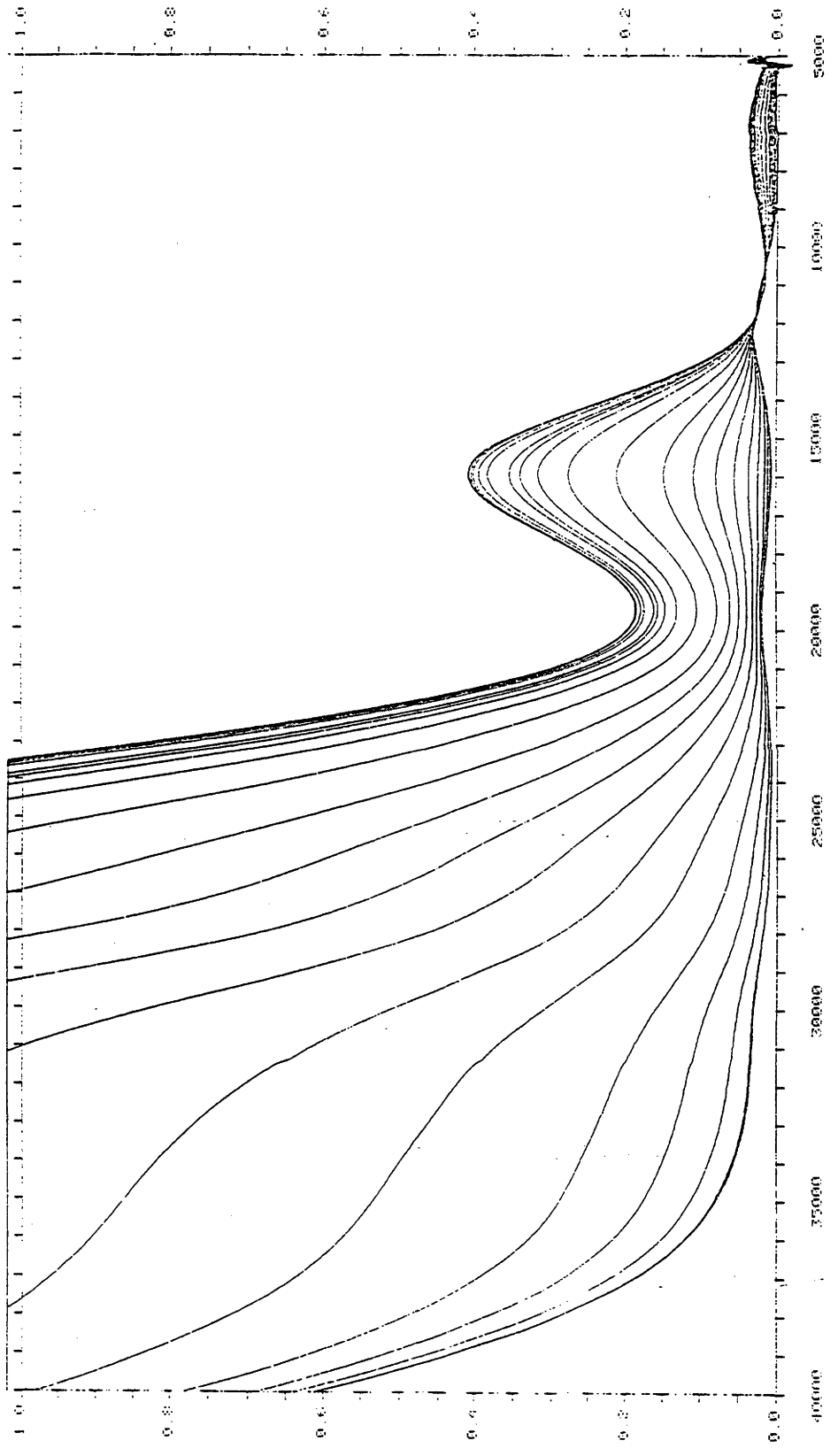

Figure A4.1.10: Electronic spectrum of $[Ni^{III}(\{NH_3^+\}_2\text{-}2,7\text{-dioxosar-}2H)]^{3+}$ in 0.1 M $NaClO_4$ at pH ~ 1 - 1.5 at 20° C.

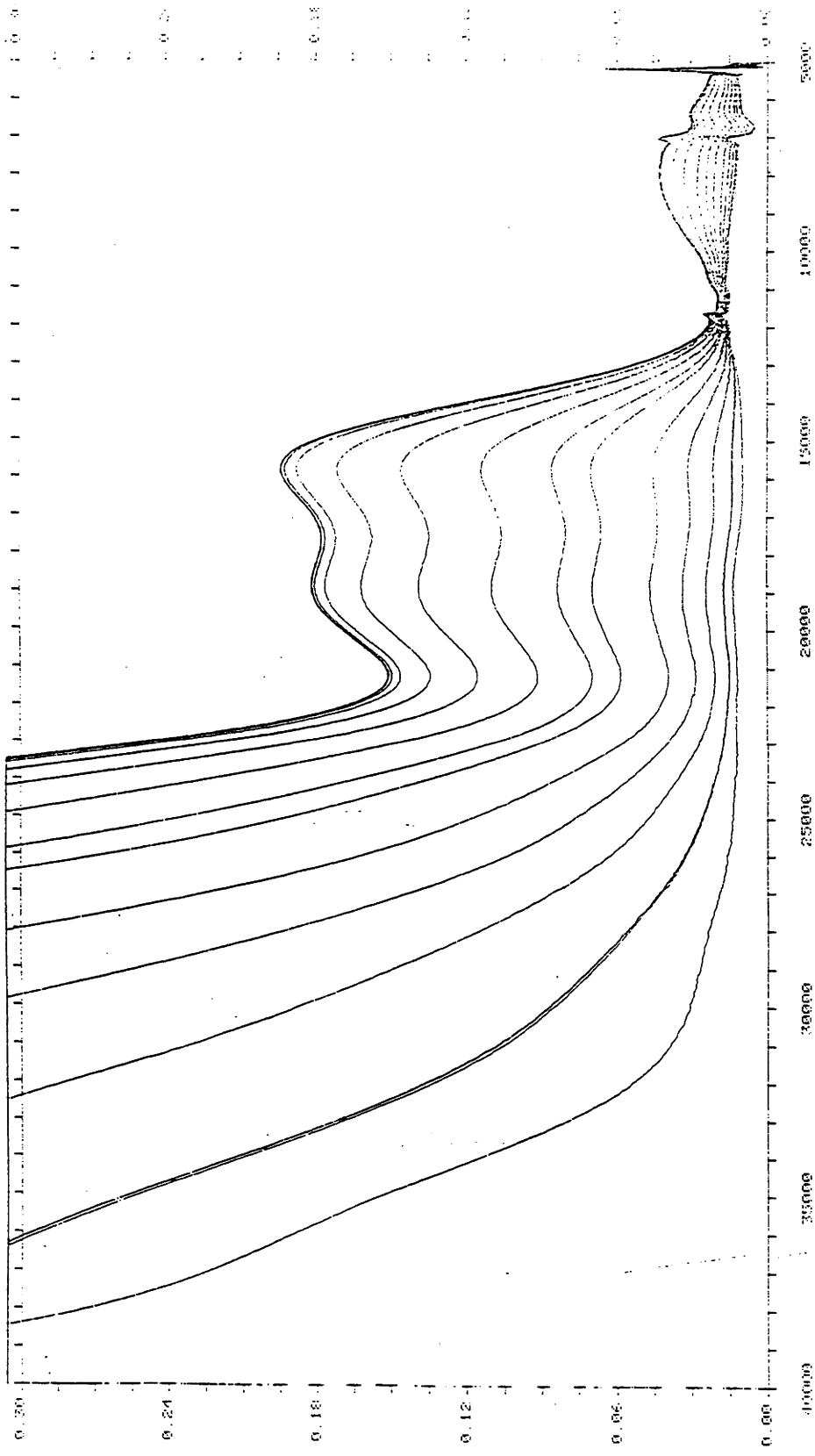

Appendix 5.1

Table A5.1.1: Crystallographic Data for $[Co^{III}(2,2',2''\text{-trioxosen-3H})].3H_2O$

Empirical formula	$C_{11}H_{27}CoN_6O_6$
Formula weight	698.30
Crystal colour, habit	orange-red, hexagonal prism
Crystal Dimensions	0.18 x 0.18 x 0.28 mm
Crystal system	hexagonal
Lattice Type	Primitive
ω Scan PWHH	0.31°
Lattice parameters	a = 8.040(3) Å
	c = 43.730(4) Å
V	2447.8(5) $Å^3$
Space group	$P6_5$ (#170)
Z Value	6
D_{calc} g/cm^3	1.621 g cm^{-3}
F_{000}	1260.00
μ(CuKα)	86.50 cm^{-1}
X-radiation	Cu-Kα
λ, Å	1.54178
T, °C	23.0
No of Data Collected	3956
No of Unique Data	1259
No Obs, (I>3.00s(I))	1090
R	0.027
R_w	0.029
Goodness of Fit	1.72

Table A5.1.2: Atomic Coordinates (non-Hydrogen atoms) for $[Co^{III}(2,2',2''\text{-trioxosen-3H})].3H_2O$

	x/a	y/b	z/c
Co(1)	0.3398(1)	0.2575(1)	0.0000
O(1)	0.0788(5)	0.3805(5)	0.06647(8)
O(2)	0.4654(5)	0.8087(5)	0.00251(8)
O(3)	0.6570(5)	0.5816(5)	0.07028(8)
O(4)	0.7134(6)	0.7875(6)	0.12633(8)
O(5)	-0.0164(5)	0.6203(5)	0.09611(8)
O(6)	-0.0363(6)	0.1995(6)	0.12345(8)
N(1)	0.2145(6)	-0.0220(6)	0.00900(10)
N(2)	0.1416(6)	0.2547(6)	0.02387(9)
N(3)	0.1925(6)	0.1962(6)	-0.03928(9)
N(4)	0.4245(6)	0.5161(6)	-0.01139(9)
N(5)	0.5653(7)	0.2576(7)	-0.01904(10)
N(6)	0.5000(6)	0.3423(6)	0.03501(9)
C(1)	0.0728(9)	-0.0673(8)	0.0341(1)
C(2)	-0.0181(8)	0.0578(8)	0.0299(1)
C(3)	0.1843(7)	0.3883(7)	0.0446(1)
C(4)	0.2036(8)	0.3693(8)	-0.0519(1)
C(5)	0.3935(8)	0.5370(8)	-0.0439(1)
C(6)	0.4306(7)	0.6397(8)	0.0081(1)
C(7)	0.7224(8)	0.3127(9)	0.0029(2)
C(8)	0.6430(8)	0.2776(8)	0.0351(1)
C(9)	0.5310(7)	0.4930(7)	0.0503(1)
C(10)	0.3900(8)	0.5674(8)	0.0422(1)
C(11)	0.4144(7)	0.7252(8)	0.0634(1)

Appendix 6.1

Table A6.1.1: Crystallographic Data for *trans*-[$Co^{III}(Et_2$-sar-2,9-diene)]$Cl_3.3H_2O$

Empirical formula	$C_{18}H_{44}Cl_3CoN_6O_4$
Formula weight	573.88
Crystal colour, habit	Yellow, block
Crystal Dimensions	0.12 x 0.14 x 0.27 mm
Crystal system	monoclinic
Lattice Type	C-centred
ω Scan PWHH	0.35°
Lattice parameters	a = 8.863(3) Å
	b = 16.369(6) Å
	c = 18.025(4) Å
	β = 96.37(2)°
V	2598(1) $Å^3$
Space group	C2/c (#15)
Z Value	4
D_{calc} g/cm^3	1.467 g cm^{-3}
F_{000}	1216.00
μ(MoKα)	10.04 cm^{-1}
X-radiation	Mo-Kα
λ, Å	0.71069
T, °C	23.0
No of Data Collected	3314
No of Unique Data	3113
No Obs, (I>3.00s(I))	2157
R	0.029
R_w	0.025
Goodness of Fit	1.65

Table A6.1.2: Atomic Coordinates (non-Hydrogen atoms) for *trans*-[$Co^{III}(Et_2$-sar-2,9-diene)]$Cl_3.3H_2O$

	x/a	y/b	z/c
Co(1)	0.5000	0.09928(3)	0.2500
Cl(1)	0.0000	-0.00281(6)	0.2500
Cl(2)	0.96077(8)	0.30560(4)	0.08510(4)
O(1)	0.4418(3)	0.3262(1)	0.1582(1)
O(2)	0.6128(3)	0.3266(2)	0.0421(1)
N(1)	0.5655(2)	0.1126(1)	0.1539(1)
N(2)	0.3542(2)	0.0116(1)	0.2200(1)
N(3)	0.3407(2)	0.1799(1)	0.2185(1)
C(1)	0.2627(4)	0.0263(2)	-0.0285(2)
C(2)	0.2151(3)	0.0907(2)	0.0248(1)
C(3)	0.3096(3)	0.0914(2)	0.1017(1)
C(4)	0.4717(3)	0.1162(1)	0.0957(1)
C(5)	0.7231(3)	0.1420(2)	0.1562(2)
C(6)	0.3105(3)	0.0065(2)	0.1377(1)
C(7)	0.4162(3)	-0.0668(1)	0.2525(1)
C(8)	0.2366(3)	0.1532(2)	0.1518(2)
C(9)	0.2582(3)	0.2064(2)	0.2829(2)

Additional Appendix

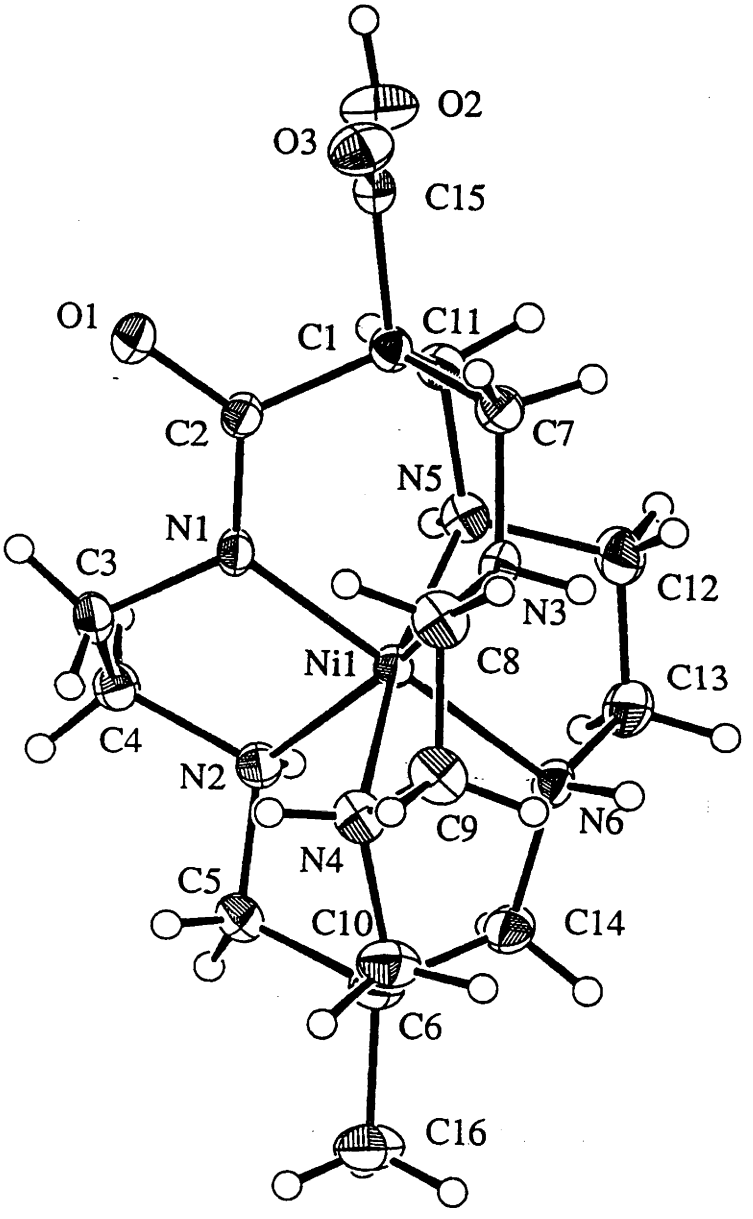

Figure AA1.1. Thermal ellipsoid diagram of $[Ni^{III}(Me,COOH\text{-}2\text{-}oxosar\text{-}H)](ClO_4)_2.H_2O$ with selected atom labelling. Ellipsoids show 30% probability levels. Hydrogen atoms are drawn as circles with small radii.

Table AA1.1: Crystallographic Data for $[Ni^{III}(Me,COOH\text{-}2\text{-}oxosar\text{-}H)](ClO_4)_2.H_2O$

Empirical formula	$C_{16}H_{33}Cl_2NiN_6O_{12}$
Formula weight	631.08
Crystal colour, habit	Dark-green, platet
Crystal Dimensions	0.45 x 0.44 x 0.20 mm
Crystal system	orthorhombic
Lattice Type	Primative
ω Scan PWHH	0.31°
Lattice parameters	a = 12.979(2) Å
	b = 18.030(2) Å
	c = 21.423(2) Å
V	5013.1(8) $Å^3$
Space group	Pbca (#1561)
Z Value	8
D_{calc} g/cm^3	1.672 g cm^{-3}
F_{000}	2632.00
μ(CuKα)	37.34 cm^{-1}
X-radiation	Cu-Kα
λ, Å	1.5478
T, °C	23.0
No of Data Collected	4186
No Obs, (I>2.0σ(I))	3350
R	0.054
R_w	0.079
Goodness of Fit	3.70

Table AA.1.2: Atomic Coordinates (non-Hydrogen atoms) for $[Ni^{III}(Me,COOH\text{-}2\text{-}oxosar\text{-}H)](ClO_4)_2.H_2O$

	x/a	y/b	z/c
Ni(1)	0.45261(2)	0.76143(2)	0.91327(1)
Cl(1)	0.2165(2)	0.5260(1)	0.8915(6)
Cl(2)	0.1990(2)	0.53417(9)	0.88578(7)
Cl(3)	0.5324(2)	0.3962(1)	0.81076(8)
Cl(4)	0.5030(2)	0.40273(9)	0.80836(7)
O(1)	0.2009(1)	0.80612(9)	1.01672(7)
O(2)	0.3291(2)	0.9350(1)	1.09809(8)
O(3)	0.3078(1)	0.82292(9)	1.13797(7)
O(4)	0.2582(2)	0.9927(2)	1.2011(1)
O(10)	0.2593(2)	0.5644(1)	0.83712(9)
O(11)	0.2748(4)	0.4736(3)	0.9206(3)
O(12)	0.1233(4)	0.4899(3)	0.8640(3)
O(13)	0.2287(6)	0.5785(3)	0.9404(2)
O(14)	0.243(1)	0.4627(5)	0.9019(6)
O(15)	0.0947(4)	0.5230(5)	0.8879(3)
O(16)	0.1686(9)	0.5905(4)	0.9253(4)
O(17)	0.1637(7)	0.4649(4)	0.8614(4)
O(18)	0.1136(5)	0.5809(4)	0.9018(3)
O(19)	0.2607(6)	0.5211(5)	0.9385(3)
O(20)	0.4723(2)	0.3327(1)	0.8281(1)
O(21)	0.5353(5)	0.4539(2)	0.8562(2)
O(22)	0.6336(4)	0.3732(3)	0.8133(3)
O(23)	0.5025(4)	0.4112(3)	0.7463(2)
O(24)	0.5823(8)	0.4380(6)	0.8457(5)
O(25)	0.5601(8)	0.4090(5)	0.7501(3)
O(26)	0.4080(7)	0.4400(7)	0.7983(6)
O(27)	0.6073(6)	0.3914(5)	0.7814(5)
O(28)	0.4486(9)	0.4418(6)	0.7628(5)
O(29)	0.4842(7)	0.4532(4)	0.8563(3)
N(1)	0.3171(1)	0.77075(9)	0.94267(8)
N(2)	0.3899(1)	0.7836(1)	0.82848(8)
N(3)	0.4925(1)	0.7257(1)	1.00172(8)
N(4)	0.4480(1)	0.6464(1)	0.89568(8)
N(5)	0.4816(1)	0.8700(1)	0.93904(8)
N(6)	0.5906(1)	0.7632(1)	0.87581(8)

Table AA.1.2 cont: Atomic Coordinates (non-Hydrogen atoms) for $[Ni^{III}(Me,COOH\text{-}2\text{-}oxosar\text{-}H)](ClO_4)_2.H_2O$

	x/a	y/b	z/c
C(1)	0.3813(1)	0.8328(1)	1.03521(9)
C(2)	0.2913(1)	0.8006(1)	0.99672(9)
C(3)	0.2385(2)	0.7604(1)	0.8933(1)
C(4)	0.2788(2)	0.8025(1)	0.83732(9)
C(5)	0.4059(2)	0.7219(1)	0.7826(1)
C(6)	0.5102(2)	0.8636(1)	0.7902(1)
C(7)	0.4606(2)	0.7747(1)	1.0541(1)
C(8)	0.4530(2)	0.6495(1)	1.0084(1)
C(9)	0.4838(2)	0.6060(1)	0.9520(1)
C(10)	0.5019(2)	0.6222(1)	0.8385(1)
C(11)	0.4313(2)	0.8963(1)	0.9975(1)
C(12)	0.5968(2)	0.8738(1)	0.9406(1)
C(13)	0.6351(2)	0.8397(1)	0.8823(1)
C(14)	0.5948(2)	0.7384(1)	0.8088(1)
C(15)	0.3346(1)	0.8633(1)	1.0962(1)
C(16)	0.5404(2)	0.6489(2)	0.7272(1)

Table AA1.3. Bond distances (Å) for $[Ni^{III}(Me,COOH\text{-}2\text{-}oxosar\text{-}H)](ClO_4)_2.H_2O$

Atom	Distance (Å)	Atom	Distance (Å)
Ni(1)-N(1)	1.876(3)	Ni(1)-N(2)	2.030(3)
Ni(1)-N(3)	2.067(4)	Ni(1)-N(4)	2.108(4)
Ni(1)-N(5)	2.069(3)	Ni(1)-N(6)	1.963(3)
Cl(1)-O(10)	1.465(5)*	Cl(1)-O(11)	1.361(9)*
Cl(1)-O(12)	1.495(9)*	Cl(1)-O(13)	1.419(9)*
Cl(2)-O(10)	1.413(4)*	Cl(2)-O(14)	1.45(1)*
Cl(2)-O(15)	1.37(1)*	Cl(2)-O(16)	1.38(1)*
Cl(2)-O(17)	1.43(1)*	Cl(2)-O(18)	1.434(9)*
Cl(2)-O(19)	1.40(1)*	Cl(3)-O(20)	1.434(5)*
Cl(3)-O(21)	1.426(7)*	Cl(3)-O(22)	1.378(9)*
Cl(3)-O(23)	1.459(8)*	Cl(4)-O(20)	1.389(4)*
Cl(4)-O(24)	1.45(1)*	Cl(4)-O(25)	1.46(1)*
Cl(4)-O(26)	1.42(1)*	Cl(4)-O(27)	1.49(1)*
Cl(4)-O(28)	1.40(1)*	Cl(4)-O(29)	1.39(1)*
O(1)-C(2)	1.252(4)	O(2)-C(151)	1.296(5)
O(3)-O(15)	1.204(5)		
N(1)-C(2)	1.320(5)	N(1)-C(3)	1.481(5)
N(2)-C(4)	1.493(5)	N(2)-C(5)	1.498(5)
N(3)-C(7)	1.486(5)	N(3)-C(8)	1.474(5)
N(4)-C(9)	1.485(5)	N(4)-C(10)	1.476(6)
N(5)-C(11)	1.490(5)	N(5)-C(12)	1.497(5)
N(6)-C(13)	1.502(5)	N(6)-C(14)	1.505(5)
C(1)-C(2)	1.542(5)	C(1)-C(7)	1.525(5)
C(1)-C(11)	1.544(5)	C(1)-C(15)	1.541(5)
C(3)-C(4)	1.513(6)	C(5)-C(6)	1.528(6)
C(6)-C(10)	1.520(6)	C(6)-C(14)	1.528(6)
C(6)-C(16)	1.538(6)	C(8)-C(9)	1.495(6)
C(12)-C(13)	1.477(6)		1.478(4)

* Restrained during refinement

Table AA1.4. Bond Angles (°) for $[Ni^{III}(Me,COOH\text{-}2\text{-}oxosar\text{-}H)](ClO_4)_2.H_2O$.

Atom	Angle (°)	Atom	Angle (°)
N(1)-Ni-N(2)	84.7(1)	N(1)-Ni-N(3)	87.4(1)
N(1)-Ni-N(4)	97.0(1)	N(1)-Ni-N(5)	89.8(1)
N(1)-Ni-N(6)	172.5(1)	N(2)-Ni-N(3)	169.1(1)
N(2)-Ni-N(4)	91.3(1)	N(2)-Ni-N(5)	97.2(1)
N(2)-Ni-N(6)	89.8(1)	N(3)-Ni-N(4)	82.2(1)
N(3)-Ni-N(5)	90.3(1)	N(3)-Ni-N(6)	98.7(1)
N(4)-Ni-N(5)	169.6(1)	N(4)-Ni-N(6)	88.2(1)
N(5)-Ni-N(6)	85.9(1)	O(10-Cl(1)-O(11)	118.8(6)
O(10)-Cl(1)-O(12)	101.5(5)*	O(10-Cl(1)-O(13)	103.3(5)*
O(11)-Cl(1)-O(12)	109.1(7)*	O(11)-Cl(1)-O(13)	93.7(8)*
O(12)-Cl(1)-O(13)	132.1(8)*	O(10)-Cl(2)-O(14)	107.5(9)*
O(10-Cl(2)-O(15)	128.9(7)*	O(10)-Cl(2)-O(16)	109.1(7)*
O(10)-Cl(2)-O(17)	104.2(7)*	O(10)-Cl(2)-O(18)	112.3(6)*
O(10)-Cl(2)-O(19)	110.0(7)*	O(14)-Cl(2)-O(15)	104(1)*
O(14)-Cl(2)-O(16)	128(1)*	O(15-Cl(2)-O(16)	79(1)*
O(17)-Cl(2)-O(18)	110.7(9)*	O(17)-Cl(2)-O(19)	109(1)*
O(18)-Cl(2)-O(19)	110.2(9)*	O(20)-Cl(3)-O(21)	114.8(5)*
O(20)-Cl(3)-O(22)	105.6(6)*	O(20)-Cl(3)-O(23)	104.4(5)*
O(21)-Cl(3)-O(22)	99.7(7)*	O(21)-Cl(3)-O(23)	121.2(6)*
O(22)-Cl(3)-O(23)	110.2(7)	O(20)-Cl(4)-O(24)	115.7(9)*
O(20)-Cl(4)-O(25)	118.6(7)*	O(20)-Cl(4)-O(26)	103(1)*
O(20)-Cl(4)-O(27)	104.8(7)*	O(20)-Cl(4)-O(28)	121.8(9)*
O(20)-Cl(4)-O(29)	108.6(7)*	O(24)-Cl(4)-O(25)	94(1)*
O(24)-Cl(4)-O(26)	120(2)*	O(25)-Cl(4)-O(26)	106(1)*
O(27)-Cl(4)-O(28)	105(1)*	O(27)-Cl(4)-O(29)	122(1)*
O(28)-Cl(4)-O(29)	96(1)*	Ni-N(1)-C(2)	124.7(2)
Ni-N(1)-C(3)	113.2(2)	C(2)-N(1)-C(3)	120.2(3)
Ni-N(2)-C(4)	108.6(2)	Ni-N(2)-C(5)	112.6(2)
C(4)-N(2)-C(5)	112.8(3)	Ni-N(3)-C(7)	115.9(2)
Ni-N(3)-C(8)	107.0(3)	C(7)-N(3)-C(8)	112.6(3)
Ni-N(4)-C(9)	109.2(3)	Ni-N(4)-C(10)	115.2(3)
C(9)-N(4)-C(10)	112.3(3)	Ni-N(5)-C(11)	116.4(2)

* Restrained during refinement

Table AA1.4 cont. Bond Angles (°) for $[Ni^{III}(Me,COOH\text{-}2\text{-}oxosar\text{-}H)](ClO_4)_2.H_2O$.

Atom	Angle (°)	Atom	Angle (°)
Ni-N(5)-C(12)	103.3(3)	C(11)-N(5)-C(12)	113.9(3)
Ni-N(6)-C(13)	109.1(2)	Ni-N(6)-C(14)	114.7(2)
C(13)-N(6)-C(14)	110.4(3)	C(2)-C(1)-C(7)	113.2(3)
C(2)-C(1)-C(11)	108.5(3)	C(2)-C(1)-C(15)	106.9(3)
C(7)-C(1)-C(11)	111.3(3)	C(7)-C(1)-C(15)	106.5(3)
C(11)-C(1)-C(15)	110.2(3)	O(1)-C(2)-N(1)	124.8(3)
O(1)-C(2)-C(1)	119.7(3)	N(1)-C(2)-C(1)	115.5(3)
N(1)-C(3)-C(4)	105.3(3)	N(2)-C(4)-C(3)	108.6(3)
N(2)-C(5)-C(6)	112.9(3)	C(5)-C(6)-C(10)	109.8(4)
C(5)-C(6)-C(14)	111.8(3)	C(5)-C(6)-C(16)	108.4(4)
C(10)-C(6)-C(14)	110.1(3)	C(10)-C(6)-C(16)	108.6(4)
C(14)-C(6)-C(16)	108.0(4)	N(3)-C(7)-C(1)	113.3(3)
N(3)-C(8)-C(9)	108.5(3)	N(4)-C(9)-C(8)	108.4(3)
N(4)-C(10)-C(6)	112.5(3)	N(5)-C(11)-C(1)	112.9(3)
N(5)-C(12)-C(13)	107.4(3)	N(6)-C(13)-C(12)	109.4(3)
N(6)-C(14)-C(6)	114.5(3)	O(2)-C(15)-O(3)	124.3(4)
O(2)-C(15)-C(1)	113.8(4)	O(3)-C(15)-C(1)	121.9(4)

* Restrained during refinement